

RESERVOIR FORMATION DAMAGE

**Fundamentals, Modeling,
Assessment, and Mitigation**

Faruk Civan

**RESERVOIR
FORMATION
DAMAGE**

This page intentionally left blank

RESERVOIR FORMATION DAMAGE

**Fundamentals, Modeling,
Assessment, and Mitigation**

Faruk Civan

University of Oklahoma



Gulf Publishing Company
Houston, Texas

Reservoir Formation Damage

Copyright ©2000 by Gulf Publishing Company, Houston, Texas.
All rights reserved. This book, or parts thereof, may not be
reproduced in any form without express written permission of
the publisher.

Gulf Publishing Company
Book Division
P.O. Box 2608 □ Houston, Texas 77252-2608

10 9 8 7 6 5 4 3 2 1

Library of Congress Cataloging-in-Publication Data

Civan, Faruk.

Reservoir formation damage : fundamentals, modeling,
assessment, and mitigation / Faruk Civan.

p. cm.

Includes bibliographical references and index.

ISBN 0-88415-301-0 (alk. paper)

1. Hydrocarbon reservoirs. 2. Petroleum—Geology. I. Title.

TN870.57.C58 2000

622'.338—dc21

00-027480

Printed in the United States of America.

Printed on acid-free paper (∞).

*Dedicated to
my family
and
Dr. C. M. Sliepcevich
with love and appreciation*

This page intentionally left blank

Contents

Preface, xv

CHAPTER 1

Overview of Formation Damage 1

Summary, 1. Introduction, 1. Common Formation Damage Problems, Factors, and Mechanisms, 4. Team for Understanding and Mitigation of Formation Damage, 6. Objectives of the Book, 6. References, 7.

PART I

Characterization of the Reservoir Rock for Formation Damage

CHAPTER 2

Mineralogy and Mineral Sensitivity of Petroleum-Bearing Formations 10

Summary, 10. Introduction, 10. Origin of Petroleum-Bearing Formations, 11. Constituents of Sedimentary Rocks, 11. Composition of Petroleum-Bearing Formations, 12. Mineral Sensitivity of Sedimentary Formations, 14. Mechanisms of Clay Swelling, 22. Models for Clay Swelling, 25. Graphical Representation of Clay Content, 42. Hayatdavoudi Hydration Index (HHI), 43. References, 44.

CHAPTER 3

Petrography and Texture of Petroleum-Bearing Formations 49

Summary, 49. Introduction, 49. Petrographical Characteristics, 49. References, 63.

CHAPTER 4

Petrophysics-Flow Functions and Parameters66
Summary, 66. Introduction, 66. Wettability Alteration, 66.
End-Point Saturations, 72. Alteration of the Flow Functions:
Capillary Pressure and Relative Permeability, 72. References, 77.

CHAPTER 5

Permeability Relationships80
Summary, 80. Introduction, 80. The Carman-Kozeny Hydraulic
Tubes Model, 80. The Modified Carman-Kozeny Equation
Incorporating the Flow Units Concept, 83. The Modified Carman-
Kozeny Equation for Porous Media Altered by Deposition, 84. The
Flow Efficiency Concept, 84. The Plugging-Nonplugging Parallel
Pathways Model, 87. Multi-Parameter Regression Models, 92.
Network Models, 92. Modified Fair-Hatch Equation, 93. Power-
Law Flow-Units Equation, 94. Effect of Dissolution/Precipitation
on Porosity and Permeability, 94. Effect of Deposition/Dissolution
and Stress on Porosity and Permeability, 95. Effect of Temperature
on Porosity and Permeability, 95. Exercises, 96. References, 97.

CHAPTER 6

**Instrumental and Laboratory Techniques for
Characterization of Reservoir Rock 102**
Summary, 102. Introduction, 102. Formation Evaluation, 103.
X-Ray Diffraction, 107. X-Ray CT Scanning, 107. X-Ray
Fluoroscopy, 108. Scanning Electron Microscope (SEM), 108.
Thin Section Petrography, 109. Petrographic Image Analysis,
109. Polarized Light Microscopy, 109. Nuclear Magnetic
Resonance Spectroscopy (NMR), 110. Acoustic Techniques,
111. Cation Exchange Capacity, 111. ξ (Zeta)-Potential, 116.
Wettability, 117. Mineral Quantification, 120. References, 123.

PART II

**Characterization of the Porous Media
Processes for Formation Damage**

CHAPTER 7

**Multi-Phase and Multi-Species Transport
in Porous Media 128**
Summary, 128. Multi-Phase and Species Systems in Porous

Media, 128. Multi-Species and Multi-Phase Macroscopic Transport Equations, 133. References, 138.

CHAPTER 8

Particulate Processes in Porous Media 140

Summary, 140. Introduction, 140. Particulate Processes, 141. Forces Acting Upon Particles, 145. Rate Equations for Particulate Processes in Porous Matrix, 148. References, 160.

CHAPTER 9

Crystal Growth and Scale Formation in Porous Media 164

Summary, 164. Introduction, 164. Inorganic Precipitation, 164. Organic Precipitation, 165. Crystallization, 166. Grain Nucleation, Growth, and Dissolution, 167. Crystallization Kinetics, 171. Particle Growth and Dissolution in Solution, 174. Scale Formation and Dissolution at the Pore Surface, 176. Crystal Surface Displacement by Dissolution and Precipitation, 178. References, 178.

PART III

Formation Damage by Particulate Processes

CHAPTER 10

Single-Phase Formation Damage by Fines Migration and Clay Swelling 183

Summary, 183. Introduction, 183. The Thin Slice Algebraic Model, 184. The Compartments-in-Series Ordinary Differential Model, 197. Simplified Partial Differential Model, 199. The Plugging-Nonplugging Parallel Pathways Partial Differential Model, 221. Model Considering the Clayey Formation Swelling and Indigeneous and External Particles, 208. Model Assisted Analysis of Experimental Data, 213. References, 235.

CHAPTER 11

Two-Phase Formation Damage by Fines Migration 238

Summary, 238. Introduction, 238. Formulation, 239. Fluid and Species Transport, 241. Wettability Transformation and Interface Transfer of Particles, 247. Particle Retention in Porous Media, 247. Filter Cake Formation on the Injection Face, 251. Model Assisted Analysis of Experimental Data, 251. References, 259.

CHAPTER 12

Cake Filtration: Mechanism, Parameters and Modeling 262

Summary, 262. Introduction, 263. Incompressive Cake Filtration, 265. Compressive Cake Filtration Including Fines Invasion, 291. References, 318.

PART IV

Formation Damage by Inorganic and Organic Processes

CHAPTER 13

Inorganic Scaling and Geochemical Formation Damage 323

Summary, 323. Introduction, 323. Geochemical Phenomena—Classification, Formulation, Reactions in Porous Media, 326. Geochemical Modeling, 335. Graphical Description of the Rock-Fluid Chemical Equilibria, 339. Geochemical Model Assisted Analysis of Solid Mineral—Aqueous Phase Interactions and Construction of Charts, 344. References, 372.

CHAPTER 14

Formation Damage by Organic Deposition 379

Summary, 379. Introduction, 379. Characteristics of Asphaltenic Oils, 382. Mechanisms of the Heavy Organic Deposition, 388. Asphaltene and Wax Phase Behavior and Deposition Envelopes, 392. Asphaltene Adsorption, 405. Empirical Algebraic Model for Formation Damage by Asphaltene Precipitation in Single Phase, 410. Simplified Analytic Model for Asphaltene-Induced Formation Damage in Single-Phase, 414. Plugging-Nonplugging Pathways Model for Asphaltene Deposition in Single-Phase, 421. Two-Phase and Dual-Porosity Model for Simultaneous Asphaltene-Paraffin Deposition, 428. Single-Porosity and Two-Phase Model for Organic Deposition, 438. References, 449.

PART V

**Assessment of the Formation
Damage Potential**

CHAPTER 15

Laboratory Evaluation of Formation Damage456

Summary, 456. Introduction, 456. Fundamental Processes of Formation Damage in Petroleum Reservoirs, 458. Selection of Reservoir Compatible Fluids, 459. Experimental Set-up for Formation Damage Testing, 459. Special Purpose Core Holders, 461. Guidelines and Program for Laboratory Formation Damage Testing, 470. Core Flood Tests, 478 Laboratory Procedures for Evaluation of Formation Damage Problems, 478. The Liquid Block Problem, 481. The Mud Damage Problem, 482. Evaluation of Drilling Muds—Damage Potential and Removal, 482. Evaluation of Hydraulic Fracturing Fluids, 488. Evaluation of Workover and Injection Fluids, 488. Evaluation of Workover Damage and Remedial Chemicals, 491. Critical Interstitial Fluid Velocity and pH for Hydrodynamic Detachment of Fines in Porous Media, 491. Scaling from Laboratory to Bottom Hole, 499. Determination of the Formation Damage Potential by Laboratory Testing, 500. References, 522.

CHAPTER 16

Simulator Development528

Summary, 528. Introduction, 528. Description of Fundamental Model Equations, 529. Numerical Solution of Formation Damage Models, 532. Ordinary Differential Equations, 533. Partial Differential Equations, 538. References, 549

CHAPTER 17

**Model Assisted Analysis and Interpretation
of Laboratory and Field Tests552**

Summary, 552. Introduction, 552. Measurement Error, 554. Error Analysis—Propagation, Impact, Estimation, 556. Sensitivity Analysis—Stability and Conditionality, 561. Model Validation, Refinement, and Parameter Estimation, 564. Determination of the Formation Damage Potential by Simulation, 570. References, 603.

PART VI

**Formation Damage Models for
Field Applications**

CHAPTER 18

**Drilling Mud Filtrate and Solids Invasion
and Mudcake Formation608**

Summary, 608. Introduction, 608. Simplified Single Phase Mud Filtrate Invasion Model, 613. Two-Phase Wellbore Mud Invasion and Filter Cake Formation Model, 617. References, 623.

CHAPTER 19

Interjectivity of the Waterflooding Wells627

Summary, 627. Introduction, 627. Injectivity Ratio, 628. Models Separating the Internal and External Filtration Processes, 632. Diagnostic-Type Curves for Water Injectivity Tests, 639. Models for Field Applications, 641. Models Coupling the Internal and External Filtration Processes, 643. References, 644.

CHAPTER 20

**Reservoir Sand Migration and Gravel-Pack Damage:
Stress-Induced Formation Damage, Sanding
Tendency, Prediction, and Control647**

Summary, 647. Introduction, 647. Sand Control, 648. Gravel Design Criteria, 651. Prediction of Sanding Conditions, 655. Massive Sand Production Model, 658. Sand Retention in Gravel-Packs, 664. References, 665.

CHAPTER 21

Formation Damage by Scale Deposition669

Summary, 669. Introduction, 669. Sulfur Deposition Model, 669. Calcite Deposition Model, 674. References, 677.

PART VII

Diagnosis and Mitigation of Formation Damage

CHAPTER 22

Field Diagnosis and Measurement of Formation Damage 680

Summary, 680. Introduction, 680. Diagnosis and Evaluation of Formation Damage in the Field, 681. Pseudo-Damage Versus Formation Damage, 684. Measures of Formation Damage, 684. Flow Efficiency, 691. Depth of Damage, 693. Model-Assisted Estimation of Skin Factor, 694. Model-Assisted Analysis of the Near-Wellbore Permeability Alteration using Pressure Transient Data, 694. Continuous Real Time Series Analysis for Detection and Monitoring Formation Damage Effects, 698. Formation Damage Expert System, 702. References, 703.

CHAPTER 23

Formation Damage Control and Remediation 706

Summary, 706. Introduction, 706. Selection of Treatment Fluids, 710. Clay Stabilization, 711. *pH*-Buffer Solutions, 714. Clay and Silt Fines, 715. Bacterial Damage, 716. Inorganic Scales, 717. Organic Deposits, 717. Mixed Organic/Inorganic Deposits, 718. Formation Damage Induced by Completion-Fluids and Crude-Oil Emulsions, 718. Wettability Alteration and Emulsion and Water Blocks, 718. Intense Heat Treatment, 719. Stimulation by Hydraulic Fracturing, 719. References, 725.

Index 730

About the Author 741

This page intentionally left blank

Preface

Formation damage is an undesirable operational and economic problem that can occur during the various phases of oil and gas recovery from subsurface reservoirs including production, drilling, hydraulic fracturing, and workover operations. Formation damage assessment, control, and remediation are among the most important issues to be resolved for efficient exploitation of hydrocarbon reservoirs. Such damage is caused by various adverse processes, including chemical, physical, biological, and thermal interactions of formation and fluids, and deformation of formation under stress and fluid shear. Formation damage indicators include permeability impairment, skin damage, and decrease of well performance. The properly designed experimental and analytical techniques presented in this book can help understanding, diagnosis, evaluation, prevention and controlling of formation damage in oil and gas reservoirs.

This book provides an understanding of the fundamentals of the relevant processes causing formation damage and reducing the flow efficiency in the near-wellbore formation during the various phases of oil and gas production; an update review of the various approaches used in the modeling and simulation of formation damage for model assisted analysis and interpretation of laboratory core tests, and for prediction and control of formation damage; and the techniques used for assessment, diagnosis, minimization, and control of formation damage in petroleum reservoirs. It focuses on the modeling and simulation of the rock, fluid, and particle interactions, fluid and particle invasion, filter cake, in-situ mobilization, migration, and deposition of fines, organic and inorganic precipitation and scale formation, alteration of porosity, permeability, and texture in laboratory cores and reservoir formations, and the effects of single and multi-phase fluid systems.

Formation damage is an interesting interdisciplinary subject that attracts many researchers. This book is a recapitulation of the present state-of-the-art knowledge in the area of formation damage. It is intended to be a convenient source of information, widely spread over different sources. I have tried to cover the relevant material with sufficient detail, without overwhelming the readers. This book can be used by those who are engaged in the various aspects of

formation damage problems associated with the production of hydrocarbons from subsurface reservoirs. It may serve as a useful reference and provides the knowledge of the theoretical and practical aspects of formation damage for various purposes, including model assisted interpretation of experimental test data, prediction and simulation of various formation damage scenarios, evaluation of alternative strategies for formation damage minimization, and scientific guidance for conducting laboratory and field tests.

Exhaustive effort has been made to gather, analyze, and systematically present the state-of-the-art knowledge accumulated over the years in the area of formation damage in petroleum reservoirs. This book is intended to provide a quick and coordinated overview of the fundamentals, and the experimental and theoretical approaches presented in selected publications. However, it should not be viewed as a complete encyclopedic documentation of the reported studies. It discusses processes causing formation damage and reducing the productivity of wells in petroleum reservoirs and systematically presents various approaches used in the diagnoses, measurement, production, and simulation of formation damage. The techniques for assessment, minimization, control, and remediation of the reservoir formation damage are described.

This book is intended for the petroleum, chemical, and environmental engineers, geologists, geochemists, and physicists involved in formation damage control, and for the undergraduate senior and graduate petroleum engineering students. Therefore, this book can be used in industry training courses and undergraduate senior and graduate level petroleum engineering courses. It is recommended for formation damage courses and as a companion for drilling, production, and stimulation courses. Readers will:

- Learn the mechanisms and theoretical background of the common formation damage processes
- Be familiar with the testing, modeling and simulation techniques available for formation damage assessment, and
- Be able to develop strategies for better management of the adverse processes to minimize and avoid formation damage in petroleum reservoirs.

The material presented in this book originates from my industry short courses and curriculum courses at the School of Petroleum and Geological Engineering at the University of Oklahoma.

I am indebted to the researchers who have contributed to the understanding and handling of the various issues and aspects of formation damage and mitigation. Their efforts have led to the accumulation of a substantial amount of knowledge and expertise on formation damage and helped develop techniques and optimal strategies for effective detection, evaluation, and mitigation of formation damage in subsurface reservoirs. Their works have been published in various literature. I am pleased to have had the opportunity to analyze,

integrate, transfer, and present the state-of-the-knowledge of formation damage in a consistent manner in one source for the readers of this book. Many of the figures, tables, and other relevant materials used in the preparation of this book were extracted from the literature published by various researchers, companies, and organizations. These include the following: Academic Press; AAPG—American Association of Petroleum Geologists; ACS—American Chemical Society; AIChE—American Institute of Chemical Engineers; American Institute of Physics; API—American Petroleum Institute; ASME—American Society of Mechanical Engineers; A.A. Balkema Publisher; Baroid Drilling Fluids, Inc.; Canadian Institute of Mining, Metallurgy and Petroleum; *Chemical Processing* magazine; Chemicky Prumysl; Computational Mechanics, Inc.; Elsevier Science, Geological Society, IEEE—Institute of Electrical and Electronics Engineers, Inc.; International Institute for Geothermal Research, Italy; Illinois State Geological Survey; John Wiley & Sons Limited; Marcel Dekker, Inc.; M-I L.L.C.; Plenum Press; Sarkeys Energy Center at the University of Oklahoma; SPE—Society of Petroleum Engineers; SPWLA—Society of Professional Well Log Analysis; Transportation Research Board; National Academies, Washington, D.C.; *Turkish Journal of Oil and Gas*; and the U.S. Department of Energy. In addition, G. Atkinson, T. Dewers, A. Hayatdavoudi, I. B. Ivanov, P. R. Johnson, P. A. Kralchevsky, R. Philip, T. S. Ramakrishnan, M. M. Reddy, G. W. Schneider, H. Tamura, and K. J. Weber allowed the use of materials from their publications. B. Seyler of the Illinois State Geological Survey provided the photographs included in the book. The permission for use of these materials in this book is gratefully acknowledged.

I am also grateful to Gulf Publishing Company, Timothy W. Calk, and Execustaff Composition Services for their support in the preparation and realization of this book. Special thanks are due to Susan Houck for her care in typing the manuscript.

Any comments, corrections, and suggestions by the readers to improve this book are welcomed.

Faruk Civan, Ph.D. P.E.
University of Oklahoma
Norman, Oklahoma

This page intentionally left blank

Chapter 1

Overview of Formation Damage

Summary

A comprehensive review of the various types of formation damage problems encountered in petroleum reservoirs is presented. The factors and processes causing these problems are described in detail. The design of a team effort necessary for understanding and controlling of the formation damage problems in the field is explained. The motivation for the writing of this book and the specific objectives are stated. The approach taken in the presentation of the materials in this book is explained. A brief executive summary of the topics covered in the book is given. The roles played by different professionals, such as the petroleum and chemical engineers, chemists, physicist, geologists, and geochemists, are described.

Introduction

Formation damage is a generic terminology referring to the impairment of the permeability of petroleum bearing formations by various adverse processes. Formation damage is an undesirable operational and economic problem that can occur during the various phases of oil and gas recovery from subsurface reservoirs including production, drilling, hydraulic fracturing, and workover operations. As expressed by Amaefule et al. (1988) "Formation damage is an expensive headache to the oil and gas industry." Bennion (1999) described formation damage as: "The impairment of the invisible, by the inevitable and uncontrollable, resulting in an indeterminate reduction of the unquantifiable!" Formation damage assessment, control, and remediation are among the most important issues to be resolved for efficient exploitation of hydrocarbon reservoirs (Energy Highlights, 1990). Formation damage is caused by physico-chemical, chemical, biological, hydrodynamic, and thermal interactions of porous formation, particles, and fluids and mechanical deformation of formation

under stress and fluid shear. These processes are triggered during the drilling, production, workover, and hydraulic fracturing operations. Formation damage indicators include permeability impairment, skin damage, and decrease of well performance. As stated by Porter (1989), "Formation damage is not necessarily reversible" and "What gets into porous media does not necessarily come out." Porter (1989) called this phenomenon "the reverse funnel effect." Therefore, it is better to avoid formation damage than to try to restore it. A verified formation damage model and carefully planned laboratory and field tests can provide scientific guidance and help develop strategies to avoid or minimize formation damage. Properly designed experimental and analytical techniques, and the modeling and simulation approaches can help understanding, diagnosis, evaluation, prevention, remediation, and controlling of formation damage in oil and gas reservoirs.

The consequences of formation damage are the reduction of the oil and gas productivity of reservoirs and noneconomic operation. Therefore, it is essential to develop experimental and analytical methods for understanding and preventing and/or controlling formation damage in oil and gas bearing formations (Energy Highlights, 1990). The laboratory experiments are important steps in reaching understanding of the physical basis of formation damage phenomena. "From this experimental basis, realistic models which allow extrapolation outside the scaleable range may be constructed" (Energy Highlights, 1990). These efforts are necessary to develop and verify accurate mathematical models and computer simulators that can be used for predicting and determining strategies to avoid and/or mitigate formation damage in petroleum reservoirs (Civan, 1994).

Confidence in formation damage prediction using phenomenological models cannot be gained without field testing. Planning and designing field test procedures for verification of the mathematical models are important. Once a model has been validated, it can be used for accurate simulation of the reservoir formation damage. Current techniques for reservoir characterization by history matching do not consider the alteration of the characteristics of reservoir formation during petroleum production. In reality, formation characteristics vary and a formation damage model can help to incorporate this variation into the history matching process for accurate characterization of reservoir systems and, hence, an accurate prediction of future performance. Formation damage is an exciting, challenging, and evolving field of research. Eventually, the research efforts will lead to a better understanding and simulation tools that can be used for model-assisted analysis of rock, fluid, and particle interactions and the processes caused by rock deformation and scientific guidance for development of production strategies for formation damage control in petroleum reservoirs.

In the past, numerous experimental and theoretical studies have been carried out for the purpose of understanding the factors and mechanisms that govern the phenomena involving formation damage. Although various results were obtained from these studies, a unified theory and approach still does not exist.

Civan (1996) explains:

A formation damage model is a dynamic relationship expressing the fluid transport capability of porous medium undergoing various alteration processes. Modeling formation damage in petroleum reservoirs has been of continuing interest. Although many models have been proposed, these models do not have the general applicability. However, an examination of the various modeling approaches reveals that these models share a common ground and, therefore, a general model can be developed, from which these models can be derived. Although modeling based on well accepted theoretical analyses is desirable and accurate, macroscopic formation damage modeling often relies on some intuition and empiricism inferred by the insight gained from experimental studies.

As J. Willard Gibbs stated in a practical manner: "The purpose of a theory is to find that viewpoint from which experimental observations appear to fit the pattern" (Duda, 1990).

Civan (1996) states:

The fundamental processes causing damage in petroleum bearing formations are: (1) physico-chemical, (2) chemical, (3) hydrodynamic, (4) thermal, and (5) mechanical. Formation damage studies are carried out for (1) understanding of these processes via laboratory and field testing, (2) development of mathematical models via the description of fundamental mechanisms and processes, (3) optimization for prevention and/or reduction of the damage potential of the reservoir formation, and (4) development of formation damage control strategies and remediation methods. These tasks can be accomplished by means of a model assisted data analysis, case studies, and extrapolation and scaling to conditions beyond the limited test conditions. The formulation of the general purpose formation damage model is presented by describing the relevant phenomena on the macroscopic scale; i.e. by representative elementary porous media averaging.

As stated by Civan (1990):

Development of a numerical solution scheme for the highly non-linear phenomenological model and its modification and verification by

means of experimental testing of a variety of cores from geological porous media are the challenges for formation damage research. As expressed by Porter (1989) and Mungan (1989), formation damage is not necessarily reversible. Thus, it is better to avoid formation damage than try to restore formation permeability using costly methods with uncertain successes in many cases. When a verified generalized formation damage model becomes available, it can be used to develop strategies to avoid or minimize formation damage.

Finally, it should be recognized that formation damage studies involve many interdisciplinary knowledge and expertise. An in-depth review of the various aspects of the processes leading to formation damage may require a large detailed presentation. Presentation of such encyclopedic information makes learning of the most important information difficult and, therefore, it is beyond the scope of this book. Instead, a summary of the well proven, state-of-the-art knowledges by highlighting the important features, are presented in a concise manner for instructional purposes. The details can be found in the literature cited at the end of the chapters.

Common Formation Damage Problems, Factors, and Mechanisms

Barkman and Davidson (1972), Piot and Lietard (1987), and Amaefule et al. (1987, 1988) have described in detail the various problems encountered in the field, interfering with the oil and gas productivity.

Amaefule et al. (1988) listed the conditions affecting the formation damage in four groups: (1) Type, morphology, and location of resident minerals; (2) In-situ and extraneous fluids composition; (3) In-situ temperature and stress conditions and properties of porous formation; and (4) Well development and reservoir exploitation practices.

Amaefule et al. (1988) classified the various factors affecting formation damage as following: (1) Invasion of foreign fluids, such as water and chemicals used for improved recovery, drilling mud invasion, and workover fluids; (2) Invasion of foreign particles and mobilization of indigenous particles, such as sand, mud fines, bacteria, and debris; (3) Operation conditions such as well flow rates and wellbore pressures and temperatures; and (4) Properties of the formation fluids and porous matrix.

Figure 1-1 by Bennion (1999) delineates the common formation damage mechanisms in the order of significance. Bishop (1997) summarized the seven formation damage mechanisms described by Bennion and Thomas (1991, 1994) as following:

1. Fluid-fluid incompatibilities, for example emulsions generated between invading oil based mud filtrate and formation water.

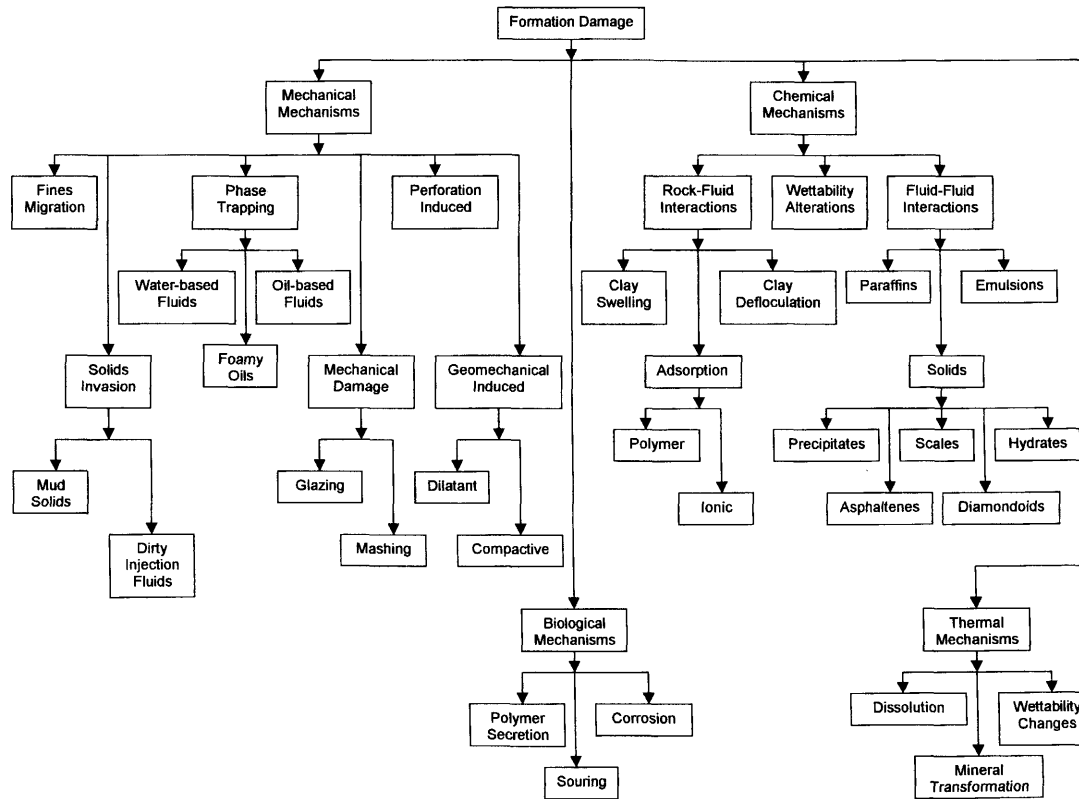


Figure 1–1. Classification and order of the common formation damage mechanisms (modified after Bennion, ©1999; reprinted by permission of the Canadian Institute of Mining, Metallurgy and Petroleum).

2. Rock-fluid incompatibilities, for example contact of potentially swelling smectite clay or deflocculatable kaolinite clay by non-equilibrium water based fluids with the potential to severely reduce near wellbore permeability.
3. Solids invasion, for example the invasion of weighting agents or drilled solids.
4. Phase trapping/blocking, for example the invasion and entrapment of water based fluids in the near wellbore region of a gas well.
5. Chemical adsorption/wettability alteration, for example emulsifier adsorption changing the wettability and fluid flow characteristics of a formation.
6. Fines migration, for example the internal movement of fine particulates within a rock's pore structure resulting in the bridging and plugging of pore throats.
7. Biological activity, for example the introduction of bacterial agents into the formation during drilling and the subsequent generation of polysaccharide polymer slimes which reduce permeability.

Team for Understanding and Mitigation of Formation Damage

Amaefule et al. (1987, 1988) stated that formation damage studies require a cooperative effort between various professionals. These and their responsibilities are described in the following: (1) Geologist and geochemist on mineralogy and diagenesis and reservoir formation characterization and evaluation; (2) Chemist on inorganic/organic chemistry, physical chemistry, colloidal and interfacial sciences, and chemical kinetics; and (3) Chemical and petroleum engineers on transport phenomena in porous media, simulator development, interpretation of laboratory core tests, scaling from laboratory to field, interpretation of field tests, and development and implementation of strategies for formation damage control.

Objectives of the Book

The focus of this book is to provide sufficient knowledge for the following purposes: (1) Understand relevant processes by laboratory and field testing; (2) Develop theories and mathematical expressions for description of the fundamental mechanisms and processes, and phenomenological mathematical modeling and obtain numerical solutions for simulator development and computer implementation; (3) Predict and simulate the consequences and scenarios of the various types of formation damage processes encountered in petroleum reservoirs; (4) Optimize for prevention and/or reduction of the damage potential of the reservoir

formation; and (5) Develop methodologies and strategies for formation damage control and remediation.

This book reviews and systematically analyzes the previous studies, addressing their theoretical bases, assumptions and limitations, and presents the state-of-the-art knowledge in formation damage in a systematic manner. The material is presented in seven parts:

- I. Characterization of the Reservoir Rock for Formation Damage—Mineralogy, Texture, Petrographics, Petrophysics, and Instrumental Techniques
- II. Characterization of the Porous Media Processes for Formation Damage—Accountability of Phases and Species, Rock-Fluid-Particle Interactions, and Rate Processes
- III. Formation Damage by Particulate Processes—Fines Mobilization, Migration, and Deposition
- IV. Formation Damage by Inorganic and Organic Processes—Chemical Reactions, Saturation Phenomena, Deposition, Dissolution
- V. Assessment of the Formation Damage Potential—Testing, Simulation, Analysis, and Interpretation
- VI. Drilling Mud Filtrate and Solids Invasion and Mudcake Formation
- VII. Diagnosis and Mitigation of Formation Damage—Measurement, Control, and Remediation

References

- Amaefule, J. O., Ajufo, A., Peterson, E., & Durst, K., "Understanding Formation Damage Processes," SPE 16232 paper, Proceedings of the SPE Production Operations Symposium, Oklahoma City, Oklahoma, 1987.
- Amaefule, J. O., Kersey, D. G., Norman, D. L., & Shannon, P. M., "Advances in Formation Damage Assessment and Control Strategies", CIM Paper No. 88-39-65, Proceedings of the 39th Annual Technical Meeting of Petroleum Society of CIM and Canadian Gas Processors Association, Calgary, Alberta, June 12–16, 1988, 16 p.
- Barkman, J. H., & Davidson, D. H., "Measuring Water Quality and Predicting Well Impairment," *Journal of Petroleum Technology*, Vol. 253, July 1972, pp. 865–873.
- Bennion, D. B., Thomas, F. B., & Bennion, D. W., "Effective Laboratory Coreflood Tests to Evaluate and Minimize Formation Damage in Horizontal Wells," presented at the Third International Conference on Horizontal Well Technology, November 1991, Houston, Texas.
- Bennion, D. B., & Thomas, F. B., "Underbalanced Drilling of Horizontal Wells: Does It Really Eliminate Formation Damage?," SPE 27352

- paper, SPE Formation Damage Control Symposium, February 1994, Lafayette, Louisiana.
- Bennion, D. F., Bietz, R. F., Thomas, F. B., & Cimolai, M. P., "Reductions in the Productivity of Oil & Gas Reservoirs due to Aqueous Phase Trapping," presented at the CIM 1993 Annual Technical Conference, May 1993, Calgary.
- Bennion, B., "Formation Damage—The Impairment of the Invisible, by the Inevitable and Uncontrollable, Resulting in an Indeterminate Reduction of the Unquantifiable!" *Journal of Canadian Petroleum Petroleum Technology*, Vol. 38, No. 2, February 1999, pp. 11–17.
- Bishop, S. R., "The Experimental Investigation of Formation Damage Due to the Induced Flocculation of Clays Within a Sandstone Pore Structure by a High Salinity Brine," SPE 38156 paper, presented at the 1997 SPE European Formation Damage Conference, The Hague, The Netherlands, June 2–3 1997, pp. 123–143.
- Civan, F., Predictability of Formation Damage: An Assessment Study and Generalized Models, Final Report, U.S. DOE Contract No. DE-AC22-90-BC14658, April 1994.
- Civan, F., "A Multi-Purpose Formation Damage Model," SPE 31101 paper, Proceedings of the SPE Formation Damage Symposium, February 14–15, 1996, pp. 311–326, Lafayette, Louisiana.
- Duda, J. L., "A Random Walk in Porous Media," *Chemical Engineering Education Journal*, Summer 1990, pp. 136–144.
- Energy Highlights, "Formation Damage Control in Petroleum Reservoirs," article provided by F. Civan, The University of Oklahoma Energy Center, Vol. 1, No. 2, p. 5, Summer 1990.
- Mungan, N., "Discussion of An Overview of Formation Damage," *Journal of Petroleum Technology*, Vol. 41, No. 11, Nov. 1989, p. 1224.
- Piot, B. M., & Lietard, O. M., "Nature of Formation Damage in Reservoir Stimulation, in Economides," M. J. and Nolte, K. S. (eds.), *Reservoir Stimulation*, Schlumberger Education Services, Houston, Texas, 1987.
- Porter, K. E., "An Overview of Formation Damage," *JPT*, Vol. 41, No. 8, 1989, pp. 780–786.

Part I

**Characterization
of the Reservoir
Rock for Formation
Damage**

**Mineralogy, Texture,
Petrographics,
Petrophysics, and
Instrumental Techniques**

Chapter 2

Mineralogy and Mineral Sensitivity of Petroleum-Bearing Formations*

Summary

The origin, mineralogy, and mineral sensitivity of petroleum-bearing formations are reviewed. The mechanisms of mineral swelling, alteration, and fines generation are described. The models for mineral sensitive properties of rock and the methods for interpretation of experimental data are presented.

Introduction

Among others, Ohen and Civan (1993) point out that fines migration and clay swelling are the primary reasons for formation damage measured as permeability impairment. Poorly lithified and tightly packed formations having large quantities of authigenic, pore filling clays sensitive to aqueous solutions, such as kaolinite, illite, smectite, chlorite, and mixed-layer clay minerals, are especially susceptible to formation damage (Amaefule et al., 1988). Formation damage also occurs as a result of the invasion of drilling mud, cements, and other debris during production, hydraulic fracturing, and workover operations (Amaefule et al., 1988).

This chapter describes the mineral content and sensitivity of typical sedimentary formations, and the relevant formation damage mechanisms involving clay alteration and migration. Analytical models for interpretation and correlation of the effects of clay swelling on the permeability and porosity of clayey porous rocks are presented (Civan, 1999). The parameters of the

* Parts of this chapter have been reprinted with permission of the Society of Petroleum Engineers from Civan (1999).

models, including the swelling rate constants, and terminal porosity and permeability that will be attained at saturation, are determined by correlating the experimental data with these models. The swelling of clayey rocks is essentially controlled by absorption of water by a water-exposed surface hindered diffusion process and the swelling-dependent properties of clayey rocks vary proportionally with their values relative to their saturation limits and the water absorption rate. These models lead to proper means of correlating and representing clayey rock properties.

Origin of Petroleum-Bearing Formations

As described by Sahimi (1995), sedimentary porous formations are formed through two primary phenomena: (1) deposition of sediments, followed by (2) various compaction and alteration processes. Sahimi (1995) states that the sediments in subsurface reservoirs have undergone four types of diagenetic processes under the prevailing in-situ stress, thermal, and flow conditions over a very long period of geological times: (1) mechanical deformation of grains, (2) solution of grain minerals, (3) alteration of grains, and (4) precipitation of pore-filling minerals, clays, cements, and other materials. These processes are inherent in determining the characteristics and formation damage potential of petroleum-bearing formations.

Constituents of Sedimentary Rocks

Many investigators, including Neasham (1977), Amaefule et al. (1988), Macini (1990), and Ezzat (1990), present detailed descriptions of the various constituents of oil and gas bearing rocks. Based on these studies, the constituents of the subsurface formations can be classified in two broad categories: (1) indigenous and (2) extraneous or foreign materials.

There are two groups of indigenous materials: (1) detrital materials, which originate during the formation of rocks and have restricted formation damage potential, because they exist as tightly packed and blended minerals within the rock matrix; and (2) diagenetic (or authigenic) materials, which are formed by various rock-fluid interactions in an existing pack of sediments, and located inside the pore space as loosely attached pore-filling, pore-lining, and pore-bridging deposits, and have greater formation damage potential because of their direct exposure to the pore fluids. Extraneous materials are externally introduced through the wells completed in petroleum reservoirs, during drilling and workover operations and improved recovery processes applied for reservoir exploitation. A schematic, pictorial description of typical clastic deposits is given in Figure 2-1 by Pittman and Thomas (1979).

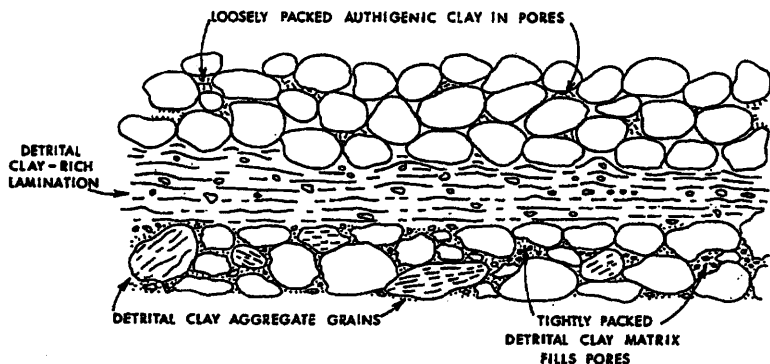


Figure 2-1. Disposition of the clay minerals in typical sandstone (after Pittman and Thomas, ©1979 SPE; reprinted by permission of the Society of Petroleum Engineers).

Composition of Petroleum-Bearing Formations

The studies of the composition of the subsurface formations by many, including Bucke and Mankin (1971) and Ezzat (1990), have revealed that these formations basically contain: (1) various mineral oxides such as SiO_2 , Al_2O_3 , FeO , Fe_2O_3 , MgO , K_2O , CaO , P_2O_5 , MnO , TiO_2 , Cl , Na_2O , which are detrital and form the porous matrix, and (2) various swelling and nonswelling clays, some of which are detrital, and the others are authigenic clays. The detrital clays form the skeleton of the porous matrix and are of interest from the point of mechanical formation damage. The authigenic clays are loosely attached to pore surface and of interest from the point of chemical and physico-chemical formation damage. Typical clay minerals are described in Table 2-1 (Ezzat, 1990).

However, the near-wellbore formation may also contain other substances, such as mud, cement, and debris, which may be introduced during drilling, completion, and workover operations, as depicted by Mancini (1991) in Figure 2-2.

“Clay” is a generic term, referring to various types of crystalline minerals described as hydrous aluminum silicates. Clay minerals occupy a large fraction of sedimentary formations (Weaver and Pollard, 1973). Clay minerals are extremely small, platy-shaped materials that may be present in sedimentary rocks as packs of crystals (Grim, 1942; Hughes, 1951). The maximum dimension of a typical clay particle is less than 0.005 mm (Hughes, 1951). The clay minerals can be classified into three main groups (Grim, 1942, 1953; Hughes, 1951): (1) Kaolinite group, (2) Smectite (or

Table 2-1
Description of the Authigenic Clay Minerals*

Mineral	Chemical Elements*†	Morphology
Kaolinite	$\text{Al}_4[\text{Si}_4\text{O}_{10}](\text{OH})_8$	Stacked plate or sheets.
Chlorite	$(\text{Mg}, \text{Al}, \text{Fe})_{12}[(\text{Si}, \text{Al})_8\text{O}_{20}](\text{OH})_{16}$	Plates, honeycomb, cabbagehead rosette or fan.
Illite	$(\text{K}_{1-1.5}\text{Al}_4[\text{Si}_{7-6.5}\text{Al}_{1-1.5}\text{O}_{20}](\text{OH})_4$	Irregular with elongated spines or granules.
Smectite	$(\frac{1}{2}\text{Ca}, \text{Na})_{0.7}(\text{Al}, \text{Mg}, \text{Fe})_4[(\text{Si}, \text{Al})_8\text{O}_{20}] \cdot n\text{H}_2\text{O}$	Irregular, wavy, wrinkled sheets, webby or honeycomb.
Mixed Layer	Illite-Smectite Chlorite-Smectite	Ribbons substantiated by filamentous morphology.

* After Ezzat, ©1990 SPE; reprinted by permission of the Society of Petroleum Engineers.

† After J. E. Welton (1984).

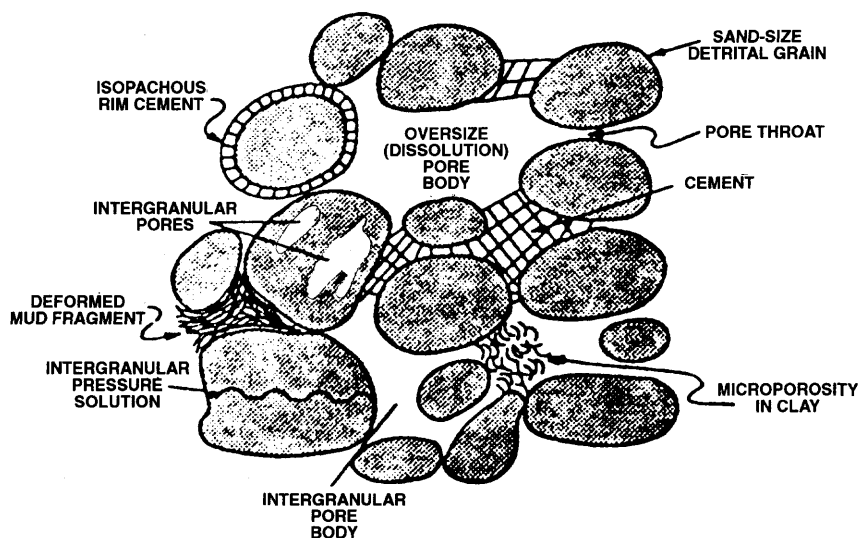


Figure 2-2. Description of the constituents in typical sandstone (after Mancini, 1991; reprinted by permission of the U.S. Department of Energy).

Montmorillonite) group, and (3) Illite group. In addition, there are mixed-layer clay minerals formed from several of these three basic groups (Weaver and Pollard, 1973).

The description of the various clay minerals of the sedimentary formations is given by Degens (1965, p. 16). The morphology and the major reservoir problems of the various clay minerals is described in Table 2-2 by Ezzat (1990).

Readers are referred to Chilingarian and Vorabutr (1981), Chapters 5 and 8, for a detailed review of the clays and their reactivity with aqueous solutions.

Mineral Sensitivity of Sedimentary Formations

Among other factors, the interactions of the clay minerals with aqueous solutions is the primary culprit for the damage of petroleum-bearing formations. Amaefule et al. (1988) state that rock-fluid interactions in sedimentary formations can be classified in two groups: (1) chemical reactions resulting from the contact of rock minerals with incompatible fluids, and (2) physical processes caused by excessive flow rates and pressure gradients.

Table 2-2
Typical Problems Caused by the Authigenic Clay Minerals[†]

Mineral	Surface Area m ² /gm*	Major Reservoir Problems
Kaolinite	20	Breaks apart, migrates and concentrates at the pore throat causing severe plugging and loss of permeability.
Chlorite	100	Extremely sensitive to acid and oxygenated waters. Will precipitate gelatinous Fe(OH) ₃ which will not pass through pore throats.
Illite	100	Plugs pore throats with other migrating fines. Leaching of potassium ions will change it to expandable clay.
Smectite	700	Water sensitive, 100% expandable. Causes loss of microporosity and permeability.
Mixed Layer	100-700	Breaks apart in clumps and bridges across pores reducing permeability.

[†] After Ezzat, ©1990 SPE; reprinted by permission of the Society of Petroleum Engineers.

* After David K. Davies—Sandstone Reservoirs—Ezzat (1990).

Amaefule et al. (1988) point out that there are five primary factors affecting the mineralogical sensitivity of sedimentary formations:

1. Mineralogy and chemical composition determine the
 - a. dissolution of minerals,
 - b. swelling of minerals, and
 - c. precipitation of new minerals.
2. Mineral abundance prevails the quantity of sensitive minerals.
3. Mineral size plays an important role, because
 - a. mineral sensitivity is proportional to the surface area of minerals, and
 - b. mineral size determines the surface area to volume ratio of particles.
4. Mineral morphology is important, because
 - a. mineral morphology determines the grain shape, and therefore the surface area to volume ratio, and
 - b. minerals with platy, foliated, acicular, filiform, or bladed shapes, such as clay minerals, have high surface area to volume ratio.
5. Location of minerals is important from the point of their role in formation damage. The authigenic minerals are especially susceptible to alteration because they are present in the pore space as pore-lining, pore-filling, and pore-bridging deposits and they can be exposed directly to the fluids injected into the near-wellbore formation.

Mungan (1989) states that clay damage depends on (1) the type and the amount of the exchangeable cations, such as K^+ , Na^+ , Ca^{2+} , and (2) the layered structure existing in the clay minerals. Mungan (1989) describes the properties and damage processes of the three clay groups as following:

1. Kaolinite has a two-layer structure (see Figure 2-3), K^+ exchange cation, and a small base exchange capacity, and is basically a nonswelling clay but will easily disperse and move.
2. Montmorillonite has a three-layer structure (see Figure 2-4), a large base exchange capacity of 90 to 150 meq/100g and will readily adsorb Na^+ , all leading to a high degree of swelling and dispersion.
3. Illites are interlayered (see Figure 2-5). Therefore, illites combine the worst characteristics of the dispersible and the swellable clays. The illites are most difficult to stabilize.

Sodium-montmorillonite swells more than calcium-montmorillonite because the calcium cation is strongly adsorbed compared to the sodium cations (Rogers, 1963). Therefore, when the clays are hydrated in aqueous

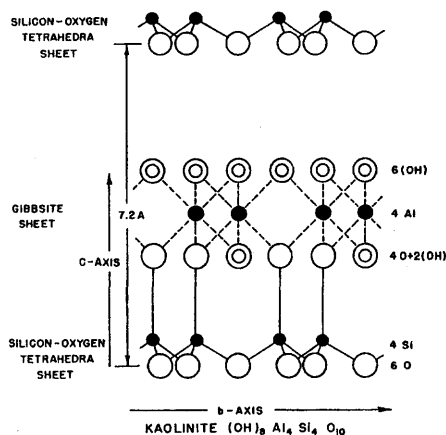


Figure 2-3. Schematic description of the crystal structure of kaolinite (after Gruner-Grim, 1942, and Hughes, 1951; reprinted courtesy of the American Petroleum Institute, 1220 L St., NW, Washington, DC 20005, Hughes, R. V., "The Application of Modern Clay Concepts to Oil Field Development," pp. 151-167, in *Drilling and Production Practice 1950*, American Petroleum Institute, New York, NY, 1951, 344 p.).

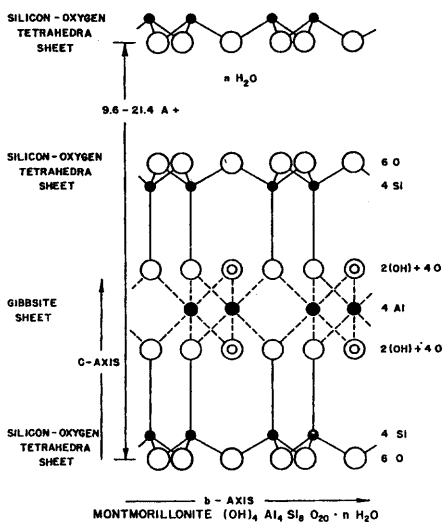


Figure 2-4. Schematic description of the crystal structure of montmorillonite (after Hoffman, Endell, and Wilm.-Grim, 1942, and Hughes, 1951; reprinted courtesy of the American Petroleum Institute, 1220 L St., NW, Washington, DC 20005, Hughes, R. V., "The Application of Modern Clay Concepts to Oil Field Development," pp. 151-167, in *Drilling and Production Practice 1950*, American Petroleum Institute, New York, NY, 1951, 344 p.).

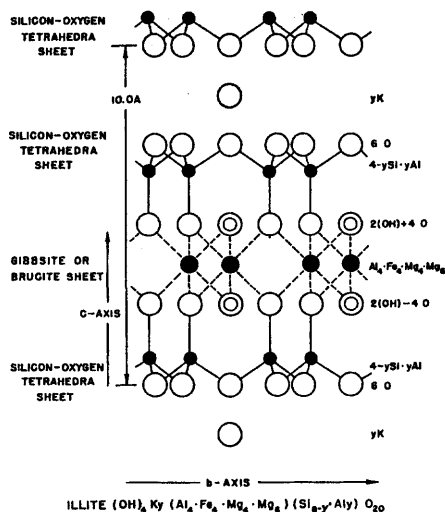


Figure 2-5. Schematic description of the crystal structure of illite (after Grim, Bray, and Bradley-Grim, 1942, and Hughes, 1951; reprinted courtesy of the American Petroleum Institute, 1220 L St., NW, Washington, DC 20005, Hughes, R. V., "The Application of Modern Clay Concepts to Oil Field Development," pp. 151-167, in *Drilling and Production Practice 1950*, American Petroleum Institute, New York, NY, 1951, 344 p.).

media, calcium-montmorillonite platelets remain practically intact, close to each other, while the sodium-montmorillonite aggregates readily swells and the platelets separate widely. Therefore, water can easily invade the gaps between the platelets and form thicker water envelopes around the sodium-montmorillonite platelets than the calcium-montmorillonite platelets (Chilangarian and Vorabutr, 1981) as depicted in Figure 2-6.

Clay damage can be prevented by maintaining high concentrations of K^+ cation in aqueous solutions. At high concentrations of K^+ cation, clay platelets remain intact, because the small size K^+ cation can penetrate the interlayers of the clay easily and hold the clay platelets together (Mondshine, 1973 and Chilangarian and Vorabutr, 1981) as depicted in Figure 2-7.

Many investigators, including Mungan (1965), Reed (1977), Khilar and Fogler (1983), and Kia et al. (1987), have determined that some degree of permeability impairment occurs in clay containing cores when aqueous solutions are flown through them. This phenomenon is referred to as the "water sensitivity."

Reed (1977) observed that young sediments are mostly friable micaceous sands and proposed a mechanism for damage. To justify his theory,

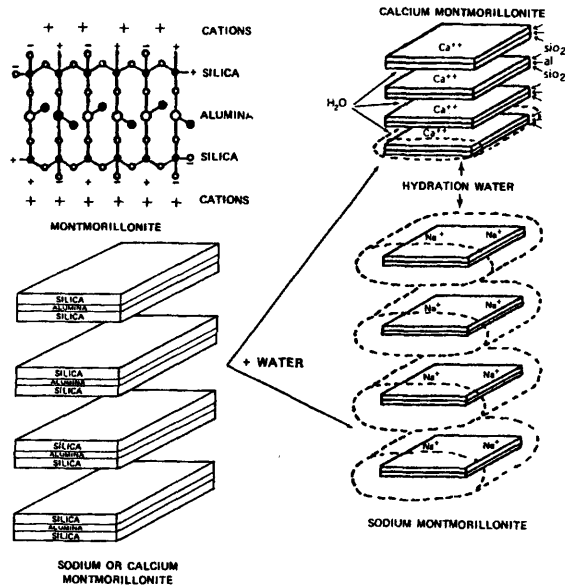


Figure 2-6. Expansion of the calcium and sodium montmorillonite by hydration (after Magcobar, ©1972, Fig. 2, p. 2; reprinted by permission of the M-I L.L.C.).

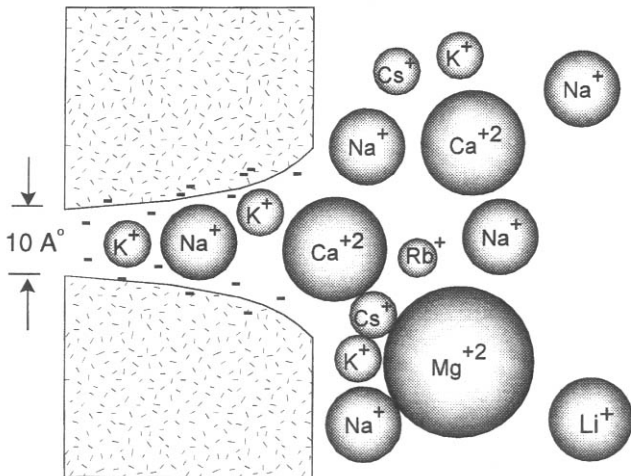


Figure 2-7. Effect of the cation size on the cation migration into a clay interlayer (modified after Baroid Mud Handbook, 1975, Fig. 12, p. 21; reprinted by permission of Baroid Drilling Fluids, Inc.).

he also conducted laboratory core tests by flowing various aqueous solutions through cores extracted from micaceous sand formations. The data shown by Figure 2-8 of Reed (1977) indicates permeability reduction. Based on the severeness of formation damage indicated by Figure 2-8, he concluded that mica alteration is a result of the exchange of K^+ cations with cations of larger sizes. Figure 2-8 shows that the deionized water caused the most damage, $CaCl_2$ solution made the least damage and damage by the $NaCl$ solution is in between. Thus, the cations involved can be ordered with respect to the most to least damaging as $H^+ > Na^+ > Ca^{++}$. Whereas, Grim (1942) determined the order of replaceability of the common cations in clays from most to least easy cations as $Li^+ > Na^+ > K^+ > Rb^+ > Cs^+ > Mg^{++} > Ca^{++} > Sr^{++} > Ba^{++} > H^+$. Hughes (1951) states: "hydrogen will normally replace calcium, which in turn will replace sodium. With the exception of potassium in illites, the firmness with which cations are held in the clay structure increases with the valence of the cation."

Reed (1977) postulated that formation damage in micaceous sands is a result of mica alteration and fines generation according to the process depicted in Figure 2-9 by Reed (1977) and later deposition in porous rock. As depicted in Figure 2-10, when clays are exposed to aqueous solutions containing no or small amounts of K^+ cation or larger cations such as H^+ , Ca^{+2} and Na^+ , the K^+ cation diffuses out of the clay platelets according to Fick's law, because there are more K^+ than the solution. In

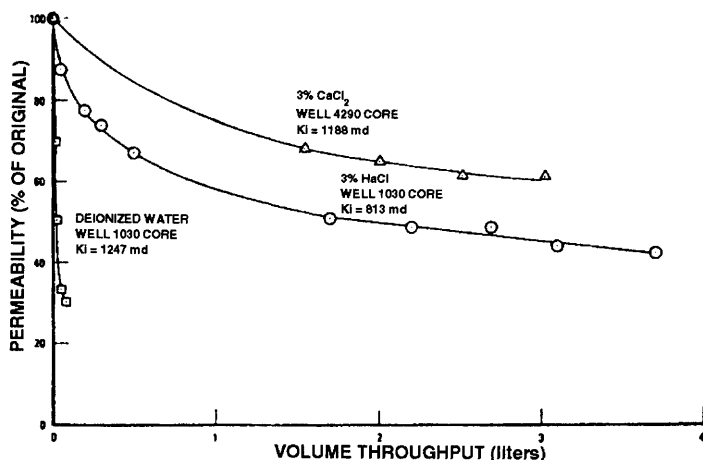


Figure 2-8. Comparison of the permeability damages by the deionized water, and calcium chloride and sodium chloride brines in field cores (after Reed, ©1977 SPE; reprinted by permission of the Society of Petroleum Engineers).

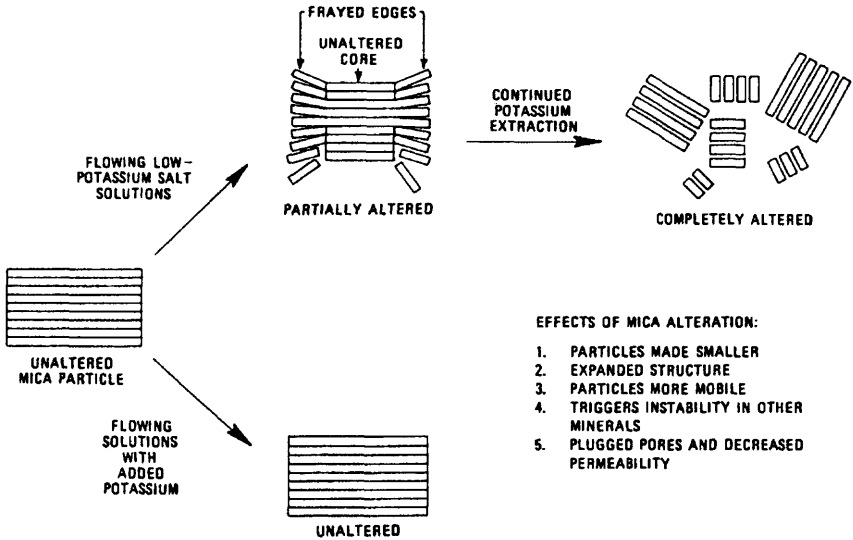


Figure 2-9. Reed's mechanism of mica alteration (after Reed, ©1977 SPE; reprinted by permission of the Society of Petroleum Engineers).

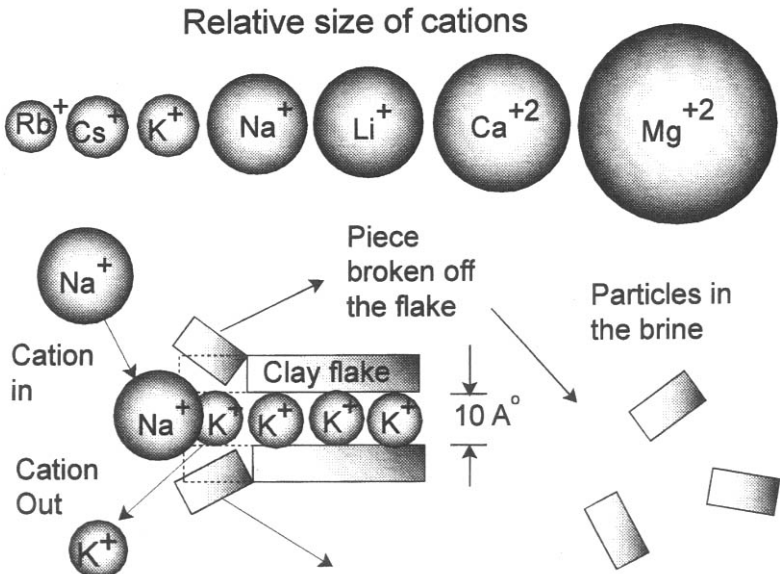


Figure 2-10. Schematic explanation of Reed's (1977) mechanism for particle generation by mica alteration during exposure to low-potassium salt brine.

contrast, the larger cations present in the aqueous solution tend to diffuse into clays because there are more of the larger cations in the solution compared to the clays. Because larger cations cannot fit into the interplanar gap depleted by K^+ cations, the edges of the friable mica flakes break off in small pieces as depicted in Figure 2-10. By a different set of experiments, Reed (1977) also demonstrated that dissolution of natural carbonate cement by aqueous salt solution can free mineral particles held by the cement. His reasoning is based on Figure 2-11, indicating increased concentrations of Ca^{+2} in the effluent while the permeability gradually decreases. The fine particles generated by mica alteration and unleashed by cement dissolution can, in turn, migrate with the flowing fluid and plug pore throats and reduce permeability.

Mohan and Fogler (1997) explain that there are three processes leading to permeability reduction in clayey sedimentary formations:

1. Under favorable colloidal conditions, non-swelling clays, such as kaolinites and illites, can be released from the pore surface and then these particles migrate with the fluid flowing through porous formation (Mohan and Fogler, 1997).
2. Whereas swelling clays, such as smectites and mixed-layer clays, first expand under favorable ionic conditions, and then disintegrate and migrate (Mohan and Fogler, 1997).

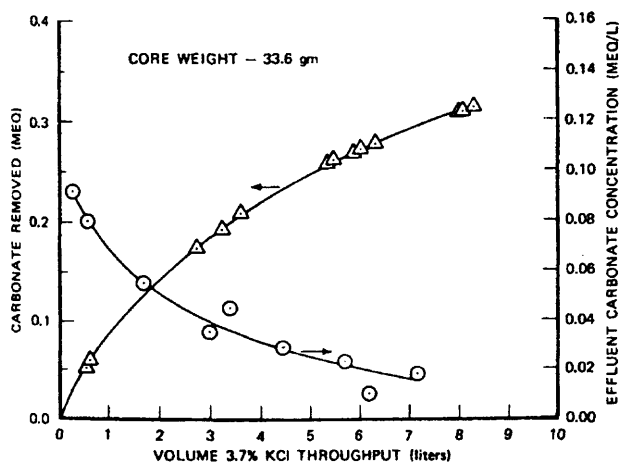


Figure 2-11. Carbonate leaching from a field core by flowing a potassium chloride brine (after Reed, ©1977 SPE; reprinted by permission of the Society of Petroleum Engineers).

3. Also, fines attached to swelling clays can be dislodged and liberated during clay swelling, the phenomenon of which is referred to as fines generation by discontinuous jumps or microquakes by Mohan and Fogler (1997).

Consequently, formation damage occurs in two ways: (1) the permeability of porous formation decreases by reduction of porosity by clay swelling (Civan and Knapp, 1987; Civan et al., 1989; and Mohan and Fogler, 1997); and (2) the particles entrained by the flowing fluid are carried towards the pore throats and captured by a jamming process. Thus, the permeability decreases by plugging of pore throats (Sharma and Yorstos, 1983; Wojtanowicz et al., 1987, 1988; Mohan and Fogler, 1997).

Khilar and Fogler (1983) have demonstrated by the flow of aqueous solutions through Berea sandstone cores that there is a “critical salt concentration (CSC)” of the aqueous solution below which colloidally induced mobilization of clay particles is initiated and the permeability of the core gradually decreases. This is a result of the expulsion of kaolinite particles from the pore surface due to the increase of the double-layer repulsion at low salt concentration (Mohan and Fogler, 1997). The critical salt concentrations for typical sandstones are given by Mohan and Fogler (1997) in Table 2–3.

Mechanism of Clay Swelling

A structural model of swelling clays having exchangeable cations, denoted by M^{z+} , is shown by Zhou et al. (1996, 1997) in Figure 2–12. Zhou et al (1996) states: “The structure layers are always deficient in positive charges due to cation substitution, and interlayer cations are required to balance the negative layer charge. Interlayer cations are exchangeable and the exchange is reversible for simple cations. The distance between two

Table 2–3
Critical Salt Concentrations in Typical Sandstone

Salt	Stevens M	Berea M
NaCl	0.50–0.25	0.07
KCl	0.3–0.2	0.03
CaCl ₂	0.3–0.2	None

* After Mohan, K. K., and Fogler, H. S., ©1997; reprinted by permission of the AIChE, ©1997 AIChE. All rights reserved.

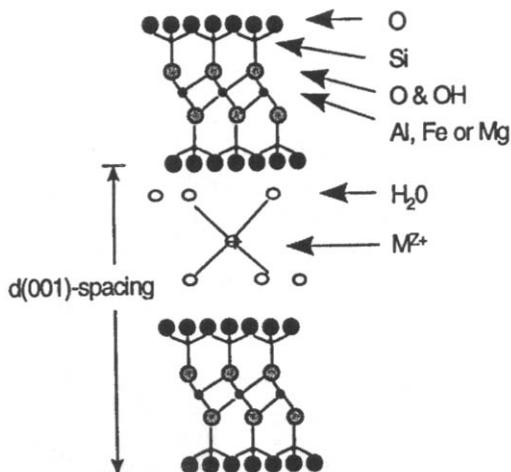


Figure 2-12. Schematic structure of a swelling clay crystal containing an exchangeable M^{2+} cation (after Zhou et al., ©1997 SPE; reprinted by permission of the Society of Petroleum Engineers).

structure layers, i.e. (001) d-spacing, is dependent on the nature (type) of the exchangeable cation, composition of the solution, and the clay composition. Clay swelling is a direct result of the d-spacing increase and volume expansion when the exchangeable cations are hydrated in aqueous solution."

As stated by Zhou (1995), "clay swelling is a result of the increase in interlayer spacing in clay particles." Clay swelling occurs when the clay is exposed to aqueous solutions having a brine concentration below the critical salt concentration (Khilar and Fogler, 1983). Therefore, Zhou (1995) concludes that "clay swelling is controlled primarily by the composition of aqueous solutions with which the clay comes into contact." Norrish (1954) have demonstrated by experiments that clay swelling occurs by crystalline and osmotic swelling processes. Zhou (1995) explains that (1) crystalline swelling occurs when the clays are exposed to concentrated brine or aqueous solutions containing large quantities of divalent or multivalent cations. It is caused by the formation of molecular water layers on the surface of clay minerals. This leads to less swelling and less damage; and (2) osmotic swelling occurs when the clays are exposed to dilute solutions or solutions containing large quantities of Na^+ cations. It is caused by the formation of an electric double layer on the surface of clay minerals. It leads to more swelling and more damage. These phenomena create repulsive forces to separate the clay flakes from each other.

Mohan and Fogler (1997) conclude that crystalline swelling occurs at high concentrations below the critical salt concentration and osmotic swelling occurs at low concentrations above the critical salt concentrations. Mohan and Fogler (1997) measured the interplanar spacing as an indication of swelling of montmorillonite in various salt solutions. Thus, according to Figures 2–13 and 2–14 given by Mohan and Fogler (1997), the crystalline and osmotic swelling regions can be distinguished by a sudden jump or discontinuity in the value of the interplanar spacing which occurs at the critical salt concentration.

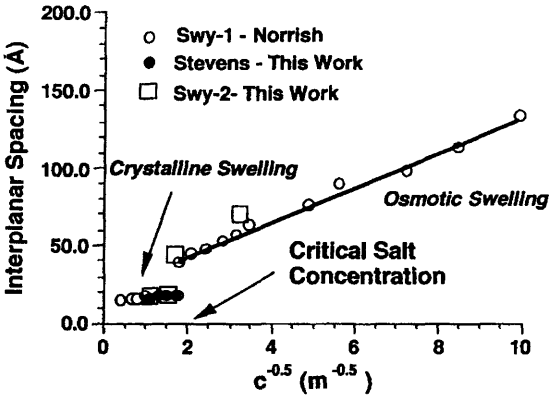


Figure 2–13. Swelling of montmorillonite in sodium chloride brine (after Mohan, K. K., and Fogler, H. S., ©1997; reprinted by permission of the AIChE, ©1997 AIChE. All rights reserved).

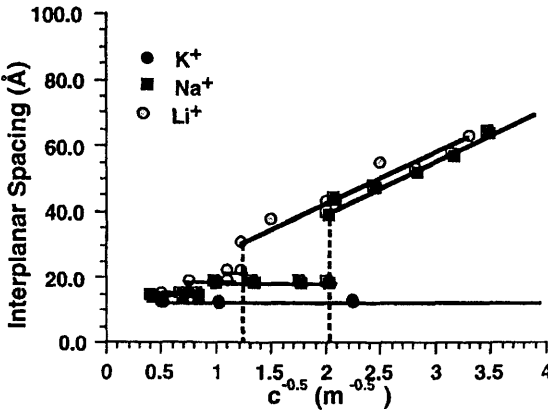


Figure 2–14. Swelling of montmorillonite in various brine (after Mohan, K. K., and Fogler, H. S., ©1997; reprinted by permission of the AIChE, ©1997 AIChE. All rights reserved).

Zhou et al. (1996, 1997) suggest the use of clay-swelling charts obtained by x-ray diffraction method similar to that given in Figures 2-15 and 2-16 to determine the compatibility of clays with mixed-electrolyte solutions. These charts indicate the cation concentrations of aqueous solutions that will cause crystalline or osmotic swelling. Consequently the cation compositions that will lead to formation damage can be identified readily in the region of the osmotic swelling, as shown in Figure 2-15, because osmotic swelling is the main cause of formation damage. Thus, Figure 2-15 provides some guidance as to the amount of Ca^{2+} necessary in the presence of Na^+ cations to prevent montmorillonite swelling in $\text{NaCl}/\text{CaCl}_2$ solutions. Figure 2-16 is a similar chart for montmorillonite in NaCl/KCl solutions given by Zhou et al (1996).

Models for Clay Swelling*

In this section, the analytical models by Civan (1999) are presented for interpretation and correlation of measurements of swelling-dependent

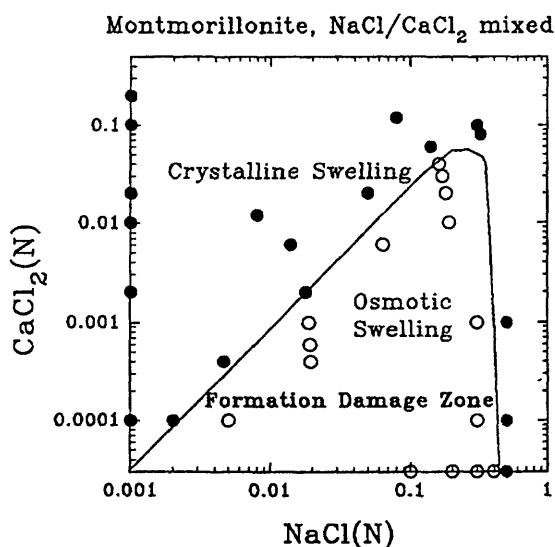


Figure 2-15. Swelling chart for montmorillonite exposed to sodium and calcium chloride brines (after Zhou et al, ©1996; reprinted by permission of the Canadian Institute of Mining, Metallurgy and Petroleum).

* After Civan, ©1999 SPE; reprinted by permission of the Society of Petroleum Engineers from SPE 52134 paper.



Figure 2-16. Swelling chart for montmorillonite exposed to sodium and potassium chloride brines (after Zhou et al., ©1996; reprinted by permission of the Canadian Institute of Mining, Metallurgy and Petroleum).

properties of reservoir formations containing swelling clays and for representing these properties in the prediction and simulation of reservoir formation damage and in well-log interpretation.

The laboratory studies by many researchers, including the ones by Zhou et al. (1997) and Mohan and Fogler (1997), have concluded that clay swelling primarily occurs by crystalline and osmotic swelling mechanisms. Civan and Knapp (1987) and Civan et al. (1989) recognized that water transfer through clayey porous media occurs by diffusion and developed the phenomenological models for permeability and porosity reduction by swelling by absorption of water via the diffusion process. Ohen and Civan (1990, 1993) and Chang and Civan (1997) incorporated these models into the simulation of formation damage in petroleum reservoirs.

Ballard et al. (1994) experimentally studied the transfer of water and ions through shales. They determined that diffusion controls the transfer process and osmosis does not have any apparent effect when pressure is not applied. Their findings reconfirms the mechanism proposed by Civan

and Knapp (1987) and Civan et al. (1989) that diffusion is the primary cause of water transfer through clayey porous formations. But, transfer rates tend to increase with pressure application. Ballard et al. (1994) observed that, beyond a certain threshold pressure, water and ions move at the same speed. This is because transfer by advection dominates and diffusion by concentration gradients becomes negligible.

The Civan and Knapp (1987) and Civan et al. (1989) models for variation of porosity and permeability by swelling assume that the external surface of the swelling clay is in direct contact with water at all times and therefore they used a Dirichlet boundary condition in the analytic solution of the models. Civan (1999) developed improved models by considering a water-exposed-surface-hindered-diffusion process and used a Neumann boundary condition in the analytical solution of the models. By means of a variety of experimental data reported in the literature, Civan (1999) demonstrated and verified that this boundary condition leads to improved analytic models which correlate the experimental data better as closely as the quality of the data permits. He has also shown that the various phenomenological parameters, such as the rate constants and the terminal porosity and permeability values that will be attained at water saturation, can be conveniently determined by fitting these models to experimental data. Civan (1999) pointed out that the laboratory swelling tests are generally carried out using aqueous solutions of prescribed concentrations. Whereas, the composition of aqueous solutions in actual reservoir formations may vary, but this effect can readily be taken into account by incorporating a time-dependent clay surface boundary condition by applying Duhamel's theorem. As a result, the effect of variable aqueous solution concentration can be adequately incorporated into the simulation of formation damage by clay swelling.

As schematically depicted in Figure 2-17, swelling clay particles can absorb water and expand to enlarge the particle size, and the clayey porous formations containing swelling clays can absorb water and expand inward to reduce its porosity and permeability. In this section various models useful for interpretation of experimental data and modeling formation damage are presented.

Osmotic Repulsive Pressure

Ladd (1960) explains that: "The exchangeable cations are attracted to the clay particles by the negative electric field arising from the negative charge on the particles. Hence, the electric field acts as a semi-permeable membrane in that it will allow water to enter the double layer but will not allow the exchangeable cations to leave the double layer." Thus, when the total ion (cations plus anions) concentration in the double-layer

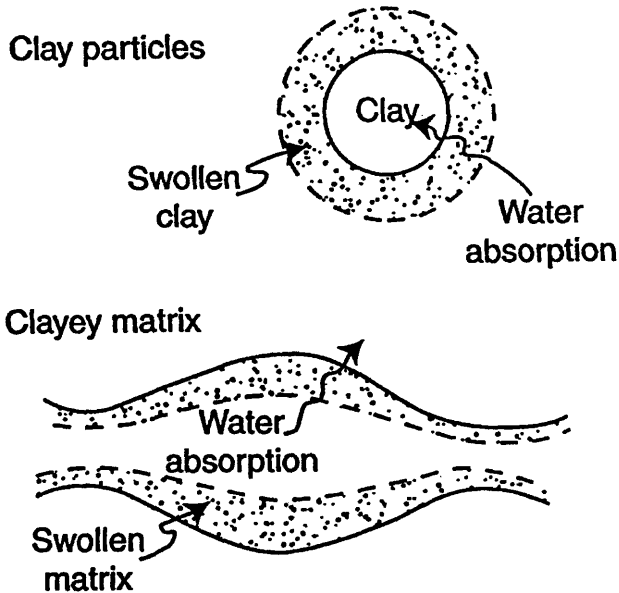


Figure 2–17. Clay particle expansion and pore space reduction by swelling (after Civan, ©1999 SPE; reprinted by permission of the Society of Petroleum Engineers).

between the clay particles is higher than that in the aqueous pore fluid, the water in the pore fluid diffuses into the double-layer to dilute its ion concentration. This phenomenon creates an osmotic repulsive pressure between the clay particles. As a result, the interparticle distance increases causing the clay to expand and swell. Therefore, the driving force for osmotic pressure is the difference of the total ion concentrations between the clay double-layer, c_c , and the surrounding pore fluid, c_f , as depicted by Figure 2–18 of Ladd (1960).

For only very dilute aqueous solutions, the van't Hoff equation given below can be used to estimate the osmotic pressure (Ladd, 1960):

$$p_{osm} = RT(c_c - c_f) \quad (2-1)$$

Non-ideal models are required for concentrate solutions.

Water Absorption Rate

Consider Figure 2–19 (Civan, 1994, 1999) showing swelling of a solid by water absorption. Civan et al. (1989) assumed that water diffuses

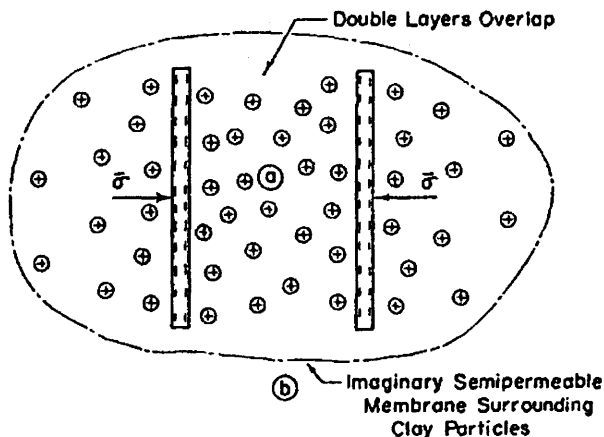


Figure 2-18. Mechanism of osmotic pressure generation between two clay particles in water (after C. C. Ladd, 1960; reprinted by permission of the Transportation Research Board, the National Academies, Washington, D.C., from C. C. Ladd, "Mechanisms of Swelling by Compacted Clay," in Highway Research Board Bulletin 245, Highway Research Board, National Research Council, Washington, D.C., 1960, pp. 10-26).

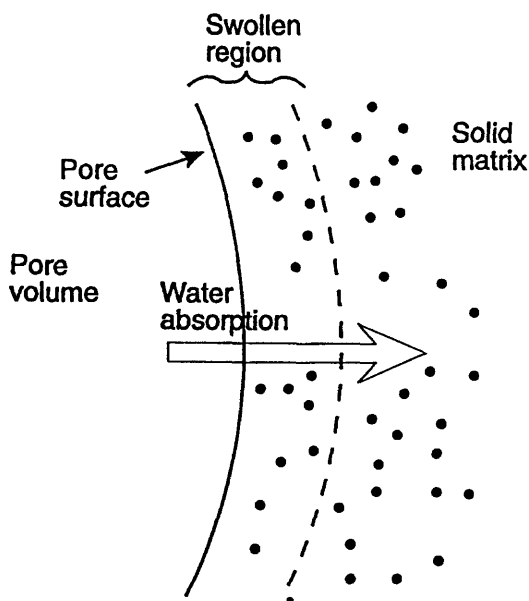


Figure 2-19. Mechanism of formation swelling by water absorption (after Civan, ©1999 SPE; reprinted by permission of the Society of Petroleum Engineers).

through the solid matrix according to Fick's second law over a short distance near the surface of the solid exposed to aqueous solution, because the coefficient of water diffusion in solid is small. Thus, the water absorption in the solid can be predicted by the one-dimensional transient-state diffusion equation:

$$\partial c / \partial t = D \partial^2 c / \partial z^2, 0 \leq z < \infty, t > 0, \quad (2-2)$$

subject to the initial and boundary conditions given, respectively, by:

$$c = c_0, 0 \leq z < \infty, t = 0 \quad (2-3)$$

$$\dot{S} \equiv -D \partial c / \partial z = k(c_1 - c), z = 0, t > 0 \quad (2-4)$$

$$c = c_0, z \rightarrow \infty, t > 0 \quad (2-5)$$

where c_0 and c are the initial and instantaneous water concentrations, respectively, in the solid, c_1 is the water concentration of the aqueous solution, z is the distance from the pore surface, t is the actual contact time, k is the film mass transfer coefficient, and D is the diffusivity coefficient in the solid matrix. Eq. 2-4 expresses that the water diffusion into clay is hindered by the stagnant fluid film over the clay surface. Thus, similar to Civan (1997), the analytical solution of Eqs. 2-2 through 2-5 can be used to express the cumulative amount of water diffusing into the solid surface as given by Crank (1956):

$$S \equiv - \int_0^t \left(-D \frac{\partial c}{\partial z} \right) dt = \frac{c_1 - c_0}{h} \left[\exp(h^2 Dt) \operatorname{erfc}(h\sqrt{Dt}) - 1 + \frac{2}{\sqrt{\pi}} h\sqrt{Dt} \right] \quad (2-6)$$

and the rate of water absorption is given by differentiation of Eq. 2-6 as:

$$\dot{S} = dS/dt = (c_1 - c_0) h D \exp(h^2 Dt) \operatorname{erfc}(h\sqrt{Dt}) \quad (2-7)$$

where $h \equiv k/D$.

Civan et al. (1989) have resorted to a simplified approach by assuming that the film mass transfer coefficient k in Eq. 2-4 is sufficiently large

so that Eq. 2-4 becomes:

$$c = c_1, z = 0, t > 0 \quad (2-8)$$

and, therefore, an analytical solution of Eqs. 2-2, 3, 8, and 5 according to Crank (1956) yields the expression for the cumulative and rate of water absorption, respectively, as:

$$S = \frac{2}{\sqrt{\pi}} (c_1 - c_0) \sqrt{Dt} \quad (2-9)$$

$$\dot{S} = \frac{D}{\sqrt{\pi}} (c_1 - c_0) \frac{1}{\sqrt{Dt}} \quad (2-10)$$

The rate of formation damage by clay swelling also depends on the variation of the water concentration in the aqueous solution flowing through porous rock. Whereas, the analytical expressions given above assume constant water concentrations in the aqueous pore fluid. However, they can be corrected for variable water concentrations by an application of Duhamel's theorem. For example, if the time-dependent water concentration at the pore surface is given by:

$$c = c_0 + (c_1 - c_0) F(t), z = 0, t > 0 \quad (2-11)$$

where $F(t)$ is a prescribed time-dependent function, the analytic solution can be obtained as illustrated, by Carslaw and Jaeger (1959). Then, using Eq. 2-10, the rate of water absorption can be expressed by:

$$\dot{S} = \frac{D(c_1 - c_0)}{2\sqrt{\pi D}} \int_0^t \frac{-F(\tau)}{(t - \tau)^{3/2}} d\tau \quad (2-12)$$

However, in the applications presented here the water concentrations involved in the laboratory experiments are essentially constant.

The preceding derivations assume a plane surface as supposed to a curved pore surface. From the practical point of view, it appears reasonable because of the very short depth of penetration of the water from the solid-fluid contact surface.

Clay Swelling Coefficient

The rate of clayey formation swelling is derived from the definition of the isothermal swelling coefficient given by (Collins, 1961):

$$\lambda_{sw} = (\partial V / \partial V_w)_T \quad (2-13)$$

V and V_w are the volumes of the solid and the water absorbed, respectively.

Ohen and Civan (1991) used the expression given by Nayak and Christensen (1970) for the swelling coefficient:

$$\lambda_{sw} = \varsigma_1 CI^m / c + \varsigma_2 \quad (2-14)$$

in which c is the water concentration in the solid and CI is the plasticity index. ς_1 and ς_2 are some empirical coefficients. m is an exponent.

Chang and Civan (1997) used the expression given by Seed et al. (1962):

$$\lambda_{sw} = k' PI^{2.44} C_c^{3.44} / (C_c - 10)^{2.44} \quad (2-15)$$

where C_c is the clay content of porous rock as weight percent, PI is the plasticity index, and k' is an empirical constant.

Water Content During Clay Swelling

The rate of water retainment of clay minerals is assumed proportional with the water absorption rate, \dot{S} , and the deviation of the instantaneous water content from the saturation water content as:

$$dw/dt = k_w \dot{S} (w_t - w) \quad (2-16)$$

subject to the initial condition

$$w = w_o, t = 0 \quad (2-17)$$

where k_w is a water retainment rate constant. w denotes the weight percent of water in clay and the subscripts o and t refer to the initial ($t = 0$) and terminal ($t \rightarrow \infty$) conditions, respectively. An analytical solution of Eqs. 2-16 and 17 yields:

$$w = w_t - (w_t - w_o) \exp(-k_w \dot{S}) \quad (2-18)$$

Osisanya and Chenevert (1996) measured the variation of the water content of the Wellington shale exposed to deionized water. Figure 2-20

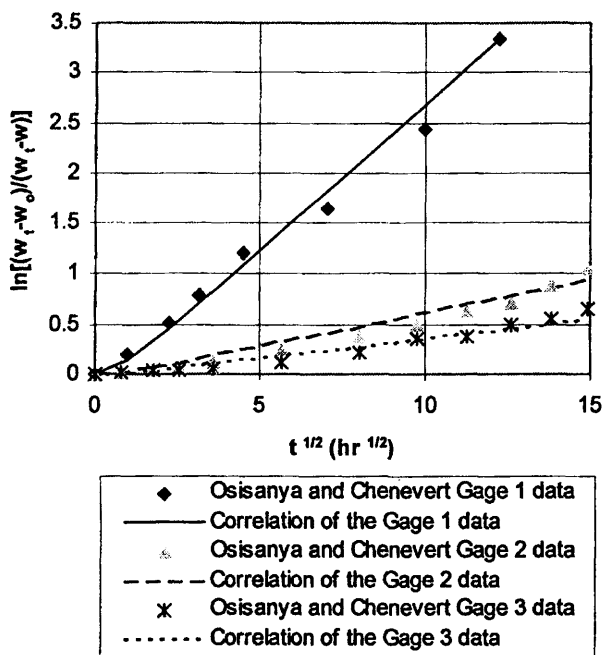


Figure 2-20. Correlation of water pickup during swelling (after Civan, ©1999 SPE; reprinted by permission of the Society of Petroleum Engineers).

shows the correlation of their data with Eq. 2-18 using Eq. 2-6. The best fits were obtained using $w_o = 2.7$ wt.%, $w_i = 3.27$ wt.%, $A = k_w(c_1 - c_0)/h = 0.26$ and $h\sqrt{D} = 1$ for their Gage 1 data, $w_o = 2.77$ wt.%, $w_i = 3.28$ wt.%, $A = 0.06$ and $h\sqrt{D} = 0.8$ for their Gage 2 data, and $w_o = 2.77$ wt.%, $w_i = 3.28$ wt.%, $A = 0.035$ and $h\sqrt{D} = 0.8$ for their Gage 3 data.

Brownell (1976) reports the data of the moisture content of a dried clay piece containing montmorillonite soaked in water. Figure 2-21 shows a correlation of the data with Eq. 2-18 using Eq. 2-6. The best fit was obtained using $w_o = 0\%$, $w_i = 14.2$ wt.%, $A = 0.2$ and $h\sqrt{D} = 0.8$.

Time-Dependent Clay Expansion Coefficient

By contact with water the swelling clay particles absorb water and expand. The rate of volume increase is assumed proportional to the water absorption rate, \dot{S} , and the deviation of the instantaneous volume from the terminal swollen volume that will be achieved at saturation, $(V_t - V)$. Therefore, the rate equation is written as:

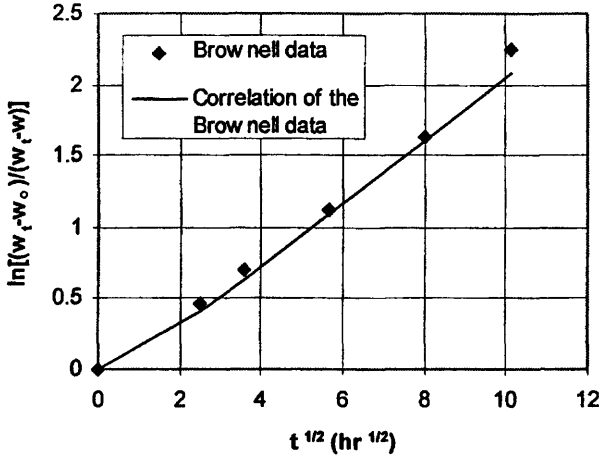


Figure 2-21. Correlation of water pickup during swelling (after Civan, ©1999 SPE; reprinted by permission of the Society of Petroleum Engineers).

$$dV/dt = k_{\alpha} \dot{S}(V_t - V) \quad (2-19)$$

subject to

$$V = V_o, t = 0, \quad (2-20)$$

k is a rate constant. Thus, solving Eqs. 2-19 and 20 yields:

$$V = V_t - (V_t - V_o) \exp(-k_{\alpha} S) \quad (2-21)$$

from which the expansion coefficient of a unit clay volume is determined as:

$$\alpha \equiv V/V_o - 1 = \alpha_t [1 - \exp(-k_{\alpha} S)] \quad (2-22)$$

where α_t is the terminal expansion coefficient at saturation. k_{α} is the rate coefficient of expansion.

Seed et al. (1962), Blomquist and Portigo (1962), Chenevert (1970), and Wild et al. (1996) measured the rates of expansion of the samples of compacted sandy clay, hydrogen soil, typical shales, and lime-stabilized kaolinite cylinders containing gypsum and ground granulated blast furnace slag, respectively. Figures 2-22 and 2-23 show the correlation of their data with Eq. 2-22 using Eq. 2-6. The best matches of the data

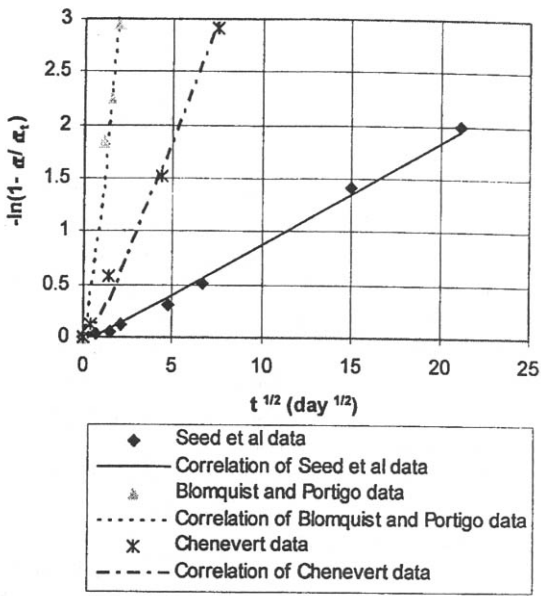


Figure 2-22. Correlation of volume change during swelling (after Civan, ©1999 SPE; reprinted by permission of the Society of Petroleum Engineers).

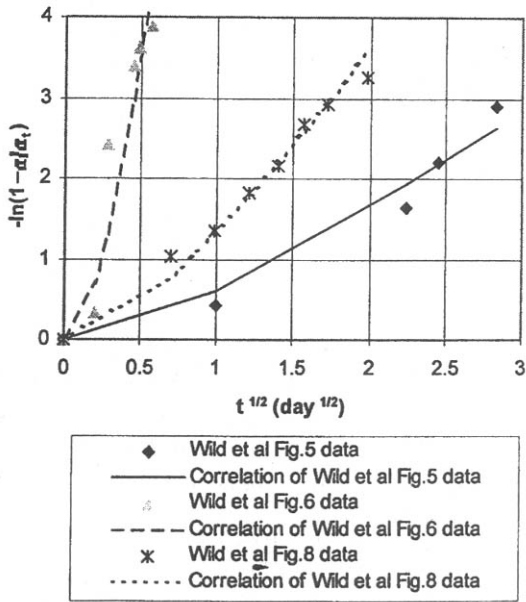


Figure 2-23. Correlation of volume change during swelling (after Civan, ©1999 SPE; reprinted by permission of the Society of Petroleum Engineers).

shown in Figure 2-22 were obtained using $A = k(c_1 - c_0)/h = 0.085$, $h\sqrt{D} = 0.67$, and $\alpha_t = 100(V_t - V_o)/V_o = 3.7$ vol.% for the Figure 2 data of Seed et al. (1962), $A = 2.2$, $h\sqrt{D} = 1.1$, and $\alpha_t = (V_t - V_o)/V_o = 95/V_o$ volume fraction for the Figure 9 data of Blomquist and Portigo (1962), and $A = 0.4$, $h\sqrt{D} = 1.37$, and $\alpha_t = 0.55\%$ for the Figure 4 (Curve F) data of Chenevert (1970). Note that the initial sample volume V_o is not given in the original data. However, this value is not required for the plots of $(1 - \alpha/\alpha_t)$ because the V_o value cancels out in the ratio of α/α_t . Note that the data points shown in Figure 2-21 are the tick-mark readings of the plots of the original reported data.

Wild et al. (1996) tested lime-stabilized compacted kaolinite cylinders containing gypsum and ground granulated blast furnace slag. After moist-curing for certain periods, they soaked these samples in water and measured the linear expansion of the samples. Figure 2-23 shows the representation of the three typical data sets selected from their Figures 5, 6, and 8 by Eq. 2-22 using Eq. 2-6. The first set of data was obtained using a 7-day moist-cured kaolinite containing 6% lime and 4% gypsum. The second set of data is for a 28-day moist-cured kaolinite containing 6% lime and 4% gypsum. The third set of data is for a 28-day moist-cured kaolinite containing 2% lime, 4% gypsum and 8% ground granulated blast furnace slug. The best fits of Eq. 2-22 using Eq. 2-6 to the first, second, and third data sets were obtained with $A = k(c_1 - c_0)/h = 1.1$, $h\sqrt{D} = 1.0$ and $\alpha_t = 10.8$ vol.%, $A = 20$, $h\sqrt{D} = 0.2$ and $\alpha_t = 1.48$ vol.%, and $A = 2.4$, $h\sqrt{D} = 0.7$ and $\alpha_t = 0.655$ vol.%, respectively.

Ladd (1960) measured the volume change and water content of the compacted Vicksburg Buckshot clay samples during swelling. For a linear plot of Ladd's data first, the S term is eliminated between Eqs. 2-18 and 22 to yield:

$$1 - \frac{\alpha}{\alpha_t} = \left(\frac{w_t - w}{w_t - w_o} \right)^{(k/k_w)} \quad (2-23)$$

Then, inferred by Eq. 2-23, Ladd's data can be correlated on a log-log scale by a straightline as shown in Figure 2-24. The best linear fit of Eq. 2-23 was obtained using $w_o = 0.8\text{g}$, $w_t = 32\text{g}$, $\alpha_t = 13.2/V_o$ and $k/k_w = 1.907$. Note that the value of V_o is not given and not required because Eq. 2-23 employs the ratio of α/α_t .

Porosity Reduction by Swelling

Based on the definition of the swelling coefficient, Civan and Knapp (1987) expressed the rate of porosity change by swelling of porous matrix as:

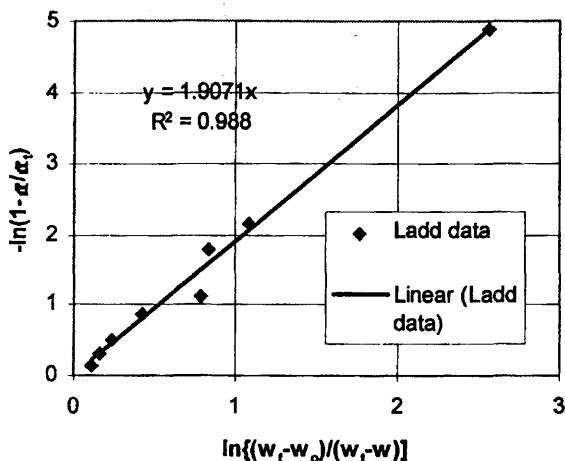


Figure 2–24. Correlation of volume change vs. water pickup during swelling (after Civan, ©1999 SPE; reprinted by permission of the Society of Petroleum Engineers).

$$\partial\phi/\partial t = -\lambda_{sw}\dot{S} \quad (2-24)$$

where ϕ is porosity, t is time, \dot{S} is the rate of water absorbed per unit bulk volume of porous medium.

Civan (1996) developed an improved equation assuming that the rate of porosity variation by swelling is proportional to the rate of water absorption and the difference between the instantaneous and the terminal or saturation porosities:

$$-d\phi/dt = k_{sw}\dot{S}(\phi - \phi_t) \quad (2-25)$$

subject to

$$\phi = \phi_o, t = 0 \quad (2-26)$$

Integrating Eqs. 2–25 and 26 yields:

$$\ln \left[\frac{\phi_o - \phi_t}{\phi - \phi_t} \right] = k_{sw} S \quad (2-27)$$

from which the porosity variation by swelling can be expressed by:

$$\Delta\phi_{sw} = \phi - \phi_o = (\phi_t - \phi_o)[1 - \exp(-k_{sw}S)] \quad (2-28)$$

where k_{sw} is the formation swelling rate constant. t is the actual time of contact with water. Therefore, the swelling rate constant can be determined by fitting Eq. 2-27. However, due to the lack of experimental data, the application of Eq. 2-28 could not be demonstrated. It is difficult to measure porosity during swelling. Permeability can be measured more conveniently. Ohen and Civan (1993) used a permeability-porosity relationship to express porosity reduction in terms of permeability reduction.

Permeability Reduction by Swelling

Civan and Knapp (1987) assumed that the rate of permeability reduction by swelling of formation depends on the rate of the water absorption and the difference between the instantaneous permeability and terminal permeability that will be attained at saturation as:

$$-dK/dt = \alpha_{sw}\dot{S}(K - K_t) \quad (2-29)$$

subject to the initial condition

$$K = K_o, t = 0 \quad (2-30)$$

where α_{sw} is a rate constant.

Thus, solving Eqs. 2-29 and 30 yield:

$$\ln\left(\frac{K_o - K_t}{K - K_t}\right) = \alpha_{sw}S \quad (2-31)$$

where α_{sw} is the rate constant for permeability reduction by swelling, from which the permeability variation by swelling is obtained as:

$$\Delta K = K_o - K = (K_o - K_t)[1 - \exp(-\alpha_{sw}S)] \quad (2-32)$$

Civan and Knapp (1987) and Civan et al. (1989) have confirmed the validity of Eq. 2-31 using the Hart et al. (1960) data for permeability reduction in the outlet region of a core subjected to the injection of a suspension of bacteria. Because bacteria is essentially retained in the inlet side of the core, the permeability reduction in the near-effluent port of the core can be attributed to formation swelling by water absorption. The

best linear, least-squares fit of Eq. 2-31 to Hart et al. (1960) data using Eq. 2-9 for S yields (Civan et al., 1989):

$$K/K_o = (K_i/K_o) + [1 - (K_i/K_o)] \exp(-B\sqrt{t}) \quad (2-33)$$

with $(K_i/K_o) = 0.57$ and $B = 2\alpha_{sw}(c_1 - c_o)\sqrt{D/\pi} = 0.81 \text{ hr}^{-1/2}$ with a correlation coefficient of $R^2 = 0.93$ as shown in Figure 2-25. However, as shown in Figure 2-25, the Hart et al. (1960) data can also be correlated using Eq. 2-6 for S . In this case, the best fit is obtained using the parameter values of $A = \alpha_{sw}(c_1 - c_o)/h = 0.95$, $h\sqrt{D} = 1$, and $K_i/K_o = 0.57$.

Ngwenya et al. (1995) conducted core flood experiments by injecting an artificial seawater into the Hopeman (Clashach) sandstone. They report that the core samples used in their experiments contained trace amounts of clays. Therefore, they concluded that the effect of clay swelling, and entrainment and deposition of clay particles to permeability impairment would be negligible. However, their Table 1 data plotted according to Eq. 2-31 in Figure 2-26 indicates a reasonably well linear trend. Consequently, it can be concluded that the swelling of some constituents of the sandstone formation should be contributing to permeability reduction. The best least-squares linear fit of Eq. 2-31 was obtained using Eq. 2-9 for S with the parameter values of $B = \alpha_{sw}(c_1 - c_g)/h = 0.038 \text{ hr}^{-1/2}$ and $(K_i/K_o) = 0.087$ with a correlation coefficient of $R^2 = 0.89$. The best

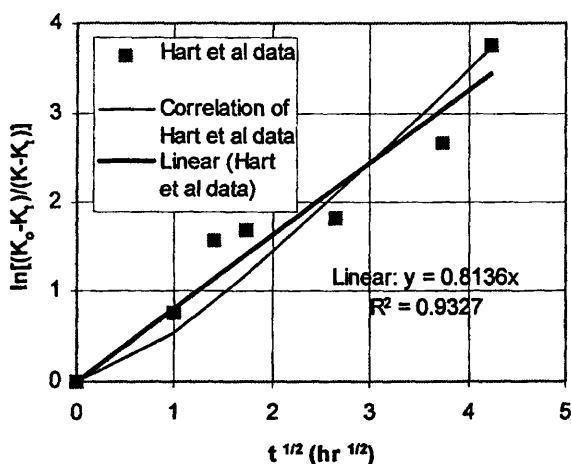


Figure 2-25. Correlation of permeability reduction during swelling (after Civan, ©1999 SPE; reprinted by permission of the Society of Petroleum Engineers).

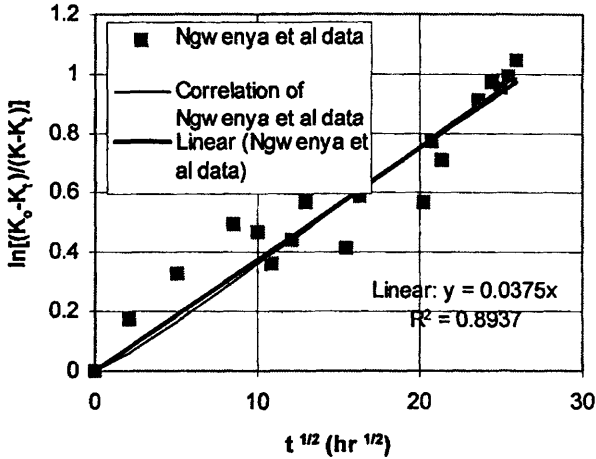


Figure 2-26. Correlation of permeability reduction during swelling (after Civan, ©1999 SPE; reprinted by permission of the Society of Petroleum Engineers).

fit of Eq. 2-31 using Eq. 2-6 for S was obtained using the parameter values of $A = \alpha_{sw} (c_1 - c_o)/h = 0.035$, $h\sqrt{D} = 1$, and $K_i/K_o = 0.087$.

It is apparent from Figures 2-25 and 26 that the quality of both the Hart et al. (1960) and the Ngwenya et al. (1995) experimental data does not permit determining whether Eqs. 2-6 or 9 with Eq. 2-31 better represents the data. Because Eq. 2-6 led to successful representation of the other data correlated in the preceding sections, it is reasonable to assume that Eq. 2-6 should also represent the permeability reduction data equally well. Therefore, Eq. 2-6 may be preferred over Eq. 2-9.

Discussion and Generalization

The preceding analyses of the various data indicate that the variation of the moisture, volume, and permeability of clayey formations during swelling by exposure to water is governed by similar rate equations, which can be generalized as (Civan, 1999):

$$-d(f - f_i)/dt = k_f \dot{S}(f - f_i) \quad (2-34)$$

subject to the initial condition

$$f = f_o, t = 0 \quad (2-35)$$

Although the validity of Eq. 2-34 for porosity variation could not be demonstrated because of the lack of experimental data, porosity variation is also expected to follow the same trend because it is a result of solid expansion by water absorption, for which case the validity of the proposed mechanism was confirmed with experimental data.

Let f denote the properties of clayey formations that vary by swelling, that is $f \in (w, \alpha, \phi, K)$, f_o and f_t denote the initial and final values of f over the swelling period, t is time, k_f is the rate constant for the property f , and S is the rate of water absorption controlled by the hindered diffusion of water into the solid according to Eq. 2-6.

The analytic solution of Eqs. 2-34 and 35 can be written in the following form:

$$\ln \left[\frac{f_o - f_t}{f - f_t} \right] = k_f S \quad (2-36)$$

As demonstrated by Eq. 2-23, it is also possible to relate a property of $f \in (w, \alpha, \phi, K)$ to another property of $g \in (w, \alpha, \phi, K)$ for $f \neq g$. This can be accomplished by first applying Eq. 2-36 for g as:

$$\ln \left[\frac{g_o - g_t}{g - g_t} \right] = k_g S \quad (2-37)$$

The quantity S can then be eliminated between Eqs. 2-36 and 37 to obtain:

$$\frac{f_o - f_t}{f - f_t} = \left[\frac{g_o - g_t}{g - g_t} \right]^{(k_f/k_g)} \quad (2-38)$$

Eq. 2-38 is particularly useful to correlate between w, α, ϕ , and K without the involvement of the time variable. For example, applying Eq. 2-38, porosity and permeability variations can be correlated by the power law equation:

$$\frac{K_o - K_t}{K - K_t} = \left[\frac{\phi_o - \phi_t}{\phi - \phi_t} \right]^{(k_K/k_\phi)} \quad (2-39)$$

where k_K and k_ϕ are the rate coefficients for permeability and porosity reduction by swelling, respectively.

Conclusions

As presented in this section,

1. Swelling of clayey porous rocks is controlled by absorption of water by a water-exposed-surface hindered diffusion process.
2. The characteristics of the swelling clayey formation, such as moisture content, volume, and permeability, vary at rates proportional to the water absorption rate and their values relative to their terminal values that would be attained at the saturation limit.
3. The rate laws of different properties allow for cross-correlation between these properties.

Civan's (1999) model provides insight into the mechanism of the clay swelling process and a proper means of interpreting and correlating the swelling-dependent characteristics of clayey formations.

Graphical Representation of Clay Content

The distribution of clays can be conveniently depicted by ternary line diagrams such as given in Figure 2-27 by Lynn and Nasr-El-Din (1998).

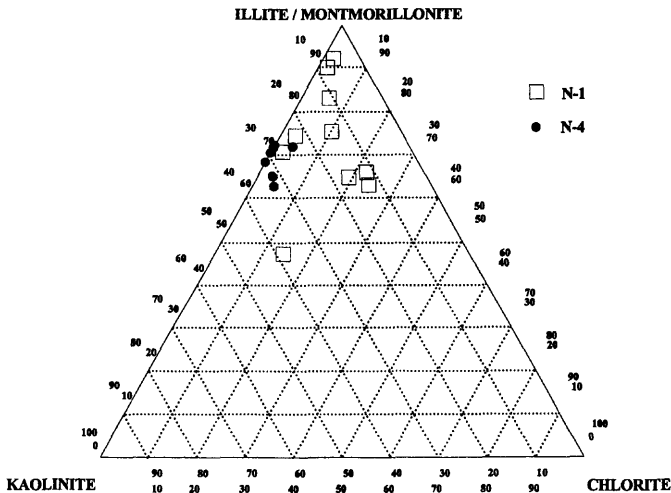


Figure 2-27. A ternary clay distribution chart (Reprinted from *Journal of Petroleum Science and Engineering*, Vol. 21, Lynn, J. D., and Nasr-El-Din, H. A., "Evaluation of Formation Damage due to Frac Stimulation of Saudi Arabian Clastic Reservoir," pp. 179–201, ©1998; reprinted with permission from Elsevier Science).

Lynn and Nasr-El-Din (1998) classified reservoir formations having less than 1 wt. % total clay and permeability higher than one Darcy as the high quality, and the low quality vice versa. Amaefule et al. (1993) measured the formation quality by the reservoir quality index defined as:

$$RQI = 10^{-2} \pi \sqrt{K/\phi} \quad (2-40)$$

Hayatdavoudi Hydration Index (HHI)

The Hayatdavoudi hydration index (HHI=[O/OH]) is defined as the ratio of the oxygen atoms to hydroxyl groups in clays and it controls the enthalpy or free energy of the clays available for the work of swelling

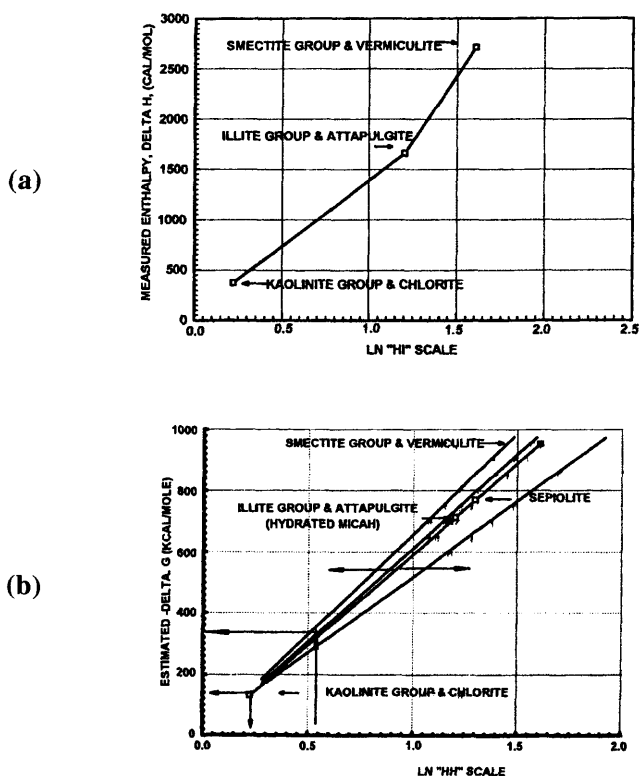


Figure 2–28. Hayatdavoudi clay hydration charts: (a) measured enthalpy versus hydration index and (b) theoretical free energy versus hydration index for various clays (after A. Hayatdavoudi, ©1999 SPE; reprinted by permission of the Society of Petroleum Engineers).

by hydration (Hayatdavoudi, 1999, 1999). Hence, higher hydration index is indicative of more clay swelling, according to (Hayatdavoudi, 1999, 1999):

$$\Delta G = \Delta H - T\Delta S = RT\ln[O/OH] \quad (2-41)$$

where G , H , S , T , and R denote the free energy, enthalpy, entropy, absolute temperature, and the universal gas constant, respectively. Figure 2–28 by Hayatdavoudi (1999) shows that all clays possess some degree of the work of swelling and therefore classification of different clays as swelling or non-swelling has no significance.

References

- Amaefule, J. O., Kersey, D. G., Norman, D. L., & Shannon, P. M., "Advances in Formation Damage Assessment and Control Strategies," CIM Paper No. 88-39-65, Proceedings of the 39th Annual Technical Meeting of Petroleum Society of CIM and Canadian Gas Processors Association, Calgary, Alberta, June 12–16, 1988, 16 p.
- Amaefule, J. O., Altunbay, M., Tiab, D., Kersey, D. G., & Keelan, D. K., "Enhanced Reservoir Description: Using Core and Log Data to Identify Hydraulic (Flow) Units and Predict Permeability in Uncored Intervals/Wells," SPE 26436 paper, Proceedings of the 68th Annual Technical Conference and Exhibition of the SPE held in Houston, Texas, October 3–6, 1993, pp. 205–220.
- Ballard, T. J., Beare, S. P., & Lawless, T. A., "Fundamentals of Shale Stabilization: Water Transport through Shales," SPE Formation Evaluation, June 1994, pp. 129–134.
- Blomquist, G. C., & Portigo, J. M., "Moisture, Density and Volume Change Relationships of Clay Soils Expressed as Constants of Proportionality," *Bull. Highway Res. Board*, No. 313, 1962, pp. 78–91.
- Brownell, W. E., *Structural Clay Products*, Springer-Verlag, New York, 1976, 231 p.
- Bucke, D. P., & Mankin, C. J., "Clay-Mineral Diagenesis Within Interlaminated Shales and Sandstones," *J. Sedimentary Petrology*, Vol. 41, No. 4, December 1971, pp. 971–981.
- Carslaw, H. S., & Jaeger, J. C., *Conduction of Heat in Solids*, Second ed., Oxford University Press, 1959, 510 p.
- Chang, F. F., & Civan, F., "Predictability of Formation Damage by Modeling Chemical and Mechanical Processes," SPE 23793 paper, Proceedings of the SPE International Symposium on Formation Damage Control, February 26–27, 1992, Lafayette, Louisiana, pp. 293–312.
- Chang, F. F., & Civan, F., "Practical Model for Chemically Induced Formation Damage," *J. of Petroleum Science and Engineering*, Vol. 17, No. 1/2, February 1997, pp. 123–137.

- Chenevert, M. E., "Shale Alteration by Water Adsorption," *JPT*, September 1970, pp. 1141–1148.
- Chilingarian, G. V., & Vorabutr, P., *Drilling and Drilling Fluids, Developments in Petroleum Science*, 11, Elsevier Scientific Publishing Co., New York, 1981.
- Civan, F., "Predictability of Formation Damage: An Assessment Study and Generalized Models," Final Report, U.S. DOE Contract No. DE-AC22-90BC14658, April 1994.
- Civan, F., "Modeling and Simulation of Formation Damage by Organic Deposition," Proceedings of the First International Symposium on Colloid Chemistry in Oil Production: Asphaltenes and Wax Deposition, IS COP'95, Rio de Janeiro, Brazil, November 26–29, 1995, pp. 102–107.
- Civan, F., "A Multi-Purpose Formation Damage Model," SPE 31101, Proceedings of the SPE Formation Damage Symposium, Lafayette, LA, February 14–15, 1996, pp. 311–326.
- Civan, F., "Interactions of the Horizontal Wellbore Hydraulics and Formation Damage," SPE 35213, Proceedings of the SPE Permian Basin Oil & Gas Recovery Conf., Midland, TX, March 27–29, 1996, pp. 561–569.
- Civan, F., "Model for Interpretation and Correlation of Contact Angle Measurements," *Jour. Colloid and Interface Science*, Vol. 192, 1997, pp. 500–502.
- Civan, F., "Interpretation and Correlations of Clay Swelling Measurements," Paper SPE 52134, Proceedings of the 1999 SPE Mid-Continent Operations Symposium, 28–31 March 1999, Oklahoma City, OK.
- Civan, F., & Knapp, R. M., "Effect of Clay Swelling and Fines Migration on Formation Permeability," SPE Paper No. 16235, Proceedings of the SPE Production Operations Symposium, OKC, 1987, pp. 475–483.
- Civan, F., Knapp, R. M., & Ohen, H. A., "Alteration of Permeability by Fine Particle Processes," *J. Petroleum Science and Engineering*, Vol. 3, Nos. 1/2, October 1989, pp. 65–79.
- Collins, E. R., *Flow of Fluids Through Porous Materials*, Penn Well Publishing Co., Tulsa, Oklahoma, 1961, 270 p.
- Crank, J., *The Mathematics of Diffusion*, Oxford University Press, London, 1956, 347 p.
- Degens, E. T., *Geochemistry of Sediments (A Brief Survey)*, Prentice-Hall, Inc., Englewood Cliffs, New Jersey, 1965, 342 p.
- Ezzat, A. M., "Completion Fluids Design Criteria and Current Technology Weaknesses, SPE 19434 paper, the SPE Formation Damage Control Symposium held in Lafayette, Louisiana, February 22–23, 1990, pp. 255–266.
- Grim, R. E., "Modern Concepts of Clay Minerals," *Jour. Geology*, Vol. 50, No. 3, April–May 1942, pp. 225–275.
- Grim, R. E., *Clay Mineralogy*, McGraw-Hill, New York, New York, 1953, 384 p.

- Hart, R. T., Fekete, T., & Flock, D. L., "The Plugging Effect of Bacteria in Sandstone Systems," *Canadian Mining and Metallurgical Bulletin*, Vol. 53, 1960, pp. 495–501.
- Hayatdavoudi, A., "Changing Chemophysical Properties of Formation and Drilling Fluid Enhances Penetration Rate and Bit Life," Paper No. SPE 50729, Proceedings of the SPE International Symposium on Oil Field Chemistry held in Houston, Texas, 16–19 February 1999, pp. 273–285.
- Hayatdavoudi, A., private communication, 1999.
- Hughes, R. V., "The Application of Modern Clay Concepts to Oil Field Development," pp. 151–167, in *Drilling and Production Practice 1950*, American Petroleum Institute, New York, NY, 1951, 344 p.
- Khilar, K. C., Fogler, H. S., "Water Sensitivity of Sandstones," *SPEJ*, February 1983, pp. 55–64.
- Kia, S. F., Fogler, H. S., & Reed, M. G., "Effect of Salt Composition on Clay Release in Berea Sandstones," SPE 16254, February 1987.
- Ladd, C. C., "Mechanisms of Swelling by Compacted Clay," in *Highway Research Board Bulletin* 245, High Research Board, National Research Council, Publication 731, Washington, D.C., 1960, pp. 10–26.
- Liu, X., Civan, F., & Evans, R. D., "Correlation of the Non-Darcy Flow Coefficient," *J. of Canadian Petroleum Technology*, Vol. 34, No. 10, 1995, pp. 50–54.
- Lynn, J. D., & Nasr-El-Din, H. A., "Evaluation of Formation Damage due to Frac Stimulation of Saudi Arabian Clastic Reservoir," *J. of Petroleum Science and Engineering*, Vol. 21, Nos. 3–4, 1998, pp. 179–201.
- Mancini, E. A., "Characterization of Sandstone Heterogeneity in Carboniferous Reservoirs for Increased Recovery of Oil and Gas from Foreland Basins," Contract No. FG07-90BC14448, in *EOR-DOE/BC-90/4 Progress Review*, No. 64, pp. 79–83, U.S. Department of Energy, Bartlesville, Oklahoma, May 1991, 129 p.
- Mohan, K. K., & Fogler, H. S., "Colloidally Induced Smectic Fines Migration: Existence of Microquakes," *AIChE J.*, Vol. 43, No. 3, March 1997, pp. 565–576.
- Mondshine, T. C., "A New Potassium Based Mud System," Paper No. SPE 4516, 48th Annual Fall Meeting of SPE of AIME, October 1973.
- Mondshine, T. C., "New Technique Determines Oil Mud Salinity Needs in Shale Drilling," *Oil and Gas J.*, July 14, 1969.
- Mungan, N., "Discussion of An Overview of Formation Damage," *JPT*, Vol. 41, No. 11, November 1989, p. 1224.
- Nayak, N. V., & Christensen, R. W., "Swelling Characteristics of Compacted Expansive Soils," *Clay and Clay Mineral*, Vol. 19, No. 4, December 1970, pp. 251–261.
- Neasham, J. W., "The Morphology of Dispersed Clay in Sandstone Reservoirs and Its Effect on Sandstone Shaliness, Pore Space and Fluid

- Flow Properties," SPE 6858, Proceedings of the 52nd Annual Fall Technical Conference and Exhibition of the SPE of AIME held in Denver, Colorado, October 9–12, 1977, pp. 184–191.
- Ngwenya, B. T., Elphick, S. C., & Shimmield, G. B., "Reservoir Sensitivity to Water Flooding: An Experimental Study of Seawater Injection in a North Sea Reservoir Analog," *AAPG Bulletin*, Vol. 79, No. 2, February 1995, pp. 285–304.
- Norrish, K., "The Swelling of Montmorillonite," *Discussions Faraday Soc.*, Vol. 18, 1954, p. 120.
- Ohen, H. A., & Civan, F., "Simulation of Formation Damage in Petroleum Reservoirs," SPE 19420 paper, Proceedings of the 1990 SPE Symposium on Formation Damage Control, Lafayette, Louisiana, February 22–23, 1990, pp. 185–200.
- Ohen, H. A., & Civan, F., "Simulation of Formation Damage in Petroleum Reservoirs," *SPE Advanced Technology Series*, Vol. 1, No. 1, pp. 27–35, April 1993.
- Osisanya, S. O., & Chenevert, M. E., "Physico-Chemical Modelling of Wellbore Stability in Shale Formations," *J. of Canadian Petroleum Technology*, Vol. 35, No. 2, February 1996, pp. 53–63.
- Pittman, E. D., & Thomas, J. B., "Some Applications of Scanning Electron Microscopy to the Study of Reservoir Rock," SPE 7550 paper, November 1979, pp. 1375–1380.
- Reed, M. G., "Formation Permeability Damage by Mica Alteration and Carbonate Dissolution," *JPT*, September 1977, pp. 1056–1060.
- Rogers, 1963.
- Sahimi, M., *Flow and Transport in Porous Media and Fractured Rock*, VCH, Weinheim, 1995, 482 p.
- Schechter, R. S., *Oil Well Stimulation*, Prentice Hall, Englewood Cliffs, New Jersey, 1992, 602 p.
- Seed, H. B., Mitchell, J. K., & Chan, C. K., "Studies of Swell and Swell Pressure Characteristics of Compacted Clays, *Bull. Highway Res. Board*, No. 313, 1962, pp. 12–39.
- Seed, H. B., Woodward, Jr., R. J., & Lundgren, R., "Prediction of Swelling Potential for Compacted Clays," *J. Soil Mech. Found. Div.*, Proc. Am. Soc. Civ. Eng., 88(SM3), June 1962, pp. 53–87.
- Sharma, M. M., & Yortsos, Y. C., "Fines Migration in Porous Media," *AIChE J.*, Vol. 33, No. 10, 1987, pp. 1654–1662.
- Simpson, J. P., "Drilling Fluid Filtration Under Simulated Downhole Conditions," SPE Paper 4779, 1974, 14 p.
- Weaver, C. E., & Pollard, L. D., *The Chemistry of Clay Minerals*, Elsevier, New York, 1973, 213 p.
- Welton, J. E., "SEM Petrology Atlas," American Association of Petroleum Geologists, Tulsa, Oklahoma, 1984, 237 p.

- Wild, S., Kinuthia, J. M., Robinson, R. B., & Humphreys, I., "Effect of Ground Granulated Blast Furnace Slag (GGBS) on the Strength and Swelling Properties of Lime-Stabilized Kaolinite in the Presence of Sulphates," *Clay Minerals*, Vol. 31, 1996, pp. 423-433.
- Wojtanowicz, A. K., Krilov, Z., & Langlinais, J. P., "Experimental Determination of Formation Damage Pore Blocking Mechanisms," Trans. of the ASME, *Journal of Energy Resources Technology*, Vol. 110, 1988, pp. 34-42.
- Wojtanowicz, A. K., Krilov, Z., & Langlinais, J. P., "Study on the Effect of Pore Blocking Mechanisms on Formation Damage," Paper SPE 16233 presented at Society of Petroleum Engineers Symposium, Oklahoma City, Oklahoma, March 8-10, 1987, pp. 449-463.
- Zhou, Z., "Construction and Application of Clay-Swelling Diagrams by Use of XRD Methods," *JPT*, April 1995, p. 306.
- Zhou, Z., Gunter, W. D., Kadatz, B., & Cameron, S., "Effect of Clay Swelling on Reservoir Quality," Paper No. 94-54, *Journal of Canadian Petroleum Technology*, Vol. 35, 1996, pp. 18-23.
- Zhou, Z., Cameron, S., Kadatz, B., & Gunter, W. D., "Clay Swelling Diagrams: Their Applications in Formation Damage Control," *SPE Journal*, Vol. 2, 1997, pp. 99-106.

Chapter 3

Petrography and Texture of Petroleum- Bearing Formations

Summary

A review of petrographical characterization of petroleum-bearing formations, critical for formation damage analysis, is presented.

Introduction

In-situ fluids and particles transport processes occur in the pore space of the subsurface formations. The subsurface formations can be classified as following (Collins, 1961; Kaviany, 1991):

1. Isotropic, anisotropic (directional dependency)
2. Homogeneous, heterogeneous (spatial dependency)
3. Consolidated, unconsolidated (cementation)
4. Single or multiple porosity, naturally fractured, nonfractured (pore structure)
5. Ordered or disordered (random)

Description of petroleum bearing formations by quantitative means is a difficult task and is presented in this chapter.

Petrographical Characteristics

The petrographical parameters are facilitated to quantitatively describe the texture or appearance of the rock minerals and the pore structure. The fundamental parameters used for this purpose are described in the following.

Fabric and Texture

Lucia (1995) emphasizes that “Pore space must be defined and classified in terms of rock fabrics and petrophysical properties to integrate geological and engineering information.” Fabric is the particle orientation in sedimentary rock (O’Brien et al., 1994). Défarge et al. (1996) defined: “Texture, i.e., the size, shape, and mutual arrangement of the constituent elements at the smaller scale of . . . sedimentary bodies, is a petrological feature that may serve to characterize and compare” them. Petrophysical classification of rock fabrics, such as shown in Figure 3–1 by Lucia (1995), distinguishes between depositional and diagenetic textures. Lucia (1995) points out that: “The pore-size distribution is controlled by the grain size in grain-dominated packstones and by the mud size in mud-dominated packstones.” Lucia (1995) explains that: “Touching-vug pore systems are defined as pore space that is (1) significantly larger than the particle size, and (2) forms an interconnected pore system of significant extent” (Figure 3–2).

Porosity

Porosity, ϕ , is a scalar measure of the pore volume defined as the volume fraction of the pore space in the bulk of porous media. The porous structure of naturally occurring porous media is quite complicated. The simplest of the pore geometry is formed by packing of near-spherical grains. When the formation contains different types of grains and fractured by stress and deformation, pore structure is highly complicated. For convenience in analytical modeling, the porous structure of a formation can be subdivided into a number of regions. Frequently, a gross classification as micropores and macropores regions according to Whitaker (1999) and Bai et al. (1993) can be used for simplification. However, in some cases, a more detailed composite description with multiple regions may be required (Cinco-Ley, 1996; Guo and Evans, 1995). Such descriptions may accommodate for natural fractures and grain packed regions of different characteristics. The various regions are considered to interact with each other (Bai et al., 1995).

Spherical Pore Space Approximation

For simplification and convenience, the shapes of the pore space and grains of porous media are approximated and idealized as spheres. The pore volume can be approximated in terms of the mean pore diameter, D , as:

$$V_p = \pi D^3/6 \quad (3-1)$$

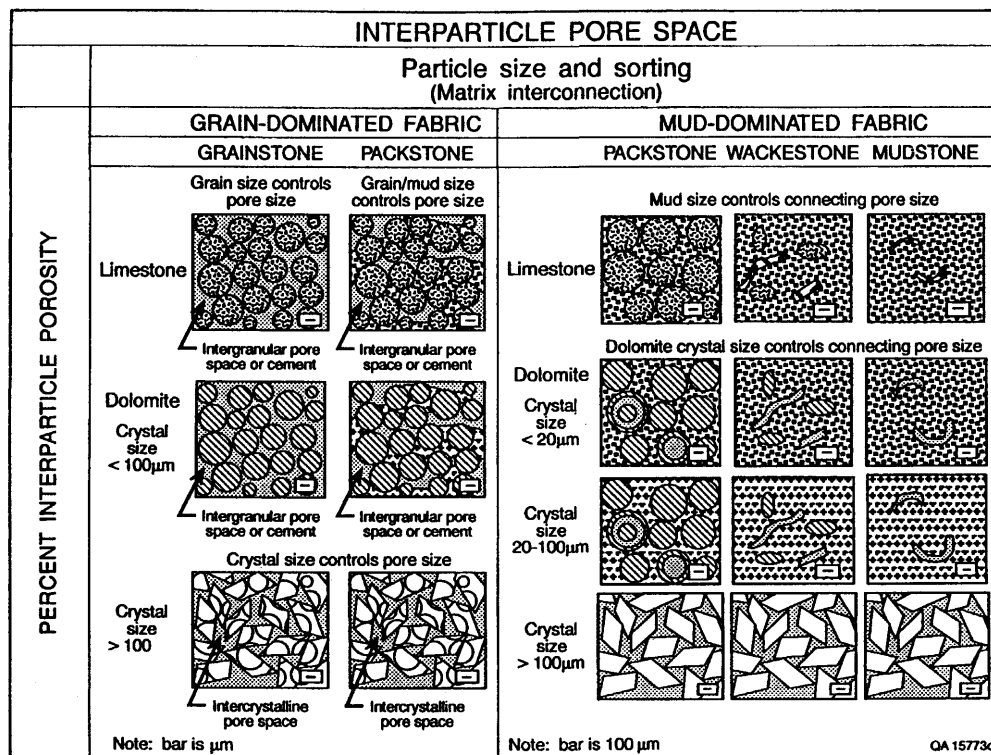
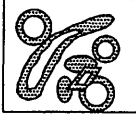

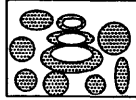
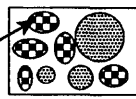

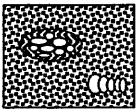
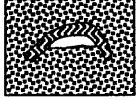

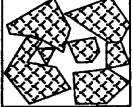
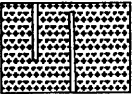
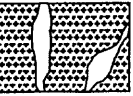
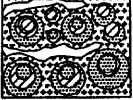


Figure 3–1. Geological and petrophysical classification of the carbonate rock interparticle pore structure (after F. J. Lucia, AAPG Bulletin, Vol. 79, No. 9, AAPG ©1995; reprinted by permission of the American Association of Petroleum Geologists whose permission is required for future use).

VUGGY PORE SPACE			
SEPARATE-VUG PORES (VUG-TO-MATRIX-TO-VUG CONNECTION)			TOUCHING-VUG PORES (VUG-TO-VUG CONNECTION)
PERCENT SEPARATE-VUG POROSITY	GRAIN-DOMINATED FABRIC	MUD-DOMINATED FABRIC	GRAIN- AND MUD-DOMINATED FABRICS
	EXAMPLE TYPES	EXAMPLE TYPES	EXAMPLE TYPES
	<p>Moldic pores</p>  <p>Composite moldic pores</p>  <p>Intrafossil pores</p>  <p>Intragranular microporosity</p> 	<p>Moldic pores</p>  <p>Intrafossil pores</p>  <p>Shelter pores</p> 	<p>Cavernous</p>  <p>Breccia</p>  <p>Fractures</p>  <p>Solution-enlarged fractures</p>  <p>Fenestral</p> 

QA 15762c

Figure 3–2. Geological and petrophysical classification of the rock vuggy pore structure (after F. J. Lucia, AAPG Bulletin, Vol. 79, No. 9, AAPG ©1995; reprinted by permission of the American Association of Petroleum Geologists whose permission is required for future use).

Then, given the bulk volume, V_B , the porosity is expressed by:

$$\phi = V_P / V_B = \frac{\pi}{6V_B} D^3 \tag{3-2}$$

The pore surface is given by:

$$A = \pi D^2 = \pi^{1/3} (6V_B)^{2/3} \phi^{2/3} \tag{3-3}$$

The specific pore surface in terms of the pore surface per pore volume is given by:

$$a = A/V_p = 6/D \quad (3-4)$$

The expressions given above for a spherical shape can be corrected for irregular pore space, respectively, as (Civan, 1996):

$$V_p = C_1 D^3 \quad (3-5)$$

$$\phi = C_2 D^3 \quad (3-6)$$

$$A = C_3 D^2 = C_4 \phi^{2/3} \quad (3-7)$$

$$a = C_5/D \quad (3-8)$$

where C_1, C_2, \dots, C_5 are some empirical shape factors.

Similarly, for the spherical idealization of a particle, the specific surface defined as the contact surface per volume sphere is given by:

$$a_p = 6/D_p \quad (3-9)$$

This can be corrected for irregular particle shape as:

$$a_p = C_6/D_p \quad (3-10)$$

where C_6 is a shape factor.

Area Open for Flow

Areosity or areal porosity is the fractional area of the bulk porous media open for flow (Liu and Masliyah, 1996). Liu and Masliyah (1996) point out that, frequently, the areal porosity has been taken equal to the volumetric porosity of porous media.

$$A_f = \phi \quad (3-11)$$

They emphasize that Equation 3-11 performs well for models considering a bundle of straight hydraulic flow pathways and nonconnecting constricted pathways. Whereas, for isotropic porous media, Liu et al. (1994) recommend that the areal porosity should be estimated as:

$$A_f = \phi^{2/3} \quad (3-12)$$

Tortuosity

Tortuosity is defined as the ration of the lengths, L_t and L , of the tortuous fluid pathways and the porous media:

$$\tau = L_t/L \quad (3-13)$$

Liu and Masliyah (1996a, b) recommend the Bruggeman (1935) equation

$$\tau^{-1} = \phi^{1/2} \quad (3-14)$$

for random packs of grains of porosity $\phi > 0.2$ and the Humble equation (Winsauer et al., 1952)

$$\tau^{-1} = 1.61 \phi^{1.15} \quad (3-15)$$

for consolidated porous media of porosity $\phi < 0.45$. They point out that the latter may have a variable accuracy and, therefore, tortuosity should be measured.

Interconnectivity of Pores

Based on their binary images shown in Figure 3-3, Davies (1990) classified the pore types in four groups (Davies, 1990, p. 74):

- “Pore Type 1:* Microspores, generally equant shape, less than 5 microns in diameter. These occur in the finest grained and shaly portions of the sand.
- Pore Type 2:* Narrow, slot like pores, generally less than 15 microns in diameter, commonly slightly to strongly curved. These represent reduced primary intergranular pores resulting from the reduction of original primary pores by extensive cementation.
- Pore Type 3:* Primary intergranular pores, triangular in shape, twenty-five to fifty microns maximum diameter. These are the original primary intergranular pores of the rock which have been affected only minimally by cementation.
- Pore Type 4:* Solution enlarged primary pores: oversized primary pores, fifty to two hundred microns maximum diameter produced through the partial dissolution of rock matrix.”

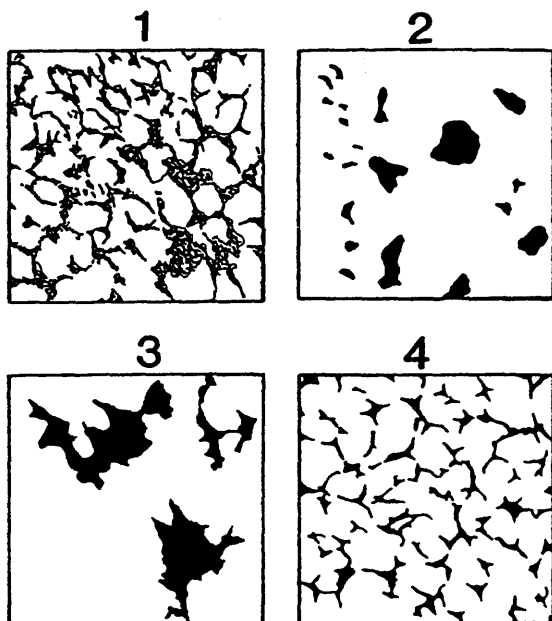


Figure 3-3. Thin-section images of various pore types (after Davies, ©1990 SPE; reprinted by permission of the Society of Petroleum Engineers).

Frequently, for convenience, pore space is perceived to consist of pore bodies connecting to other pore bodies by means of the pore necks or throats as depicted in Figure 3-4. Many models facilitate a network of pore bodies connected with pore throats as shown in Figure 3-5. However, in reality, it is an formidable task to distinguish between the pore throats and pore bodies in irregular porous structure (Lymeropoulos and Payatakes, 1992).

Interconnectivity of pores is a parameter determining the porosity of the porous media effective in its fluid flow capability. In this respect, the pores of porous media, as sketched in Figure 3-6, are classified in three groups:

1. Connecting pores which have flow capability or permeability (conductor),
2. Dead-end pores which have storage capability (capacitor), and
- 2 Non-connecting pores which are isolated and therefore do not contribute to permeability (nonconductor).

The interconnectivity is measured by the coordination number, defined as the number of pore throats emanating from a pore body. Typically, this

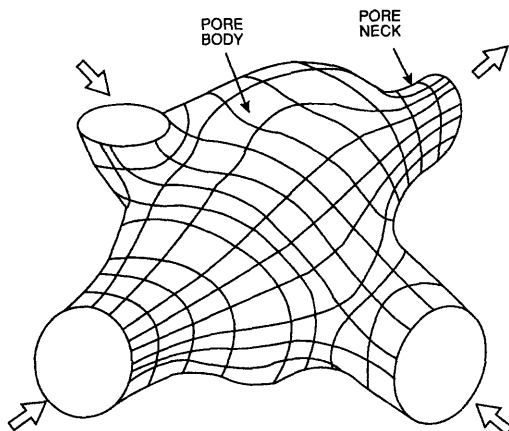


Figure 3-4. Description of the pore volume attributes (after Civan, ©1994; reprinted by permission of the U.S. Department of Energy).

number varies in the range of $6 \leq Z \leq 14$ (Sharma and Yortsos, 1987). For cubic packing, $Z = 6$ and $\phi = 1 - \pi/6$. The coordination number can be determined by nitrogen sorption measurements (Liu and Seaton, 1994).

Pore and Pore Throat Size Distributions

Typical measured pore body and pore throat sizes, given by Ehrlich and Davies (1989) are shown in Figure 3-7. Figure 3-8 shows the pore throat size distribution measured by Al-Mahtot and Mason (1996). The mathematical representation of the distribution of the pore body and pore throat sizes in natural porous media can be accomplished by various statistical means. The three of the frequently used approaches are the following:

1. Log-Normal Distribution (not representative)
2. Bi-Model Distribution (fine and course fractions)
3. Fractal Distribution

Log-Normal Distribution. Because of its simplicity, the log-normal distribution function given below has been used by many, including Ohen and Civan (1991):

$$F(D) = (2\pi s_d D)^{-1/2} \exp\left\{-\frac{1}{2}\left[\ln(D/D_m)/s_d\right]^2\right\}, 0 \leq D \leq \infty \quad (3-16)$$

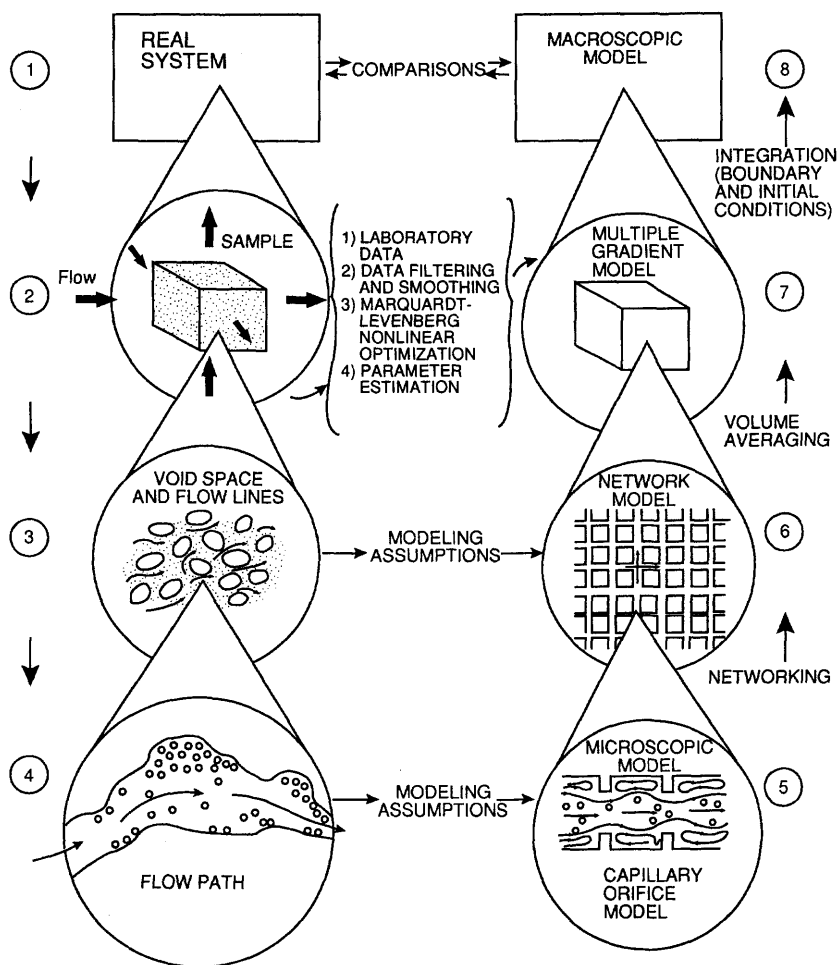


Figure 3-5. An integrated modeling approach to characterization of porous formation and processes (after Civan, ©1994; reprinted by permission of the U.S. Department of Energy).

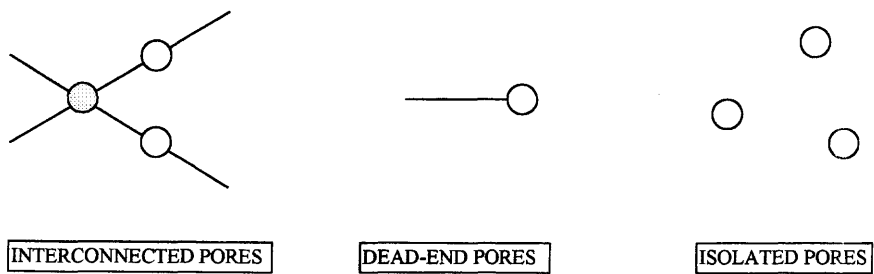


Figure 3-6. Interconnectivity of pores.

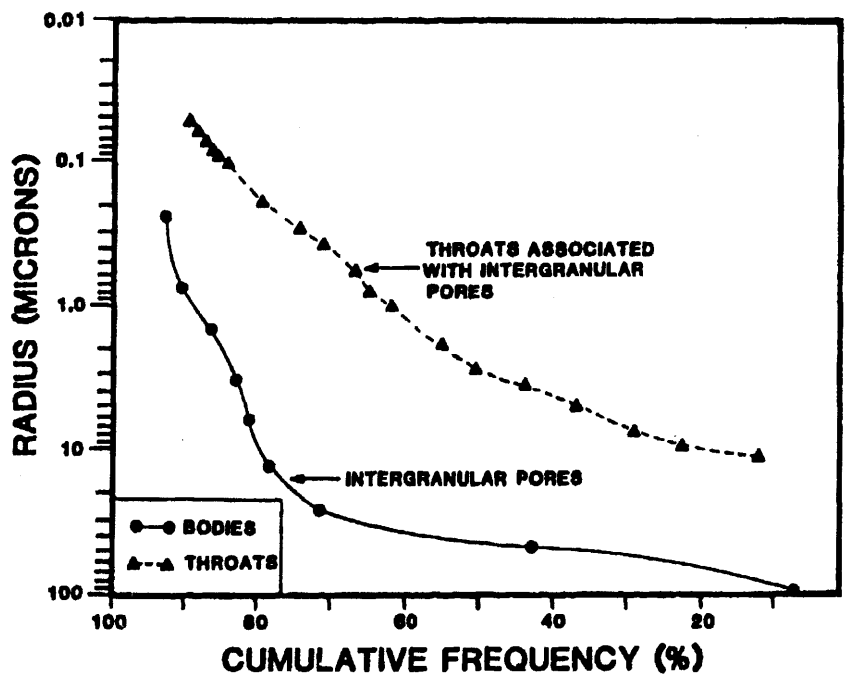


Figure 3-7. Typical cumulative pore body and pore throat size distributions in porous formation (after Ehrlich and Davies, ©1989 SPE; reprinted by permission of the Society of Petroleum Engineers).

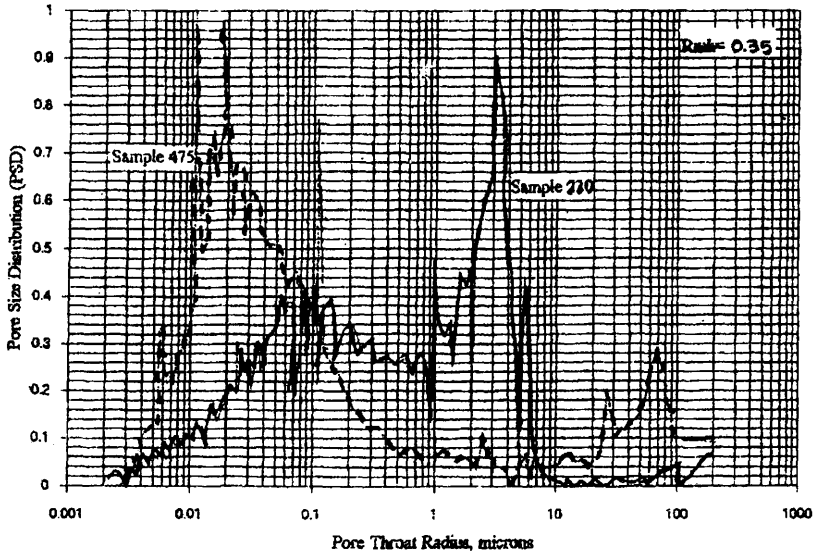


Figure 3–8. Typical bimodal pore throat size distributions in porous formation (after Al-Mahtot and Mason, ©1996; reprinted by permission of the *Turkish Journal of Oil and Gas*).

where D is the diameter of the pores approximated by spheres, D_m is the mean pore diameter calculated by:

$$D_m = \int_{D_{\min}}^{D_{\max}} DF(D)dD \quad (3-17)$$

and s_d is the standard deviation, and D_{\min} and D_{\max} denote the smallest and largest diameters.

Bi-Modal Distribution. Typically, the pore body and pore throat sizes vary over finite ranges and the size distributions can display a number of peaks corresponding to various fractions of pore bodies and pore throats in porous media. If only two groups, such as the fine and coarse fractions, are considered, a bi-modal distribution function according to Popplewell et al. (1989) can be used for mathematical representation of the size distribution:

$$f(D) = wf_1(D) + (1 - w)f_2(D) \quad (3-18)$$

where D denotes the diameter, $f_1(D)$ and $f_2(D)$ are the distribution functions for the fine and coarse fractions, and w is the fraction of the fine fractions.

Popplewell et al. (1988, 1989) used the β -distribution function to represent the skewed size distribution, because the diameters of the smallest and the largest particles are finite in realistic porous media. For convenience, they expressed the β -distribution function in the following modified form:

$$f(x) = x^{am}(1-x)^m \bigg/ \int_0^1 x^{am}(1-x)^m dx \quad (3-19)$$

in which x denotes a normalized diameter defined by:

$$x = (D - D_{\min}) / (D_{\max} - D_{\min}) \quad (3-20)$$

D_{\min} and D_{\max} are the smallest and the largest diameters, respectively. a and m are some empirical power coefficients. The mode, x_m , and the spread, σ^2 , for Equation 3-19 are given, respectively, by:

$$x_m = a / (a + 1) \quad (3-21)$$

and

$$\sigma^2 = \frac{(am+1)(m+1)}{[(a+1)m+2]^2[(a+1)m+3]} \quad (3-22)$$

Chang and Civan (1991, 1992, 1997) used this approach successfully in a model for chemically induced formation damage.

Fractal Distribution. Fractal is a concept used for convenient mathematical description of irregular shapes or patterns, such as the pores of rocks, assuming self-similarity. The pore size distributions measured at different scales of resolution have been shown to be adequately described by empirically determined power law functions of the pore sizes (Garrison et al., 1993; Verrecchia, 1995; Karacan and Okandan, 1995; Perrier et al., 1996). The expression given by Perrier et al. (1996) for the differential pore size distribution can be written in terms of the pore diameter as:

$$-\frac{dV}{dD} = \beta(e-d)D^{e-d-1}, \quad 0 < d < e \quad (3-23)$$

where, D denotes the pore diameter, V represents the volume of pores whose diameter is greater than D , d is the fractal dimension (typically $2 < d < 3$), e is the Euclidean space dimension ($e = 3$) and β is a positive constant. Thus, integrating Equation 3-23, Perrier et al. (1996) derived the following expression for the pore size distribution:

$$V = V_o - \beta D^{e-d}, \quad 0 < d < e \quad (3-24)$$

in which V_o is the constant of integration. Perrier et al. (1996) then considered a range of pore size as $D_{\min} \leq D \leq D_{\max}$. Thus, applying Equation 3-24, the total pore volume, V_p , is given by (Perrier et al., 1996):

$$V_p = V_o - \beta D_{\min}^{e-d} \quad (3-25)$$

Because $V_p = 0$ for $D = D_{\max}$, Equation 3-24 leads to (Perrier et al., 1996):

$$V_o = \beta D_{\max}^{e-d} \quad (3-26)$$

Textural Parameters

Nolen et al. (1992) have described the textural appearance of reservoir formation by four parameters:

1. Median grain size, defined as:

$$d_g = \int_{d_{\min}}^{d_{\max}} dF(d)d(d) \quad (3-27)$$

2. Grain shape factor, defined as:

$$\Psi = \left(\frac{d_v}{d_A} \right)^2 = 6^{2/3} \pi^{1/3} V^{2/3} / A \quad (3-28)$$

in which volume and volume based diameter, d_v , are given, respectively, by:

$$V = \frac{\pi d_v^3}{6}, \quad d_v = \left(\frac{6V}{\pi} \right)^{1/3} \quad (3-29)$$

and the surface area and surface area based diameter, d_A , are given, respectively, by:

$$A = \pi d_A^2, d_A = \left(\frac{A}{\pi} \right)^{1/2} \quad (3-30)$$

Note that $\psi = 1$ for spherical particles.

3. Sorting, defined by:

$$\delta = \frac{d_g - d_o}{\sigma} \quad (3-31)$$

where d_g is the average grain diameter, d_o is the mode diameter, and σ is the standard deviation.

4. Packing, which is the volume fraction of the solid matrix, given by:

$$\beta = 1 - \phi \quad (3-32)$$

where ϕ denotes the porosity in fraction.

Triangular diagrams, such as shown in Figure 3-9 by Hohn et al. (1994), are convenient ways of presenting the relationships between packing,

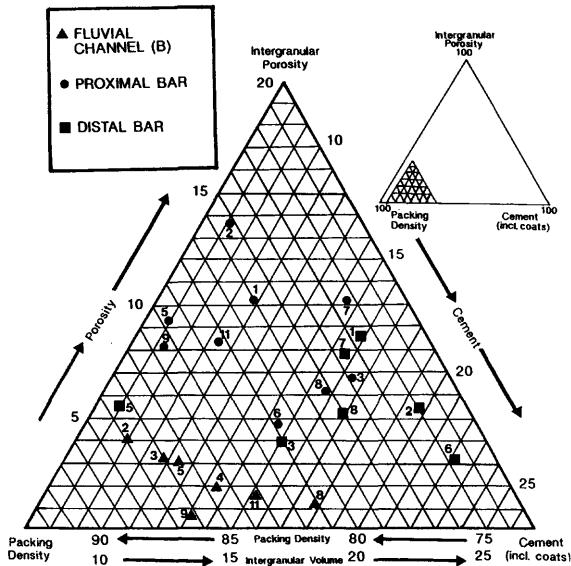


Figure 3-9. A ternary chart showing the relationship between packing density, intergranular pore space, and cement in Granny Creek wells nos. 1-9, 11, and 12 (after Hohn et al., ©1994; reprinted by permission of the U.S. Department of Energy).

density, cement, and intergranular volume at various locations of reservoir formations. Such diagrams provide useful insight into the heterogeneity of reservoirs. Coskun et al. (1993) shows the relationships between composition, texture, porosity, and permeability for a typical sandstone reservoir.

References

- Al-Mahtot, O. B., & Mason, W. E., "Reservoir Description: Use of Core Data to Identify Flow Units for a Clastic North Sea Reservoir," *Turkish Journal of Oil and Gas*, Vol. 2, No. 1, February 1996, pp. 33–43.
- Bai, M., Elsworth, & Roegiers, J. C., "Multiporosity/Multipermeability Approach to the Simulation of Naturally Fractured Reservoirs," *Water Resources Research*, Vol. 29, No. 6, 1993, pp. 1621–1633.
- Bai, M., Bouhroum, A., Civan, F., & Roegiers, J. C., "Improved Model for Solute Transport in Heterogeneous Porous Media," *J. Petroleum Science and Engineering*, Vol. 14, 1995, pp. 65–78.
- Bruggeman, D. A. G. "Berechnung verschiedener physikalischer Konstanten von heterogenen Substanzen," *Ann. Phys. (Leipzig)*, Vol. 24, 1935, pp. 636–679.
- Chang, F. F., & Civan, F., "Modeling of Formation Damage due to Physical and Chemical Interactions between Fluids and Reservoir Rocks," SPE 22856 paper, Proceedings of the 66th Annual Technical Conference and Exhibition of the Society of Petroleum Engineers, October 6–9, 1991, Dallas, Texas.
- Chang, F. F., & Civan, F., "Predictability of Formation Damage by Modeling Chemical and Mechanical Processes," SPE 23793 paper, Proceedings of the SPE International Symposium on Formation Damage Control, February 26–27, 1992, Lafayette, Louisiana, pp. 293–312.
- Chang, F. F., & Civan, F., "Practical Model for Chemically Induced Formation Damage," *J. of Petroleum Science and Engineering*, Vol. 17, No. 1/2, February 1997, pp. 123–137.
- Cinco-Ley, H., "Well-Test Analysis for Naturally Fractured Reservoirs," *Journal of Petroleum Technology*, January 1996, pp. 51–54.
- Collins, E. R., *Flow of Fluids Through Porous Materials*, Penn Well Publishing Co., Tulsa, Oklahoma, 1961, 270 p.
- Coskun, S. B., Wardlaw, N. C., & Haverslew, B., "Effects of Composition, Texture and Diagenesis on Porosity, Permeability and Oil Recovery in a Sandstone Reservoir," *Journal of Petroleum Science and Engineering*, Vol. 8, 1993, pp. 279–292.
- Davies, D. K., "Image Analysis of Reservoir Pore Systems: State of the Art in Solving Problems Related to Reservoir Quality, SPE 19407, the SPE Formation Damage Control Symposium held in Lafayette, Louisiana, February 22–23, 1990, pp. 73–82.

- Défarage, C., Trichet, J., Jaunet, A-M., Robert, M., Tribble, J., & Sansone, F. J., "Texture of Microbial Sediments Revealed by Cryo-Scanning Electron Microscopy," *Journal of Sedimentary Research*, Vol. 66, No. 5, September 1996, pp. 935-947.
- Ehrlich, R. and Davies, D. K., "Image Analysis of Pore Geometry: Relationship to Reservoir Engineering and Modeling," SPE 19054 paper, Proceedings of the SPE Gas Technology Symposium held in Dallas, Texas, June 7-9, 1989, pp. 15-30.
- Ertekin, T., & Watson, R. W., "An Experimental and Theoretical Study to Relate Uncommon Rock-Fluid Properties to Oil Recovery," Contract No. AC22-89BC14477, in *EOR-DOE/BC-90/4 Progress Review*, No. 64, pp. 68-71, U.S. Department of Energy, Bartlesville, Oklahoma, May 1991, 129 p.
- Garrison, Jr., J. R., Pearn, W. C., & von Rosenberg, D. U., "The Fractal Menger Sponge and Sierpinski Carpet as Models for Reservoir Rock/Pore Systems: I. Theory and Image Analysis of Sierpinski Carpets and II. Image Analysis of Natural Fractal Reservoir Rocks, *In-Situ*, Vol. 16, No. 4, 1992, pp. 351-406, and Vol. 17, No. 1, 1993, pp. 1-53.
- Guo, G., & Evans, R. D., "Geologic and Stochastic Characterization of Naturally Fractured Reservoirs," SPE 27025 paper, presented at 1994 SPE III Latin American & Caribbean Petroleum Engineering Conference, Buenos Aires, Argentina, April 27-29, 1994.
- Hohn, M. E., Patchen, D. G., Heald, M., Aminian, K., Donaldson, A., Shumaker, R., & Wilson, T., "Report Measuring and Predicting Reservoir Heterogeneity in Complex Deposystems," Final Report, work performed under Contact No. DE-AC22-90BC14657, U.S. Department of Energy, Bartlesville, Oklahoma, May 1994.
- Karacan, C. Ö., & Okandan, E., "Fractal Analysis of Pores from Thin Sections and Estimation of Permeability Therefrom," *Turkish Journal of Oil and Gas*, Vol. 1, No. 2, October 1995, pp. 52-58.
- Kaviany, M., *Principles of Heat Transfer in Porous Media*, Springer-Verlag, New York, 1991, 626 p.
- Liu, H., & Seaton, N. A., "Determination of the Connectivity of Porous Solids from Nitrogen Sorption Measurements—III. Solids Containing Large Mesopores," *Chemical Engineering Science*, Vol. 49, No. 11, 1994, pp. 1869-1878.
- Liu, S., Afacan, A., & Masliyah, J. H., *Chemical Engineering Science*, Vol. 49, 1994, pp. 3565-3586.
- Liu, S., & Masliyah, J. H., "Principles of Single-Phase Flow Through Porous Media," Chapter 5, pp. 227-286, in *Suspensions, Fundamentals and Applications in the Petroleum Industry*, Advances in Chemistry Series 251, L. L. Schramm (ed.), American Chemical Society, Washington, DC, 1996a, 800 p.

- Liu, S. and Masliyah, J. H., Single Fluid Flow in Porous Media, *Chem. Engng. Commun.*, Vol. 148–150, 1996b, pp. 653–732.
- Lucia, F. J., “Rock-Fabric/Petrophysical Classification of Carbonate Pore Space for Reservoir Characterization,” *AAPG Bulletin*, Vol. 79, No. 9, September 1995, pp. 1275–1300.
- Lymberopoulos, D. P., & Payatakes, A. C., “Derivation of Topological, Geometrical, and Correlational Properties of Porous Media from Pore-Chart Analysis of Serial Section Data,” *Journal of Colloid and Interface Science*, Vol. 150, No. 1, 1992, pp. 61–80.
- Nolen, G., Amaefule, J. O., Kersey, D. G., Ross, R., & Rubio, R., “Problems Associated with Permeability and V_{clay} Models from Textural Properties of Unconsolidated Reservoir Rocks,” SCA 9225 paper, 33rd Annual Symposium of SPWLA Society of Core Analysts, Oklahoma City, Oklahoma, June 15–17, 1992.
- O’Brien, N. R., Brett, C. E., & Taylor, W. L., “Microfabric and Taphonomic Analysis in Determining Sedimentary Processes in Marine Mudstones: Example from Silurian of New York,” *Journal of Sedimentary Research*, Vol. A64, No. 4, October 1994, pp. 847–852.
- Perrier, E., Rieu, M., Sposito, G., & de Marsily, G., “Models of the Water Retention Curve for Soils with a Fractal Pore Size Distribution,” *Water Resources Research Journal*, Vol. 32, No. 10, October 1996, pp. 3025–3031.
- Popplewell, L. M., Campanella, O. H., & Peleg, M., “Simulation of Bimodal Size Distributions in Aggregation and Disintegration Processes,” *Chem. Eng. Progr.*, August 1989, pp. 56–62.
- Sharma, M. M. and Yortsos, Y. C., “Transport of Particulate Suspensions in Porous Media: Model Formulation,” *AIChE J.*, pp. 1636–1643, Vol. 33, No. 10, Oct. 1987.
- Verrecchia, E. P., “On the Relation Between the Pore-Throat Morphology Index (“a”) and Fractal Dimension (D_f) of Pore Networks in Carbonate Rocks-Discussion,” *Journal of Sedimentary Research*, Vol. A65, No. 4, October 1995, pp. 701–702.
- Whitaker, S., *The Method of Volume Averaging*, Kluwer Academic Publishers, Boston, 1999, 219 p.
- Winsauer, W. O., Shearin, H. M., Masson, P. H., and Williams, M., “Resistivity of Brine Saturated Sands in Relation to Pore Geometry,” *Bull. Amer. Ass. Petrol. Geol.*, Vol. 36(2), 1952, pp. 253–277.

Chapter 4

Petrophysics–Flow Functions and Parameters

Summary

A review of the petrophysical properties involving formation damage is presented in this chapter.

Introduction

The distribution and behavior of multiphase fluid systems in petroleum reservoirs are strongly influenced by the petrophysical properties of sedimentary formations. Ucan et al. (1997) state: “Petrophysical properties of multiphase flow systems in porous rock are complex functions of the morphology and topology of the porous medium, interactions between rock and fluids, phase distribution, and flow pattern and regimes. The effect of these properties on the flow behavior is lumped in the form of empirically determined relative permeability and capillary pressure functions which are used as the primary flow parameters for the macroscopic description of multiphase flow in porous media.”

During formation damage, petrophysical properties vary due to rock, fluid, and particle interactions. Therefore, dynamic relationships are required to take the varying petrophysical properties into account in predicting the fluid behavior during formation damage. This chapter presents a review of the primary petrophysical properties that influence the fluid behavior and formation damage in petroleum reservoirs.

Wettability Alteration

Kaminsky and Radke (1997) stated that the wettability of reservoirs is “loosely defined as the preferential affinity of the solid matrix for either the aqueous or oil phases.”

Wettability is an important property of sedimentary formations that affects the fluid distribution, capillary pressure, relative permeability, and behavior of fluids in reservoirs (Dubey and Waxman, 1991). Wettability is a measure of the preferential tendency of immiscible fluids to spread over a solid surface (Civan and Donaldson, 1987; Grattoni et al., 1995). Thus, the solid is called a water-wet material when water tends to spread out to cover the solid surface, and oil-wet vice versa. Contact angle is a good indication of the spreadability and wetting characteristics of fluids over simple continuous surfaces. A smaller contact angle, $\theta < 90^\circ$, indicates stronger wettability, and a larger contact angle, $\theta > 90^\circ$, indicates weaker wettability. $\theta \sim 90^\circ$ indicates intermediate wettability and the probability of a fluid to have exactly $\theta = 90^\circ$ is very small.

The wettability of porous materials may be two types: (1) uniform or homogeneous and (2) nonuniform or heterogeneous (Cuiec, 1991; Kovscek et al., 1992; McDougall and Sorbie, 1995). Uniformly wet porous materials have either a completely water-wet or oil-wet pore surface throughout the porous media. Whereas, most sedimentary formations are nonuniform because they typically contain separate portions of water- and oil-wet regions. Two types of wettability nonuniformity may be distinguished in a sedimentary rock: (1) mixed-wettability and (2) fractional-wettability (McDougall and Sorbie, 1995). Mixed-wettability describes the rocks having only the larger pores being oil-wet and only the smaller pores being water-wet, as indicated by McDougall and Sorbie (1995). This mixed-wettability condition is created by oil migration preferentially into larger pores followed by organic deposition, such as asphaltene, paraffins, and resins, to transform the water-wet to oil-wet types (McDougall and Sorbie, 1995). On the other hand, fractional-wettability describes the rocks having sites of different surface characteristics due to the differences in the type of surface mineralogy. Therefore, as depicted by McDougall and Sorbie (1995), the water-wet and oil-wet pores may encompass over all sizes of pores in a fractionally-wet formation.

As pointed out by Hirasaki (1991): "The wettability of a rock/brine/oil system cannot be described by a single contact angle because it is the multitude of contact angles at the various three-phase contact regions in the pore spaces that determines system wettability. A complete wettability description requires a morphological description of the pore space with the contact angles as a boundary condition for the fluid distribution." Therefore, characterization of the wettability of porous materials is a difficult task. As stated by Robin et al. (1995): "The contact angle is a macroscopic concept." Jerauld and Rathmell (1997) consider a formation preferentially water-wet when the apparent (as measured) contact angle $\theta < 30^\circ$, preferentially oil-wet when $\theta > 150^\circ$ and mixed-wet when $30^\circ < \theta < 150^\circ$.

A practical approach to quantify wettability is to facilitate the work involving the fluid displacement processes (Sharma, 1985). As stated by Grattoni et al. (1995), the displacement process is referred to as imbibition when the wetting phase saturation increases and drainage when the wetting phase saturation decreases. The work of displacement per unit bulk volume is equal to the area indicated by the capillary pressure curve (Yan et al., 1997):

$$W = \phi \int p_c dS_w \quad (4-1)$$

Therefore, Donaldson et al. (1980) have alleviated the difficulty of defining the wettability of porous media in a practical manner, by defining a wettability index as the logarithm of the ratio of the areas, A^+ and A^- , of the capillary pressure curve above and below the zero capillary pressure line, as [the USBM Method by Donaldson and Crocker (1980)]

$$WI = \log_{10}(A^+/A^-) \quad (4-2)$$

Thus, according to Equation 4-2, porous materials are classified as following:

1. $WI > 0$, water-wet,
2. $WI \approx 0$, intermediately-wet, and
3. $WI < 0$, oil-wet.

Many studies have reported wettability variation during formation damage due to alteration of pore surface characteristics by rock, fluid, and particle interactions. Figure 4-1, by Donaldson (1985), shows that the capillary pressure curves of the sandstone and therefore the wettability variation by clay fines plugging.

Alternatively, the wettability can be expressed in terms of the Amott (1959) indices to water and oil. As stated by Jerauld and Rathmell (1997), "The Amott (1959) index of a phase is defined by the ratio of the volume spontaneously imbibed to the sum of that imbibed and forced." Thus,

$$I_j = \frac{\Delta S_{j,imb}}{\Delta S_{j,imb} + \Delta S_{j,disp}} ; j = \text{water or oil} \quad (4-3)$$

Then, the Amott-Harvey wettability index is defined as:

$$WI = I_w - I_o \quad (4-4)$$

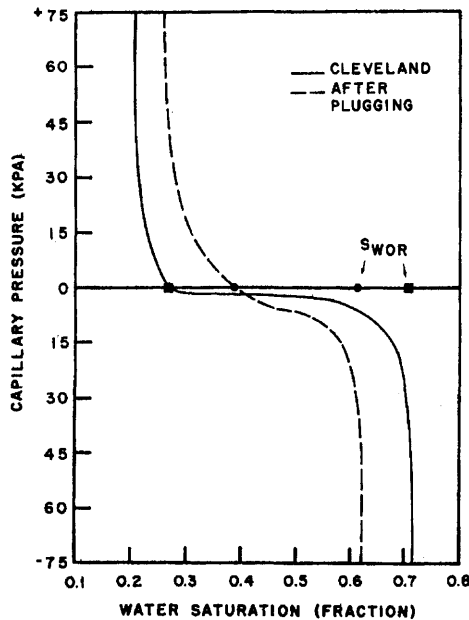


Figure 4-1. Effect of pore plugging by clay particles on capillary pressure (Donaldson, ©1985 SPE; reprinted by permission of the Society of Petroleum Engineers).

Jerauld and Rathmell (1997) show that the Amott-Harvey wettability index correlates linearly and increases with the initial saturation for Prudhoe. Ertekin and Watson (1991) show that the wettability index correlates linearly and decreases with the average pore-throat length. Figure 4-2 by Leontaritis et al. (1992) describes the alteration of wettability towards oil-wet by adsorption of organic matters, such as asphaltenes. Figure 4-3 by Yan et al. (1997) clearly indicates that the wettability index decreases as the adsorption of asphaltenes progresses.

Durand and Rosenberg (1998) have determined by cryo-scanning electron microscopy that the bulk or apparent wettability of clay-bearing formations is significantly influenced by the type, morphology, quantity, and location of the clay minerals, and the trapment of fluids in the pore space. They explain that, when water-wet kaolinite and platy illite are aged in oil, these minerals absorb some oil components to become oil-wet. Whereas, the fibrous illite does not show any affinity toward oil and it remains water-wet. However, even a small amount of kaolinite or platy illite can make a clay-bearing sandstone oil-wet after aging with oil. Once transformed into an oil-wet system, as depicted by Durand and Rosenberg

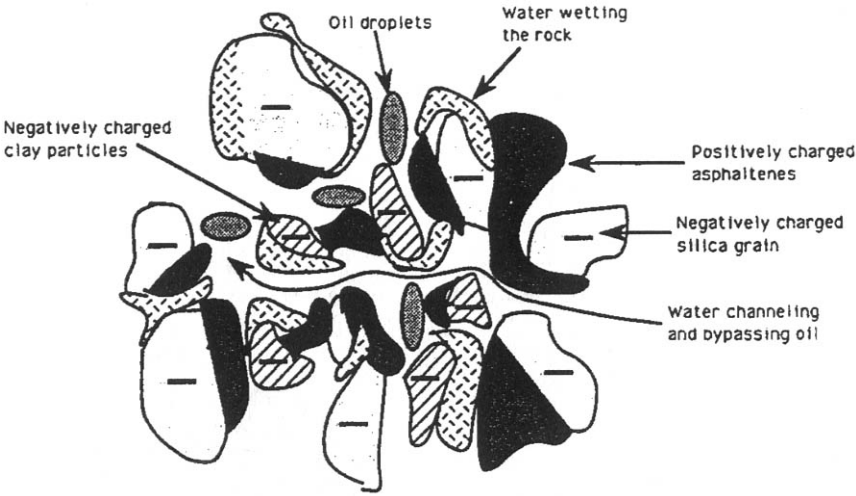


Figure 4–2. Mechanism of wettability alteration by asphaltene adsorption (Leontaritis et al., ©1992 SPE; reprinted by permission of the Society of Petroleum Engineers).

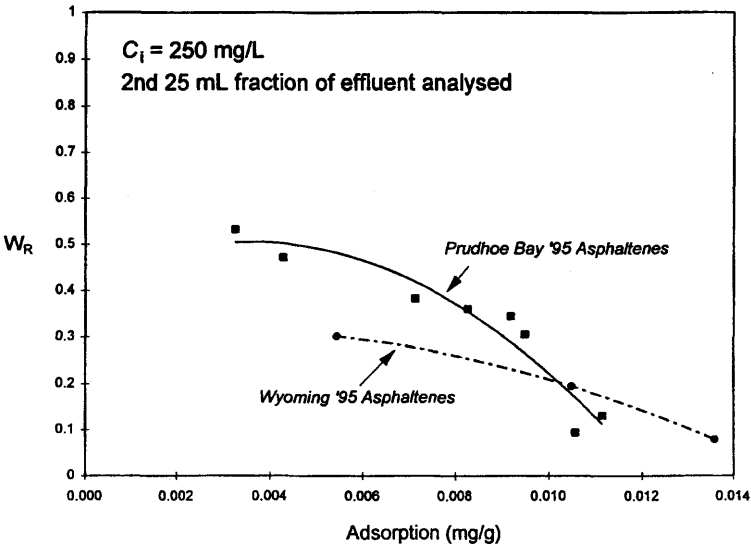


Figure 4–3. Variation of the wettability index by asphaltene adsorption in Berea sandstone (Yan et al., ©1997 SPE; reprinted by permission of the Society of Petroleum Engineers).

(1998) schematically in Figure 4–4b, clay-bearing sandstone retains oil due to large capillary forces and becomes water repellent. They determined that, when aged with water, the fibrous illite in an oil-saturated formation transforms to become water-wet. Therefore, they have concluded that adsorption and capillary forces act together to transform a clay-bearing formation from water-wet to oil-wet or vice-versa, depending

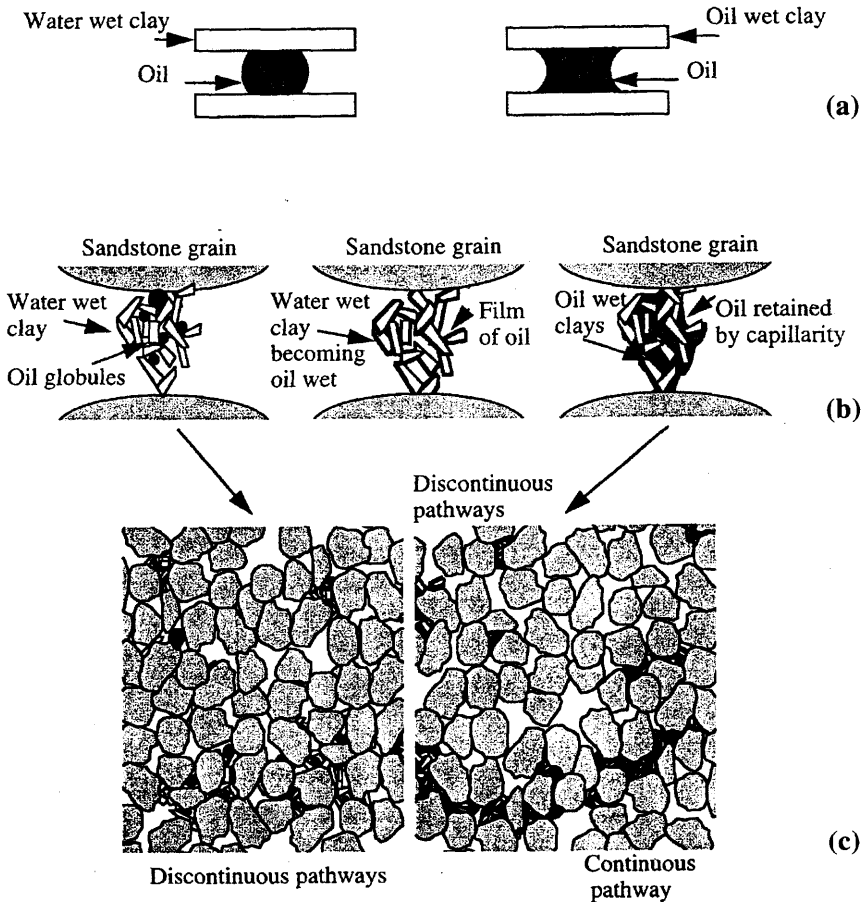


Figure 4–4. Schematic description of the wettability effect at different scales: a) between clay particles, b) at microscopic scale between sandstone grains, and c) at bulk porous formation scale (Reprinted from *Journal of Petroleum Science and Engineering*, Vol. 19, Durand, C., and Rosenberg, E., “Fluid Distribution in Kaolinite- or Illite-Bearing Cores: Cryo-SEM Observation Versus Bulk Measurements,” pp. 65–72, ©1998, with permission from Elsevier Science).

on the amount of the oil and water affine clay minerals existing in the formation, and the morphology of illite which behaves hydrophilic in fibrous form and hydrophobic in platy form.

End-Point Saturations

The end-point saturations determine the mobile fluid saturation range for the flow functions. The end-point saturations, S_{wc} , S_{gr} , and S_{or} , for an oil-gas-water system represent the connate water, trapped gas, and residual oil saturations which vary as a result of the packing of particles during formation damage. The values of these quantities are larger for ordered packing of particles (~40%) and smaller for disordered packing of particles (~10%). They can be correlated with permeability. For a given type, however, they decrease by increasing permeability or porosity. For example, as shown by Collins (1961), the connate water saturation decreases linearly with increasing logarithmic permeability in sandstones. Thus, the end-point (also known as irreducible, residual, or immobile) fluid saturations can be approximated by:

$$S_{rj} = a_j - b_j \log_{10} K: j = \text{gas, oil, water} \quad (4-5)$$

where j denotes the gas, oil, or water phases, r denotes the end-point saturation condition, K is permeability and a_j and b_j are some empirically determined parameters.

Alteration of the Flow Functions: Capillary Pressure and Relative Permeability

Capillary pressure and relative permeability vary by (1) the pore surface properties including wettability, end-point saturations and contact angle, and (2) the net overburden stress effecting the tortuosity, porosity and interconnectivity of pores. Marle (1981) points out that capillary pressure and relative permeability are complicated functions of the properties of the fluids and porous media. By dimensional analysis of an oil-water system in porous media, Marle (1981) has shown that these flow functions can be correlated by means of the pertinent dimensionless groups as:

$$\frac{lp_c}{\sigma} = f_{p_c} \left[\frac{(\rho_1 - \rho_2)gl^2}{\sigma}, \theta, S_1, M \right] \quad (4-6)$$

and

$$k_{rj} = f_{kr} \left[\frac{(\rho_1 - \rho_2)gl^2}{\sigma}, \theta, S_1, \frac{\rho_1}{\rho_2}, \frac{\mu_1}{\mu_2}, \frac{\mu_1 u}{\sigma}, \frac{\rho_1 l u}{\mu_1} \right] \quad (4-7)$$

: $j = \text{fluid 1 or 2}$

where l is a characteristic dimension of pores, such as the mean pore diameter proportional to $\sqrt{k/\phi}$, ρ_1 and ρ_2 , and μ_1 and μ_2 denote the densities and viscosities of the fluid phases 1 and 2, respectively, g is the gravitational acceleration, p_c is capillary pressure, σ is interfacial tension between the fluid phases 1 and 2, θ is the contact angle, S is the saturation of the fluid phase 1, k_{rj} denotes the relative permeability of phase j , $j = 1$ for fluid 1 and 2 for fluid 2, and M represents all other characteristics of porous media pertaining to the morphology of pores.

In lack of a better approach, frequently, the Leverett (1941) J-function analogy is facilitated to estimate the capillary pressure for an oil/water system during formation damage according to:

$$p_c = J(S_w) \sigma \cos \theta / \sqrt{K/\phi}; S_{wc} < S_w < (1 - S_{or}) \quad (4-8)$$

where $J(S_w)$ is the empirical Leverett J-function, which is a dimensionless function of the water saturation, S_w . Marle (1981) points out that using Equation 4-8 is not rigorously correct because grouping σ and θ as $\sigma \cos \theta$ is only valid for cylindrical capillary tubes. Gupta and Civan (1994) have shown that the porous media representative value of the $\cos \theta$ term depends on the wettability. The surface tension varies by temperature and species concentration. A quick remedy to apply Equation 4-8 for a nonuniformly-wet porous formation is to define a weighted average of the various wetting fractions of pores as, extending the approach by Cassie and Baxter (1944) and Paterson et al. (1998).

$$\cos \bar{\theta} = \sum_i \alpha_i \cos \theta_i, \quad \sum_i \alpha_i = 1 \quad (4-9)$$

where θ_i are the contact angles of the different wetting pore surfaces. α_i are the surface fractions of different wetting pores, defined by McDougall and Sorbie (1995).

As a simplistic approach, assuming that the Leverett J-function remains unchanged during formation alteration, Equation 4-8 can be applied at a reference state and denoted by subscript "o" and at an instantaneous state during formation damages to obtain:

$$\frac{P_c}{P_{c_o}} = \frac{\sigma \cos \theta}{\sigma_o \cos \theta_o} \sqrt{\frac{K/\phi}{K_o/\phi_o}} \quad (4-10)$$

for which K/ϕ can be estimated using one of the methods presented in Chapter 5, such as by the Carman-Kozeny equation.

Ajufo et al. (1993) have demonstrated that the capillary pressure data is sensitive to overburden pressure. In poorly sorted and cemented formations, the effect of overburden may create an irreversible decay of the formation integrity.

Frequently, the capillary pressure and relative permeability data are correlated by Corey type power law empirical expressions of the normalized saturation given, respectively, by (Mohanty et al., 1995):

$$p_{cj} = \sigma_{jo} \bar{S}_j^{n_j} \quad (4-11)$$

and

$$k_{rj} = k_{rj}^o \bar{S}_j^{b_j} \quad (4-12)$$

where σ_{jo} is the interfacial tension of the j^{th} fluid phase with oil, k_{rj}^o is the permeability at the end-point saturation of the j^{th} phase, b_j and n_j are some correlation exponents, and \bar{S}_j is the normalized saturation of the j^{th} phase defined as:

$$\bar{S}_j = (S_j - S_{rj}) / \left(1 - \sum_k S_{rk} \right) \quad (4-13)$$

Chang et al. (1997) have resorted to Sigmund and McCaffery (1979) type formulae to represent relative permeabilities, which can be generalized as:

$$k_{rj} = k_{rj}^o \left[\frac{\bar{S}_j^{m_j} + a_j \bar{S}_j}{1 + a_j} \right] \quad (4-14)$$

where m_j and a_j are some empirical parameters. Chang et al. (1997) have used the following expression to represent the capillary pressure function:

$$p_{cj} = \Gamma \sigma_{jo} (K/\phi)^{1/2} \bar{S}_j^{-1/\beta_j} \quad (4-15)$$

where Γ is a scaling factor for the capillary pressure and β_j is an empirical parameter.

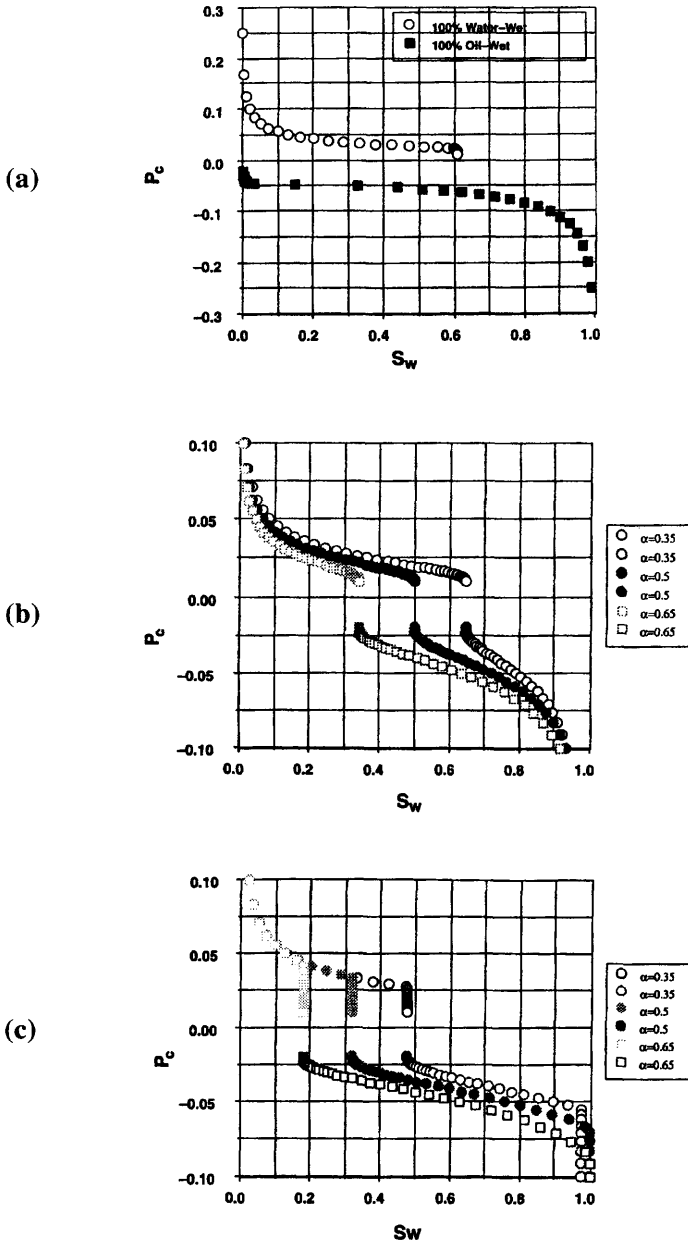


Figure 4-5. Capillary pressure curves for a) 100% water-wet and 100% oil-wet systems, b) three fractionally-wet systems, and c) three mixed-wet systems (McDougall and Sorbie, ©1995 SPE; reprinted by permission of the Society of Petroleum Engineers).

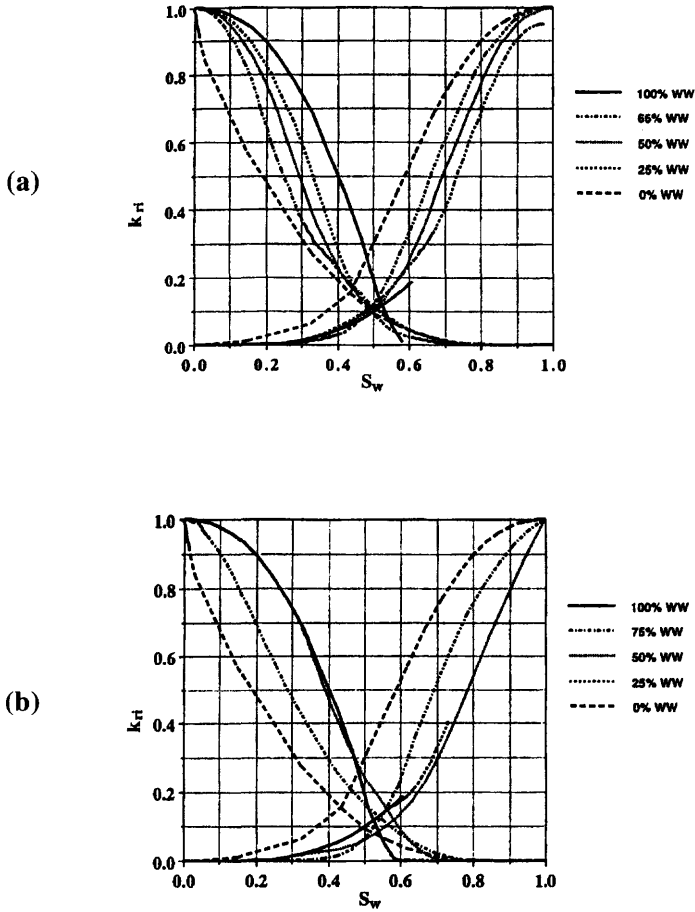


Figure 4-6. Relative permeability curves for a range of a) fractionally-wet and b) mixed-wet systems (McDougall and Sorbie, ©1995 SPE; reprinted by permission of the Society of Petroleum Engineers).

Donaldson et al. (1987) propose a hyperbolic expression for capillary pressure as:

$$p_{cj} = \frac{A + B\bar{S}_j}{1 + C\bar{S}_j} \quad (4-16)$$

where A , B , and C are some correlation parameters.

During formation damage the wettability index and the capillary pressure and relative permeability curves vary continuously. Therefore,

it is reasonable to assume that the parameters of Eqs. 4–14, 15 and 16 can be correlated with respect to the wettability index to obtain dynamic correlations. Figures 4–5 and 4–6 obtained by simulation by McDougall and Sorbie (1995) demonstrate the effect of wettability on capillary pressure and relative permeability.

Wang (1988) shows the effect of a wettability alteration on imbibition relative permeability. Tielong et al. (1996) have demonstrated that the oil and water relative permeabilities of cores before and after polymer treatment can be correlated by Eq. 4–12. Tielong et al. (1996) determined the values of the exponents of Eq. 4–12 before and after polymer treatment and showed that they varied. However, they did not determine the exponent values at various intervals during polymer treatment. Therefore, a correlation cannot be derived from their data.

Neasham (1977) studied the affect of the morphology of dispersed clay on fluid flow properties in sandstone cores. Neasham present the mineralogical, petrographical and petrophysical properties of the sandstones tested. Neasham demonstrates that different sandstones indicate significantly different capillary pressure behavior.

References

- Ajufo, A. O., Daneshjou, D. H., & Warne, J. D., "Capillary Pressure Characteristics of Overburden Pressure Using the Centrifuge Method," SPE 26148 paper, Proceedings of the SPE Gas Technology Symposium, Calgary, Alberta, Canada (June 28–30 1993) pp. 107–117.
- Amott, E., "Observations Relating to the Wettability of Porous Rock," *Trans. AIME*, Vol. 216, 1959, pp. 156–162.
- Cassie, A. B. D., & Baxter, S., "Wettability of Porous Surfaces," *Trans. Faraday Soc.*, Vol. 40, 1944, pp. 546–551.
- Chang, Y. C., Mohanty, K. K., Huang, D. D., & Honarpour, M. M., "The Impact of Wettability and Core-Scale Heterogeneities on Relative Permeability," *J. of Petroleum Science and Engineering*, Vol. 18, Nos. 1/2, 1997, pp. 1–19.
- Civan, F., & Donaldson, E. C., "Relative Permeability from Unsteady-State Displacements: An Analytical Interpretation," SPE Paper 16200, Proceedings of the SPE Production Operations Symposium held in Oklahoma City, Oklahoma, March 8–10, 1987, pp. 139–155.
- Collins, E. R., *Flow of Fluids Through Porous Materials*, Penn Well Publishing Co., Tulsa, Oklahoma, 1961, 270 p.
- Cuiec, L. E., "Evaluation of Reservoir Wettability and Its Effect on Oil Recovery," in *Interfacial Phenomena in Petroleum Recovery*, N. R. Morrow (ed.), Marcel Dekker Inc., New York, Ch. 9, 1991, pp. 319–373.

- Donaldson, E. C., "Use of Capillary Pressure Curves for Analysis of Production Well Formation Damage," SPE 13809 paper, Proceedings of the SPE Production Operations Symposium held in Oklahoma City, Oklahoma, March 10–12, 1985, pp. 157–163.
- Donaldson, E. C., & Crocker, M. E., "Characterization of the Crude Oil Polar Compound Extract," DOE/BETC/RI-80/5, NTIS, Springfield, Virginia 22161, 1980, 27 p.
- Donaldson, E. C., Ewall, N., & Singh, B., "Characteristics of Capillary Pressure Curves," *Journal of Petroleum Science and Engineering*, Vol. 6, No. 3, 1991, pp. 249–261.
- Donaldson, E. C., Kendall, R. F., Pavelka, E. A., & Crocker, M. E., "Equipment and Procedures for Fluid Flow and Wettability Tests of Geological Materials," Bartlesville Energy Technology Center, Report No. DOE/BETC/IC-79/5, U.S. DOE, May 1980.
- Durand, C., & Rosenberg, E., "Fluid Distribution in Kaolinite- or Illite-Bearing Cores: Cryo-SEM Observation Versus Bulk Measurements," *Journal of Petroleum Science and Engineering*, Vol. 19, Nos. 1/2, 1998, pp. 65–72.
- Ertekin, T., & Watson, D., EOR, DOE/BC-90/4 Progress Review, September 30, 1990.
- Grattoni, C. A., Chiotis, E. D., & Dawe, R. A., "Determination of Relative Wettability of Porous Sandstones by Imbibition Studies," *J. Chem. Tech. Biotechnol.*, Vol. 64, 1995, pp. 17–24.
- Gupta, A., & Civan, F., "An Improved Model for Laboratory Measurement of Matrix to Fracture Transfer Function Parameters in Immiscible Displacement," SPE 28929 paper, Proceedings of the 68th Annual Technical Conference and Exhibition (September 25–28, 1994), New Orleans, Louisiana, pp. 383–396.
- Hirasaki, G. J., "Wettability: Fundamentals and Surface Forces," *SPE Formation Evaluation*, June 1991, pp. 217–226.
- Jerauld, G. R., & Rathmell, J. J., "Wettability and Relative Permeability of Prudhoe Bay: A Case Study in Mixed-Wet Reservoirs," *SPE Reservoir Engineering*, February 1997, pp. 58–65.
- Kaminsky, R., & Radke, C. J., "Asphaltenes, Water Films, and Wettability Reversal," *SPE Journal*, Vol. 2, December 1997, pp. 485–493.
- Kovscek, A. R., Wong, H., & Radke, C. J., "A Pore-Level Scenario for the Development of Mixed-Wettability in Oil Reservoirs," Project Report DOE/BC/92001062, U.S. Dept. of Energy, Bartlesville, OK 74005, September 1992, 52 p.
- Leontaritis, K. J., Amaefule, J. O., and Charles, R. E., "A Systematic Approach for the Prevention and Treatment of Formation Damage Caused by Asphaltene Deposition," SPE Paper 23810, Proceedings of the SPE International Symposium on Formation Damage Control, Lafayette, LA, February 26–27, 1992, pp. 383–395.

- Leverett, M. C., "Capillary Behavior in Porous Solids," *Trans. AIME*, Vol. 142, 1941, pp. 152-169.
- Marle, C. M., *Multiphase Flow in Porous Media*, Gulf Publ. Co., Houston, Texas, 1981, 257 p.
- McDougall, S. R., & Sorbie, K. S., "The Impact of Wettability on Waterflooding: Pore Scale Simulation," *SPE Reservoir Engineering*, August 1995, pp. 208-213.
- Mohanty, K. K., Masino Jr., W. H., Ma, T. D., & Nash, L. J., "Role of Three-Hydrocarbon-Phase Flow in a Gas-Displacement Process," *SPE Reservoir Engineering*, August 1995, pp. 214-221.
- Neasham, J. W., "The Morphology of Dispersed Clay in Sandstone Reservoirs and Its Effect on Sandstone Shaliness, Pore Space and Fluid Flow Properties," SPE 6858, Proceedings of the 52nd Annual Fall Technical Conference and Exhibition of the SPE of AIME held in Denver, Colorado, October 9-12, 1977, pp. 184-191.
- Paterson, A., Robin, M., Fermigier, M., Jenffer, P., and Hulin, J. P., "Effect of Density and Spatial Distribution of Wettability Heterogeneities on Contact Angle," *Journal of Petroleum Science and Engineering*, Vol. 20, No. 3/4, pp. 127-132, 1998.
- Robin, M., Rosenberg, E., & Fassi-Fihri, O., "Wettability Studies at the Pore Level: A New Approach by use of Cryo-SEM," *SPE Formation Evaluation*, March 1995, pp. 11-19.
- Sharma, R., "On the Application of Reversible Work to Wetting/Dewetting of Porous Media," *Colloids and Surfaces*, Vol. 16, No. 1, 1985, pp. 87-91.
- Sigmund, P. M., & McCaffery, F. G., "An Improved Unsteady-State Procedure for Determining the Relative Permeability Characteristics of Heterogeneous Porous Media," *Soc. Pet. Eng. J.*, Vol. 19, 1979, pp. 15-28.
- Tielong, C., Yong, Z., Kezong, P., & Wanfeng, P., "Experimental Studies and Field Trials of Relative Permeability Modifier for Water Control of Gas Wells in Low Permeability Reservoir," SPE Paper 35617, Proceedings of the SPE Gas Technology Conference held in Calgary, Alberta, Canada, April 28-May 1, 1996, pp. 385-392.
- Wang, F. H. L., "Effect of Wettability Alteration on Water/Oil Relative Permeability, Dispersion, and Flowable Saturation in Porous Media," *SPE Reservoir Engineering*, May 1988, pp. 617-628.
- Yan, J., Plancher, H., & Morrow, N. R., "Wettability Changes Induced by Adsorption of Asphaltenes," SPE paper 37232, Proceedings of the 1997 SPE International Symposium on Oilfield Chemistry held in Houston, TX, February 18-21, 1997, pp. 213-227.

Chapter 5

Permeability Relationships

Summary

A review of the permeability relationships considering the formation damage effects in petroleum reservoirs is presented.

Introduction

The permeability relationships can be classified in two groups: static and dynamic. The static correlations have been derived using the properties of various porous materials that have not been subjected to formation damage processes. The dynamic correlations or models consider porous media undergoing alteration due to rock-fluid interactions during formation damage and, therefore, are preferred for formation damage prediction.

In the following, selected models pertaining to formation damage are reviewed and presented with some modifications for consistency and applications in the formation damage prediction.

The Carman-Kozeny Hydraulic Tubes Model

The hydraulic tubes model was derived based on the analogy between the flow of fluids through porous media and parallel flow through a bundle of tortuous capillary tubes (Carman-Kozeny, 1938).

The number, diameter, and the tortuous length of the hydraulic tubes are denoted by n , D_h , and L_h , respectively. The porosity, specific pore or grain surface, and length of the porous media are ϕ , Σ , and L . V_p and V_b denote the pore and bulk volumes, respectively.

The tortuosity of porous media is expressed as the ratio of the actual tortuous tube length to the length of porous media:

$$\tau = L_h / L \quad (5-1)$$

The pore volume can be expressed in terms of the total volume of hydraulic tubes as:

$$V_p = V_b \phi = n \frac{\pi D_h^2}{4} L_h \quad (5-2)$$

The pore surface, Σ_p , can be expressed in terms of the total cylindrical surface of the hydraulic tubes as:

$$\Sigma_p = V_b \Sigma_b = n \pi D_h L_h \quad (5-3)$$

Dividing Eqs. 5-2 and 3 leads to:

$$D_h = 4\phi / \Sigma_b \quad (5-4)$$

The pore surface per unit bulk volume, Σ_b , can be expressed in terms of the pore surface per unit volume of the solid porous matrix, Σ_g , as:

$$\Sigma_b = \Sigma_g (1 - \phi) \quad (5-5)$$

Thus, invoking Eq. 5-5 into 4, the hydraulic tube diameter can be expressed as:

$$D_h = \frac{4\phi}{\Sigma_g (1 - \phi)} \quad (5-6)$$

If the grains making up the porous media are assumed of the spherical shape, then the specific grain surface is given by:

$$\Sigma_g = \pi D_g^2 / \frac{1}{6} \pi D_g^3 = 6 / D_g \quad (5-7)$$

where D_g is the grain diameter.

Next consider that the laminar flows through porous media and the bundle of tortuous tubes can be described by the Darcy and the Hagen-Poiseuille laws given, respectively, as:

$$q = \frac{KA_b}{\mu} \frac{\Delta p}{L} \quad (5-8)$$

$$q = n \frac{\pi D_h^4}{128\mu} \frac{\Delta p}{L_h} \quad (5-9)$$

K is the intrinsic permeability of porous media. The cross-sectional area of porous media open for flow can be expressed by:

$$A_p = A_b \phi = n\pi D_h^2 / 4 \quad (5-10)$$

Therefore, equating Eqs. 5-9 and 10, and substituting Eqs. 5-1 and 10 results in the following relationship for the mean hydraulic tube diameter:

$$D_h = 4\sqrt{2\tau} \sqrt{K/\phi} \quad (5-11)$$

Equating Eqs. 5-6 and 11 leads to the following Carman-Kozeny equation (1938):

$$\sqrt{\frac{K}{\phi}} = \frac{1}{\sqrt{2\tau\Sigma_g}} \left(\frac{\phi}{1-\phi} \right) \quad (5-12)$$

Two alternative forms can also be derived. Substitution of Eq. 5-7 into 12 yields:

$$\sqrt{\frac{K}{\phi}} = \frac{D_g}{6\sqrt{2\tau}} \left(\frac{\phi}{1-\phi} \right) \quad (5-13)$$

or substituting Eq. 5-5 into Eq. 5-12 and then rearranging yields a power law type relationship given as (Kozeny, 1927):

$$K = \frac{1}{2\tau\Sigma_b^2} \phi^3 \quad (5-14)$$

Based on the analysis of data by Jacquín (1964), Adler et al. (1990) suggested a power law correlation of permeability with respect to porosity as:

$$K \propto \phi^n \quad (5-15)$$

Bourbie et al. (1986) determined that $n \cong 7$ for $\phi < 0.05$ and $n \cong 3$ for $0.08 \leq \phi \leq 0.25$. In view of this evidence and Eq. 5-14, the Carman-Kozeny equation appears to be valid for the $0.08 \leq \phi \leq 0.25$ fractional porosity range. Reis and Acock (1994) warn that these exponents may be low "because the permeabilities were not corrected for the Klinkenberg effect."

The Modified Carman-Kozeny Equation Incorporating the Flow Units Concept

The derivation of the Carman-Kozeny equation presented in the preceding section inherently assumed uniform diameter cylindrical flow tubes analogy. Therefore, for applications to nonuniform diameter flow tubes, the Carman-Kozeny equation has been modified by inserting a geometric shape factor, F_s (Amaefule et al., 1993), as:

$$\sqrt{\frac{K}{\phi}} = \left[\frac{1}{\sqrt{F_s \tau \Sigma_g}} \right] \left(\frac{\phi}{1-\phi} \right) \quad (5-16)$$

Hearn et al. (1984, 1986) introduced the "flow units" concept and Amaefule et al. (1993) defined a lumped parameter as following, called the "flow zone indicator" to combine the three unknown parameters, F_s , τ and Σ_g , into one unknown parameter:

$$FZI = \frac{1}{\sqrt{F_s \tau \Sigma_g}} \quad (5-17)$$

Therefore, a plot of experimental data based on the logarithmic form of Eq. 5-16 (Amaefule et al., 1993)

$$\log\left(\frac{K}{\phi}\right) = \log(FZI^2) + 2 \log\left(\frac{\phi}{1-\phi}\right) \quad (5-18)$$

should yield a straightline with a slope of two. Hence, the FZI^2 value can be obtained as the value of K/ϕ at the $\phi = 0.5$ value.

Implicit in Eq. 5-18 is the assumption that formations with similar flow characteristics can be represented by the same characteristic flow zone indicator parameter values. Consequently, formations having distinct flow zone parameters can be identified as different flow units.

The Modified Carman-Kozeny Equation for Porous Media Altered by Deposition

Based on the Carman-Kozeny model, Eq. 5-14, Adin's (1978) correlation of experimental data leads to a permeability-porosity model as:

$$\frac{K}{K_o} = \left[1 - \left(\frac{\varepsilon}{\phi_o} \right)^{1/2} \right]^3 \quad (5-19)$$

where the volumetric fraction of bulk porous media occupied by the deposits is given by:

$$\varepsilon = \phi_o - \phi \quad (5-20)$$

This equation facilitated the following expression for the porosity reduction by deposition:

$$\frac{\phi}{\phi_o} = 1 - \left(\frac{\varepsilon}{\phi_o} \right)^{1/2} \quad (5-21)$$

The alternative empirical expression proposed by Arshad (1991) can be modified as (Civan, 1998):

$$\frac{\phi}{\phi_o} = 1 - \alpha \left(\frac{\varepsilon}{\phi_o} \right)^n \quad (5-22)$$

where α and n are some empirical parameters. Arshad's equation accounts for the formation of the dead-end pores during deposition, which do not conduct fluids.

The Flow Efficiency Concept

Rajani (1988) concluded that permeability function can be separated into and expressed as a product of a function incorporating the pore geometry and a function of porosity as:

$$K = Cf(\phi) \quad (5-23)$$

This approach is particularly useful in porous media undergoing alteration during formation damage. Frequently, the Carman-Kozeny equation fails to represent the cases where the pore throats are plugged without significant porosity reduction.

This problem can be alleviated by introducing a flow efficiency factor, γ , in view of Eq. 5-19 (Ohen and Civan, 1993; Chang and Civan, 1991, 1992, 1997). Hence, the permeability variation can be expressed by (Chang and Civan, 1997):

$$\frac{K}{K_o} = a\gamma^b \left(\frac{\phi}{\phi_o} \right)^c \quad (5-24)$$

where a , b , and c are some empirically determined parameters and K_o and ϕ_o denote the permeability and porosity at some initial or reference state. The flow efficiency factor, γ , can be interpreted as a measure of the fraction of the open pore throats allowing fluid flow. Thus, when the pore throats are plugged, then $\gamma = 0$, and therefore $K = 0$, even if $\phi \neq 0$. This phenomenon is referred to as the "gate or valve effect" of the pore throats (Chang and Civan, 1997; Ochi and Vernoux, 1998).

In order to estimate the flow efficiency factor, Ohen and Civan (1993) assumed that, although the pore throat sizes vary with time, they always remain log-normally distributed:

$$f(y) = (2\pi s_d y)^{-1/2} \exp \left\{ -0.5 \left[\ln(y/d_t)/s_d \right]^2 \right\} \quad (5-25)$$

in the range of $d_t \leq y \leq d_h$, where s_d is the standard deviation and d_t is the mean pore throat diameter.

Then, assuming that the pore throats smaller than the size, d_p , of the suspended particles will be plugged, the flow efficiency factor is estimated by the fraction of pores remaining open at a given time:

$$\gamma = 1 - E_p \int_{d_t}^{d_p} f(y) dy / \int_{d_t}^{d_h} f(y) dy \quad (5-26)$$

where E_p is the plugging efficiency factor. Particles that are sticky and deformable can mold into the shape of pore throats and seal them. Then, the plugging is highly efficient and E_p is close to unity. Particles that are rigid and nonsticky cannot seal the pore throats effectively and still allow for some fluid flow. Thus, $E_p < 1$ for such plugs.

The lower and upper bounds of the pore throat size range are estimated by a simultaneous solution of the non-linear integral equations given by:

$$\int_{d_l}^{d_h} f(y) dy = 1 \quad (5-27)$$

$$\int_{d_l}^{d_h} y f(y) dy = d_t \quad (5-28)$$

for which the mean pore throat size is estimated by solving the following equation which relates the pore throat size variation to the rate of deposition:

$$\partial d_t / \partial t = -k_6 \partial \epsilon_p / \partial t, \quad t > 0 \quad (5-29)$$

where k_6 is a rate constant and ϵ_p is the volume of deposition per unit bulk volume, subject to the initial mean pore throat diameter, either determined from the initial pore throat size distribution using Eq. 5-28, or estimated as a fraction of the mean pore diameter using:

$$d_{t_o} = \eta \sqrt{K_o / \phi_o}, \quad t = 0 \quad (5-30)$$

Note that η is not a fraction because it is a lumped coefficient including the mentioned fraction, some unit conversion factors, and the shape factor.

Chang and Civan (1991, 1992, 1997) considered that the pore throat and particle diameters can be better represented by bimodal distribution functions over finite diameter ranges, given by Popplewell et al. (1989) as:

$$f(y) = w f_1(y) + (1 - w) f_2(y) \quad (5-31)$$

where w is an adjustable weighting factor in the range of $0 \leq w \leq 1$, and $f_1(y)$ and $f_2(y)$ denote the distribution functions for the fine and coarse fractions, each of which are described by:

$$f(y) = \frac{(y - d_\ell)^{\alpha m} (d_h - y)^m}{\int_{d_l}^{d_h} (y - d_\ell)^{\alpha m} (d_h - y)^m dy} \quad (5-32)$$

with different values of the parameters α , m , d_l , and d_h . Chang and Civan (1991, 1992, 1997) used the critical particle diameter, $(d_p)_{cr}$, necessary for pore throat jamming, determined according to the criteria described in Chapter 8.

For applications with multiphase flow systems, Liu and Civan (1993, 1994, 1995, 1996) used a simplified empirical equation for permeability reduction in porous media as:

$$\frac{K}{K_o} = \left[(1-f)K_f + f \frac{\phi}{\phi_o} \right]^3 \quad (5-33)$$

where K_o and ϕ_o are the reference permeability and porosity, K_f is the residual permeability of plugged formation, and f is a flow efficiency factor given by:

$$f = 1 - \sum_i k_i \sum_l (\epsilon_{i,l})_t \quad (5-34)$$

where i and l denote the species and phases, k_i are some rate constants and $(\epsilon_{i,l})_t$ are the quantity of the pore throat deposits. The instantaneous porosity is given by:

$$\phi = \phi_o - \sum_i \sum_l [(\epsilon_{i,l})_t + (\epsilon_{i,l})_s] \quad (5-35)$$

where $(\epsilon_{i,l})_s$ is amount of surface deposits.

The Plugging–Nonplugging Parallel Pathways Model

The porous media realization is based on the plugging and nonplugging pathways concept according to Gruesbeck and Collins (1982). Relatively smooth and large diameter flowpaths mainly involve surface deposition and are considered nonplugging. Flowpaths that are highly tortuous and having significant variations in diameter are considered plugging. In the plugging pathways, retainment of deposits is assumed to occur by jamming and blocking of pore throats when several particles approach narrow flow constrictions. Deposits that are sticky and deformable usually seal the flow constrictions (Civan, 1990, 1994, 1996). Therefore, conductivity of a flow path may diminish without filling the pore space completely. Fluid seeks alternative flow paths until all the flow paths are eliminated.

Then the permeability diminishes even though the porosity may be nonzero. Another important issue is the criteria for jamming of pore throats. As demonstrated by Gruesbeck and Collins (1982) experimentally for perforations, the probability of jamming of flow constrictions depends strongly on the particle concentration of the flowing suspension and the flow constriction-to-particle diameter ratio.

The pore plugging mechanisms are analyzed considering an infinitesimally small width slice of the porous core. The total cross-sectional area, A , of the porous slide can be separated into two parts: (1) the area A_p , containing pluggable paths in which plug-type deposition and pore filling occurs, and (2) the area, A_{np} , containing nonplugging paths in which nonplugging surface deposition occurs. Thus, the total area of porous media facing the flow is given by:

$$A = A_p + A_{np} \quad (5-36)$$

The fractions of the bulk volume containing the plugging and nonplugging pathways can be estimated by (Civan, 1995, 1996):

$$f_p = A_p / A \approx \phi_p / \phi \quad (5-37)$$

$$f_{np} = A_{np} / A \approx \phi_{np} / \phi \quad (5-38)$$

where ϕ_p , ϕ_{np} , and ϕ denote the porosities of the plugging, nonplugging, and overall flow pathways.

Thus, by definition:

$$f_p + f_{np} = 1 \quad (5-39)$$

The fraction of the plugging pathways is a characteristic property of porous media and the particles of the critical size, comparable or larger than the pore throat size (Gruesbeck and Collins, 1982; Schechter, 1992). As explained in Chapter 8, the pore size distribution of the porous medium and the size distribution of the particles determine its value. However, its value varies because the nonplugging pathways undergo a transition to become plugging during formation damage.

The volumetric flow rate, q , can also be expressed as a sum of the flow rates, q_p and q_{np} , through the pluggable and nonpluggable paths as:

$$q = q_p + q_{np} \quad (5-40)$$

The volumetric flows and volumetric fluxes are related by the following expressions:

$$q = Au \quad (5-41)$$

$$q_p = A_p u_p \quad (5-42)$$

$$q_{np} = A_{np} u_{np} \quad (5-43)$$

Thus, by means of Eqs. 5-36 through 43 the total superficial flow is expressed as (Gruesbeck and Collins, 1982):

$$u = f_p u_p + f_{np} u_{np} \quad (5-44)$$

Applying the Darcy law, the volumetric fluxes through the porous media and the pluggable and nonpluggable paths can be expressed as:

$$u = (K/\mu)(-\partial p/\partial x) \quad (5-45)$$

$$u_p = (K_p/\mu)(-\partial p/\partial x)_p \quad (5-46)$$

$$u_{np} = (K_{np}/\mu)(-\partial p/\partial x)_{np} \quad (5-47)$$

K_p and K_{np} represent the permeabilities of the pluggable and nonpluggable fractions of the core. Assuming that the plugging and nonplugging paths are interconnective and hydraulically communicating, the pressure gradients are taken equal:

$$(-\partial p/\partial x)_p = (-\partial p/\partial x)_{np} = (-\partial p/\partial x) \quad (5-48)$$

Then, it can be shown that, the average permeability of the porous medium is given by (Civan, 1992; Schechter, 1992):

$$K = f_p K_p + f_{np} K_{np} \quad (5-49)$$

and the superficial flows in the plugging and nonplugging pathways are given respectively, by:

$$u_p = uK_p / K \quad (5-50)$$

$$u_{np} = uK_{np} / K \quad (5-51)$$

Let ϕ_{p_o} and ϕ_{np_o} denote the initial pore volume fractions of the plugging and nonplugging pathways of the porous media (Civan, 1995) and ε_p and ε_{np} represent the fractions of the bulk volume occupied by the deposits in the respective pathways. Thus, the instantaneous porosities in the plugging and nonplugging pathways are given by:

$$\phi_p = \phi_{p_o} - \varepsilon_p \quad (5-52)$$

$$\phi_{np} = \phi_{np_o} - \varepsilon_{np} \quad (5-53)$$

Total instantaneous and initial porosities are given, respectively, by:

$$\phi = \phi_p + \phi_{np} \quad (5-54)$$

$$\phi_o = \phi_{p_o} + \phi_{np_o} \quad (5-55)$$

The total deposit volume fraction and the instantaneous available porosity are given by:

$$\varepsilon = \varepsilon_p + \varepsilon_{np} \quad (5-56)$$

$$\phi = \phi_o - \varepsilon \quad (5-57)$$

The permeabilities of the plugging and nonplugging pathways are given by the following empirical relationships by Civan (1994) by generalizing the expressions given by Gruesbeck and Collins (1982):

$$K_p = K_{p_o} \exp \left[-\alpha (\phi_{p_o} - \phi_p)^{n_1} \right] = K_{p_o} \exp (-\alpha \varepsilon_p^{n_1}) \quad (5-58)$$

and

$$K_{np} = K_{np_o} \left(\phi_{np} / \phi_{np_o} \right)^{n_2} = K_{np_o} \left(1 - \varepsilon_{np} / \phi_{np_o} \right)^{n_2} \quad (5-59)$$

where n_1 and n_2 are the permeability reduction indices, α is a coefficient and K_{p_o} and K_{np_o} are the permeabilities at the reference porosities ϕ_{p_o} and ϕ_{np_o} of the plugging and nonplugging pathways, respectively. Eq. 5-58 represents the snow-ball effect of plugging on permeability, while Eq. 5-59 expresses the power-law effect of surface deposition on permeability. Eqs. 5-58 and 5-59 have been also verified by Gdanski and Shuchart (1998) and Bhat and Kovscek (1999), respectively, using experimental data. Bhat and Kovscek (1999) have shown that the power-law exponent in Eq. 5-59 can be correlated as a function of the coordination number and the pore body to throat aspect ratio, applying the statistical network theory for silica deposition in silicaous diatomite formation. Note that, for $n_2 < 0$ and $\epsilon_{np}/\phi_{np_o} \ll 1$, Eq. 5-59 simplifies to the expression given by Gruesbeck and Collins (1982):

$$K_{np} \cong K_{np_o} / (1 + b\epsilon_{np}) \quad (5-60)$$

where $b = n_2/\phi_{np_o}$. Eq. 5-60 is a result of a truncated series approximation of Eq. 5-59.

Thus, substitution of Eqs. 5-58 and 59 into Eq. 5-49 results in the following expression for the permeability of the porous media (Civan, 1994, 1996):

$$K = f_p K_{p_o} \exp(-\alpha \epsilon_p^{n_1}) + f_{np} K_{np_o} (1 - \epsilon_{np}/\phi_{np_o})^{n_2} \quad (5-61)$$

Cernansky and Siroky (1985) proposed an empirical relationship as:

$$1 - \frac{\phi}{\phi_o} = \frac{\epsilon}{\phi_o} = E \left(1 - \frac{K}{K_o} \right) + \frac{1-E}{\exp G - 1} \left\{ \exp \left[G \left(1 - \frac{K}{K_o} \right) \right] - 1 \right\} \quad (5-62)$$

where E and G are some empirical constants. It can be shown that $K = K_o$ for $\epsilon = 0$. Civan (2000) pointed out that, when $E = 1$, Eq. 5-62 yields a linear model as:

$$\frac{\epsilon}{\phi_o} = 1 - \frac{K}{K_o} \quad (5-63)$$

When $E = 0$, Eq. 5-62 yields a nonlinear model as:

$$\frac{\varepsilon}{\phi_o} = \frac{\exp \left[G \left(1 - \frac{K}{K_o} \right) \right] - 1}{\exp G - 1} \quad (5-64)$$

In view of the Gruesbeck and Collins (1982) plugging and nonplugging pathways approach, Civan (2000) concluded that the E coefficient can be analogous to the fraction of the nonplugging pathways and Eqs. 5–63 and 64 can be attributed to the nonplugging and plugging pathways in porous media, respectively.

Multi-Parameter Regression Models

Efforts for development of empirical correlations and theoretical models for prediction of the permeability of porous media are being pursued by many investigators because the applications of the theoretical models in the formation damage prediction have had limited success. Because of their inherent simplifications, these models are not able to represent the complicated nature of the relationship of the permeability to the petrographical, petrophysical, and mineralogical parameters of geological porous materials. Empirical models, such as by Nolen et al. (1992) have been shown to incorporate such parameters to accurately predict permeability. However, the mathematical form of such models varied in the literature. Extending the Nolen et al. approach, Civan (1996) proposed two general empirical correlations:

$$K = b \prod_i x_i^{a_i} \quad (5-65)$$

$$K = b \prod_i \exp(a_i x_i) \quad (5-66)$$

in which $x_i; i=1,2,\dots,m$ represent the various petrographical, petrophysical, and mineralogical variables, and b and $a_i; i=1,2,\dots,m$ are empirically determined parameters.

Network Models

Network models facilitate representations of porous media by prescribed networks of nodes (pore bodies) connected with bonds (pore throats). Network models have been used by many researchers, including

Sharma and Yortsos (1987), Rege and Fogler (1987, 1988), and Bhat and Kovscek (1999). Although, network models may serve as useful research tools, their implementation in routine simulations of formation damage problems may be cumbersome and computationally demanding. Therefore, they are not included in this chapter.

Modified Fair-Hatch Equation

Liu et al. (1997) formulated the texture, porosity, and permeability relationship for scale formation. Here, their approach is presented in a manner consistent with the formulation given in this section. By definition of fractional volumes ϕ , ϕ_s , and ϕ_r occupied in the bulk volume, respectively, by the pore space, deposited scales, and the non-reacting rock grains, we can write

$$\phi + \phi_s + \phi_r = 1 \quad (5-67)$$

If the mineral grains forming the scales and the rock are assumed of spherical shapes, the i^{th} grain volume can be approximated by:

$$v_i = \pi D_i^3 / 6 \quad (5-68)$$

Consider that there are a total of n_i of the i^{th} grains and the number of different mineral grains is N_m . Therefore, Liu et al. (1997) express Eq. 5-67 as:

$$\phi + \sum_{i=1}^{N_m} n_i v_i = 1 \quad (5-69)$$

and use a modified form of the Fair-Hatch equation (Bear, 1972, p. 134) to relate the texture, porosity, and permeability as:

$$K = \phi^3 \left\{ J(1-\phi)^2 \left[\sum_{i=1}^{N_m} \frac{2\theta_i n_i v_i}{D_i} \right]^2 \right\} \quad (5-70)$$

in which $J(\sim 5)$ is a packing factor and $\theta_i(\sim 6)$ for spherical grains) is a geometric factor.

Power-Law Flow-Units Equation

Civan (1996, 2000) expressed the mean-pore diameter as a three-parameter power-law function of the pore volume to solid volume ratio:

$$\sqrt{\frac{K}{\phi}} = \gamma \left(\frac{\phi}{\alpha - \phi} \right)^{\beta} \quad (5-71)$$

in which α , β and γ are empirical parameters, and usually $\alpha = 1$. β and γ depend on the pore connectivity and can be correlated as a function of the coordination number, Z , respectively, by:

$$\beta^{-1}/\beta^{-1}_{\infty} = 1 - \exp(-CZ + D) \quad (5-72)$$

$$\gamma/\gamma_{\infty} = 1 - \exp(-AZ + B) \quad (5-73)$$

The interconnectivity parameter can also be approximated by a power law function of porosity as (Civan, 1996):

$$\gamma = c\phi^n \quad (5-74)$$

in which c and n are empirical parameters. γ is zero when the pores are blocked by deposition. Civan (2000) verified the validity of Eqs. 5-71 through 74 using the data by Rajani (1988), Verlaan et al. (1999), and Bhat and Kovscek (1999).

Effect of Dissolution/Precipitation on Porosity and Permeability

Civan (2000) expressed the precipitation/dissolution rate by:

$$\frac{d\varepsilon}{dt} = k_1(F-1)(\phi_o - \varepsilon)^n \quad (5-75)$$

subject to the initial condition

$$\varepsilon = \varepsilon_o, t = 0 \quad (5-76)$$

where, t is time, k_1 is a rate constant, ϕ_o is the initial porosity, ε is the volume fraction of deposits in porous media, F is the solution

saturation ratio, and n is a process rate exponent. The porosity, ϕ , and the volume fraction of the deposits in the pore volume, σ , are related, respectively, by:

$$\phi_o = \phi + \varepsilon \quad (5-77)$$

$$\varepsilon = \phi_o \sigma \quad (5-78)$$

Once the porosity is calculated, the permeability can be determined by Eq. 5-71. Civan (2000) verified this approach using the Koh et al. (1996) data for permeability impairment by silica deposition.

Effect of Deposition/Dissolution and Stress on Porosity and Permeability

Civan (2000) modified the equations of Adin (1978), Arshad (1991), Tien et al. (1997), and Civan (1998) as:

$$\frac{\phi_o - \phi_\infty}{\phi - \phi_\infty} = (1 - \alpha_1 \varepsilon^{\alpha_2}) (1 + \alpha_3 p_{eff})^{\alpha_4} \quad (5-79)$$

$$\frac{K_o - K_\infty}{K - K_\infty} = (1 + \alpha_5 \varepsilon^{\alpha_6}) (1 + \alpha_7 p_{eff})^{\alpha_8} \quad (5-80)$$

in which, the subscripts o and ∞ indicate the initial and terminal porosity and permeability values, $\alpha_i; i=1,2,\dots,8$ are empirical parameters, and p_{eff} denotes the effective overburden stress given according to Nieto et al. (1994) and Bustin (1997) as:

$$p_{eff} = p_{ob} - \alpha p_{pf} \quad (5-81)$$

in which α is Biot's constant, and p_{ob} and p_{pf} are the overburden stress and pore fluid pressure, respectively. Civan (2000) verified these equations using the data by Nieto et al. (1994) and Bustin (1997).

Effect of Temperature on Porosity and Permeability

Gupta and Civan (1994) and then Civan (2000) formulated the variation of porosity and permeability by temperature. Representing the volumetric thermal expansion coefficient of the porous media grains by the linear equation

$$\beta_{gV} = a + b(T - T_o) \quad (5-82)$$

where T and T_o denote the temperature and a reference temperature, respectively, and a and b are empirical parameters, Civan (2000) derived:

$$\frac{1 - \phi}{1 - \phi_o} = \exp[a(T - T_o) + (b/2)(T - T_o)^2] \quad (5-83)$$

and

$$\frac{K}{K_o} = \left\{ \frac{1 - (1 - \phi_o) \exp[a(T - T_o) + (b/2)(T - T_o)^2]}{\phi_o} \right\}^3 \quad (5-84)$$

$$\exp\{-(5/3)[a(T - T_o) + (b/2)(T - T_o)^2]\}$$

Civan (2000) verified this formulation using the Okoye et al. (1990) data.

Exercises

1. The plugging and nonplugging parallel pathways model by Gruesbeck and Collins (1982) assumed Darcy flow. However, deposition and deformation in porous media reduces the flow passages causing the fluids to accelerate. Therefore, Darcy's law is modified as following, considering the inertial effects (Civan, 1996):

$$u = -\mu^{-1} N_{nd} K \partial p / \partial x \quad (5-85)$$

where K is the permeability, p is the fluid pressure, and the non-Darcy number is given by:

$$N_{nd} = (1 + \text{Re})^{-1} \quad (5-86)$$

in which the porous media Reynolds number is given by:

$$\text{Re} = v^{-1} u K \beta \quad (5-87)$$

and β is the inertial flow coefficient given by an appropriate empirical correlation, such as by Liu et al. (1995):

$$\beta = \frac{8.91 \times 10^8 \tau}{\phi K} \quad (5-88)$$

ν is the kinematic viscosity of the fluid. Determine the expression of the average permeability to be used instead of Eq. 5-49, which considers $N_{nd} = 1$ for Darcy flow.

2. Gdanski and Shuchart (1998) have correlated their permeability vs. porosity measurements obtained during sandstone-acidizing by:

$$\log_{10} K = (670 \phi)^{1/3.5} - 2 \quad (5-89)$$

They pointed out that Eq. 5-89 is remarkably similar to Civan's (1994) equation (Eq. 5-58). Note that, for permeability enhancement by acid stimulation, Eq. 5-58 can be written as:

$$K_p = K_{p_o} \exp \left[\alpha (\phi_p - \phi_{p_o})^{n_1} \right] \quad (5-90)$$

By comparison of Eqs. 5-89 and 5-90, show that the parameter values are $K_{p_o} = 0.01$ md, $\phi_{p_o} = 0$, $\alpha = 15$ and $n_1 = 0.29$ (Civan, 2000).

3. Show that Eq. 5-60 can be derived by a truncated series approximation of Eq. 5-59 for $n_2 < 0$ and $\varepsilon_{np}/\phi_{np_o} \ll 1$ (Civan, 1994).

References

- Adin, A., "Prediction of Granular Water Filter Performance for Optimum Design," *Filtration and Separation*, Vol. 15, No. 1, 1978, p. 55-60.
- Adler, P. M., Jacquin, C. G., & Quiblier, J. A., "Flow in Simulated Porous Media," *Int. J. Multiphase Flow*, Vol. 16, No. 4, 1990, pp. 691-712.
- Amaefule, J. O., Altunbay, M., Tiab, D., Kersey, D. G., & Keelan, D. K., "Enhanced Reservoir Description: Using Core and Log Data to Identify Hydraulic (Flow) Units and Predict Permeability in Uncored Intervals/Wells," SPE 26436, Proceedings of the 68th Annual Technical Conference and Exhibition of the SPE held in Houston, TX, October 3-6, 1993, pp. 205-220.
- Arshad, S. A., "A Study of Surfactant Precipitation in Porous Media with Applications in Surfactant-Assisted Enhanced Oil Recovery Processes," Ph.D. Dissertation, University of Oklahoma, 1991, 285 p.
- Bear, J., *Dynamics of Fluids in Porous Media*, American Elsevier Publ. Co., Inc., New York, New York, 1972, 764 p.
- Bhat, S. K., & Kovscek, A. R., "Statistical Network Theory of Silica Deposition and Dissolution in Diatomite," *In-Situ*, Vol. 23, No. 1, 1999, pp. 21-53.

- Bourbié, T., Coussy, O., & Zinszner, B., *Acoustique des Milieux Poreux*, Technip, Paris, 1986.
- Bustin, R. M., "Importance of Fabric and Composition on the Stress Sensitivity of Permeability in Some Coals, Northern Sydney Basin, Australia: Relevance to Coalbed Methane Exploitation, *AAPG Bulletin* (November 1997) Vol. 81, No. 11, 1894–1908.
- Carman, P. C., "The Determination of the Specific Surfaces of Powders. I," July 1938, pp. 225–234.
- Carman, P. C., *Flow of Gases Through Porous Media*, Butterworths, London, 1956.
- Cernanský, A., & Šíroký, R., "Deep-bed Filtration on Filament Layers on Particle Polydispersed in Liquids," *Chemický Průmysl*, Vol. 32 (57), No. 8, pp. 397–405, 1982.
- Cernanský, A., & Šíroký, R., "Deep-bed Filtration on Filament Layers on Particle Polydispersed in Liquids," *Int. Chem. Eng.*, Vol. 25, No. 2, 1985, pp. 364–375.
- Chang, F. F., & Civan, F., "Predictability of Formation Damage by Modeling Chemical and Mechanical Processes," SPE 23793 paper, Proceedings of the SPE International Symposium on Formation Damage Control, February 26–27, 1992, Lafayette, Louisiana, pp. 293–312.
- Chang, F. F., & Civan, F., "Modeling of Formation Damage due to Physical and Chemical Interactions between Fluids and Reservoir Rocks," SPE 22856 paper, Proceedings of the 66th Annual Technical Conference and Exhibition of the Society of Petroleum Engineers, October 6–9, 1991, Dallas, Texas.
- Chang, F. F., & Civan, F., "Practical Model for Chemically Induced Formation Damage," *J. of Petroleum Science and Engineering*, Vol. 17, No. 1/2, February 1997, pp. 123–137.
- Civan, F., "A Generalized Model for Formation Damage by Rock-Fluid Interactions and Particulate Processes," SPE 21183 paper, Proceedings of the SPE 1990 Latin American Petroleum Engineering Conference, October 14–19, 1990, Rio de Janeiro, Brazil, 11 p.
- Civan, F., "Evaluation and Comparison of the Formation Damage Models," SPE 23787 paper, Proceedings of the SPE International Symposium on Formation Damage Control, February 26–27, 1992, Lafayette, Louisiana, pp. 219–236.
- Civan, F., "A Multi-Phase Mud Filtrate Invasion and Well Bore Filter Cake Formation Model," SPE Paper No. 28709, Proceedings of the SPE International Petroleum Conference & Exhibition of Mexico, October 10–13, 1994, Veracruz, Mexico, pp. 399–412.
- Civan, F., Predictability of Formation Damage: An Assessment Study and Generalized Models, Final Report, U.S. DOE Contract No. DE-AC22-90BC14658, April 1994.

- Civan, F., "Modeling and Simulation of Formation Damage by Organic Deposition," Proceedings of the First International Symposium on Colloid Chemistry in Oil Production: Asphaltenes and Wax Deposition, IS COP'95, Rio de Janeiro, Brazil, November 26–29, 1995, pp. 102–107.
- Civan, F., "A Multi-Purpose Formation Damage Model," SPE 31101, Proceedings of the SPE Formation Damage Symposium, Lafayette, Louisiana, February 14–15, 1996, pp. 311–326.
- Civan, F., "Interactions of the Horizontal Wellbore Hydraulics and Formation Damage," SPE 35213, Proceedings of the SPE Permian Basin Oil & Gas Recovery Conf., Midland, TX, March 27–29, 1996, pp. 561–569.
- Civan, F., "Practical Model for Compressive Cake Filtration Including Fine Particle Invasion," *AIChE J.* (November 1998) 44, No. 11, 2388–2398.
- Civan, F., "Predictability of Porosity and Permeability Alterations by Geochemical and Geomechanical Rock and Fluid Interactions," Paper SPE 58746, Proceedings of the SPE International Symposium on Formation Damage held in Lafayette, Louisiana, 23–24 February 2000.
- Collins, E. R., *Flow of Fluids Through Porous Materials*, Penn Well Publishing Co., Tulsa, Oklahoma, 1961, 270 p.
- Gdanski, R. D., & Shuchart, C. E., "Advanced Sandstone-Acidizing Designs with Improved Radial Models," *SPE Production & Facilities Journal*, November 1998, pp. 272–278.
- Gruesbeck, C., & Collins, R. E., "Particle Transport Through Perforations," *SPEJ*, December 1982, pp. 857–865.
- Gruesbeck, C., & Collins, R. E., "Entrainment and Deposition of Fine Particles in Porous Media," *SPEJ*, December 1982, pp. 847–856.
- Gupta, A., and Civan, F., "Temperature Sensitivity of Formation Damage in Petroleum Reservoirs," paper SPE 27368, Proceedings of the 1994 SPE Formation Damage Control Symposium, Lafayette, Louisiana, February 9–10, 1994, 301–328.
- Hearn, C. L., Ebanks Jr., W. J., Tye, R. S., & Ranganathan, V., "Geological Factors Influencing Reservoir Performance of the Hartzog Draw Field, Wyoming," *Journal of Petroleum Technology*, Vol. 36, No. 9, August 1984, pp. 1335–1344.
- Hearn, C. L., Hobson, J. P., & Fowler, M. L., "Reservoir Characterization for Simulation, Hartzog Draw Field, Wyoming," In: *Reservoir Characterization*, pp. 341–372, L. W. Lake & H. B. Carroll, Jr. (Eds.), Academic Press, Inc., Orlando, Florida, 1986, 659 p.
- Jacquin, C. G., "Corrélation Entre la Perméabilité et les Caractéristiques Géométriques du Grès de Fontainebleau," *Revue Inst. Fr Pétrole*, Vol. 19, 1964, pp. 921–937.
- Koh, C. J., Dagenais, P. C., Larson, D. C., and Murer, A. S., "Permeability Damage in Diatomite Due to In-Situ Silica Dissolution/Precipitation," paper SPE/DOE 35394, proceedings of the 1996 SPE/DOE Tenth

- Symposium on Improved Oil Recovery held in Tulsa, Oklahoma, April 21–24, 1996, 511–517.
- Kozeny, J., "Über Kapillare Leitung des Wasser im Boden," Sitzungsber, Akad. Wiss. Wien, No. 136, 1927, pp. 271–106.
- Liu, X., & Civan, F., "Characterization and Prediction of Formation Damage in Two-Phase Flow Systems, SPE 25429 paper, Proceedings of the SPE Production Operations Symposium, March 21–23, 1993, Oklahoma City, Oklahoma, March 21–23, 1993, pp. 231–248.
- Liu, X., & Civan, F., "Formation Damage and Skin Factors Due to Filter Cake Formation and Fines Migration in the Near-Wellbore Region," SPE 27364 paper, Proceedings of the 1994 SPE Formation Damage Control Symposium, February 9–10, 1994, Lafayette, Louisiana, pp. 259–274.
- Liu, X., & Civan, F., "Formation Damage by Fines Migration Including Effects of Filter Cake, Pore Compressibility and Non-Darcy Flow—A Modeling Approach to Scaling from Core to Field," SPE Paper No. 28980, SPE International Symposium on Oilfield Chemistry, February 14–17, 1995, San Antonio, TX.
- Liu, X., & Civan, F., "Formation Damage and Filter Cake Buildup in Laboratory Core Tests: Modeling and Model-Assisted Analysis," *SPE Formation Evaluation J.*, Vol. 11, No. 1, March 1996, pp. 26–30.
- Liu, X., Civan, F., & Evans, R. D., "Correlation of the Non-Darcy Flow Coefficient, *J. of Canadian Petroleum Technology*, Vol. 34, No. 10, 1995, pp. 50–54.
- Liu, X., Ormond, A., Bartko, K., Li, Y., & Ortoleva, P., "A Geochemical Reaction-Transport Simulator for Matrix Acidizing Analysis and Design," *Jour. of Petroleum Science and Engineering*, Vol. 17, No. 1/2, February 1997, pp. 181–196.
- Nieto, J. A., Yale, D. P., and Evans, R. J., "Improved Methods for Correcting Core Porosity to Reservoir Conditions," *The Log Analyst* (May-June 1994) 21–30.
- Nolen, G., Amaefule, J. O., Kersey, D. G., Ross, R., & Rubio, R., "Problems Associated with Permeability and V_{clay} Models from Textural Properties of Unconsolidated Reservoir Rocks," SCA 9225 paper, 33rd Annual Symposium of SPWLA Society of Core Analysts, Oklahoma City, Oklahoma, June 15–17, 1992.
- Ochi, J., and Vernoux, J.-F., "Permeability Decrease in Sandstone Reservoirs by Fluid Injection-Hydrodynamic and Chemical Effects," *J. of Hydrology* (1998) 208, 237–248.
- Okoye, C. U., Onuba, N. L., Ghalambor, A., and Hayatdavoudi, A., "Characterization of Formation Damage in Heavy Oil Formation During Steam Injection," paper SPE 19417, presented at the 1990 SPE

- Formation Damage Control Symposium, Lafayette, Louisiana, February 22–23, 1990.
- Ohen, H. A., & Civan, F. "Simulation of Formation Damage in Petroleum Reservoirs," *SPE Advanced Technology Series*, Vol. 1, No. 1, April 1993, pp. 27–35.
- Popplewell, L. M., Campanella, O. H., & Peleg, M., "Simulation of Bimodal Size Distributions in Aggregation and Disintegration Processes," *Chem. Eng. Progr.*, August 1989, pp. 56–62.
- Rajani, B. B., "A Simple Model for Describing Variation of Permeability with Porosity for Unconsolidated Sands," *In Situ*, Vol. 12, No. 3, 1988, pp. 209–226.
- Rege, S. D., & Fogler, H. S., "Network Model for Straining Dominated Particle Entrapment in Porous Media," *Chemical Engineering Science*, Vol. 42, No. 7, 1987, pp. 1553–1564.
- Rege, S. D., & Fogler, H. S., "A Network Model for Deep Bed Filtration of Solid Particles and Emulsion Drops," *AIChE J.*, Vol. 34, No. 11, 1988, pp. 1761–1772.
- Reis, J. C., & Acock, A. M., "Permeability Reduction Models for the Precipitation of Inorganic Solids in Berea Sandstone," *In Situ*, Vol. 18, No. 3, 1994, pp. 347–368.
- Schechter, R. S., *Oil Well Stimulation*, Prentice Hall, Englewood Cliffs, New Jersey, 1992, 602 p.
- Sharma, M. M., & Yortsos, Y. C., "A Network Model for Deep Bed Filtration Processes," *AIChE J.*, Vol. 33, No. 10, 1987, pp. 1644–1653.
- Verlaan, M. L., Dijkgraaf, H. K., and van Kruijsdijk, C.P.J.W., "Effect of a Wetting Immobile Phase on Diffusion and Macroscopic Dispersion in Unconsolidated Porous Media," paper SPE 56417, presented at the 1999 SPE Annual Technical Conference and Exhibition held in Houston, Texas, October 3–6, 1999, 13 p.
- Tien, C., Bai, R., & Ramarao, B. V., "Analysis of Cake Growth in Cake Filtration: Effect of Fine Particle Retention," *AIChE J.*, Vol. 43, No. 1, January 1997 pp. 33–44.

Chapter 6

Instrumental and Laboratory Techniques for Characterization of Reservoir Rock

Summary

Reservoir rock evaluation is a very extensive task requiring a multi-disciplinary effort and knowledge of instrumentation, testing and interpretation, and cross-correlation of various types of data. It is a continuously evolving area of science and engineering.

In this chapter, the frequently used techniques for determination of the characteristics of petroleum-bearing rocks and their operating principles are briefly reviewed. Correct application of each technique requires well-trained personnel, who developed expertise and skills through testing of a variety of reservoir rock samples and by getting acquainted with the operation of the specific equipment, instrument, or procedure, and the interpretation methods. This usually requires a long-term effort and hands-on training on the job and/or by special courses. A detailed treatment of each technique is beyond the scope of this book. The intent of this chapter is to familiarize readers with the commonly used techniques and the capabilities and functions of these techniques. More specific and detailed information may be found in the literature and/or in users' manuals provided by the manufacturers.

Introduction

Evaluation of reservoir formation sensitivity to changing conditions during petroleum reservoir exploitation requires a multi-disciplinary team effort and the integration of various instrumental and analytical approaches

(Kersey, 1986; Amaefule et al., 1988; Unalmsir and Funk, 1998). Some methods, such as well test interpretation, may be used to infer for limited information on a few critical parameters of reservoir formation. However, direct measurements of core properties at reservoir conditions are preferred, because they provide the most realistic information about the petroleum-bearing formations.

The fundamental analytical techniques available for laboratory evaluation of core samples for sensitivity and damage potential are briefly described in this chapter. For operational principles and detailed descriptions, the readers are referred to manufacturers' manuals and other pertinent sources.

Formation Evaluation

Knowledge of reservoir formation characteristics is essential information required for studies of reservoir formation damage and interpretation of laboratory and field tests. As stated by Doublet et al. (1995), "Reservoir properties and heterogeneities can be effectively defined using four scale levels (Doublet et al., 1995 credit; Kelkar, 1991, 1993 for this information):

- *Microscopic*
 - micro scale data
 - pore and grain size distributions
 - pore throat radius
 - rock lithology
- *Macroscopic*
 - core scale data
 - permeability
 - porosity
 - saturation
 - wettability
- *Megascopic*
 - simulator grid block scale data
 - wireline logs
 - seismic data
- *Gigascopeic*
 - reservoir scale data
 - pressure transient tests
 - geologic model"

The extent of the information required depends on the scale of the studies planned. Various techniques are being developed for measurement

of reservoir formation properties. Figure 6-1 by Weber (1986) describes the various types of information that can be acquired by different logging techniques. However, Weber (1986) cautions that: "Combination of modern logs can give much information in non-cored wells, but only after proper calibration via core studies."

Characterization and quantification of the properties of the rocks, pore, and fluid systems require an integration of disciplines (Gunter et al., 1997). Skopec (1992) defines that "Reservoir characterization is a process for quantitatively predicting reservoir properties to reduce geological

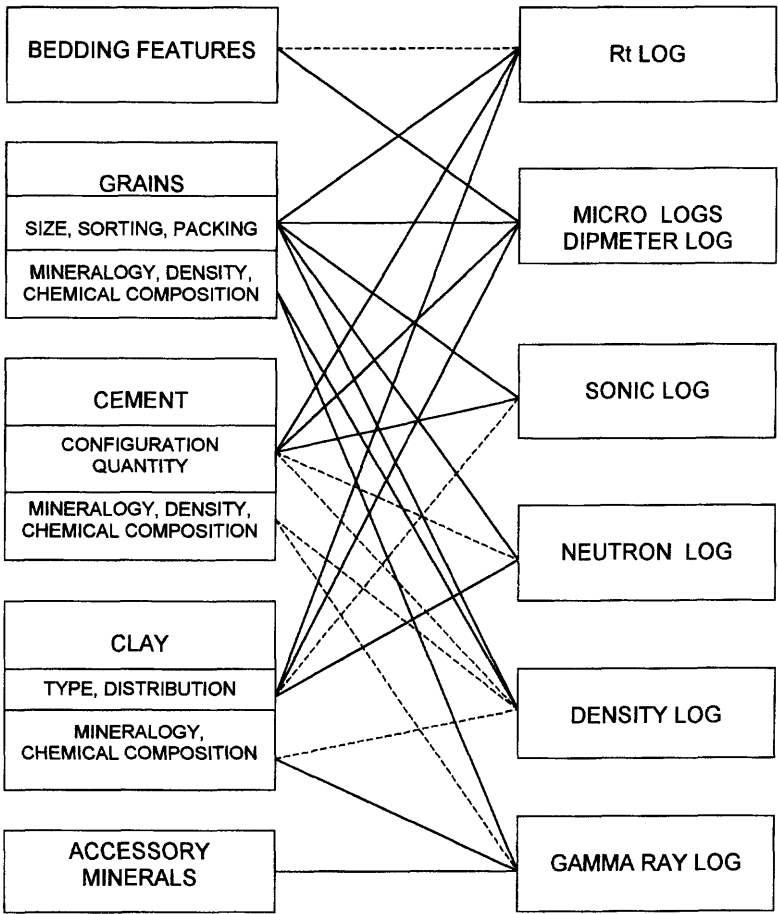


Figure 6-1. Logging techniques available for determination of formation characteristics (after Weber, 1986; reprinted by permission of the author and Academic Press).

uncertainties and define reservoir spatial variability.” Skopec (1992) adds that “Rock characterization is one component in the reservoir characterization scheme.” Figure 6–2 by Skopec (1992) describes the multidisciplinary effort necessary for rock characterization. The overall process of petrophysical integration is described in Figure 6–3 by Gunter et al. (1997). As explained in Figure 6–3, the petrophysical integration tasks can be grouped into three stages: (1) characterization of the rock and pore types, and the fluids and the flow functions, (2) construction of a petrophysical model, and (3) testing of the reservoir description by various approaches. Typical instrumental techniques used for characterization of core samples are described in the following.

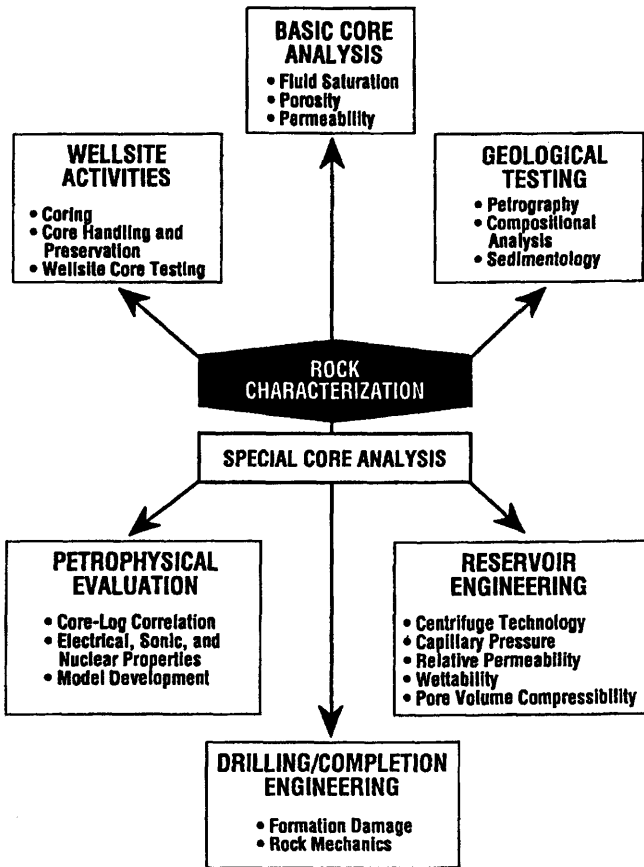


Figure 6–2. Elements of the integrated rock characterization (after Skopec, ©1992; reprinted by permission of SPWLA).

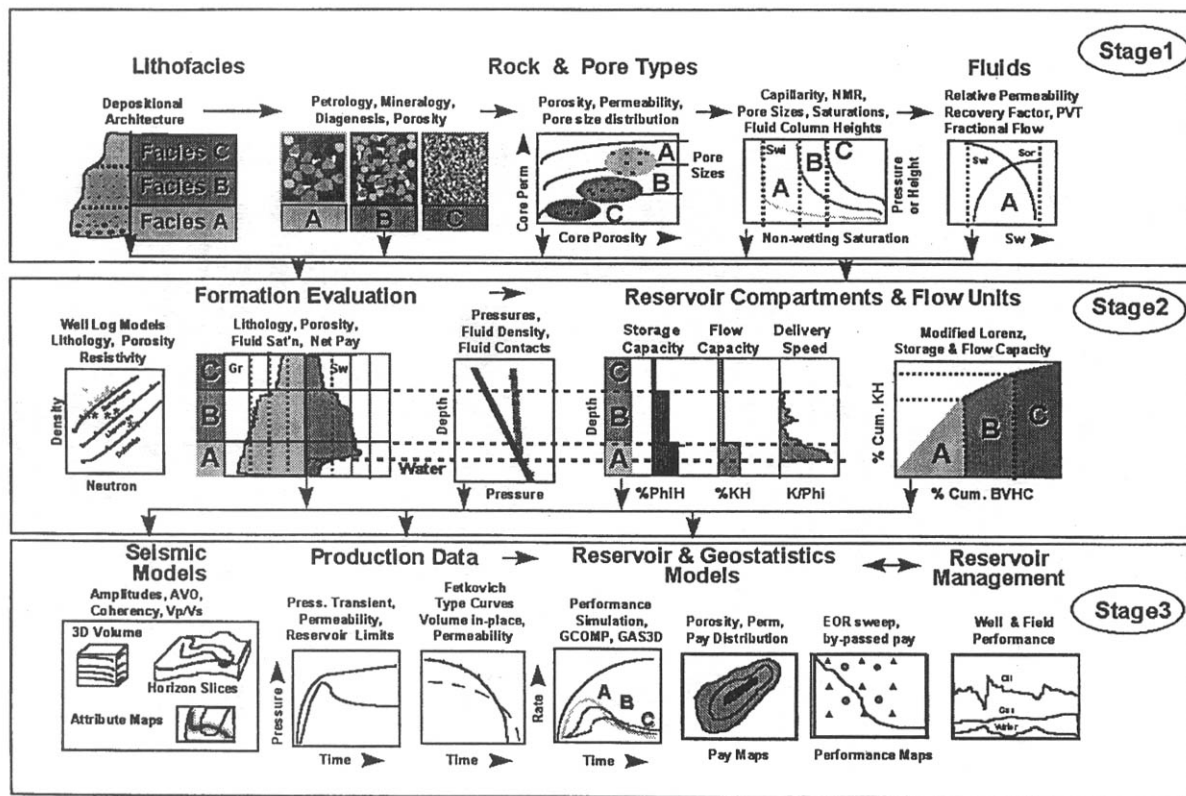


Figure 6-3. Petrophysical integration in formation characterization and evaluation (Gunter et al., ©1997 SPE; reprinted by permission of the Society of Petroleum Engineers).

X-Ray Diffraction (XRD)

The X-ray powder diffraction analysis (XRD) is a nondestructive technique that can provide a rapid and accurate mineralogical analysis of less than 4 micron size, bulk and clay contents of sedimentary rock samples (Amaefule et al., 1988). This is accomplished by separately analyzing the clays and the sand/silt constituents of the rock samples (Kersey, 1986). The X-ray diffraction technique is not particularly sensitive for noncrystalline materials, such as amorphous silicates and, therefore, an integrated application of various techniques, such as polarized light microscopy, X-ray diffraction, and SEM-EDS analyses, are required (Braun and Boles, 1992). Hayatdavoudi (1999) shows the typical X-ray diffraction patterns of the bulk and the smaller than 4 micron size clay fractions present in a core sample.

X-Ray CT Scanning (XRCT)

X-Ray CT (computer-assisted tomography) scanning is a nondestructive technique, which provides a detailed, two- and three-dimensional examination of unconsolidated and consolidated core samples during the flow of fluids, such as drilling muds, through core plugs and determines such data like the atomic number, porosity, bulk density, and fluid saturations (Amaefule et al., 1988; Unalmiser and Funk, 1998). This technique has been adapted from the field of medical radiology (Wellington and Vinegar, 1987).

As depicted by Hicks Jr. (1996), either an X-ray source is rotated around a stationary core sample or the core sample is rotated while the X-ray source is kept stationary. The intensity of the X-rays passing through the sample is measured at various angles across different cross sections of the core and used to reconstruct the special features of the porous material. The operating principle is Beer's law, which relates the intensity of the X-ray, through the linear attenuation coefficient, to the physical properties of materials and different fluid phases in the sample (Wellington and Vinegar, 1987; Hicks Jr., 1996). A schematic of a typical X-ray scanning apparatus is shown by Coles et al. (1998). The image patterns can be constructed using the linear attenuation coefficient measured for sequential cross-sectional slides along the core sample as shown by Wellington and Vinegar (1987). These allow for reconstruction of vertical and horizontal, cross-sectional images, such as shown by Wellington and Vinegar (1987). Three-dimensional images can be reconstructed from the slice images as illustrated by Coles et al. (1998). Tremblay et al. (1998) show the cross-sectional and longitudinal images of a typical wormhole, perceived as a high permeability channel, growing

in a sand-pack. Such images provide valuable insight and understanding of the alteration of porous rock by various processes.

X-Ray Fluorescopy (XRF)

The X-Ray fluorescence technique is used for determining the drilling mud invasion profiles in unconsolidated and consolidated core samples and it is especially convenient for testing unconsolidated, sleeved core samples (Amaefule et al., 1988). Amaefule et al. (1988) show a typical X-ray fluorescent image.

Scanning Electron Microscope (SEM)

The rock and fluid interactions causing formation damage is a result of direct contact of the pore filling and pore lining minerals present in the pore space of petroleum-bearing formations. The mineralogical analysis, abundance, size, and topology and morphology of these minerals can be observed by means of the scanning electron microscopy (SEM) (Kersey, 1986; Amaefule et al., 1988). Braun and Boles (1992) caution that, although the SEM can provide qualitative and quantitative chemical analyses, it should be combined with other techniques, such as the polarized light microscopy (PLM) and the X-ray diffraction (XRD) to characterize the crystalline and noncrystalline phases, because amorphous materials do not have distinct morphological properties. An energy dispersive spectroscopy (EDS) attachment can be used during SEM analysis to determine the iron-bearing minerals (Amaefule et al., 1988). Various specific implementations of the SEM are evolving. For example, the environmental SEM has been used to visualize the modification of the pore structure by the retention of deposits in porous media (Ali and Barrufet, 1995). The cryo-scanning electron microscopy has been used to visualize the distribution of fluids in regard to the shape and spatial distribution of the grains and clays in the pore space (Durand and Rosenberg, 1998). The SEM has also been used for investigation of the reservoir-rock wettability and its alteration (Robin and Cuiec, 1998; Durand and Rosenberg, 1998).

The SEM operates based on the detection and analysis of the radiations emitted by a sample when a beam of high energy electrons is focused on the sample (Ali and Barrufet, 1995). It allows for determination of various properties of the sample, including its composition and topography (Ali and Barrufet, 1995).

Typical SEM photomicrographs are shown by Amaefule et al. (1988). The environmental SEM images shown by Ali and Barrufet (1995) illustrate the modification of the pore structure by polymer retention in

porous media. As can be seen by these examples, the SEM can provide very illuminating insight into the alteration of the characteristics of the porous structure and its pore filling and pore lining substances.

Thin Section Petrography (TSP)

The thin section petrography technique can be used to examine the thin sections of core samples to determine the texture, sorting, fabric, and porosity of the primary, secondary, and fracture types, as well as the location and relative abundance of the detrital and authigenic clay minerals and the disposition of matrix minerals, cementing materials, and the porous structure (Kersey, 1986; Amaefule et al., 1988). Amaefule et al. (1988) show the examples of typical thin section photomicrographs.

Petrographic Image Analysis (PIA)

As stated by Rink and Schopper (1977), "The physical properties of sedimentary rocks strongly depend on the geometrical structure of their pore space. Thus, a geometrical analysis of the pore structure can provide valuable information in formation evaluation." The petrographic image analysis (PIA) technique analyzes the photographs of the cuttings, thin sections, or slabs of reservoir core samples using high-speed image analysis systems to infer for important petrophysical properties, including textural parameters, grain size and distribution, topography, directional dependency of textural features, pore body and pore throat sizes, porosity, permeability, capillary pressure, and formation factor (Amaefule et al., 1988; Rink and Schopper, 1997; Oyno et al., 1998).

The images of the rock surfaces can be obtained by photographing on paper using standard cameras or digital video cameras attached to a microscope, but computer-aided digital storage and analysis of images provide many advantages (Oyno et al., 1998). Saner et al. (1996) show typical thin section photomicrographs of typical carbonate lithofacies. The photographs shown by Ehrlich et al. (1997) indicate the packing flaws in typical sandstone samples. Coskun and Wardlaw (1996) show the pore size spectra and binary images of five pore types of some North Sea sandstones. Such images can be analyzed by various techniques to determine the textural attributes and to derive the petrophysical characteristics of the petroleum-bearing formation (Rink and Schopper, 1977; Ehrlich et al., 1997; Coskun and Wardlaw, 1993, 1996; Ioannidis et al., 1996).

Polarized Light Microscopy (PLM)

The polarized light microscopy (PLM) technique can be utilized for effectively detecting amorphous substances in porous media because,

being optically isotropic, amorphous substances can be distinguished from the majority of the crystalline matter, except for the optically isotropic halides (Braun and Boles, 1982). The polarized light microscopy is based on distinguishing between various substances by the difference in their refractive indices. Braun and Boles (1982) recommend supporting the PLM method by at least another method, such as the scanning electron microscopy combined with the energy dispersive X-ray spectrometry (SEM-EDS) and the X-ray diffraction (XRD) method.

Nuclear Magnetic Resonance Spectroscopy (NMR)

The nuclear magnetic resonance spectroscopy is a nondestructive technique, which measures the spin-lattice and spin-spin relaxation times by means of the radio-frequency resonance of protons in a magnetic field to infer for the petrophysical parameters, including porosity, permeability, and free and bound fluids using specially derived correlations (Unalmsir and Funk, 1998; Rueslåtten et al., 1998). Because fines mobilization, migration, and retention in porous media causes porosity variation, the NMR can also be used for examination of core plugs during fines invasion. For example, Fordham et al. (1993) examined the invasion of clay particles within natural sedimentary rocks by injection of suspension of clay particles using the NMR imaging technique. Fordham et al. (1993) show that the proton spin-lattice relaxation time profiles measured at different times indeed indicate the effect of clay fines invasion into core plugs. This information can be used to determine the penetration depth of the clay fines and the effect of fines invasion to permeability. Xiao et al. (1999) state that:

The NMR (nuclear magnetic resonance) techniques, namely NMRI (nuclear magnetic resonance imaging) and NMRR (nuclear magnetic resonance relaxation), can support the observations obtained with the return permeability tests, helping in the identification and comprehension of the formation damage mechanisms caused by solids and filtrate invasion in the pores of a reservoir rock.

However, the NMR techniques are expensive and time consuming, and better suited for in depth studies (Xiao et al., 1999). Xiao et al. (1999) show typical NMR images and relaxation time curves on invasion of a typical bentonite/mixed metal hydroxide (MMH)/sized carbonate mud system into a core plug. The core plug images provided visual inspections for the core initially saturated with a 3% NH_4Cl brine, then contaminated by mud invasion, and finally back flushed with brine for mud removal, respectively.

Acoustic Techniques (AT)

The acoustic techniques facilitate acoustic-velocity signatures and correlations of the acoustic properties of rocks to construct acoustic velocity tomograms to image the rock damage by deformation, such as elastic and dilatant deformations, pore collapse, and normal consolidation processes (Scott et al., 1998). Scott et al. (1998) describe the acoustic velocity behaviors during compaction of reservoir rock samples. Scott et al. (1998) show a schematic of a confined-indentation experiment used and the acoustic velocity tomograms obtained by the indentation tests.

Cation Exchange Capacity (CEC)

The total amount of ions (anions and cations) that are present at the clay surface and exchangeable with the ions in an aqueous solution in contact with the clay surface, is referred to as the ion-exchange capacity (*IEC*) of the clay minerals and it is measured in meq/100 g (Kleven and Alstad, 1996). The total ion-exchange capacity is therefore equal to the sum of the cation-exchange capacity (*CEC*) and the anion-exchange capacity (*AEC*):

$$IEC = CEC + AEC \quad (6-1)$$

During reservoir exploitation, when brines of different composition than the reservoir brines enter the reservoir formation, an ion-exchange process may occur, activating various processes leading to formation damage (see Chapter 13). In the literature, more emphasis has been given to the measurement of the cation-exchange capacity, because it is the primary culprit, responsible for water sensitivity of clayey formations (Hill and Milburn, 1956; Thomas, 1976; Huff, 1987; Muecke, 1979; Khilar and Fogler, 1983, 1987).

The mechanisms, by which aqueous ions interact with the clay minerals present in petroleum-bearing rock, have been the subject of many studies. Kleven and Alstad (1996) identified two different mechanisms: (1) lattice substitutions and (2) surface edge reactions. The first mechanism involves the ion-exchange within the lattice structure itself, by substitution of Al^{3+} for Si^{4+} , Mg^{2+} for Al^{3+} , as well as other ions to a lesser degree, and does not depend on the ionic strength and *pH* of the aqueous solution (Kleven and Alstad, 1996).

The second mechanism involves the reactions of the functional groups present along the edges of the silica-alumina units and it is affected by the ionic strength and *pH* of the aqueous solution (Kleven and Alstad, 1996). The relative contributions of these mechanisms vary by the clay mineral types. It appears that montmorillonite and illite primarily undergo

lattice substitutions, and surface edge reactions are dominant for kaolinite and chlorite (Kleven and Alstad, 1996). Expansion of swelling clays, such as montmorillonite, increases their surface area of exposure and, therefore, their cation-exchange capacity (Kleven and Alstad, 1996). Theoretical description of the ion-exchange reactions between the aqueous phase and the sedimentary formation minerals is very complicated because of various effects, including ion composition, pH , and temperature (Kleven and Alstad, 1996).

The methods used for measurement of the ion-exchange capacity vary by the reported studies. For example, Kleven and Alstad (1996) measured the CEC of clays using Ca^{2+} brines without the presence of $NaCl$ and measured the AEC using SO_4^{2-} brines. Rhodes and Brown (1994) point out the CEC measurement of clays by commonly used methods, such as the ammonium ion and methylene blue dye adsorption methods, have inherent shortcomings, leading to inaccurate results. Therefore, Rhodes and Brown (1994) have used the adsorption of the colored $Co(H_2O)_6^{2+}$ ion, which yields a very stable hydrated $Co(II)$ complex. Rhodes and Brown (1994) have determined that the $CECs$ of four different Na^+ -montmorillonites measured by three different adsorption methods differ appreciably. The methylene blue adsorption method generates significantly different results from the cobalt and ammonium ion adsorption methods, which agree with each other within acceptable tolerance.

Because the ion-exchange reactions in petroleum-bearing rock are usually treated as equilibrium reactions for practical purposes, ion-exchange isotherms relating the absorbed and the aqueous phase ion contents in equilibrium conditions are desirable. For example, Kleven and Alstad (1996) determined the cation-exchange isotherms shown in Figures 6-4, 6-5, and 6-6, respectively, for single cation-exchange reactions involving



and



and binary cation exchange reactions involving



Similarly, Figure 6-7 by Kleven and Alstad (1996) shows the typical anion-exchange isotherms for a single anion-exchange reaction involving $SO_4^{2-} \rightarrow Cl^-$. When more than one ions are present in the system, some are preferentially more strongly adsorbed than the others depending on

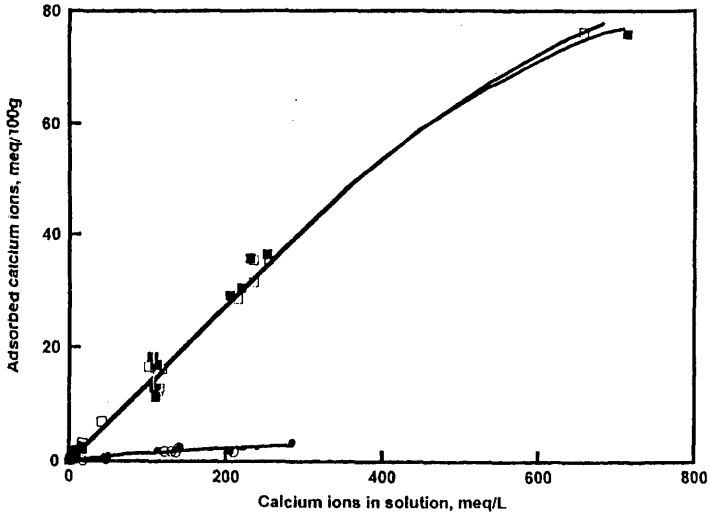


Figure 6-4. Calcium-sodium ion-exchange isotherms (circles = kaolinite, squares = montmorillonite, open figures = 20°C, and closed figures = 70°C) (Reprinted from *Journal of Petroleum Science and Engineering*, Vol. 15, Kleven, R., and Alstad, J., "Interaction of Alkali, Alkaline-Earth and Sulphate Ions with Clay Minerals and Sedimentary Rocks," pp. 181-200, ©1996, with permission from Elsevier Science).

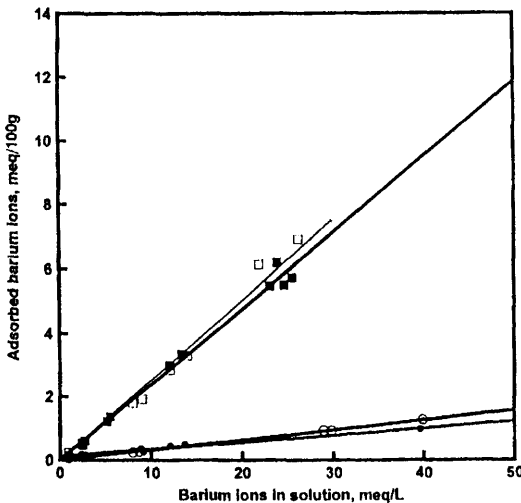


Figure 6-5. Barium-sodium ion-exchange isotherms (circles = kaolinite, squares = montmorillonite, open figures = 20°C, and closed figures = 70°C) (Reprinted from *Journal of Petroleum Science and Engineering*, Vol. 15, Kleven, R., and Alstad, J., "Interaction of Alkali, Alkaline-Earth and Sulphate Ions with Clay Minerals and Sedimentary Rocks," pp. 181-200, ©1996, with permission from Elsevier Science).

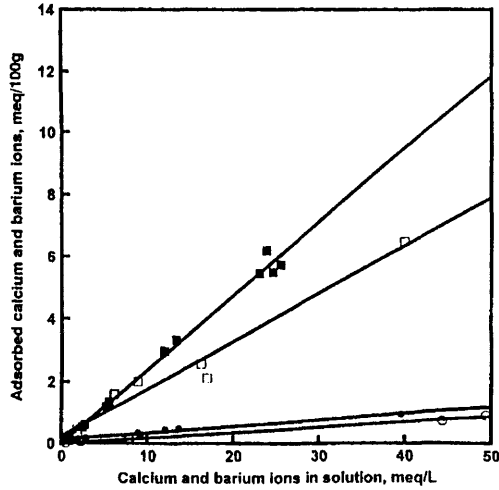


Figure 6-6. Calcium (open figures) and barium (closed figures) ion-exchange isotherms at 70°C (circles = kaolinite and squares = montmorillonite) (Reprinted from *Journal of Petroleum Science and Engineering*, Vol. 15, Kleven, R., and Alstad, J., "Interaction of Alkali, Alkaline-Earth and Sulphate Ions with Clay Minerals and Sedimentary Rocks," pp. 181-200, ©1996, with permission from Elsevier Science).

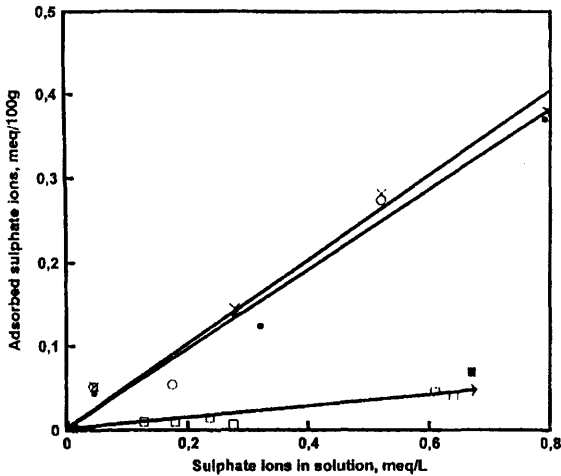


Figure 6-7. Sulfate-chloride ion-exchange isotherms at low sulfate concentrations (circles = kaolinite, squares = montmorillonite, open figures = 20°C, and closed figures = 70°C) (Reprinted from *Journal of Petroleum Science and Engineering*, Vol. 15, Kleven, R., and Alstad, J., "Interaction of Alkali, Alkaline-Earth and Sulphate Ions with Clay Minerals and Sedimentary Rocks," pp. 181-200, ©1996, with permission from Elsevier Science).

the affinities of the clay minerals for different ions. This phenomenon is referred to as the selectivity. Kleven and Alstad (1996) have determined that the kaolinite and montmorillonite clays prefer Ba^{2+} over Ca^{2+} , as indicated by the normalized cation-exchange isotherms shown in their Figure 6–8. Similarly, their Figure 6–9 showing the normalized anion-exchange isotherms indicate that the kaolinite clay prefers SO_4^{2-} over Cl^- . Figure 6–8 also shows that the selectivity is also influenced by the swelling properties of clays. It is apparent that the affinity of divalent cations (such as Ca^{2+}) over monovalent cations (such as Na^+) is much higher for kaolinite (nonswelling clay) than montmorillonite (swelling clay).

Petroleum-bearing formations contain various metal oxides, including Fe_2O_3 , Fe_3O_4 , MnO_2 , and SiO_2 . Tamura et al. (1999) propose a hydroxylation mechanism that the exposure of metal oxides to aqueous solutions causes water to neutralize the strongly base lattice oxide ions to transform them to hydroxide ions, according to



Hence, the ion-exchange capacity of the metal oxides can be measured by determining the hydroxyl site densities on metal oxides by various

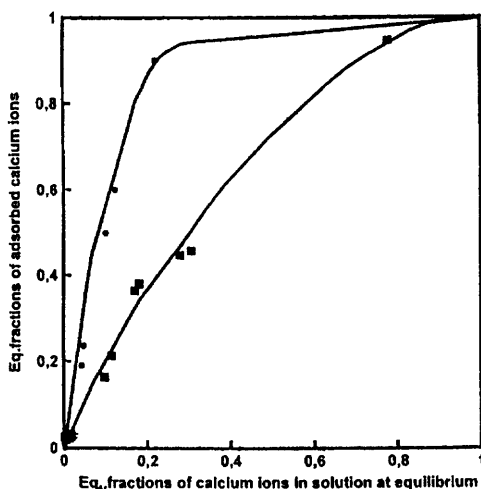


Figure 6–8. Normalized calcium-sodium ion-exchange isotherms (circles = kaolinite, squares = montmorillonite, open figures = 20°C, and closed figures = 70°C) (Reprinted from *Journal of Petroleum Science and Engineering*, Vol. 15, Kleven, R., and Alstad, J., "Interaction of Alkali, Alkaline-Earth and Sulphate Ions with Clay Minerals and Sedimentary Rocks," pp. 181–200, ©1996, with permission from Elsevier Science).

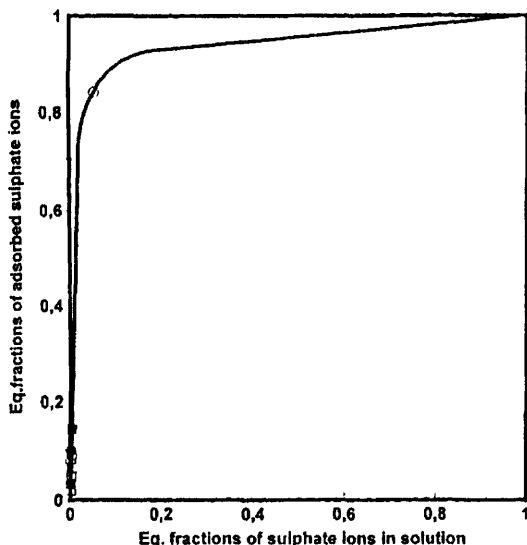


Figure 6-9. Normalized sulfate-chloride ion-exchange isotherms (circles = kaolinite, squares = montmorillonite, open figures = 20°C, and closed figures = 70°C) (Reprinted from *Journal of Petroleum Science and Engineering*, Vol. 15, Kleven, R., and Alstad, J., "Interaction of Alkali, Alkaline-Earth and Sulphate Ions with Clay Minerals and Sedimentary Rocks," pp. 181-200, ©1996, with permission from Elsevier Science).

methods, including reactions with Grignard reagents, acid-base ion-exchange reactions, dehydration by heating, infra-red (IR) spectroscopy, tritium exchange by hydroxyl, and crystallographic calculations (Tamura et al., 1999). Figure 6-10 by Tamura et al. (1999) shows a typical isotherm for OH^- ion for hematite. Figure 6-11 by Arcia and Civan (1992) show that the cation-exchange capacity of the cores extracted from reservoirs may vary significantly by the clay content.

ζ (Zeta)-Potential

When an electrolytic solution flows through the capillary paths in porous media, an electrostatic potential difference is generated along the flow path because of the relative difference of the anion and cation fluxes. Because the mobility of the ions is affected by the surface charge, this potential difference, called the zeta-potential, can be used as a measure of the surface charge (Sharma, 1985). The zeta-potential can be measured by various methods, including potentiometric titration, electrophoresis, and streaming potential.

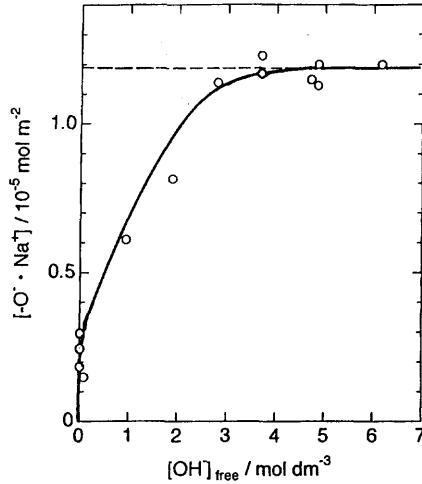


Figure 6-10. Hydroxyl-hematite ion-exchange isotherm indicating the amount of hydroxyl ion consumed per unit surface area of hematite vs. the hydroxyl ion concentration in solution (after Tamura et al., 1999; reprinted by permission of the authors and Academic Press).

The Helmholtz-Smoluchowski equation of the zeta-potential for granular porous media is given by Johnson (1999) as:

$$\zeta = \frac{4\pi\mu L}{\epsilon\epsilon_0\phi A\zeta R} \frac{dU}{dp} \quad (6-6)$$

based on the cylindrical capillary bundle of tubes model. In Eq. 6-6, ζ denotes the zeta-potential of the capillary surface, μ is the viscosity, ($\epsilon\epsilon_0$) is the permittivity, (dU/dp) is the streaming potential pressure gradient, U is the streaming potential, p is pressure, A and L are the cross-sectional area and length of porous media, respectively, ϕ is the porosity, and R is the electrical resistance. Figures 6-12 and 6-13 by Johnson (1999) show the dependency of the zeta-potential on the ionic strength and pH of the aqueous solution, obtained by the electrophoresis and streaming potential methods.

Wettability

Wettability of the pore surface is one of the important factors influencing the distribution and transport of various fluid phases and therefore the extent of formation damage in petroleum-bearing formations. Because

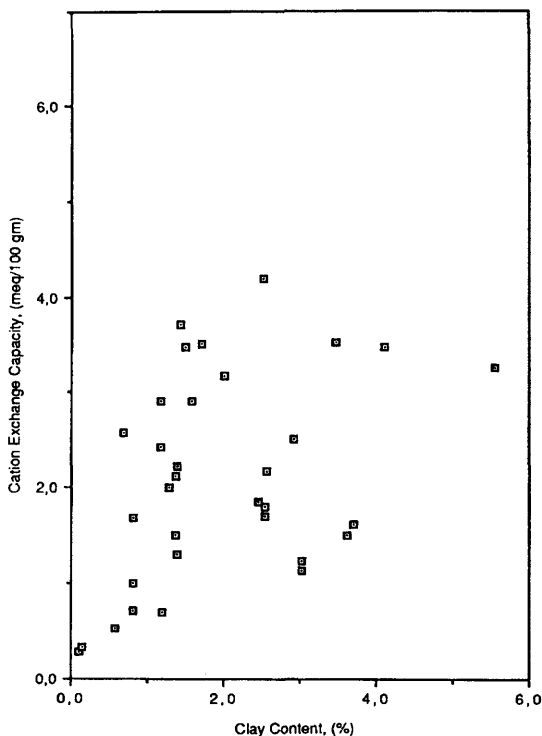


Figure 6-11. Cation exchange capacity of the various Ceuta field core samples by Maraven S. A., Venezuela (Arcia and Civan, ©1992; reprinted by permission of the Canadian Institute of Mining, Metallurgy and Petroleum).

the wettability of rocks is altered by the rock and fluid interactions and variations of the reservoir fluid conditions, prediction of its effects on formation damage is a highly complicated issue. Although mineral matters forming the reservoir rocks are generally water-wet, deposition of heavy organic matter, such as asphaltenes and paraffines, over a long reservoir lifetime may render them mixed-wet or oil-wet, depending on the composition of the oil and reservoir conditions. Wettability may be expressed by various means, including the Amott and USBM indices. (See Chapter 4.) During reservoir exploitation, wettability may vary by various reasons. For example, Figure 6-14 by Burchfield and Bryant (1988) is an evidence of the alteration of the wettability of a water-wet berea sandstone to a stronger water-wet state in contact with microbial solutions. Madden and Strycker (1988) determined that the wettability of the Berea sandstone saturated with oils vary by their asphaltene and polar components content

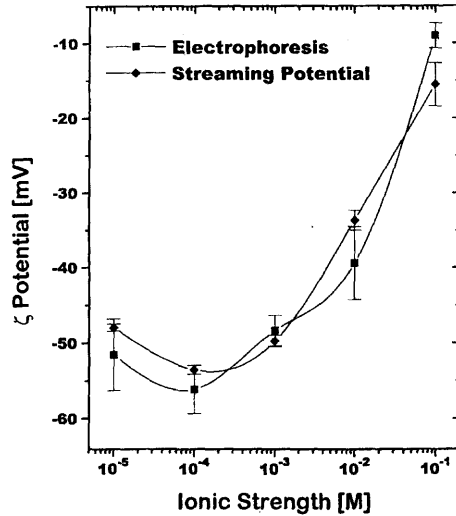


Figure 6–12. Comparison of electrokinetic measurement methods at various KCl ionic strengths in the 4.4–5.8 pH range (Johnson, 1999; reprinted by permission of the author and Academic Press).

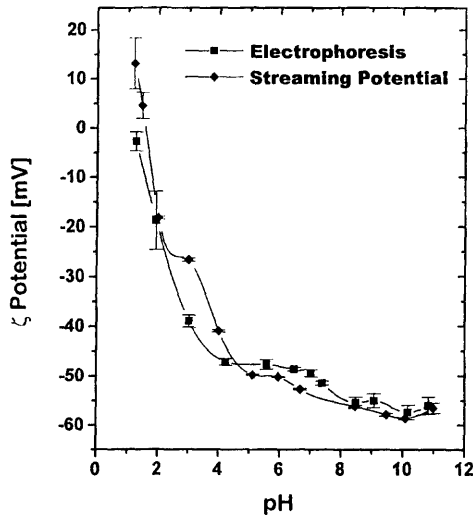


Figure 6–13. Comparison of electrokinetic measurement methods at various pH values, with the initial solution of 10^{-3} M KCl (Johnson, 1999; reprinted by permission of the author and Academic Press).

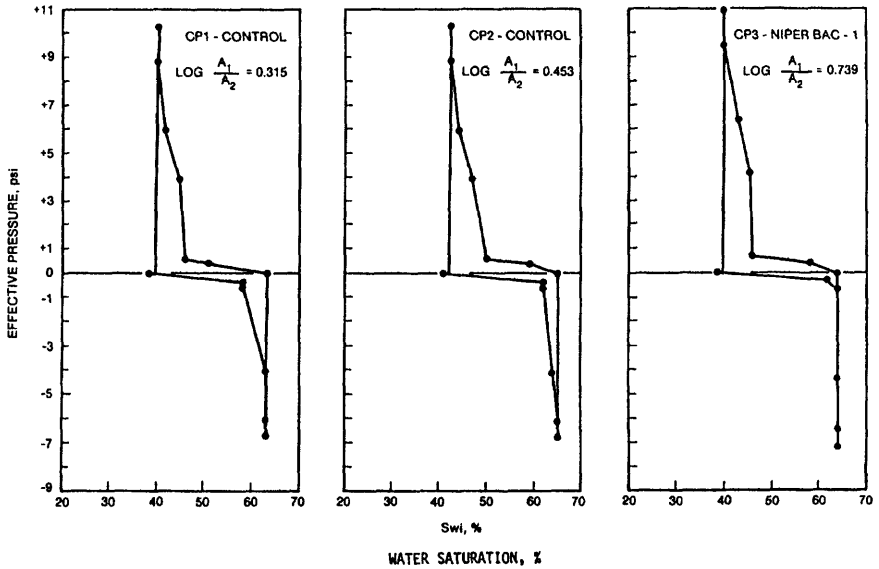


Figure 6-14. Effect of microbial solutions on the capillary pressure curve and wettability index (after Burchfield and Bryant, 1989; reprinted by permission of the U.S. Department of Energy).

and temperature. Figure 6-15 by Madden and Strycker (1988) depicts the shifting of the wettability curves by temperature.

Mineral Quantification

Knowledge of the types, quantities, and conditions of the minerals forming the petroleum-bearing rocks is important for assessment of their formation damage potential and design preventive and stimulation techniques to alleviate formation damage. As stated by Chakrabarty and Longo (1997), "Minerals are usually quantified using mineral properties available from published data and rock properties measured in the laboratory used cored samples or in the field using geochemical well logs." In the literature, several approaches have been proposed for this purpose. For example, the rapid mineral quantification method developed by Chakrabarty and Longo (1997) can be used for quantification of minerals both in the laboratory and downhole. They begin by expressing each measured rock property, y_i , as a mass fraction, f_i , weighted sum

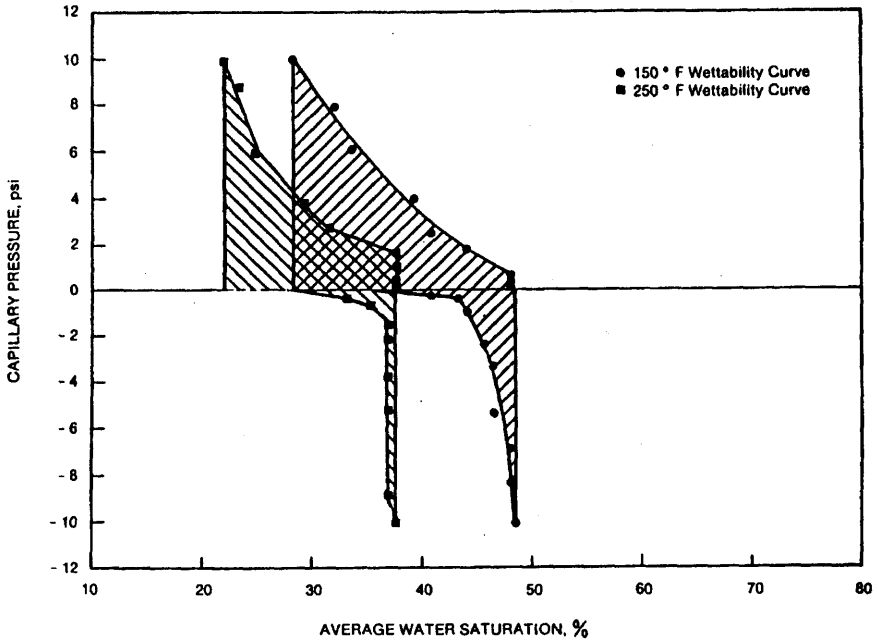


Figure 6-15. Effect of temperature on the capillary pressure curve (Madden and Strycker, 1989; reprinted by permission of the U.S. Department of Energy).

of the properties, x_{ij} , of the minerals present in the rock by the property balance equation:

$$y_i = \sum_j x_{ij} f_j + e_i, \quad i = 1, 2, \dots, n \text{ and } j = 1, 2, \dots, p \quad (6-7)$$

or in matrix form

$$y = X \cdot f + e \quad (6-8)$$

where n and p denote the number of rock properties measured and the number of different mineral phases present in the rock, respectively, and e_i denotes the measurement error. Because, the mineral properties, x_{ij} , can be obtained from the literature, the mineral compositions, $f_j: 1, 2, \dots, n$, can be calculated by solving the set of linear algebraic equations formed by Eq. 6-7. The system, represented by Eq. 6-8, is under-determined when the number of measured rock properties is less than the number of

different minerals present in the rock, and over-determined, otherwise, and determined when they are equal. In order to handle both of these cases and alleviate any instability problems associated with the solution of Eq. 6–8, Chakrabarty and Longo (1997) supplemented the property balance equation (Eq. 6–8) with the following constraining equation:

$$c = C \cdot f + u \quad (6-9)$$

This equation incorporates any prior information available or initial guesses on the fractional compositions of the minerals present in rocks, in which c is a vector of the initial guesses of the mineral fractions, C is a unit diagonal matrix, and u is a vector of errors associated with the initial guesses of the fractions of the various minerals.

Chakrabarty and Longo (1997), then, combines Eqs. 6–8 and 9 as:

$$\begin{bmatrix} y \\ c \end{bmatrix} = \begin{bmatrix} X \cdot f \\ C \cdot f \end{bmatrix} + \begin{bmatrix} e \\ u \end{bmatrix} \quad (6-10)$$

from which, the estimates of the mineral fractions is expressed by:

$$f^* = \left[X^T \cdot \{V(e)\}^{-1} \cdot X + C^T \cdot \{V(u)\}^{-1} \cdot C \right]^{-1} \cdot \left[X^T \cdot \{V(e)\}^{-1} \cdot y + C^T \cdot \{V(u)\}^{-1} \cdot c \right] \quad (6-11)$$

The superscripts “ T ” and “ -1 ” refer to the transpose and inverse of the matrices, respectively. $V(e)$ and $V(u)$ are diagonal matrices, whose elements are the error variances (standard deviations) of the measured rock properties and the initial guesses of the mineral fractions, respectively.

Chakrabarty and Longo (1997) expressed the variances of the mineral fractions by:

$$V(f^*) = \left[X^T \cdot \{V(e)\}^{-1} \cdot X + C^T \cdot \{V(u)\}^{-1} \cdot C \right]^{-1} \quad (6-12)$$

which is the same as the first part of Eq. 6–11.

Using Eq. 6–8 without the error term and Eq. 6–11, the rock properties are estimated by:

$$y^* = X \cdot f^* \quad (6-13)$$

and therefore the deviations of the measured and estimated rock properties are given by:

$$e = f - f^* \quad (6-14)$$

Then, Chakrabarty and Longo (1997) determine the goodness of the estimates of the mineral fractions by the following sum of the squares of the deviations:

$$J = e^T \cdot e \quad (6-15)$$

As stated by Chakrabarty and Longo (1997), the chemical laboratories measuring the rock properties usually also provide the standard deviations of the measured properties. Similarly, the service companies running the wireline logs can provide the standard deviations of the geochemical well logging. They suggest that the XRD pattern can provide the initial estimates of the mineral fractions. Otherwise, a reasonable initial guess, such as evenly distributed mineral fractions can be used.

Chakrabarty and Longo (1997) demonstrated their method, called the modified matrix algebra-based method, by several examples. Chakrabarty and Longo (1997) show satisfactory comparisons of the measured and predicted properties of the various rock samples.

References

- Ali, L., & Barrufet, M. A., "Study of Pore Structure Modification Using Environmental Scanning Electron Microscopy," *Journal of Petroleum Science and Engineering*, Vol. 12, 1995, pp. 323–338.
- Amaefule, J. O., Kersey, D. G., Norman, D. L., & Shannon, P. M., "Advances in Formation Damage Assessment and Control Strategies," CIM Paper No. 88-39-65, Proceedings of the 39th Annual Technical Meeting of Petroleum Society of CIM and Canadian Gas Processors Association, Calgary, Alberta, June 12–16, 1988, 16 p.
- Appel, M., Stallmach, F., & Thomann, H., "Irreducible Fluid Saturation Determined by Pulsed Field Gradient NMR," *Journal of Petroleum Science and Engineering*, Vol. 19, 1998, pp. 45–54.
- Arcia, E. M., & Civan, F., "Characterization of Formation Damage by Particulate Processes," *Journal of Canadian Petroleum Technology*, Vol. 31, No. 3, 1992, pp. 27–33.
- Braun, G., & Boles, J. L., "Characterization and Removal of Amorphous Aluminosilicate Scales," SPE 24068 paper, Proceedings of the SPE Western Regional Meeting, Bakersfield, California, March 30–April 1, 1982, pp. 389–398.

- Burchfield, T. E., & Bryant, R. S., "Development of MEOR Processes for Use in Field Applications," 1988 Annual Report, Work Performed Under Cooperative Agreement No. FC22-83FE60149, for the U.S. Department of Energy, Bartlesville Project Office, Bartlesville, Oklahoma, September 1989, pp. 69-73.
- Chakrabarty, T., & Longo, J. M., "A New Method for Mineral Quantification to Aid in Hydrocarbon Exploration and Exploitation," *Journal of Canadian Petroleum Technology*, Vol. 36, No. 11, pp. 15-21.
- Coles, M. E., Hazlett, R. D., Spanne, P., Soll, W. E., Muegge, E. L., & Jones, K. W., "Pore Level Imaging of Fluid Transport Using Synchrotron X-Ray Microtomography," *Journal of Petroleum Science and Engineering*, Vol. 19, 1998, pp. 55-63.
- Coskun, S. B., & Wardlaw, N. C., "Estimation of Permeability from Image Analysis of Reservoir Sandstones—Image analysis for estimating ultimate oil recovery efficiency by waterflooding for two sandstone reservoirs," *Journal of Petroleum Science and Engineering*, Vol. 10, 1993, pp. 1-16, Vol. 15, 1996, pp. 237-250.
- Cuic, L., & Robin, M., "Two SEM Techniques to Investigate Reservoir-Rock Wettability," *Journal of Petroleum Technology*, November 1998, pp. 77-79.
- Doublet, L. E., Pande, P. K., Clark, M. B., Nevans, J. W., Vessell, R., & Blasingame, T. A., SPE 29594 paper, Proceedings of the 1995 SPE Joint Rocky Mountain and Low Permeability Reservoirs Symposium, Denver, Colorado, March 19-22, 1995, pp. 13-38.
- Durand, C., & Rosenberg, E., "Fluid Distribution in Kaolinite- or Illite-Bearing Cores: Cryo-SEM Observations Versus Bulk Measurements," *Journal of Petroleum Science and Engineering*, Vol. 19, Nos. 1/2, 1998, pp. 65-72.
- Ehrlich, R., Prince, C., & Carr, M. B., "Sandstone Reservoir Assessment and Production is Fundamentally Affected by Properties of a Characteristic Porous Microfabric," SPE 38712 paper, Proceedings of the 1997 SPE Annual Technical Conference and Exhibition, San Antonio, Texas, October 5-8, 1997, pp. 591-599.
- Fordham, E. J., Horsfield, M. A., Hall, L. D., & Maitland, G. C., "Depth Filtration of Clay in Rock Cores Observed by One-Dimensional ^1H NMR Imaging," *Journal of Colloid and Interface Science*, Vol. 156, 1993, pp. 253-255.
- Gunter, G. W., Pinch, J. J., Finneran, J. M., & Bryant, W. T., "Overview of an Integrated Process Model to Develop Petrophysical Based Reservoir Description," SPE 38748 paper, Proceedings of the 1997 SPE Annual Technical Conference and Exhibition, San Antonio, Texas, October 5-8, 1997, pp. 475-479.

- Hayatdavoudi, A., "Changing Chemophysical Properties of Formation and Drilling Fluid Enhances Penetration Rate and Bit Life," SPE 50729 paper, Proceedings of the 1999 SPE International Symposium on Oilfield Chemistry, Houston, Texas, February 16–19, 1999, pp. 273–285.
- Hicks Jr., P. J., "X-Ray Computer-Assisted Tomography for Laboratory Core Studies," *Journal of Petroleum Technology*, December 1996, pp. 1120–1122.
- Ioannidis, M. A., Kwiecien, M. J., & Chatzis, I., "Statistical Analysis of the Porous Microstructure as a Method of Estimating Reservoir Permeability," *Journal of Petroleum Science and Engineering*, Vol. 16, 1996, pp. 251–261.
- Johnson, P. R., "A Comparison of Streaming and Microelectrophoresis Methods for Obtaining the ζ Potential of Granular Porous Media Surfaces," *Journal of Colloid and Interface Science*, Vol. 209, 1999, pp. 264–267.
- Kelkar, M., "Introduction to Geostatistics," tutorial paper, presented at the 1991 International Reservoir Characterization Conference, Tulsa, Oklahoma.
- Kelkar, M., *Applied Geostatistics for Reservoir Characterization*, draft, University of Tulsa, Tulsa, Oklahoma, 1993.
- Kersey, D. G., "The Role of Petrographic Analysis in the Design of Non-damaging Drilling, Completion, and Stimulation Programs," SPE 14089 paper, presented at the 1986 SPE Intl. Meeting on Petroleum Engineering, Beijing, March 17–20.
- Khilar, K. C., & Fogler, H. S., "Colloidally Induced Fines Migration in Porous Media," in Amundson, N. R., & Luss, D. (Eds.), *Reviews in Chemical Engineering*, Freund Publishing House LTD., London, England, January–June 1987, Vol. 4, Nos. 1 and 2, pp. 41–108.
- Khilar, K. C., & Fogler, H. S., "Water Sensitivity of Sandstones," *SPEJ*, pp. 55–64, February 1983.
- Kleven, R., & Alstad, J., "Interaction of Alkali, Alkaline-Earth and Sulphate Ions with Clay Minerals and Sedimentary Rocks," *Journal of Petroleum Science and Engineering*, Vol. 15, 1996, pp. 181–200.
- Madden, M. P., & Strycker, A. R., "Thermal Processes for Light Oil Recovery," 1988 Annual Report, Work Performed Under Cooperative Agreement No. FC22-83FE60149, for the U.S. Department of Energy, Bartlesville Project Office, Bartlesville, Oklahoma, September 1989, pp. 205–218.
- Muecke, T. W., "Formation Fines and Factors Controlling their Movement in Porous Media," *JPT*, pp. 147–150, Feb. 1979.
- Oyno, L., Tjetland, B. C., Esbensen, K. H., Solberg, R., Scheie, A., & Larsen, T., "Prediction of Petrophysical Parameters Based on Digital

- Video Core Images," *SPE Reservoir Evaluation and Engineering*, February 1998, pp. 82–87.
- Rhodes, C. N., & Brown, D. R., "Rapid Determination of the Cation Exchange Capacity of Clays Using Co(II)," *Clay Minerals Journal*, Vol. 29, 1994, pp. 799–801.
- Rink, M., & Schopper, J. R., "On the Application of Image Analysis to Formation Evaluation," *The Log Analyst*, January–February 1978, pp. 12–22.
- Rueslåtten, H., Eidesmo, T., Lehne, K. A., & Relling, O. M., "The Use of NMR Spectroscopy to Validate NMR Logs from Deeply Buried Reservoir Sandstones," *Journal of Petroleum Science and Engineering*, Vol. 19, 1998, pp. 33–43.
- Saner, S., Al-Harathi, A., & Htay, M. T., "Use of Tortuosity for Discriminating Electro-Facies to Interpret the Electrical Parameters of Carbonate Reservoir Rocks," *Journal of Petroleum Science and Engineering*, Vol. 16, 1996, pp. 237–249.
- Scott Jr., T. E., Zaman, M. M., & Roegiers, J.-C., "Acoustic-Velocity Signatures Associated with Rock-Deformation Processes," *Journal of Petroleum Technology*, June 1998, pp. 70–74.
- Sharma, M. M., "Transport of Particulate Suspensions in Porous Media," Ph.D. Dissertation, University of Southern California, 1985, 342 p.
- Skopec, R.A., "Recent Advances in Rock Characterization," *The Log Analyst*, May–June 1992, pp. 270–284.
- Tamura, H., Tanaka, A., Mita, K.-Y., & Furuichi, R., "Surface Hydroxyl Site Densities on Metal Oxides as a Measure for the Ion-Exchange Capacity," *Journal of Colloid and Interface Science*, Vol. 209, 1999, pp. 225–231.
- Tremblay, B., Sedgwick, G., & Vu, D., "CT-Imaging of Wormhole Growth Under Solution-Gas Drive," SPE 39638 paper, Proceedings of the 1998 SPE/DOE Improved Oil Recovery Symposium, Tulsa, Oklahoma, April 19–22, 1998, pp. 367–382.
- Unalmiser, S., & Funk, J. J., "Engineering Core Analysis," *Journal of Petroleum Technology*, April 1998, pp. 106–114.
- Weber, K. J., "How Heterogeneity Affects Oil Recovery," in *Reservoir Characterization*, L. W. Lake & H. B. Carroll, Jr. (eds.), Academic Press, Inc., Orlando, Florida, 1986, pp. 487–544.
- Wellington, S. L., & Vinegar, H. J., "X-Ray Computerized Tomography," *Journal of Petroleum Technology*, August 1987, pp. 885–898.
- Xiao, L., Piatti, C., Giacca, D., Nicula, S., & Gallino, G., "Studies on the Damage Induced by Drilling Fluids in Limestone Cores," SPE 50711 paper, Proceedings of the 1999 SPE International Symposium on Oilfield Chemistry, Houston, Texas, February 16–19, 1999, pp. 105–117.

Part II

Characterization of the Porous Media Processes for Formation Damage

**Accountability of Phases
and Species, Rock–Fluid–
Particle Interactions, and
Rate Processes**

Chapter 7

Multi-Phase and Multi-Species Transport in Porous Media*

Summary

The fundamental concepts, definitions, expression of species content, and conservation laws in multi-phase and species environments in porous media are presented in this chapter by expanding the overview and developments given by Civan (1993, 1996).

Multi-Phase and Species Systems in Porous Media

The reservoir formation is considered in three parts: (1) the stationary or deforming solid phase containing (a) porous matrix made from detrital grains, minerals and clays, and (b) the immobile materials attached to the pore surface including authigenic or diagenetic minerals and clays; various deposits; scale forming precipitates such as wax, asphaltene, sulfur, and gels; trapped gas, connate water and residual oil; (2) the flowing or mobile fluid phases including (a) gas, (b) oil, (c) brine, and (d) chemicals used for improved recovery; (3) various types of species that the solid and fluid phases may contain.

Typical species are (1) ions including the anions such as Cl^- , HCO_3^- , CO_3^{2-} , SO_4^{2-} and the cations such as K^+ , Na^+ , Ca^{+2} , Ba^{+2} , Mg^{+2} ; (2) molecules such as CH_4 , CO_2 , H_2S , N_2 , molasses, polymers, surfactants, paraffin, asphaltene, and resins; (3) pseudocomponents such as gas, oil, and brine with prescribed compositions; (4) particulates such as minerals, clays,

* After Civan, ©1996 SPE; parts reprinted by permission of the Society of Petroleum Engineers from SPE 31101 paper.

sand, gels, paraffin, asphaltene, sulfur, precipitates, crystalline matter, mud fines, debris, and bacteria; and (5) associates such as the pairs of ions and molecules, coagulates of various particulates, micelles, and microemulsions.

The characteristics of the particulates play an important role in formation damage. Based on their characteristics, particles can be classified as: (1) indigenous, in-situ generated, or externally introduced; (2) dissolved or nondissolved; (3) water-wet, mixed-wet, or oil-wet; (4) deformable (soft) or nondeformable (hard); (5) sticky or nonsticky; (6) swelling or nonswelling; (7) organic or inorganic; (8) reactive or inert; (9) biological or nonbiological; (10) growing or nongrowing; and (11) associating or nonassociating.

The species content of a system can be expressed in a variety of alternative ways:

1. mass concentration (all species)

$$c_i = \frac{\text{mass of } i}{\text{volume of mixture}} \quad (7-1)$$

2. molar concentration (preferred for dissolved species)

$$C_i = \frac{c_i}{M_i} = \frac{\text{mass concentration of } i}{\text{molecular weight of } i} = \frac{\text{mole of } i}{\text{volume of mixture}} \quad (7-2)$$

3. mass fraction (all species)

$$w_i = \frac{c_i}{\rho} = \frac{\text{mass concentration of } i}{\text{density of mixture}} = \frac{\text{mass of } i}{\text{mass of mixture}} \quad (7-3)$$

4. mole fraction (preferred for dissolved species)

$$x_i = \frac{\text{moles of } i}{\text{moles of mixture}} \quad (7-4)$$

5. volume fraction (preferred for particulates)

$$\sigma_i = \frac{c_i}{\rho_i} = \frac{\text{mass concentration of } i}{\text{density of } i} = \frac{\text{volume of } i}{\text{volume of mixture}} \quad (7-5)$$

6. volume ration (preferred for particulates)

$$n_{ik} = \frac{\text{volume of } i}{\text{volume of } k} \quad (7-6)$$

The relationship between volume fraction and volume ratio is given by:

$$\sigma_i = \frac{n_i}{1 + \sum_j n_j} \quad (7-7)$$

Frequently, conversion between the various ways of expressing the species content are required for various purposes. Some of these are presented in the following.

The conversion between mole and mass fractions are given by:

$$x_i = (w_i/M_i) / \sum_j (w_j/M_j) \quad (7-8)$$

and

$$w_i = x_i M_i / \left(\sum_j x_j M_j \right) \quad (7-9)$$

The mass concentration of species i in a mixture can be expressed per unit volume of another species k as:

$$\tilde{c}_{ik} = w_i / (w_k / \rho_k) = \frac{\text{mass of } i}{\text{volume of } k} \quad (7-10)$$

The mass concentration of species i in a mixture can be expressed in terms of its mass fraction as:

$$c_i = w_i / \sum_j (w_j / \rho_j) \quad (7-11)$$

The volume fraction of species i in a mixture can also be expressed in terms of its mass fraction as:

$$\sigma_i = (w_i / \rho_i) / \sum_j (w_j / \rho_j) \quad (7-12)$$

The volume fraction of species i can be expressed in terms of the volume ratio as:

$$\sigma_i = \frac{n_{ik}}{1 + \sum_{j \neq k} n_{jk}} \quad (7-13)$$

In the following formulations, the various phases (solid and fluid) in porous media are denoted by j , s denotes the solid phase, n is the total number of phases, ϵ_j is the volume fraction of the j^{th} phase in porous media, ϕ is the porosity of porous media, and S_j is the saturation or volume fraction of j^{th} phase in the pore space.

The following equations can be written:

$$\epsilon_s = 1 - \phi \quad (7-14)$$

$$\epsilon_j = \phi S_j : j = w, o, g \quad (7-15)$$

$$\sum_j^n \epsilon_j = 1.0, \sum_j^{n-s} S_j = 1.0, \sum_i w_{ij} = 1.0, \sum_i \sigma_{ij} = 1.0, \sum_i x_{ij} = 1.0 \quad (7-16)$$

$$\sum_i c_{ij} = \rho_j \quad (7-17)$$

The density and velocity of a mixture is given by the volume fraction weighted averages, respectively, as:

$$\rho = \sum_i \sigma_i \rho_i \quad (7-18)$$

and

$$\rho v = \sum_i \sigma_i \rho_i v_i \quad (7-19)$$

Therefore, the density and velocity of a mixture are variable when the composition varies even if the constituents are incompressible.

For incompressible systems, it is more convenient to use volumetric balance equations. Therefore, Eqs. 7-18 and 7-19 are replaced by:

$$1 = \sum_i \sigma_i \quad (7-20)$$

$$v = \sum_i \sigma_i v_i \quad (7-21)$$

Several other relationships, which may be convenient to use in the formulation of the transport phenomena in porous media, are given in the following:

The volume flux, u_j , and the velocity, v_j , of a phase j are related by:

$$\bar{u}_j = (\epsilon_j - \epsilon_{jr}) \bar{v}_j \quad (7-22)$$

where ϵ_{jr} is the volume fraction of the irreducible phase j in porous media. When an irreducible residual fluid saturation, S_{jr} exists in porous media, Eq. 7-22 should be substituted into Eq. 7-15 for the flowing phase volume flux as:

$$\bar{u}_j = \phi (S_j - S_{jr}) \bar{v}_j \quad (7-23)$$

In deforming porous media, the volumetric flux of the solid phase can be expressed in terms of the velocity according to the following equation:

$$\bar{u}_s = \epsilon_s \bar{v}_s \quad (7-24)$$

where ϵ_s and v_s denote the solid phase volume fraction and velocity, respectively.

Substituting Eq. 7-14, Eq. 7-24 becomes:

$$\bar{u}_s = (1 - \phi) \bar{v}_s \quad (7-25)$$

Accounting for the immobile fluid fraction, ϵ_{jr} , in deforming porous media, the volumetric flux of the fluid relative to the deforming solid phase is given by Civan (1994, 1996):

$$\bar{u}_{rj} = (\epsilon_j - \epsilon_{jr}) (\bar{v}_j - \bar{v}_s) = \bar{u}_j - \left(\frac{\epsilon_j - \epsilon_{jr}}{\epsilon_s} \right) \bar{u}_s \quad (7-26)$$

The volume fraction of species i of phase j in the bulk system is given by:

$$\epsilon_{ij} = \epsilon_j \sigma_{ij} \quad (7-27)$$

or by

$$\rho_i \epsilon_{ij} = \epsilon_{kj} \tilde{c}_{ikj} \quad (7-28)$$

The mass concentration of species i in phase j is given by:

$$c_{ij} = \rho_i \sigma_{ij} \quad (7-29)$$

The molar concentration of species i in phase j is given by:

$$C_{ij} = c_{ij} / M_i \quad (7-30)$$

The volume flux of species i in phase j is given by:

$$u_{ij} = \sigma_{ij} u_{rj} \quad (7-31)$$

where u_{rj} is the volume flux of phase j .

The mass flux of species i in phase j is given by:

$$m_{ij} = c_{ij} u_{rj} = \tilde{c}_{ikj} u_{rkj} \quad (7-32)$$

Multi-Species and Multi-Phase Macroscopic Transport Equations

The macroscopic description of transport in porous media is obtained by elemental volume averaging (Slattery, 1972). The formulations of the macroscopic equations of conservations in porous media have been carried out by many researchers. A detailed review of these efforts is presented by Whitaker (1999). The mass balances of various phases are given by (Civan, 1996, 1998):

$$\partial/\partial t (\epsilon_j \rho_j) + \vec{\nabla} \cdot (\rho_j \vec{u}_j) = \vec{\nabla} \cdot (\epsilon_j \vec{D}_j \cdot \vec{\nabla} \rho_j) + \epsilon_j \dot{m}_j \quad (7-33)$$

where u_{rj} is the fluid flux relative to the solid phase, t is the time and $\vec{\nabla} \cdot$ is the divergence operator. ρ_j is the phase density. \dot{m}_j is the net mass rate of the phase j added per unit volume of phase j . \vec{D}_j is the hydraulic dispersion coefficient which has been omitted in the petroleum engineering literature.

The species i mass balance equations for the water, oil, gas and solid phases are given by:

$$\partial/\partial t(\epsilon_j \rho_j w_{ij}) + \bar{\nabla} \cdot (\rho_j w_{ij} \bar{u}_{rj}) + \bar{\nabla} \cdot \bar{j}_{ij} = \epsilon_j \dot{m}_{ij} \quad (7-34)$$

in which w_{ij} is the mass fraction of species i in the j^{th} phase. \bar{j}_{ij} denotes the spontaneous or dispersive mass flux of species i in the j^{th} phase given by modifying the equation by Olson and Litton (1992):

$$\bar{j}_{ij} = -\epsilon_j \rho_j \left[\bar{D}_{ij} \cdot \bar{\nabla} w_{ij} + \frac{w_{ij}}{kT} \bar{D}_{ij} \cdot \bar{\nabla} \Phi_{ij} + \sum_s \frac{w_{ij}}{w_{sj}} \bar{D}_{sj} \cdot \bar{\nabla} w_{sj} \right] \quad (7-35)$$

where \bar{D}_{ij} is the coefficient of dispersion of species i in the j^{th} phase, k is the Boltzmann constant, and T is temperature. The first term represents the ordinary dispersive transport by concentration gradient. For particulate species of relatively large sizes the first term may be neglected. The second term represents the dispersion induced by the gradient of the potential interaction energy, Φ_{ij} . When the particles are subjected to uniform interaction potential field then the second term drops out. The third term represents the induced dispersion of bacterial species by substrate or nutrient, S , concentration gradient due to the chemotaxis phenomena (Chang et al., 1992). \bar{D}_{sj} is the substrate dispersion coefficient.

Incorporating Eq. 7-33 into Eq. 7-34 leads to the following alternative form:

$$\rho_j \left(\epsilon_j \partial w_{ij} / \partial t + \bar{u}_{rj} \cdot \bar{\nabla} w_{ij} \right) + \bar{\nabla} \cdot \bar{j}_{ij} = \epsilon_j \left(\dot{m}_{ij} - w_{ij} \dot{m}_j \right) \quad (7-36)$$

Adding Eq. 7-34 over all the phases gives the total species i mass balance equation as:

$$\partial/\partial t \left(\sum_{j=1}^n \epsilon_j \rho_j w_{ij} \right) + \bar{\nabla} \cdot \left(\sum_{j=1}^n \rho_j w_{ij} \bar{u}_{rj} \right) + \bar{\nabla} \cdot \left(\sum_{j=1}^n \bar{j}_{ij} \right) = \sum_{j=1}^n \epsilon_j \dot{m}_{ij} \quad (7-37)$$

Considering the possibility of the inertial flow effects due to the narrowing of pores by formation damage, the Forchheimer (1901) equation is used for the momentum balance. Although more elaborate forms of the macroscopic equation of motion are available, Blick and Civan (1988) have shown that Forchheimer's equation is satisfactory for all practical

purposes. The Forchheimer equation for multi-dimensional and multi-phase fluids flow can be written for the j^{th} phase as (Civan, 1994; Tutu et al., 1983; Schulenberg and Müller, 1987):

$$-\bar{\nabla}\Psi_j = v_j K_{rj}^{-1} \bar{K}^{-1} \cdot \bar{u}_{rj} + |\bar{u}_{rj}| \eta_{rj}^{-1} \bar{\eta}^{-1} \cdot \bar{u}_{rj} + \rho_j^{-1} S_j^{-1} \bar{F}_j \quad (7-38)$$

in which \bar{F}_j is the interfacial drag force, $\eta_{rj} = k_{rj}$ (Liu et al., 1995), $\eta = 1/\beta$ and Ψ is the flow potential given by:

$$\Psi = \int_{p_o}^p \frac{dp}{\rho} + g(z - z_o) + \Omega \quad (7-39)$$

where the first term is the fluid-content-dependent potential or simply the negative of the “effective stress” due to the interactions of the fluid with the pore surface, g is the gravitational acceleration, $g(z - z_o)$ is the potential of fluid due to gravity, z is the positive upward distance measured from a reference at z_o , and Ω is the overburden potential, which is the work of a vertical displacement due to the addition of fluid into porous media (Smiles and Kirby, 1993).

\bar{K} and $\bar{\beta}$ denote the Darcy or laminar permeability and the non-Darcy or inertial flow coefficient tensors, respectively. K_{rj} and β_{rj} are the relative permeability and relative inertial flow coefficient, respectively.

Eq. 7-38 can be written as, for convenience

$$\bar{u}_{rj} = -v_j^{-1} K_{rj} \bar{N}_{ndj} \cdot \bar{K} \cdot \bar{\nabla}\Psi_j \quad (7-40)$$

in which v is the kinematic viscosity (or momentum diffusivity) given by

$$v_j = \mu_j / \rho_j \quad (7-41)$$

and \bar{N}_{nd} is the non-Darcy number for anisotropic porous media given by, neglecting the interfacial drag force F_j :

$$\bar{N}_{ndj} = [\bar{I} + \bar{Re}_j]^{-1}, \quad \bar{O} \leq \bar{N}_{ndj} \leq \bar{I} \quad (7-42)$$

where \bar{I} denotes a unit tensor and \bar{Re}_j is the tensor Reynolds number for flow of phase j in an anisotropic porous media given by

$$\bar{Re}_j = v_j^{-1} |\bar{u}_{rj}| \cdot \bar{K} \cdot \bar{\beta} \quad (7-43)$$

$$|\vec{u}_{rj}| = (u_{rx}^2 + u_{ry}^2 + u_{rz}^2)^{1/2} \quad (7-44)$$

The permeability and inertial flow coefficient for porous materials are determined by means of laboratory core flow data and thus correlated empirically (Civan and Evans, 1998). Liu et al. (1995) give:

$$\beta = \frac{8.91 \times 10^8 \tau}{\phi k} \quad (7-45)$$

where β is in ft^{-1} , k is in mD , and ϕ is in fraction.

The energy balance equations for the water, oil, gas, and solid phases are given by:

$$\begin{aligned} \partial/\partial t (\epsilon_j \rho_j H_j) + \vec{\nabla} \cdot (\rho_j H_j \vec{u}_{rj}) &= \vec{\nabla} \cdot (\epsilon_j \vec{k}_j \cdot \vec{\nabla} T_j) \\ + \partial/\partial t (\epsilon_j p_j) + \vec{u}_{rj} \cdot \vec{\nabla} p_j + \epsilon_j &\left(q_j + \sum_{\substack{\alpha=1 \\ \alpha \neq j}}^n q_{j,\alpha} \right) \end{aligned} \quad (7-46)$$

q_j and $q_{j,\alpha}$ denote the external and interface heat transfer to the phase j per unit volume of phase j ; \vec{k}_j is the thermal conductivity of phase j . Note that the enthalpy H_j and internal energy U_j per unit mass of phase j are related according to:

$$H_j = U_j + p_j/\rho_j \quad (7-47)$$

Thus, Eq. 7-46 can also be written as:

$$\begin{aligned} \partial/\partial t (\epsilon_j \rho_j U_j) + \vec{\nabla} \cdot (\rho_j H_j \vec{u}_{rj}) \\ = \vec{\nabla} \cdot (\epsilon_j \vec{k}_j \cdot \vec{\nabla} T_j) + \vec{u}_{rj} \cdot \vec{\nabla} p_j + \epsilon_j &\left(q_j + \sum_{\substack{\alpha=1 \\ \alpha \neq j}}^n q_{j,\alpha} \right) \end{aligned} \quad (7-48)$$

When the system is at thermal equilibrium (i.e. $T_w = T_o = T_g = T_s = T$) then Eq. 7-48 can be written for each phase and then added to obtain the total energy balance equation as:

$$\begin{aligned}
& \partial/\partial t \left(\sum_{j=1}^n \epsilon_j \rho_j U_j \right) + \bar{\nabla} \cdot \left(\sum_{j=1}^n \rho_j H_j \bar{u}_{rj} \right) \\
& = \bar{\nabla} \cdot \left[\left(\sum_{j=1}^n \epsilon_j \bar{k}_j \right) \cdot \bar{\nabla} T \right] + \sum_{j=1}^n \bar{u}_{rj} \cdot \bar{\nabla} p_j + \sum_{j=1}^n \epsilon_j q_j
\end{aligned} \tag{7-49}$$

Invoking Eq. 7-33, Eq. 7-46 can be written in an alternative form as:

$$\begin{aligned}
& \rho_j \left[\epsilon_j \partial H_j / \partial t + \bar{u}_{rj} \cdot \bar{\nabla} H_j \right] = \partial / \partial t (\epsilon_j p_j) + \bar{u}_{rj} \cdot \bar{\nabla} p_j + \\
& \bar{\nabla} \cdot (\epsilon_j \bar{k} \cdot \bar{\nabla} T_j) + \epsilon_j (q_j + \sum_{\substack{\alpha=1 \\ \alpha \neq j}} q_{j,\alpha} - H_j \dot{m}_j)
\end{aligned} \tag{7-50}$$

The equation of motion given by Chase and Willis (1992), for deforming porous matrix can be written as following:

$$\epsilon_s \nabla \wp_s - \sum_j \epsilon_j \nabla \wp_j + \nabla \cdot \bar{\tau}_s + \left(\epsilon_s \rho_s - \sum_j \epsilon_j \rho_j \right) \bar{g} = 0 \tag{7-51}$$

where $\bar{\tau}_s$ is the shear stress tensor for the solid matrix.

The jump mass balance equations, given by Slattery (1972) can be simplified to express the boundary conditions as:

$$\left[\rho_s (\bar{u}_s - \bar{u}^\sigma) \cdot \bar{n}^\sigma \right] = r_s^\sigma \tag{7-52}$$

$$\left[\rho_j (\bar{u}_j - \bar{u}^\sigma) \cdot \bar{n}^\sigma \right] = r_j^\sigma \tag{7-53}$$

$$\left[\rho_{ij} (\bar{u}_j - \bar{u}^\sigma) \cdot \bar{n}^\sigma \right] = r_{ij}^\sigma \tag{7-54}$$

The superscript σ denotes a quantity associated with the dividing surface, which is moving at a macroscopic velocity of \bar{u}^σ , and \bar{n}^σ is the unit vector normal to the dividing surface. r_s^σ , r_j^σ and r_{ij}^σ are the rates of addition of mass of the porous matrix, the j^{th} phase, and the species i

in the j^{th} phase, respectively. $\llbracket \dots \rrbracket$ denotes a jump in a quantity across a dividing surface defined by:

$$\llbracket \dots \rrbracket \equiv (\dots)^+ - (\dots)^- \quad (7-55)$$

where the signs + and - indicate the post and fore sides, respectively, of the dividing surface.

Exercises

1. Show that the balance of species i in phase j can also be expressed in the following forms:

$$\frac{\partial}{\partial t}(\epsilon_j c_{ij}) + \nabla \cdot (c_{ij} \mathbf{u}_{rj}) = \nabla \cdot [\epsilon_j \rho_j D_{ij} \cdot \nabla (c_{ij} / \rho_j)] + \epsilon_j \dot{m}_{ij} \quad (7-56)$$

$$\begin{aligned} & \frac{\partial}{\partial t}(\epsilon_j \rho_i \sigma_{ij}) + \nabla \cdot (\rho_i \sigma_{ij} \mathbf{u}_{rj}) \\ &= \nabla \cdot [\epsilon_j \rho_j D_{ij} \cdot \nabla (\rho_i \sigma_{ij} / \rho_j)] + \epsilon_j \dot{m}_{ij} \end{aligned} \quad (7-57)$$

2. Show that, for incompressible flow and incompressible species, Eq. 7-56 simplifies as

$$\frac{\partial}{\partial t}(\epsilon_j \sigma_{ij}) + \nabla \cdot (\sigma_{ij} \mathbf{u}_{rj}) = \nabla \cdot (\epsilon_j D_{ij} \cdot \nabla \sigma_{ij}) + \epsilon_j \dot{m}_{ij} / \rho_i \quad (7-58)$$

References

- Blick, E. F., & Civan, F., "Porous Media Momentum Equation for Highly Accelerated Flow," *SPE Reservoir Engineering*, Vol. 3, No. 3, 1988, pp. 1048-1052.
- Chang, M.-M., Bryant, R. S., Stepp, A. K., & Bertus, K. M. "Modeling and Laboratory Investigations of Microbial Oil Recovery Mechanisms in Porous Media," Topical Report No. NIPER-629, FC22-83FE60149, U.S. Department of Energy, Bartlesville, Oklahoma, 1992, p. 27.
- Chase, G. G., & Willis, M. S., "Compressive Cake Filtration," *Chem. Eng. Sci.*, Vol. 47, 1992, pp. 1373-1381.

- Civan, F., "Waterflooding of Naturally Fractured Reservoirs—An Efficient Simulation Approach," SPE Production Operations Symposium, March 21–23, 1993, Oklahoma City, Oklahoma, pp. 395–407.
- Civan, F. Predictability of Formation Damage: An Assessment Study and Generalized Models, Final Report, U.S. DOE Contract No. DE-AC22-90-BC14658, April 1994.
- Civan, F. "A Multi-Phase Mud Filtrate Invasion and Well Bore Filter Cake Formation Model," SPE Paper No. 28709, Proceedings of the SPE International Petroleum Conference & Exhibition of Mexico, October 10–13, 1994, Veracruz, Mexico, pp. 399–412.
- Civan, F. "A Multi-Purpose Formation Damage Model," SPE 31101 paper, Proceedings of the SPE Formation Damage Symposium, Lafayette, LA, February 14–15, 1996, pp. 311–326.
- Civan, F., "Quadrature Solution for Waterflooding of Naturally Fractured Reservoirs," *SPE Reservoir Evaluation and Engineering*, April 1998, pp. 141–147.
- Civan, F., & Evans, R. D., "Determining the Parameters of the Forchheimer Equation from Pressure-Squared vs. Pseudopressure Formulations," *SPE Reservoir Evaluation and Engineering*, February 1998, pp. 43–46.
- Forchheimer, P., "Wasserbewegung durch Boden," *Zeitz. ver. Deutsch Ing.* Vol. 45, 1901, pp. 1782–1788.
- Liu, X., Civan, F., & Evans, R. D. "Correlation of the Non-Darcy Flow Coefficient," *J. of Canadian Petroleum Technology*, Vol. 34, No. 10, 1995, pp. 50–54.
- Olson, T. M., & Litton, G. M. "Colloid Deposition in Porous Media and an Evaluation of Bed-Media Cleaning Techniques," Chapter 2, pp. 14–25, in *Transport and Remediation of Subsurface Contaminants, Colloidal, Interfacial, and Surfactant Phenomena*, Sabatini, D. A. and R. C. Knox (Eds.), ACS Symposium Series 491, American Chemical Society, Washington, DC (1992).
- Schulenberg, T., & Müller, U., "An Improved Model for Two-Phase Flow Through Beds of Coarse Particles," *Int. J. Multiphase Flow*, Vol. 13, No. 1, 1987, pp. 87–97.
- Slattery, J. C. *Momentum, Energy and Mass Transfer in Continua*, McGraw-Hill Book Co., New York, 1972, pp. 191–197.
- Smiles, D. E., & Kirby, J. M., "Compressive Cake Filtration—A Comment," *Chem. Eng. Sci.*, Vol. 48, No. 19, 1993, pp. 3431–3434.
- Tutu, N. K., Ginsberg, T., & Chen, J. C., "Interfacial Drag for Two-Phase Flow Through High Permeability Porous Beds," *Interfacial Transport Phenomena*, Chen, J. C. & Bankoff, S. G., (eds.), ASME, New York, pp. 37–44.
- Whitaker, S., *The Method of Volume Averaging*, Kluwer Academic Publishers, Boston, 1999, 219 p.

Chapter 8

Particulate Processes in Porous Media

Summary

Physico-chemical, chemical, hydrodynamic, and mechanical processes frequently lead to the mobilization, generation, migration and deposition of fine particles, which in turn cause formation damage in petroleum bearing formations.

This chapter is devoted to the review of the various types of internal particulate processes that occur in porous media, and the factors and forces affecting these processes.

Introduction

There are three primary sources of fine particles in petroleum bearing formations:

1. Invasion of foreign particles carried with the fluids injected for completion, workover, and improved recovery purposes,
2. Mobilization of in-situ formation particles due to the incompatibility of the fluids injected into porous media and by various rock-fluid interactions, and
3. Production of particulates by chemical reactions, and inorganic and organic precipitation.

Fluids injected into petroleum reservoirs usually contain iron colloids produced by oxidation and corrosion of surface equipment, pumps, steel casing, and drill string (Wojtanowicz et al., 1987). Brine injected for waterflooding may contain some fine sand and clay particles. Mud fines can invade the formation during overbalanced drilling. These are some examples of the externally introduced particles.

Petroleum bearing formation usually contains various types of clay and other mineral species attached to the pore surface. These species can be

released by colloidal forces or mobilized by hydrodynamic shear of the fluid flowing through porous media. Fine particles can also be generated by deformation of rock during compression and dilatation. This is due to variation of the net overburden stress and loss of the integrity of rock grains. Fine particles are unleashed and liberated because of the integrity loss of rock grains by chemical dissolution of the cementing materials in porous rock, such as by acidizing or caustic flooding. These are the typical internal sources of indigenous fine particles.

Particulate matter can be produced by various chemical reactions such as the salt formation reactions that occur when the seawater injected for waterflooding mixes with the reservoir brine, and formation of elemental sulfur during corrosion. Particulate matter can also be produced by precipitation due to the change of the thermodynamic conditions and of the composition of the fluids by dissolution or liberation of light gases (Amaefule et al., 1988). These are typical mechanisms of particle production in porous media.

Once entrained by the fluids flowing through porous media, the various particles migrate by four primary mechanisms (Wojtanowicz et al., 1987):

1. Diffusion
2. Adsorption
3. Sedimentation
4. Hydrodynamics

The transport of the fine particles are affected by six factors (Wojtanowicz et al., 1987):

1. Molecular forces
2. Electrokinetic interactions
3. Surface tension
4. Fluid pressure
5. Friction
6. Gravity

As the fine particles move along the tortuous flow pathways existing in porous media, they are captured, retained, and deposited within the porous matrix. Consequently, the texture of the matrix is adversely altered to reduce its porosity and permeability. Frequently, this phenomena is referred to as formation damage measured as the permeability impairment.

Particulate Processes

The various particulate processes, schematically depicted in Figure 8–1, can be classified in two groups as the internal and external processes.

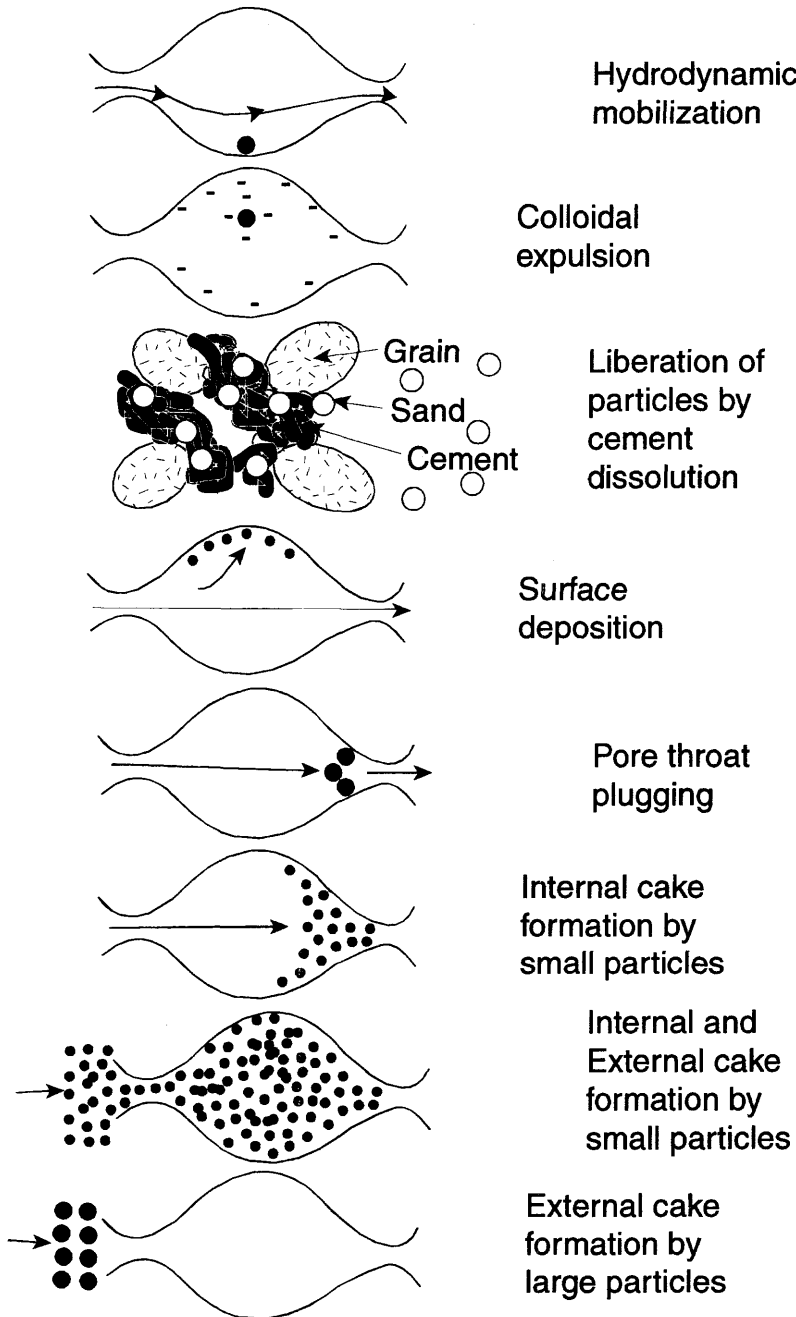


Figure 8-1. Various particulate processes.

The external processes occur over the formation face and are discussed in Chapter 12. The internal processes occur in the porous media and can be classified in three groups as (Civan, 1990, 1994, 1996):

1. Pore Surface Processes
 - a. Deposition
 - b. Removal
2. Pore Throat Processes
 - a. Plugging (screening, bridging, sealing, Figure 8–2)
 - b. Unplugging
3. Pore Volume Processes
 - a. In-Situ Cake Formation
 - b. In-Situ Cake Depletion
 - c. Migration
 - d. Generation and Consumption (chemical reactions, rock deformation and crushing, liberation of fine particles by chemical dissolution of cement, coagulation/disintegration)
 - e. Interphase Transport or Exchange

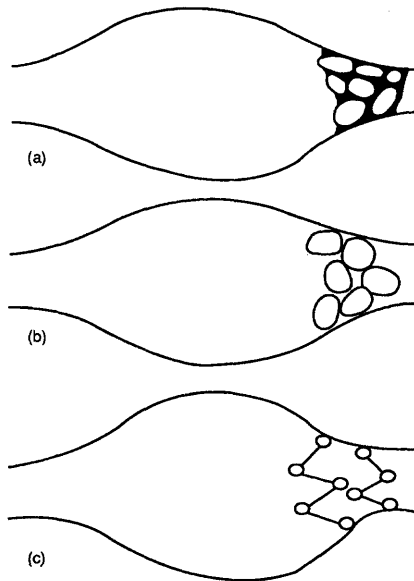


Figure 8–2. Mechanism of pore throat blocking: **a)** plugging and sealing, **b)** flow restriction, **c)** bridging (after Civan, 1994; reprinted by permission of the U.S. Department of Energy).

The net amount of particles deposited in porous media is expressed by:

Instantaneous amount of particles in porous matrix = initial amount of particles in porous matrix + net amount of particles deposited on pore surface + net amount of particles deposited behind pore throats.

The various particulate processes are depicted in Figure 8-3.
The fundamental particle generation mechanisms are:

1. Hydrodynamic mobilization
2. Colloidal expulsion
3. Liberation of particles due to the loss of integrity of rock grains by chemical dissolution of cement or by rock compression, crushing, and deformation
4. Chemical and physico-chemical formation

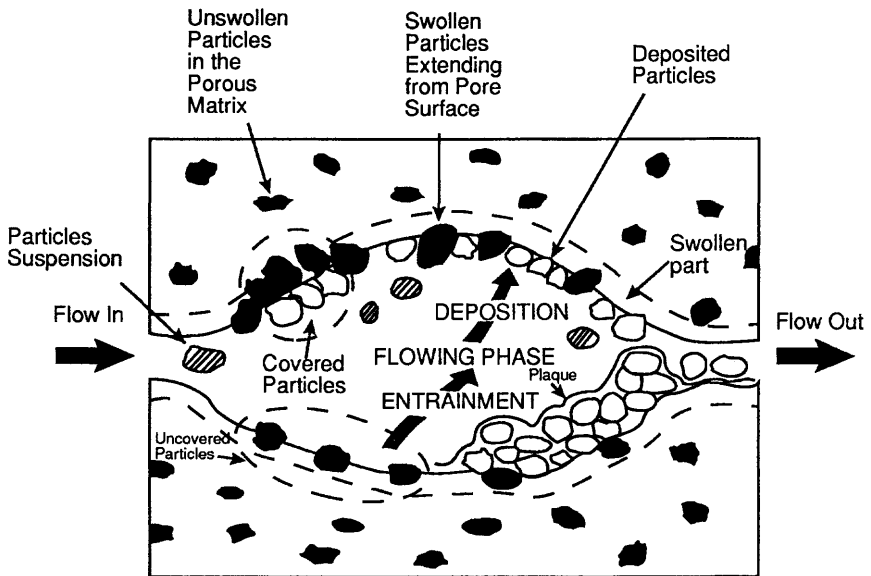


Figure 8-3. Particulate processes in porous media (after Civan, 1994; reprinted by permission of the U.S. Department of Energy, modified after Civan et al. 1989, from *Journal of Petroleum Science and Engineering*, Vol. 3, "Alteration of Permeability by Fine Particle Processes," pp. 65-79, ©1989, with permission from Elsevier Science).

The fundamental particle retention mechanisms are:

1. Surface deposition (physico-chemical)
2. Pore throat blocking (physical jamming)
3. Pore filling and internal filter cake formation (physical)
4. Screening and external filter cake formation (physical)

Forces Acting Upon Particles

Ives (1985) classified the various forces acting on particles in a flowing suspension in three categories as (a) forces related to the transport mechanisms, (b) forces related to the attachment mechanisms, and (c) forces related to the detachment mechanisms, and characterized them in terms of the relevant dimensionless groups.

Forces Related to the Transport Mechanisms

The important relevant quantities governing the particle behavior in a suspension can be summarized as following: d and D are particle and porous media grain diameters, respectively; ρ_s is the density of particles; ρ and μ are the density and viscosity of the carrier liquid, respectively; v_a is the convective velocity; g is the gravitational acceleration coefficient; and T is the absolute temperature.

Inertia Force. The inertia of a particle forces it to maintain motion in a straight line. The inertia force can be expressed by the dimensionless group as (Ives, 1985):

$$I = \frac{\rho_s d^2 v_a}{18\mu D} \quad (8-1)$$

Gravity Force. As a result of the density difference between the particle and the carrier liquid, particles tend to move in the gravity direction according to Stokes' law. The velocity of a spherical particle undergoing a Stokes' motion is given by:

$$v_s = (\rho_s - \rho)gd^2/(18\mu) \quad (8-2)$$

The gravity force acts upward when particles are lighter and, therefore, buoyant. The gravity force acts downward when particles are heavier and, therefore, tend to settle. The gravity force can be expressed by a

dimensionless group, which relates the Stokes and convection velocities as (Ives, 1985):

$$G_g = \frac{g(\rho_s - \rho)d^2}{18\mu v_a} \quad (8-3a)$$

Centrifugal Forces. The centrifugal forces are generated by external acceleration. The centrifugal force created with an angular velocity of ω and a radius of R is expressed in dimensionless form by

$$G_c = \frac{R\omega^2(\rho_s - \rho)d^2}{18\mu v_a} \quad (8-3b)$$

Diffusion Force. Particles smaller than 1 mm diameter tend to move irregularly in a liquid media and disperse randomly. This phenomena is called the Brownian motion. The diffusivity of fine particles undergoing a Brownian motion is given by Einstein (McDowell-Boyer et al., 1986):

$$D = KT/(3\pi\mu d) \quad (8-4)$$

The diffusion force can be expressed by the Peclet number as the ratio of the convection velocity to the average Brownian velocity given by (Ives, 1985).

$$Pe = \frac{3\pi\mu d v_a}{KT} \quad (8-5)$$

where $\pi = 3.1459\dots$ and $K = 1.38 \times 10^{-23}$ is Boltzmann's constant.

Hydrodynamic Force. Hydrodynamic forces are the fluid shearing and pressure forces (Wojtanowicz et al., 1987, 1988). Ives (1985) explains that during fluid flow secondary circulation flows can be formed around the particles, which can generate out-of-balance hydrodynamic forces acting on the particles to move them across the flow field. Ives (1985) states that a proper dimensionless group rigorously expressing the hydrodynamic force is not available. Ives (1985) points out that the Reynolds number given by:

$$Re = \frac{v_a D \rho}{\mu} \quad (8-6)$$

and its other forms such as those “relating to the shear gradient, the relative velocity between particle and liquid, the angular velocity of the rotating particle, and the frequency of pulsation liquid have been suggested.”

Khilar and Fogler (1987) expressed the hydrodynamic lift force pulling a spherical particle off the pore surface by the following equation given by Hallow (1973):

$$F_L \cong 8d^2(\mu\rho K)^{1/2}u_s \quad (8-7)$$

where u_s is the slip velocity, K is the linearized velocity gradient near the particle, and d is the diameter of the spherical particle.

Forces Related to the Attachment Mechanisms

These forces act on the particles when they are near the grain surface less than a 1 μm distance (Ives, 1985). These forces and the characteristic dimensionless groups are described below.

London—van der Waals Force. This is the attractive force due to the electromagnetic waves generated by the electronic characteristics of atoms and molecules. The attraction force is expressed by (Ives, 1985):

$$F_{vw}(s) = \frac{1}{(s-2)^2} F_n \left(\frac{s-2}{\bar{\lambda}} \right) \quad (8-8)$$

in which $\bar{\lambda}$ is a dimensionless wavelength of the dispersion force divided by πd product and F_n is a function assuming different forms for $(s-2)/\bar{\lambda}$ less and greater than unity.

Friction—Drag Force and Hydrodynamic Thinning. Particles approaching the grain surfaces experience a flow resistance because they must displace the liquid at the surface radially as they attach to the grain surface (Ives, 1985; Khilar and Fogler, 1987).

Forces Related to the Detachment Mechanisms

Shearing Force. This is the friction or drag force. When the shear stress of the liquid flowing over the deposited particles creates a shearing force greater than those attaching the particles to the grain surface, then the particles can be detached and mobilized (Ives, 1985):

$$\tau = \mu \frac{dv}{dr} \quad (8-9)$$

Electrostatic Double-Layer Force. These forces are created due to the ionic conditions measured by pH and ionic strength. When the particle and grain surfaces carry the electrostatic charges of the same sign, they repel each other. The repulsive force is expressed by (Ives, 1985):

$$F_R(s) = \frac{\exp[-kd(s-2)]}{1 + \exp[-kd(s-2)]} \quad (8-10)$$

where s is the dimensionless separation distance expressed as the ratio of the radial separation distance divided by the particle radius ($d/2$), k is the Debye reciprocal double-layer thickness, and d is the particle diameter. When the ionic strength is higher, then the double-layer thickness is smaller, and hence k is larger.

Born Repulsion Force. This force is generated as a result of the overlapping of the electron clouds (Wojtanowicz et al., 1987, 1988).

Rate Equations for Particulate Processes in Porous Matrix

Ohen and Civan (1993) classified the indigenous particles that are exposed to solution in the pore space in two groups: lump of total expansive (swelling, that is, total authigenic clay that is smectitic) and lump of total nonexpansive (nonswelling) particles, because of the difference of their rates of mobilization and sweepage from the pore surface. They considered that the particles in the flowing suspension are made of a combination of the indigenous particles of porous media entrained by the flowing suspension and the external particles introduced to the porous media via the injection of external fluids. They considered that the particles of the flowing suspension can be redeposited and reentrained during their migration through porous media and the rates of mobilization of the redeposited particles should obey a different order of magnitude than the indigenous particles of the porous media. Further, they assumed that the deposition of the suspended particles over the indigenous particles of the porous media blocks the indigenous particles and limits their contact and interaction with the flowing suspension in the pore space. They considered that the swelling clays of the porous media can absorb water and swell to reduce the porosity until they are mobilized by the flowing suspension.

The rate at which the various particulate processes occur in porous media can be expressed by empirical equations. These equations can also be considered as the particulate material balance equations for the porous matrix. Here they are written as volume balance of particles.

Surface Deposition

The rate of surface deposition is proportional to the particle mass flux, $u\sigma_p$, where σ_p is the particle volume concentration in the flowing suspension, and the pore surface available for deposition that relates to $\phi^{2/3}$ (Lichtner, 1992; Civan, 1995, 1996); k_d is a deposition rate constant; α is a stationary deposition factor expressing deposition at stationary conditions; and ε_d is the volume fraction of the particles in the bulk media retained at the pore surface. Thus, the surface deposition rate equation is given by:

$$\frac{d\varepsilon_d}{dt} = k_d(\alpha + u)\sigma_p\phi^{2/3} \quad (8-11)$$

subject to

$$\varepsilon_d = \varepsilon_{do}, t = 0 \quad (8-12)$$

Pore Filling After Pore Throat Plugging

As stated by Chang and Civan (1991, 1992, 1997) and Ochi and Vernoux (1998), pore throats act like gates connecting the pores and create a “gate or valve effect,” indicated by a severe reduction of permeability as they are plugged by particles and shut off (see Figure 8-2). Let ε_t represent the volume fraction of the particles in the bulk media captured and retained behind the pore throats. The pore filling following the pore throat plugging leads to an internal cake formation at a rate proportional to the particle flux, $u\sigma_p$, and the pore volume, ϕ , available.

$$\frac{\partial \varepsilon_t}{\partial t} = k_t u \sigma_p \phi \quad (8-13)$$

subject to

$$\varepsilon_t = \varepsilon_{to}, t = 0 \quad (8-14)$$

k_t is a pore filling rate constant given by:

$$k_t \neq 0 \text{ for } t > t_{cr} \text{ when } \beta < \beta_{cr} \quad (8-15)$$

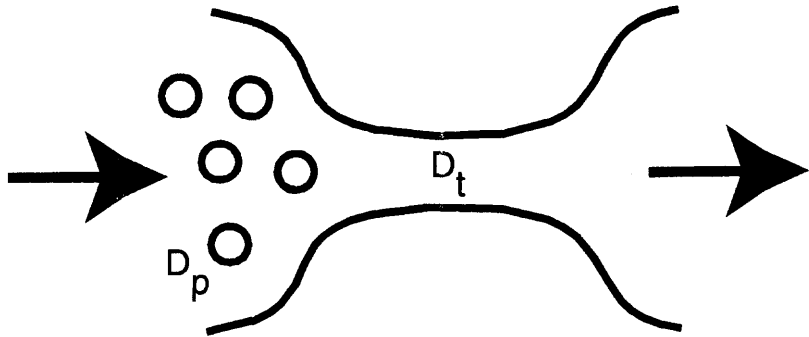


Figure 8-4. Particles approaching a pore throat.

and

$$k_t = 0 \text{ otherwise} \quad (8-16)$$

t_{cr} represents the critical time when the pore throats are first jammed by particles.

This time is similar to the screen-factor. Himes et al. (1991) define the screen-factor as:

A screen-factor value is the time for a given volume of a solution to pass through a network of five 100-U.S.-mesh screens stacked together and normalized to the time taken for the carrier fluid alone (usually water). A higher screen-factor value means less mobility and poor injectivity. A value of one indicates equal mobility to the carrier fluid.

β is the pore throat to particle diameter ration given by (see Figure 8-4):

$$\beta = D_t / D_p \quad (8-17)$$

and β_{cr} is the critical value below which pore throat blocking can occur.

One of the factors affecting the particle migration through a pore throat is the particle size relative to the pore throat size. The hydraulic tube diameter is given by the Carman-Kozeny equation:

$$D = 4\sqrt{2} \sqrt{\frac{K}{\phi}} \quad (8-18)$$

The pore throat diameter can be estimated as a fraction, f , of the hydraulic tube diameter according to (Ohen and Civan, 1990, 1993):

$$D_t = fD \quad (8-19)$$

Then, the ration of the particle to pore throat diameters can be approximated by:

$$F_s \equiv \frac{1}{\beta} = \frac{D_p}{D_t} = \frac{D_p(\mu m)}{(0.18f/\sqrt{\phi})\sqrt{K(md)}} \quad (8-20)$$

King and Adegbesan (1997) state that the ratio of the median particle diameter to pore throat diameter is given by (Dullien, 1979):

$$F_s = \frac{D_p(\mu m)}{0.95\sqrt{K(md)}} \quad (8-21)$$

A comparison of Eqs. 8-20 and 21 implies that, even if $f=1.0$, Eq. 8-21 is applicable for tight porous media with a porosity of the order of $\phi \approx 0.04$.

The value of the parameter F_s or its reciprocal β indicates that the flow of a particulate suspension into porous media may lead to one of the following phenomena (King and Adegbesan, 1997):

- a. $\beta < 3$, external filtercake formation
- b. $3 < \beta < 7$, internal filtercake formation
- c. $\beta > 7$, negligible filtercake involvement

Pautz et al. (1989) point out that these rules-of-thumb have been derived based on experimental observations. The values 3 and 7 denote the critical values or β_{cr} . Note these values are very close to the values of 2 and 6 indicated by Figure 8-5 given by Gruesbeck and Collins (1982) for bridging of particles in perforations.

Civan (1990, 1996) determined β_{cr} empirically by correlating between two dimensionless numbers. In the pore throat plugging process, the mean pore throat diameter, D_t , mean particle diameter, D_p , particle mass concentration, c_p , viscosity of suspension, μ , and the interstitial velocity of suspension, $v = u/\phi$, are the important quantities. Therefore, a dimensional analysis among these variables leads to two dimensionless groups (Civan, 1996). The first is an aspect ratio representing the critical pore throat to particle diameter ratio necessary for plugging given by:

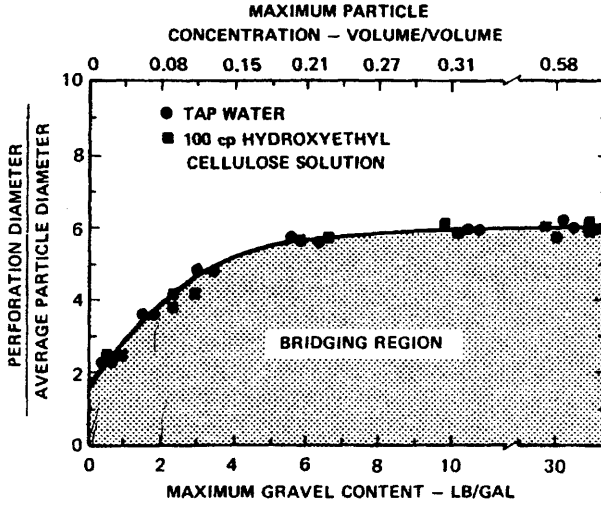


Figure 8-5. Chart for determination of the particle bridging conditions for perforations (Gruesbeck and Collins, ©1982 SPE; reprinted by permission of the Society of Petroleum Engineers).

$$\beta_{cr} = (D_t/D_p)_{cr} \quad (8-22)$$

and the second is the particle Reynolds number given by:

$$Re_p = c_p u D_p / (\mu \phi) \quad (8-23)$$

The relationship between β_{cr} and Re_p can be developed using experimental data. Inferred by the Gruesbeck and Collins (1982) data for perforation plugging, and by Rushton (1985) and Civan (1990, 1996), such a relationship is expected to obey the following types of expressions:

$$\beta_{cr} = A[1 - \exp(-B Re_p)] + C \quad (8-24)$$

or

$$\beta_{cr} = A(Re_p)^B + C \quad (8-25)$$

where A , B , and C are some empirical parameters. Figure 8-6 shows a plot of Eq. 8-24.

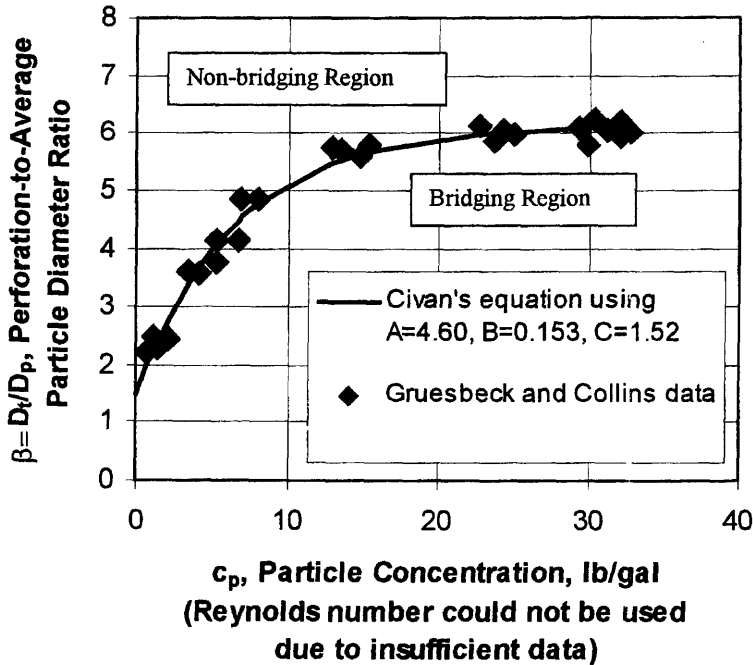


Figure 8–6. Chart for determination of the particle bridging conditions using the aspect ratio and particle Reynolds number (modified after Civan, 1994; reprinted by permission of the U.S. Department of Energy).

The above formulation is a simplistic approach. In reality, the pore and pore throat sizes are distribution functions, which vary by damage or stimulation, as shown in Figure 8–7. This can be considered by the methods developed by Ohen and Civan (1993) and Chang and Civan (1997), as described in Chapter 5.

Dislodgment and Redeposition of Particles at Pore Throats

Gruesbeck and Collins (1982) observed that the effluent particle concentration tended to fluctuate during constant flow rate experiments. Such phenomena did not occur during constant pressure difference experiments, which are more representative of the producing well conditions.

They explain this behavior by consecutive dislodgment and formation of plugs at the pore throats. They postulate that, in heterogeneous systems, when a suspension of particles of various sizes flow through a porous media made of a wide range of grain sizes, narrow pathways are likely to be plugged first, diverting the flow to wider pathways, which transfer

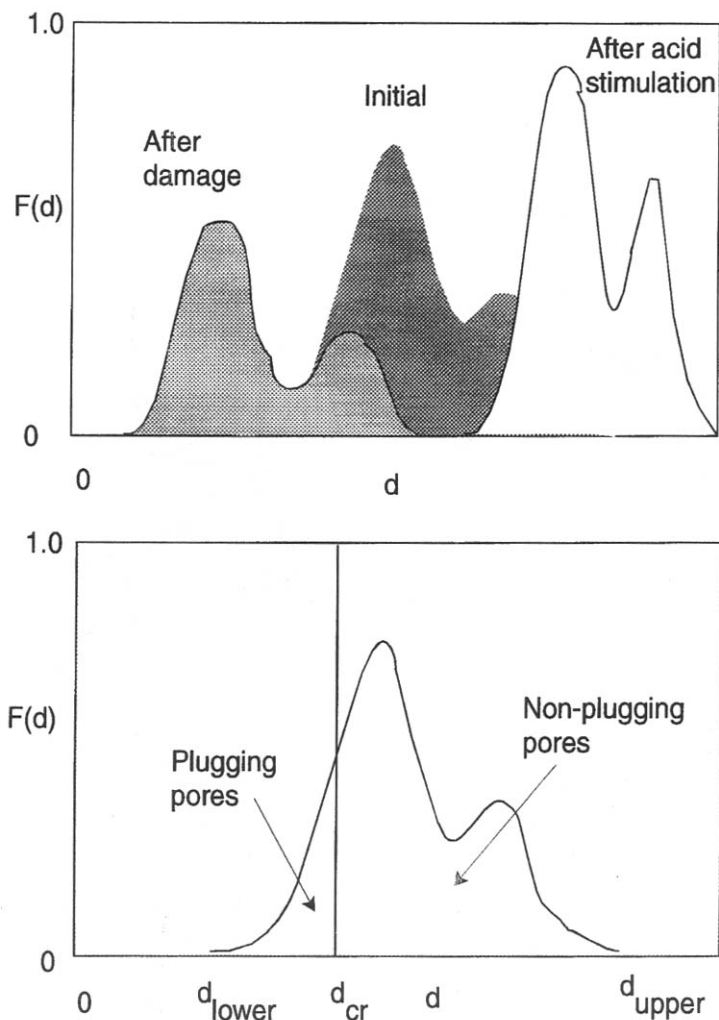


Figure 8-7. Alteration of pore throat size distribution by formation damage and acid stimulation

the particles to the effluent more effectively. However, as the flow paths are plugged, the pressure difference across the porous media may exceed the critical stress necessary to break some of the plugs. Therefore, these plugs break and release particles into the flowing media increasing its particle concentration. Subsequently, the deposition process progresses to form new plugs during which the flowing media particle concentration

decreases. Gruesbeck and Collins (1982) also observed a similar phenomena in systems of homogeneous grain sizes subjected to a constant rate injection of a suspension of particles.

Millan-Arcia and Civan (1992) have reported frequent fluctuations in the effluent fluid concentrations and pH during injection of brine into sandstone (see Figure 8–8).

Colloidal Release and Mobilization

Colloidal mobilization is a result of the physico-chemical reactions that involve electro-kinetic forces, zeta potential, and ionic strength (Wojtanowicz et al., 1987). Let ϵ_p denote the volume fraction of porous media occupied by the particles available for mobilization over the pore surface. The rate of colloidal expulsion or mobilization of particles at the pore surface is proportional to the excess critical salt concentration ($c_{cr} - c$),

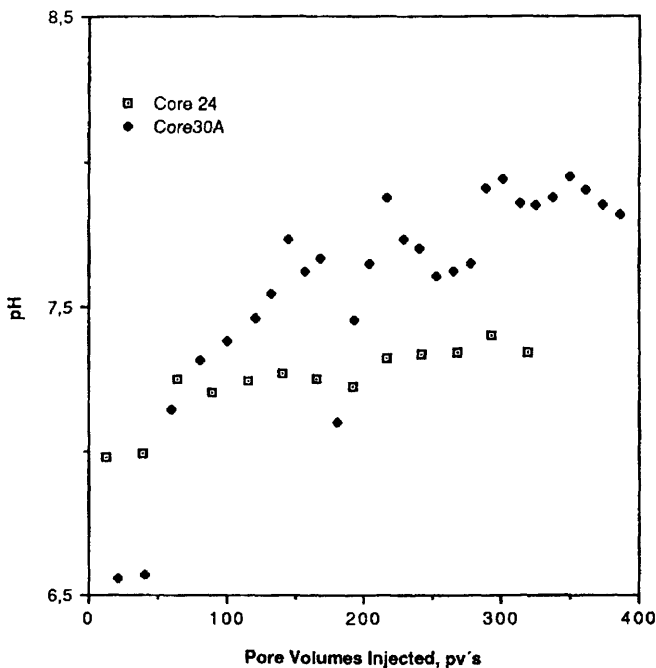


Figure 8–8. Effect of frequent pore throat plugging and unplugging by particles on the effluent solution pH (Arcia and Civan, ©1992; reprinted by permission of the Canadian Institute of Mining, Metallurgy and Petroleum).

and the amount of the unblocked particles at the pore surface available for mobilization, $\epsilon_p \eta_e$.

$$\frac{\partial \epsilon_r}{\partial t} = -(1 + \alpha) k_r \epsilon_p \eta_e \phi^{2/3} (c_{cr} - c) \quad (8-26)$$

subject to

$$\epsilon_r = \epsilon_{ro}, t = 0 \quad (8-27)$$

α is the volumetric expansion coefficient for swelling clays as described in Chapter 2; $\alpha = 0$ for nonswelling particles; c_{cr} is the critical salt concentration; and η_e is the fraction of the unblocked particles approximated by (see Figure 8-3) (Civan et al., 1989; Ohen and Civan, 1993; Civan, 1996):

$$\eta_e = \exp \left(-\lambda \sum_p \epsilon_p \right) \quad (8-28)$$

λ is an empirical constant; $\sum_p \epsilon_p$ represents the total volume of various types of particles retained within the pore space; k_r is a particle release rate constant given by (Khilar and Fogler, 1987, 1983; Kia et al., 1987):

$$k_r \neq 0 \text{ when } c < c_{cr} \quad (8-29)$$

and

$$k_r = 0 \text{ otherwise} \quad (8-30)$$

Hydraulic Erosion and Mobilization

The rate of hydraulic mobilization of the particles at the pore surface is proportional to the excess pore wall shear stress, $(\tau_w - \tau_{cr})$, and the amount of the unblocked particles available for mobilization at the pore surface (Gruesbeck and Collins, 1982; Khilar and Fogler, 1987; Cernansky and Siroky, 1985; Civan, 1992, 1996).

$$\frac{\partial \epsilon_e}{\partial t} = -(1 + \alpha) k_e \epsilon_p \eta_e \phi^{2/3} (\tau - \tau_{cr}) \quad (8-31)$$

subject to

$$\varepsilon_e = \varepsilon_{eo}, t = 0 \quad (8-32)$$

τ_{cr} is the critical shear stress and k_e is an erosion rate constant given by (Khilar and Fogler, 1987):

$$k_e \neq 0 \text{ when } \tau_w > \tau_{cr} \quad (8-33)$$

and

$$k_e = 0 \text{ otherwise} \quad (8-34)$$

There are several alternative ways of expressing the hydraulic force. The Rabinowitsch-Mooney equation for non-Newtonian fluid wall shear stress, τ_w , in pipes is given by (Metzner and Reed, 1955):

$$\tau_w = \frac{D}{4} \left(-\frac{\partial p}{\partial x} \right) = k' \left(\frac{8v}{D} \right)^{n'} \quad (8-35)$$

The non-Darcy equation can be modified by applying the capillary tubes analogy and the procedure by Ikoku and Ramey, Jr. (1979):

$$u^{n'} = (v\phi)^{n'} = \frac{N_{nd}K}{\mu_e} \left(-\frac{\partial p}{\partial x} \right) \quad (8-36)$$

where μ_e is the effective viscosity given by

$$\mu_e = N_{nd} 2^{(2+3n')} k' K / \left[D^{(1+n')} \phi^{n'} \right] \quad (8-37)$$

k' and n' are some empirical parameters, which assume $k' = \mu$ and $n' = 1$ for Newtonian fluids.

The critical shear stress, τ_{cr} , is a function of the particle stickiness to the surface characterized by the k_τ constant and the particle concentration at pore surface (Civan, 1990, 1996):

$$\tau_{cr} = k_\tau c_p^\alpha \quad (8-38)$$

where α is an empirical constant.

Based on Eqs. 8–35 and 8–36, the excess shear stress can be correlated for one-dimensional horizontal flow:

$$(\tau_w - \tau_{cr}) \sim \left[\frac{D}{4} \left(-\frac{\partial p}{\partial x} \right) - \tau_{cr} \right] \sim \left[\frac{u' \mu_e D}{4 N_{nd} K} - \tau_{cr} \right] \quad (8-39)$$

The previous studies are mostly limited to one-dimensional Newtonian fluid flow and they typically used (Civan et al., 1989; Khilar and Folger, 1987; Gruesbeck and Collins, 1982; Cernansky and Siroky, 1985; Ohen and Civan, 1989, 1990):

$$\begin{aligned} (\tau_w - \tau_{cr}) &\sim \left[(-\partial p / \partial x) - (-\partial p / \partial x)_{cr} \right] \sim \\ &\left[(u \mu / K) - (u \mu / K)_{cr} \right] \sim (u - u_{cr}) \end{aligned} \quad (8-40)$$

In general, for multi-dimensional flow (Civan, 1996)

$$(\tilde{\tau}_w - \tilde{\tau}_{cr}) \cdot \tilde{\delta} \sim \left[-1/4 \rho \tilde{D} \cdot \tilde{\nabla} \psi - \tilde{\tau}_{cr} \cdot \tilde{\delta} \right] \quad (8-41)$$

where ψ is the flow potential and \tilde{D} is the hydraulic tube diameter tensor for anisotropic media. $\tilde{\delta}$ is a unit vector.

Particle Transfer Across Fluid-Fluid Interfaces

The driving force for particle transfer between two fluid phases is the wettability of the fluid phases relative to the wettability of the particles. Particles prefer to be in the phase that wets them (Muecke, 1979) (see Figure 8–9 by Civan, 1994). But, mixed-wet particles tend to remain on the interface where they are most stable (Ivanov et al., 1986) (see Figure 8–10). In the region involving the interface between wetting and non-wetting phases, it can be postulated that particles A in a weaker wettability phase-1 first move to the interface and then migrate from the interface to a stronger wettability phase-2 according to the following consecutive processes (Civan, 1996):

$$\text{Nonwetting phase} - 1 \rightarrow \text{Interface} \rightarrow \text{Wetting phase} - 2 \quad (8-42)$$

Therefore, the following power-law rate expressions can be proposed:

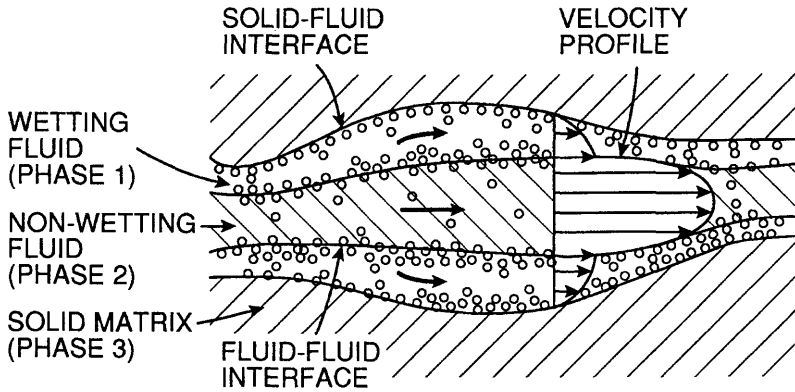


Figure 8-9. Particle retention at solid-fluid and fluid-fluid interfaces and the velocity profiles in multi-phase systems (after Civan, 1994; reprinted by permission of the U.S. Department of Energy).

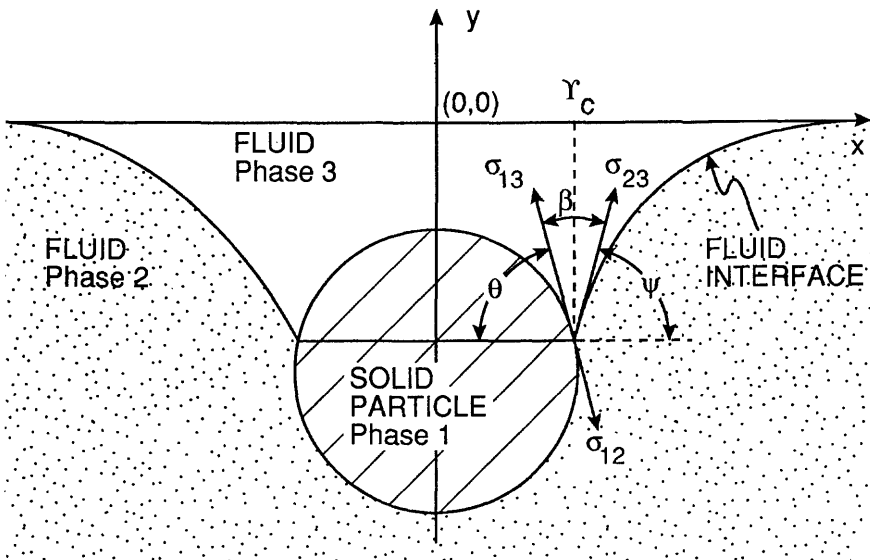


Figure 8-10. A particle stabilized at a fluid-fluid interface (modified after Ivanov et al., 1986; reprinted by permission of the author and Academic Press; after Civan, 1994; reprinted by permission of the U.S. Department of Energy).

$$\dot{R}_{A1} \equiv \frac{dR_{A1}}{d(t-t_{A1})} = -\lambda_{A1} R_{A1}^{\alpha_A} \quad (8-43)$$

$$\dot{R}_{A12} \equiv \frac{dR_{A12}}{d(t-t_{A12})} = \lambda_{A1} R_{A1}^{\alpha_A} - \lambda_{A2} R_{A12}^{\beta_A} \quad (8-44)$$

$$\dot{R}_{A2} \equiv \frac{dR_{A2}}{d(t-t_{A2})} = \lambda_{A2} R_{A12}^{\beta_A} \quad (8-45)$$

λ_{A1} and λ_{A2} are some rate constants; α_A and β_A are some empirical exponents of intensities; and t_{A1} , t_{A12} , and t_{A2} are the time delays due to the inertia of the respective transfer processes. The initial conditions are:

$$R_{A1} = R_{A1}^{\circ} \quad R_{A12} = R_{A12}^{\circ} \quad R_{A2} = R_{A2}^{\circ}, \quad t = 0 \quad (8-46)$$

The rate of particle transfer can be expressed per unit volume of the ℓ^{th} phase according to the following expression:

$$\dot{m}_{A\ell} = \dot{R}_{A\ell} / (\phi S_{\ell} \rho_{\ell}), \quad \ell = 1, 2 \quad (8-47)$$

The particles captured at the interface are assumed to migrate at a speed determined by the relative speed of the fluid phases.

Exercise

1. Using Einstein's equation, Eq. 8-4, estimate the Brownian diffusivity of a $1\mu\text{m}$ diameter fine particle in water at 20°C temperature. (Answer: $D = 4.3 \times 10^{-9} \text{ cm}^2/\text{s}$; McDowell-Boyer et al., 1986)

References

- Amaefule, J. O., Kersey, D. G., Norman, D. L., & Shannon, P. M., "Advances in Formation Damage Assessment and Control Strategies," CIM Paper No. 88-39-65, Proceedings of the 39th Annual Technical Meeting of Petroleum Society of CIM and Canadian Gas Processors Association, June 12-16, 1988, Calgary, Alberta, 16 p.
- Cernansky, A., & Siroky, R., "Deep-bed Filtration on Filament Layers on Particle Polydispersed in Liquids," *Int. Chem. Eng.*, Vol. 25, No. 2, 1985, pp. 364-375.

- Chang, F. F., & Civan, F., "Modeling of Formation Damage due to Physical and Chemical Interactions between Fluids and Reservoir Rocks," SPE 22856 paper, Proceedings of the 66th Annual Technical Conference and Exhibition of the Society of Petroleum Engineers, October 6–9, 1991, Dallas, Texas.
- Chang, F. F., & Civan, F., "Predictability of Formation Damage by Modeling Chemical and Mechanical Processes," SPE 23793 paper, Proceedings of the SPE International Symposium on Formation Damage Control, February 26–27, 1992, Lafayette, Louisiana, pp. 293–312.
- Chang, F. F., & Civan, F., "Practical Model for Chemically Induced Formation Damage," *J. of Petroleum Science and Engineering*, Vol. 17, No. 1/2, February 1997, pp. 123–137.
- Civan, F., "A Generalized Model for Formation Damage by Rock-Fluid Interactions and Particulate Processes," SPE Paper 21183, Proceedings of the SPE 1990 Latin American Petroleum Engineering Conference, October 14–19, 1990, Rio de Janeiro, Brazil, 11 p.
- Civan, F., "Evaluation and Comparison of the Formation Damage Models," SPE Paper 23787, Proceedings of the SPE International Symposium on Formation Damage Control, February 26–27, 1992, Lafayette, Louisiana, pp. 219–236.
- Civan, F., "Predictability of Formation Damage: An Assessment Study and Generalized Models," Final Report, U.S. DOE Contract No. DE-AC22-90BC14658, April 1994.
- Civan, F., "A Multi-Phase Mud Filtrate Invasion and Well Bore Filter Cake Formation Model," SPE 28709 paper, Proceedings of the SPE International Petroleum Conference & Exhibition of Mexico, October 10–13, 1994, Veracruz, Mexico, pp. 399–412.
- Civan, F., "Modeling and Simulation of Formation Damage by Organic Deposition," Proceedings of the First International Symposium on Colloid Chemistry in Oil Production: Asphaltenes and Wax Deposition, ISCO'95, Rio de Janeiro, Brazil, November 26–29, 1995, pp. 102–107.
- Civan, F., "A Multi-Purpose Formation Damage Model," SPE 31101 paper, Proceedings of the SPE Formation Damage Symposium, Lafayette, Louisiana, February 14–15, 1996, pp. 311–326.
- Civan, F., Knapp, R. M., & Ohen, H. A., "Alteration of Permeability by Fine Particle Processes," *J. Petroleum Science and Engineering*, Vol. 3, Nos. 1/2, October. 1989, pp. 65–79.
- Dullien, F. A. L., *Porous Media Fluid Transport and Pore Structure*, Academic Press, London (1979), 396 p.
- Gruesbeck, C., & Collins, R. E., "Particle Transport Through Perforations," *SPEJ*, December 1982, pp. 857–865.
- Gruesbeck, C., R. E. Collins, "Entrainment and Deposition of Fine Particles in Porous Media," *SPEJ*, December 1982, pp. 847–856.

- Hallow, J. S., "Incipient Rolling, Sliding, and Suspension of Particles in Horizontal and Inclined Turbulent Flow," *Chem. Eng. Sci.*, Vol. 28, 1973, pp. 1-12.
- Himes, R. E., Vinson, E. F., & Simon, D. E., "Clay Stabilization in Low-Permeability Formations," *SPE Production Engineering*, August 1991, pp. 252-258.
- Ikoku, C. U., & Ramey, Jr., H. J., "Transient Flow of Non-Newtonian Power-Law Fluids in Porous Media," Supri-TR-9, Report No. E(04-3)1265, U.S. Department of Energy (February 1979) 257.
- Ivanov, I. B., Kralchevsky, P. A., & Nikolov, A. D., "Film and Line Tension Effects on the Attachment of Particles to an Interface," *J. Colloid and Interface Sci.*, Vol. 112, No. 1, 1986, pp. 97-107.
- Ives, K. J., "Deep Bed Filters," in Rushton, A. (Ed.) *Mathematical Models and Design Methods in Solid-Liquid Separation*, 1985 Martinus Nijhoff Publishers, pp. 90-332.
- Khilar, K. C., & Fogler, H. S., "Colloidally Induced Fines Migration in Porous Media," in Amundson, N. R. and Luss, D. (Eds.), *Reviews in Chemical Engineering*, Freund Publishing House LTD., London, England, January-June 1987, Vol. 4, Nos. 1 and 2, pp. 41-108.
- Khilar, K. C., & Fogler, H. S., "Water Sensitivity of Sandstones," *SPEJ*, February 1983, pp. 55-64.
- Kia, S. F., Fogler, H. S., & Reed, M. G., "Effect of Salt Composition on Clay Release in Berea Sandstones," SPE 16254, February 1987.
- King, R. W., and Adegbesan, K. O., "Resolution of the Principal Formation Damage Mechanisms Causing Injectivity and Productivity Impairment in the Pembina Cardium Reservoir," SPE Paper 38870, Proceedings of the 1997 Annual Technical Conference and Exhibition held in San Antonio, Texas, October 5-8, 1997, pp. 277-288.
- Lichtner, *Water Resources Research*, Vol. 28, No. 12, December 1992, pp. 3135-3155.
- McDowell-Boyer, L. M., Hunt, J. R., & Sitar, N., "Particle Transport Through Porous Media," *Water Resources Research*, Vol. 22, No. 13, December 1986, pp. 1901-1921.
- Metzner, A. B., & Reed, J. C., "Flow of Non-Newtonian Fluids—Correlation of the Laminar, Transition, and Turbulent Flow Regions," *AIChE J.*, Vol. 1, No. 4, 1955, pp. 434-440.
- Millan-Arcia, E., Civan, F. "Characterization of Formation Damage by Particulate Processes," *J. Canadian Petroleum Technology*, Vol. 31, No. 3, March 1992, pp. 27-33.
- Muecke, T. W., "Formation Fines and Factors Controlling their Movement in Porous Media," *JPT*, April 1979.
- Ochi, J., & Vernoux, J.-F., "Permeability Decrease in Sandstone Reservoirs by Fluid Injection-Hydrodynamic and Chemical Effects," *J. of Hydrology*, Vol. 208, 1998, pp. 237-248.

- Ohen, H. A., & Civan, F., "Predicting Fines Generation, Migration and Deposition Near Injection and Production Wells," Proceedings of the First Regional Meeting, American Filtration Society, Houston, Texas, October 30–November 1, 1989, pp. 161–164.
- Ohen, H. A., & Civan, F., "Simulation of Formation Damage in Petroleum Reservoirs," SPE 19420 paper, Proceedings of the 1990 SPE Symposium on Formation Damage Control, Lafayette, Louisiana, February 22–23, 1990, pp. 185–200.
- Ohen, H. A., & Civan, F., "Simulation of Formation Damage in Petroleum Reservoirs," *SPE Advanced Technology Series*, Vol. 1, No. 1, April 1993, pp. 27–35.
- Pautz, J. F., Crocker, M. E., & Walton, C. G., "Relating Water Quality and Formation Permeability to Loss of Injectivity," SPE 18888 paper, Proceedings of the SPE Production Operations, Oklahoma City, Oklahoma, March 13–14, 1989, pp. 565–576.
- Rushton, A., "Mathematical Models and Design Methods in Solid-Liquid Separation," *NATO ASI*, 1985, No. 88, Ed. A. Rushton, Martinus Nijhoff.
- Wojtanowicz, A. K., Krilov, Z. and Langlinais, J. P., "Study on the Effect of Pore Blocking Mechanisms on Formation Damage," Paper SPE 16233, presented at Society of Petroleum Engineers Production Operations Symposium, Oklahoma City, Oklahoma, March 8–10, 1987, pp. 449–463.
- Wojtanowicz, A. K., Krilov, Z. and Langlinais, J. P., "Experimental Determination of Formation Damage Pore Blocking Mechanisms," Trans. of the ASME, *Journal of Energy Resources Technology*, Vol. 110, 1988, pp. 34–42.

Chapter 9

Crystal Growth and Scale Formation in Porous Media*

Summary

In this chapter, the inorganic and organic precipitation/dissolution phenomena, and their effect on the size of the suspended particles and porosity variation are discussed and formulated.

Introduction

Civan (1996) describes that:

Injection of fluids and chemicals for improved recovery, and liberation of dissolved gases, such as CO_2 and light hydrocarbons from the reservoir fluids approaching the wellbore during production, and variation of fluid saturations can alter the temperature, pressure, and composition of the fluids in the near wellbore region and tubing. Consequently, the thermodynamic and chemical balance may change in favor of precipitate separation, aggregation of precipitates, crystal growth, and scale formation. Precipitates cause formation damage by changing the wettability and permeability of petroleum bearing rock and cause scale formation and clogging in tubing and pore throats.

Inorganic Precipitation

Typical inorganic precipitates include anhydrate (CaCO_3), gypsum ($\text{CaSO}_4 \cdot 2\text{H}_2\text{O}$), hemihydrate ($\text{CaSO}_4 \cdot \frac{1}{2}\text{H}_2\text{O}$), barite (BaSO_4), celestite

* Parts reprinted by permission of the Society of Petroleum Engineers from Civan, ©1996 SPE, SPE 31101 paper.

($SrSO_4$), magnesium sulfide ($MgSO_4$) originating from mixing sea water with brine, and rock and brine interactions (Oddo and Tomson, 1994; Atkinson and Mecik, 1997); ironhydroxide gel ($Fe(OH)_3$) originating from the acid dissolution and precipitation of iron minerals such as pyrrhotite (FeS), pyrite (FeS_2), hematite (Fe_2O_3), magnetite (Fe_3O_4), and siderite ($FeCO_3$) (Rege and Fogler, 1989); silicium tetra hydroxide gel ($Si(OH)_4$) originating from the alkaline dissolution and precipitation of minerals in shaly sandstones such as quartz and kaolinite (Labrid, 1990); and polymeric substances produced by in-situ gelation (Todd et al., 1993), alcohol induced crystallization (Zhu and Tiab, 1993), separation of elemental sulfur (Roberts, 1997); and surfactant precipitation (Arshad and Harwell, 1985).

Following Oddo and Tomson (1994), precipitation/dissolution reactions can be symbolically represented by:



where Me represents a cation or metal ion such as Sr^{+2} , Ca^{+2} , Mg^{+2} , An represents an anion such as CO_3^{-2} , SO_4^{-2} , and Pr represents a solid precipitate such as $CaCO_3$, $MgCO_3$, $BaSO_4$, $Fe(OH)_3$, $Si(OH)_4$. ν_1 , ν_2 , and ν_3 are some stoichiometric coefficients.

Oddo and Tomson (1994) correlated the saturation solubility product, K_{sp} , empirically as a function of temperature, T , pressure, p , and ionic strength, S_i , for typical systems. Hence, the saturation ratio given by the following equation can be used to determine whether the conditions are favorable for precipitation (Oddo and Tomson, 1994):

$$F_s = [Me]^{\nu_1} [An]^{\nu_2} / K_{sp} \quad (9-2)$$

$F_s < 1$ indicates an undersaturated solution, condition unfavorable for scaling, if $F_s = 1$, the solution is at equilibrium with the solid scale, and $F_s > 1$ indicates a supersaturated solution, condition favorable for scaling.

Organic Precipitation

Typical organic precipitates encountered in petroleum production are paraffins and asphaltenes. Paraffins are inert and asphaltenes are reactive substances. They are both sticky, thick, and deformable precipitates (Chung, 1992; Ring et al., 1994). Therefore, they can seal the pore throats and reduce the permeability to zero without needing to reduce the porosity to zero and their deposition at the pore surface and tubing wall is irreversible unless a solvent treatment is applied (Leontaritis et al., 1992):

The saturation ratio is given by:

$$F_s = x_A / (x_A)_s \quad (9-3)$$

where $F_s < 1$ for undersaturated solution, $F_s = 1$ for saturated solution, and $F_s > 1$ for supersaturated solution. x_A is the mole fraction of the dissolved organic in oil and $(x_A)_s$ is the organic solubility at saturation conditions. $(x_A)_s$ is predicted using the thermodynamic model by Chung (1992).

Crystallization

Majors (1999) explains that “Crystallization is the arrangement of atoms from a solution into an orderly solid phase.” and “Growth is simply the deposition of material at growth sites on an existing crystal face.” The process is called primary nucleation if there are no crystals present in the solution to start with and crystallization is occurring for the first time. Primary nucleation can be homogeneous or heterogeneous (Majors, 1999). Homogeneous nucleation occurs inside the solution without contact with any surface. Heterogeneous nucleation occurs over a solid surface. The process is called secondary nucleation if there are already some crystals present in the system over which further deposition can occur. The schematic chart given in Figure 9-1 by Majors (1999) describes the concentration-temperature relationship for nucleation. As can be seen, the primary nucleation process requires a sufficiently high concentration of

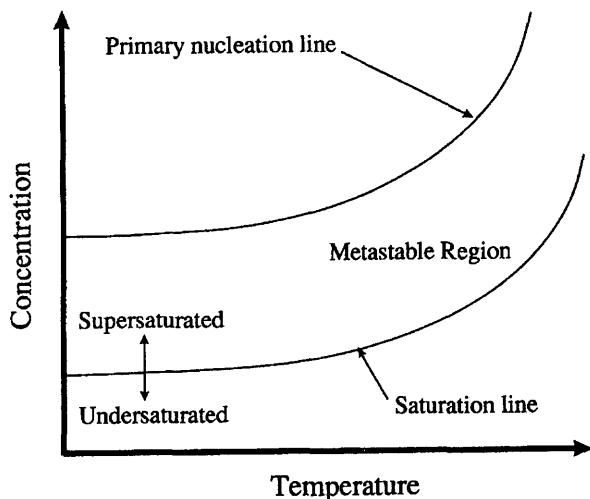


Figure 9-1. Concentration vs. temperature diagram for crystal formation (after Majors, 1999; reprinted by permission of the *Chemical Processing Magazine*).

supersaturated solution. Whereas, secondary nucleation can occur at relatively lower concentrations above the saturation line. The metastable region represents the favorable conditions for crystal growth (Majors, 1999).

The schematic chart given in Figure 9–2 by Majors (1999) describes the effect of the supersaturation ratio on the crystal growth and nucleation rates. Crystal growth rate is a low-order function of supersaturation and can be represented by a linear relationship, while nucleation rate is a high-order function of supersaturation and requires a more difficult nonlinear relationship (Majors, 1999). Majors (1999) explains that “Crystal growth is a dynamic process. While most of the crystals in the solution will grow, some may dissolve.”

Grain Nucleation, Growth, and Dissolution

The formation of crystalline particulates from aqueous solutions of salts involves a four step phase change process (Dunning, 1969):

1. Alteration of chemical and/or physical conditions to lead to supersaturation of the solution,
2. Initiation of the first small nuclei of the crystals,
3. Crystal growth, and
4. Relaxation leading to coagulation of crystalline particles.

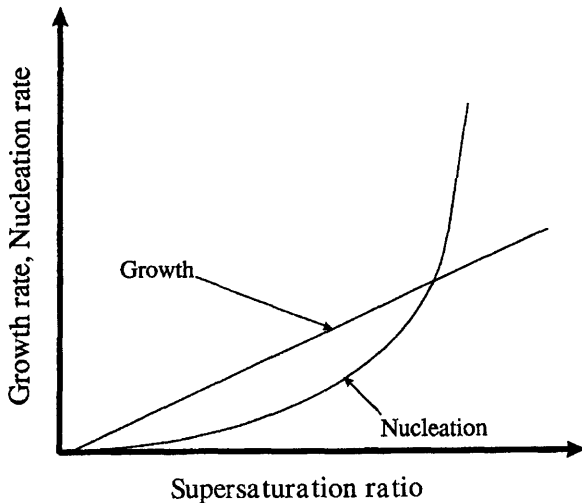


Figure 9–2. Effect of saturation ration of the crystal growth and nucleation rates (after Majors, 1999; reprinted by permission of the *Chemical Processing Magazine*).

The process is called homogeneous or heterogeneous crystal nucleation depending on the absence or presence, respectively, of some impurities, seed crystals, or contact surfaces, called substrates (see Figure 9–3 by Leetaru, 1996). As stated by Schneider (1997), “Nucleation commonly occurs at sites of anomalous point defects on the grain surface, at structural distortions caused by edge or screw dislocations, or at irregular surface features produced by dissolution and etching.” Because, Schneider (1997) adds, “When nucleation occurs at one of these sites, the free energy of the defect, dislocation, or surface irregularity can contribute to help overcome any energy barrier to nucleation.” Also, the mineral grain surfaces serve as seed for nucleation if the mineral crystal lattice structure matches that of the precipitating substance (Schneider, 1997).

The free energy change associated with heterogeneous nucleation at a surface is expressed by (Schneider, 1997):

$$\Delta G = \Delta G_{\text{volume}} + \Delta G_{\text{surface}} + \Delta G_{\text{strain}} \quad (9-4)$$

where ΔG_{strain} is the change of the strain volume free energy of shrinking of a nucleus.

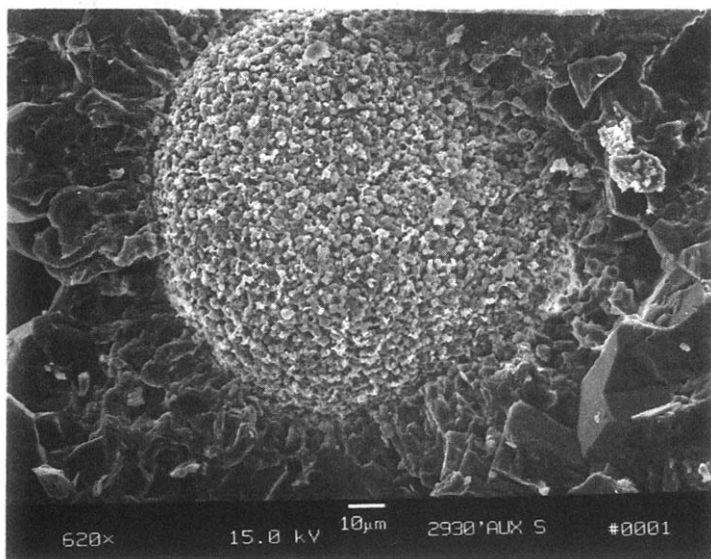


Figure 9–3. SEM photomicrograph of a calcite cement nucleating at a site in an Aux Vases sandstone sample (after Leetaru, 1996; reprinted by permission of the Illinois State Geological Survey).

Stumm and Morgan (1996) expressed the interface free energy change by

$$\Delta G_{\text{interface}} = A_{cw}\sigma_{cw} + A_{cs}(\sigma_{cs} - \sigma_{sw}) \quad (9-5)$$

Thus Eq. 9-4 becomes:

$$\Delta G = V\Delta G_v + A_{cw}\sigma_{cw} + A_{cs}(\sigma_{cs} - \sigma_{sw}) + V\varepsilon \quad (9-6)$$

where cw , cs , and sw denote the deposit-water, deposit-substrate, and substrate-water interfaces, respectively. A denotes the surface area and σ denotes the interfacial free energy. σ_{cs} and σ_{cw} denote the surface energies per unit surface area of the deposited particle-substrate interface and the deposited particle-solution interface, respectively. ε is the strain energy per unit volume. V is the volume of particle formed by precipitation. σ is the surface energy per unit particle surface. ΔG_v is the change of volume free energy from solution to solid phases per unit particle volume, given by (Stumm and Morgan, 1996):

$$\Delta G_v = -\frac{k_b T}{v} \ln\left(\frac{a}{a_o}\right) \quad (9-7)$$

where k_b is the Boltzmann constant, T is absolute temperature, v is the molar volume, and a and a_o are the activity of the mineral dissolved in solution and its theoretical activity at saturation, respectively.

Considering a semi-spherical deposition of radius r over a planar substrate surface as an approximation, such that (see Figure 9-3)

$$V = \frac{1}{2} \left(\frac{4}{3} \pi r^3 \right) \quad (9-8)$$

$$A_{cw} = \frac{1}{2} (4 \pi r^2) \quad (9-9)$$

$$A_{cs} = \pi r^2 \quad (9-10)$$

By combining the various efforts, Eq. 9-6 can be expressed as (Walton, 1969; Putnis and McConnell, 1980; Richardson and McSween, 1989; Schneider, 1997; and Stumm and Morgan, 1996):

$$\Delta G(r) = \left\{ \frac{1}{2} \left(\frac{4}{3} \pi r^3 \right) \Delta G_v \right\} + \left\{ \frac{1}{2} (4 \pi r^2) \sigma_{cw} + \pi r^2 (\sigma_{cs} - \sigma_{sw}) \right\} + \left\{ \frac{1}{2} \left(\frac{4}{3} \pi r^3 \right) \epsilon \right\} \quad (9-11)$$

The depositing substance and the substrate surface match well when $\sigma_{cs} < \sigma_{cw}$, and σ_{cs} is negligible and $\sigma_{sw} = \sigma_{cw}$ for perfect matching (Schneider, 1997).

Thus, the critical minimum radius necessary for formation of stable particles can be determined by equating the derivative of Eq. 9-11 with respect to the radius to zero as:

$$r_c = - \frac{\sigma_{cs} + 2\sigma_{cw} - \sigma_{sw}}{\Delta G_v + \epsilon} \quad (9-12)$$

Then, substituting Eq. 9-12 into Eq. 9-11 yields the expression for the activation energy necessary for formation of stable particles as:

$$\Delta G_{cr} = \frac{\pi (\sigma_{cs} + 2\sigma_{cw} - \sigma_{sw})^3}{3(\Delta G_v + \epsilon)^2} \quad (9-13)$$

For homogeneous nucleation, $A_{cs} = 0$ and Eq. 9-6 simplifies to

$$\Delta G = V \Delta G_v + A_{cw} \sigma_{cw} + V \epsilon \quad (9-14)$$

Approximating the shape of the deposit by a sphere of radius r such that

$$V = \frac{4}{3} \pi r^3 \quad (9-15)$$

$$A_{cw} = 4 \pi r^2 \quad (9-16)$$

Eq. 9-14 can be written as

$$\Delta G(r) = \frac{4}{3} \pi r^3 (\Delta G_v + \epsilon) + 4 \pi r^2 \sigma_{cw} \quad (9-17)$$

The minimum critical particle radius for a homogeneous nucleus to form a stable deposit at a given super saturation state can be estimated by equating the derivative of Eq. 9-17 to zero:

$$r_{cr} = -\frac{2\sigma_{cw}}{\Delta G_v + \epsilon} \quad (9-18)$$

Thus, the activation energy necessary for starting homogeneous nucleation can be estimated by substituting Eq. 9-18 into Eq. 9-17 as:

$$\Delta G_{cr} = \frac{16\pi\sigma_{cw}^3}{3(\Delta G_v + \epsilon)^2} \quad (9-19)$$

Crystallization Kinetics

The time necessary to initiate nucleation of crystals from a super-saturated solution is called “induction time” (Reddy, 1995). It is a function of the solution supersaturation, that is, the ratio of the ion activity product to the solubility product of the precipitating crystalline matter as demonstrated in Figure 9-4 by Reddy (1995) for calcium carbonate nucleation in the presence of magnesium ions. Figure 9-4 indicates that the induction time is lower for higher supersaturation. Below the supersaturation value of about 10, the induction time for calcium carbonate nucleation is very long. In this region, the solution is at a “metastable” condition and, therefore, calcium carbonate crystals cannot be formed without the aid of a matching growth surface or substrate (Reddy, 1995). It can also be observed that the presence of magnesium ions increases the induction time for calcium carbonate nucleation and therefore has a retardation and/or inhibition effect. Reddy (1995) explains the magnesium ion inhibition of calcium carbonate nucleation by adsorption of the magnesium ions and thus, the occupation of some crystal growth sites on the calcium carbonate crystal surface. For a quantitative interpretation of this phenomenon, Reddy (1986; 1995) resorts to a growth rate analysis and a Langmuir adsorption isotherm model using experimental data obtained by a seeded growth method. He expressed the crystal growth rate as being proportional to the surface available for crystal growth and the square of the driving force for precipitation:

$$dN/dt = kSN^2 \quad (9-20)$$

where N represents the calcium carbonate crystal concentration in the solution in moles/liter, t denotes the time measured from the time of

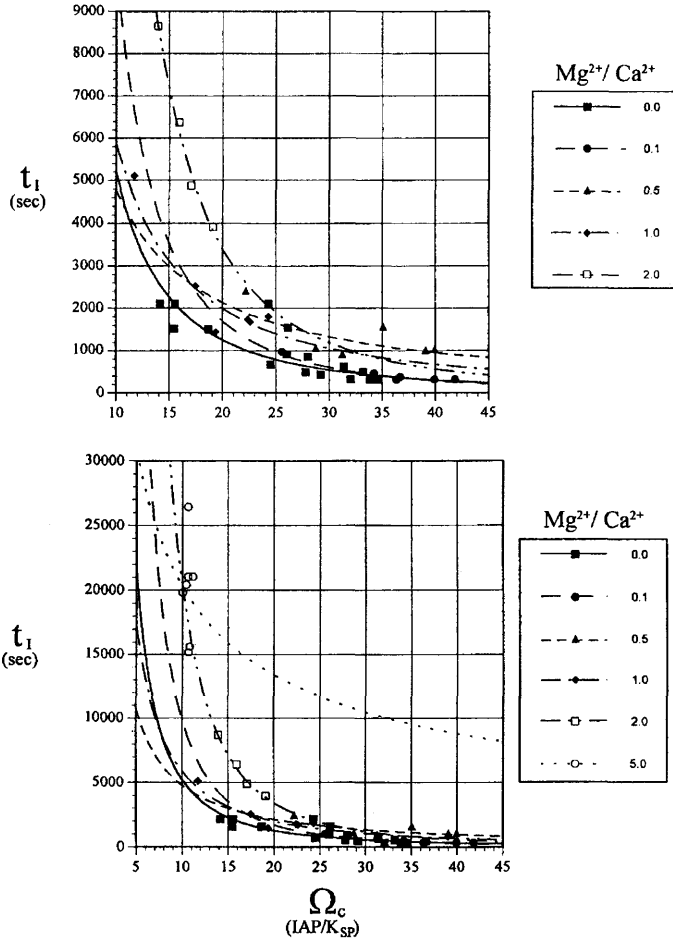


Figure 9-4. Calcium carbonate induction time vs. the supersaturation for solutions containing magnesium to calcium ion concentrations ratios of a) 0 to 2, and b) 0 to 5 (after Reddy, ©1995; reprinted by permission of the author and Plenum Press).

initiation of the crystallization by seeding, s is the concentration of the seed added to provide the surface area for growth in mg/liter, and k is the crystal growth-rate constant. If N_o denotes the initial theoretical crystal concentration that would be produced by precipitation from a stable supersaturated solution at the time of seeding, the integration of Eq. 9-20 yields (Reddy, 1986):

$$N^{-1} - N_o^{-1} = ks t \quad (9-21)$$

The plot of the calcium carbonate growth data given by Reddy (1995) in Figure 9-5 confirms the validity of Eq. 9-21 and indicates that the presence of magnesium ions reduces the slopes of the straight lines and, thus the crystallization rate constant and inhibits the calcite formation. Figure 9-6 by Reddy (1995) shows a rapid decline of the crystallization rate constant by the increasing magnesium ions presence. The plot of data according to the Langmuir model

$$k_o / (k_o - k) = 1 + k_d (k_a T_{Mg^{2+}})^{-1} \quad (9-22)$$

given in Figure 9-7 by Reddy (1995) clearly indicates that the mechanism of the inhibition of the calcite crystal growth is the magnesium ion adsorption on the growth sites, where k_a and k_d denote the rate constants for adsorption and desorption of the magnesium ions at the growth sites, k_o and k are the crystallization growth-rate constants without and with the presence of magnesium ions, and $T_{Mg^{2+}}$ is the total concentration of the magnesium ions present in the system.

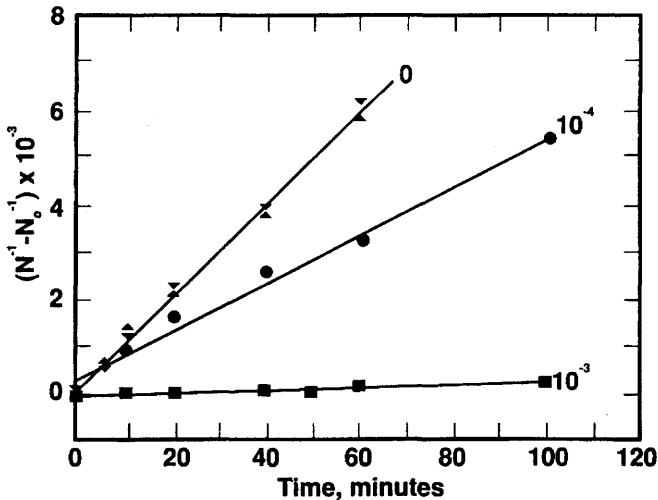


Figure 9-5. Effect of the magnesium ions on the calcite crystal growth rate for different magnesium ion concentrations indicated at the end of each line (after Reddy, ©1995; reprinted by permission of the author and Plenum Press).

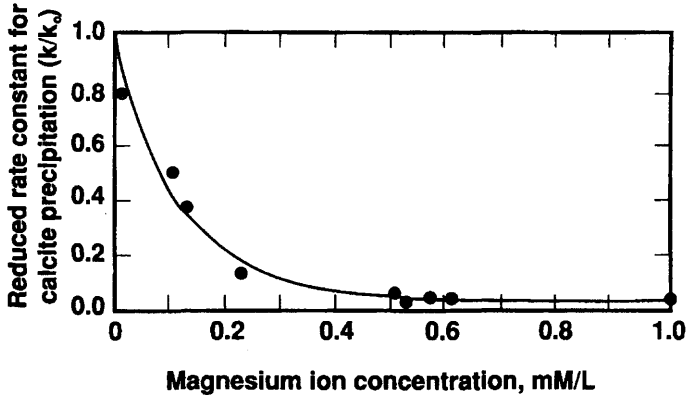


Figure 9-6. Effect of the magnesium ion concentration on the calcite precipitation rate constant (after Reddy, ©1995; reprinted by permission of the author and Plenum Press).

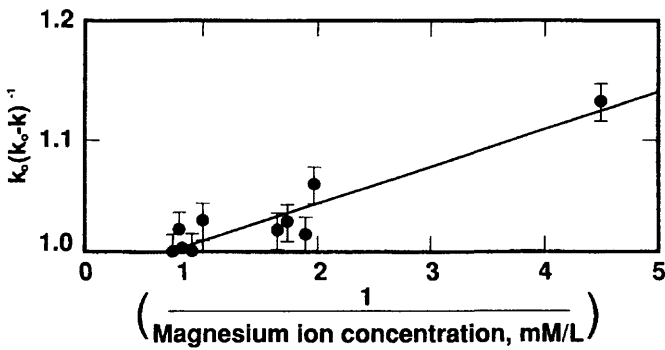


Figure 9-7. Langmuir isotherm plotted against the reciprocal added magnesium ion concentration for calcite precipitation (after Reddy, ©1995; reprinted by permission of the author and Plenum Press).

Particle Growth and Dissolution in Solution

The particle growth is assumed to occur at a rate proportional to the surface, A_c , available for growth and the deviation of the saturation ratio from unity (Chang and Civan, 1992; Civan, 1996):

$$\frac{dm_c}{dt} = k_c A_c (F_s - 1) \quad (9-23)$$

for which the initial amount of crystals present per unit bulk medium is given by

$$m_c = m_c^o, \quad t = 0 \quad (9-24)$$

Relating the crystal shape to spherical shape, the mass and surface area of the crystalline particle is given, respectively, by:

$$m_c = \rho_c \frac{\pi D_c^3}{6} C_1 \quad (9-25)$$

and

$$A_c = \pi D_c^2 C_2 \quad (9-26)$$

in which C_1 and C_2 are the shape factors, ρ_c , is the density, and D_c is the diameter. k_c is a crystallization rate constant. Thus, Eqs. 9-23 through 9-26 lead to the following model in which the shape factors and the constant ($1/2$) have been incorporated into the constant k'_c :

$$\rho_c \frac{dD_c}{dt} = k'_c (F_s - 1) \quad (9-27a)$$

subject to

$$D_c = D_{c_o}, \quad t = 0 \quad (9-27b)$$

where

$$F_s \begin{cases} > 1 \text{ crystal growth} \\ = 1 \text{ equilibrium} \\ < 1 \text{ crystal dissolution} \end{cases} \quad (9-28)$$

For constant saturation, Eqs. 9-27a, b yield:

$$D_c = D_{c_o} + kt \quad (9-29)$$

For example, $D_{c_o} = 5 \mu\text{m}$, and $k \equiv k'_c (F_s - 1) / \rho_c$ is equal to 1.4 and 10.3 $\mu\text{m/s}$ for calcium carbonate crystal growth at 25 and 50°C, respectively, using the Dawe and Zhang (1997) data.

Scale Formation and Dissolution at the Pore Surface

The rate of scale formation at the pore surface can be expressed similarly to crystal growth. The pore volume relates to the diameter of an equivalent spherical shape pore space by (Civan, 1996):

$$\phi = C_3 D^3 \quad (9-30)$$

indicating that

$$D = (\phi / C_3)^{1/3} \quad (9-31)$$

Thus, the pore surface relates to the porosity according to:

$$A = C_4 D^2 = C_4 (\phi / C_3)^{2/3} = C_5 \phi^{2/3} \quad (9-32)$$

C_3 and C_4 are some shape factors and $C_5 = C_4 / C_3^{2/3}$. The porosity of the solid porous matrix can be expressed as a sum of the instantaneous porosity, ϕ , and the pore space occupied by the scales, ϕ_s , as:

$$\phi_r = \phi + \phi_s \quad (9-33)$$

Therefore, the mass of the scale formed over the pore surface is given by

$$m_c = \rho_s \phi_s = \rho_s (\phi_r - \phi) \quad (9-34)$$

Therefore, substituting Eqs. 9-32 and 9-34 into Eq. 9-23 yields (Civan, 1996):

$$-\rho_s \frac{d\phi}{dt} = k'_c \phi^{2/3} (F_s - 1) \quad (9-35)$$

subject to

$$\phi = \phi_o, \quad t = 0 \quad (9-36)$$

where

$$F_s \begin{cases} > 1 \text{ scale formation} \\ = 1 \text{ equilibrium} \\ < 1 \text{ scale dissolution} \end{cases} \quad (9-37)$$

and k'_c is a scale formation rate constant incorporating the above mentioned shape factors and some constants. The minus sign in Eq. 9-35 is for the reduction of porosity by scale formation at the pore surface. Thus, assuming the rock porosity, ϕ_r , remains constant and substituting Eq. 9-33 into 9-35 leads to an equation similar to Ortoleva et al. (1987):

$$-\rho_s \frac{d\phi_s}{dt} = k'_c (\phi_r - \phi_s)^{2/3} (F_s - 1) \quad (9-38)$$

subject to

$$\phi_s = \phi_r - \phi_o, \quad t = 0 \quad (9-39)$$

Assume that the surface area of crystal available for growth can be expressed empirically by:

$$A_c = f(\phi) m_c \quad (9-40)$$

in which $f(\phi)$ is the specific surface of the mineral-fluid contact area (surface area per unit mineral mass) expressed as a function of porosity. Civan (1996) approximated this function according to Eq. 9-32. Thus, substituting Eq. 9-40 into Eq. 9-23 leads to Holstad's (1995) equation:

$$-\frac{dm_c}{dt} = k_c m_c f(\phi) (1 - F_s) \quad (9-41)$$

Holstad (1995) expressed the temperature dependency of the crystallization rate constant by the Arrhenius equation:

$$k_c = F_M A_M \exp\left(-\frac{E_M}{RT}\right) \quad (9-42)$$

where F_M , A_M , and E_M denote an empirical mineral property factor, an Arrhenius pre-factor, and the activation energy. Liu et al. (1997) used a similar equation

$$k_c = k_c^o \exp\left(-\frac{E_M}{RT}\right) \quad (9-43)$$

where k_c^o is the high-temperature ($T \rightarrow \infty$) limit of the rate constant.

The effects of various conditions on dissolution rates, including lithologic variation, hydrodynamics, ionic strength, saturation state, mixed-kinetic control, and surface treatment, have been investigated by Raines and Dewers (1997, 1997), Hajash Jr. et al. (1998), and Merino and Dewers (1998).

Crystal Surface Displacement by Dissolution and Precipitation

The dissolution and precipitation of a crystalline matter in contact with a solution can be studied by measuring the progress of the crystal surface as a function of time. Hunkeler and Bohni (1981) and Dunn et al. (1999) used this technique. Civan (2000) determined that the position of the progressing crystal surface could be correlated by:

$$\ln \left[\frac{x_o - x_t}{x - x_t} \right] = kM \quad (9-44)$$

for which x , x_o , and x_t are the instantaneous, initial, and final surface positions, respectively, k is a rate constant, and M is the amount of solute precipitated or dissolved, given by:

$$M = \frac{2}{\sqrt{\pi}} (c_1 - c_o) \sqrt{Dt} \quad (9-45)$$

where t is time, c_o and c_1 are the solute concentrations of the solution at the beginning and equilibrium, respectively, and D is the diffusion coefficient of the solute. Civan (2000) verified this model using the Dunn et al. (1999) measurements of the pit depth during barite dissolution.

References

- Arshad, A., & Harwell, J. H., "Enhanced Oil Recovery by Surfactant-Enhanced Volumetric Sweep Efficiency," SPE 14291, Annual Technical Conference and Exhibition of SPE, Las Vegas, Nevada, September 22–25, 1985.
- Atkinson, G., & Mecik, M., "The Chemistry of Scale Prediction," *J. of Petroleum Science and Engineering*, Vol. 17, No. 1/2, February 1997, pp. 113–121.

- Chang, F. F., & Civan, F., "Predictability of Formation Damage by Modeling Chemical and Mechanical Processes," SPE 23793 paper, Proceedings of the SPE International Symposium on Formation Damage Control, February 26–27, 1992, Lafayette, Louisiana, pp. 293–312.
- Chung, T.-H., "Thermodynamic Modeling for Organic Solid Precipitation," SPE 24851, Proceedings of the 67th Annual technical Conference and Exhibition of the SPE held in Washington, D.C., October 4–7, 1992, pp. 869–878.
- Civan, F., "Correlation of the Pit Depth in Crystal Etching by Dissolution," *J. of Colloid and Interface Science*, Vol. 222, No. 1, pp. 156–158, 2000.
- Civan, F., "A Multi-Purpose Formation Damage Model," SPE 31101 paper, SPE Formation Damage Symposium, Lafayette, Louisiana, February 14–15, 1996, pp. 311–329.
- Dawe, R. A. and Zhang, Y., "Kinetics of Calcium Carbonate Scaling Using Observations from Glass Micromodels," *Journal of Petroleum Science and Engineering*, Vol. 18, No. 3/4, pp. 179–187, 1997.
- Dunn, K., Daniel, E., Shuler, P. J., Chen, H. J., Tang, Y., and Yen, T. F., "Mechanism of Surface Precipitation and Dissolution of Barite: A Morphology Approach," *J. Colloid Interface Sci.* Vol. 214, 1999, pp. 427–437.
- Dunning, W. J., "General and Theoretical Introduction," *Nucleation*, Zettlemoyer, A.C. (Ed.), M. Dekker, Inc., New York, New York, 1969, pp. 1–67.
- Hajash Jr., A., Carpenter, T. D., & Dewers, T. A., "Dissolution and Time-Dependent Compaction of Albite Sand: Experiments at 100°C and 160°C in pH-buffered Organic Acids and Distilled Water," *Tectonophysics*, Vol. 295, 1998, pp. 93–115.
- Holstad, A., "Mathematical Modeling of Diagenetic Processes in Sedimentary Basins," *Mathematical Modeling of Flow Through Porous Media*, Bourgeat, A. P., Carasso, C., Luckhaus, S., and Mikelić, A., (Eds.), World Scientific Publ. Co. Pte. Ltd., 1995, pp. 418–428.
- Hunkeler, F. and Bohni, H., "Determination of Pit Growth Rates on Aluminum Using a Metal Foil Technique," *Corrosion*, Vol. 37(11), 1981, pp. 645–650.
- Labrid, J., "Modeling of High pH Sandstone Dissolution," Proceedings of the International Technical Meeting held jointly by the Petroleum Society of CIM and the SPE in Calgary, June 10–13, 1990, pp. 81/1–21.
- Leetaru, H. E., "Reservoir Characteristics and Oil Production in the Cypress and Aux Vases Formations at Storms Consolidated Field in White County, Illinois," *Illinois Petroleum Series 150*, 1996, Department of Natural Resources, Illinois State Geological Survey, 47 p.
- Leontaritis, K. J., Amaefule, J. O., & Charles, R. E., "A Systematic Approach for the Prevention and Treatment of Formation Damage

- Caused by Asphaltene Deposition," SPE 23810 paper, Proceedings of the SPE International Symposium on Formation Damage Control, Lafayette, Louisiana, February 26–27, 1992, pp. 383–395.
- Liu, X., & Ortoleva, P., "A General-Purpose, Geochemical Reservoir Simulator," SPE 36700 paper, Proceedings of the 1996 SPE Annual Technical Conference and Exhibition, Denver, Colorado, October 6–9, 1996, pp. 211–222.
- Liu, X., Ormond, A., Bartko, K., Li, Y., & Ortoleva, P., "A Geochemical Reaction-Transport Simulator for Matrix Acidizing Analysis and Design," *J. of Petroleum Science and Engineering*, Vol. 17, No. 1/2, February 1997, pp. 181–196.
- Majors, J., "Crystallization and the Bottom Line," Chemical Processing, Vol. 62, No. 2, 1999, pp. 55–59.
- Merino, E., & Dewers, T., "Implications of Replacement for Reaction-Transport Modeling," *Journal of Hydrology*, Vol. 209, 1998, pp. 137–146.
- Oddo, J. E., & Tomson, M. B., "Why Scale Forms and How to Predict It," SPE Production Facilities, February 1994, pp. 47–54.
- Ortoleva, P., Chadam, J., Merino, E., & Sen, A., "Geochemical Self-Organization II: The Reactive-Infiltration Instability," *Amer. J. Sci.*, Vol. 287, 1987, pp. 1008–1040.
- Putnis, A., & McConnell, J. D. C., *Principles of Mineral Behaviour*, Blackwell Scientific Publ., Boston, 1980.
- Raines, M. A., & Dewers, T. A., "Mixed Transport/Reaction Control of Gypsum Dissolution Kinetics in Aqueous Solutions and Initiation of Gypsum Karst," *Chemical Geology*, Vol. 140, 1997, pp. 29–48.
- Raines, M. A., & Dewers, T. A., "Mixed Kinetics Control of Fluid-Rock Interactions in Reservoir Production Scenarios," *J. of Petroleum Science and Engineering*, Vol. 17, No. 1/2, February 1997, pp. 139–155.
- Reddy, M. M., "Effect of Magnesium Ion on Calcium Carbonate Nucleation and Crystal Growth in Dilute Aqueous Solutions at 25° Celsius, in Studies in Diageneses, Denver, F. A. Mumpton (Ed.), Colorado, U.S. Geological Survey," Bulletin 1578, 1986, pp. 169–182.
- Reddy, M. M., "Carbonate Precipitation in Pyramid Lake, Nevada, Probable Control by Magnesium Ion," in Mineral Scale Formation and Inhibition (Z. Amjad, ed.), Plenum Press, New York, 1995, pp. 21–32.
- Rege, S. D., & Fogler, H. S., "Competition Among Flow, Dissolution and Precipitation in Porous Media," *AIChE J.*, Vol. 35, No. 7, 1989, pp. 1177–1185.
- Richardson, S. M., & McSween, H. Y., *Geochemistry: Pathways and Processes*, Prentice Hall, Inc., New York, New York, 1989.
- Ring, J. N., Wattenbarger, R. A., Keating, J. F., & Peddibhotla, S., "Simulation of Paraffin Deposition in Reservoirs," *SPE Production & Facilities*, February 1994, pp. 36–42.

- Roberts, B. E., "The Effect of Sulfur Deposition on Gaswell Inflow Performance," *SPE Reservoir Engineering*, May 1997, pp. 118–123.
- Schneider, G. W., "A Geochemical Model of the Solution-Mineral Equilibria Within a Sandstone Reservoir," M.S. Thesis, The University of Oklahoma, 1997, 157 p.
- Stumm, W., & Morgan, J. J., *Aquatic Chemistry: Chemical Equilibria and Rates in Natural Waters*, John Wiley and Sons, New York, New York, 1996.
- Todd, B. J., Willhite, G. P., & Green, D. W., "A Mathematical Model of In-situ Gelation of Polyacrylamide by a Redox Process," *SPE Reservoir Engineering*, February 1993, pp. 51–58.
- Walton, A. G., "Nucleation in Liquids and Solutions," *Nucleation*, Zettlemoyer, A. C. (Ed.), M. Dekker, Inc., New York, New York, 1969, pp. 225–307.
- Zhu, T., & Tiab, D., "Improved Sweep Efficiency by Selective Plugging of Highly Watered Out Zones by Alcohol Induced Precipitation," *JCPT*, Vol. 32, No. 9, November 1993, pp. 37–43.

Part III

Formation Damage by Particulate Processes

Fines Mobilization, Migration, and Deposition

Chapter 10

Single-Phase Formation Damage by Fines Migration and Clay Swelling*

Summary

A review of the primary considerations and formulations of the various single-phase models for formation damage by fines migration and clay swelling effects is presented. The applicability and parameters of these models are discussed.

Introduction

The majority of the formation damage models were developed for single phase fluid systems. This assumption is valid only for very specific cases such as the production of particles with oil flow and for special core tests. Nevertheless, it is instructive to understand these models before looking into the multi-phase effects. Therefore, the various processes involving single-phase formation damage are discussed and the selected models available are presented along with some modifications and critical evaluation as to their practical applicability and limitations. The methodology for determination of the model parameters are presented. The parameters that can be measured directly are identified. The rest of the parameters are determined by means of a history matching technique. The applications of the models and the parameter estimation method are demonstrated using several examples.

* Parts reprinted by permission of the Society of Petroleum Engineers from Civan, ©1992 SPE, SPE 23787 paper, and by permission of the U.S. Department of Energy from Civan, 1994.

An evaluation and comparison of six selected models bearing direct relevance to formation damage prediction for petroleum reservoirs are carried out. The modeling approaches and assumptions are identified, interpreted, and compared. These models are applicable for special cases involving single-phase fluid systems in laboratory core tests.

Porous media is considered in two parts: (1) the flowing phase, denoted by the subscript f , consists of a suspension of fine particles flowing through and (2) the stationary phase, denoted by the subscript s , consists of the porous matrix and the particles retrained.

The Thin Slice Algebraic Model

Model Formulation

Wojtanowicz et al. (1987, 1988) considered a thin slice of a porous material and analyzed the various formation damage mechanisms assuming one distinct mechanism dominates at a certain condition. Porous medium is visualized as having tortuous pathways represented by N_h tubes of the same mean hydraulic equivalent diameter, D_h , located between the inlet and outlet ports of the core as depicted in Figure 10-1. The cross-sectional area of the core is A and the length is L . The tortuosity factor for the tubes is defined as the ratio of the actual tube length to the length of the core.

$$\tau = L_h / L \quad (10-1)$$

The cross-sectional area of the hydraulic tubes are approximated by

$$A_h = C_1 \pi D_h^2 \quad (10-2)$$

in which C_1 is an empirical shape factor that incorporates the effect of deviation of the actual perimeter from a circular perimeter.

As a suspension of fine particles flows through the porous media, tubes having narrow constrictions are plugged and put out of service. If the number of nonplugged tubes at any given time is denoted by N_{np} and the plugged tubes by N_p , then the total number of tubes is given by:

$$N_h = N_p + N_{np} \quad (10-3)$$

The area open for flow is given by

$$A_f = N_{np} A_h \quad (10-4)$$

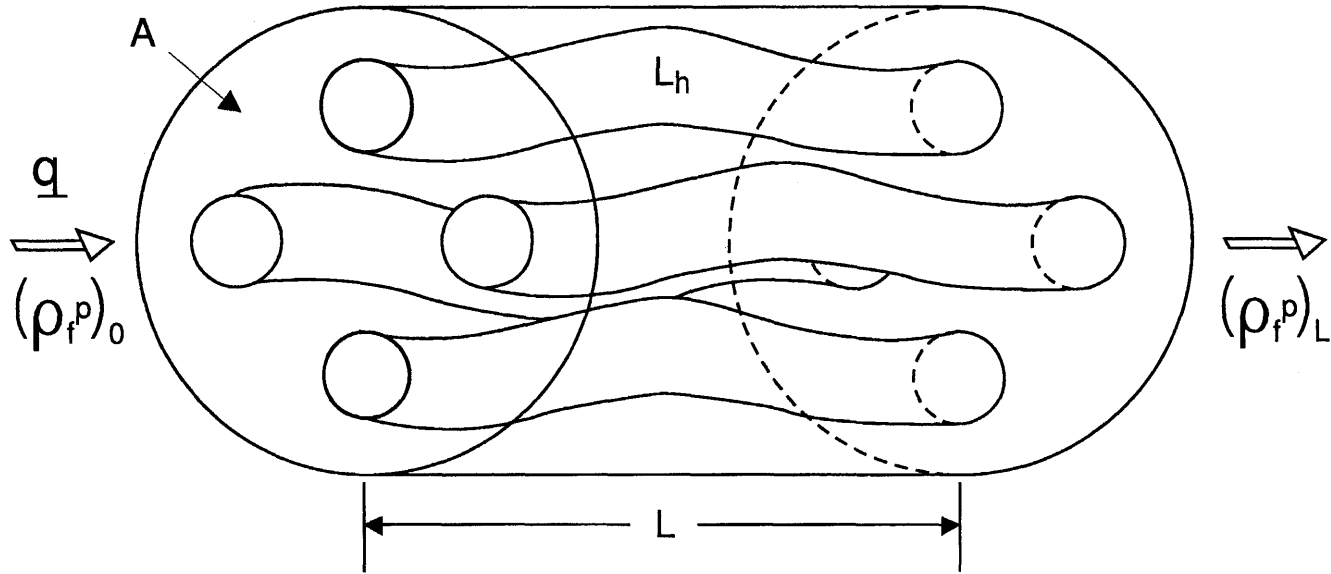


Figure 10–1. Hydraulic tubes realization of flow paths in a core (after Civan, 1994; reprinted by permission of the U.S. Department of Energy; after Civan 1992 SPE, reprinted by permission of the Society of Petroleum Engineers).

The Darcy and Hagen-Poiseuille equations given respectively by

$$\Delta p = q\mu L / (KA) \quad (10-5)$$

and

$$\Delta p = 32q\mu L_h / (A_f D_h^2) \quad (10-6)$$

are considered as two alternative forms of the porous media momentum equations. q is the flowrate of the flowing phase and Δp is the pressure differential across the thin core slice. Thus, equating Eqs. 10-5 and 10-6 and using Eqs. 10-1 and 10-2 the relationship between permeability, K , and open flow area, A_p , is obtained as:

$$K = A_f A_h / C_2^2 \quad (10-7)$$

in which the new constant is defined by

$$C_2^2 \equiv 32A\tau\pi C_1 \quad (10-8)$$

The permeability damage in porous media is assumed to occur by three basic mechanisms: (1) gradual pore reduction (pore narrowing, pore lining) by surface deposition, (2) single pore blocking by screening (pore throat plugging) and (3) pore volume filling by straining (internal filter cake formation by the snowball effect).

Gradual pore reduction is assumed to occur by deposition of particles smaller than pore throats on the pore surface to reduce the cross-sectional area, A , of the flow tubes gradually as depicted in Figure 10-2. Thus, the number of tubes open for flow, N_{np} , at any time remains the same as the total number of tubes, N_h , available. Hence,

$$N_h = N_{np}, N_p = 0 \quad (10-9)$$

Then, using Eq. 10-9 and eliminating A between Eqs. 10-4 and 10-7 leads to the following equation for the permeability to open flow area relationship during the surface deposition of particles:

$$A_f = C_3 K^{1/2} \quad (10-10)$$

in which the new constant is defined by

$$C_3 = C_2 N_h^{1/2} \quad (10-11)$$

Single pore blocking is assumed to occur by elimination of flow tubes from service by plugging of a pore throat or constriction, that may exist

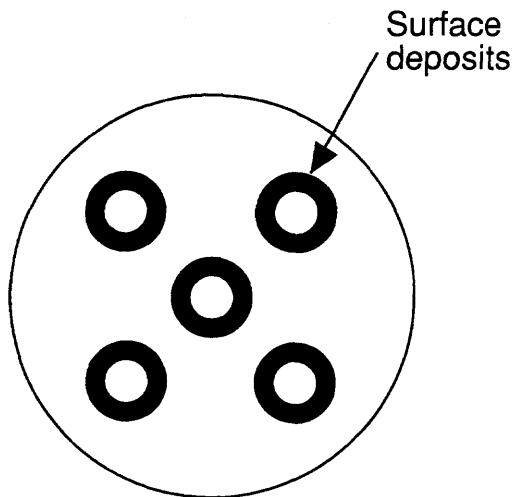


Figure 10-2. Pore surface deposition in a core (after Civan, 1994; reprinted by permission of the U.S. Department of Energy; after Civan 1992 SPE; reprinted by permission of the Society of Petroleum Engineers).

somewhere along the tube, by a single particle to stop the flow through that particular tube. Therefore, the cross-sectional areas of the individual tubes, A_h , do not change. But, the number of tubes, N_{np} , open for the flow is reduced as depicted in Figure 10-3. The area of the tubes eliminated from service is given by:

$$A_p = N_p A_h \quad (10-12)$$

The number of tubes plugged is estimated by the ratio of the total volume of pore throat blocking particles to the volume of a single particle of the critical size.

$$N_p = \left(qf_d \int_0^t \rho_{pf} dt / \rho_p \right) / (\pi d^3 / 6) \quad (10-13)$$

The critical particle size, d , is defined as the average size of the critical pore constrictions in the core. f_d is the volume fraction of particles in the flowing phase, having sizes comparable or greater than d . ρ_p is the particle grain density. ρ_{pf} is the mass concentration of particles in the flowing suspension of particles. Because A_h is a constant, Eq. 10-7 leads to the following permeability to open flow area relationship:

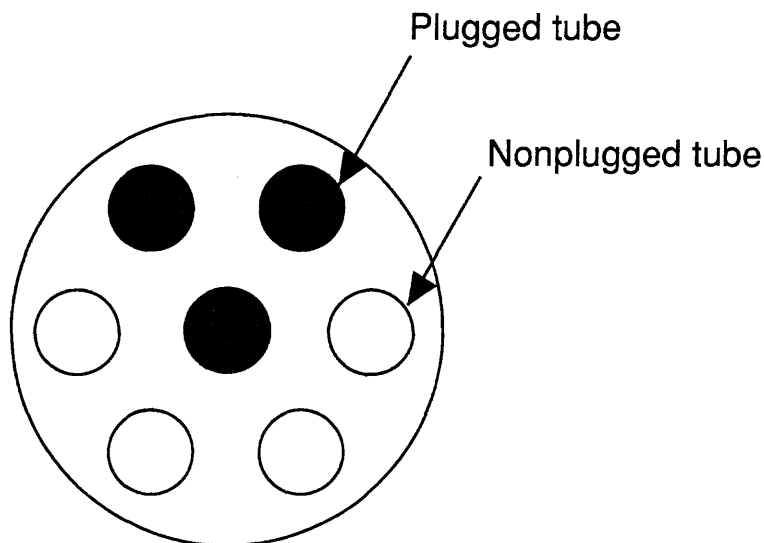


Figure 10-3. Pore throat plugging in a core (after Civan, 1994; reprinted by permission of the U.S. Department of Energy; after Civan 1992 SPE; reprinted by permission of the Society of Petroleum Engineers).

$$A_f = C_4 K \quad (10-14)$$

in which the new constant is given by:

$$C_4 = C_2^2 / A_h \quad (10-15)$$

Pore filling occurs near the inlet face of the core when a suspension of high concentration of particles in sizes larger than the size of the pore throats is injected into the core as depicted in Figure 10-4. The permeability, K_c , of the particle invaded region decreases by accumulation of particles. But, in the uninvaded core region near the outlet, the permeability of the matrix, K_m , remains unchanged. The harmonic mean permeability, K , of a core section (neglecting the cake at the inlet face) can be expressed in terms of the permeability, K_c , of the L_c long pore filling region and the permeability, K_m , of the L_m long uninvaded region as

$$L / K(t) = L_c / K_c(t) + L_m / K_m \quad (10-16)$$

which can be written as:

$$K(t) = L / [L_c R_c(t) + L_m R_m] \quad (10-17)$$

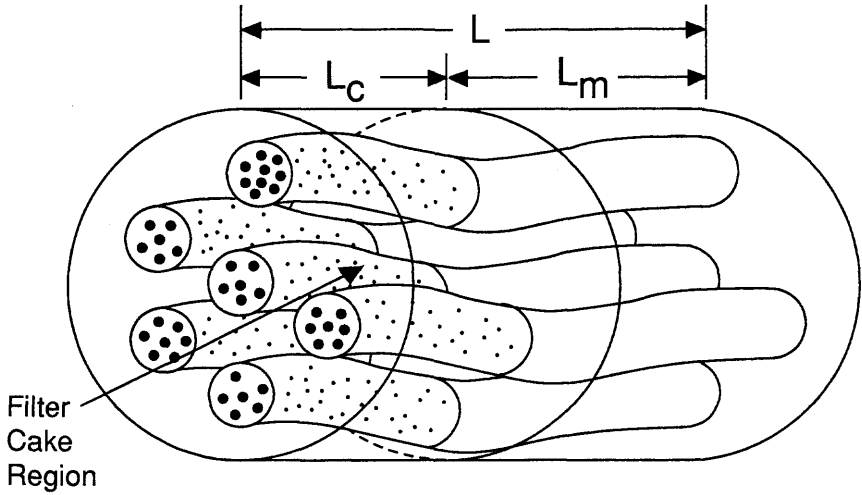


Figure 10-4. Pore filling and internal filter cake formation in a core (after Civan, 1994; reprinted by permission of the U.S. Department of Energy; after Civan 1992 SPE; reprinted by permission of the Society of Petroleum Engineers).

$R_c(t)$ and R_m are the resistances of the pore filling and uninvaded regions defined by

$$R_c(t) = 1/K_c(t) \quad (10-18)$$

$$R_m = 1/K_m \quad (10-19)$$

The rate of increase of the filtration resistance of the pore filling particles is assumed proportional to the particle mass flux of the flowing phase according to:

$$dR_c/dt = (k_c/L_c)(q/A)\rho_{pf} \quad (10-20)$$

subject to the initial condition

$$R_c = R_m, t = 0 \quad (10-21)$$

Then, solving Eqs. 10-20 and 21 yields:

$$R_c(t) = R_m + \int_0^t (k_c/L_c)(q/A)\rho_{pf} dt \quad (10-22)$$

k_c is the pore filling particles resistance rate constant.

The instantaneous porosity of a given cross-sectional area is given by:

$$\phi = \phi_o - \varepsilon_p \quad (10-23)$$

ϕ_o and ϕ denote the initial and instantaneous porosity values. ε_p is the fractional bulk volume of porous media occupied by the deposited particles, given by

$$\varepsilon_p = m_p / \rho_p \quad (10-24)$$

m_p is the mass of particles retained per unit volume of porous media and ρ_p is the particle grain density. For convenience, these quantities can be expressed in terms of initial and instantaneous open flow areas, A_{fo} and A_p , and the area covered by the particle deposits, A_p , as

$$\phi = A_f / A \quad (10-25)$$

$$\phi_o = A_{fo} / A \quad (10-26)$$

$$\varepsilon_p = A_p / A \quad (10-27)$$

Substituting Eqs. 10-25 through 10-27, Eqs. 10-23 and 24 become, respectively

$$A_{fo} = A_f + A_p \quad (10-28)$$

$$A_p = Am_p / \rho_p \quad (10-29)$$

The particle mass balance for a thin core slice is given by:

$$d/dt [AL(\phi \rho_{pf} + m_p)] + q(\rho_{pf})_{out} - q(\rho_{pf})_{in} = 0 \quad (10-30)$$

subject to the initial conditions:

$$(\phi \rho_{pf} + m_p) = (\phi \rho_{pf} + m_p)_o, t = 0 \quad (10-31)$$

$(\rho_{pf})_{in}$ and $(\rho_{pf})_{out}$ are the particle mass concentrations in the flowing phase at the inlet and outlet of the core. Wojtanowicz et al. (1987, 1988) omitted the accumulation of particles in the thin core slice and simplified Eq. 10-30 to express the concentration of particles leaving a thin section by:

$$(\rho_{pf})_{out} = (\rho_{pf})_{in} - (AL/q) dm_p/dt \quad (10-32)$$

The rate of particle retention on the pore surface is assumed proportional to the particle mass concentrations in the flowing phase according to:

$$r_r \equiv (dm_p/dt)_r = k_r \rho_{pf} \quad (10-33)$$

The rate of entrainment of the surface deposited particles by the flowing phase is assumed proportional to the mass of particles available on the pore surface according to:

$$r_e \equiv (dm_p/dt)_e = k_e m_p \quad (10-34)$$

Then, the net rate of deposition is given as the difference between the retention and entrainment rates as:

$$dm_p/dt = k_r \rho_{pf} - k_e m_p \quad (10-35)$$

subject to the initial condition given by:

$$m_p = (m_p)_o, t = 0 \quad (10-36)$$

Diagnostic Equations for Typical Cases

Wojtanowicz et al. (1987, 1988) have analyzed and developed diagnostic equations for two special cases of practical importance:

1. Deposition of the externally introduced particles during the injection of a suspension of particles
2. Mobilization and subsequent deposition of the indigeneous particles of porous medium during the injection of a particle free solution

Deposition of Externally Introduced Particles

Three distinct permeability damage mechanisms are analyzed for a given injection fluid rate and particle concentration. As depicted in Figure 10-4, particles are retained mainly in the thin core section near the inlet face. In this region the concentration of the flowing phase is assumed the same as the injected fluid (i.e., $\rho_{pf} \equiv (\rho_{pf})_{in}$).

Gradual pore reduction by surface deposition occurs when the particles of the injected suspension are smaller than the pore constrictions. Assume that the surface deposition is the dominant mechanism compared to the entrainment, that is, $k_r \gg k_e$.

Then, the solution of Eqs. 10–35 and 36 yields:

$$m_p = k_r (\rho_{pf})_{in} t \quad (10-37)$$

A substitution of Eq. 10–37 into Eq. 10–29 leads to the following expression for the area occupied by the surface deposits

$$A_p = \left[Ak_r (\rho_{pf})_{in} / \rho_p \right] t \quad (10-38)$$

Substitution of Eqs. 10–10 and 38 into Eq. 10–28 yields the following diagnostic equation:

$$(K/K_o)^{1/2} = 1 - C_5 t \quad (10-39)$$

in which the empirical constant is given by

$$C_5 = \frac{Ak_r (\rho_{pf})_{in}}{C_3 K_o^{1/2} \rho_p} \quad (10-40)$$

Single pore blocking occurs when the size of the particles in the injected fluid are comparable or bigger than the size of the pore constrictions. A substitution of Eqs. 10–12, 13, and 14 into Eq. 10–28 yields the following diagnostic equation:

$$K/K_o = 1 - C_6 t \quad (10-41)$$

in which the empirical constant is given by:

$$C_6 = 6A_h q f_d (\rho_{pf})_{in} / (C_4 K_o \rho_p \pi d^3) \quad (10-42)$$

Cake formation near the inlet face of the porous media occurs when the particles in the injected solutions are large relative to the pore size and at high a concentration. Combining Eqs. 10–22 and 17 yields the following diagnostic equation:

$$K_o/K = 1 + C_7 t \quad (10-43)$$

in which

$$C_7 = k_c q (\rho_{pf})_{in} / (ALR_m) \quad (10-44)$$

Mobilization and Subsequent Deposition of Indigeneous Particles

This case deals with the injection of a clear (particle free) solution into a porous media. A core is visualized as having two sections designated as the inlet and outlet sides. The particles of the porous media entrained by the flowing phase in the inlet part are recaptured and deposited at the outlet side of the core.

Near the inlet port, the mobilization and entrainment of particles by the flowing phase is assumed to be the dominant mechanism compared to the particles retention (i.e., $k_e \gg k_r$). Thus, dropping the particle retention term, Eqs. 10–35 and 36 yield the following solution for the mass of particles remaining on the pore surface

$$m_p = m_{p_o} \exp(-k_e t) \quad (10-45)$$

Substituting Eq. 10–45 and $(\rho_{pf})_{in} = 0$, Eq. 10–32 yields the following expression for the particle concentration of the flowing phase passing from the inlet to the outlet side of the core as

$$\rho_{pf} = [k_e A L m_{p_o} / q] \exp(-k_e t) \quad (10-46)$$

Depending on the particle concentration and size of the flowing phase entering the core, the outlet side diagnostic equations for three permeability damage mechanisms mentioned previously are derived next.

Gradual Pore Reduction by Surface Deposition and Sweeping

Assume that the mass of the indigeneous or previously deposited particles on the pore surface is m_p^* . Then, the area occupied by these particles is given by Eq. 10–29 as

$$A_p^* = A m_p^* / \rho_p \quad (10-47)$$

and the area open for flow is given by Eq. 10–28 as

$$A_{f_o} = A_f + A_p^* \quad (10-48)$$

A_{f_o} denotes the open flow area when all the deposits are removed.

If simultaneous, gradual pore surface deposition and sweeping are occurring near the outlet region, then both the entrainment and retention terms are considered equally important. Thus, substituting Eq. 10–46, Eq. 10–35 yields the following ordinary differential equation:

$$dm_p/dt + k_e m_p = [k_r k_e AL m_{p_o}/q] \exp(-k_e t) \quad (10-49)$$

The solution of Eq. 10-49, subject to the initial condition $m_p = m_p^*$ (previously deposited particles), is obtained by the integration factor method as:

$$m_p = (m_p^* + C_{11}) \exp(-k_e t) \quad (10-50)$$

in which

$$C_{11} = k_r k_e AL m_p / q \quad (10-51)$$

Then, the area occupied by the remaining particles is given by Eq. 10-29 as:

$$A_p = (Am_p^* / \rho_p) [1 + (C_{11} / m_p^*) t] \exp(-k_e t) \quad (10-52)$$

and the area open for flow is given by Eq. 10-28 as:

$$A_{fo} = A_f + A_p \quad (10-53)$$

Eliminating A_{fo} between Eqs. 10-48 and 53, substituting Eqs. 10-47 and 52 for A_p^* and A_p , and then applying Eq. 10-10 for A_f and A_f^* yields the following diagnostic equation:

$$(K/K^*)^{1/2} = 1 + C_7 - (C_7 + C_8 t) \exp(-k_e t) \quad (10-54)$$

in which

$$C_7 = Am_p^* / (C_3 K^{*1/2} \rho_p) \quad (10-55)$$

and

$$C_8 = C_{11} / m_p^* = k_r k_e AL m_{p_o} / (q m_p^*) \quad (10-56)$$

Normally, $m_{p_o} = m_p^*$. Wojtanowicz et al. (1987) simplified Eq. 10-54 by substituting $C_7 = 0$ when the mass of the particles initially available on the pore surface is small compared to the mass of particles deposited later (i.e., $m_p^* \cong 0$).

If only pore sweeping occurs, then $k_r \ll k_e$. Thus, substitute $k_r = 0$ in Eq. 10-56 to obtain $C_8 = 0$ and Eq. 10-54 becomes:

$$(K/K^*)^{1/2} = 1 + C_7[1 - \exp(-k_e t)] \quad (10-57)$$

If only gradual surface deposition is taking place in the outlet region, then $k_r \gg k_e$. Therefore, dropping the particle retention term and substituting Eq. 10-46, Eqs. 10-35 and 36 for $m_{p_o} = 0$ are solved to obtain the amount of particles retained as:

$$m_p = [k_r A L m_{p_o} / q][1 - \exp(-k_e t)] \quad (10-58)$$

Then, substituting Eqs. 10-58, 29, and 10 into Eq. 10-28 yields the following diagnostic equation:

$$(K/K_o)^{1/2} = 1 - C_9[1 - \exp(-k_e t)] \quad (10-59)$$

in which

$$C_9 = k_r A^2 L m_{p_o} / (C_3 K_o^{1/2} q \rho_p) \quad (10-60)$$

Single Pore Blocking

If the permeability damage is solely due to single pore blocking, then substituting Eqs. 10-46, 12, 13 and 14 into Eq. 10-28 yields the following diagnostic equation:

$$K/K_o = 1 - C_7[1 - \exp(-k_e t)] \quad (10-61)$$

in which

$$C_7 = 6 f_d A L m_{p_o} / (\pi d^3 \rho_p C_4) \quad (10-62)$$

Cake Formation

If the permeability damage is by cake formation, then substituting Eqs. 10-46 and 22 into Eq. 10-17 yields the following diagnostic equation

$$K_o/K = 1 + C_{10}[1 - \exp(-k_e t)] \quad (10-63)$$

in which

$$C_{10} = k_c m_{p_o} / R_m \quad (10-64)$$

A list of the diagnostic equations derived in this section are summarized in Table 10-1 for convenience.

Table 10-1
Diagnostic Equations for Typical Permeability Damage Mechanisms*

Injection Fluid	Permeability Damage Mechanisms	Diagnostic Equation	Straight Line Plotting Scheme	Eq. #
Particulate Suspension	Pore surface deposition	$(K/K_o)^{1/2} = 1 - C_5 t$	$(K/K_o)^{1/2}$ vs. t	T1-1
	Pore throat plugging	$K/K_o = 1 - C_6 t$	(K/K_o) vs. t	T1-2
	Pore filling	$K_o/K = 1 + C_7 t$	(K_o/K) vs. t	T1-3
Particle-free solution	Simultaneous pore surface deposition and sweeping	$(K/K_o)^{1/2} = 1 + C_7$ $-(C_7 + C_8 t)e^{-k_e t}$	Least squares fit	T1-4a
	Simplified pore surface deposition and sweeping for negligible initial particle content	$(K/K_o)^{1/2} = 1 - C_8 t e^{-k_e t}$	$\ln \left\{ \left[1 - (K/K_o)^{1/2} \right] / t \right\}$ vs. t	T1-4b
	Pore surface sweeping	$(K/K_o)^{1/2} = 1 + C_7$ $(1 - e^{-k_e t})$	$\ln \left\{ 1 - \left[(K/K_o)^{1/2} - 1 \right] / C_7 \right\}$ vs. t	T1-5
	Pore surface deposition	$(K/K_o)^{1/2} = 1 - C_9$ $(1 - e^{-k_e t})$	$\ln \left\{ 1 + \left[(K/K_o)^{1/2} - 1 \right] / C_9 \right\}$ vs. t	T1-6
	Pore throat blocking	$K/K_o = 1 - C_7$ $(1 - e^{-k_e t})$	$\ln \left\{ 1 + \left[(K/K_o) - 1 \right] / C_7 \right\}$ vs. t	T1-7
	Pore filling	$K_o/K = 1 + C_{10}$ $(1 - e^{-k_e t})$	$\ln \left\{ 1 - \left[(K_o/K) - 1 \right] / C_{10} \right\}$ vs. t	T1-8

* After Wojtanowicz et al., 1987, 1988; Civan, ©1992 SPE; reprinted by permission of the Society of Petroleum Engineers, and Civan, 1994; reprinted by permission of the U.S. Department of Energy.

The Compartments-in-Series Ordinary Differential Model

Khilar and Fogler (1987) divided a core into n -compartments as depicted in Figure 10-5. The contents of these compartments are assumed well-mixed. Therefore, the composition of the flow stream leaving the compartments should be the same as the contents of the compartments. However, because particles having sizes comparable or larger than the pore throats are trapped within the porous media, the particle concentration of the stream leaving a compartment will be a fraction, γ , of the concentration of the fluid in the compartment. γ is called the particle transport efficiency factor.

Pore surfaces are considered as the source of in-situ mobilized particles and the pore throats are assumed the locations of particle capture. A particle mass balance over a thin slice yields

$$d/dt \left[AL(\phi \rho_{pf} + m_p + m_p^*) \right]_j + q(\rho_{pf})_{out} - q(\rho_{pf})_{in} = 0 \quad (10-65)$$

m_p and m_p^* denote the mass of particles captured at the pore throats and the indigeneous particles remaining on pore surfaces, respectively. In Eq. 10-65

$$(\rho_{pf})_{in} = (\gamma \rho_{pf})_{j-1} \quad (10-66)$$

$$(\rho_{pf})_{out} = (\gamma \rho_{pf})_j \quad (10-67)$$

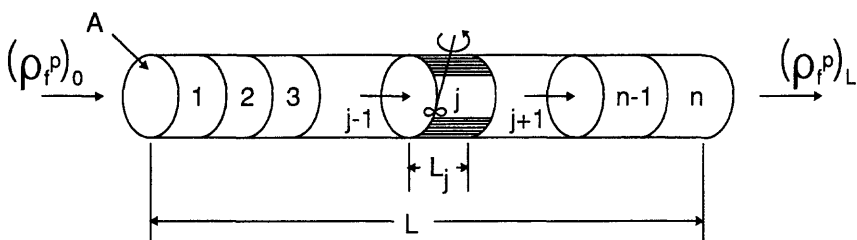


Figure 10-5. Continuously stirred compartments in series realization in a core (after Civan, 1994; reprinted by permission of the U.S. Department of Energy; after Civan 1992 SPE; reprinted by permission of the Society of Petroleum Engineers).

Substituting Eqs. 10–66 and 67, and rearranging Eq. 10–65 becomes:

$$AL_j d/dt(\phi \rho_{pf})_j = q(\gamma \rho_{pf})_{j-1} - q(\gamma \rho_{pf})_j - AL_j d/dt(m_{pj}) \quad (10-68)$$

subject to the initial condition given by:

$$(\phi \rho_{pf})_j = \phi_o \rho_{pfo}, j = 1, 2, \dots, n, t = 0 \quad (10-69)$$

and the boundary condition given by:

$$\rho_{pff} = \rho_{pfo}, j = 0, t > 0 \quad (10-70)$$

The mass balance of particles captured at the pore throats is given by:

$$dm_p/dt = r_r \quad (10-71)$$

subject to

$$m_p = 0, t = 0 \quad (10-72)$$

The mass balance of indigenous particles remaining on pore surfaces is

$$dm_p^*/dt = -r_e \quad (10-73)$$

subject to

$$m_p^* = m_{po}^*, t = 0 \quad (10-74)$$

where m_{po}^* is the mass of particles initially available on pore surface.

The rate of particle entrainment by the flowing phase is assumed both colloiddally and hydrodynamically induced.

$$r_e = \alpha_c m_p^* + \alpha_h (\tau - \tau_c) a_s \quad (10-75)$$

τ is shear stress. a_s is the specific pore surface area. α_c is the colloiddally induced release coefficient given by (Khilar and Fogler, 1983):

$$\alpha_c \neq 0 \text{ for } C_s < C_{sc} \quad (10-76)$$

$$\infty_c = 0 \text{ for } C_s \geq C_{sc} \quad (10-77)$$

C_s is the salt concentration. C_{sc} is the critical salt concentration for particle expulsion. ∞_h is the hydrodynamically induced release coefficient given by (Gruesbeck and Collins, 1982):

$$\infty_h \neq 0 \text{ for } \tau > \tau_c \quad (10-78)$$

$$\infty_h = 0 \text{ for } \tau \leq \tau_c \quad (10-79)$$

τ_c is the critical shear stress required to mobilize particles on pore surface.

The rate of capture of particles at pore throats is assumed proportional to the flowing phase particle concentration:

$$r_c = \beta_t \rho_{pf} \quad (10-80)$$

β_t is the capture coefficient.

Let ρ_{pfc} be the critical particle concentration above which bridging at pore throats occur and particles cannot travel between pore bodies. If the particle concentration is below ρ_{pfc} , then no trapping at pore throats takes place. Therefore,

$$\gamma = 1, \beta_t = 0 \text{ for } \rho_{pf} < \rho_{pfc} \quad (10-81)$$

$$\gamma = 0, \beta_t \neq 0 \text{ for } \rho_{pf} > \rho_{pfc} \quad (10-82)$$

The correlation between entrapment and permeability reduction is based on the Hagen-Poiseuille flow assumption of flow through the pore throat

$$K/K_o = [1 - Bm_p/m_{po}^*]^2 \quad (10-83)$$

where B is a characteristic constant and K_o is the initial permeability.

Simplified Partial Differential Model

Čerňanský and Šíroky (1985) considered injection of a low particle concentration suspension at a constant rate into porous media made of a bed of filaments. Neglecting the diffusion of particles and the contribution of the small amount of particles in the flowing suspension, they expressed the total mass balance of particles similar to Gruesbeck and Collins' (1982) simplified mass balance equation. Thus, for incompressible liquid

and particles and constant injection rate, the total volumetric particle balance equation is given by:

$$\partial \varepsilon / \partial t + u \partial \sigma / \partial x = 0 \quad (10-84)$$

subject to

$$\varepsilon = \varepsilon_o, \quad \sigma = \sigma_o = 0, \quad 0 \leq x \leq L, \quad t = 0 \quad (10-85)$$

and

$$\sigma = \sigma_{in}, \quad x = 0, \quad t > 0 \quad (10-86)$$

Čerňanský and Široký (1985) expressed the net rate of particle deposition in porous media as the difference between the deposition by pore throat plugging and entrainment by hydrodynamic mobilization. Considering the critical shear stress necessary to mobilize the deposited particles in porous media, Civan et al. (1989) modified their rate equation as:

$$\partial \varepsilon / \partial t = k_p u \sigma \phi - k_e \varepsilon (\tau - \tau_{cr}) \quad (10-87)$$

in which the shear-stress is expressed as

$$\tau = \frac{D}{4} \left(-\frac{\partial p}{\partial x} \right) \quad (10-88)$$

where D is the hydraulic tube diameter, and the pressure gradient is represented by Darcy's law:

$$-\partial p / \partial x = u \mu / K \quad (10-89)$$

The instantaneous porosity is given by:

$$\phi = \phi_o - \varepsilon \quad (10-90)$$

where ϕ_o is the initial porosity. Thus, substituting Eqs. 10-88 through 10-90 into Eq. 10-87 yields:

$$\partial \varepsilon / \partial t = k_p u \sigma (\phi_o - \varepsilon) - k'_e \varepsilon (u \mu / K - \tau'_{cr}) \quad (10-91)$$

in which $k'_e = k_e D/4$ and $\tau'_{cr} = 4\tau_{cr}/D$ are the redefined entrainment coefficient and critical shear-stress. $k'_e = 0$ when $u \mu / K < \tau'_{cr}$. At equilibrium, $\partial \varepsilon / \partial t = 0$.

Based on their experimental studies, Čerňanský and Široký (1985) proposed an empirical permeability-porosity relationship as:

$$\frac{\varepsilon}{\phi_o} = 1 - \frac{\phi}{\phi_o} = E \left(1 - \frac{K}{K_o} \right) + \frac{1-E}{\exp G - 1} \left\{ \exp \left[G \left(1 - \frac{K}{K_o} \right) \right] - 1 \right\} \quad (10-92)$$

where E and G are some empirical constants.

The Plugging-Nonplugging Parallel Pathways Partial Differential Model

Gruesbeck and Collins (1982a) developed a partial differential model based on the concept of parallel flow of a suspension of particles through plugging and nonplugging pathways, as depicted in Figure 10-6. Relatively smooth and large diameter flowpaths mainly involve surface deposition and are considered nonplugging. Flowpaths that are highly tortuous and having significant variations in diameter are considered plugging. In the plugging pathways, retainment of particles occurs by jamming and blocking of pore throats when several particles approach narrow flow constrictions. Sticky and deformable deposits usually seal the flow constrictions (Civan, 1994, 1996). Therefore, conductivity of a flow path may diminish without filling the pore space completely. Thus, the fluid seeks alternative flow paths until all the flow paths are eliminated. Then the permeability diminish even though the porosity may be nonzero. Another important issue is the criteria for jamming of pore throats. As demonstrated by Gruesbeck and Collins (1982b) experimentally for perforations, the probability of jamming of flow constrictions strongly depends on the particle concentration of the flowing suspension and the flow constriction-to-particle diameter ratio. Gruesbeck and Collins (1982a) assumed that the liquid and particles have constant physical properties. The porous media is incompressible, homogeneous and isotropic. There is hydraulic communication through the interconnectivity of the plugging and nonplugging pathways and therefore the pressure gradients and the particle concentrations of the suspension flowing through the plugging and nonplugging pathways are the same. The volume flux through the core is constant and only the external particle invasion is considered. The flow through porous media was assumed to obey the Darcy Law. In this section, the Gruesbeck and Collins (1982) model is presented with the modifications and improvements made by Civan (1995).

ϕ_{p_o} and ϕ_{np_o} denote the initial pore volume fractions of the plugging and nonplugging pathways of the porous media (Civan, 1994, 1995).

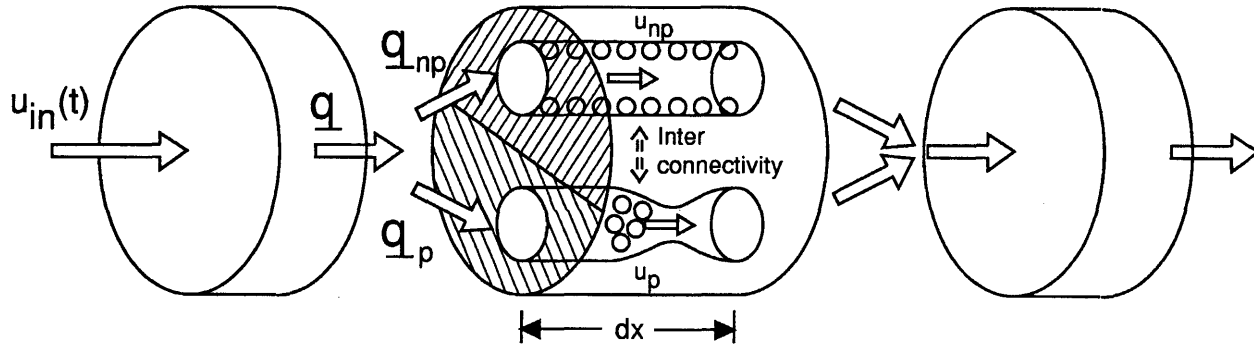


Figure 10–6. Non-plugging and plugging paths realization in a core (after Civan, 1994; reprinted by permission of the U.S. Department of Energy; after Civan 1992 SPE; reprinted by permission of the Society of Petroleum Engineers).

These values can be determined experimentally for a given porous media and the particle size distribution. ϵ_p and ϵ_{np} represent the fractions of the bulk volume occupied by the deposits. Thus, the instantaneous porosities are:

$$\phi_p = \phi_{p_o} - \epsilon_p \quad (10-93)$$

$$\phi_{np} = \phi_{np_o} - \epsilon_{np} \quad (10-94)$$

The fractions of the bulk volume containing the plugging and nonplugging pathways can be approximated, respectively, by:

$$f_p \cong \phi_p / \phi \quad (10-95)$$

$$f_{np} \cong \phi_{np} / \phi \quad (10-96)$$

However, Gruesbeck and Collins (1982) assume a constant value for f_p (and therefore for $f_{np} = 1 - f_p$), which is a characteristic of the porous medium and the particles. Total instantaneous and initial porosities are given, respectively, by:

$$\phi = \phi_p + \phi_{np} \quad (10-97)$$

$$\phi_o = \phi_{p_o} + \phi_{np_o} \quad (10-98)$$

The total deposit volume fraction and the instantaneous available porosity are given, respectively, by:

$$\epsilon = \epsilon_p + \epsilon_{np} \quad (10-99)$$

$$\phi = \phi_o - \epsilon \quad (10-100)$$

The rate of deposition in the plugging pathways is given by assuming the pore filling mechanism:

$$\partial \epsilon_p / \partial t = k_p u_p \sigma_p \phi_p \quad (10-101)$$

$$\epsilon_p = \epsilon_{p_o}, \quad t = 0 \quad (10-102)$$

where σ_p is the volume fraction of the particles flowing through the plugging pathways, $k_p = 0$ when $t < t_p$. t_p is the time at which the pore throats are blocked by forming particle bridges and jamming. This occurs

when the pore throat-to-particle diameter ratio is below its critical value. Civan (1990, 1994) recommended the following empirical correlation:

$$D_t/D_p \left(D_t/D_p \right)_{cr}, \left(D_t/D_p \right)_{cr} = A \left[1 - \exp(-B \text{Re}_p) \right] + C \quad (10-103)$$

which is determined empirically as a function of the particle Reynolds number:

$$\text{Re}_p = \rho_p \sigma_p u D_p / (\mu \phi) \quad (10-104)$$

The rate of deposition in the nonplugging tubes is given as the difference between the rates of surface deposition and sweeping of particles (Civan, 1994):

$$\partial \varepsilon_{np} / \partial t = k_d u_{np} \sigma_{np} \phi_{np}^{2/3} - k_e \varepsilon_{np} \phi_{np}^{2/3} \eta_e (\tau_{np} - \tau_{cr}) \quad (10-105)$$

subject to the initial condition

$$\varepsilon_{np} = \varepsilon_{np_0}, t = 0 \quad (10-106)$$

where σ_{np} is the volume fraction of particles in the suspension of particles flowing through the nonplugging pathways. k_d and k_e are the surface deposition and mobilization rate constants. $k_e = 0$ when $\tau_w < \tau_{cr}$. η_e is the fraction of the uncovered deposits that can be mobilized from the pore surface, estimated by:

$$\eta_e = \exp(-k \varepsilon_{np}) \quad (10-107)$$

τ_{cr} is the minimum shear stress necessary to mobilize the surface deposits. τ_{np} is the wall shear-stress in the nonplugging tubes, given by the Rabinowitsch-Mooney equation (Metzner and Reed, 1955):

$$\tau_{np} = k' (8 v_{np} / D_{np})^{n'} \quad (10-108)$$

in which the interstitial velocity, v_{np} , is related to the superficial velocity, u_{np} , by:

$$v_{np} = u_{np} / \phi_{np} \quad (10-109)$$

and the mean pore diameter is given by:

$$D_{np} = C4\sqrt{2}\left(K_{np}/\phi_{np}\right)^{1/2} \quad (10-110)$$

where C is an empirical shape factor.

It can be shown that Eqs. 10-101 and 105 simplify to the deposition rate equations given by Gruesbeck and Collins (1982):

$$\partial\epsilon_p/\partial t = (c_1 + c_2\epsilon_p)u_p\sigma \quad (10-111)$$

$$\partial\epsilon_{np}/\partial t = c_3\sigma_{np} - c_4(u_{np} - u_c)\epsilon_{np} \quad (10-112)$$

where c_1, c_2, c_3 , and c_4 are some empirically determined coefficients.

This requires that the effects of the permeability and porosity changes be negligible, the fraction of the uncovered deposits be unity, the suspension of particles be Newtonian, and the particle volume fractions of the suspensions flowing through the plugging and nonplugging pathways be the same, that is,

$$\sigma_p = \sigma_{np} = \sigma \quad (10-113)$$

The permeabilities of the plugging and nonplugging pathways are given by the following empirical relationships (Civan, 1994):

$$K_p = K_{p_o} \exp\left[-\alpha(\phi_{p_o} - \phi_p)^{n_1}\right] = K_{p_o} \exp(-\alpha\epsilon_p^{n_1}) \quad (10-114)$$

and

$$K_{np} = K_{np_o} \left(\phi_{np}/\phi_{np_o}\right)^{n_2} = K_{np_o} \left(1 - \epsilon_{np}/\phi_{np_o}\right)^{n_2} \quad (10-115)$$

Then, the average permeability of the porous medium is given by:

$$K = f_p K_p + f_{np} K_{np} \quad (10-116)$$

Note that Eq. 10-116 was derived independently by Civan (1992) and Schechter (1992) and is different than the expression given by Gruesbeck and Collins (1982).

The superficial flows in the plugging and nonplugging pathways are given, respectively, by:

$$u_p = uK_p/K \quad (10-117)$$

$$u_{np} = uK_{np}/K \quad (10-118)$$

Considering that the physical properties of the particles and the carrier liquid are constant, the volumetric balance of particles in porous media is given by:

$$\partial/\partial t(\phi\sigma + \varepsilon) + \partial/\partial x(\sigma u) = 0 \quad (10-119)$$

Substituting Eq. 10-100 into Eq. 10-119, and then rearranging, an alternative convenient form of Eq. 10-119 can be obtained as:

$$(\phi_o - \varepsilon)\partial\sigma/\partial t + \partial/\partial x(\sigma u) + (1 - \sigma)\partial\varepsilon/\partial t = 0 \quad (10-120)$$

Following Gruesbeck and Collins (1982), Eq. 10-120 can be simplified for cases where ε and σ are small compared to ϕ_o and unity, respectively, and for constant injection rate, as:

$$\phi_o \frac{\partial\sigma}{\partial t} + u \frac{\partial\sigma}{\partial x} + \frac{\partial\varepsilon}{\partial t} = 0 \quad (10-121)$$

The initial particle contents of the flowing solution and porous media are assumed zero:

$$\sigma = \sigma_0 = 0, \quad \varepsilon = \varepsilon_0, \quad 0 \leq x \leq L, \quad t = 0 \quad (10-122)$$

where L is the length of porous medium. The particle content of the suspension of particles injected into the porous media is prescribed as:

$$\sigma = \sigma_{in}, \quad x = 0, \quad t > 0 \quad (10-123)$$

Alternatively, the pressures of the inlet and outlet ends of the porous media instead of the flow rate can be specified. Then, the volumetric flux can be estimated by the Darcy law:

$$u = (K/\mu)(-\partial p/\partial x) \quad (10-124)$$

Substituting Eq. 10-124 into the volumetric equation of continuity

$$\partial\phi/\partial t + \partial u/\partial x = 0 \quad (10-125)$$

results in the pressure equation

$$\frac{\partial}{\partial x} \left(\frac{K}{\mu} \frac{\partial p}{\partial x} \right) = \frac{\partial \phi}{\partial t} \quad (10-126)$$

subject to the boundary conditions

$$p = p_{in}, \quad x = 0 \quad (10-127)$$

$$p = p_{out}, \quad x = L \quad (10-128)$$

Then, the pressure obtained by solving Eqs. 10-126 through 10-128 is substituted into Eq. 10-124 to determine the volume flux.

The preceding formulation of Eq. 10-119 or 120 applies to the overall system following Gruesbeck and Collins' (1982) assumption that the particle concentrations in the plugging and nonplugging pathways are the same according to Eq. 10-113. When different concentrations are considered, Eq. 10-120 should be applied separately for the plugging and nonplugging paths, respectively, as suggested by Civan (1995):

$$\begin{aligned} & (\phi_{p_o} - \varepsilon_p) \partial \sigma_p / \partial t + \partial / \partial x (\sigma_p u_p) + (1 - \sigma_p) \partial \varepsilon_p / \partial t = \\ & k(\sigma_p - \sigma_{np}) \end{aligned} \quad (10-129)$$

$$\begin{aligned} & (\phi_{np_o} - \varepsilon_{np}) \partial \sigma_{np} / \partial t + \partial / \partial x (\sigma_{np} u_{np}) + (1 - \sigma_{np}) \partial \varepsilon_{np} / \partial t = \\ & -k(\sigma_p - \sigma_{np}) \end{aligned} \quad (10-130)$$

subject to

$$\sigma_p = 0, \quad \sigma_{np} = 0, \quad 0 \leq x \leq L, \quad t = 0 \quad (10-131)$$

$$\sigma_p = \sigma_{np} = \sigma_{in}, \quad x = 0, \quad t > 0 \quad (10-132)$$

k is a particle exchange rate coefficient. A solution of Eqs. 10-129 through 132 along with the particle deposition rate equations, Eqs. 10-101 and 105, yields the particle volume fractions in the plugging and nonplugging flow paths.

Model Considering the Clayey Formation Swelling and Indigeneous and External Particles

Civan et al. (1989) and Ohen and Civan (1991, 1993) considered the formation damage by clayey formation swelling and migration of externally injected and indigeneous particles. They assumed constant physical properties of the particles and the carrier fluid in the suspension. They also considered the effect of fluid acceleration during the narrowing of the flow passages by formation damage. Ohen and Civan (1993) classified the indigeneous particles that are exposed to solution in the pore space in two groups: lump of total expansive (swelling, i.e. total authigenic clay that is smectitic) and lump of total nonexpansive (nonswelling) particles, because of the difference of their rates of mobilization and sweepage from the pore surface. They considered that the particles in the flowing suspension are made of a combination of the indigeneous particles of porous media entrained by the flowing suspension and the external particles introduced to the porous media via the injection of external fluids. They considered that the particles of the flowing suspension can be redeposited and reentrained during their migration through porous media and the rates of mobilization of the redeposited particles should obey a different order of magnitude than the indigeneous particles of the porous media. Further, they assumed that the deposition of the suspended particles over the indigeneous particles of the porous media blocks the indigeneous particles and limits their contact and interaction with the flowing suspension in the pore space. They considered that the swelling clays of the porous media can absorb water and swell to reduce the porosity until they are mobilized by the flowing suspension. They assumed that permeability reduction is a result of the porosity reduction by net particle deposition and formation swelling and by formation plugging by size exclusion. The Ohen and Civan (1993) formulation is applicable for dilute and concentrated suspensions, whereas, Gruesbeck and Collins' (1982) model applies to dilute suspensions.

The mass balance equations for the total water (flowing plus absorbed) in porous media and the total particles (suspended plus deposited) in porous media are given, respectively, by:

$$\partial/\partial t[(\phi\sigma_w + \varepsilon_w)\rho_w] + \partial/\partial x(\sigma_w u \rho_w) = 0 \quad (10-133)$$

$$\partial/\partial t[(\phi\sigma_p + \varepsilon_p + \varepsilon_p^*)\rho_p] + \partial/\partial x(\sigma_p u \rho_p) = 0 \quad (10-134)$$

Thus, adding Eqs. 10–133 and 134 yields the total mass balance equation for the water and particles in porous media as:

$$\begin{aligned} & \partial/\partial t \left[\phi (\sigma_w \rho_w + \sigma_p \rho_p) + \epsilon_w \rho_w + (\epsilon_p + \epsilon_p^*) \rho_p \right] \\ & + \partial/\partial x \left[(\sigma_w \rho_w + \sigma_p \rho_p) u \right] = 0 \end{aligned} \quad (10-135)$$

In Eqs. 10-133- through 135, ϕ is the instantaneous porosity, ρ_w and ρ_p are the densities of water and particles, u is the volumetric flux of the flowing suspension of particles, ϵ_w , ϵ_p , and ϵ_p^* represent the volume fraction of porous media containing the absorbed water, particles deposited from the flowing suspension, and the indigenous particles in the pore space, respectively, and σ_w and σ_p denote the volume fractions of the water and particles, respectively, in the flowing suspension. Thus,

$$\sigma_w + \sigma_p = 1 \quad (10-136)$$

According to Eq. 10-135 the density of the flowing suspension is given as a volumetric weighted sum of the densities of the water and particles by:

$$\rho = \sigma_w \rho_w + \sigma_p \rho_p = \rho_w + (\rho_p - \rho_w) \sigma_p \quad (10-137)$$

For simplification purposes, assume constant densities for the water and particles. However, note that the density of suspension is not a constant, because it is variable by the particle and water volume fractions based on Eq. 10-137. Therefore, Eqs. 10-134 and 135 can be expressed, respectively, as:

$$\partial/\partial t (\phi \sigma_p) + \partial/\partial x (\sigma_p u) + \partial \epsilon_p / \partial t + \partial \epsilon_p^* / \partial t = 0 \quad (10-138)$$

$$\begin{aligned} & \partial/\partial t (\phi \rho) + \partial/\partial x (\rho u) + \rho_p (\partial \epsilon_p / \partial t + \partial \epsilon_p^* / \partial t) \\ & + \rho_w \partial \epsilon_w / \partial t = 0 \end{aligned} \quad (10-139)$$

Considering the rapid flow of suspension as the flow passages narrow during the formation damage, the Forchheimer equation is used as the momentum balance equation:

$$u = -(\mu/\rho)^{-1} N_{nd} K \partial \psi / \partial x \quad (10-140)$$

where ψ is the flow potential defined as:

$$\Psi = \int_{p_o}^p \frac{dp}{\rho} + g(z - z_o) \sin \theta \quad (10-141)$$

in which θ is the inclination angle and z_o is a reference level. N_{nd} is the non-Darcy number given by

$$N_{nd} = (1 + \rho u \beta K / \mu)^{-1} \quad (10-142)$$

The inertial flow coefficient, β can be estimated by the Liu et al. (1995) correlation:

$$\beta = \frac{8.91 \times 10^8 \tau}{\phi K} \quad (10-143)$$

Brinkman's application of Einstein's equation is used to estimate the viscosity of the suspension:

$$\mu = \mu_w (1 - \sigma_p)^{2.5} \quad (10-144)$$

where μ_w is the viscosity of water.

Substituting Eq. 10-140 into Eq. 10-139 yields the following equation for the flow potential:

$$\begin{aligned} \partial/\partial x \left[(\rho^2/\mu) N_{nd} K \partial \Psi / \partial x \right] &= \partial/\partial t (\phi \rho) \\ + \rho_p (\partial \epsilon_p / \partial t + \partial \epsilon_p^* / \partial t) &+ \rho_w \partial \epsilon_w / \partial t \end{aligned} \quad (10-145)$$

The particle volume fraction and the flow potential can be calculated by solving Eqs. 10-138 and 145 simultaneously, using an appropriate numerical method such as the finite difference method used by Ohen and Civan (1993), subject to the initial and boundary conditions given by:

$$\sigma_p = \sigma_{p_o}(x), \quad \Psi = \Psi_o(x), \quad 0 \leq x \leq L, \quad t = 0 \quad (10-146)$$

$$\sigma_p = (\sigma_p)_{in}, \quad \Psi = \Psi_{in} \text{ or } u = u_{in}, \quad x = 0, \quad t > 0 \quad (10-147)$$

$$\Psi = \Psi_{out}, \quad x = L, \quad t > 0 \quad (10-148)$$

The volumetric rate of water absorption is estimated by (Civan et al., 1989):

$$\partial \epsilon_w / \partial t = B t^{-1/2} \quad (10-149)$$

where t is the actual contact time of flowing water with the porous media and B is an absorption rate constant.

The porosity change by clayey formation swelling is estimated by (Civan and Knapp, 1987; Ohen and Civan, 1990, 1993):

$$\partial \epsilon_{sw} / \partial t = \lambda \partial \epsilon_w / \partial t \quad (10-150)$$

where λ is the swelling coefficient determined by an appropriate empirical correlation such as by those given by Seed et al. (1962) and Nayak and Christensen (1970).

The volume balance of particles (indigenous and/or external types) of the flowing suspension deposited in porous media is given as the difference of the deposition by the pore surface and pore throat deposition processes and the re-entrainment rates by the colloidal and hydrodynamic processes as (Civan, 1996, 1996):

$$\begin{aligned} \partial \epsilon_p / \partial t = & k_d(a+u)\sigma_p \phi^{2/3} + k_p u \sigma_p \phi \\ & - k_r \epsilon_p \eta_e (c_{cr} - c) - k_e \epsilon_p \eta_e \phi^{2/3} (\tau - \tau_{cr}) \end{aligned} \quad (10-151)$$

where

$$k_p = 0 \text{ for } t < t_p \quad (10-152)$$

$$k_r = 0 \text{ for } c > c_r \quad (10-153)$$

$$k_e = 0 \text{ for } \tau < \tau_{cr} \quad (10-154)$$

The initial condition is given by:

$$\epsilon_p = \epsilon_{p_0}, \quad 0 \leq x \leq L, \quad t = 0 \quad (10-155)$$

Let single and double primes denote the nonswelling and swelling clays. The volume balances of the nonmobilized indigenous nonswelling and swelling clays remaining in porous media is given in terms of the colloidal and hydrodynamic mobilization rates, respectively, by:

$$\partial \epsilon_p^* / \partial t = -k'_e \epsilon_p^* \eta'_e (c'_{cr} - c) - k'_e \epsilon_p^* \eta'_e \phi^{2/3} (\tau - \tau'_{cr}) \quad (10-156)$$

$$\begin{aligned} \partial \epsilon_p^{*''} / \partial t &= (1 + \alpha) \\ \left[-k_r'' \epsilon_p^{*''} \eta_e'' (c_{cr}'' - c) - k_e'' \epsilon_p^{*''} \eta_e'' \phi^{2/3} (\tau - \tau_{cr}'') \right] \end{aligned} \quad (10-157)$$

where α is the expansion coefficient of a unit clay volume, estimated by (see Chapter 2):

$$\alpha = \alpha_s - (\alpha_s - 1) \exp(-2k_4 B \sqrt{t}) \quad (10-158)$$

in which α_s is the expansion coefficient at saturation. The initial conditions are given by:

$$\epsilon_p^{*'} = \epsilon_{p_o}^{*'}, \quad \epsilon_p^{*''} = \epsilon_{p_o}^{*''}, \quad 0 \leq x \leq L, \quad t = 0 \quad (10-159)$$

Therefore,

$$\partial \epsilon_p^{*} / \partial t = \partial \epsilon_p^{*'} / \partial t + \partial \epsilon_p^{*''} / \partial t \quad (10-160)$$

and

$$\epsilon_p^{*} = \epsilon_p^{*'} + \epsilon_p^{*''} \quad (10-161)$$

Note $k_r' = 0$ for $c > c_{cr}'$, $k_r'' = 0$ for $c > c_{cr}''$, $k_e' = 0$ for $\tau < \tau_{cr}'$, and $k_e'' = 0$ for $\tau < \tau_{cr}''$.

$$\eta_e' = e^{-k_s \epsilon_p} \quad (10-162)$$

$$\eta_e'' = e^{-k_s' \epsilon_p} \quad (10-163)$$

The instantaneous porosity is given by:

$$\phi = \phi_o - \Delta \epsilon_{sw} - \Delta \epsilon_p + \Delta \epsilon_p^{*} \quad (10-164)$$

where ϕ_o is the initial porosity.

The instantaneous permeability is estimated by means of the modified Kozeny-Carman equation (see Chapter 5 for derivation).

$$\frac{K}{K_o} = \gamma \left(\frac{\phi}{\phi_o} \right)^3 \quad (10-165)$$

where K_o and ϕ_o are the initial permeability and porosity and γ is the flow efficiency factor, which is a measure of the fraction of the pore throats remaining open (see Figure 10-3). Thus, when all the pore throats are closed, then $\gamma = 0$ and $K = 0$, even if $\phi \neq 0$.

The cumulative volume of fluid injected at $x = 0$, expressed in terms of the initial undamaged pore volume, is given by

$$Q_o = (L\phi_o)^{-1} \int_0^t u_o dt \quad (10-166)$$

u_o is the injection volumetric flux.

The cumulative fines production at $x = L$, in the effluent is

$$Q_{pL} = A \int_0^t \sigma_{pL} u_L dt \quad (10-167)$$

u_L and σ_{pL} are the effluent volumetric flux and particle fraction, respectively.

The harmonic mean average permeability of the core of length L is calculated by

$$K_m = L / \int_0^L (1/K) dx \quad (10-168)$$

The linear flow model presented above can be converted to the radial flow model by the application of the transformation given by (Ohen and Civan, 1991):

$$x = \ln(r/r_w) \quad (10-169)$$

r and r_w denote the radial distance and the well bore radius, respectively.

Model Assisted Analysis of Experimental Data

Without the theoretical analysis and understanding, laboratory work can be premature, because the analyst may not exactly know what to look for and what to measure. The theoretical analysis of various processes involved in formation damage provide a scientific guidance in designing the experimental tests and helps in selecting a proper, meaningful set of variables that should be measured. Having studied the various issues involving formation damage by fines migration, we are prepared to

conduct laboratory experiments in a manner to extract useful information. Here, the analysis of experimental data by means of the mathematical models developed in this chapter is illustrated by several examples taken from the literature.

Applications of the Wojtanowicz et al. Model

In general, formation damage may be a result of a number of mechanisms acting together with different relative contributions. But the Wojtanowicz et al. (1987, 1988) analysis of experimental data is based on the assumption that one of the potential formation damage mechanisms is dominant under certain conditions. Therefore, by testing the various diagnostic equations given in Table 10-1 derived by Wojtanowicz et al. for possible mechanisms involving the laboratory core damage, the particular governing damage mechanism can be identified. They have demonstrated that portions of typical laboratory data can be represented by different equations, indicating that different mechanisms are responsible for damage. For example, as indicated by Figures 10-7 and 10-8, the initial and later

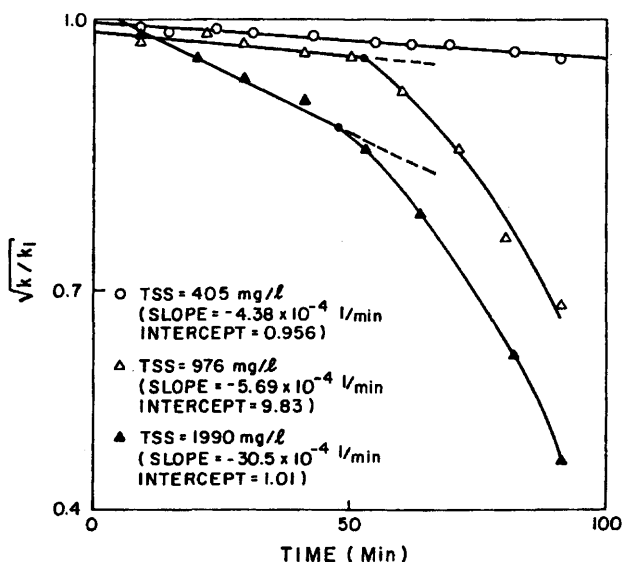


Figure 10-7. Diagnostic chart for gradual pore blockage by external particles invasion (after Wojtanowicz et al., ©1987 SPE; reprinted by permission of the Society of Petroleum Engineers and after Wojtanowicz et al., ©1988, reprinted by permission of the ASME).

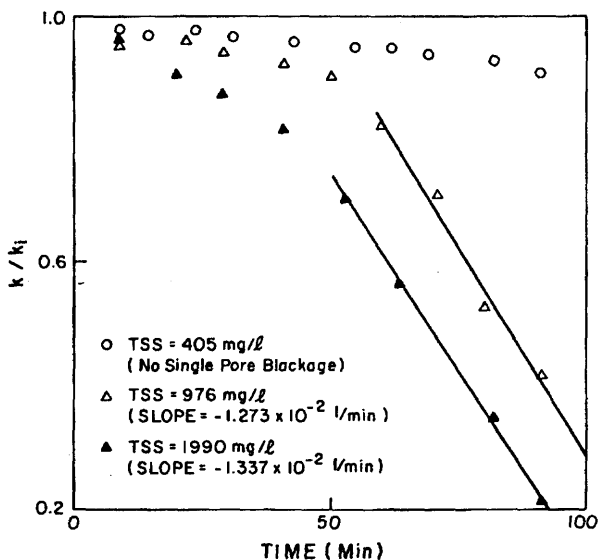


Figure 10-8. Diagnostic chart for gradual pore blockage by external particles invasion (after Wojtanowicz et al., ©1987 SPE; reprinted by permission of the Society of Petroleum Engineers and after Wojtanowicz et al., ©1988, reprinted by permission of the ASME).

portions of the experimental data for damage by foreign particles invasion with low particle concentration drilling muds (0.2%, 0.5%, and 1.0% by weight) can be represented by Eqs. T1-1 and 2, successfully, revealing that the pore surface deposition and pore throat plugging mechanisms are dominant during the early and late times, respectively. Figure 10-9 shows that Eq. T1-3 provides an accurate straight-line representation of the core damage with injection of suspensions of high concentration drilling muds (2% and 3% by weight) of foreign particles, revealing that the dominant formation damage mechanism should be the pore filling and internal cake formation. The data plotted in Figure 10-10 shows that the sizes and concentrations of the particles of the injected suspension significantly affect the durations and extent of the initial formation damage by pore surface deposition (Eq. T1-1) and later formation damage by pore throat plugging (Eq. T1-2) mechanisms.

Figure 10-11 shows that the damage of the core by a particle-free calcium chloride-based completion fluid is due to the plugging of pore throats by particles mobilized by brine incompatibility, because Eq. T1-7 can represent the data satisfactorily by a straight-line. Figures 10-12 and

(text continued on page 218)

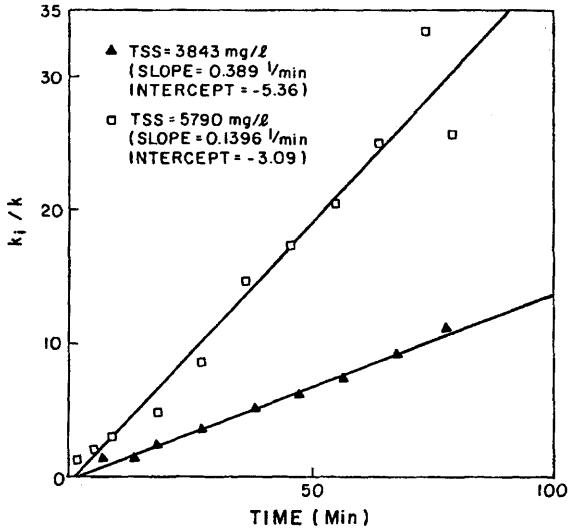


Figure 10-9. Diagnostic chart for cake forming by external particles invasion (after Wojtanowicz et al., ©1987 SPE; reprinted by permission of the Society of Petroleum Engineers and after Wojtanowicz et al., ©1988, reprinted by permission of the ASME).

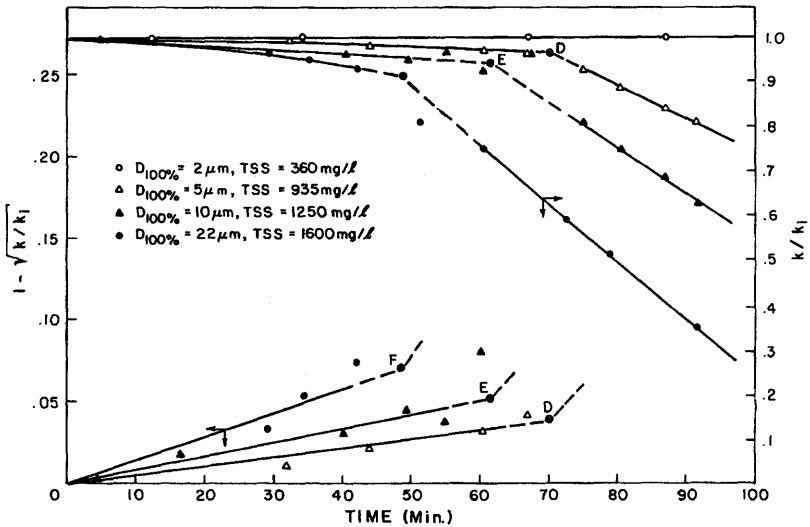


Figure 10-10. Diagnostic chart for transition from gradual pore blockage to single pore blockage during external particles invasion (after Wojtanowicz et al., ©1987 SPE; reprinted by permission of the Society of Petroleum Engineers and after Wojtanowicz et al., ©1988, reprinted by permission of the ASME).

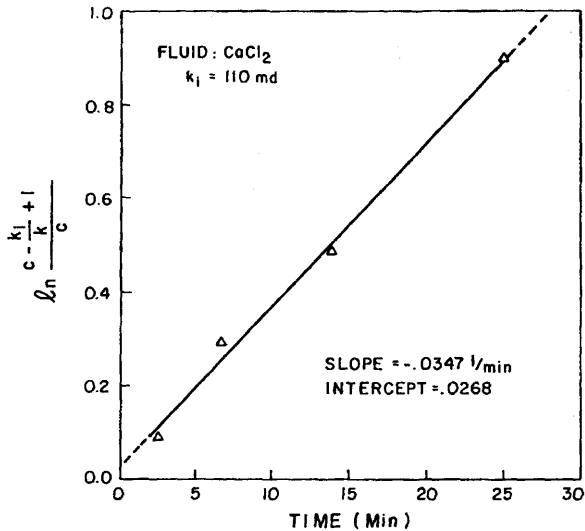


Figure 10-11. Diagnostic chart for cake forming by calcium chloride-based completion fluid invasion (after Wojtanowicz et al., ©1987 SPE; reprinted by permission of the Society of Petroleum Engineers and after Wojtanowicz et al., ©1988, reprinted by permission of the ASME).

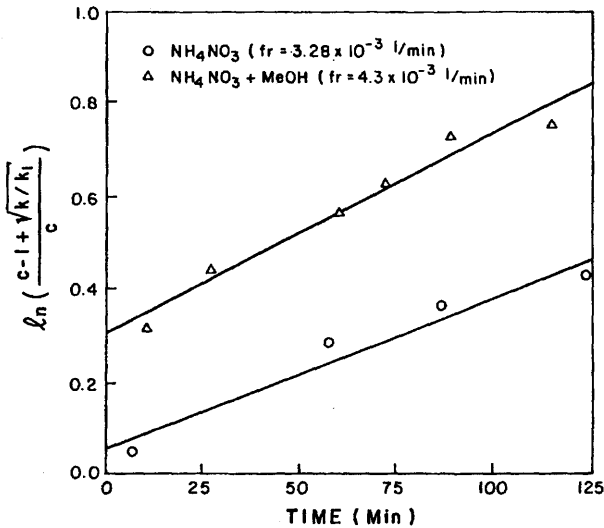


Figure 10-12. Diagnostic chart for gradual pore blocking by ammonium nitrate/alcohol-based completion fluid invasion (after Wojtanowicz et al., ©1987 SPE; reprinted by permission of the Society of Petroleum Engineers and after Wojtanowicz et al., ©1988, reprinted by permission of the ASME).

(text continued from page 215)

10–13 show that the damage of the core by particle-free ammonium nitrate/alcohol-based completion fluids are due to pore surface deposition and pore surface sweeping, because the data can be satisfactorily fitted by straight-lines according to Eqs. T1–6 and 5, respectively. Figure 10–14 showing the plot of data for the combined effects of pore surface deposition and sweeping according to Eq. T1–4, indicates the effect of the flow rate on damage. As can be seen, the rate of formation damage increases by the flow rate. Wojtanowicz et al. (1987) explain this increase due to about a fivefold increase in the value of the release coefficient, k_e , as a result of about a threefold increase in the flow rate from 3 to 10 ml/min.

The best estimates of the intercept and slope values obtained by the least-squares regression analysis for the cases analyzed are presented by Wojtanowicz et al. (1987) in Figures 10–7 through 10–14. Using these parameters in the relevant equations representing these cases, the relative retained permeability curves vs. t are plotted in Figure 10–15 for comparison. As can be seen, pore filling by cake formation causes the most severe damage.

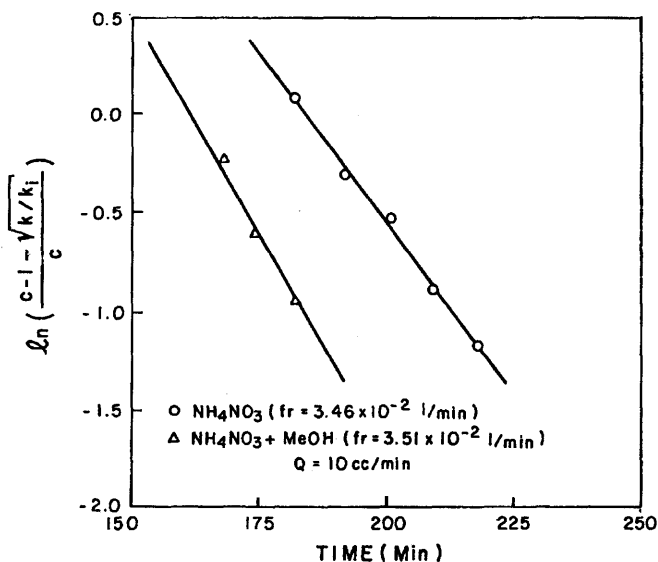


Figure 10–13. Diagnostic chart for gradual pore sweeping by ammonium nitrate/alcohol-based completion fluid invasion (after Wojtanowicz et al., ©1987 SPE; reprinted by permission of the Society of Petroleum Engineers and after Wojtanowicz et al., ©1988, reprinted by permission of the ASME).

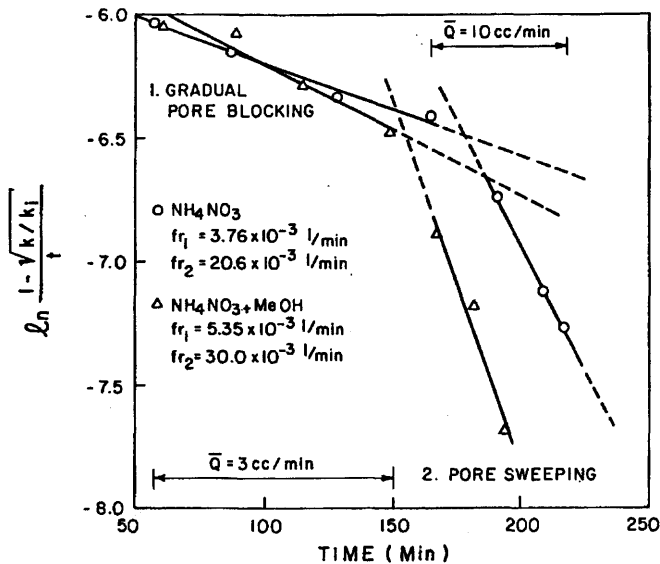


Figure 10-14. Diagnostic chart for combined effects of gradual pore blocking and sweeping (after Wojtanowicz et al., ©1987 SPE; reprinted by permission of the Society of Petroleum Engineers and after Wojtanowicz et al., ©1988, reprinted by permission of the ASME).

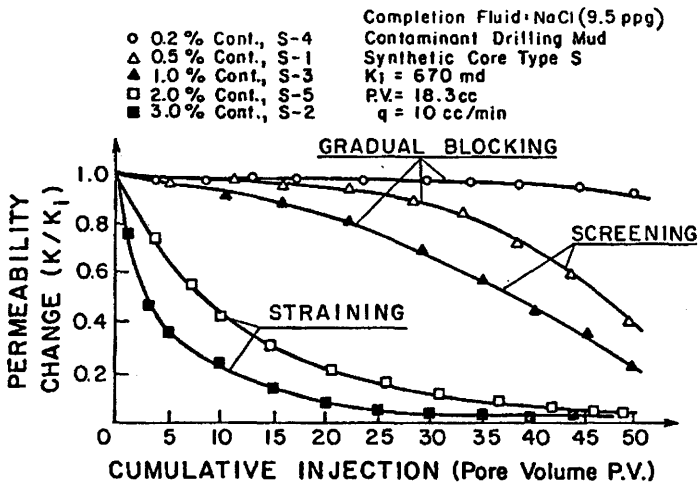


Figure 10-15. Comparison of the effects of gradual blocking, screening, and straining on permeability reduction (after Wojtanowicz et al., ©1987 SPE; reprinted by permission of the Society of Petroleum Engineers and after Wojtanowicz et al., ©1988, reprinted by permission of the ASME).

Applications of the Černanský and Široký Model

The objectives of the experimental studies were threefold:

1. Determine an empirical relationship between permeability and porosity in the form of Eq. 10–92.
2. Determine the values of the deposition and entrainment rate constants, k_p and k'_e .
3. Study the effects of the length of porous media and the rate and concentration of the particle suspension injected into the porous media.

The pressure difference across the porous media and the particle concentration of the effluent were measured as functions of time during the injection of a suspension of finely ground limestone particles at a given concentration and rate.

The porous material was prepared by using nonwoven felt of filaments of polypropylene. The porous material samples of 4 cm diameter and 0.5, 1.0, 1.5, and 2.0 cm lengths were used. The particle suspension was prepared using finely ground limestone of $2,825 \text{ kg/m}^3$ density in water. The porosity was determined by the weighting method. The discrete times at which measurements are taken are denoted by the subscript $i = 2, 3, \dots, N$ and the initial time is denoted by $i = 1$. The permeability was determined by Darcy's equation by neglecting the effect of gravity for short samples:

$$K_i = u\mu L / \Delta p_i : i = 2, 3, \dots, N \quad (10-170)$$

The volume of particles deposited per unit volume of porous media was calculated, by integrating Eq. 10–84 and applying the mean value theorem:

$$\left(\frac{\partial \varepsilon}{\partial t} \right)_{\text{avg}} \equiv \frac{1}{L} \int_0^L \frac{\partial \varepsilon}{\partial t} dx = \frac{(\sigma_{in} - \sigma_{out}) u}{L} \quad (10-171)$$

from which

$$\varepsilon = \varepsilon_o + \frac{u}{L} \int_0^t (\sigma_{in} - \sigma_{out}) dt \quad (10-172)$$

where $\varepsilon_o = 0$ for an initially particle-free porous material. Eq. 10–172 is evaluated numerically by applying the trapezoidal rule of integration as, for a constant injection suspension particle concentration:

$$\varepsilon_i = \varepsilon_o + \frac{u}{L} \sum_{i=2}^N \left[\sigma_{in} - \frac{(\sigma_{out})_{i-1} + (\sigma_{out})_i}{2} \right] \Delta t_i : i = 2, 3, \dots, N \quad (10-173)$$

Eqs. 10-170 and 173 were applied at different times and the data were plotted in Figure 10-16. As shown in Figure 10-16, virtually the same results were obtained for different injection velocities of $u = 0.5$ and 1.0 cm/s.

The E and G parameter values were determined as a function of the length of porous media by nonlinear regression of Eq. 10-92 to the data given in Figure 10-16. Plot of E and G vs. the length are given in Figure 10-17. Exponential regressions of these data indicate that $E \cong 0.14$ and $G \cong 5.3$ as the length approaches zero, although the data are of low

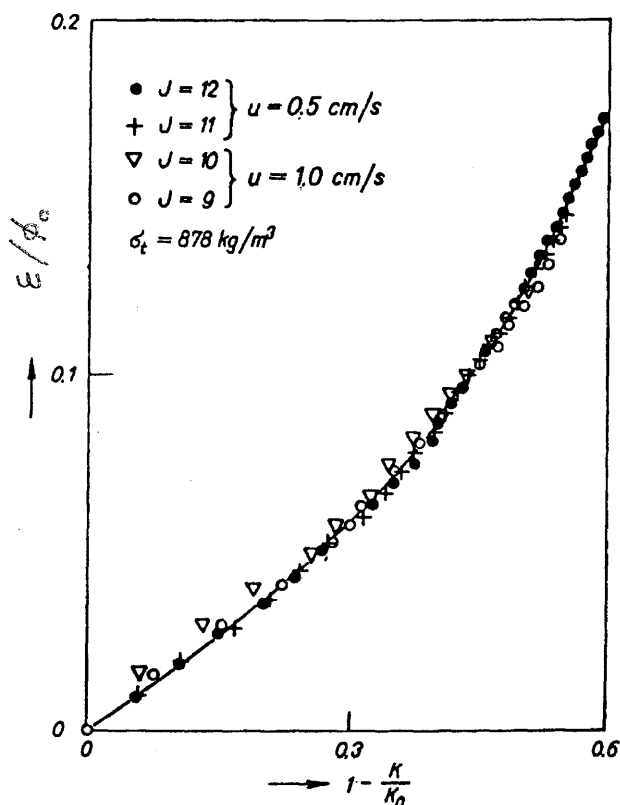


Figure 10-16. Correlation of the deposit fraction and permeability for material POP 1, using a 5 mm thick porous material and $c_o = 0.1$ kg/m³ (Cerňanský, A., & Šíroky, R., 1985; reprinted by permission of the AIChE, ©1985 AIChE, all rights reserved, and after Cerňanský and Šíroky, 1982, reprinted by permission).

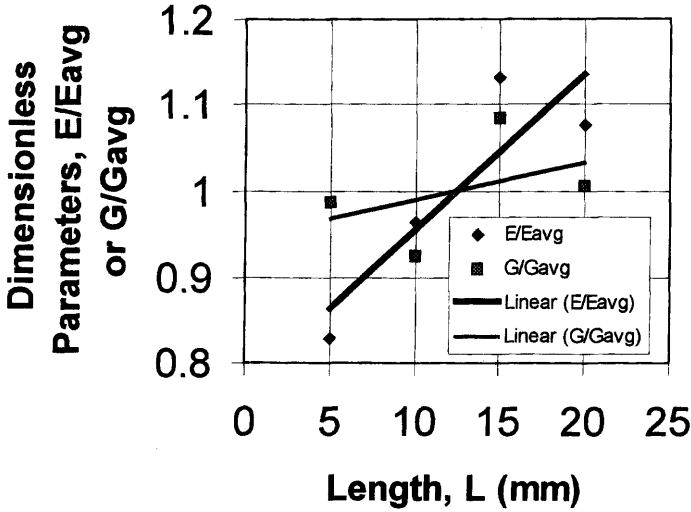


Figure 10-17. Correlation of the Čerňanský and Široký (1985) data for variation of the E and G parameters by the length of porous media for material POP 1. $E_{avg} = 0.179$ and $G_{avg} = 5.66$.

quality, as indicated by the coefficients of regressions $R^2 = 0.78$ and $R^2 = 0.18$, respectively.

The mean diameter of particles is $20.2\mu\text{m}$ and the estimated dimension of pores $50\mu\text{m}$. The porosity is $\phi_o = 0.31$. The concentration of the injected suspension is $c_{in} = 0.1\text{kg}/\text{m}^3$ or $\sigma_{in} = (0.1\text{kg}/\text{m}^3)/(2,825\text{kg}/\text{m}^3) = 3.54 \times 10^{-5} \text{m}^3/\text{m}^3$.

To determine the deposition and entrainment rate constants, in Eq. 10-91 $\tau'_{cr} = 0$ was substituted and the derivative with respect to time was evaluated numerically using the central and backward finite difference approximations given below, respectively, for the interior and the final points (see Chapter 16 for derivation):

$$\frac{\partial \epsilon_i}{\partial t} \cong \frac{\epsilon_{i+1} - \epsilon_{i-1}}{2\Delta t_i} : i = 2, 3, \dots, N-1 \quad (10-174)$$

$$\frac{\partial \epsilon_N}{\partial t} \cong \frac{\epsilon_{N-2} - 4\epsilon_{N-1} + 3\epsilon_N}{2\Delta t_N} \quad (10-175)$$

The average concentration was estimated as the logarithmic mean value of the injection and the effluent suspension concentrations according to:

$$\sigma_i = \frac{\sigma_{in} - (\sigma_{out})_i}{\ln \left[\frac{\sigma_{in}}{(\sigma_{out})_i} \right]} : i = 2, 3, \dots, N: \quad (10-176)$$

The rate parameters, k_p and k'_e , in Eq. 10-91 were determined for different injection velocities using the method of least squares with the values calculated by Eqs. 10-170 and 174-176. The results presented in Figure 10-18 indicate that the retention rate coefficient, k_p , decreases and the entrainment rate coefficient, k_e , increases with the injection velocity.

These calculations were repeated for different length porous media and the results are summarized in Figure 10-19. These values can be extrapolated to zero core length, however, again the quality of data is not good.

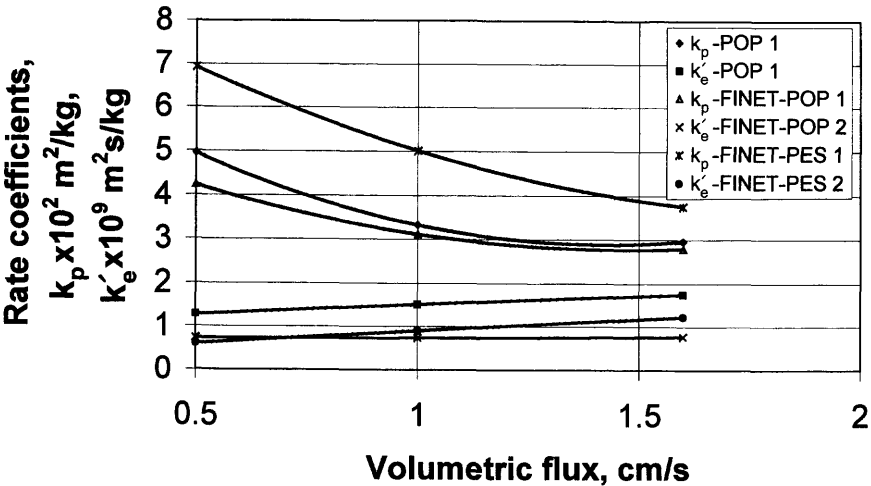


Figure 10-18. Correlation of the Čerňanský and Široký (1985) data for variation of the rate coefficients by volumetric flux.

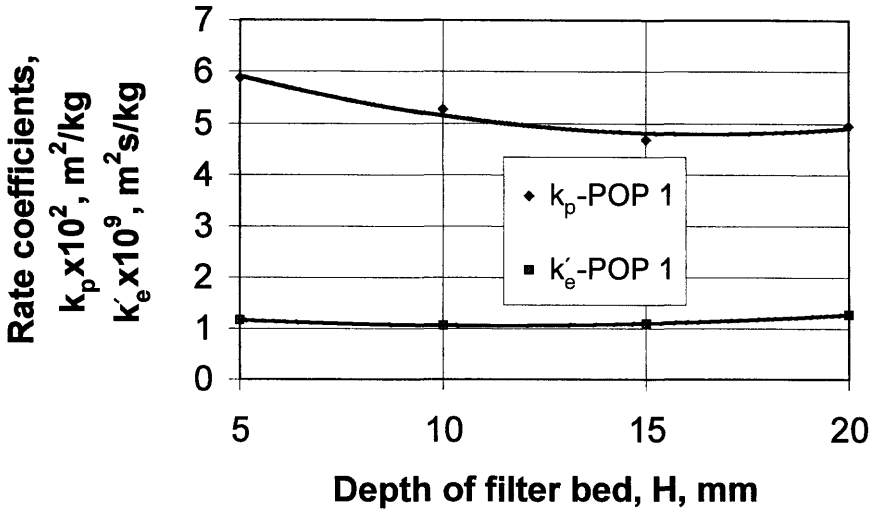


Figure 10–19. Correlation of the Čerňanský and Široký (1985) data for variation of the rate coefficients by the thickness of porous media.

The effect of the suspension particle concentration and particle size on the pressure drop is shown in Figure 10–20.

For a given injection suspension particle concentration and rate, at equilibrium, Eq. 10–91 for $\tau'_{cr} = 0$ yields

$$k_p \sigma_{in} (\phi_o - \varepsilon^*) - k'_e \varepsilon^* \mu / K^* = 0 \quad (10-177)$$

in which the permeability is determined by:

$$K^* = u \mu L / \Delta p^* \quad (10-178)$$

Figure 10–21 shows the equilibrium ε^* and K^* values calculated by Eqs. 10–177 and 178, which are attained during the injection of $\sigma_{in} = 0.1 kg/m^3$ concentration suspension at various constant injection rates.

Applications of the Gruesbeck and Collins Model

Gruesbeck and Collins (1982) conducted core flow tests under constant rate and pressure difference conditions and studied the formation damage effects and determined the relevant rate constants. Their data analysis methods and results are presented in the following.

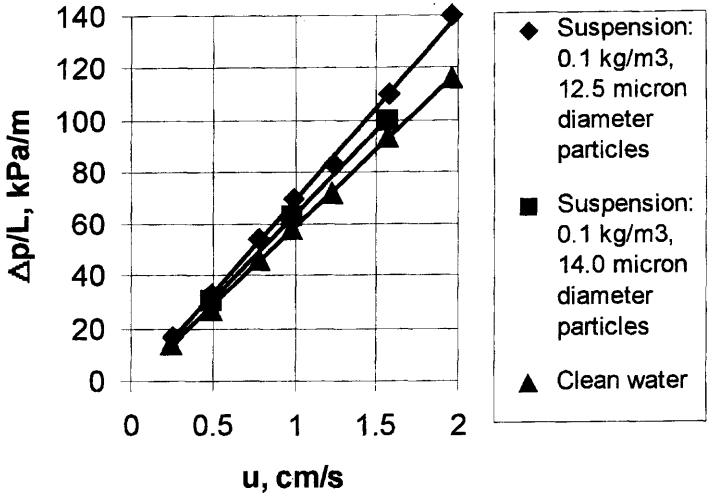


Figure 10-20. Plot of the Čerňanský and Široký (1985) data for the effect of suspension concentration and particle size on pressure drop.

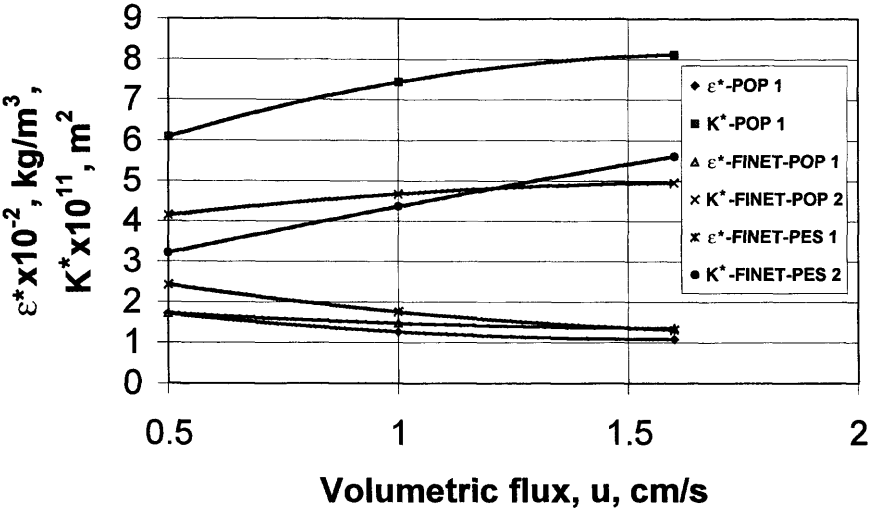


Figure 10-21. Correlation of the Čerňanský and Široký (1985) data for variation of the limiting saturation values for $c_o = 0.1$ kg/m³ by the volumetric flux.

I—Constant-Flow-Rate Tests

Assuming that ϕ and σ essentially remained constant with time during their experiments, Gruesbeck and Collins simplified Eq. 10-119 for a constant injection rate as:

$$\partial \varepsilon / \partial t + u \partial \sigma / \partial x = 0 \quad (10-179)$$

and designed special experiments to verify their model as described in the following.

Case 1—Particle Deposition and Mobilization in Nonplugging Pathways. First they considered a case where particle mobilization does not occur, and the particle deposition rate is proportional to the particle concentration of the suspension according to

$$\partial \varepsilon / \partial t = \beta \sigma \quad (10-180)$$

Then, Eqs. 10-179 and 180 can be solved subject to the conditions

$$\varepsilon = \varepsilon_o, \quad 0 \leq x \leq L, \quad t = 0 \quad (10-181)$$

and

$$\sigma = \sigma_{in}, \quad x = 0, \quad t > 0 \quad (10-182)$$

to obtain the following analytic solutions:

$$\sigma = \sigma_{in} \exp(-\beta x / u) \quad (10-183)$$

$$\varepsilon = \varepsilon_o + \beta \sigma t \quad (10-184)$$

An application of Eq. 10-183 over the length of the porous media yields:

$$\beta = -\frac{u}{L} \ln \left(\frac{\sigma_{out}}{\sigma_{in}} \right) \quad (10-185)$$

Gruesbeck and Collins (1982) injected a low concentration of a suspension of $CaCO_3$ particles into a column of clean, unconsolidated sand pack. Under these conditions, they assumed that removal of deposited particles was negligible. They measured the concentration of particles in the

effluent. Applying Eq. 10-185 with their data given in Figure 10-22, Gruesbeck and Collins determined the same β value on the average for different flow rates. Therefore, they concluded that the rate law postulated by Eq. 10-180 is valid.

Second, Gruesbeck and Collins neglected the deposition rate and considered that the mobilization phenomena is dominant. Thus, integrating Eq. 10-179 over the length of the porous media and applying the mean value theorem yields:

$$\left(\frac{\partial \epsilon}{\partial t} \right)_{avg} \equiv \frac{1}{L} \int_0^L \frac{\partial \epsilon}{\partial t} dx = \frac{(\sigma_{in} - \sigma_{out})u}{L} \quad (10-186)$$

where $\sigma_{in} = 0$ for injection of a particle free solution.

In order to test the validity of Eq. 10-186, Gruesbeck and Collins prepared a sand pack by mixing sand and a suspension of $CaCO_3$ particles into a column. Then, a particle free KCl solution was injected into the column.

In Figures 10-23 and 10-24 of Gruesbeck and Collins, their experimental data and plots of Eq. 10-186 are given, respectively. Based on Figure 10-24, they concluded that the particle mobilization rate can be represented by

$$\frac{\partial \epsilon}{\partial t} = \alpha \sigma (u - u_c) \quad (10-187)$$

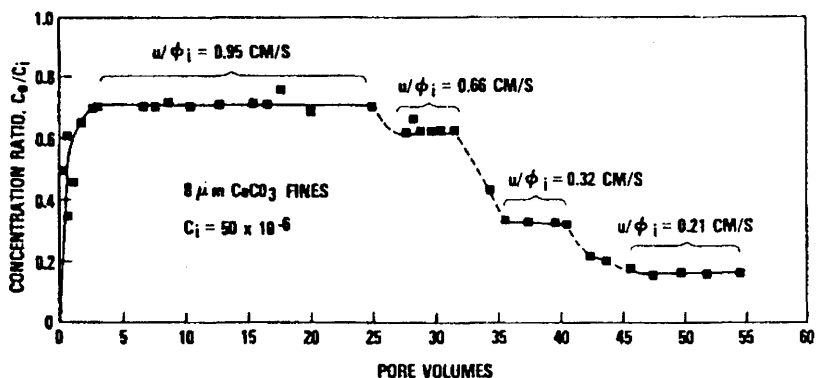


Figure 10-22. Deposition of fines in a porous medium of 30.48 cm pack of 840–2000 mm diameter sand grains (after Gruesbeck and Collins, ©1982 SPE; reprinted by permission of the Society of Petroleum Engineers).

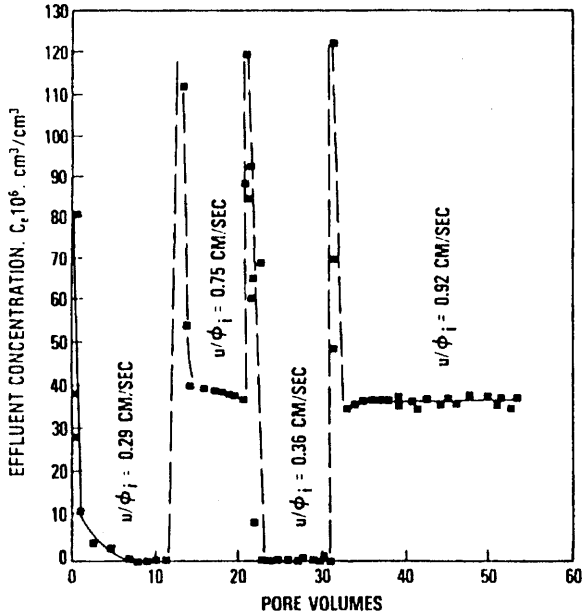


Figure 10-23. Entrainment of 0.5%, initially deposited, 8 mm CaCO_3 fines in a porous medium of 60.96 cm pack of 840–2000 mm diameter sand grains (after Gruesbeck and Collins, ©1982 SPE; reprinted by permission of the Society of Petroleum Engineers).

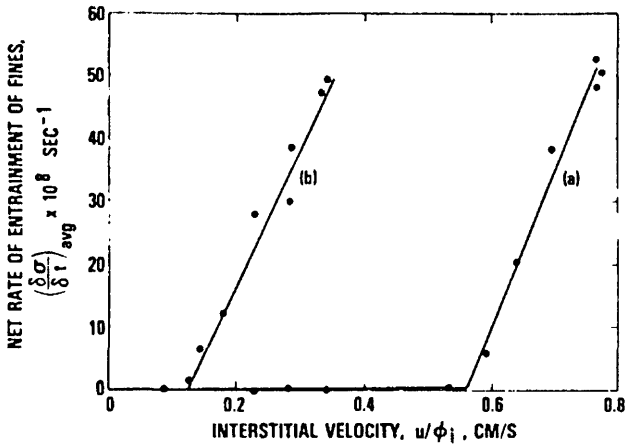


Figure 10-24. Net entrainment rate of fines in a porous medium: Line (a) from data given in Figure 10-23, and Line (b) similar data obtained using a 10 mPa.s viscosity fluid (after Gruesbeck and Collins, ©1982 SPE; reprinted by permission of the Society of Petroleum Engineers).

where

$$\alpha = 0 \text{ when } u < u_c \quad (10-188)$$

where u_c is the critical flux below which mobilization does not occur.

Case 2—Particle Deposition in Plugging Pathways. To verify their plugging rate equation, they considered sand packs and suspension of glass particles of various sizes. They estimated the effective pore diameter of the passages between the closest packing of sand grains as the grain diameter, d_g , divided by 6.5, $d_g/6.5$.

The data of sand grain and glass particle sizes as well as the estimated effective pore diameter to particle diameter ratio are presented in Table 10-2. They measured the pressure difference across the sand pack as a function of the pore volume of the suspension of glass beads injected at a constant rate. They classified the deposition type as indicated in Table 10-2 based on the observed variation of the pressure difference. The deposition process was considered mainly as the pore surface deposition when the variation of the pressure difference was small, and indicated by "S" in Table 10-2. The deposition was considered due to the pore throat plugging, when the pressure difference indicated a monotonic increase and indicated by "P" in Table 10-2. A rise in pressure difference

Table 10-2
Deposition of 5- to 10- μ m Glass Beads in Sandpacks*

Sand Grain Diameter d_g (μ m)	Effective Pore Size d_s (μ m)	Glass Bead Diameter d_f (μ m)	d_s / d_f	Deposition Type**
840 to 2000	218†	5 to 10	29.1 ξ	S
840 to 2000	218	8 to 25	13.2	S
420 to 840	97	5 to 10	12.9	S
420 to 840	97	8 to 25	5.9	S and P
250 to 297	42	5 to 10	5.6	S and P
250 to 297	42	8 to 10	2.6	FC
177 to 210	30	5 to 10	4.0	P
104 to 124	18	5 to 10	2.4	FC

*After Gruesbeck and Collins, 1982 SPE; reprinted by permission of the Society of Petroleum Engineers.

**S = surface, P = plugging, FC = filter cake

† = $(1/2)(840 + 2000) / 6.5 = 218$ for closest packing of spheres

$\xi = 218 / [(1/2)(5+10)] = 29.1$

to a plateau was an indication of simultaneous pore surface deposition and pore throat plugging, and indicated by "S and P" in Table 10-2. Filter cake deposition was indicated by "FC" in Table 10-2.

Gruesbeck and Collins carried out experiments under conditions favorable for simultaneous surface deposition and pore throat plugging. For this purpose, suspensions of glass beads were injected into columns of clean sand packs. The effluent glass beads concentration, pressure difference across the sand pack, and cumulative glass bead deposit in the sand pack were measured as a function of the pore volume of suspension of glass beads injected at constant rates. The experimental data are presented in Figure 10-25. Next, they have solved their model equations, Eqs. 10-121, 111, 112, 114, 115, 116, numerically by assuming trial

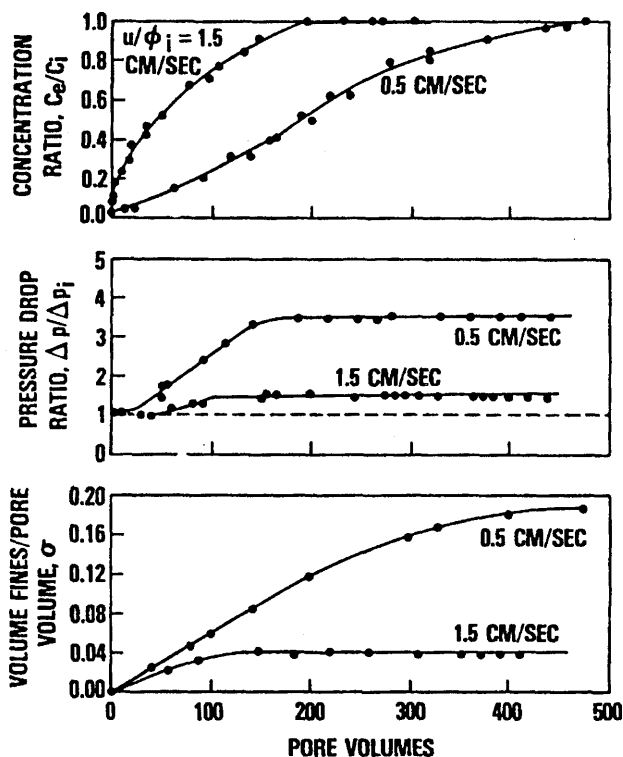


Figure 10-25. Deposition and entrainment of 5–10 mm diameter glass beads in a porous medium of 15.24 cm pack of 250–297 mm diameter sand grains for 9.5×10^{-4} injection suspension concentration (after Gruesbeck and Collins, ©1982 SPE; reprinted by permission of the Society of Petroleum Engineers).

values for the various phenomenological parameters to match the measurements. The simulation results are shown in Figure 10-26. The fact that their model reasonably predicts the experimental observations indicates that their model based on the plugging and nonplugging pathways concept is valid for their experimental systems.

When the plugging pathways are eliminated by particle retention, the flow is diverted to the nonplugging pathways. Then the particle retainment continues in the nonplugging pathways as pore surface deposition until a dynamic equilibrium is attained. At this condition, Eq. 10-112 yields the following expression for the equilibrium amount of the deposits in the nonplugging pathways as:

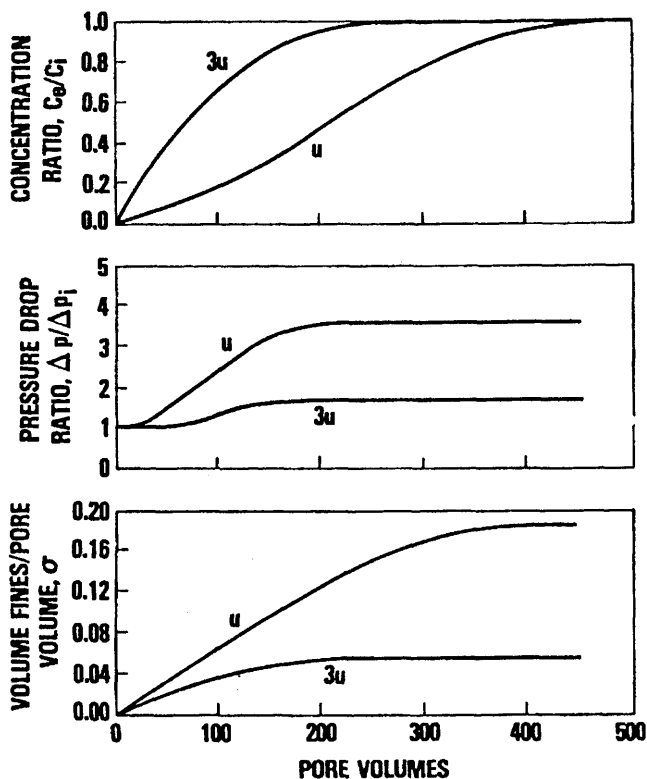


Figure 10-26. Numerical simulation of the deposition and entrainment experimental results presented in Figure 10-25 (after Gruesbeck and Collins, ©1982 SPE; reprinted by permission of the Society of Petroleum Engineers).

$$\varepsilon_{np}^* = \frac{c_3 \sigma_{np}}{c_4 (u_{np} - u_c)} \quad (10-189)$$

in which

$$\sigma_{np} = \sigma, \quad u_{np} = u \quad (10-190)$$

because all flow goes through the plugging pathways.

The fact that the cumulative amounts of deposits reach certain limiting values as shown in Figure 10-25 is indicative of attainment of such equilibrium conditions. Note, however, that the amounts shown in Figure 10-25 are the cumulative amounts including the amount of deposits in the plugging pathways. Therefore at equilibrium

$$\varepsilon^* = \varepsilon_p^* + \varepsilon_{np}^* \quad (10-191)$$

II—Constant-Pressure-Difference Tests

Constant pressure tests are more representative of the producing well conditions.

Gruesbeck and Collins (1982) flowed suspensions of glass particles through sand packs at constant pressure differences by applying relatively high pressure difference to a column of fine sand pack and relatively low pressure difference to a column of coarse sand pack. The results are reported in Figure 10-27. In the fine sand packs, they observed more deposition near the injection side, and the mean permeability of the sand

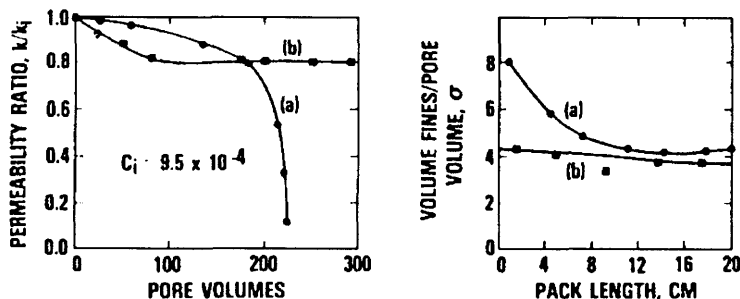


Figure 10-27. Constant pressure deposition and entrainment of 5–10 mm diameter glass beads in a pack of (a) 177–210 mm diameter sand grains subjected to 900 kPa/m pressure gradient and (b) 250–297 mm diameter sand grains subjected to 450 kPa/m pressure gradient (after Gruesbeck and Collins, ©1982 SPE; reprinted by permission of the Society of Petroleum Engineers).

pack decreased to zero. Because, in the fine sand pack, almost all the pathways are of the plugging type. Whereas, in coarse sand packs, the deposition tended to occur almost uniformly along the sand pack and the mean permeability of the sand pack decreased to an equilibrium value. Because, in the coarse sand pack, most of the pathways are of the nonplugging types.

Gruesbeck and Collins (1982) state that their computer simulation produced results similar to measurement reported in Figure 10-27. Civan et al. (1989), and Ohen and Civan (1990, 1993) also simulated these experiments successfully.

Consolidated Core Tests. Gruesbeck and Collins tested Berea and field cores. First, the Berea cores were tested using

1. 2% *KCl* brine in a dry core (single phase system)
2. 2% *KCl* brine and white oil at a 50/50 ratio in a dry core (two phase system)
3. white oil in a dry core (single phase system)
4. white oil in a core at connate 2% *KCl* brine saturation (two phase)

Cores were tested at various constant injection rates over a period of time determined by a prescribed, cumulative pore volume amount of the injection fluid. During each test, the pressure difference was measured and the permeability was calculated using Darcy's law. Typical results obtained using a 2% *KCl* brine in a Berea core are presented in Figure 10-28. As can be seen, the permeability remained unchanged at the low flow rate of $0.0367\text{cm}^3/\text{s}$, while it decreased further at each of the increased high flow rates of 0.0682, 0.1002, 0.1310, and $0.1702\text{cm}^3/\text{s}$. The final permeability values attained after each of the high flow rates are used to calculate the permeability reductions from the initial state, which are then plotted against these high flow rates as shown in Figure 10-29. The results shown in Figure 10-29 are indicative of surface particle removal, similar to Figure 10-24. They stated that the removal of indigeneous particles in the cores from the pore surface and subsequent redeposition at the pore throats caused the permeability reduction.

Second, core samples were taken from an oil field, indicating an abnormal decline of productivity in some wells. These cores were tested using

1. white oil in a dry core
2. white oil in a core at connate 2% *KCl* brine saturation.

The experimental results presented in Figure 10-30 indicate a trend similar to Figure 10-29.

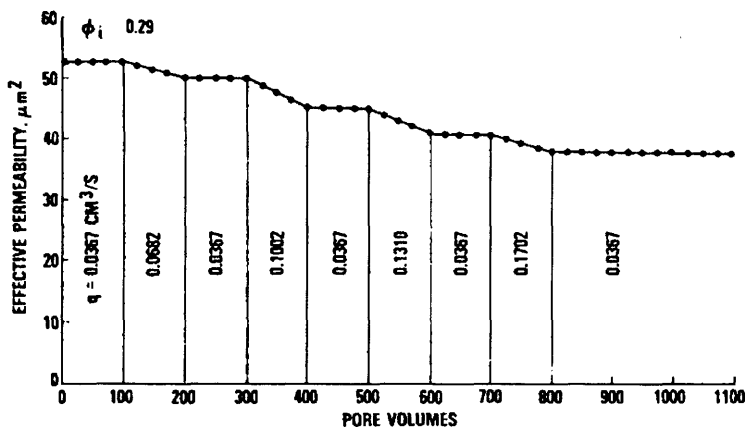


Figure 10-28. Effect of fluid velocity on the entrainment and redeposition of fines in a 3.81 cm diameter and 3.0 cm long Berea core during a 2% KCl solution injection (after Gruesbeck and Collins, ©1982 SPE; reprinted by permission of the Society of Petroleum Engineers).

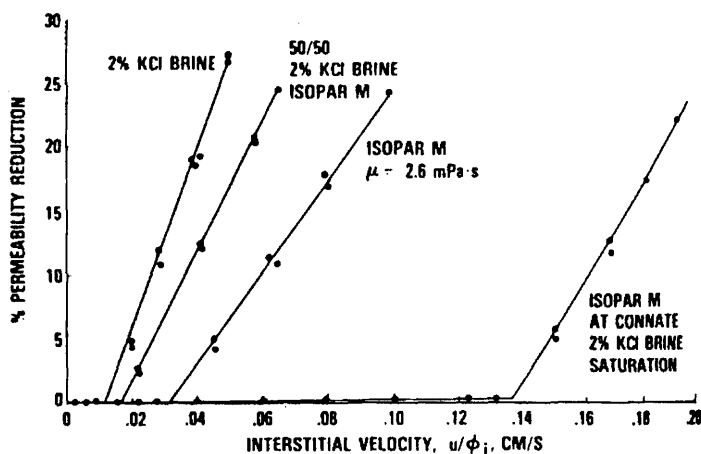


Figure 10-29. Permeability reduction as a function of the interstitial velocity determined using the Figure 10-28 data (after Gruesbeck and Collins, ©1982 SPE; reprinted by permission of the Society of Petroleum Engineers).

The results presented in Figures 10-29 and 10-30 indicate that the indigenous particles of Berea and field cores are water wet. This is apparent by the effect of the two phases on the critical velocity values required to initiate particle mobilization. The implication of this is that variation of the fluid system from oil to oil/water can reduce the critical

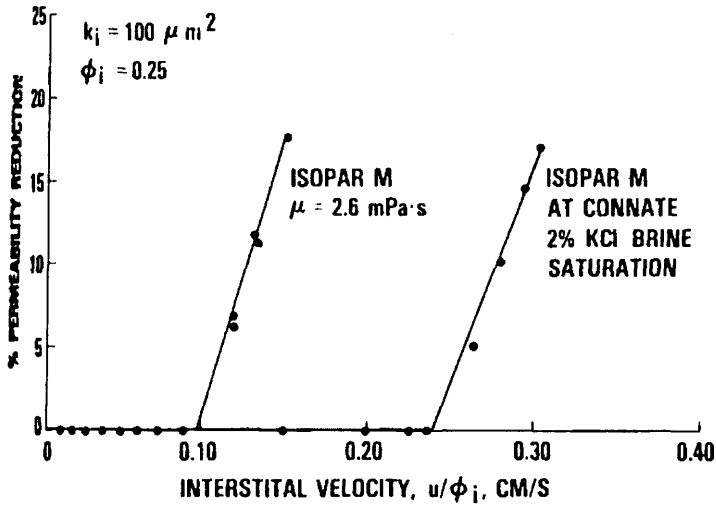


Figure 10-30. Permeability reduction as a function of the interstitial velocity determined using a 3.81 cm diameter and 3.0 cm long field core sample (after Gruesbeck and Collins, ©1982 SPE; reprinted by permission of the Society of Petroleum Engineers).

velocity, induce surface particle mobilization, and increase permeability damage in the near well bore formation.

References

- Čerňanský, A., & Šíroký, R. "Deep-bed Filtration on Filament Layers on Particle Polydispersed in Liquids," *Int. Chem. Eng.*, Vol. 25, No. 2, 1985, pp. 364–375.
- Čerňanský, A., & Šíroký, R., "Hlbkova Filtracia Polydisperzných Castic z Kvapalin na Vrstvach z Vlákien," *Chemický Prumysl*, Vol. 32 (57), No. 8, 1982, pp. 397–405.
- Civan, F. "A Generalized Model for Formation Damage by Rock-Fluid Interactions and Particulate Processes," SPE Paper 21183, Proceedings of the SPE 1990 Latin American Petroleum Engineering Conference, October 14–19, 1990, Rio de Janeiro, Brazil, 11 p.
- Civan, F. "Evaluation and Comparison of the Formation Damage Models," SPE 23787 paper, Proceedings of the SPE International Symposium on Formation Damage Control, February 26–27, 1992, Lafayette, Louisiana, pp. 219–236.
- Civan, F., & Knapp, R. M. "Effect of Clay Swelling and Fines Migration on Formation Permeability," SPE Paper No. 16235, Proceedings of the

- SPE Production Operations Symposium, Oklahoma City, Oklahoma, 1987, pp. 475–483.
- Civan, F. "A Multi-Phase Mud Filtrate Invasion and Well Bore Filter Cake Formation Model," SPE Paper No. 28709, Proceedings of the SPE International Petroleum Conference & Exhibition of Mexico, October 10–13, 1994, Veracruz, Mexico, pp. 399–412.
- Civan, F., Knapp, R. M., & Ohen, H. A. "Alteration of Permeability by Fine Particle Processes," *J. Petroleum Science and Engineering*, Vol. 3, Nos. 1/2, October 1989, pp. 65–79.
- Civan, F., Predictability of Formation Damage: An Assessment Study and Generalized Models, Final Report, U.S. DOE Contract No. DE-AC22-90BC14658, April 1994.
- Civan, F. "Modeling and Simulation of Formation Damage by Organic Deposition," Proceedings of the First International Symposium on Colloid Chemistry in Oil Production: Asphaltenes and Wax Deposition, IS COP'95, Rio de Janeiro, Brazil, November 26–29, 1995, pp. 102–107.
- Civan, F. "A Multi-Purpose Formation Damage Model," SPE 31101, Proceedings of the SPE Formation Damage Symposium, Lafayette, Louisiana, February 14–15, 1996, pp. 311–326.
- Civan, F. "Interactions of the Horizontal Wellbore Hydraulics and Formation Damage," SPE 35213, Proceedings of the SPE Permian Basin Oil & Gas Recovery Conf., Midland, Texas, March 27–29, 1996, pp. 561–569.
- Gruesbeck, C., & Collins, R. E. "Particle Transport Through Perforations," *SPEJ*, December 1982b, pp. 857–865.
- Gruesbeck, C., & Collins, R. E. "Entrainment and Deposition of Fine Particles in Porous Media," *SPEJ*, December 1982a, pp. 847–856.
- Khilar, K. C., & Fogler, H. S. "Colloidally Induced Fines Migration in Porous Media," in Amundson, N. R. & Luss, D. (Eds.), *Reviews in Chemical Engineering*, Freund Publishing House LTD., London, England, January–June 1987, Vol. 4, Nos. 1 and 2, pp. 41–108.
- Khilar, K. C., & Fogler, H. S. "Water Sensitivity of Sandstones," *SPEJ*, February 1983, pp. 55–64.
- Liu, X., Civan, F., & Evans, R. D. "Correlation of the Non-Darcy Flow Coefficient," *J. of Canadian Petroleum Technology*, Vol. 34, No. 10, 1995, pp. 50–54.
- Metzner, A. B., & Reed, J. C. "Flow of Non-Newtonian Fluids—Correlation of the Laminar, Transition, and Turbulent Flow Regions," *AIChE J.*, Vol. 1, No. 4, 1955, pp. 434–440.
- Nayak, N. V., & Christensen, R. W. "Swelling Characteristics of Compacted Expansive Soils," *Clay and Clay Mineral*, Vol. 19, No. 4, December 1970, pp. 251–261.
- Ohen, H. A., & Civan, F. "Predicting Fines Generation, Migration and Deposition Near Injection and Production Wells," Proceedings of the

- First Regional Meeting, American Filtration Society, Houston, Texas, October 30–November 1, 1989, pp. 161–164.
- Ohen, H. A., & Civan, F. "Simulation of Formation Damage in Petroleum Reservoirs," *SPE Advanced Technology Series*, Vol. 1, No. 1, April 1993, pp. 27–35.
- Ohen, H. A., & Civan, F. "Simulation of Formation Damage in Petroleum Reservoirs," SPE 19420 paper, Proceedings of the 1990 SPE Symposium on Formation Damage Control, Lafayette, Louisiana, February 22–23, 1990, pp. 185–200.
- Schechter, R. S., *Oil Well Stimulation*, Prentice Hall, Englewood Cliffs, New Jersey, 1992, 602 p.
- Seed, H. B., Woodward, Jr., R. J., & Lundgren, R. "Prediction of Swelling Potential for Compacted Clays," *J. Soil Mech. Found. Div.*, Proc. Am. Soc. Civ. Eng., 88(SM3), June 1962, pp. 53–87.
- Wojtanowicz, A. K., Krilov, Z., & Langlinais, J. P. "Study on the Effect of Pore Blocking Mechanisms on Formation Damage," SPE 16233 paper, presented at Society of Petroleum Engineers Production Operations Symposium, Oklahoma City, Oklahoma, March 8–10, 1987, pp. 449–463.
- Wojtanowicz, A. K., Krilov, Z., & Langlinais, J. P. "Experimental Determination of Formation Damage Pore Blocking Mechanisms," Trans. of the ASME, *Journal of Energy Resources Technology*, Vol. 110, 1988, pp. 34–42.

Chapter 11

Two-Phase Formation Damage by Fines Migration

Summary

Most reservoirs contain multi-phase fluid systems. Formation damage processes in such reservoirs are more complicated because of the effects of the relative wettabilities of fine particles and formation, interface transport, relative permeabilities, and capillary pressures. There are only a few models available for multi-phase systems. These models have been developed for and tested with two phase laboratory core flow data. This chapter discusses the additional processes on top of those involving single-phase formation damage that need to be considered for multi-phase formation damage by fines migration. A systematic analysis and formulation of the relevant processes involving fines migration and formation damage during two-phase fluid flow through sedimentary formations is presented, as well as applications to typical laboratory core damage tests. The formulation can be readily extended for the multi-phase and multi-dimensional systems and the actual fluid conditions existing in reservoir formations.

Introduction

Several investigators including Muecke (1979), Sarkar (1988), and Sarkar and Sharma (1990) have determined that fine particles behave differently in a multi-phase fluid environment and formation damage follows a different course than the single-phase systems. However, the reported studies on the two-phase formation damage are very limited. Sutton and Roberts (1974) and Sarkar and Sharma (1990) have experimentally observed that formation damage in two-phase is less severe than in single-phase. Liu and Civan (1993, 1995, 1996) have shown that two-phase

formation damage requires the consideration of other factors, such as the wettability affect and partitioning of particles between various phases.

In this chapter, mutual interactions and affects between the two-phase flow systems, fine particles, and porous matrix are described mathematically to develop a predictive model for formation damage by fines migration in two-phase systems flowing through porous formations. The formulation is carried out by extending the Liu and Civan (1993, 1994, 1995, 1996) model for more realistic applications. The tests and case studies used by Liu and Civan (1995, 1996) are presented for demonstration and verification of the model. Although the model presented here involves some simplifications pertaining to the laboratory core damage experiments, it can be readily modified and generalized for the actual conditions encountered in petroleum reservoirs.

Formulation

The equations describing the various aspects for formation damage by fines migration during two-phase fluid flow through porous formations are formulated here. However, the formulation can be extended readily to multi-phase fluid systems. It is safe to assume that the gas phase does not carry any solid particles (i.e., it is nonwetting for all particles).

For convenience in modeling, the bulk porous media is considered in four phases as schematically depicted in Figure 11-1: (1) the solid matrix, (2) the wetting fluid, (3) the nonwetting fluid, and (4) the interface region. These phases are indicated by S , W , N , and I , respectively. The porous matrix is assumed nondeformable. Therefore, it is stationary and its volumetric flux is zero. The wetting and nonwetting phases flow at the volumetric fluxes denoted, respectively, by u_w and u_N . The interface region is located between the wetting and nonwetting phases and is assumed to move at a flux equal to the absolute value of the difference between the fluxes of the wetting and nonwetting phases (i.e., its flux is $u_I = |u_w - u_N|$).

The various particles involving the formation damage are classified as (1) the foreign particles introduced externally at the wellbore, (2) the indigeneous particles existing in the porous formation, and (3) the particles generated inside the pore space by various processes, such as the wettability alteration considered in this chapter. Another classification of particles is made with reference to the wettability as (1) the wetting particles, (2) the nonwetting particles, and (3) the intermediately wetting particles. These particles are identified, respectively, by wp , np , and ip . The latter classification is more significant from the modeling point of view. Because, as explained by Muecke (1979), the wettability affects the behavior of these particles in a multi-phase fluid system. By means of

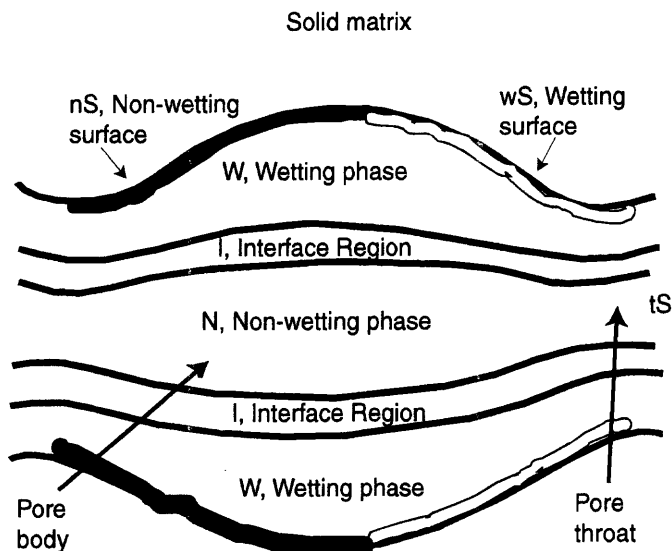


Figure 11-1. Multi-phase system in porous media.

experimental investigations, Muecke (1979) has observed that particles tend to remain in the phases that can wet them. Ku and Henry, Jr. (1987) have shown that intermediately wet particles accumulate at the interface of the wetting and nonwetting phases, because they are most stable there. Therefore, in the following formulation, an interface region containing the intermediately wet particles is perceived to exist in between the wetting and nonwetting phases as schematically indicated in Figure 11-1. Further, it is reasonable to consider that the wettability of some particles may be altered by various processes, such as asphaltene, paraffin, and inorganic precipitation or by other mechanisms such as the turbulence created by rapid flow in the near-wellbore region. Consequently, these altered particles should tend to migrate into the phases that wet them as inferred by the experimental studies of Ku and Henry, Jr. (1979).

In addition to the particles, the various phases may contain a number of dissolved species. The salt content of the aqueous phase is particularly important, because it can lead to conditions for colloiddally induced release of clay particles when its salt concentration is below a critical salt concentration (Khilar and Fogler, 1983).

For convenience in formulation, the locations for particles retention can be classified in three categories: (1) the wetting pore surface, (2) the nonwetting pore surface, and (3) the pore space behind the plugging pore

throats. These regions are denoted by wS , nS , and tS , respectively, as indicated schematically in Figure 11-1. The areal fractions of the wetting and nonwetting sites can vary as a result of the various rock, fluid, and particle interactions during formation damage, such as by asphaltene, paraffin, and inorganic deposition. Therefore, a parameter f_{kS} indicating the fraction of the pore surface, that is wetting for species k , is introduced in the formulation.

Because the applications to describe and interpret the laboratory core damage data, conducted at mild temperature and pressure conditions are intended, the formulation is carried out for one-dimensional flow in homogeneous core plugs, isothermal conditions, and incompressible particles and fluids. This allows the use of a simplified formulation based on volumetric balances and a fractional flow concept. However, the derivation can be readily extended for compressible systems encountered at the prevailing elevated pressure conditions of the reservoir formations.

Fluid and Species Transport

Assuming incompressible species, the volumetric balance of species j transported via phase J through porous media is given by:

$$\frac{\partial}{\partial t}(\epsilon_J \sigma_{jJ}) + \frac{\partial}{\partial x}(u_J \sigma_{jJ}) + q_{jJ} = \frac{\partial}{\partial x} \left[\epsilon_J \rho_J D_{jJ} \frac{\partial}{\partial x} \left(\frac{\sigma_{jJ}}{\rho_J} \right) \right]; \quad (11-1)$$

$$J = W, N, I, wS, nS, tS \text{ and } j = w, n, wp, np, ip$$

where ϵ_J indicates the volume fraction of phase J in porous media, σ_{jJ} is the volume fraction of species j in phase J , u_J is the volumetric flux of phase J through porous media and q_{jJL} represents the volume rate of transfer of species j from phase J to phase L . D_{jJ} denotes the coefficient of dispersion of species j in phase J , and ρ_J is the density of phase J , which varies by its composition even if the individual constituent species may be considered incompressible. x and t denote the distance along the flow direction and time. The dispersion term for particles is usually neglected.

The volumetric rate of particle lost per unit bulk media by various processes is given by:

$$q_{jJ} = \sum_{l \neq j} q_{jJl} + \sum_{J \neq L} q_{jJL} \quad (11-2)$$

in which q_{jJl} denotes the volume rate of transformation of species j type to species l type in phase J expressed per unit bulk volume. Summing

Eq. 11-1 over all species j in phase J and considering that the dispersion terms of various species j cancel each other out in a given phase, the volumetric equation of continuity for phase J is obtained as:

$$\frac{\partial \epsilon_J}{\partial t} + \frac{\partial u_J}{\partial x} + q_J = 0 ; J = W, N, wS, nS, tS \quad (11-3)$$

in which the volumetric loss of all types of particles from phase J is given by:

$$q_J = \sum_j q_{jJ} \quad (11-4)$$

Finally, by summing Eq. 11-3 for all phases J , the total equation of continuity for the multi-phase fluid system is obtained as:

$$\frac{\partial \phi}{\partial t} + \frac{\partial u}{\partial x} + q = 0 \quad (11-5)$$

where the total volumetric flux and all types of particles lost by the multi-phase fluid system are given, respectively, by:

$$u = \sum_J u_J \quad (11-6)$$

$$q = \sum_J q_J \quad (11-7)$$

Considering the possibility of the generation of inertial effects by rapid flow due to the narrowing of pores during formation damage, the volumetric flux of phase J is represented by the non-Darcy flow equation given by:

$$u_J = -\frac{Kk_{rJ}N_{ndJ}}{\mu_J} \left(\frac{\partial p_J}{\partial x} + \rho_J g \sin \theta \right) ; J = W, N \quad (11-8)$$

where θ is the angle of inclination of the flow path and p_J and μ_J are the pressure and viscosity of phase J . k_{rJ} is the relative permeability of phase J and K is the permeability of porous media. N_{ndJ} is the phase J non-Darcy number given according to the Forchheimer equation as:

$$N_{ndJ} = (1 + \text{Re}_J)^{-1} , 0 \leq N_{ndJ} \leq 1 \quad (11-9)$$

in which Re_J is the phase J Reynolds number given by (Ucan and Civan, 1996):

$$Re_J = K\beta\rho_J u_J/\mu_J \quad (11-10)$$

where β is the inertial flow coefficient given by a suitable correlation, such as by Liu et al. (1995).

Determination of Fluid Saturations and Pressures

Two alternative convenient formulations can be taken for solution of the equations of continuity and motion given by Eqs. 11-3 and 8 for pressures and saturations of the various phases flowing through porous media. In the first approach, Eq. 11-8 is substituted into Eq. 11-3 to obtain:

$$\frac{\partial}{\partial x} \left[\frac{1}{\mu_J} N_{ndJ} k_{rJ} K \left(\frac{\partial p_J}{\partial x} + \rho_J g \sin \theta \right) \right] = \frac{\partial \epsilon_J}{\partial t} + q_J ; J = W, N \quad (11-11)$$

The capillary pressure is defined as the difference between the nonwetting and wetting phase pressures according to:

$$p_{cNW} = p_N - p_W \quad (11-12)$$

The phase J volume fraction is given by:

$$\epsilon_J = \phi S_J \quad (11-13)$$

where ϕ is porosity and S_J is the saturation of phase J .

Thus, substituting Eqs. 11-12 and 11-13 into Eq. 11-11 yields the following equations for the wetting and nonwetting phases, respectively:

$$\frac{\partial}{\partial x} \left[\frac{N_{ndW} k_{rW} K}{\mu_W} \left(\frac{\partial p_W}{\partial x} + \rho_W g \sin \theta \right) \right] = \frac{\partial (\phi S_W)}{\partial t} + q_W \quad (11-14)$$

$$\begin{aligned} \frac{\partial}{\partial x} \left[\frac{N_{ndN} k_{rN} K}{\mu_N} \left(\frac{\partial p_W}{\partial x} + \frac{dp_{cNW}}{dS_W} \frac{\partial S_W}{\partial x} + \rho_N g \sin \theta \right) \right] \\ = \frac{\partial (\phi S_N)}{\partial t} + q_N \end{aligned} \quad (11-15)$$

Note that the saturations add up to one:

$$S_w + S_N = 1 \quad (11-16)$$

Therefore, adding Eqs. 11-14 and 11-15 yields the following equation:

$$\begin{aligned} & \frac{\partial}{\partial x} \left[\left(\frac{N_{ndW} k_{rW}}{\mu_w} + \frac{N_{ndN} k_{rN}}{\mu_N} \right) K \frac{\partial p_w}{\partial x} \right] \\ & + \frac{\partial}{\partial x} \left[\frac{N_{ndN} k_{rN} K}{\mu_N} \frac{dp_{cNW}}{dS_w} \frac{\partial S_w}{\partial x} + (\rho_w + \rho_N) g \sin \theta \right] = \frac{\partial \phi}{\partial t} + q \end{aligned} \quad (11-17)$$

where the total volumetric loss of particles from the two-phase system is given by:

$$q = q_w + q_N \quad (11-18)$$

Eqs. 11-14 and 17 can be solved simultaneously to determine the wetting phase pressure and saturation, p_w and S_w .

A second and more convenient approach facilitates the fractional flow formulation. This is especially suitable for incompressible systems described by the equation of continuity given by Eq. 11-3. Civan's (1996) formulation based on Richardson's (1961) formulation can be modified as the following to include the loss terms and inertia flow affect in the saturation equation:

$$\begin{aligned} & \phi \frac{\partial S_w}{\partial t} + \frac{dF_w}{dS_w} u \frac{\partial S_w}{\partial x} + \frac{\partial}{\partial x} \left(D_w N_{ndW} K \frac{\partial S_w}{\partial x} \right) \\ & - \frac{\partial}{\partial x} (T_w N_{ndW} K \sin \theta) - F_w q + q_w + (S_w - F_w) \frac{\partial \phi}{\partial t} = 0 \end{aligned} \quad (11-19)$$

for which the capillary and gravity dispersion coefficients are given, respectively, by:

$$D_w = F_w \frac{k_{rN}}{\mu_N} \frac{dp_{cNW}}{dS_w} \quad (11-20)$$

$$T_w = F_w \frac{k_{rN}}{\mu_N} (\rho_w - \rho_N) g \quad (11-21)$$

The zero capillary pressure and zero gravity fractional flow term is given by:

$$F_w = \left[1 + \frac{k_{rN} \mu_w}{k_{rW} \mu_N} \right]^{-1} \quad (11-22)$$

In the fractional flow formulation, the saturation of the wetting phase is calculated by solving Eq. 11-19. But the pressure of the wetting phase is still determined by solving Eq. 11-17.

As explained by Civan (1996), the solution of equations presented above requires the capillary pressure and relative permeability data for the two-phase system. These data continuously vary during formation damage and empirical models, such as those given in Chapter 4, are required to incorporate these affects in the solution. This problem can be alleviated in a practical manner by resorting to an end-point mobility ratio formulation similar to Civan (1996) and Luan (1995), by extending and generalizing the unit mobility ratio formulations given by Craig (1971), Collins (1961) and Dake (1978). In view of the uncertainties in determining the exact nature of the variations of these data, it is reasonable to make the following assumptions.

First, similar to Liu and Civan (1996), the capillary pressure affect can be neglected. Second, the relative permeabilities can be approximated by linear relationships with respect to the phase saturations as (Yokoyama and Lake, 1981):

$$k_{rJ} = k_{rJ}^o \bar{S}_J \quad ; \quad J = W, N \quad (11-23)$$

where k_{rJ}^o is the end-point relative permeability. Third, the end-point mobility ratio parameter as defined below can be implemented:

$$M = \frac{k_{rW}^o \mu_N}{\mu_w k_{rN}^o} \quad (11-24)$$

Under these conditions, Eqs. 11-20 and 22, respectively, become:

$$D_w = 0 \quad (11-25)$$

and

$$F_w = \frac{M\bar{S}_w}{1 + (M-1)\bar{S}_w} \quad (11-26)$$

Consequently, Eq. 11-19 can be simplified significantly by substituting Eqs. 11-25 and 11-26. In addition, the non-Darcy effect can be neglected by substituting

$$N_{ndJ} = 1.0 ; J = W, N \quad (11-27)$$

The end-point relative permeabilities and fluid densities may be replaced by average values as:

$$\left(\frac{\bar{k}_r^o}{\mu} \right) \equiv \frac{k_{rw}^o}{\mu_w} \equiv \frac{k_{rN}^o}{\mu_N} \equiv \frac{1}{2} \left(\frac{k_{rw}^o}{\mu_w} + \frac{k_{rN}^o}{\mu_N} \right) \quad (11-28)$$

$$\bar{\rho} \equiv \rho_w \equiv \rho_N = \frac{\rho_w + \rho_N}{2} \quad (11-29)$$

As a result of substituting Eqs. 11-27 and 11-28, Eq. 11-5 can be simplified as (Civan, 1996):

$$\left(\frac{\bar{k}_r^o}{\mu} \right) \frac{\partial}{\partial x} \left(K \frac{\partial p_w}{\partial x} \right) + \bar{\rho} g \frac{\partial}{\partial x} (\sin \theta) = \frac{\partial \phi}{\partial t} + q \quad (11-30)$$

Determination of Species Concentrations in Various Phases

Once the phase saturations are determined, then the species concentrations can be determined by solving the following equation obtained by combining Eqs. 11-1 and 11-3:

$$\epsilon_J \frac{\partial \sigma_{jJ}}{\partial t} + u_J \frac{\partial \sigma_{jJ}}{\partial x} + \sigma_{jJ} q_J + q_{jJ} = \frac{\partial}{\partial x} \left[\epsilon_J \rho_J D_J \frac{\partial}{\partial x} \left(\frac{\sigma_{jJ}}{\rho_J} \right) \right]; \quad (11-31)$$

$J = W, N, I, wS, nS, iS$ and $j = w, n, wp, np, ip$

The dispersion term is considered for dissolved species, such as those contained in the aqueous phase, but it is usually neglected for the particles.

In accordance with the experimental observations by Muecke (1979), Liu and Civan (1993, 1995, 1996) have assumed that wettable particles remain in the wetting phase and nonwettable particles remain in the nonwetting phase and the intermediately wet particles are situated along the interface. They did not consider the possibility of wettability alteration of the particles and the pore surface in porous media and they assumed that the dispersion terms are negligible for the particles. They considered that the porous media has uniform wetting properties. Under these circumstances, Eq. 11–31 simplifies significantly because $q_{jL} = 0$ and the particle loss only occurs from the fluid phases to the solid matrix (i.e., $q_J = q_{jJ} = q_{jJS}$; $J = W, N$).

Liu and Civan (1996) considered a water/oil system flowing through a homogeneous (i.e., one type—either water-wet or oil-wet—porous media). They assumed that the wettability of the porous medium does not change during the short period of time involving the typical laboratory core tests.

Wettability Transformation and Interface Transfer of Particles

The literature on studies of the mechanisms of wettability alteration and interface particle transfer is rather limited and insufficient to formulate these processes accurately and rigorously. Therefore, Liu and Civan (1996) have resorted to a simplified approach, which yielded reasonably good results. They have combined the rate processes of the wettability transformation and the phase to phase particle transfer into one step assuming that the particles would immediately migrate into the phases, which wet them once their wettabilities change from one type to another. Based on the experimental observations and the studies of the mechanisms of interface particle transfer of Ku and Henry (1987), Liu and Civan (1996) assumed that the rate of the combined processes of wettability transformation and interface transfer of particles can be expressed as being proportional to the particle concentration according to:

$$q_{jLL} = k_{jLL} \sigma_{jJ} \quad (11-32)$$

Particle Retention in Porous Media

Although particle retentions may occur at various locations in porous media by various mechanisms, only the most likely mechanisms are considered here. The wetting and nonwetting particles preferentially

deposit over the similar wettability type pore surfaces. They can also be captured at and detained behind the pore throats under favorable conditions. The intermediately wet particles most likely move directly towards the pore throats and are captured there under certain conditions, because they migrate along the interface.

Surface Deposition

The volumetric rate of deposition of the particle species j from phase J over a similar wetting pore surface can be expressed by (Civan, 1996):

$$q_{jJS} \equiv d \epsilon_{jJS} / dt = k_{djJS} (\alpha_J + u_J) \sigma_{jJ} \phi^{2/3} f_{jS} \quad (11-33)$$

subject to the initial condition

$$\epsilon_{jJS} = \epsilon_{jJS}^o, \quad t = 0 \quad (11-34)$$

In Eq. 11-33, k_{djJS} is a deposition rate constant, α_J is a stationary deposition constant, ϕ is a porosity, and f_{jS} is the fraction of the pore surface of the same wettability type of the particle species j .

Similar to Gruesbeck and Collins (1982), Liu and Civan (1996) assumed that the porosity variation by deposition of small amounts of particles is negligible (i.e., ϕ is a constant). Liu and Civan (1996) considered a homogeneous wettability porous media, hence $f_{jS} = 1$, and neglected the stationary deposition, therefore $\alpha_J = 0$.

Pore Throat Plugging

The volumetric rate of retention of particles in the pore space following the pore throat plugging can be expressed by (Gruesbeck and Collins, 1982, Civan, 1996):

$$q_{jJS} \equiv d \epsilon_{jJS} / dt = k_{tjJS} u_J \sigma_{jJ} \phi \quad (11-35)$$

subject to the initial condition

$$\epsilon_{jJS} = \epsilon_{jJS}^o, \quad t = 0 \quad (11-36)$$

Liu and Civan (1996) assumed the porosity change is negligible in Eq. 11-35 (i.e., $\phi = \text{constant}$). In Eq. 11-35, k_{tjJS} denotes the rate

constant for deposition by pore throat plugging. Civan (1990, 1996) proposed a dimensionless correlation to determine the conditions favorable for pore throat plugging in single phase fluid media. This equation determines the critical ratio of the pore throat-to-particle diameters below which pore throat plugging by jamming of particles occurs. Thus,

$$k_{tjts} = 0, \text{ when } D_t/D_p \leq (D_t/D_p)_{cr} \quad (11-37)$$

For multi-phase flow, this equation can be modified as:

$$\beta_{cr} = A \left[1 - \exp(-B \text{Re}_p) \right] + C \quad (11-38)$$

where the pore throat-to-particle diameter ratio and the particle Reynolds numbers are given, respectively, by:

$$\beta_{cr} = \overline{D}_t / \overline{D}_p \quad (11-39)$$

$$\text{Re}_p = \frac{\overline{c_p u} \overline{D}_p}{\overline{\mu} \phi} \quad (11-40)$$

in which the total particle mass flux is given by:

$$\overline{c_p u} = \sum_J \sum_j \rho_j u_j \sigma_{jJ} \quad (11-41)$$

and the saturation weighted average particle diameter is given by:

$$\overline{D}_p = \sum_J S_J \sum_j \sigma_{jJ} D_{jJ} \quad (11-42)$$

Liu and Civan (1993, 1995, 1996) have resorted to a simplified approach in an adhoc manner and demonstrated by comparison of the results with experimental data that it works. They assumed that the fraction of the plugged pore throats is proportional to the amount of particles detained behind the plugged pore throats. Therefore, their expression for the fraction of the nonplugged pore throats can be written as:

$$f_t = 1 - \sum_J \sum_j k_{tjJ} \sigma_{jJ} \quad (11-43)$$

where k_{tjJ} are some empirical coefficients. They considered that there is a minimum characteristic value of $(f_t)_{\min}$ for which the pore throat blocking happens. Thus,

$$k_{tjJ} = 0, \text{ when } f \leq (f_t)_{\min} \quad (11-44)$$

Colloidal Mobilization

The volumetric rate of colloidally induced surface particle release can be expressed as, by modifying the formulations by Khilar and Fogler (1983) and Civan (1996):

$$q_{jJJS} = d \in_{ejJJS} / dt = -k_{ejJJS} \sigma_{JS} \eta_e f_{JS} (c_{crJ} - c_J) \quad (11-45)$$

subject to the initial condition

$$\in_{ejJJS} = \in_{ejJJS}^o, \quad t = 0 \quad (11-46)$$

Liu and Civan (1996) assumed $\eta_e = 1$ and $f_{JJ} = 1$. Note that

$$k_{ejJJS} = 0, \text{ when } c_J < c_{crJ} \quad (11-47)$$

Hydraulic Mobilization

The volumetric rate of surface particle mobilization by the fluid shearing force can be expressed by modifying the formulations by Khilar and Fogler (1983) and Civan (1996) as:

$$q_{hjJJS} \equiv d \in_{hjJJS} / dt = -k_{hjJJS} \sigma_{JS} \eta_e \phi^{2/3} f_{JS} (\tau_J - \tau_{crJ}) \quad (11-48)$$

subject to the initial condition

$$\in_{hjJJS} = \in_{hjJJS}^o, \quad t = 0 \quad (11-49)$$

Liu and Civan (1993, 1995, 1996) assumed $\eta_e = 1$, $f_{JS} = 1$ and $\phi \approx \text{constant}$ and used $(\tau_J - \tau_{crJ}) \sim (u_J - u_{crJ})$. Note

$$k_{hjJJS} = 0, \text{ when } \tau_J < \tau_{crJ} \text{ or } u_J < u_{crJ} \quad (11-50)$$

Porosity and Permeability Variation

The porosity is expressed by (Liu and Civan, 1996):

$$\phi = \phi_o + \sum_j \sum_s \sum_j \Delta \epsilon_{jsj} \quad (11-51)$$

and the permeability is estimated by (Liu and Civan, 1996)

$$K = K_o \left[(1 - f_i) K_p + f_i \phi / \phi_o \right] \quad (11-52)$$

Filter Cake Formation on the Injection Face

When the suspended particles existing in the injected fluid are large enough they cannot invade the formation or when a sufficient amount of fine particles are deposited in the porous formation to prevent particle invasion, a filter cake formation begins over the injection face. Liu and Civan (1995, 1996) applied a rate equation for the filter cake buildup similar to (Peng and Peden, 1992):

$$(1 - \phi_c) \rho_p \frac{dL_c}{dt} = u_{in} c_{in} - k_e \tau \quad (11-53)$$

Model Assisted Analysis of Experimental Data*

In this section, the application of the model to the analysis of formation damage in a variety of core tests is demonstrated. The model was validated and model parameters were determined using the data of core tests.

Damage by Formation Fines Migration

Sarkar and Sharma (1990) examined fines migration in two Berea core samples, one of them containing residual oil (ROS). Data for the two core tests are given in Table 11-1. The core samples were first saturated with 3% NaCl brine. Formation damage due to fines migration took place upon fresh water injection. Values of some model parameters were gathered from Khilar and Fogler (1983) while the others were obtained by matching the model responses to the measured data, as summarized in Table 11-2.

* Reproduced by permission from Liu and Civan, ©1996 SPE; reprinted by permission of the Society of Petroleum Engineers.

Table 11-1
Core Test Data for Fines Migrations*

Data	Core without ROS	Core with ROS
Core diameter (cm)	2.54	2.54
Core length (cm)	8.30	8.30
Initial porosity (fraction)	0.21	0.21
Initial permeability (Darcy)	0.0654	0.0825
Residual oil saturation	0.0	0.367
End-point relative permeability	1.0	0.038
Injection velocity (cm/s)	4.31×10^{-4}	4.31×10^{-4}
Water viscosity (cp)	1.0	1.0

* Information extracted from Sarkar and Sharma, 1990. After Liu and Civan, ©1996 SPE; reprinted by permission of the Society of Petroleum Engineers.

Table 11-2
Model Parameters for Fines Migrations*

Parameter	Core without ROS	Core with ROS
σ_{fpo} (gm/cm ³)	0.025	0.02
C_{sc} (mole/liter)	7.0×10^{-3}	7.0×10^{-3}
$k_{cr,fp,w}$ (s · liter/mole)	0.435	0.28
$k_{hr,fp,w}$ (cm ⁻¹)	0.0	0.0
$k_{pt,fp,w}$ (cm ⁻¹)	5.25	5.25
$k_{fe,fp}$ (cm ³ /gm)	35.4	35.4
f_{min}	0.0	0.0
k_p	0.0	0.0

* After Liu and Civan, ©1996 SPE; reprinted by permission of the Society of Petroleum Engineers.

Figure 11-2 shows that the simulation results favorably represent the experimental data for the two core tests. The simulation study also confirms that formation damage in the presence of oil is less pronounced. As can be seen in Table 11-2, the amount of formation fines that can be released from the pore surface, σ_{fpo} , is 20% less and the rate constant for fines release due to colloidal effects, $k_{cr,fp,w}$, is 35% lower in the presence of residual oil.

Sarkar (1988) conducted a laboratory test using a Berea core of 8.27 cm in length to investigate fines migration in two-phase flow. The core porosity and permeability initially were 0.21 fraction and 0.122 Darcy, respectively. The core saturated with crude oil was displaced with 3%

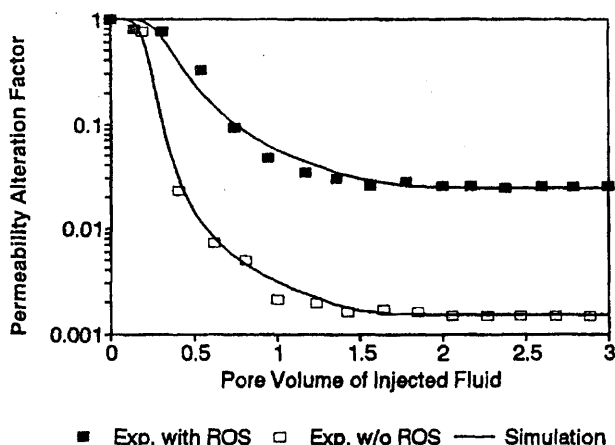


Figure 11-2. Instantaneous to initial permeability ratio (or permeability alteration factor) vs. pore volume during formation fines migration in single-phase flow (Liu and Civan, ©1996 SPE; reprinted by permission of the Society of Petroleum Engineers).

NaCl brine. Berea sandstones generally do not suffer from permeability reduction during a brine flood. Neglecting the effects of capillary pressure, the model was used to simulate the two-phase flow test. Relative permeability data were obtained by matching the simulated results with the measured pressure drop across the core as shown in Figure 11-3. An oil flood was then carried out to reestablish the connate water saturation. The core was finally displaced with fresh water and formation damage took place due to fines migration in two-phase flow. Using the relative permeabilities obtained from the two-phase flow test without formation damage, simulation was carried out to match measured pressure drop as shown in Figure 11-4. Alteration in the rock permeability, predicted in Figure 11-5, indicates that formation damage due to fines migration in two-phase flow of oil and fresh water is similar to that of single-phase flow of fresh water in the presence of residual oil. Detailed information on core data and model parameters in this case is presented elsewhere (Liu and Civan, 1995).

Damage by Particle Invasion

Experimental data of two similar core samples conducted by Eleri and Ursin (1992) were used to analyze formation damage due to particle invasion. The two samples were labeled as Core #26 and Core #27 in the Eleri and Ursin (1992) study. Prior to flow tests, the core samples

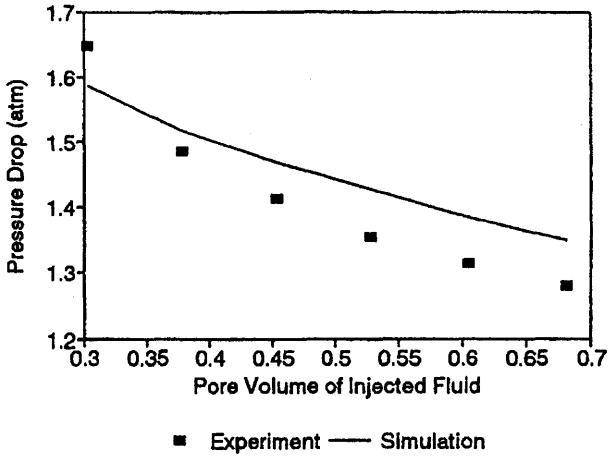


Figure 11-3. Pressure drop across an undamaged core vs. pore volume during two-phase flow (Liu and Civan, ©1996 SPE; reprinted by permission of the Society of Petroleum Engineers).

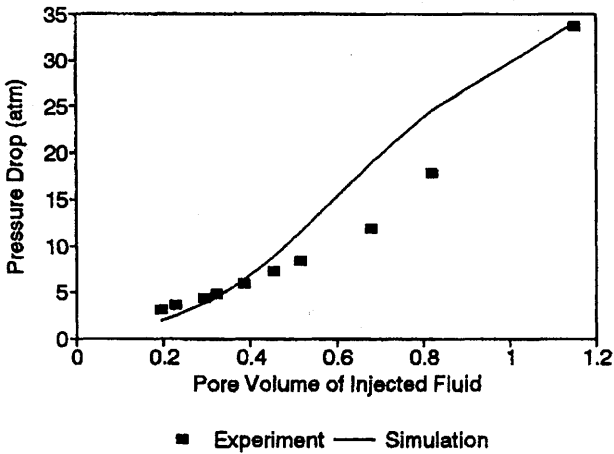


Figure 11-4. Pressure drop across a damaged core vs. pore volume during two-phase flow (Liu and Civan, ©1996 SPE; reprinted by permission of the Society of Petroleum Engineers).

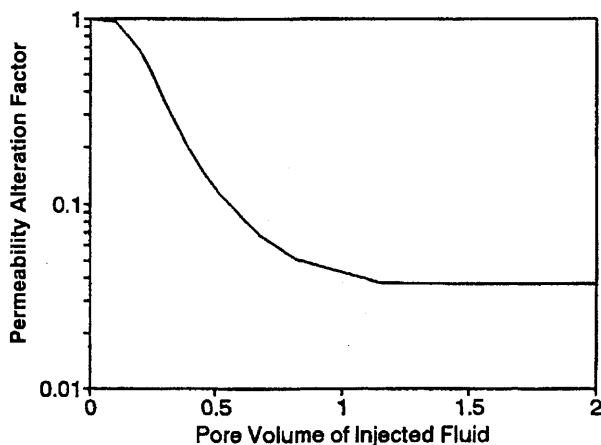


Figure 11-5. Predicted instantaneous to initial permeability ratio (or permeability alteration factor) vs. pore volume during formation fines migration in two-phase flow (Liu and Civan, ©1996 SPE; reprinted by permission of the Society of Petroleum Engineers).

were treated to eliminate formation fines migration. Latex particles of less than 3 microns in size suspended in water were injected into Core #26 at the concentration of 0.5×10^{-4} gm/cm³ and into Core #27 at the concentration of 2.0×10^{-4} gm/cm³. Simulations were performed to examine the two tests. Permeability alteration versus cumulative volume of injected fluid is illustrated in Figure 11-6 including a comparison between experimental and simulated results. Detailed information on core data and model parameters in this case is presented by Liu and Civan (1993). All model parameters for the two core tests are the same except that $f_{min} = 0.58$ for Core #26 and $f_{min} = 0.41$ for Core #27. The difference reveals that higher particle concentration causes more pores being plugged. Both experimental and simulation results indicate that particle concentration is a major factor for formation damage caused by particle invasion.

Damage by Mud Filtration

Rahman and Marx (1991) studied formation damage by mud filtration. A core sample was contaminated by circulating a drilling fluid over the surface of core inlet under a constant differential pressure of 34.54 atm across the core. Before mud filtration, the core was saturated with 1.5% KCl water to prevent formation fines migration. Permeability

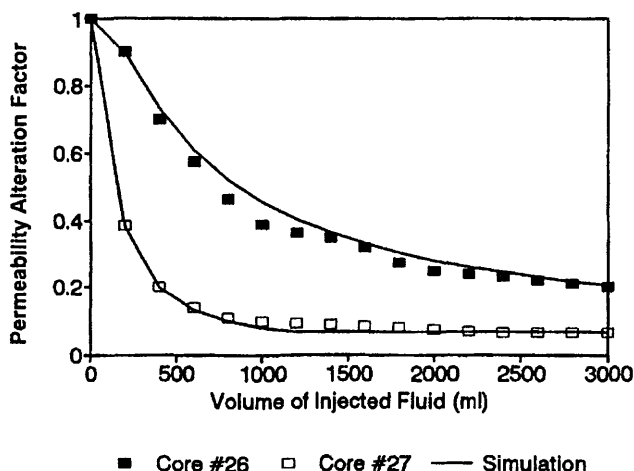


Figure 11-6. Instantaneous to initial permeability ratio (or permeability alteration factor) vs. pore volume during external fines invasion (Liu and Civan, ©1996 SPE; reprinted by permission of the Society of Petroleum Engineers).

alteration along the core was measured after one hour of mud contamination. Data for the core test and values of model parameters for simulation are presented elsewhere by Liu and Civan (1993). Experimental and simulated results for drilling fluid loss versus time and permeability alteration versus core distance after one hour of mud contamination are illustrated in Figures 11-7 and 11-8. Simulation results indicate that the model can favorably represent the process of mud filtration.

Another laboratory test involving dynamic mud filtration was conducted by Jiao and Sharma (1992). A fresh water-based mud was circulated over the surface of core inlet and infiltrated into a Berea core under an average differential pressure of 6.29 atm across the system. This Berea core sample was previously saturated with 3% NaCl brine. Formation damage in this test is caused by external solid invasion and formation fines migration. Pressure taps were placed at different locations along the core of 20.34 cm in length to measure permeability change during the test. Experimental and simulated mud filtration volumes are in good agreement, as presented in Figure 11-9. As shown in Figure 11-10, experimental results of permeability alteration in the core section between 6.35 cm and 11.43 cm from core inlet compare quite well with simulation results. Further discussion on the simulation of this test is presented elsewhere (Liu and Civan, 1993).

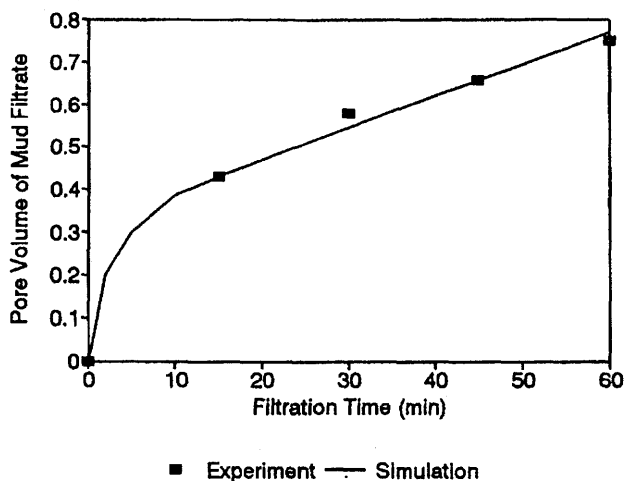


Figure 11-7. Cumulative fluid loss vs. filtration time during mud filtration (Liu and Civan, ©1996 SPE; reprinted by permission of the Society of Petroleum Engineers).

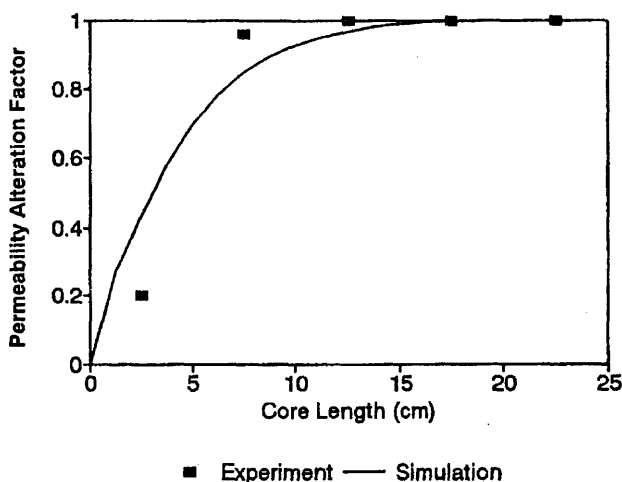


Figure 11-8. Instantaneous to initial permeability ratio (or permeability alteration factor) vs. core length after one hour of filtration time during mud filtration (Liu and Civan, ©1996 SPE; reprinted by permission of the Society of Petroleum Engineers).

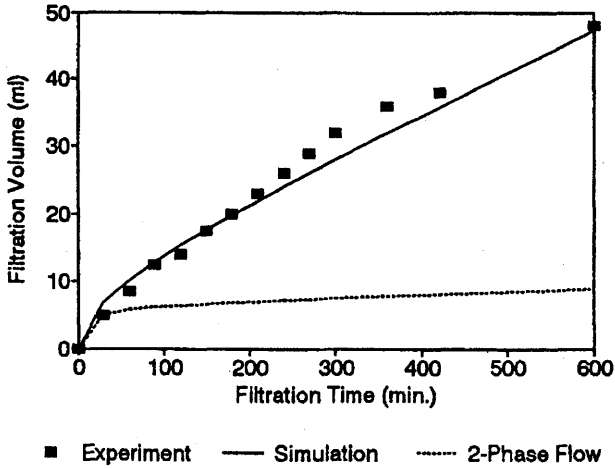


Figure 11-9. Cumulative fluid loss vs. filtration time during dynamic mud filtration (Liu and Civan, ©1996 SPE; reprinted by permission of the Society of Petroleum Engineers).

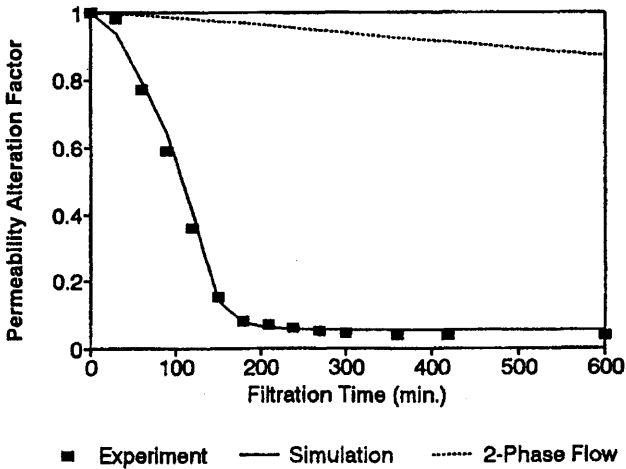


Figure 11-10. Instantaneous to initial permeability ratio (or permeability alteration factor) vs. filtration time during dynamic mud filtration (Liu and Civan, ©1996 SPE; reprinted by permission of the Society of Petroleum Engineers).

Prediction of formation damage due to dynamic mud filtration in two-phase flow was also carried out to demonstrate the capacity and application of the model and to provide a comparison with single-phase flow results. If the core studied by Jiao and Sharma (1992) was saturated by oil prior to mud filtration, the invasion of the water-based mud would lead to two-phase flow of oil and water in the rock. The same model parameters determined above for mud filtration in single-phase flow were used. Additional data necessary for simulation, including connate water saturation, residual oil saturation and relative permeabilities, are adapted from the case of fines migration in two-phase flow that was also simulated above. The predicted mud filtration volume and permeability alteration in two-phase flow are also plotted in Figures 11-9 and 11-10, as denoted by the dashed lines. These results indicate that filtration volume and formation damage are significantly less when a water-based mud invades an oil-bearing formation. This is because the total mobility for simultaneous two-phase flow of water and oil is usually less than that of single phase of water in formations, especially in Berea sandstones, which are generally strongly water-wet and have a very low permeability for water phase with the presence of oil in the formations.

References

- Civan, F., "A Generalized Model for Formation Damage by Rock-Fluid Interactions and Particulate Processes," SPE Paper 21183, Proceedings of the SPE 1990 Latin American Petroleum Engineering Conference, October 14-19, 1990, Rio de Janeiro, Brazil, 11 p.
- Civan, F., Predictability of Formation Damage: An Assessment Study and Generalized Models, Final Report, U.S. DOE Contract No. DE-AC22-90-BC14658, April 1994.
- Civan, F., "A Multi-Phase Mud Filtrate Invasion and Well Bore Filter Cake Formation Model," SPE Paper No. 28709, Proceedings of the SPE International Petroleum Conference & Exhibition of Mexico, October 10-13, 1994, Veracruz, Mexico, pp. 399-412.
- Civan, F., "A Multi-Purpose Formation Damage Model," SPE 31101 paper, Proceedings of the SPE Formation Damage Symposium, Lafayette, Louisiana, February 14-15, 1996, pp. 311-326.
- Civan, F., "Convenient Formulations for Immiscible Displacement in Porous Media," SPE Paper 36701, Proceedings of the 71st SPE Annual Tech. Conf. and Exhibition, Denver, Colorado, October 6-9, 1996, pp. 223-236.
- Collins, E. R., *Flow of Fluids Through Porous Materials*, Penn Well Publishing Co., Tulsa, Oklahoma, 1961, 270 p.

- Craig, F. F., Jr., *The Reservoir Engineering Aspects of Waterflooding*, Third Printing, November 1980, Society of Petroleum Engineers of AIME, New York, 1971, 134 p.
- Dake, L. P., *Fundamentals of Reservoir Engineering*, Elsevier Scientific Publ. Co., New York, 1978, 443 p.
- Eleri, O. O., & Ursin, J-R., "Physical Aspects of Formation Damage in Linear Flooding Experiments," SPE 23784 paper, presented at the SPE Intl. Symposium on Formation Damage Control, Lafayette, Louisiana, February 26–27, 1992.
- Gruesbeck, C., & Collins, R. E., "Particle Transport Through Perforations," *SPEJ*, December 1982, pp. 857–865.
- Gruesbeck, C., & Collins, R. E., "Entrainment and Deposition of Fine Particles in Porous Media," *SPEJ*, December 1982, pp. 847–856.
- Jiao, D., & Sharma, M. M., "Formation Damage Due to Static and Dynamic Filtration of Water-Based Muds," SPE 23823 paper, presented at the SPE Intl. Symposium on Formation Damage Control, Lafayette, Louisiana, February 26–27, 1992.
- Khilar, K. C., & Fogler, H. S., "Water Sensitivity of Sandstones," *SPEJ*, February 1983, pp. 55–64.
- Ku, C-A., & Henry, Jr., J. D., "Mechanisms of Particle Transfer from a Continuous Oil to a Dispersed Water Phase, *J. Colloid and Interface Sci.*, 1987, Vol. 116, No. 2, pp. 414–422.
- Liu, X., & Civan, F., "Characterization and Prediction of Formation Damage in Two-Phase Flow Systems, SPE 25429 paper, Proceedings of the SPE Production Operations Symposium, March 21–23, 1993, Oklahoma City, Oklahoma, March 21–23, 1993, pp. 231–248.
- Liu, X., & Civan, F., "Formation Damage and Skin Factors Due to Filter Cake Formation and Fines Migration in the Near-Wellbore Region," SPE 27364 paper, Proceedings of the 1994 SPE Formation Damage Control Symposium, February 9–10, 1994, Lafayette, Louisiana, pp. 259–274.
- Liu, X., & Civan, F., "Formation Damage by Fines Migration Including Effects of Filter Cake, Pore Compressibility and Non-Darcy Flow—A Modeling Approach to Scaling from Core to Field," SPE Paper #28980, SPE International Symposium on Oilfield Chemistry, February 14–17, 1995, San Antonio, TX.
- Liu, X., & Civan, F., "Formation Damage and Filter Cake Buildup in Laboratory Core Tests: Modeling and Model-Assisted Analysis," *SPE Formation Evaluation J.*, Vol. 11, No. 1, March 1996, pp. 26–30.
- Liu, X., Civan, F., & Evans, R. D., "Correlation of the Non-Darcy Flow Coefficient, *J. of Canadian Petroleum Technology*, Vol. 34, No. 10, 1995, pp. 50–54.

- Luan, Z., "Splitting Pseudospectral Algorithm for Parallel Simulation of Naturally Fractured Reservoirs," SPE Paper 30723, Proceedings of the Annual Tech. Conf. & Exhibition held in Dallas, TX, October 22–25.
- Muecke, T. W., "Formation Fines and Factors Controlling their Movement in Porous Media," *JPT*, pp. 147–150, Feb. 1979.
- Peng, S. J., & Peden, J. M., "Prediction of Filtration Under Dynamic Conditions," paper SPE 23824 presented at the SPE Intl. Symposium on Formation Damage Control held in Lafayette, LA, February 26–27, 1992, pp. 503–510.
- Rahman, S. S., & Marx, C., "Laboratory Evaluation of Formation Damage Caused by Drilling Fluids and Cement Slurry," *J. Can. Pet. Tech.*, November–December, 1991, pp. 40–46.
- Richardson, J. G., "Flow Through Porous Media," In: V. L. Streeter (Editor), *Handbook of Fluid Dynamics*, Section 16, McGraw-Hill, New York, 1961, pp. 68–69.
- Sarkar, A. K., "An Experimental Investigation of Fines Migration in Two-Phase Flow," MS Thesis, U. of Texas, Austin, 1988.
- Sarkar, A. K., & Sharma, M. M., "Fines Migration in Two-Phase Flow," *JPT*, May 1990, pp. 646–652.
- Sutton, G. D., & Roberts, L. D., "Paraffin Precipitation During Fracture Stimulation," *JPT*, September 1974, pp. 997–1004.
- Ucan, S., & Civan, F., "Simultaneous Estimation of Relative Permeability and Capillary Pressure for Non-Darcy Flow-Steady-State," SPE Paper 35271, Proceedings of the 1996 SPE Mid-Continent Gas Symposium, Amarillo, TX, April 29–30, 1996, pp. 155–163.
- Yokoyama, Y., & Lake, L. W., "The Effects of Capillary Pressure on Immiscible Displacements in Stratified Porous Media," SPE 10109 paper, presented at the 56th Annual Fall Technical Conference and Exhibition of the Society of Petroleum Engineers of AIIME, San Antonio, TX, October 5–7, 1981.

Chapter 12

Cake Filtration: Mechanism, Parameters and Modeling*

Summary

Models for interpretation and prediction of incompressible and compressible filter cake thickness, and filtrate volume and rate data for linear and radial filtration cases, and at static and dynamic filtration conditions are presented. Effects of compressibility and small particle invasion and deposition inside the cake and formation, as well as the Darcy versus non-Darcy flow regimes, are considered. Methods and diagnostic charts for determining the model parameters from experimental filtration data are presented. Applications for radial and linear filtration cases are presented and the results are compared for constant rate and constant pressure drive filtration. Model assisted analyses of experimental data demonstrate the diagnostic and predictive capabilities of the models. The parametric studies indicate that the particle screening efficiency of the formation is an important factor on the filter cake properties and filtration rate, the differences between the linear and radial cake filtration performances are more pronounced, and the cake thickness and filtrate volume are smaller, for constant pressure filtration than constant rate filtration. The present thickness-averaged ordinary differential models are shown to reproduce the predictions of the previous partial differential model rapidly with significantly less computational effort. Because of the simplicity of the equations and reduction of computational effort, the thickness-averaged

* Parts of this chapter have been reprinted with permission of the American Institute of Chemical Engineers and the Society of Petroleum Engineers from Civan (1998a,b, and 1999a, b).

linear and radial filter cake formation models offer significant advantages over the partial differential models for the analysis, design, and optimization of the cake filtration processes involving the well-bore and hydraulically created fracture surfaces. Simplified models considering incompressible particles and carrier fluids and analytical solutions for incompressible cakes without fines invasion are also presented. These models provide insight into the mechanism of cake filtration and offer practical means of interpreting experimental data, estimating the model parameters, and simulating the linear and radial filtration processes.

Introduction

Cake filtration occurs inherently in many in-situ hydrocarbon reservoir exploitation processes. For example, hydraulic fracturing of petroleum bearing rock and overbalanced drilling of wells into petroleum reservoirs usually cause a cross-flow filtration, which leads to a filter cake build-up over the face of the porous rock and filtrate invasion into the reservoir (Civan, 1994, 1996). When the slurry contains particles of different sizes, the larger particles of the slurry form the skeleton of the filter cake and the smaller particles can migrate into and deposit within the porous cake formed by the large particles. Simultaneously, the cake may undergo a compaction process under the effect of the fluid drag as the suspension of smaller particles flow through the cake (Tien et al., 1997). Consequently, the porosity, permeability, and thickness of the cake vary, which in turn effect the performance of the filtration process. Static filtration occurs when a slurry is applied to a filter without cross-flow. Therefore, the particles are continuously deposited to form thicker filter cakes. Dynamic filtration involves some cross-flow. Therefore, the filter cake thickness varies until the particle deposition and erosion rates equal.

Model assisted analyses, interpretation of experimental data and optimization and simulation of the filtration processes are of continuing interest for the industry. The majority of the previous modeling efforts has been limited to linear filtration applications, in spite of the fact that many industrial filtration processes facilitate radial filtration applications. Linear filtration models can closely approximate radial filtration only when the thicknesses of the filter and filter cake are sufficiently small relative to the radius of the filter surface exposed to slurry. Otherwise, radial models should be used for radial filtration.

Because of their simplicity, empirical correlations such as those reviewed by Clark and Barbat (1989) are frequently used for static and dynamic filtration. Xie and Charles (1997) have demonstrated that the use of a set of properly selected dimensionless groups leads to improved empirical correlations. Simple models, are preferred in many applications because

of their convenience and the reduced computational effort. The applicability of the majority of the previously reported simple analytical models, such as by Collins (1961), Hermia (1982), and de Nevers (1992), are usually limited to linear and constant rate filtration. However, models for constant pressure filtration are also required for certain applications. Civan (1998a) developed and verified improved linear and radial filtration models applicable for incompressible cake filtration without fines invasion at static and dynamic conditions.

Simplified models omit the internal details of the filtration processes and, therefore, may lead to incorrect results if applied for conditions beyond the range of the experimental data used to obtain the empirical correlations. In many applications, the phenomenological models describing the mechanisms of the cake formation, based on the conservation laws and rate equations, are preferred for filter cake build-up involving small particle migration and deposition and cake compaction, because these models allow for extrapolation beyond the range of data used to test and calibrate the models. Chase and Willis (1992), Sherman and Sherwood (1993), and Smiles and Kirby (1993) presented partial differential models for compressible filter cakes without particle intrusion. Liu and Civan (1996) developed a partial differential model for incompressible filter cake build-up, and filtrate and fine particle invasion into petroleum bearing rock at dynamic condition. Tien et al. (1997) have developed a partial differential model for compressible filter cakes considering small particle retention inside the cake at static condition. The solutions of such partial differential models require complicated, time consuming, and computationally intensive numerical schemes. To alleviate this difficulty, Corapcioglu and Abboud (1990), Abboud (1993), and Civan (1994) have resorted to formulations facilitating cake thickness averaging. Consequently, the partial differential filtration models have been reduced to ordinary differential equations requiring much less computational effort. Such mathematically simplified models are particularly advantageous because ordinary differential equations can be solved rapidly, accurately, and conveniently by readily available and well established numerical methods. The thickness-averaged models developed by Corapcioglu and Abboud (1990) and Abboud (1993) consider a constant porosity and linear cake filtration at static condition. The constant porosity assumption was justified by their filtration experiments because they used very dilute suspensions of particles and low pressure filtration, near the atmospheric pressure. Their models would not be applicable for high pressure filtration of thick slurries considered by Tien et al. (1997). Further, they assumed the same values for the rates of deposition of the small and large particles over the progressing filter cake surface. This assumption is invalid for most applications.

Civan (1998b) developed improved ordinary differential, linear and radial filtration models incorporating the effects of filter cake compaction, small particle invasion and retention at static and dynamic conditions. He applied filter cake thickness averaging by extending the methodology by Corapcioglu and Abboud (1990) and Civan (1994, 1996). The new models alleviate the aforementioned problems associated with the previous models. Civan (1998b) also derived the simplified forms of his models, considering that the particles and carrier fluid can be assumed incompressible for many practical applications. He presented the applications to radial and linear filtration processes and compared the results. The thickness-averaged ordinary differential filter cake model reproduced the predictions of the Tien et al. (1997) partial differential model rapidly with less computational effort.

In most filtration models, the flow through porous media is represented by Darcy's law. Consequently, the applicability of these models is limited to filtration undergoing at low flow rate or low pressure difference conditions. Civan (1999a,b) also developed linear and radial filtration models incorporating a non-Darcy flow behavior and applicable at static and dynamic filtration conditions by extending Civan's (1998a,b) model considering Darcy behavior. The non-Darcy behavior is represented by Forchheimer's (1901) law. In this chapter, the filtration models are presented by including the non-Darcy effects. However, the models also apply for Darcy flow because the non-Darcy effects diminish at low flow rates. Civan (1998a) also developed and verified several methods for determining the parameters of these incompressible cake filtration models from experimental data by constructing diagnostic charts of linear types. However, some parameters should be either directly measured or determined by a least-squares regression of experimental data with the filtration models as demonstrated by Civan (1998a,b). In this chapter, Civan's (1998a,b, 1999a,b) filtration models are presented.

Incompressible Cake Filtration

In this section, models for interpretation and prediction of incompressible filter cake thickness, and filtrate volume and rate data for linear and radial filtration cases, at static and dynamic conditions, are presented. Methods for determining the model parameters from experimental filtration data are presented. Model assisted analyses of three sets of experimental data demonstrate the diagnostic and predictive capabilities of the model. These models provide insight into the mechanism of incompressible cake filtration and offer practical means of interpreting experimental data, estimating the model parameters, and simulating the linear and radial filtration processes.

Linear Filter Cake Model

A schematic of the formation of a filter cake over a hydraulically created fracture is shown in Figure 12-1. Figure 12-2 shows the simplified, one-dimensional linear cake filtration problem considered in this section. The locations of the mud slurry side cake surface and the slurry and effluent side surfaces of the porous medium are denoted, respectively, by x_c , x_w , and x_e . Consistent with laboratory tests using core plugs, the cross-sectional area is denoted by a and the core length by $L \equiv x_e - x_w$.

The mass balance of particles in the filter cake is given by (Civan, 1996, 1998a)

$$-(\rho_p \epsilon_s)_c dx_c/dt = R_{ps} \quad (12-1)$$

where ρ_p is the particle density, t is time, ϵ_s is the volume fraction of particles of the cake that can be expressed as a function of the porosity ϕ_c of the cake as

$$\epsilon_s = 1 - \phi_c \quad (12-2)$$

and R_{ps} is the net mass rate of deposition of particles of the slurry to form the cake given by (Civan, 1998b, 1999a,b)

$$R_{ps} = k_d u_c c_p - k_e (\epsilon_s \rho_p)_c (\tau_s - \tau_{cr}) U(\tau_s - \tau_{cr}) \quad (12-3)$$

The first term on the right of Eq. 12-3 expresses the rate of particle deposition as being proportional to the mass of particles carried toward the filter by the filtration volumetric flux u_c , normal to the filter surface, given by

$$u_c = q/a \quad (12-4)$$

where q is the carrier fluid filtration flow rate and a is the area of the cake surface. c_p is the mass of particles contained per unit volume of the carrier fluid in the slurry. k_d is the deposition rate coefficient. The second term on the right of Eq. 12-3 expresses the rate of erosion of the cake particles from the cake surface on the slurry side. Erosion takes place only when the shear-stress τ_s applied by the slurry to the cake surface exceeds a minimum critical shear stress τ_{cr} necessary for detachment of particles from the cake surface. The shear-stress is given by (Metzner and Reed, 1955)

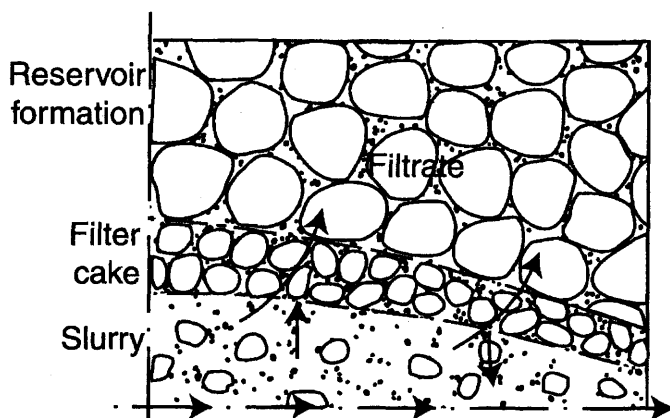


Figure 12-1. Filter cake buildup over a hydraulically created fracture surface (after Civan, ©1999 SPE; reprinted by permission of the Society of Petroleum Engineers).

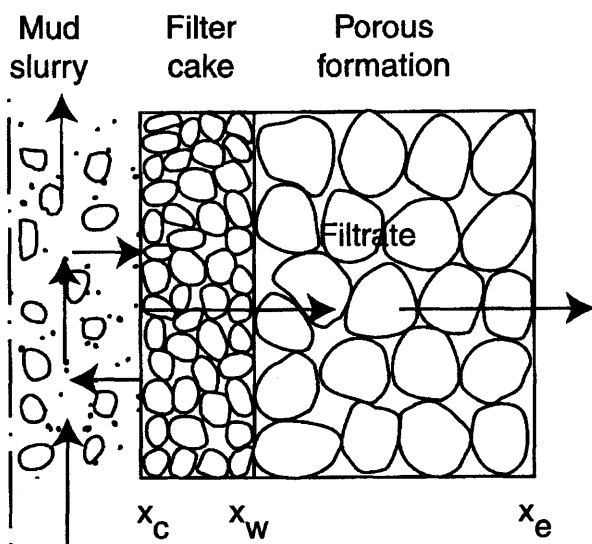


Figure 12-2. Linear filter cake over a flat surface of a core plug (after Civan, ©1999 SPE; reprinted by permission of the Society of Petroleum Engineers).

$$\tau_s = k'(8\nu)^{n'} \quad (12-5)$$

where k' and n' denote, respectively, the consistency constant and flow index. The critical shear-stress is dependent on various factors, including surface roughness and particle stickiness (Civan, 1998a,b) and aging (Ravi et al., 1992) and it should be measured directly. The deposition and erosion rate constants depend on the properties of the particles and carrier fluid, and the conditions of the slurry, such as particle concentration, flow rate, and pressure.

Ravi et al. (1992) have determined that the following equation proposed by Potanin and Uriev (1991) predicts the critical shear stress with the same order of magnitude accuracy of their experimental measurements:

$$\tau_{cr} = H/(24dl^2) \quad (12-6)$$

where $H = 3.0 \times 10^{-13}$ erg is the Hamaker coefficient, $d(\text{cm})$ is the average particle diameter, and $l(\text{cm})$ is the separation distance between the particle surfaces in the filter cake. However, the values calculated from Eq. 12-6 is only a first order accurate estimate because Eq. 12-6 has been derived from an ideal theory. The ideal theory does not take into account the effect of the other factors, such as aging (Ravi et al., 1992), surface roughness, and particle stickiness (Civan, 1996), on the particle detachment. Therefore, the actual value of the critical shear stress may be substantially different than that predicted by Eq. 12-6 using the particle size and separation distance data. Hence, Ravi et al. (1992) recommend experimental determination of the critical shear stress.

$U(\tau_s - \tau_{cr})$ is the Heaviside step function [$U(\tau_s - \tau_{cr}) = 0$ when $\tau_s < \tau_{cr}$, and $U(\tau_s - \tau_{cr}) = 1$ when $\tau_s \geq \tau_{cr}$].

$(\epsilon_s \rho_p)_c$ is the mass of particles contained per unit bulk volume of the slurry side cake surface. The erosion rate is related also to the particle content of the cake $(\epsilon_s \rho_p)_c$ and erosion cannot occur if there is no cake, that is if $(\epsilon_s \rho_p)_c = 0$. Here, the cake properties are assumed constant.

$$(\epsilon_s \rho_p)_c = \epsilon_s \rho_p = \text{constant} \quad (12-7)$$

Therefore, k_e and $(\epsilon_s \rho_p)_c$ can be combined into one coefficient as (Civan, 1999a)

$$\tilde{k}_e \equiv k_e (\epsilon_s \rho_p)_c \quad (12-8)$$

Then, Eq. 12-3 can be simplified to Civan's (1999a) equation as

$$R_{ps} = k_d u_c c_p - \tilde{k}_e (\tau_s - \tau_{cr}) U(\tau_s - \tau_{cr}) H(\epsilon_s) \quad (12-9)$$

in which $H(\epsilon_s) = 0$ when $\epsilon_s = 0$ (no cake) and $H(\epsilon_s) = 1$ when $\epsilon_s > 0$. The function $H(\epsilon_s)$ can be expressed in terms of the cake thickness, δ , as $H(\delta) = 0$ when $\delta = 0$ and $H(\delta) = 1$ when $\delta > 0$, because $\epsilon_s = 0$ when $\delta = 0$.

The filter cake thickness δ is given by

$$\delta = x_w - x_c \quad (12-10)$$

Note the slurry side filter surface position x_w is fixed.

Substituting Eqs. 12-2, 4, 9 and 10, Eq. 12-1 can be written as (Civan, 1998a)

$$d\delta/dt = Aq - B, 0 \leq \delta \quad (12-11)$$

where

$$A = k_d c_p / [(1 - \phi_c) \rho_p a] \quad (12-12)$$

$$\begin{aligned} B &= \tilde{k}_e (\tau_s - \tau_{cr}) U(\tau_s - \tau_{cr}) H(\delta) / [(1 - \phi_c) \rho_p] \\ &= k_e (\tau_s - \tau_{cr}) U(\tau_s - \tau_{cr}) H(\delta) \end{aligned} \quad (12-13)$$

The initial condition for Eq. 12-11 is

$$\delta = 0, t = 0 \quad (12-14)$$

The rapid filtration flow of the carrier fluid through the cake and filter can be expressed by Forchheimer's (1901) equation

$$-\frac{\partial p}{\partial x} = \frac{\mu}{K} u + \rho \beta u^2 \quad (12-15)$$

The inertial flow coefficient is given by the Liu et al. (1995)

$$\beta = 2.92 \times 10^4 \tau / (\phi K) \quad (12-16)$$

where β is the inertial flow coefficient in cm^{-1} , K is the permeability in Darcy, and τ is the tortuosity (dimensionless). Substituting Eq. 12-4 into Eq. 12-15 yields

$$-\frac{\partial p}{\partial x} = \frac{\mu}{aK} q + \frac{\rho\beta}{a^2} q^2 \quad (12-17)$$

As explained by Civan (1998a,b), the instantaneous carrier fluid filtration flow rate q is the same everywhere in the cake and filter irrespective of whether the process is undergoing a constant pressure or a constant rate filtration. In the following, the formulations for variable and constant rate filtration processes are derived.

For variable rate filtration occurring under an applied pressure difference, integrating Eq. 12-17 for conditions existing prior to and during the process of formation of a filter cake leads to, respectively:

$$p_c - p_e = \frac{q_o \mu L_f}{aK_f} + \frac{\rho\beta_f L_f q_o^2}{a^2} \quad (12-18)$$

and

$$\begin{aligned} p_c - p_e &= (p_c - p_w) + (p_w - p_e) \\ &= \left(1 + \frac{K_f \delta}{K_c L_f}\right) \frac{q \mu L_f}{aK_f} + \left(1 + \frac{\beta_c \delta}{\beta_f L_f}\right) \frac{\rho\beta_f L_f q^2}{a^2} \end{aligned} \quad (12-19)$$

Consequently, eliminating $(p_c - p_e)$ between Eqs. 12-18 and 19, and then solving for q , yields for Darcy flow ($\beta_f = \beta_c = 0$)

$$q = -\tilde{\gamma}/\tilde{\beta} \quad (12-20a)$$

and for non-Darcy flow:

$$q = \frac{-\tilde{\beta} + \sqrt{\tilde{\beta}^2 - 4\tilde{a}\tilde{\gamma}}}{2\tilde{a}} \quad (12-20b)$$

in which

$$\tilde{a} = (\beta_f L_f + \beta_c \delta) \frac{\rho}{a^2} \quad (12-21)$$

$$\tilde{\beta} = \left(1 + \frac{K_f \delta}{K_c L_f} \right) \frac{\mu L_f}{a K_f} \quad (12-22)$$

$$\tilde{\gamma} = - \left(\frac{q_o \mu L_f}{a K_f} + \frac{\rho \beta_f L_f q_o^2}{a^2} \right) \quad (12-23)$$

Alternatively, eliminating $(p_c - p_e)$ between Eqs. 12-18 and 12-19 and then solving for δ yields:

$$\delta = \frac{\frac{\mu L_f q_o}{a K_f} \left(1 - \frac{q}{q_o} \right) + \frac{\rho \beta_f L_f q_o^2}{a^2} \left[1 - \left(\frac{q}{q_o} \right)^2 \right]}{\frac{\mu q}{a K_c} + \frac{\rho \beta_c q^2}{a^2}} \quad (12-24)$$

Notice that Eq. 12-24 yields $\delta = 0$ when $q = q_o$. Differentiating Eq. 12-24 with respect to time and then substituting into Eq. 12-11 yields

$$\begin{aligned} & - \left\{ \left(\frac{\mu L_f}{a K_f} + \frac{2 \rho \beta_f L_f q}{a^2} \right) \left(\frac{\mu q}{a K_c} + \frac{\rho \beta_c q^2}{a^2} \right) \right. \\ & \left. + \left[\frac{\mu L_f q_o}{a K_f} \left(1 - \frac{q}{q_o} \right) + \frac{\rho \beta_f L_f q_o^2}{a^2} \left(1 - \frac{q^2}{q_o^2} \right) \right] \right\} \\ & \left(\frac{\mu}{a K_c} + \frac{2 \rho \beta_c q}{a^2} \right) \frac{dq}{dt} = \left(\frac{\mu q}{a K_c} + \frac{\rho \beta_c q^2}{a^2} \right)^2 (Aq - B) \end{aligned} \quad (12-25)$$

The initial condition for Eq. 12-25 is

$$q = q_o, t = 0 \quad (12-26)$$

Substituting Eq. 12-20 and considering the initial condition given by Eq. 12-14, Eq. 12-11 can be solved using a numerical scheme, such as the Runge-Kutta-Fehlberg four (five) method (Fehlberg, 1969). Eqs. 12-25 and 12-26 can also be solved numerically using the same method.

The relationships between filtrate flow rate and cumulative filtrate volume are given by

$$Q = \int_0^t q dt \quad (12-27)$$

$$q = dQ/dt \quad (12-28)$$

Note that Eqs. 12-24 and 25 simplify to Eqs. 12-29 and 12-33 (Civan, 1998a), respectively, when the inertial effects are neglected, that is, for $\beta_c = \beta_f = 0$.

$$\delta = C/q - D \quad (12-29)$$

where

$$C = q_o D \quad (12-30)$$

$$D = L_f K_c / K_f \quad (12-31)$$

$$u_c = q/a \quad (12-32)$$

and

$$dq/dt = -(1/C)q^2(Aq - B) \quad (12-33)$$

subject to

$$q = q_o, t = 0 \quad (12-34)$$

Then, the analytical solutions for the filtrate flow rate and cumulative volume as well as the filter cake thickness can be derived as demonstrated by Civan (1998a, 1999a).

The analytical solution of Eqs. 12-33 and 34 is (Civan, 1998a)

$$t = -\frac{C}{B} \left\{ \frac{A}{B} \ln \left[\frac{\frac{A}{B} - \frac{1}{q}}{\frac{A}{B} - \frac{1}{q_o}} \right] + \frac{1}{q} - \frac{1}{q_o} \right\} \quad (12-35)$$

Eliminating q between Eqs. 12–29 and 12–35 yields another expression as:

$$t = -\frac{C}{B} \left\{ \frac{A}{B} \ln \left[\frac{\frac{A}{B} - \frac{\delta + D}{C}}{\frac{A}{B} - \frac{\delta_o + D}{C}} \right] + \frac{\delta - \delta_o}{C} \right\} \quad (12-36)$$

in which, usually, $\delta_o = 0$ at $t = 0$ (i.e., no initial filter cake).

Eq. 12–36 is different from Eq. 7-96 of Collins (1961) because Collins did not consider the filter cake erosion. Therefore, Collins' equation applies for static filtration. To obtain Collins' result, $k_e = 0$ or $B = 0$ must be substituted in Eq. 12–11. Thus, eliminating q between Eqs. 12–29 and 12–11, and then integrating, yields the following equation for the filter cake thickness (Civan, 1998a):

$$(1/2)\delta^2 + D\delta = ACt \quad (12-37)$$

which results in Eqs. 7-96 of Collins (1961) by invoking Eqs. 12–18 for $\beta_f = 0$, Eqs. 12–30, 12–31, and 12–12 and expressing the mass of suspended particles per unit volume of the carrier fluid in terms of the volume fraction, σ_p , of the particles in the slurry according to:

$$c_p = \rho_p \sigma_p / (1 - \sigma_p) \quad (12-38)$$

Civan (1998a) derived the expressions for the filtrate flow rate and the cumulative filtrate volume by integrating Eq. 12–33 for $B = 0$ and applying Eq. 12–27, respectively, as:

$$q = q_o / \sqrt{1 + (2Aq_o^2/C)t} \quad (12-39)$$

and

$$Q = (C/A)(q^{-1} - q_o^{-1}) \quad (12-40)$$

Eq. 12–39 expresses that the filtrate rate declines by time due to static filter cake build-up. Donaldson and Chernoglazov (1987) used an empirical decay function:

$$q = q_o \exp(-\beta t) \quad (12-41)$$

in which β is an empirically determined coefficient.

For constant rate filtration, Eq. 12-11 subject to Eq. 12-14 can be integrated numerically for varying shear-stress τ_s . When the shear-stress is constant or does not vary significantly, an analytical solution can be obtained as (Civan, 1999a):

$$\delta = (Aq - B)t \quad (12-42)$$

in which $B=0$ because $\tau=0$ for static conditions and $B \neq 0$ because $\tau \neq 0$ for dynamic conditions. The cumulative filtrate volume is given by, for both the static and dynamic filtration

$$Q = qt \quad (12-43)$$

Then, the pressure difference $(p_c - p_e)$ or the slurry injection pressure p_c , when the back pressure at the effluent side of the porous filter media p_e is prescribed, can be calculated by Eq. 12-19. The following conventional filtration equation (Hermia, 1982; de Nevers, 1992) can be derived by invoking Eq. 12-43 into Eq. 12-40:

$$\frac{t}{Q} = \frac{A}{C}Q + \frac{1}{q_o} \quad (12-44)$$

Radial Filter Cake Model

A schematic of the formation of a filter cake over the sand face during over-balanced mud circulation in a wellbore is shown in Figure 12-3. Figure 12-4 is a quadrant areal view of the problem. The radii of the mud slurry side cake surface, the sand face over which the cake is built up, and the external surface considered for the region of influence are denoted by r_c , r_w , and r_e , respectively. The formation thickness is h .

The particle mass balance equation is given by (Civan, 1994, 1998a)

$$-(\rho_p \epsilon_s)_c dr_c/dt = R_{ps} \quad (12-45)$$

The filter cake thickness is given by

$$\delta = r_w - r_c \quad (12-46)$$

R_{ps} is given by Eq. 12-9. The slurry shear-stress at the cake surface is given by the Rabinowitsch-Mooney equation (Metzner and Reed, 1955)

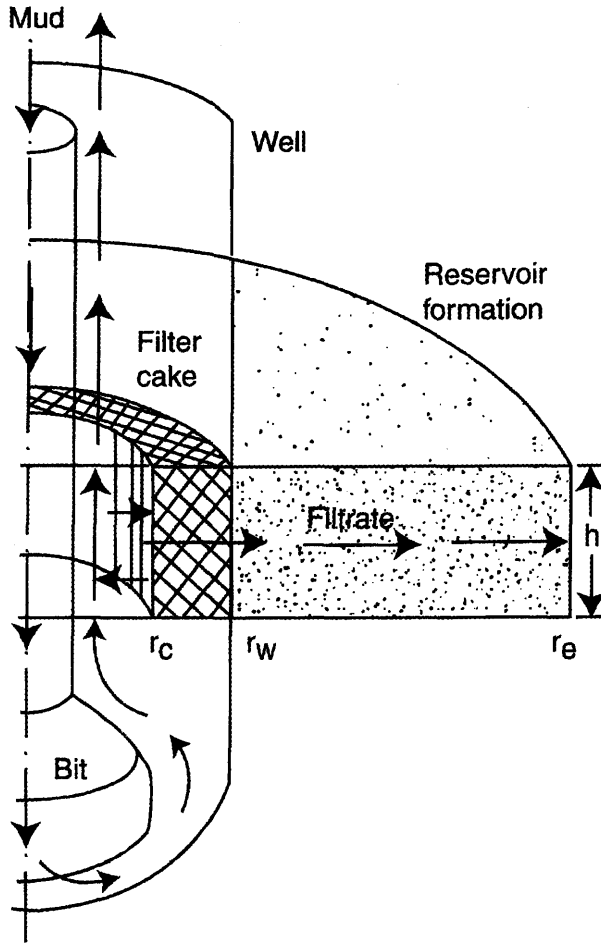


Figure 12-3. Mud-cake buildup over a wellbore sandface (after Civan, ©1999 SPE; reprinted by permission of the Society of Petroleum Engineers).

$$\tau_s = k'(4v/r_c)^{n'} \quad (12-47)$$

The carrier fluid filtration flux u_c at the filter cake surface in terms of the filtration flow rate is given by

$$u_c = \frac{q}{2\pi r_c h} \quad (12-48)$$

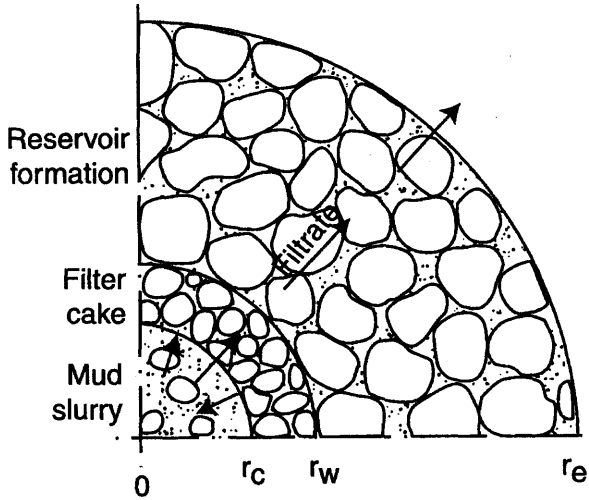


Figure 12-4. Radial filter cake over a wellbore sandface (after Civan, ©1999 SPE; reprinted by permission of the Society of Petroleum Engineers).

Substituting Eqs. 12-2, 12-9, 12-46, and 12-48 into Eq. 12-45 results in (1999a)

$$\frac{d\delta}{dt} = A \frac{q}{r_w - \delta} - B, 0 \leq \delta \leq r_w \quad (12-49)$$

where

$$A = \frac{k_d c_p}{2\pi h (1 - \phi_c) \rho_p} \quad (12-50)$$

and B is given by Eq. 12-13. The initial condition for Eq. 12-49 is

$$\delta = 0, t = 0 \quad (12-51)$$

Forchheimer's (1901) equation for radial flow of the carrier fluid reads as

$$-\frac{\partial p}{\partial r} = \frac{\mu}{K} u + \beta \rho u^2 \quad (12-52)$$

The radial volumetric flux of the carrier fluid is given by

$$u = \frac{q}{2\pi rh} \quad (12-53)$$

Thus, substituting Eq. 12-53 into Eq. 12-52 results in

$$-\frac{\partial p}{\partial r} = \frac{\mu}{2\pi h K} \frac{q}{r} + \frac{\rho\beta}{(2\pi h)^2} \left(\frac{q}{r}\right)^2 \quad (12-54)$$

Integration of Eq. 12-54 for conditions prevailing prior to and during filter cake formation leads to the following expressions, respectively (Civan, 1999a)

$$p_c - p_e = \frac{q_o \mu}{2\pi h K_f} \ln\left(\frac{r_e}{r_w}\right) + \frac{\rho\beta_f q_o^2}{(2\pi h)^2} \left(\frac{1}{r_w} - \frac{1}{r_e}\right) \quad (12-55)$$

and

$$\begin{aligned} p_c - p_e = & \frac{q\mu}{2\pi h K_f} \left[\ln\left(\frac{r_e}{r_w}\right) + \frac{K_f}{K_c} \ln\left(\frac{r_w}{r_c}\right) \right] \\ & + \frac{\rho\beta_f q^2}{(2\pi h)^2} \left[\frac{1}{r_w} - \frac{1}{r_e} + \frac{\beta_c}{\beta_f} \left(\frac{1}{r_c} - \frac{1}{r_w}\right) \right] \end{aligned} \quad (12-56)$$

Thus, eliminating $(p_c - p_e)$ between Eqs. 12-55 and 56, substituting Eq. 12-46, and then solving for q , yields for Darcy flow ($\beta_f = \beta_c = 0$):

$$q = -\tilde{\gamma}/\tilde{\beta} \quad (12-57a)$$

and for non-Darcy flow:

$$q = \frac{-\tilde{\beta} + \sqrt{\tilde{\beta}^2 - 4\tilde{\alpha}\tilde{\gamma}}}{2\tilde{\alpha}} \quad (12-57b)$$

in which

$$\tilde{\alpha} = \frac{\rho}{(2\pi h)^2} \left[\beta_f \left(\frac{1}{r_w} - \frac{1}{r_e}\right) + \beta_c \left(\frac{1}{r_w - \delta} - \frac{1}{r_w}\right) \right] \quad (12-58)$$

$$\tilde{\beta} = \frac{\mu}{2\pi h K_f} \left[\ln \left(\frac{r_e}{r_w} \right) + \frac{K_f}{K_c} \ln \left(\frac{r_w}{r_w - \delta} \right) \right] \quad (12-59)$$

$$\tilde{\gamma} = - \left[\frac{q_o \mu}{2\pi h K_f} \ln \left(\frac{r_e}{r_w} \right) + \frac{\rho \beta_f q_o^2}{(2\pi h)^2} \left(\frac{1}{r_w} - \frac{1}{r_e} \right) \right] \quad (12-60)$$

Substituting Eq. 12-57 and considering the initial condition given by Eq. 12-51, Eq. 12-49 can be solved using a numerical scheme, such as the Runge-Kutta-Fehlberg four (five) method (Fehlberg, 1969).

The cumulative filtrate volume is given by Eq. 12-27. The pressure difference $(p_c - p_e)$, or the slurry injection pressure p_c when the back pressure p_e is prescribed, can be calculated by Eq. 12-56.

When the inertial flow terms are negligible, equating Eqs. 12-55 and 12-56 and rearranging leads to (Civan, 1998a):

$$\ln(r_w/r_c) = (q_o/q - 1) (K_c/K_f) \ln(r_e/r_w) \quad (12-61)$$

Equation 12-61 can be written as:

$$r_c/r_w = \exp(-C/q + D) \quad (12-62)$$

where

$$C = q_o D / K_f \quad (12-63)$$

where q_o is the injection rate given by Eq. 12-55 for $\beta_f = 0$ before the filter cake buildup and

$$D = (K_c/K_f) \ln(r_e/r_w) \quad (12-64)$$

Thus, substituting Eqs. 12-46 and 12-62 into Eq. 12-49 and rearranging yield the filtration flow rate equation as (Civan, 1998a):

$$dq/dt = (-1/C) q^2 [Aq \exp(C/q - D) - B] \exp(C/q - D) \quad (12-65)$$

subject to the initial condition given by:

$$q = q_o, t = 0 \quad (12-66)$$

The wall shear-stress is calculated by Eq. 12-47 for the varying cake radius, $r_c = r_c(t)$. The filter cake thickness is calculated by means of Eqs. 12-46 and 62. Equations 12-65 and 66 can be solved numerically using an appropriate method such as the Runge-Kutta method. However, for thin cakes, it is reasonable to assume that the wall-shear stress is approximately constant, because $r_c \cong r_w$. Then, Eq. 12-65 can be integrated as (Civan, 1998a):

$$t = -C \int_{q_0}^q \left\{ q^2 \exp(C/q - D) [Aq \exp(C/q - D) - B] \right\}^{-1} dq \quad (12-67)$$

For constant rate filtration, Eq. 12-49 subject to Eq. 12-51 can be integrated numerically for varying shear-stress τ_s . When the filter cake is thin, the variation of the shear-stress τ_s by the cake radius r_c can be neglected and an analytical solution can be obtained as for dynamic filtration conditions ($B \neq 0$) (Civan, 1999a):

$$t = -\frac{\delta}{B} + \frac{Aq}{B^2} \ln \left[\frac{r_w - \delta - \frac{Aq}{B}}{r_w - \frac{Aq}{B}} \right] \quad (12-68)$$

The solution for static filtration conditions ($B = 0$) is obtained as (Civan, 1999a):

$$t = \frac{1}{Aq} \left(r_w \delta - \frac{1}{2} \delta^2 \right) \quad (12-69)$$

Eq. 12-68 and 12-69 apply irrespective of whether the flow is Darcy or non-Darcy.

Determination of Model Parameters and Diagnostic Charts

The majority of the reported filtration studies have not made attempts at measuring a full set of measurable parameters. The filtration models presented in this chapter may provide some guidance for the types of parameters needed for simulation.

As listed in Table 12-1, Civan's (1998a, 1999a) filtration models require the values of 20 parameters for simulation. Only five of these parameters may not be directly or conveniently measurable with the

Table 12-1
Data for the Laboratory Filtration Applications^{†}**

Parameters	Radial Flow Fisk et al.(1991)	Linear Flow Jiao and Sharma (1994)	Linear Flow Willis et al. (1983)
Suspension type	Seawater-based partially hydrolyzed poly-acrylamide drilling mud	Fresh water bentonite suspension	Lucite in water suspension
Filter permeability, K_f (darcy)	6 [*]	0.104 [†]	—
Cake permeability, K_c (darcy)	1.35×10^{-6}	2.1×10^{-4}	—
Cake porosity, ϕ_c	0.40 [‡]	0.40 [‡]	0.388 [*]
Filter length, L_f (cm)	—	20.34 [†]	—
Filter diameter, D (cm)	—	2.54 [†]	—
Slurry injection side filter radius, r_w (cm)	2.5 [*]	—	—
Filtrate outlet side filter radius, r_e (cm)	3.8 [*]	—	—
Filter width, h (cm)	1.9 [*]	—	—
Filtrate density, ρ_w (gm/cm ³)	1.0	1.0	0.997 [*]
Particle density, ρ_p (gm/cm ³)	2.5 [‡]	2.5 [‡]	1.18 [*]
Particle mass per carrier fluid volume, c_p (gm/cm ³)	0.56 [*]	0.04 [†]	0.055 [*]
Deposition rate constant, k_d	1.1	4.3	—
Erosion rate constant, k_e (s/cm)	3×10^{-6}	7.4×10^{-7}	—
Critical shear-stress, τ_w (dyne/cm ²)	0.5	5.0	—
Filtrate (water) viscosity, μ (cp)	1.0	1.0	0.969 [*]
Consistency constant, k' (dyne/cm ² /s ⁿ)	8.0 [†]	8.0 [†]	—
Flow index, n'	0.319 [†]	0.319 [†]	—
Slurry tangential velocity, v (cm/s)	125 [*]	8.61 [†]	—
Slurry application pressure, p_c (atm)	34 [*]	6.89 [†]	1.7 [*]
Filter outlet side back pressure, p_e (atm)	1.	1.	1. [*]

‡ Data assumed; *Data from Fisk et al. (1991);

† Data from Jiao and Sharma (1994); Willis et al. (1983); **After Civan, F., 1998a; reprinted by permission of the AIChE, ©1998 AIChE, All Rights reserved.

conventional techniques. These are the permeability K_c and porosity ϕ_c of the filter cake, and the deposition and erosion rate constants k_d and k_e , and the critical shear-stress τ_{cr} for the particles. However, given the experimental measurements of the filtrate volume $Q(\text{cm}^3)$, or rate q (cm^3/s), and the filter cake thickness δ as functions of the filtration time t , some of these parameters can be determined by means of the diagnostic charts constructed as described in the following. These are presented separately for the linear and radial filtration processes obeying Darcy's law according to Civan (1998a).

Linear Filtration

A plot of Eq. 12-11 for $d\delta/dt$ versus q yields a straight line. Substituting the slope (A) and intercept ($-B$) of this line into Eqs. 12-12 and 13 yields, respectively, the following expressions for the particle deposition and erosion rate constants:

$$k_d = Aa(1 - \phi_c)\rho_p/c_p \quad (12-70)$$

$$k_e = B(1 - \phi_c)\rho_p/(\tau - \tau_{cr}) \quad (12-71)$$

In dynamic filtration, the filter cake thickness attains a certain limit value, δ_∞ , when the particle deposition and erosion rates equate. Simultaneously, the filtration rate also reaches a limiting value, determined by Eq. 12-11 as:

$$q_\infty = B/A \quad (12-72)$$

At this condition, Eq. 12-29 yields the limiting value of the filter cake thickness as:

$$\delta_\infty = C/q_\infty - D \quad (12-73)$$

Consequently, substituting Eqs. 12-30, 12-31, 12-12 and 12-13 for A , B , C , and D into Eqs. 12-72 and 12-73 leads to the following relationships for the cake permeability and the ratio of the erosion and deposition rate constants, respectively, as:

$$K_c = \delta_\infty K_f / [L_f(q_o/q_\infty - 1)] \quad (12-74)$$

$$k_e/k_d = c_p q_\infty / [a(\tau - \tau_{cr})] \quad (12-75)$$

Equation 12-33 can be rearranged in a linear form as:

$$-\frac{d}{dt}\left(\frac{1}{q}\right) = \frac{1}{q^2} \frac{dq}{dt} = -\frac{A}{C}q + \frac{B}{C} \quad (12-76)$$

Thus, the intercept (B/C) and slope ($-A/C$) of the straight-line plot of Eq. 12-76 can be used with Eqs. 12-30, 12-31, 12-12, and 12-13 to obtain the following expressions:

$$\frac{k_e}{k_d} = \frac{(B/C)c_p}{(A/C)(\tau - \tau_{cr})a} \quad (12-77)$$

$$k_d = \frac{(A/C)(1 - \phi_c)\rho_p a q_o q_\infty \delta_\infty}{c_p(q_o - q_\infty)} \quad (12-78)$$

Comparing Eqs. 12-75 and 12-77 yields an alternative expression for determination of the limit filtrate rate as:

$$q_\infty = (B/C)/(A/C) \quad (12-79)$$

Eq. 12-79 can be used to check the value of q_∞ obtained by Eq. 12-72. Equation 12-74 can be used to determine the filter cake permeability, K_c . Equations 12-70 and 12-75 or 12-77 and 12-78 can be used to calculate the particle deposition and erosion rates k_d and k_e , if the cake porosity ϕ_c and the critical shear stress τ_{cr} are known. ϕ_c can be measured. τ_{cr} can be estimated by Eq. 12-6, but the ideal theory may not yield a correct value as explained previously by Ravi et al. (1992) and in this chapter. Therefore, Ravi et al. (1992) suggested that τ_{cr} should be measured directly.

Radial Filtration

Given the filter cake thickness δ , the progressing surface cake radius r_c can be calculated by Eq. 12-46. Then a straight line plot of $\ln(r_c/r_w)$ vs. $(1/q)$ data according to Eq. 12-62 yields the values of C and D as the slope and intercept of this line, respectively. A straightline plot of $[d\delta/dt]$ versus $[q/(r_w - \delta)]$ data according to Eq. 12-49 yields the values of A and B as the slope and intercept of this line, respectively. At static filtration conditions, $v = 0$ and $\tau = 0$ according to Eq. 12-47. Therefore,

$B=0$ according to Eq. 12-13. Consequently, substituting $B=0$ and Eq. 12-63, Eq. 12-65 can be expressed in the following linear form:

$$\begin{aligned}\ln\left\{d/dt\left[1/(2q^2)\right]\right\} &= \ln\left[-q^{-3} dq/dt\right] \\ &= \left[\ln(A/C) - 2CK_f/q_o\right] + 2C/q\end{aligned}\quad (12-80)$$

Thus, a straightline plot of $\ln\left[-q^{-3} dq/dt\right]$ versus $(1/q)$ yields the values of $(2C)$ and $\left[\ln(A/C) - 2CK_f/q_o\right]$ as the slope and intercept of this line, respectively. This allows for determination of the A and C coefficients only. The determination of a full set of A, B, C , and D from Eqs. 12-49 and 12-65 requires both the filtrate flow rate (or volume) and the cake thickness versus the filtration time data. Once these coefficients are determined, then their values can be used in Eqs. 12-50, 12-13, 12-63, and 12-64 to determine the values of the deposition and erosion rate constants k_d and k_e . The discussion of the linear filtration about the determination of τ_{cr} by Eq. 12-6 is valid also in the radial filtration case.

At dynamic equilibrium, the filter cake thickness and the filtrate flow rate attain certain limiting values δ_∞ and q_∞ . Then, substituting Eq. 12-46 into Eqs. 12-49 and 62 yields the following relationships, respectively:

$$Aq_\infty = B(1 - \delta_\infty/r_w) \quad (12-81)$$

$$1 - \delta_\infty/r_w = \exp(-C/q_\infty + D) \quad (12-82)$$

The filter cake permeability is determined by Eq. 12-64 as:

$$K_c = DK_f/\ln(r_e/r_w) \quad (12-83)$$

The equations and the linear plotting schemes developed in this section allow for determination of the parameters of the filtration models, mentioned at the beginning of this section, from experimental filtrate flow rate (or volume) and/or filter cake thickness data. The remaining parameters should be either directly measured or estimated. In the following applications, the best estimates of the missing data have been determined by adjusting their values to fit the experimental data. This is an exercise similar to several other studies, including Liu and Civan (1996) and Tien et al. (1997). They have resorted to a model assisted estimation of the parameters because there is no direct method of measurement for some of these parameters.

Applications

The numerical solutions of the present models require the information on the characteristics of the slurries, particulates, carrier fluids, filters and filter cakes, the actual conditions of the tests conducted, and the measurements of all the system parameters and variables. The reported studies of the slurry filtration have measured only a few parameters and the filtrate volumes or rates and do not offer a complete set of suitable data that is needed for full scale experimental verification of the present models. Civan (1998a) used the Willis et al. (1983) and Jiao and Sharma (1994) data for linear filtration, and the Fisk et al. (1991) data for radial filtration, because these data provide more information than the other reported studies. The data is presented in Table 12-1 in consistent Darcy units, which are more convenient for flow through porous media.

Linear Filtration Applications

Jiao and Sharma (1994) carried out linear filtration experiments using concentrated bentonite suspensions. They only measured the filtrate volume and predicted the filter cake thickness using a simple algebraic model. These data are given in their Figures 3 and 10, respectively. In Figures 12-5 to 12-7, their data are plotted according to the linear plotting schemes presented in the previous section for determination of parameters. As can be seen from these figures, the coefficients of Eqs. 12-76, 12-29, and 12-11 obtained by the least-squares regression method and the corresponding coefficients of regression are given, respectively, by:

$$A/C = 8.297 \text{ min/cm}^6, B/C = 0.1136 \text{ cm}^{-3}, R^2 = 0.8713 \quad (12-84)$$

$$C = 0.0034 \text{ cm}^4/\text{min}, D = 0.0076 \text{ cm}, R^2 = 0.949 \quad (12-85)$$

$$A = 0.0229 \text{ cm}^{-2}, B = 0.0003 \text{ cm/min}, R^2 = 0.9873 \quad (12-86)$$

The coefficients of regressions very close to 1.0 indicate that the present equations closely represent the data. The coefficient of regression $R^2 = 0.8713$ indicated by Figure 12-5 and Eq. 12-84 is lower than those indicated by Figures 12-6 and 12-7 and Eqs. 12-85 and 12-86, inferring the possibility of larger measurement errors involved in the filtrate volume data. Another source of errors may be due to the three-point finite difference numerical differentiation of the filtrate volume data to obtain the filtrate flow rate data used to construct Figure 12-5. The data necessary for Figure 12-5 were obtained by a series of numerical procedures, first

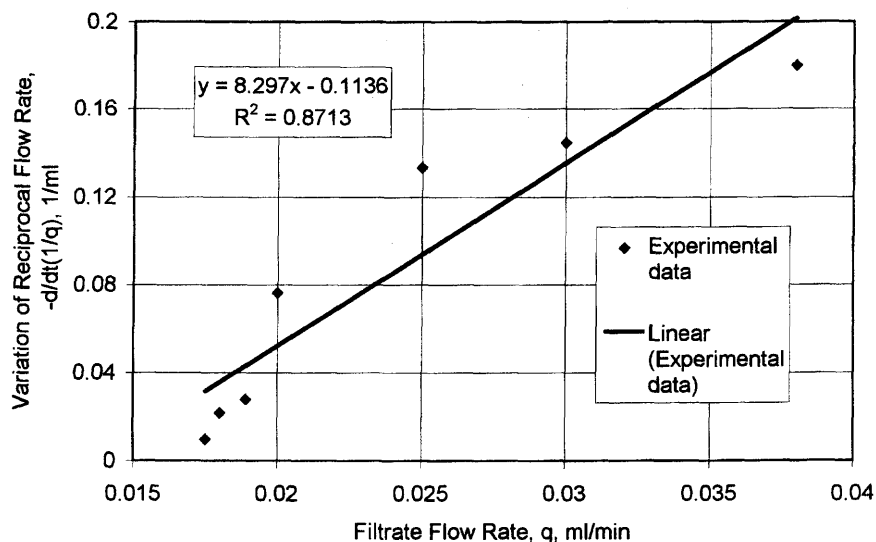


Figure 12-5. Correlation of Jiao and Sharma (1994) experimental data (Civan, F., 1998; reprinted by permission of the AIChE, ©1998a AIChE. All rights reserved).

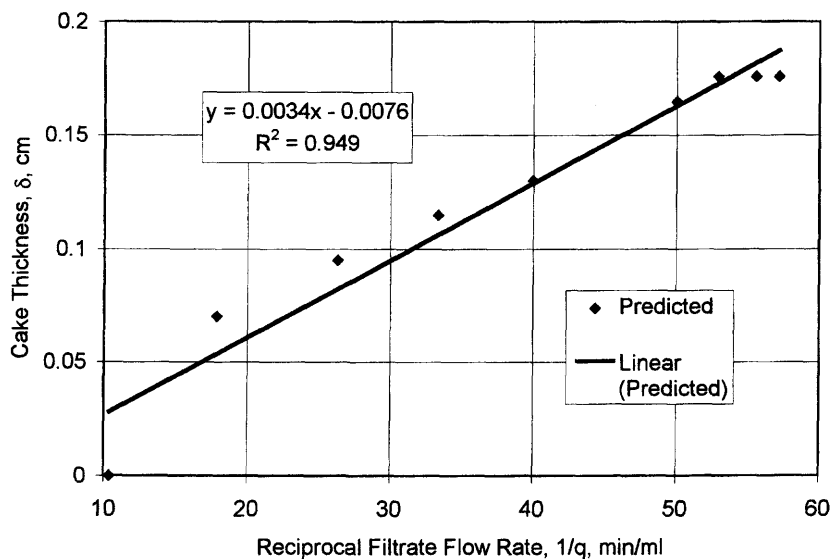


Figure 12-6. Correlation of Jiao and Sharma (1994) predicted filter cake thickness data (Civan, F., 1998; reprinted by permission of the AIChE, ©1998a AIChE. All rights reserved).

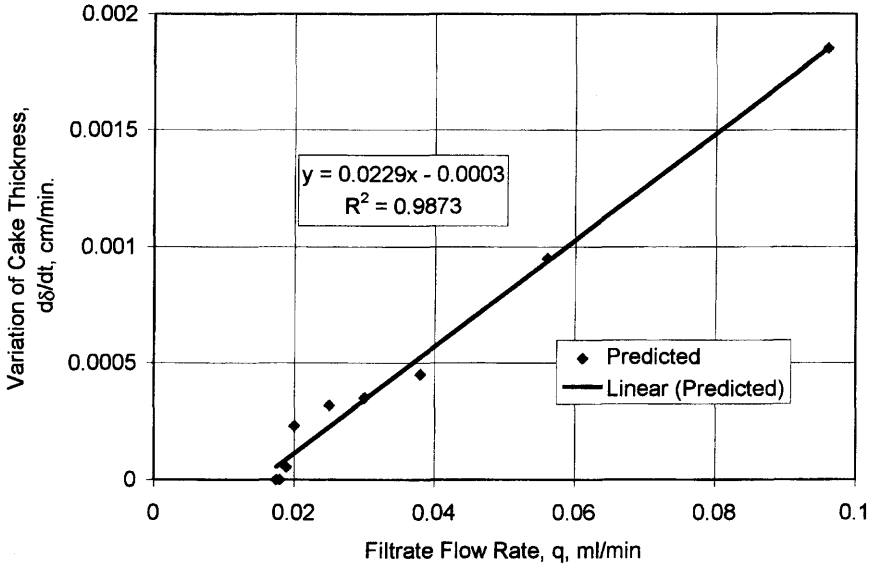


Figure 12-7. Correlation of Jiao and Sharma (1994) predicted filter cake thickness data (Civan, F., 1998a; reprinted by permission of the AIChE, ©1998 AIChE. All rights reserved).

to calculate $q = dQ/dt$ from the filtrate volume Q data, and then $(1/q)$ and $[d/dt(1/q)]$.

The initial filtrate volume rate is obtained as $q_o = 0.096 \text{ mL/min}$ by a three-point forward differentiation of the measured, initial filtrate volume data. This data is expected to involve a larger error because of the possibility of relatively larger errors involved in the early filtrate volume data. The noisy data had to be smoothed prior to numerical differentiation, which may have introduced further errors. Because of the propagation of the significantly larger measurement errors involved in the early filtrate volume data, the first two of the $[d/dt(1/q)]$ values degenerated and deviated significantly from the expected straightline trend. Therefore, these two data points formed the outliers for linear regression and had to be discarded.

Substituting the values given in Eq. 12-84 into Eq. 12-79 yields the limiting filtrate flow rate as $q_\infty = 0.014 \text{ mL/min}$. On the other hand, substituting the values given in Eq. 12-86 into Eq. 12-72 yields $q_\infty = 0.013 \text{ mL/min}$. These two values obtained from the filtrate flow rate and cake thickness data, respectively, are very close to each other. The limiting filtrate volume rate q_∞ estimated by an extrapolation of the

derivatives of the filtrate volume data beyond the range of the experimental data is $q_{\infty} = 0.017 \text{ mL/min}$ and close to the values obtained by the regression method. This is an indication of the validity of the filtration model.

Using $q_{\infty} = 0.014 \text{ mL/min}$ in Eq. 12-29 yields the limiting filter cake thickness as $\delta_{\infty} = 0.24 \text{ cm}$. The predicted cake thickness data presented in Figure 10 of Jiao and Sharma (1994) indicates a value of approximately 0.17 cm . Therefore, their prediction of the limiting filter cake thickness appears to be an underestimate compared to the 0.24 cm value obtained by Civan (1998a).

The above obtained values can now be used to determine the values of the model parameters as following. The filter cake permeability can be calculated by Eq. 12-74. Equations 12-70, 12-71, 12-75, 12-77, and 12-78 form a set of alternative equations to determine the deposition and erosion rate constants, k_d and k_e . Here, Eqs. 12-70 and 12-75 were selected for this purpose. However, Jiao and Sharma (1994) do not offer any data on the cake porosity ϕ_c and the critical shear stress τ_{cr} necessary for detachment of the particles from the progressing cake surface. Therefore, the ϕ_c and τ_{cr} parameters had to be estimated and used with Eqs. 12-70 and 12-75 to match the filtration data over the period of the filtration process. Then, the ϕ_c and τ_{cr} values obtained this way were used in Eqs. 12-70 and 12-75 to calculate the k_d and k_e values.

Using the slurry tangential velocity of $v = 8.61 \text{ cm/s}$, the typical particle diameter of $d = 2.5 \times 10^{-4} \text{ cm}$, and the particle separation distance of $l = 2. \times 10^{-7} \text{ cm}$ in Eq. 12-5, the critical shear stress for particle detachment is estimated to be $\tau_{cr} = 1.25 \times 10^3 \text{ dyne/cm}^2$. Whereas, the prevailing shear stress calculated by Eq. 12-5 is only $\tau = 16 \text{ dyne/cm}^2$. Under these conditions, theoretically the cake erosion should not occur because $\tau \ll \tau_{cr}$. Therefore, the value of the coefficient B should be zero. In contrast, as indicated by Eq. 12-86, the present analysis of the data has led to a small but nonzero value of $B = 3. \times 10^{-4} \text{ cm/min}$. Recall that we used this value in Eq. 12-72 to calculate the limiting flow rate of $q_{\infty} = 0.013 \text{ mL/min}$. This value was shown to be very close to the $q_{\infty} = 0.014 \text{ mL/min}$ value calculated by Eq. 12-79 and the approximate value of $q_{\infty} = 0.017 \text{ mL/min}$ obtained by extrapolating the filtrate flow rate data beyond the range of the experimental data. Thus, it is reasonable to assume that $B = 3. \times 10^{-4} \text{ cm/min}$ is a meaningful value and not just a numerical result of the least-squares regression of Eq. 12-11 to data, because the coefficient of regression $R^2 = 0.9873$ is very close to one. Hence, it can be inferred that $\tau > \tau_{cr}$ and the cake erosion occurred in the actual experimental conditions of Jiao and Sharma (1994). In view of this discussion, it becomes apparent that the theoretical value obtained by Eq. 12-6 is not realistic.

The Jiao and Sharma (1994) data and the missing parameter values, which have been approximated by fitting the experimental data, are given in Table 12-1. The results presented in Figure 12-8 indicate that the model represents the measured filtrate volumes over the complete range of 600 min of filtration time as closely as the quality of their experimental data permits. However, they did not measure the cake thickness, but predicted it using a simple algebraic model. As shown in Figure 12-9, the cake thicknesses predicted by Jiao and Sharma (1994) and Civan (1998a) are close to each other.

Willis et al. (1983) conducted linear filtration experiments using a suspension of lucite in water. As shown in Table 12-1, they reported only a few parameter values. They only provide some measured filtrate flow rate and cake thickness data in their Table 2. However, the filtration time data is missing. Therefore, a full scale simulation of their filtration process as a function of time could not be carried out by Civan (1998a). Only the linear plotting of the measured data according to Eq. 12-29 could be accomplished. As indicated by Figure 12-10, the best linear fit of Eq. 12-29 with the least-squares method has been obtained with a coefficient of regression of $R^2 = 0.9921$, very close to 1.0. This reconfirms the validity of the filtration model.

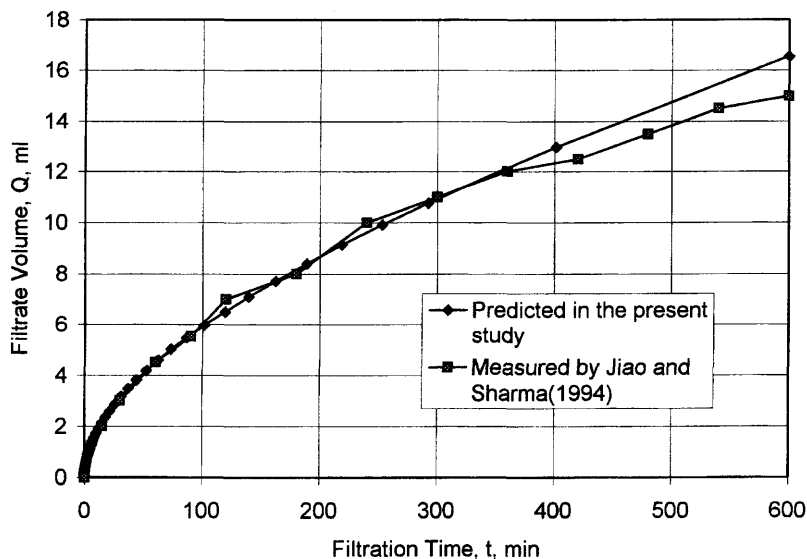


Figure 12-8. Comparison of the predicted and measured filtrate volumes for linear filtration of fresh water bentonite suspension (Civan, F., 1998; reprinted by permission of the AIChE, ©1998a AIChE. All rights reserved).

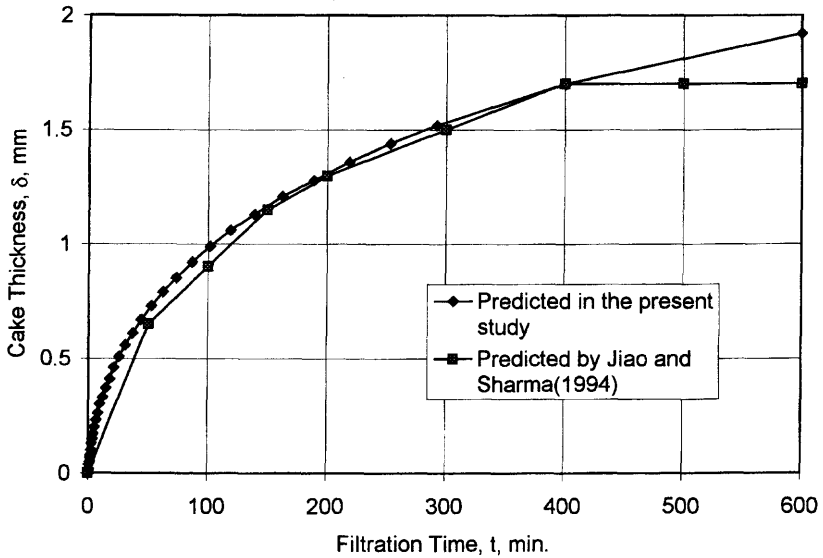


Figure 12-9. Comparison of the predicted cake thicknesses for linear filtration of fresh water bentonite suspension (Civan, F., 1998a; reprinted by permission of the AIChE, ©1998 AIChE. All rights reserved).

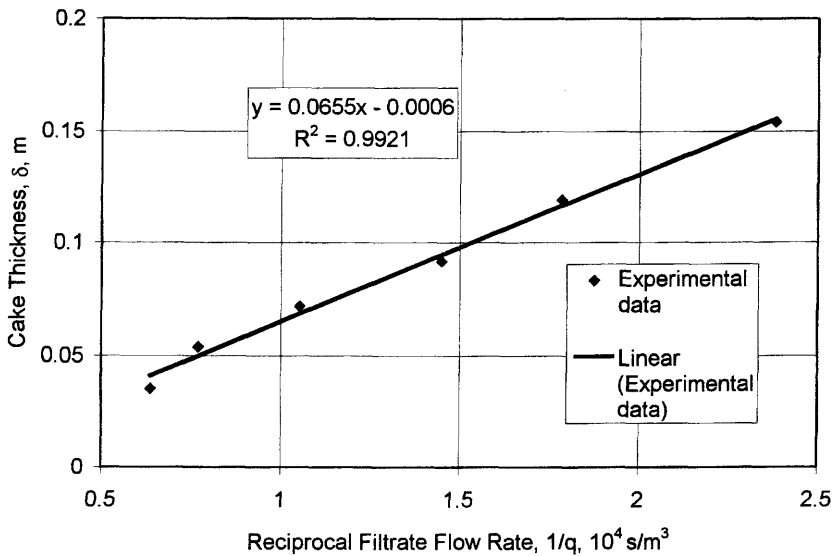


Figure 12-10. Correlation of Willis et al. (1983) measured filter cake thickness data (Civan, F., 1998; reprinted by permission of the AIChE, ©1998a AIChE. All rights reserved).

Radial Filtration Applications

Fisk et al. (1991) conducted radial filtration experiments using a seawater-based partially hydrolized polyacrylamide mud. Their Figure 4 provides the measured dynamic and static filtrate volumes versus filtration time data. Judging by their Figure 4, their static filtration data contains only three distinct measured values. This data is insufficient to extract meaningful information on the values of the A and C coefficients by regression of Eq. 12–80, because the calculation of $\ln[-q^{-3} dq/dt]$ requires a two step, sequential numerical differentiation—first to obtain the filtrate flow rate $q = dQ/dt$ by differentiating the filtrate volume Q , and then differentiating q to obtain dq/dt . On the other hand, their dynamic filtration data is limited to the filtrate volume. As explained in the previous section on the determination of parameters, the determination of all coefficients of A , B , C , and D by means of Eqs. 12–49 and 12–65 requires both the filtration volume and filter cake thickness measurements. Therefore, the Fisk et al. (1991) radial filtration data has more missing parameter values, which had to be approximated as given in Table 12–1. Figure 12–11 shows, the model predicts the measured dynamic and static

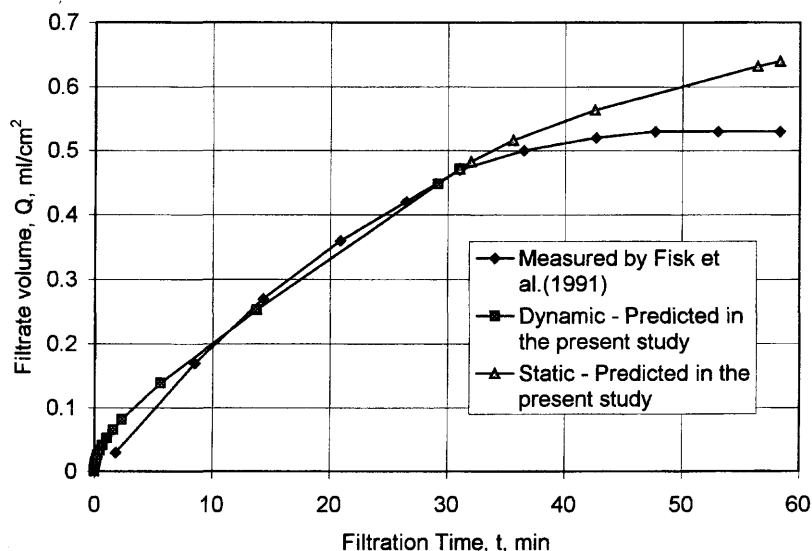


Figure 12–11. Comparison of the predicted and measured filtrate volumes for radial filtration of a sea-water based partially hydrolized polyacrylamide drilling mud (Civan, F., 1998; reprinted by permission of the AIChE, ©1998a AIChE. All rights reserved).

filtrate volumes with reasonable accuracy in view of the uncertainties involved in the estimated values of the missing data. Fisk et al. (1991) did not report any results on the filter cake thickness and therefore a comparison of the cake thicknesses could not be made by Civan (1998a) in the radial filtration case.

Conclusion

The models presented in this section offer practical means of interpreting experimental data, estimating the model parameters, and simulating the linear and radial, incompressive cake filtration processes at static and dynamic filtration conditions. The simplified forms of these models conform with the well-recognized simplified models reported in the literature. These models are capable of capturing the responses of typical laboratory filtration tests while providing insight into the governing mechanisms.

Compressive Cake Filtration Including Fines Invasion

The applicability of the majority of the previous models, such as those by Corapcioglu and Abboud (1990), Liu and Civan (1996), Tien et al. (1997) and Civan (1998b), is limited to low rate or low pressure difference filtration processes because these models facilitate Darcy's law to describe flow through porous media. However, filtration at high flow rates and high overbalance pressure differences may involve some inertial flow effects, especially during the initial period of the filter cake formation. In the literature, the initial non-linear relationships of the filtrate volume versus the square root of time has been attributed to invasion and clogging of porous media by fine particles during filtrate flow into porous media prior to filter cake formation. The cumulative volume of the carrier fluid (filtrate) lost into porous media during this time is usually referred to as the spurt loss (Darley, 1975).

Based on an order of magnitude analysis of the relevant dimensionless groups of the general mass and momentum balances of the multiphase systems involving the cake buildup, Willis et al. (1983) concluded that non-parabolic filtration behavior is not caused by non-Darcy flow. Instead, it is a result of the reduction of the permeability of porous media by clogging by fine particles. Their claim is valid under the conditions of their experimental test conditions. The phenomenological models for filter cake buildup involving fine particle invasion have been presented by Liu and Civan (1996) and Civan (1998b) for low rate filtration. However, a close examination of most filtration data reveal some non-Darcian flow effect during the short, initial period of filtration depending on the magnitude of the filtration flow rate and/or the applied pressure difference.

The large flow rates encountered during this period usually promote a non-Darcy effect. Willis et al. (1983) investigated the non-parabolic filtration behavior, but concluded that the non-parabolic behavior is a result of the impairment of the permeability of porous media by invasion and clogging by fine particles rather than by the non-Darcy flow effect. This conclusion is justified for their experimental conditions, however, some reported experimental data appear to involve a non-Darcy flow effect during the initial period of filter cake buildup.

Civan (1998b, 1999b) developed linear and radial filtration models and verified them by means of experimental data. These models are more generally applicable because of the following salient features:

1. A cake-thickness-averaged formulation leads to a convenient and computationally efficient representation of the filtration processes by means of a set of ordinary differential equations;
2. The nonhomogeneous-size particles of the slurry are classified into the groups of the large and fine particles, and the large particles form the cake matrix and the fine particles deposit inside the cake matrix;
3. The flow through porous cake and formation, which acts as a filter, is represented by Forchheimer's (1901) law to account for the inertial flow effects encountered during the early filtration period;
4. The dynamic and static filtration conditions encountered with and without the slurry flowing tangentially over the cake surface, respectively, are considered;
5. The variation of the filter cake porosity and permeability by compaction due to the drag of the fluid flowing through the cake matrix and deposition of fine particles within the cake matrix is considered;
6. An average fluid pressure is used to determine the fluid drag force applied to the cake matrix;
7. The formulations are presented for general purposes, but applied for commonly encountered cases involving incompressible particles and carrier fluids; and
8. The constant and variable rate filtration processes can be simulated.

The model presented in this section incorporates empirical constitutive relationships for the permeability and porosity variations of compressible cakes retaining fine particles. The simulation of a series of filtration scenarios are presented to demonstrate the parametric sensitivity of the model. It is determined that permeability impairment by fine particles retainment and pore throat clogging in the filter cake is increasingly induced by cake compression. It was also determined that constant pressure filtration limits the filtrate invasion more effectively than constant rate filtration and the non-Darcy flow effect is more significant

during the initial period of the filter cake formation. The cake formation models developed in this section can be used for predicting the effects of the compressible filter cakes involving the drilling muds and fracturing fluids.

The applications of the improved models are illustrated by typical case studies.

Radial Filtration Formulation

Consider that a slurry is applied to the inner surface of a drum filter and the filtrate leaves from its outer surface (see Figure 12-4). The model developed here is also equally applicable for the reverse operation. The filter cake is located between the filter inner surface radius r_w (cm), over which the cake is formed, and the slurry side cake surface radius r_c (cm), and its thickness is denoted by $h = r_w - r_c$. The external surface radius of the filter from which the filtrate leaves is r_e (cm) and the filter width is indicated by w (cm), such that the area of the inner filter surface over which the cake is formed is $2\pi r_w w$. The slurry flows over the cake surface at a tangential or cross-flow velocity of v_f (cm/s) and the filtrate flows into the filter at a filtration velocity of u_f (cm³/cm²·s) normal to the filter face due to the overbalance of the pressure between the slurry and the effluent sides of the filter. The flowing suspension of particles and the filter cake (solid) are denoted by the subscripts f and s , respectively. The carrier phase (liquid) and the particles are denoted, respectively, by l and p . Following Tien et al. (1997), the slurry is considered to contain particles larger than the filter medium pore size that form the filter cake and the particles smaller than the pore sizes of the filter cake and the filter medium, which can migrate into the cake and the filter to deposit there. All particles (small plus large) are denoted by p , and the large and small particles are designated by p_1 and p_2 , respectively.

Civan (1998b, 1999b) developed the filtration models by considering the cake-thickness averaged volumetric balance equations for

1. The total (fine plus large) particles of the filter cake;
2. The fine particles of the filter cake;
3. The carrier fluid of the suspension of fine particles flowing through the filter cake; and
4. The fine particles carried by the suspension of fine particles flowing through the filter cake.

The radial mass balances of all particles forming the cake, the small particles retained within the cake, the carrier fluid, and the small particles suspended in the carrier fluid are given, respectively, by (Civan, 1998b):

$$\frac{d}{dt} \left[(r_w^2 - r_c^2) \overline{\epsilon_s \rho_p} \right] = 2r_c R_{ps}^\sigma + (r_w^2 - r_c^2) \bar{R}_{p2s} \quad (12-87)$$

$$\frac{d}{dt} \left[(r_w^2 - r_c^2) \overline{\epsilon_s c_{p2s}} \right] = 2r_c R_{p2s}^\sigma + (r_w^2 - r_c^2) \bar{R}_{p2s} \quad (12-88)$$

$$\begin{aligned} \frac{d}{dt} \left[(r_w^2 - r_c^2) \overline{\epsilon_l \rho_l} \right] + (\rho_l \epsilon_l)_{slurry} \frac{dr_c^2}{dt} \\ = 2r_c (\rho_l u_l)_{slurry} - 2r_w (\rho_l u_l)_{filter} \end{aligned} \quad (12-89)$$

$$\begin{aligned} \frac{d}{dt} \left[(r_w^2 - r_c^2) \overline{\epsilon_l c_{p2l}} \right] + (\epsilon_l c_{p2l})_{slurry} \frac{dr_c^2}{dt} \\ = 2r_c (c_{p2l} u_l)_{slurry} - 2r_w (c_{p2l} u_l)_{filter} \\ - 2r_c R_{p2s}^\sigma - (r_w^2 - r_c^2) \bar{R}_{p2s} \end{aligned} \quad (12-90)$$

Eqs. 12-87 to 90 apply over the cake, located within $r_c \leq r \leq r_w$, and for $t > 0$. ϵ_s and ϵ_l denote the volume fractions of the bulk cake system occupied by the cake forming particles and the carrier fluid, respectively. ρ_p and ρ_l are the densities of the particles and the carrier fluid (g/cm^3). u_s and u_l are the volumetric fluxes of the compressing filter cake and the carrier fluid flowing through the cake ($\text{cm}^3/\text{cm}^2 \cdot \text{s}$). c_{p2s} and c_{p2l} denote the small particle masses contained per unit volume of the cake-forming particles and the carrier fluid flowing through the cake (g/cm^3). t and r denote the time and radial distance (cm), respectively.

R_{ps}^σ is the mass rate of particle deposition from the slurry over to the moving cake surface ($\text{g}/\text{s}/\text{cm}^3$) given by:

$$R_{ps}^\sigma = R_{p1s}^\sigma + R_{p2s}^\sigma \quad (12-91)$$

where R_{p1s}^σ and R_{p2s}^σ denote, respectively, the mass rates of large and small particles deposition from the slurry over the cake surface ($\text{g}/\text{s}/\text{cm}^3$). R_{p2s}^σ is usually negligible unless the small particles are retained by a process of jamming of small particles across the pores of the large particles, such as described by Civan (1994, 1996) and Liu and Civan (1996).

The variation of the filter cake thickness (cm) $h = r_w - r_c$ can be calculated using the variable radius, $r_c = r_c(t)$, of the slurry side filter cake surface.

For many practical applications, it is reasonable to assume that the particles and the carrier fluid are incompressible. The volumetric retention rates of the large and small particles are given, respectively, by:

$$N_{is}^\sigma = R_{is}^\sigma / \rho_p : i = p, p1, p2 \quad (12-92)$$

$$N_{p2s} = R_{p2s} / \rho_p \quad (12-93)$$

The volumetric concentration (or fraction) of species i in phase j , the volume fraction of species i of phase j in the bulk of the cake system, and the superficial velocity of species i of phase j are given, respectively, by:

$$\sigma_{ij} = c_{ij} / \rho_i \quad (12-94)$$

$$\epsilon_{ij} = \epsilon_j \sigma_{ij} \quad (12-95)$$

$$u_{ij} = u_j \sigma_{ij} \quad (12-96)$$

t denotes the time; $\bar{\phi}$, $\bar{\epsilon}_{p2s}$, and $\bar{\epsilon}_{p2l}$ are the cake-thickness-average porosity, the fine particle volume fractions of the cake matrix and the suspension of fine particles flowing through the cake matrix, respectively; $(\epsilon_{pl})_{slurry}$ is the volume fraction of the total (fine plus large) particles in the slurry; and $(u_l)_{slurry}$ and $(u_l)_{filtrate}$ denote the volume fluxes of the carrier fluid entering and leaving the filter cake, respectively.

Substituting Eqs. 12-92 to 12-96 into Eqs. 12-87 to 12-90 leads to the following volumetric balance equations, respectively (Civan, 1999b):

$$\frac{d}{dt} [(r_w^2 - r_c^2) (1 - \bar{\phi})] = 2r_c N_{ps}^\sigma + (r_w^2 - r_c^2) \bar{N}_{p2s} \quad (12-97)$$

$$\frac{d}{dt} [(r_w^2 - r_c^2) \bar{\epsilon}_{p2s}] = 2r_c N_{p2s}^\sigma + (r_w^2 - r_c^2) \bar{N}_{p2s} \quad (12-98)$$

$$\begin{aligned} \frac{d}{dt} [(r_w^2 - r_c^2) (\bar{\phi} - \epsilon_{pl})] + \left[1 - (\epsilon_{pl})_{slurry} \right] \frac{dr_c^2}{dt} \\ = 2r_c (u_l)_{slurry} - 2r_w (u_l)_{filtrate} \end{aligned} \quad (12-99)$$

$$\begin{aligned} \frac{d}{dt} \left[(r_w^2 - r_c^2) \bar{\epsilon}_{p2l} \right] + (\epsilon_{p2l})_{slurry} \frac{dr_c^2}{dt} = 2r_c (u_{p2l})_{slurry} \\ - 2r_w (u_{p2l})_{filtrate} - 2r_c N_{p2s}^\sigma - (r_w^2 - r_c^2) \bar{N}_{p2s} \end{aligned} \quad (12-100)$$

Eqs. 12-97 through 100 can be solved numerically subject to the initial conditions given by:

$$r_c = r_w, \quad \bar{\epsilon}_{p2s} = \bar{\epsilon}_{p2l} = 0, \quad t = 0 \quad (12-101)$$

Linear Filtration Formulation

The radial filter cake equations derived above can be readily converted to linear filter cake equations by means of the transformation given by:

$$x = r^2, \quad h = x_w - x_c = r_w^2 - r_c^2 \quad (12-102)$$

Thus, application of Eq. 12-102 to Eqs. 12-87 through 90 yields, respectively, the following thickness-averaged mass balance equations for the linear cake formation (Civan, 1998b):

$$\frac{d}{dt} (h \overline{\epsilon_s \rho_p}) = R_{ps}^\sigma + h \bar{R}_{p2s} \quad (12-103)$$

$$\frac{d}{dt} (h \overline{\epsilon_s c_{p2s}}) = R_{p2s}^\sigma + h \bar{R}_{p2s} \quad (12-104)$$

$$\frac{d}{dt} (h \overline{\epsilon_l \rho_l}) - (\epsilon_l \rho_l)_{slurry} \frac{dh}{dt} = (\rho_l u_l)_{slurry} - (\rho_l u_l)_{filter} \quad (12-105)$$

$$\begin{aligned} \frac{d}{dt} (h \overline{\epsilon_l c_{p2l}}) - (\epsilon_l c_{p2l})_{slurry} \frac{dh}{dt} \\ = (c_{p2l} u_l)_{slurry} - (c_{p2l} u_l)_{filter} - R_{p2s}^\sigma - h \bar{R}_{p2s} \end{aligned} \quad (12-106)$$

Similarly, Eqs. 12-97 through 100, respectively, become (Civan, 1999b):

$$\frac{d}{dt} [(x_w - x_c)(1 - \bar{\phi})] = N_{ps}^\sigma + (x_w - x_c) \bar{N}_{p2s} \quad (12-107)$$

$$\frac{d}{dt}[(x_w - x_c)\bar{\epsilon}_{p2s}] = N_{p2s}^\sigma + (x_w - x_c)\bar{N}_{p2s} \quad (12-108)$$

$$\begin{aligned} \frac{d}{dt}[(x_w - x_c)(\bar{\phi} - \epsilon_{p2l})] + \left[1 - (\epsilon_{pl})_{slurry}\right] \frac{dx_c}{dt} \\ = (u_l)_{slurry} - (u_l)_{filtrate} \end{aligned} \quad (12-109)$$

$$\begin{aligned} \frac{d}{dt}[(x_w - x_c)\epsilon_{p21}] + (\epsilon_{p21})_{slurry} \frac{dx_c}{dt} \\ = (u_{p21})_{slurry} - (u_{p21})_{filtrate} - N_{p2s}^\sigma - (x_w - x_c)\bar{N}_{p2s} \end{aligned} \quad (12-110)$$

Eqs. 12-107 through 110 can be solved numerically, subject to the initial conditions given by:

$$x_c = x_w, \quad \bar{\epsilon}_{p2s} = \bar{\epsilon}_{p2l} = 0, \quad t = 0 \quad (12-111)$$

The volume fractions of the filter cake solids and pore fluid can be expressed in terms of the cake porosity, respectively, as

$$\bar{\epsilon}_s = 1 - \bar{\phi} \quad (12-112)$$

$$\bar{\epsilon}_f = \epsilon_l + \epsilon_{p2l} = \bar{\phi} \quad (12-113)$$

where $\bar{\phi}$ is the average cake porosity (cm^3/cm^3). The following expressions for the small particle volume flux and mass per carrier fluid volume can be written according to Eqs. 12-94 through 96, respectively, as:

$$u_{p2l} = u_l \epsilon_{p2l} / \epsilon_l = u_l c_{p2l} / \rho_p \quad (12-114)$$

$$c_{p2l} = \rho_p \epsilon_{p2l} / \epsilon_l \quad (12-115)$$

Note that Eqs. 18, 28, and 24 of Corapcioglu and Abboud (1990) correspond to the present Eqs. 12-103, 12-109, and 12-106, respectively, with some differences. Equation 12-103 simplifies to their Eq. 18,

assuming ρ_p is constant and substituting Eq. 12-112. The present Eqs. 12-106 and 12-109 simplify to their Eqs. 24 and 28, substituting Eq. 12-113 for $\epsilon_{p2l} \ll \epsilon_l$. Also, Corapcioglu and Abboud (1990) did not distinguish between the rates of deposition of small and all (large plus small) particles over the progressing cake surface (i.e., R_{p2s}^σ and R_{ps}^σ) and used $R_{p2s}^\sigma = R_{ps}^\sigma$ in their Eq. 24. This assumption is not valid because most small particles migrate into the cake and only a little fraction of the small particles can deposit by the jamming process over the slurry side of the filter cake, such as described by Civan (1996). The filter cake is essentially formed by the deposition of the large particles and the deposition of the small particles over the progressing cake surface is negligible. The deposition of the small particles more dominantly occurs within the cake matrix as the suspension of small particles flows through the cake. Therefore, there is a large order of magnitude difference between the rates of the small and large particles deposition over the filter cake (i.e., $R_{p1s}^\sigma \gg R_{p2s}^\sigma$ and, thus, $R_{ps}^\sigma \cong R_{p1s}^\sigma$). However, it is more accurate to use Eq. 12-91.

Pressure-Flow Relationships

The slurry carrier fluid flow rate u_l ($\text{cm}^3/\text{cm}^2 \cdot \text{s}$) can be expressed using the effluent fluid pressure p_e (atm) at the outlet side of the filter, the pressure p_c (atm) at the slurry side cake surface, and the harmonic average permeability of the cake and filter system.

Forchheimer's (1901) law of flow through porous media for the linear case is given by

$$-\frac{\partial p}{\partial x} = \frac{\mu}{k} u + \rho \beta u^2 \quad (12-116)$$

The pressure differences over the filter cake and the porous media can be expressed by integrating Eq. 12-116, respectively, as (Civan, 1999b):

$$p_c - p_w = \left[\frac{\mu}{k_c} \bar{u}_c + \rho_c \bar{\beta}_c \bar{u}_c^2 \right] (x_w - x_c) \quad (12-117)$$

$$p_w - p_e = \left[\frac{\mu}{k_f} \bar{u}_f + \rho_f \bar{\beta}_f \bar{u}_f^2 \right] (x_e - x_w) \quad (12-118)$$

The instantaneous volumetric fluxes and densities of the suspensions of fine particles flowing through the cake matrix and porous formation are

assumed the same. Then, adding Eqs. 12-117 and 118, and rearranging and solving, yields (Civan, 1999b) for Darcy flow ($\beta_f = \beta_c = 0$):

$$\bar{u}_c = \bar{u}_f \equiv u_c = -\tilde{\gamma}/\tilde{\beta} \quad (12-119a)$$

and for non-Darcy flow:

$$\bar{u}_c = \bar{u}_f \equiv u_c = \frac{(u_l)_{slurry}}{1 - (\epsilon_{pl})_{slurry}} = \frac{-\tilde{\beta} + \sqrt{\tilde{\beta}^2 - 4\tilde{\alpha}\tilde{\gamma}}}{2\tilde{\alpha}} \quad (12-119b)$$

in which

$$\tilde{\alpha} = \rho [\bar{\beta}_c(x_w - x_c) + \beta_f(x_e - x_w)] \quad (12-120)$$

$$\tilde{\beta} = \mu \left[\frac{x_w - x_c}{\bar{k}_c} + \frac{x_e - x_w}{\bar{k}_f} \right] \quad (12-121)$$

$$\tilde{\gamma} = -(p_c - p_e) \quad (12-122)$$

Although the preceding approach yields a reasonably good accuracy, a more rigorous treatment should facilitate

$$u_c = \bar{u}_c - (x_w - x_c) \frac{d\bar{u}_c}{dx_c} \quad (12-123)$$

Forchheimer's law (1901) for the radial flow case is given by

$$-\frac{\partial p}{\partial r} = \frac{\mu}{k} u + \rho \beta u^2 \quad (12-124)$$

The volumetric flux and flow rate are related by

$$u = \frac{q}{2\pi r h} \quad (12-125)$$

where h is the formation thickness. Thus, invoking Eq. 12-125 into Eq. 12-124 yields

$$-\frac{\partial p}{\partial r} = \frac{\mu}{2\pi h k} \left(\frac{q}{r} \right) + \frac{\rho \beta}{(2\pi h)^2} \left(\frac{q}{r} \right)^2 \quad (12-126)$$

The pressure differences over the filter cake and porous media can be expressed by integrating Eq. 12-126, respectively, as (Civan, 1999b):

$$p_c - p_w = \frac{\mu \bar{q}_c}{2\pi h \bar{k}_c} \ln \left(\frac{r_w}{r_c} \right) + \frac{\rho \bar{\beta}_c \bar{q}_c^2}{(2\pi h)^2} \left(\frac{1}{r_c} - \frac{1}{r_w} \right) \quad (12-127)$$

$$p_w - p_e = \frac{\mu \bar{q}_f}{2\pi h \bar{k}_f} \ln \left(\frac{r_e}{r_w} \right) + \frac{\rho \bar{\beta}_f \bar{q}_f^2}{(2\pi h)^2} \left(\frac{1}{r_w} - \frac{1}{r_e} \right) \quad (12-128)$$

The densities and instantaneous flow rates of the suspensions of fine particles flowing through the cake matrix and porous formation are assumed the same. Then, adding Eqs. 12-127 and 12-128, and rearranging and solving, yields (Civan, 1999b) for Darcy flow ($\beta_f = \beta_c = 0$):

$$\bar{q}_c = \bar{q}_f \cong q_c = -\tilde{\gamma}/\tilde{\beta} \quad (12-129a)$$

and for non-Darcy flow:

$$\begin{aligned} \bar{q}_c = \bar{q}_f \cong q_c &= \frac{u_c}{2\pi r_c h} = \frac{(u_l)_{slurry}}{2\pi r_c h [1 - (\epsilon_{pl})_{slurry}]} \\ &= \frac{-\tilde{\beta} + \sqrt{\tilde{\beta}^2 - 4\tilde{\alpha}\tilde{\gamma}}}{2\tilde{\alpha}} \end{aligned} \quad (12-129b)$$

in which

$$\tilde{\alpha} = \frac{\rho}{(2\pi h)^2} \left[\bar{\beta}_c \left(\frac{1}{r_c} - \frac{1}{r_w} \right) + \beta_f \left(\frac{1}{r_w} - \frac{1}{r_e} \right) \right] \quad (12-130)$$

$$\tilde{\beta} = \frac{\mu}{2\pi h} \left[\frac{1}{k_c} \ln \left(\frac{r_w}{r_c} \right) + \frac{1}{k_f} \ln \left(\frac{r_e}{r_w} \right) \right] \quad (12-131)$$

$$\tilde{\gamma} = -(p_c - p_e) \quad (12-132)$$

Although this approach leads to a reasonably good estimate, a more rigorous approach should employ

$$q_c = \bar{q}_c - \left[\frac{r_w^2 - r_c^2}{2r_c} \right] \frac{d\bar{q}_c}{dr_c} \quad (12-133)$$

The inertial flow coefficient is estimated by the Liu et al. (1995) correlation given by Eq. 12-16.

Particle Deposition Rates

The rate of deposition of the particles of the slurry over the slurry side cake surface is assumed proportional to the particle mass flux approaching the filter cake. The rate of erosion of the particles from the slurry side cake surface is assumed proportional to the tangential, excess shear stress above the critical stress necessary for particle mobilization. Therefore, for dynamic filtration involving cross flow, the net mass rate of all particles (large plus small) deposition per unit area of the slurry side cake surface is given by the difference between the deposition and erosion rates as (Civan, 1996, 1998b):

$$R_{ps}^{\sigma} = k_d^{\sigma} (u_l c_{pl})_{slurry} - k_e^{\sigma} (\epsilon_s \rho_p)_c (\tau - \tau_{cr}) U(\tau - \tau_{cr}) \quad (12-134)$$

where u_l is the carrier fluid filtration flux normal to the cake surface ($\text{cm}^3/\text{cm}^2 \cdot \text{s}$) and c_{pl} is the slurry particle concentration expressed as the particle mass per unit volume of the carrier fluid in the slurry.

For small particles retention over the slurry side of the cake, an expression similar to Eq. 12-134 can be written as:

$$R_{p2s}^{\sigma} = k_{d2}^{\sigma} (u_l c_{p2l})_{slurry} - k_{e2}^{\sigma} (\epsilon_s c_{p2s})_c (\tau - \tau_{cr2}) U(\tau - \tau_{cr2}) \quad (12-135)$$

in which $(c_{p2l})_{slurry}$ denotes the mass of small particles per volume of the carrier fluid in the slurry.

The net mass rate of deposition of small particles within the filter cake is given by:

$$\bar{R}_{p2s} = \bar{k}_d \bar{\epsilon}_l \bar{c}_{p2l} - \bar{k}_e \bar{\epsilon}_s \bar{c}_{p2s} \quad (12-136)$$

which is similar to Eq. 33 of Corapcioglu and Abboud (1990), but the deposition and the mobilization terms are more consistently expressed.

The rate expressions given by Eqs. 12-134 through 136 for the deposition of the total (fine plus large) and fine particles of the slurry over the progressing cake surface and the retention of the fine particles of the flowing suspension within the cake matrix can be expressed in terms of the volumetric rates, respectively, as (Civan, 1999b):

$$N_{ps}^{\sigma} = k_d^{\sigma} \left[\frac{u_l \epsilon_{pl}}{1 - \epsilon_{pl}} \right]_{slurry} - k_e^{\sigma} (1 - \phi_c) (\tau_s - \tau_{cr}) U(\tau_s - \tau_{cr}) \quad (12-137)$$

$$N_{p2s}^{\sigma} = k_{d2}^{\sigma} \left[\frac{u_l \epsilon_{p2l}}{1 - \epsilon_{pl}} \right]_{slurry} - k_{e2}^{\sigma} (\epsilon_{p2s})_c (\tau_s - \tau_{cr2}) U(\tau_s - \tau_{cr2}) \quad (12-138)$$

$$\bar{N}_{p2s} = \bar{k}_d \bar{\epsilon}_{p2l} - \bar{k}_e \bar{\epsilon}_{p2s} \quad (12-139)$$

In Eqs. 12-10 through 12, the slurry shear-stress, τ_s , acting over the progressing cake surface is estimated using the Rabinowitsch-Mooney equation (Metzner and Reed, 1955). This equation can be expressed for linear and radial flow cases, respectively, as follows:

$$\tau_s = k'(8v)^{n'} \quad (12-140)$$

$$\tau_s = k'(4v/r_c)^{n'} \quad (12-141)$$

where k' and n' are the consistency ($\text{dyne/cm}^2/\text{s}^{n'}$) and flow (dimensionless) indices, which are equal to the fluid viscosity, μ , and unit for Newtonian fluids, respectively, and v is the tangential velocity of the slurry over the filter cake surface. For static filtration, $v = 0$ and therefore

$\tau = 0$, and the second term on the right side of Eq. 12-134 drops out, leading to an expression similar to Corapcioglu and Abboud (1990) and Tien et al. (1997).

τ_{cr} is the minimum slurry shear-stress necessary for detachment of particles from the progressing cake surface. Following Ravi et al. (1992), the critical shear stress necessary for detachment of the deposited particles from the progressing cake surface can be estimated according to Potanin and Uriev (1991) by Eq. 12-6. However, the actual critical stress can be substantially different than predicted by Eq. 12-6, because the ideal theory neglects the effects of the other factors, including aging (Ravi et al., 1992), surface roughness, and particle stickiness (Civan, 1996) on the particle detachment. Therefore, Ravi et al. (1992) recommend that the critical shear stress be determined experimentally. $U(\tau_s - \tau_{cr})$ is the Heaviside unit step function. It is equal to zero when $\tau_s < \tau_{cr}$ and one for $\tau_s \geq \tau_{cr}$. k_d^σ and k_e^σ are the rate coefficients for the total (fine plus large) particles deposition and detachment at the progressing cake surface. k_{d2}^σ and k_{e2}^σ are the rate coefficients for the fine particles deposition and detachment at the progressing cake surface. \bar{k}_d and \bar{k}_e are the cake-thickness-average rate coefficients for the deposition and mobilization of the fine particles within the filter cake matrix.

Porosity and Permeability Relationships

Incorporating the effects of fine particles deposition according to Arshad (1991) and cake compaction according to Tien et al. (1997), Civan (1998a) estimates the cake-thickness-average porosity by the following constitutive equation:

$$\frac{\bar{\Phi}}{\Phi^o} = \left[1 - \alpha \left(\frac{\bar{\epsilon}_{p2s}}{\Phi^o} \right)^n \right] \left[\frac{1}{\Phi^o} - \left(\frac{1}{\Phi^o} - 1 \right) \left(1 + \frac{\bar{p}_s}{p_a} \right)^\beta \right] \quad (12-142)$$

Considering the fine particles deposition and cake compaction, Civan (1998a) estimates the cake-thickness-average permeability by the Tien et al. (1997) constitutive equation:

$$\bar{k}_c / k_c^o = \left(1 + \alpha_1 \bar{\epsilon}_{p2s}^{\alpha_2} \right)^{-1} \left(1 + \bar{p}_s / p_a \right)^{-\delta} \quad (12-143)$$

In Eqs. 12-142 and 143, Φ^o and k_c^o represent the fine particles-free and non-compacted cake porosity and permeability; respectively, α , n , p_a , β , α_1 , α_2 , and δ are the empirically determined parameters.

Thickness-Averaged Fluid Pressure and Cake Porosity

The average fluid pressure in the filter cake for linear filtration can be expressed similar to Dake (1978) as:

$$\bar{p} = \int_{x_c}^{x_w} p \phi dx / \int_{x_c}^{x_w} \phi dx \quad (12-144)$$

The average cake porosity is given by:

$$\bar{\phi} = \int_{x_c}^{x_w} \phi dx / \int_{x_c}^{x_w} dx \quad (12-145)$$

The following expression can be derived from Eqs. 12-144 and 12-145:

$$\bar{p}\bar{\phi} = \int_{x_c}^{x_w} p \phi dx / \int_{x_c}^{x_w} dx \quad (12-146)$$

Note x_w is a constant, but $x_c = x_c(t)$ varies by time.

Similarly, the following three expressions can be written for radial flow:

$$\bar{p} = \int_{r_c}^{r_w} p \phi r dr / \int_{r_c}^{r_w} \phi r dr \quad (12-147)$$

$$\bar{\phi} = \int_{r_c}^{r_w} \phi r dr / \int_{r_c}^{r_w} r dr \quad (12-148)$$

$$\bar{p}\bar{\phi} = \int_{r_c}^{r_w} p \phi r dr / \int_{r_c}^{r_w} r dr \quad (12-149)$$

Eq. 12-147 is given by Dake (1978). Note that r_w is a constant, but $r_c = r_c(t)$ varies by time.

Eqs. 12-146 and 149 define the average fluid pressure, but they cannot be used directly because the pressure distribution over the cake thickness is not a priori known. Civan (1998b, 1999b) circumvented this problem by applying a procedure similar to Jones and Roszelle (1978) to express a local function value in terms of its average.

The local cake porosity at the slurry side of the cake can be expressed in terms of the cake-thickness-average porosity. For linear filtration Civan (1998b) differentiated Eq. 12-145 to obtain:

$$\phi_c = \bar{\phi} - (x_w - x_c) \frac{d\bar{\phi}}{dx_c} \quad (12-150)$$

For radial filtration, Eq. 12-148 yields (Civan, 1999b):

$$\phi_c = \bar{\phi} - \left[\frac{r_w^2 - r_c^2}{2r_c} \right] \frac{d\bar{\phi}}{dr_c} \quad (12-151)$$

Similar to Tiller and Crump (1985), the cake-thickness-average drag force, \bar{p}_s , created by the flow of the suspension of fine particles through the filter cake is determined using

$$\bar{p}_s = p_c - \bar{p} \quad (12-152)$$

in which p_c is the pressure of the slurry applying at the progressing filter cake surface and \bar{p} is the cake-thickness-average pressure of the suspension of fine particles flowing through the cake. For linear filtration, p_c and \bar{p} can be related by differentiating Eq. 12-146 and then substituting Eq. 12-150 to obtain (Civan, 1998b):

$$\bar{p}\bar{\phi} - (x_w - x_c) \frac{d(\bar{p}\bar{\phi})}{dx_c} = p_c \left(\bar{\phi} - (x_w - x_c) \frac{d\bar{\phi}}{dx_c} \right) \quad (12-153)$$

For computational convenience, Eq. 12-153 can be reformulated in a form of an ordinary differential equation as (Civan, 1999b):

$$\frac{d\bar{p}}{dt} = (p_c - \bar{p}) \left[\frac{-1}{x_w - x_c} \frac{dx_c}{dt} + \frac{1}{\bar{\phi}} \frac{d\bar{\phi}}{dt} \right] \quad (12-154)$$

Differentiating Eq. 12-149 and then substituting Eq. 12-151 for radial flow, Eqs. 12-153 and 12-154 are replaced, respectively, by (Civan, 1998b):

$$\bar{p}\bar{\phi} - \left[\frac{r_w^2 - r_c^2}{2r_c} \right] \frac{d(\bar{p}\bar{\phi})}{dr_c} = p_c \left\{ \bar{\phi} - \left[\frac{r_w^2 - r_c^2}{2r_c} \right] \frac{d\bar{\phi}}{dr_c} \right\} \quad (12-155)$$

$$\frac{d\bar{p}}{dt} = (p_c - \bar{p}) \left[\frac{-2r_c}{r_w^2 - r_c^2} \frac{dr_c}{dt} + \frac{1}{\bar{\phi}} \frac{d\bar{\phi}}{dt} \right] \quad (12-156)$$

Eqs. 12-154 or 12-156 can be solved numerically subject to the initial condition

$$\bar{p} = p_c, t = 0 \quad (12-157)$$

Applications

The applications of the linear and radial filter cake buildup models are illustrated using the data given in Table 12-2.

Corapcioglu and Abboud (1990) obtained a numerical solution for the linear constant rate filtration problem involving small particle invasion at static condition, assuming that the cake is incompressible, the cake porosity remains constant and all particles are filtered. Abboud (1993) repeated a similar calculation, but also considered the effect of small particles migration into the filter. Tien et al. (1997) considered both constant rate and constant pressure-driven compressive cake filtrations in a linear and static case only.

In the following, the applications by Civan (1998b, 1999b) to constant rate and constant pressure-driven filtration processes in linear and radial cases are presented and compared. The data considered are composed from the data used by Corapcioglu and Abboud (1990), Tien et al. (1997), and the missing data estimated by Civan (1998b), given in Table 12-2. Civan obtained the best estimates of the missing data by fitting the model to data as practiced by Liu and Civan (1996) and Tien et al. (1997).

The numerical solutions of the ordinary differential equations, Eqs. 12-107, 108, and 110 for the linear model and Eqs. 12-97, 98, and 100 for the radial model, are obtained using the Runge-Kutta-Fehlberg four (five) method (Fehlberg, 1969) to determine the filter cake thickness, $h \equiv x_w - x_c$ for the linear and $h \equiv r_w - r_c$ for radial cases, and the volume fractions of the small particles retained in the cake and suspended in the flowing slurry, $\bar{\epsilon}_{p2s}$ and $\bar{\epsilon}_{p2l}$, respectively. Eqs. 12-109 and 99 are used to determine the filtrate carrier fluid volumetric flux, $(u_l)_{\text{filter}}$, for the linear and radial cases, respectively. First, using the data given in Table 12-2, identified as Data I, the numerical solutions are carried out with the present, improved model for both linear and radial constant rate filtrations. The results for all particles filtered, for which $(c_{p2l})_{\text{filter}} = 0$, as expected from an efficient filter, are compared and the effect of fine

(text continued on page 310)

Table 12-2
Model Input Parameters*

Parameter	Symbol	Data I	Data II
Cake porosity without compaction and small particle retention, cm^3 pore volume/ cm^3 bulk volume	$\phi^o = 1 - \epsilon_s^o$	0.39 ^b	0.73 ^c
Cake particle volume fraction cm^3 particle/ cm^3 bulk volume	$\epsilon_s^o = 1 - \phi^o$	0.61 ^c	0.27 ^d
Particle density, g/cm^3	ρ_p	1.18 ^b	1.18 ^a
Carrier fluid (water) density, g/cm^3	ρ_l	0.97 ^b	0.97 ^a
Slurry total particle mass fraction, $\text{g particles}/\text{g slurry}$	$(w_{pf})_{slurry}$	0.101 ^b	—
Slurry total particle volume fraction, cm^3 particles/ cm^3 slurry	$(\sigma_{pf})_{slurry}$	—	0.2 ^d
Slurry total particle mass per carrier fluid volume, $\text{g particle}/\text{cm}^3$ carrier fluid	$(c_{pl})_{slurry} = \frac{(w_{pf})_{slurry} \rho_l}{1 - (w_{pf})_{slurry}}$ $= \rho_p \left[\frac{1}{(\epsilon_l)_{slurry}} - 1 \right]$	0.109 ^c	0.295 ^c
Slurry carrier fluid volume fraction, cm^3 carrier fluid/ cm^3 slurry	$(\epsilon_l)_{slurry} = \left[1 + (c_{pl})_{slurry} / \rho_p \right]^{-1}$ $= 1 - (\sigma_{pf})_{slurry}$	0.915 ^c	0.8 ^c
Slurry carrier fluid volumetric flux, cm^3 carrier fluid/ $(\text{cm}^2 \text{ cake surface} \cdot \text{s})$	$(u_l)_{slurry}$	2.0×10^{-3} _b	2.0×10^{-3} _d
Slurry injection pressure, atm	p_c	8.9 ^a	8.9 ^d
Filter outlet pressure, atm	p_e	1.0 ^a	1.0 ^d

* Civan, F., 1998b; reprinted by permission of the AIChE, ©1998 AIChE—All rights reserved.

Table 12-2 (continued)

Parameter	Symbol	Data I	Data II
Slurry small particles mass per carrier fluid volume, g small particles/cm ³ carrier fluid	$(c_{p2l})_{slurry} = (\rho_p \sigma_{p2l})_{slurry}$	0.049 ^a	0.059 ^a
Slurry small particles volume per carrier fluid volume, cm ³ small particles/cm ³ carrier fluid	$(\sigma_{p2l})_{slurry} = (c_{p2l}/\rho_p)_{slurry}$	0.415 ^c	0.05 ^d
Filtrate small particle mass per carrier fluid volume, g small particle/cm ³ carrier fluid	$(c_{p2l})_{filter}$	0, 0.005 ^a	0, 0.005 ^a
Filter thickness, cm	L_f	0.5 ^a	0.5 ^a
Slurry side filter radius, cm	r_w	5.08 ^a	—
Filtrate side filter radius, cm	r_e	2.54 ^a	—
Rate constant for small particle deposition within the cake, s ⁻¹	\bar{k}_d	6.5×10^{-3b}	1.0×10^{-3a} , 1.0×10^{-6a} ,
Rate constant for small particle entrainment within the cake, s ⁻¹	\bar{k}_e	4.35×10^{-5}	5.0×10^{-5a} , 5.0×10^{-7a} ,
Rate constant for total particle deposition over the slurry side cake surface, dimensionless	k_d^σ	1.0 ^a	1.4 ^{a,r} 75. ^{a,p}
Rate constant for total particle erosion over the slurry side cake surface, cm ⁻¹ .s	k_e^σ	0. ^s	0. ^s
Rate constant for small particle deposition over the slurry side cake surface, dimensionless	k_{d2}^σ	0.1 ^a	0.05 ^{a,r} 0. ^{a,p}
Rate constant for small particle erosion over the slurry side cake surface, cm ⁻¹ .s	k_{e2}^σ	0. ^s	0. ^s
Parameter dimensionless	α_1	30. ^a	30.0 ^d

Table 12-2 (continued)

Parameter	Symbol	Data I	Data II
Parameter dimensionless	α_2	1. ^a	1.0 ^d
Parameter dimensionless	β	0.09 ^a	0.07 ^a
Parameter dimensionless	δ	0.49 ^a	0.47 ^a
Cake permeability without compaction and small particle deposition, darcy	k_c^o	3.5×1.0^{-3a}	3.5×1.0^{-3d}
Filter permeability, darcy	k_f	1.0×1.0^{-4a}	1.0×1.0^{-4a}
Viscosity of carrier fluid (water), <i>cp</i>	μ	1.0 ^a	1.0 ^a
Parameter dimensionless	α	1.0 ^f	1.0 ^f
Parameter dimensionless	n	1/2 ^f	1/2 ^f
An empirical constant, atm	p_a	∞^a	0.0118 ^d
A constant, <i>dynes/cm²/s^{n'}</i>	k'	1.0 ^a	1.0 ^a
A constant, dimensionless	n'	1.0 ^a	1.0 ^a
Tangential velocity of the injected slurry, <i>cm/s</i>	v	0, 0.01 ^a	0, 0.01 ^a

- a : Data assumed
 b : Corapcioglu and Abboud (1990)
 c : Data calculated
 d : Tien, et al.(1997)
 f : Adin (1978)
 p : Data for the constant pressure case
 r : Data for the constant rate case
 s : Static filtration

(text continued from page 306)

particle invasion into an inefficient filter is demonstrated by assuming a value of $(c_{p2l})_{filter} = 0.005 \text{ g/cm}^3$ in Figures 12–12 through 12–16. Civan's (1998b) results have similar trends, but different values than the results of Corapcioglu and Abboud (1990) and Abboud (1993), because of the simplifying assumptions involved in their calculations, such as incompressible cake and constant cake porosity and the use of the same rates of deposition for small and all (large plus small) particles over the progressing cake surface. Also, the average porosity of the filter cake can vary significantly in actual cases as described by Tien et al. (1997). Next, Civan (1998b) obtained the numerical solution for the constant pressure drive filtration. Corapcioglu and Abboud (1990) and Abboud (1993) did not present any results for this case. The flow rate is allowed to vary according to Eqs. 12–129 and 12–119 for the radial and linear cases, respectively. In Figures 12–17 through 12–21, Civan's (1998b) results for the linear and radial cases are compared. The results presented in Figures 12–12 through 12–21 indicate that fine particle invasion into the filter plays an important role. The differences between the radial and linear

(text continued on page 315)

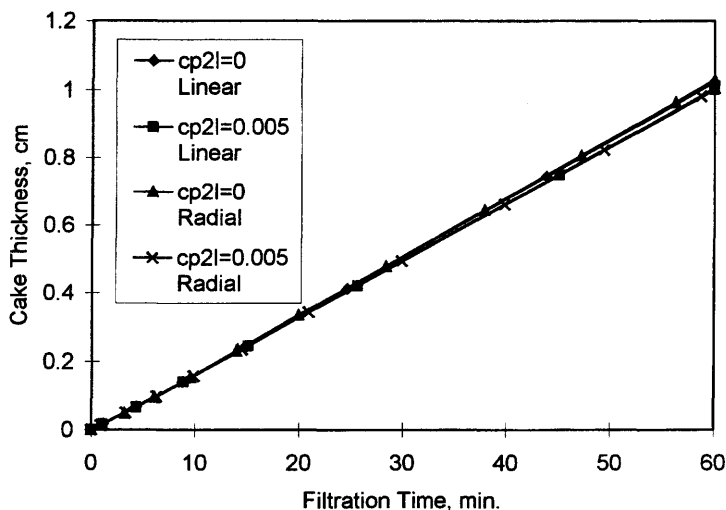


Figure 12–12. Comparison of the cake thickness for linear and radial constant rate filtration (Civan, F., 1998b; reprinted by permission of the AIChE, ©1998 AIChE. All rights reserved).

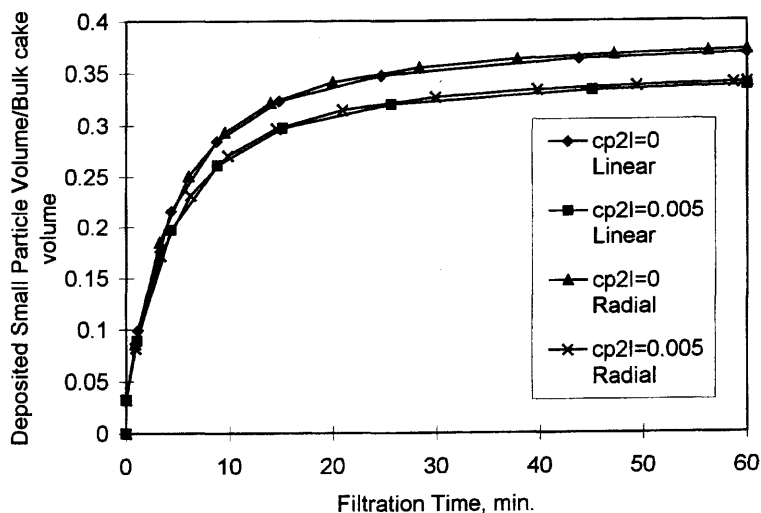


Figure 12-13. Comparison of the small particle deposition for linear and radial constant rate filtration (Civan, F., 1998b; reprinted by permission of the AIChE, ©1998 AIChE. All rights reserved).

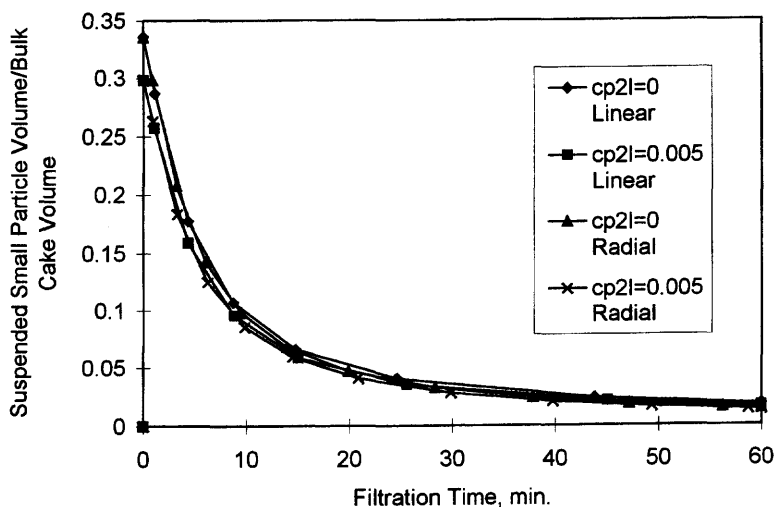


Figure 12-14. Comparison of the suspended small particles for linear and radial constant rate filtration (Civan, F., 1998b; reprinted by permission of the AIChE, ©1998 AIChE. All rights reserved).

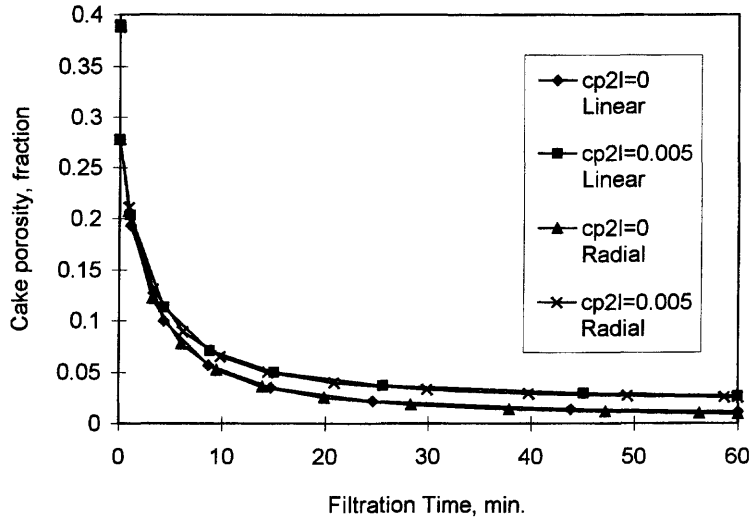


Figure 12-15. Comparison of the cake porosity for linear and radial constant rate filtration (Civan, F., 1998b; reprinted by permission of the AIChE, ©1998b AIChE. All rights reserved).

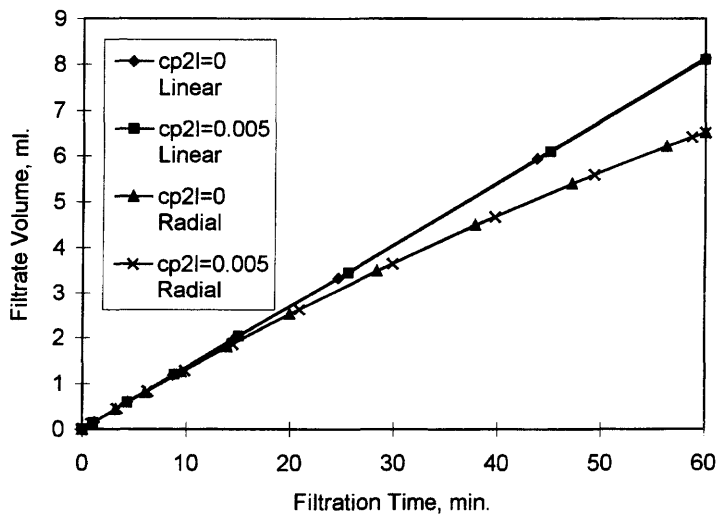


Figure 12-16. Comparison of the filtrate volume for linear and radial constant rate filtration (Civan, F., 1998b; reprinted by permission of the AIChE, ©1998b AIChE. All rights reserved).

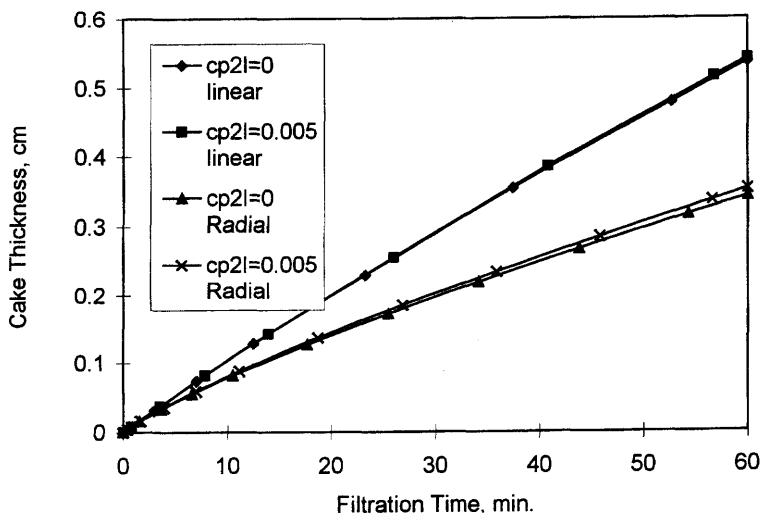


Figure 12-17. Comparison of the cake thickness for linear and radial constant pressure filtration (Civan, F., 1998b; reprinted by permission of the AIChE, ©1998 AIChE. All rights reserved).

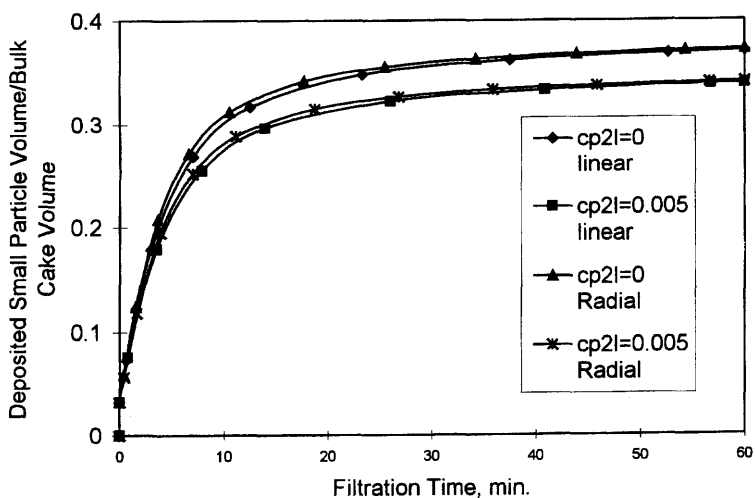


Figure 12-18. Comparison of the small particle deposition for linear and radial constant pressure filtration (Civan, F., 1998b; reprinted by permission of the AIChE, ©1998 AIChE. All rights reserved).

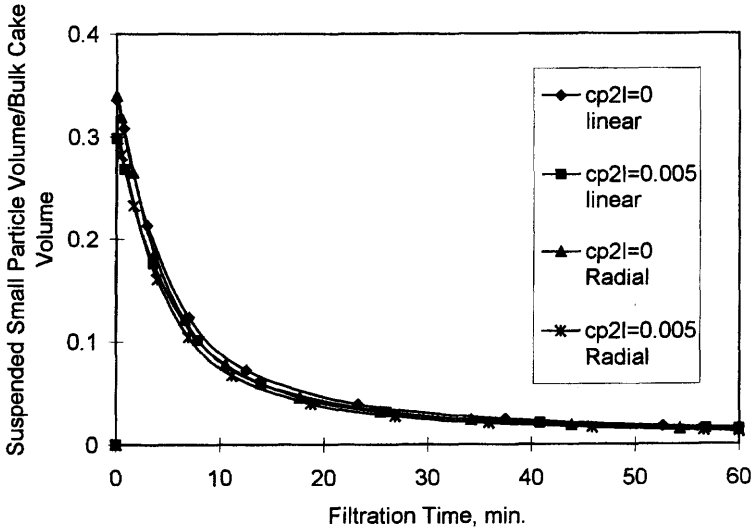


Figure 12-19. Comparison of the suspended small particles for linear and radial constant pressure filtration (Civan, F., 1998b; reprinted by permission of the AIChE, ©1998 AIChE. All rights reserved).

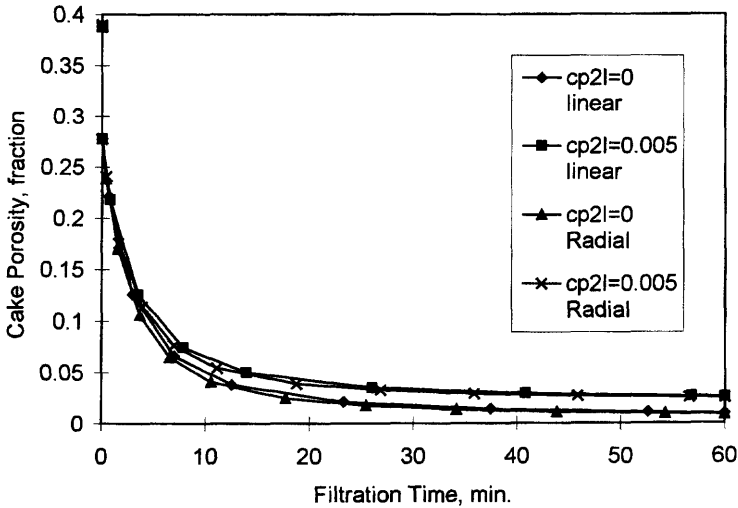


Figure 12-20. Comparison of the cake porosity for linear and radial constant pressure filtration (Civan, F., 1998b; reprinted by permission of the AIChE, ©1998 AIChE. All rights reserved).

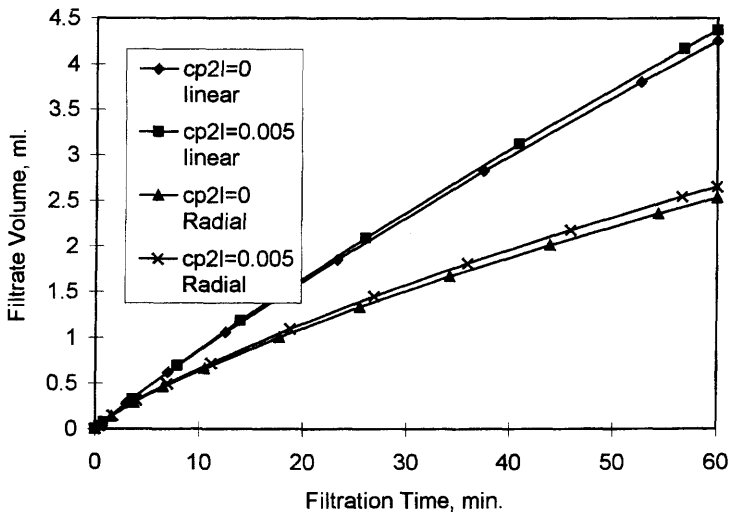


Figure 12-21. Comparison of the filtrate volume for linear and radial constant pressure filtration (Civan, F., 1998b; reprinted by permission of the AIChE, ©1998 AIChE. All rights reserved).

(text continued from page 310)

filtration results are more pronounced and the cake thickness and filtrate volume are less for the constant pressure filtration.

Tien et al. (1997) have solved their partial differential model numerically using a ready-made Fortran subroutine for linear filtration at static condition and reported numerical solutions along the filter cake only at the 100- and 1000-seconds times. Their model generates numerical solutions over the thickness of the filter cake, whereas, Civan's (1998b, 1999b) models calculate the thickness-averaged values. Therefore, Civan averaged the profiles predicted by Tien et al. (1997) over the cake thickness and used for comparison with the solutions obtained with the thickness-averaged filter cake model. Because Tien et al. (1997) reported numerical solutions at only two time instances, this resulted in only two discrete values. Civan generated the numerical solutions with the linear filtration model using the data identified as Data II in Table 12-2 for constant rate and constant pressure filtrations. As can be seen by Civan's (1998b) results presented in Figures 12-22 through 12-25, his ordinary differential model can closely reproduce the results of the Tien et al.

(text continued on page 318)

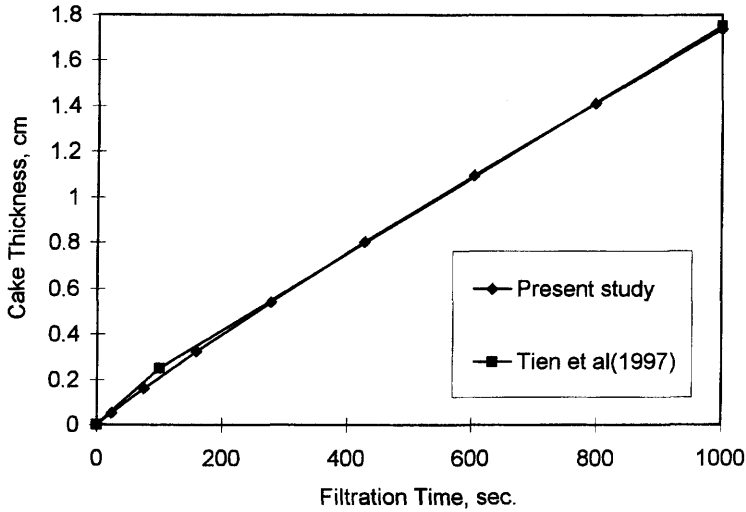


Figure 12-22. Comparison of the cake thickness for constant rate filtration (Civan, F., 1998b; reprinted by permission of the AIChE, ©1998 AIChE. All rights reserved).

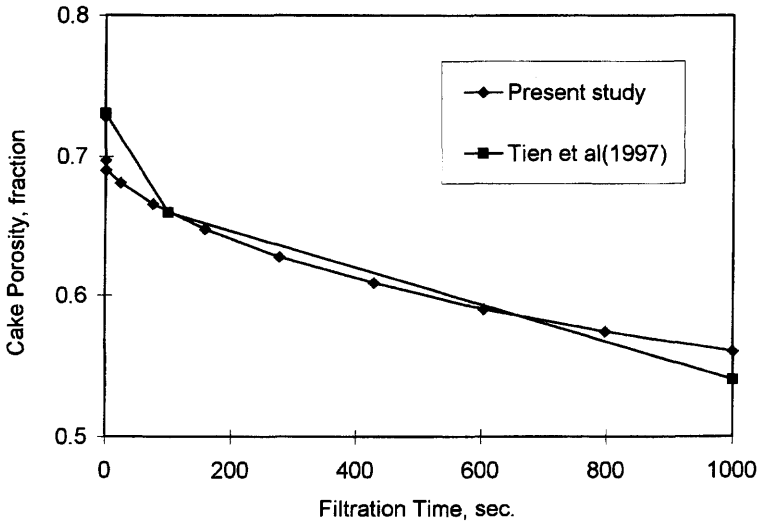


Figure 12-23. Comparison of the cake porosity for constant rate filtration (Civan, F., 1998b; reprinted by permission of the AIChE, ©1998 AIChE. All rights reserved).

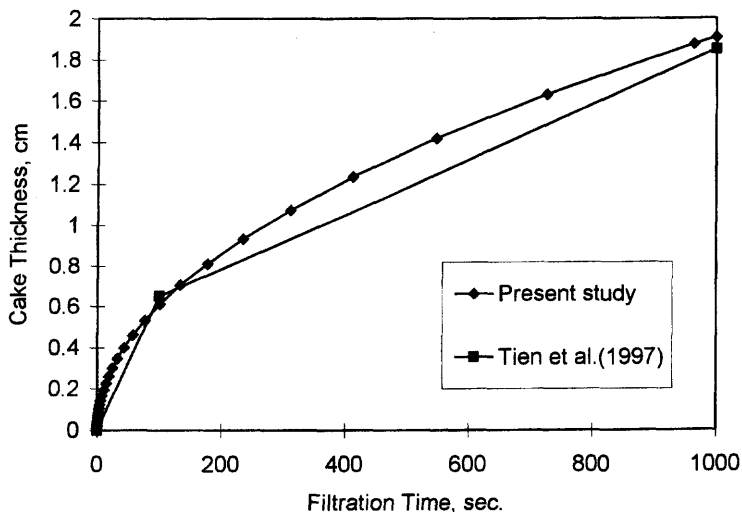


Figure 12-24. Comparison of the cake thickness for constant pressure filtration (Civan, F., 1998b; reprinted by permission of the AIChE, ©1998 AIChE. All rights reserved).

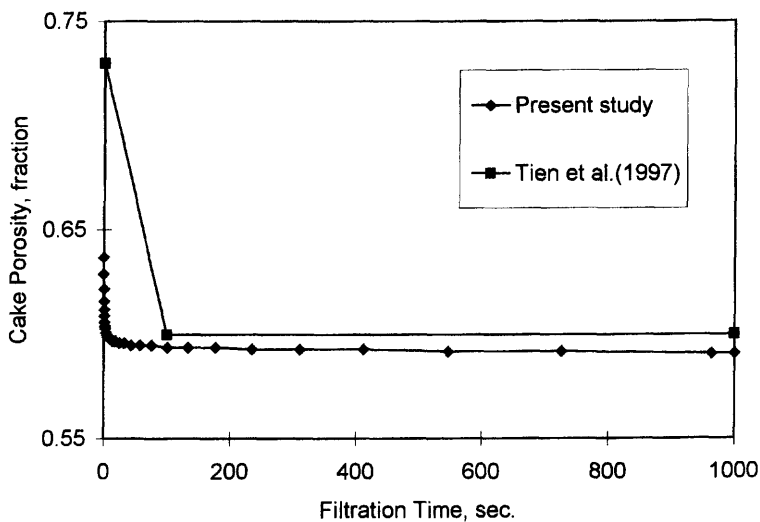


Figure 12-25. Comparison of the cake porosity for constant pressure filtration (Civan, F., 1998b; reprinted by permission of the AIChE, ©1998 AIChE. All rights reserved).

(text continued from page 315)

(1997) partial differential model. Note that, as indicated in Table 12-2, the values of the parameters at the present cake thickness-averaged level should be different than those for the formulation at the local level considering the spatial variations, such as by Tien et al. (1997).

Conclusions

Because of the improved phenomenological description and convenient cake thickness-averaged formulation, the ordinary differential models can provide faster numerical solutions with reduced computational effort and, therefore, offer certain practical advantages over the partial differential models for the analysis, design, and optimization of the cake filtration processes.

The applicability of the models by Corapcioglu and Abboud (1990) and Abboud (1993) is limited to static and low pressure filtration of dilute suspensions and their assumption of the same rates for the deposition of the small and large particles over the progressing cake surface is not reasonable. The Tien et al. (1997) model can alleviate these problems but it is computationally intensive and also limited to static filtration. These models are for linear filtration and may sufficiently approximate radial filtration only when the cake and the filter are much thinner compared to the radius of the filter surface exposed to the slurry. However, the radial model developed by Civan (1998a,b, 1999a,b) can better describe the radial filtration involving thick filter cake and filter media.

The filtration models presented in this section provide insight into the mechanism of compressive cake filtration and a convenient means of simulation with additional features.

References

- Abboud, N. M., "Formation of Filter Cakes with Particle Penetration at the Filter Septum," *Particulate Science and Technology*, Vol. 11, 1993, pp. 115-131.
- Adin, A., "Prediction of Granular Water Filter Performance for Optimum Design," *Filtration and Separation*, Vol. 15, No. 1, 1978, pp. 55-60.
- Arshad, S. A., "A Study of Surfactant Precipitation in Porous Media with Applications in Surfactant-Assisted Enhanced Oil Recovery Processes," Ph.D. Dissertation, University of Oklahoma, 1991, 285 p.
- Chase, G. G., & Willis, M. S., "Compressive Cake Filtration," *Chem. Engng. Sci.*, Vol. 47, No. 6, 1992, pp. 1373-1381.

- Chen, W., "Solid-Liquid Separation via Filtration," *Chemical Engineering*, Vol. 104, February 1997, pp. 66–72.
- Civan, F., "A Multi-Phase Mud Filtrate Invasion and Well Bore Filter Cake Formation Model," SPE 28709 paper, Proceedings of the SPE International Petroleum Conference & Exhibition of Mexico, Veracruz, Mexico, October 10–13, 1994, pp. 399–412.
- Civan, F., "A Multi-Purpose Formation Damage Model," SPE 31101 paper, Proceedings of the SPE Formation Damage Control Symposium held in Lafayette, Louisiana, February 14–15, 1996, pp. 311–326.
- Civan, F., "Incompressive Cake Filtration: Mechanism, Parameters, and Modeling," *AIChE J.*, Vol. 44, No. 11, November 1998a, pp. 2379–2387.
- Civan, F., "Practical Model for Compressive Cake Filtration Including Fine Particle Invasion," *AIChE J.*, Vol. 44, No. 11, November 1998b, pp. 2388–2398.
- Civan, F., "Predictive Model for Filter Cake Buildup and Filtrate Invasion with Non-Darcy Effects," SPE 52149 paper, Proceedings of the 1999 SPE Mid-Continent Operations Symposium held in Oklahoma City, Oklahoma, March 28–31, 1999a.
- Civan, F., "Phenomenological Filtration Model for Highly Compressible Filter Cakes Involving Non-Darcy Flow," SPE 52147 paper, Proceedings of the 1999 SPE Mid-Continent Operations Symposium held in Oklahoma City, Oklahoma, March 28–31, 1999b.
- Clark, P. E., & Barbat, O., "The Analysis of Fluid-Loss Data," SPE 18971 paper, Proc., SPE Joint Rocky Mountain Regional/Low Permeability Reservoirs Symposium and Exhibition, Denver, Colorado, March 6–8, 1989, pp. 437–444.
- Collins, E. R., *Flow of Fluids Through Porous Materials*, Penn Well Publishing Co., Tulsa, Oklahoma, 1961, 270 p.
- Corapcioglu, M. Y., & Abboud, N. M., "Cake Filtration with Particle Penetration at the Cake Surface," *SPE Reservoir Engineering*, Vol. 5, No. 3, August 1990, pp. 317–326.
- Dake, L. P., *Fundamentals of Reservoir Engineering*, Elsevier Scientific Publishing Co., New York, 1978, 443 p.
- Darcy, H., "Les Fontaines Publiques de la Ville de Dijon," Dalmount, Paris (1856).
- Darley, H. C. H., "Prevention of Productivity Impairment by Mud Solids," *Petroleum Engineer*, September 1975, pp. 102–110.
- de Nevers, N., "Product in the Way Processes," *Chemical Engineering Education*, Summer 1992, pp. 146–151.
- Donaldson, E. C., & Chernoglazov, V., "Drilling Mud Fluid Invasion Model," *J. Pet. Sci. Eng.*, Vol. 1, No. 1, 1987, pp. 3–13.

- Fehlberg, E., "Low-Order Classical Runge-Kutta Formulas with Stepsize Control and their Application to Some Heat Transfer Problems," NASA TR R-315, Huntsville, Alabama, July 1969.
- Fisk, J. V., Shaffer, S. S., & Helmy, S., "The Use of Filtration Theory in Developing a Mechanism for Filter-Cake Deposition by Drilling Fluids in Laminar Flow," *SPE Drilling Engineering*, Vol. 6, No. 3, September 1991, pp. 196–202.
- Forchheimer, P., "Wasserbewegung durch Boden," *Zeitz. ver. Deutsch Ing.* Vol. 45, 1901, pp. 1782–1788.
- Hermia, J., "Constant Pressure Blocking Filtration Laws—Application to Power-Law Non-Newtonian Fluids," *Trans. IChemE*, Vol. 60, 1982, pp. 183–187.
- Jiao, D., & Sharma, M. M., "Mechanism of Cake Buildup in Crossflow Filtration of Colloidal Suspensions," *J. Colloid and Interface Sci.*, Vol. 162, 1994, pp. 454–462.
- Jones, S. C., & Roszelle, W. O., "Graphical Techniques for Determining Relative Permeability from Displacement Experiments," *Journal of Petroleum Technology, Trans AIME*, Vol. 265, 1978, pp. 807–817.
- Liu, X., & Civan, F., "Formation Damage and Filter Cake Buildup in Laboratory Core Tests: Modeling and Model-Assisted Analysis," *SPE Formation Evaluation J.*, Vol. 11, No. 1, March 1996, pp. 26–30.
- Liu, X., Civan, F., and Evans, R. D., "Correlation of the Non-Darcy Flow Coefficient," *Journal of Canadian Petroleum Technology*, Vol. 34, No. 10, December 1995, pp. 50–54.
- Metzner, A. B., & Reed, J. C., "Flow of Non-Newtonian Fluids—Correlation of the Laminar, Transition, and Turbulent Flow Regions," *AIChE J.*, Vol. 1, No. 4, 1955, pp. 434–440.
- Peng, S. J., & Peden, J. M., "Prediction of Filtration Under Dynamic Conditions," SPE 23824 paper, presented at the SPE Intl. Symposium on Formation Damage Control held in Lafayette, Louisiana, February 26–27, 1992, pp. 503–510.
- Potantin, A. A., & Uriev, N. B., "Micro-rheological Models of Aggregated Suspensions in Shear Flow," *J. Coll. Int. Sci.*, Vol. 142, No. 2, 1991, pp. 385–395.
- Ravi, K. M., Beirute, R. M., & Covington, R. L., "Erodability of Partially Dehydrated Gelled Drilling Fluid and Filter Cake," SPE 24571 paper, Proceedings of the 67th Annual Technical Conference and Exhibition of the SPE held in Washington, DC, October 4–7, 1992, pp. 219–234.
- Sherman, N. E., & Sherwood, J. D., "Cross-Flow Filtration: Cakes With Variable Resistance and Capture Efficiency," *Chemical Engineering Science*, Vol. 48, No. 16, 1993, pp. 2913–2918.
- Smiles, D. E., & Kirby, J. M., "Compressive Cake Filtration—A Comment," *Chem. Engng. Sci.*, Vol. 48, No. 19, 1993, pp. 3431–3434.

- Tien, C., Bai, R., & Ramarao, B. V., "Analysis of Cake Growth in Cake Filtration: Effect of Fine Particle Retention, *AIChE J.*, Vol. 43, No. 1, January 1997 pp. 33–44.
- Tiller, F. M., & Crump, J. R., "Recent Advances in Compressible Cake Filtration Theory," in *Mathematical Models and Design Methods in Solid-Liquid Separation*, A. Rushton, ed., Martinus Nijhoff, Dordrecht, 1985.
- Willis, M. S., Collins, R. M., & Bridges, W. G., "Complete Analysis of Non-Parabolic Filtration Behavior," *Chem. Eng. Res. Des.*, Vol. 61, March 1983, pp. 96–109.
- Xie, X., & Charles, D. D., "New Concepts in Dynamic Fluid-Loss Modeling of Fracturing Fluids," *J. Petroleum Science and Engineering*, Vol. 17, No. 1/2, February 1997, pp. 29–40.

Part IV

Formation Damage by Inorganic and Organic Processes

**Chemical Reactions,
Saturation Phenomena,
Deposition, and
Dissolution**

Chapter 13

Inorganic Scaling and Geochemical Formation Damage

Summary

Various processes leading to inorganic scaling and formation damage are discussed. Special attention is given to formation damage caused by the adverse reactions encountered during acid stimulation, brine incompatibility in seawater injection for water flooding, precipitation caused by CO_2 and light hydrocarbon gases near wellbore, and sulfur deposition. The alterations of thermodynamic and chemical balances in favor of precipitation, precipitate aggregation, crystal growth, and inorganic scale formation are discussed and mathematically formulated. The rate processes governing the cation exchange, adsorption/desorption, and dissolution/precipitation reactions are formulated. The criteria for precipitate forming conditions are derived. Typical applications to above mentioned inorganic precipitation and scale formation processes are presented.

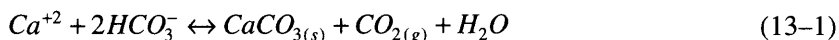
Introduction

Inorganic scaling is a process of deposition of scales from aqueous solutions of minerals, referred to as brines, when they become supersaturated as a result of the alteration of the state of their thermodynamic and chemical equilibria (Amaefule et al., 1988). Inorganic scaling can occur in the well tubings and near well bore formations of the production and injection wells.

Amaefule et al. (1988) explain that conditions leading to supersaturation can be created by various mechanisms at different stages of reservoir exploitation. Scaling is caused essentially by mixing incompatible fluids during well development operations, such as drilling, completion, work-over, such as acidizing. Scaling is caused by a decrease of pressure and

temperature during the production of reservoir fluids. Scaling associated with the improved recovery processes, such as water, carbonated water, alkaline water, and carbon dioxide injection, may be caused by mixing incompatible fluids and/or pressure and temperature variations.

The scale formation mechanisms can be classified as: (1) natural scaling and (2) induced scaling (Amaefule et al., 1988). These mechanisms can be best explained by means of scale precipitation charts, such as those given by Shaughnessy and Kline (1982, 1983), who developed practical charts depicting the relationships between dissolved calcium (Ca^{+2}) and bicarbonate (HCO_3^-) ions, calcium carbonate ($CaCO_3$) precipitate, CO_2 partial and total pressures, and temperature, based on the equilibrium relationship for the calcium carbonate scale formation by the reaction



The chart given in Figure 13-1 by Shaughnessy and Kline (1982) shows the calcium carbonate precipitation regions located above the equilibrium curves of the 2.8 MPa (400 psi) and 3.4 MPa (500 psi) CO_2 partial pressures at 93°C (200°F) temperature. Natural scaling occurs mostly in the near production wellbore regions as a result of the liberation of dissolved light gases from the formation brine by high drawdown (Amaefule et al., 1988). Consequently, the loss of the CO_2 gas from the brine promotes calcium carbonate precipitation. Amaefule et al. (1988) explained this phenomenon by the Le Chatelier principle. Because H_2O

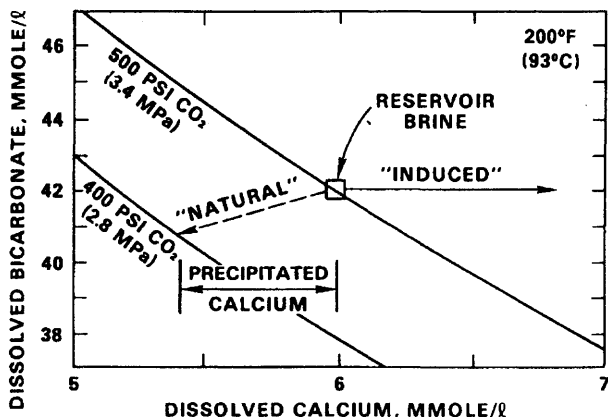


Figure 13-1. Natural and induced scale damage mechanisms (Shaughnessy and Kline, ©1983 SPE; reprinted by permission of the Society of Petroleum Engineers).

is in abundance, its concentration can be taken constant. Then, the chemical equilibrium constant for Eq. 13-1 reads as:

$$K_{eq} = \frac{[CaCO_3][CO_2]}{[Ca^{+2}][HCO_3^-]^2} \quad (13-2)$$

Therefore, applying Le Chatelier's cause-and-effect principle, when CO_2 is liberated and removed by pressure reduction, the CO_2 concentration will reduce. To compensate this effect, more $CaCO_3$ will be produced to maintain the constant K_{eq} .

Amaefule et al. (1988) explain that induced scaling occurs by mixing the formation brine with extraneous incompatible fluids invading the reservoir formation during drilling, cementing, completion, and workover operations. The same may occur by injection of fluids for enhanced recovery purposes. Any increase of the dissolved calcium (Ca^{+2}) ion concentration caused by these operations is compensated by calcium carbonate ($CaCO_3$) precipitation according to Eq. 13-1, following Le Chatelier's principle of the cause-and-effect.

Dewers et al. (2000) draw attention to some important phenomena that have been overlooked for the most part. First, the presence of oil and gas phases may effect the thermodynamics and chemistry of aqueous phases. Second, scale formation in the near wellbore formation is more kinetically controlled than thermodynamically controlled because the rapid flow that occurs around wellbores compared to the rest of the reservoir does not allow for sufficient time to attain equilibrium. This may result with an incomplete release of the light dissolved gases, such as carbon dioxide, from the aqueous phase. Hence, the saturation conditions at the actual near-wellbore fluid pressure may not be attained and the partitioning of various light gases between the liquid and gas phases may not reach the equilibrium condition. Dewers et al. (2000) caution that these phenomena should be considered for accurate scale prediction.

Geochemical interactions of the aqueous phase and the solid porous matrix result in alterations of minerals and the texture, porosity and permeability of porous formation. As stated by Lichtner (1985), geochemical systems involve various reversible and irreversible chemical interactions, such as oxidation-reduction reactions, ion complexing, mineral dissolution/precipitation, and adsorption. Dissolution of solid minerals is a slow process and complete dissolution cannot occur within the convection time scale of the flow in the near wellbore (Nordstrom and Munoz, 1994). However, alteration of the composition and saturation of the aqueous phase and the fluid shear can induce the entrainment,

migration, and redeposition of fine mineral particles and therefore cause formation damage (Chang and Civan, 1991, 1992, 1997).

Formation damage resulting from the injection of incompatible waters into reservoirs can be avoided if the initial rock-fluid equilibria and, hence, the initial reservoir quality can be maintained (Schneider, 1997). Injecting oxygenated waters into reservoirs and can oxidize the reduced *Fe* and *S* species present in the pore water and can cause precipitation and plugging of pores (Schneider, 1997). Geochemical models are important for predicting the complications that will result from the interactions of the various drilling and production fluids with the reservoir formation (Schneider, 1997).

Yeboah et al. (1993) draw attention to the fact that most models use limited solubility or thermodynamical data and ignore the effects of ion pairs, presence of other ions (such as magnesium) on the solubility, and the kinetic and transport phenomena factors. Therefore, Yeboah et al. (1993) caution that “the available models predict only scaling tendency and with a high degree of uncertainty,” but “a positive scaling potential does not necessarily imply that scale will form.”

Geochemical Phenomena—Classification, Formulation, Modeling, and Software

Fluids and minerals in petroleum-bearing formations may undergo various interactive chemical reactions in response to the alteration of the in-situ conditions by various operations, including drilling, workover, and improved recovery. Geochemical models provide scientific guidance for controlling adverse reactions that may result from rock-fluid interactions.

Excellent treaties of the geochemical reaction modeling are available from several sources, including Melchior and Bassett (1990), Ortoleva (1994), and Bethke (1996). This subject is extremely complex, therefore, only the fundamentals of the overall subject are outlined here. The readers are encouraged to resort to literature for details and to use ready-made software available from various sources.

Petroleum-bearing formations can be generally viewed as being geochemical systems in which fluids consisting of oil, gas, water, and immobile solid phases formed from an assemblage of minerals interact through various chemical reactions. Lichtner (1985) classified such reactions into four categories: (1) aqueous ion complexing, (2) oxidation and reduction, (3) mineral precipitation and dissolution, and (4) ion exchange and adsorption reactions. As stated by Kharaka et al. (1988) and Amaefule et al. (1988), such reactions occur in response to changing temperature, pressure, and fluid composition by various factors, including

the addition of incompatible fluids during drilling, workover and improved recovery processes and liberation of light gases, such as CH_4 , CO_2 , H_2S , and NH_3 , during pressure-drawdown. Changes in temperature and pressure often cause the variation of the pH of the reservoir aqueous phase, which in turn induces adverse processes such as the precipitation of iron and silica gels (Kharaka et al., 1988; Rege and Fogler, 1989; Labrid and Bazin, 1993). Geochemical reactions can also be classified as homogeneous and heterogeneous depending on whether the reaction occurs inside a phase or with another phase, respectively. Geochemical reactions can also be classified as reversible and irreversible. As explained by Lichtner (1985), the rates of reversible reactions are independent of the surface area. Reversible reactions can attain local equilibrium over a sufficiently long period of time, at which time, the reaction rates terms vanish in the transport equations. However, Lichtner (1985) adds that irreversible reactions require kinetic or rate expressions, in terms of the pertinent driving forces, that is chemical affinity, and/or the surface available for reactions.

Detailed geochemical description is a very cumbersome task and often unnecessary and unjustified in view of the lack of the basic thermodynamic and kinetic data required for description. Rather, geochemical models are constructed to emphasize the chemical reactions of the important aqueous species and minerals, which are essential for adequate description of the rock-water interactions, and neglect all other reactions. This is done to compromise between the quality of description and the effort necessary to gather basic thermodynamic and kinetic data and to carry out the numerical computations.

Among the various alternatives, the kinetic and equilibrium models are extensively utilized. The kinetic models describe the rate of change of the amount of mineral and aqueous species in porous media in terms of the relevant driving forces and factors, such as deviation from equilibrium concentration and mineral-aqueous solution contact surface. The proportionality constant is called the rate constant. The equations formed in this way are called the rate laws or kinetic equations. The equilibrium models assume geochemical equilibrium between the pore water and the minerals of porous formation. Since equilibrium can be reached over a sufficiently long time, equilibrium models represent the closed systems at steady-state conditions. Mathematically, the equilibrium models can be derived from kinetic models in the limit of infinitely large rate constants. Hence, rapid reactions reach equilibrium faster. Therefore, the equilibrium models represent the limiting conditions and yield conservative predictions (Schneider, 1997). Equilibrium models are particularly advantageous for determining the mineral stability and graphical representations of the mineral and aqueous species interactions (Bjørkum and Gjelsvik, 1988; Stumm and Morgan, 1996; Schneider, 1997).

Because of the highly intensive numerical computations involved, the geochemical models of the rock-water interactions are usually implemented by computer-coded software. The geochemical computer software is constantly evolving and becoming more robust and accurate as a result of the advancement in computer technology, availability of accurate thermodynamic data, and development of efficient numerical solution methods. The engineers responsible for developing operational strategies and procedures for scale control in petroleum reservoirs should rely on such software. However, efficient use of the ready-made software requires some familiarity with the fundamental concepts, theories, and methods involved in the treatment and formulation of geochemical reactions. This information is usually provided with the user's guide and/or by relevant publications. In the following, a brief review of the description and graphical representation of aqueous and mineral species reactions and various approaches to geochemical modeling are presented.

Reactions in Porous Media

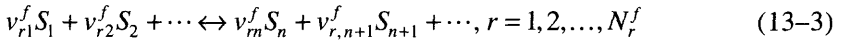
The various chemical reactions occurring in the pore space can be classified into the groups of homogeneous and heterogeneous reactions (Lichtner, 1992). The reactions occurring within the aqueous fluid phase are called the homogeneous or aqueous reactions. The reactions of the aqueous phase species with the solid minerals of porous formation, occurring at the pore surface, are called the heterogeneous or mineral reactions. A convenient treatment of the geochemical reactions can be achieved by grouping the various reacting solute species into the primary and secondary sets of species (Kandiner and Brinkley, 1950; Lichtner, 1992). The primary set of species is formed by selecting a minimum, critical number of reacting aqueous species, S_α , necessary for adequate description of the homogeneous and heterogeneous reactions. Thus, all other species form the set of the secondary species. The secondary species are derived from the primary species by means of the equations of the relevant chemical reactions.

Aqueous Phase Reactions

Lichtner (1992) classifies the homogeneous reactions into three categories: (a) ion pairing/exchange reactions, (b) complexing reactions, and (c) redox reactions. The aqueous phase reactions are generally rapid relative to the mineral reactions (Liu et al., 1997). The rapid rates of aqueous phase reactions require kinetic descriptions with significantly large rate constants. Thus, for all practical purposes, these reactions can be assumed instantaneous and a transport controlled, local chemical

equilibrium assumption is usually considered reasonable (Walsh et al., 1982; Lichtner, 1992; Liu et al., 1997; Liu and Ortaleva, 1996, 1996).

Consider an aqueous phase undergoing a total of N_r^f chemical aqueous reactions. $r = 1, 2, \dots, N_r^f$ denotes the index for the various aqueous reactions. N_r represents the total number of aqueous species involved in the r^{th} aqueous or homogeneous reaction. $S_\alpha: \alpha = 1, 2, \dots, N_r$ denotes the various aqueous species involved in the r^{th} aqueous reaction. Then, the aqueous reactions can be typically represented by (Walsh et al., 1982; Liu et al., 1996):



or simply as

$$\sum_{\alpha=1}^{N_r} v_{r\alpha}^f S_\alpha = 0, r = 1, 2, \dots, N_r^f \quad (13-4)$$

where $v_{r\alpha}^f$ denotes the stoichiometric coefficient of species α involved in the r^{th} aqueous reaction. Note $v_{r\alpha}^f$ is negative for the reactants and positive for the products.

Applying the mass action law of Prigogine and DeFay (1954), the chemical equilibria between the products and reactants of the r^{th} reaction can be expressed as (Walsh et al., 1982; Liu et al., 1996):

$$K_r^f = \prod_{\alpha=1}^{N_r} a_{\alpha}^{v_{r\alpha}^f}, r = 1, 2, \dots, N_r^f \quad (13-5)$$

K_r^f denotes the thermodynamic equilibrium constant for the r^{th} aqueous reaction given as the ratio of the rate constants k_{rf}^f and k_{rb}^f of the forward and backward reactions represented by Eq. 13-3:

$$K_r^f = k_{rf}^f / k_{rb}^f \quad (13-6)$$

a_α is the chemical activity of the aqueous species α , which can be expressed in terms of the molal concentration, C_α , of species α as:

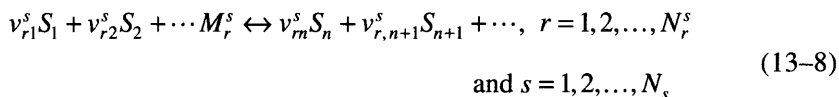
$$a_\alpha = \gamma_\alpha C_\alpha \quad (13-7)$$

in which γ_α is the activity coefficient determined by the Debye-Hückel theory (Helgeson et al., 1970).

Mineral Reactions

The reactions of the aqueous phase species with the solid mineral matter of the porous matrix are referred to as the mineral reactions. Most mineral reactions are typically hydrolysis reactions. The interactions of minerals and aqueous species are generally slow relative to the aqueous phase reactions (Lichtner, 1992). Their reaction kinetics are controlled by the external mineral surface area contacting the aqueous phase. The mineral surface area is determined by the sizes of the grains of the porous formation. The rates of mineral reactions are gradual and, therefore, require kinetic descriptions with finite reaction rate constants.

Consider a porous formation containing a total of N_s different mineral species and undergoing a total of N_r^s different chemical reactions between its minerals species and the aqueous phase species. $s = 1, 2, \dots, N_s$ denotes the index for the participating mineral species of the porous formation. N_r denotes the total number of aqueous species involved in the r^{th} heterogeneous reaction. M_r^s denotes the s^{th} mineral species undergoing the r^{th} heterogeneous reaction. S_α : $\alpha = 1, 2, \dots, N_r$ denotes the various aqueous species involved in the r^{th} mineral reaction. Then, the reactions between porous formation minerals and aqueous species can be typically represented by (Lichtner, 1992, Liu et al., 1996):



or simply by

$$M_r^s + \sum_{\alpha=1}^{N_r} v_{r\alpha}^s S_\alpha = 0, \quad r = 1, 2, \dots, N_r^s$$

(13-9)

and $s = 1, 2, \dots, N_s$

where $v_{r\alpha}^s$ denotes the stoichiometric coefficients associated with the aqueous phase species per one participating mineral species. Note that $v_{r\alpha}^s$ is negative for the reactants and positive for the products.

Applying the mass action law (Prigogine and DeFay, 1954), and assuming that the activity of the solid minerals is equal to one, the chemical equilibria between the minerals of the porous formation and the aqueous species of the r^{th} reaction can be expressed in terms of the equilibrium saturation solubility product as (Walsh et al., 1982):

$$K_{rs}^{sp} = \prod_{\alpha=1}^{N_r} a_{\alpha}^{v_{\alpha r}^s}, \quad r = 1, 2, \dots, N_r^s \quad (13-10)$$

and $s = 1, 2, \dots, N_s$ minerals

For a mineral s undergoing a dissolution/precipitation reaction r , the reaction driving force is given by (Liu et al., 1996):

$$\Delta G_{rs} = k_{rs} \left\{ \prod_{\alpha=1}^{N_r} a_{\alpha}^{|v_{\alpha r}^s|} - (1/K_{rs}^{sp}) \prod_{\alpha=1}^{N_r} a_{\alpha}^{v_{\alpha r}^s} \right\} \quad (13-11)$$

$v_{\alpha r}^s < 0$ $v_{\alpha r}^s > 0$

$\Delta G_{rs} > 0$ for mineral dissolution and $\Delta G_{rs} < 0$ for mineral precipitation. k_{rs} denotes the dissolution rate constant of the r^{th} reaction of the s^{th} mineral.

Approximating the shape of the mineral grains by a sphere, and assuming that the mineral reactions are kinetic reactions, Liu et al. (1996) express the rate of dissolution or precipitation of the s^{th} mineral by the r^{th} reaction by:

$$W_r^s = n_s \rho_s 4\pi R_s^2 \Delta G_{rs} \quad (13-12)$$

as being proportional to the number of the s^{th} mineral grains per formation bulk volume, n_s , the surface area of the s^{th} mineral grain, $4\pi R_s^2$, and the reaction driving force, ΔG_{rs} . The grain mass density of the s^{th} mineral, ρ_s , is inserted to express the mass rate of dissolution or precipitation of the i^{th} mineral grain. R_s represents the radius of the s^{th} mineral grain. Thus, Liu et al. (1996) express the rate of change of the s^{th} grain radius by dissolution and/or precipitation by various reactions as:

$$\frac{\partial R_s}{\partial t} = \sum_{r=1}^{N_r} \Delta G_{rs} \quad (13-13)$$

The mass conservation equation for species α undergoing transport through porous media by various mechanisms is given by Eq. 7-34 derived in Chapter 7. The rate of generation of the α^{th} aqueous species per bulk formation volume, required for Eq. 7-34, is given by Liu et al. (1996) as:

$$r_{\alpha} = \sum_{r=1}^{N_r^f} v_{\alpha r}^f W_r^f + \sum_{r=1}^{N_r^s} v_{\alpha r}^s W_r^s + q_{\alpha}, \quad \alpha = 1, 2, \dots, N_{\alpha} \quad (13-14)$$

where N_α is the total number of aqueous species involved; N_r^f and N_r^s denote the total number of aqueous and mineral reactions, respectively; W_r^f and W_r^s represent the rates of the r^{th} aqueous and mineral reactions, respectively; $v_{\alpha r}^f$ and $v_{\alpha r}^s$ denote the stoichiometric coefficients of the species α in the aqueous and mineral reactions, respectively, and q_α represents the rate of species α addition per bulk formation volume by means of direct injection of fluids through wells completed in the reservoir.

Ion Exchange and Adsorption Reactions

Ion exchange and adsorption are surface chemical or surface complexation processes leading to the exchange of chemical species between the aqueous solution and mineral surfaces present in geological porous formations (Jennings and Kirkner, 1984; Lichtner, 1985; Kharaka et al., 1988). Kharaka et al. (1988) explain the difference between ion exchange and adsorption as following: "The ion exchange model treats the exchange of cations or anions on a constant charge surface" and "the adsorption model simulates the exchange process on a surface where the surface charge is developed due to the ionization of surface sites at the solution-surface interface." Therefore, adsorption is a more general concept and ion exchange is a special case of adsorption (Lichtner, 1985; Sahai and Sverjensky, 1998). Among the various surface complexation models, Sahai and Sverjensky (1998) facilitate the triple-layer model (Yates et al., 1974) for describing the electrical charge near mineral surfaces, as described in Figure 13-2 (Sahai and Sverjensky, 1998) according to Westall (1986). As indicated in Figure 13-2, this model considers the mineral surface, referred to as the O -plane, for adsorption of hydroxide ions and protons and at a short distance near the mineral surface, referred to as the β -plane, for adsorption of electrolyte ions and the surface charge is generated by adsorption of the electrolyte ions and protons (Sahai and Sverjensky, 1998).

Clays present in geological porous formations have many active ion exchange sites, α , occupied by various cations and cation exchange takes place for replacement of the cations in the order of the replacing tendency of $Ca^{+2} > Mg^{+2} > K^+ > Na^+$ (Li et al., 1997). The cation exchange capacity (CEC) of rocks can be expressed as the total number of moles of exchange sites α per unit mass of rock, Q_{ex}^α , or per unit volume of rock, w_α , which are related by (Lichtner, 1985):

$$w_\alpha = (1 - \phi) \rho_s Q_{ex}^\alpha \quad (13-15)$$

Lichtner (1985) points out that "precipitation/dissolution reactions can alter the exchange capacity of the porous medium by creating or destroy-

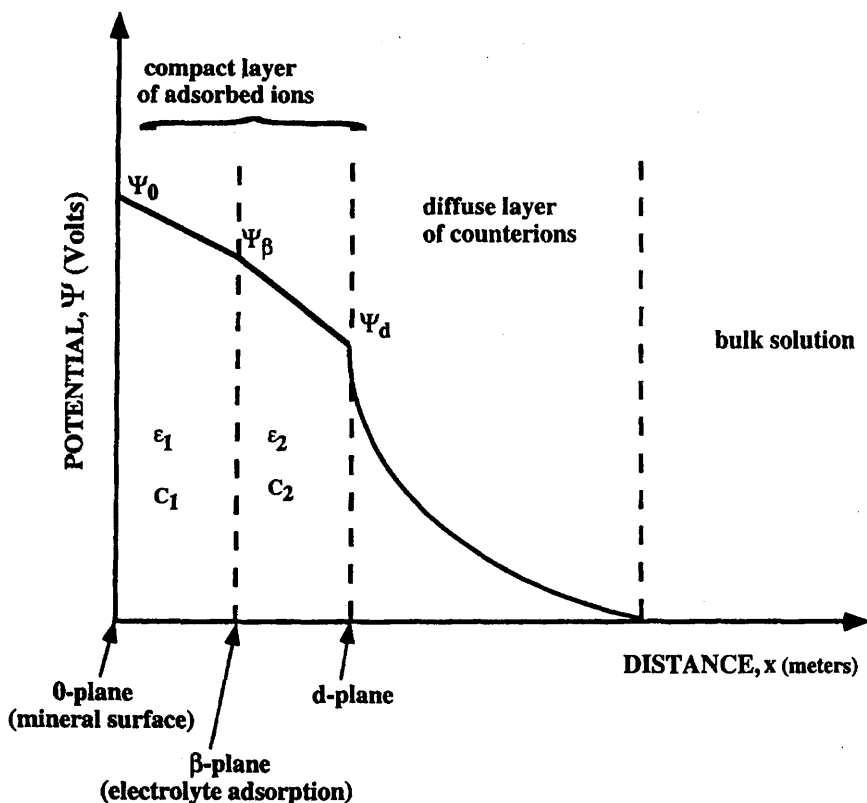
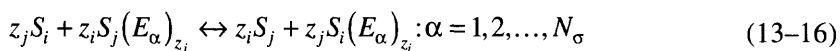


Figure 13-2. Triple-layer description of the potential vs. distance from the mineral surface (Reprinted from *Journal of Computers and Geosciences*, Vol. 24, Sahai, N., & Sverjensky, D. A., "GEOSURF: A Computer Program for Modeling Adsorption on Mineral Surfaces from Aqueous Solution," pp. 853–873, ©1998, with permission from Elsevier Science).

ing exchange sites," but this effect has not been taken into account in most reported studies. In Eq. 13-15, ϕ and ρ_s denote the porosity and the grain density of the rock, respectively. Represent the exchange sites by α , the total number of different exchange sites by N_σ , an exchange site of type α with unit charge by E_α , the i^{th} cation species with valence z_i by S_i , and the concentration of the i^{th} species attached to the exchange sites α by C_i^α , expressed in moles per unit bulk volume. Lichtner (1985) then describes the chemical reactions at mineral surfaces by



and the conservation of the ion exchange sites by

$$\omega_{\alpha} = \sum_{k=1}^N z_k C_k^{\alpha} \quad (13-17)$$

where N is the total number of chemically reacting species. $S_j(E_{\alpha})_{z_j}$ and $S_i(E_{\alpha})_{z_i}$ represent the cations attached to the active exchange sites. Sears and Langmuir (1982) report that ion exchange and adsorption reactions in soils typically require a time of seconds to days to attain equilibrium. Therefore, Jennings and Kirkner (1984) describe these reactions by rate equations for full kinetic modeling. Applying their approach to Eq. 13-16 according to Chang and Civan (1997) yields the following kinetic expression for the rates of consumption of $S_j(E_{\alpha})_{z_j}$ and production of $S_i(E_{\alpha})_{z_i}$, respectively:

$$\begin{aligned} -z_i \frac{\partial S_i}{\partial t} &= -z_j \frac{\partial [S_j(E_{\alpha})_{z_j}]}{\partial t} = z_j \frac{\partial S_j}{\partial t} = z_i \frac{\partial [S_i(E_{\alpha})_{z_i}]}{\partial t} \\ &= \phi k_f^{ij} S_i^{z_j} S_j^{z_i} (E_{\alpha})_{z_j} - \phi k_r^{ij} S_j^{z_i} S_i^{z_j} (E_{\alpha})_{z_i} \end{aligned} \quad (13-18)$$

where ϕ is the porosity and k_f^{ij} and k_r^{ij} denote the rate coefficients for the forward and reverse reactions, respectively. If I_{ij}^{α} is the reaction rate for the exchange of the i^{th} cation present in aqueous solution with the j^{th} cation attached to the α^{th} site on the mineral surface, and I_r is the rate of the reactions of the i^{th} cation of the aqueous solution other than adsorption, the transport equation for the i^{th} cation present in aqueous solution is given by (Lichtner, 1985):

$$\frac{\partial}{\partial t} (\epsilon_a c_i) + \bar{\nabla} \cdot \bar{J}_i = - \sum_{\alpha=1}^{N_{\alpha}} \sum_{\substack{j=1 \\ j \neq i}}^N z_j I_{ij}^{\alpha} + \sum_{r=1}^M v_{ir} I_r : i = 1, 2, \dots, N \quad (13-19)$$

where ϵ_a denotes the volume fraction of the aqueous phase in the bulk of porous formation and c_i denotes the concentration of the i^{th} cation in the aqueous solution, expressed in moles per unit volume of the aqueous phase.

The balance of the i^{th} cation adsorbed on the α^{th} site of the mineral surface is given by (Litchner, 1985):

$$\frac{\partial C_i^{\alpha}}{\partial t} = \sum_{\substack{j=1 \\ j \neq i}}^N z_j I_{ij}^{\alpha} : i = 1, 2, \dots, N \text{ and } \alpha = 1, 2, \dots, N_{\alpha} \quad (13-20)$$

where C_i^α is the concentration of the i^{th} species attached to the exchange sites α expressed in moles per unit bulk volume. Because

$$I_{ij}^\alpha \equiv \frac{\partial S_i}{\partial t} \quad (13-21)$$

$$I_{ji}^\alpha \equiv \frac{\partial S_j}{\partial t} \quad (13-22)$$

$$\text{then, } z_j I_{ij}^\alpha = -z_i I_{ji}^\alpha \quad (13-23)$$

Thus, Lichtner (1985) combined Eqs. 13–19 and 20 into the following convenient form by summing Eq. 13–20 over all the exchange sites α , adding the resultant equation to Eq. 13–19, and eliminating the exchange reaction rates by means of Eq. 13–23:

$$\frac{\partial}{\partial t} \left(\varepsilon_a c_i + \sum_{\alpha=1}^{N_\alpha} C_i^\alpha \right) + \vec{\nabla} \cdot \vec{J}_i = \sum_{r=1}^M v_{ir} I_r : i = 1, 2, \dots, N \quad (13-24)$$

Geochemical Modeling

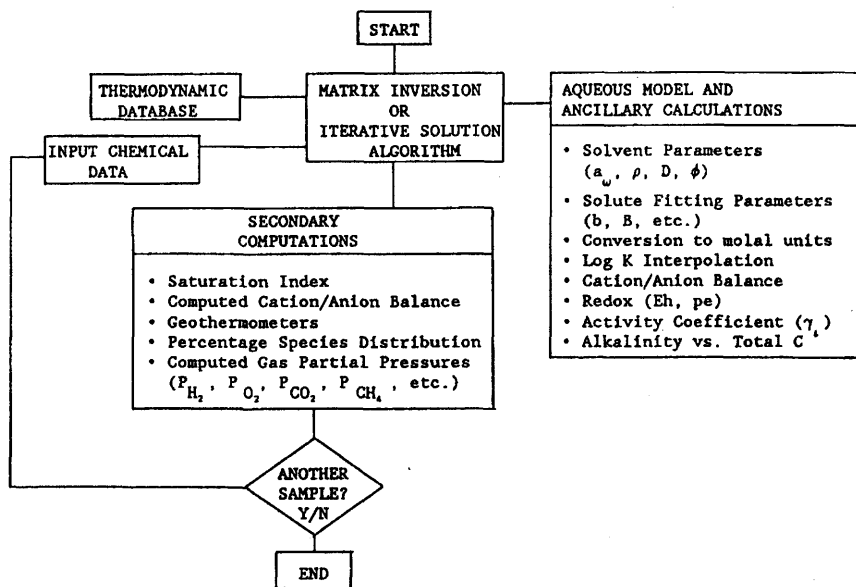
As stated by Plummer (1992)*: “Geochemical modeling attempts to interpret and (or) predict chemical reactions of minerals, gases, and organic matter with aqueous solutions in real or hypothetical water-rock systems.” Figure 13–3 by Bassett and Melchior (1990) outlines the basic constituents and options of most geochemical models.

Plummer (1992)* classified the various geochemical modeling efforts into four groups:

1. Aqueous speciation models for geochemical applications,
2. Inverse geochemical modeling techniques for interpreting observed hydrochemical data,
3. Forward geochemical modeling techniques for simulating the chemical evolution of water-rock systems, and
4. Reaction-transport modeling for the coupling of geochemical reaction modeling with equations describing the physics of fluid flow and solute transport processes.

Brief descriptions of these models are presented in the following, according to Plummer (1992).

* Reprinted from “Water-Rock Interaction,” Proceedings of the 7th international symposium, WRI-7, Park City, Utah, 13–18 July 1992 Kharaka, Y. K. & A. S. Maest (eds.), 90 5410 075 3, 1992, 25 cm, 1730 pp., 2 vols., EUR 209.00/US\$246.00 GBP147. Please order from: A. A. Balkema, Old Post Road, Brookfield, Vermont 05036 (telephone: 802-276-3162; telefax: 802-276-3837; e-mail: info@ashgate.com).



OPTIONS AND EVOLUTIONARY CHANGES

- Mixing of Waters
- Titration of Solids and Gases
- Outgassing
- Samples at Multiple Temperatures
- Organic Ligands
- Adsorption Models
- Reaction Path Simulation
- Adherence to Phase Boundaries
- Isotope Mass Balance
- Pressure Correction for Log K
- Pseudo-Kinetic Expressions
- Fitzer Ion-Interaction Expression
- Mixed Redox Couples

Figure 13-3. Common elements of aqueous chemical models (Reprinted with permission from Bassett, R. L., & Melchior, D. C., "Chemical Modeling of Aqueous Systems—An Overview," Chapter 1, pp. 1-14, in *Chemical Modeling of Aqueous Systems II*, Melchior, D. C. & Bassett, R. L. (eds.), ACS Symposium Series 416, ACS, Washington, 1990, Figure 2, page 6; ©1990 American Chemical Society).

Aqueous Speciation Models

Aqueous speciation models describe the thermodynamic properties of aqueous solutions and they are an integral part of the geochemical models. Plummer (1992)* summarizes the constituents of these models as:

1. Mass balance equations for each element,
2. Mass action equations and their equilibrium constants, for complex-ion formation, and
3. Equations that define individual ion-activity coefficients.

Two types of aqueous specification models are popular: (a) ion-association models and (b) specific interaction models. The ion association and the specific interaction models facilitate, respectively, the extensions and a complex expansion of the Debye-Hückel theory to estimate the individual ion activity coefficients of aqueous species (Plummer, 1992). The specific interaction models are preferred for highly concentrated solutions of mixed-electrolytes (Plummer, 1992). As pointed out by Plummer (1992), aqueous geochemical models can be used for forward and inverse geochemical modeling.

Geochemical Modeling—Inverse and Forward

Plummer (1992)* summarizes that “Two approaches to geochemical modeling have evolved—“inverse modeling,” which uses water and rock compositions to identify and quantify geochemical reactions, and “forward modeling,” which uses hypothesized geochemical reactions to predict water and rock compositions.” However, the application of these models is rather difficult because the basic data necessary for these models are often incomplete and/or uncertain (Plummer, 1992).

Plummer (1992)* describes the most essential information necessary for geochemical modeling and its applications as following:

1. The mineralogy, and its spatial variation in the system,
2. The surface area of reactants in contact with aqueous fluids in ground-water systems,
3. The chemical and isotopic composition of reactants and products in the system,
4. The hydrology of the system,
5. The extent to which the system is open or closed,

* Reprinted from “Water-Rock Interaction,” Proceedings of the 7th international symposium, WRI-7, Park City, Utah, 13–18 July 1992 Kharaka, Y. K. & A. S. Maest (eds.), 90 5410 075 3, 1992, 25 cm, 1730 pp., 2 vols., EUR 209.00/US\$246.00 GBP147. Please order from: A. A. Balkema, Old Post Road, Brookfield, Vermont 05036 (telephone: 802-276-3162; telefax: 802-276-3837; e-mail: info@ashgate.com).

6. The temporal variation of these properties,
7. The fundamental knowledge on the kinetics and mechanisms of important water-rock reactions,
8. The kinetics of sorption processes, and
9. The degradation pathways of organic matter.

Inverse Geochemical Modeling

Plummer (1992)* explains that "Inverse geochemical modeling combines information on mineral saturation indices with mass-balance modeling to identify and quantify mineral reactions in the system." The mass-balance modeling requires (Plummer, 1992):

1. Element mass balance equations,
2. Electron conservation equations,
3. Isotope mass balance equations, when applicable,
4. Aqueous compositional and isotopic data, and
5. Mineral stoichiometry data for all reactants and products.

Plummer (1992)* warns that "The inverse-modeling approach is best suited for steady-state regional aquifers, where effects of hydrodynamic dispersion can often be ignored."

Forward Geochemical Modeling

The objective of the forward geochemical modeling is to predict mineral solubilities, mass transfers, reaction paths, *pH* and *pe* by using available solid-aqueous data in aqueous specification models (Plummer, 1992). Some of the important features of the advanced forward geochemical models are cited by Plummer (1992) as:

1. Access to a large thermodynamic data base,
2. Generalized reaction-path capability,
3. Provision for incorporation of reaction kinetics in both dissolution and precipitation,
4. A variety of activity coefficient models,
5. Treatment of solid solutions,
6. Calculation of *pH* and *pe*,

* Reprinted from "Water-Rock Interaction," Proceedings of the 7th international symposium, WRI-7, Park City, Utah, 13-18 July 1992 Kharaka, Y. K. & A. S. Maest (eds.), 90 5410 075 3, 1992, 25 cm, 1730 pp., 2 vols., EUR 209.00/US\$246.00 GBP147. Please order from: A. A. Balkema, Old Post Road, Brookfield, Vermont 05036 (telephone: 802-276-3162; telefax: 802-276-3837; e-mail: info@ashgate.com).

7. Calculation of mineral solubilities with and without accompanying irreversible reaction,
8. Calculation of boiling, cooling, wall-rock alteration, ground-water mixing with hot waters and evaporation, and
9. Equilibrium or partial equilibrium states in gas-solid-aqueous systems.

Plummer (1992)* states that forward geochemical modeling can be used "in developing reaction models that can account for the observed compositional-mineralogical relations in the deposit, if there are no aqueous or solid data for the system."

Reaction-Transport Geochemical Modeling

The reaction-transport models describe the geochemical reactions under the influence of fluid flow and convective and dispersive transport of various species in geological porous media. These models couple the geochemical reaction and the fluids and species transport submodels to accomplish temporal and spatial prediction of the evolution of geochemical reactions in compositionally-complex geological systems (Plummer, 1992). These models are more applicable in most petroleum reservoir exploitation and scale formation studies.

Graphical Description of the Rock-Fluid Chemical Equilibria

Properly designed charts provide convenient means of describing the equilibrium chemical reactions of the rock-fluid systems. Frequently, the $pe - pH$, activity-activity, and saturation index charts are facilitated for convenient description of equilibrium chemical systems. The construction of these charts are based on the description of chemical systems at thermodynamic equilibrium. In this section, the theoretical bases, characteristics, and utilization of these charts are described according to Schneider (1997).

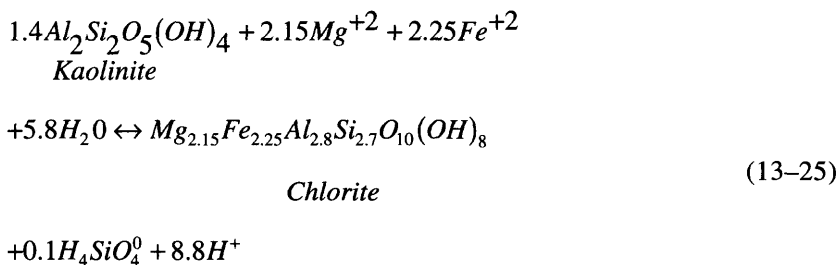
Saturation Index or Mineral Stability Charts

Mineral stability charts are convenient means of representing the various equilibrium reactions of the solid minerals and aqueous solutions in geological porous media in terms of the saturation index concept.

* Reprinted from "Water-Rock Interaction," Proceedings of the 7th international symposium, WRI-7, Park City, Utah, 13-18 July 1992 Kharaka, Y. K. & A. S. Maest (eds.), 90 5410 075 3, 1992, 25 cm, 1730 pp., 2 vols., EUR 209.00/US\$246.00 GBP147. Please order from: A. A. Balkema, Old Post Road, Brookfield, Vermont 05036 (telephone: 802-276-3162; telefax: 802-276-3837; e-mail: info@ashgate.com).

Mineral stability charts can be more meaningfully developed by considering the incongruent equilibrium reactions of various solid phases including the igneous and metamorphic reactions (Schneider, 1997).

Incongruent reactions represent the direct relationships of the various solid minerals involved in aqueous solution systems. The expressions of the incongruent reactions are derived from a combination of the relevant mineral dissolution/precipitation reactions in a manner to conserve certain key elements of the solid minerals so that the aqueous ionic species of these elements do not explicitly appear in the final equation. For example, the incongruent reactions of the alumino silicate minerals, including clay minerals, feldspars, and chlorites, are usually expressed to conserve the aluminum element (Fletcher, 1993; Schneider, 1997). Aluminum is a natural choice as the conserved element because this element is mostly immobile and the activities of the aqueous aluminum species are relatively low (Hayes and Boles, 1992; Schneider, 1997). Consequently, the incongruent mineral reaction equations do not involve the potential dissolved aluminum species such as Al^{+3} , $Al(OH)_2^+$, $Al(OH)_4^-$, $Al(OH)^{+2}$, and $Al(OH)_3^0$ (Schneider, 1997). Thus, the aluminum element conserving incongruent reaction to form the chlorite mineral from the kaolinite mineral reads as (Schneider, 1997, p. 119):



The reactions for electrolyte dissolution in water can be represented by (Schneider, 1997):



Substituting unity for the activity of the solid phase, the expression of the reaction quotient leads to the actual ion activity product, given by:

$$K_{ap} = \left[a_{A_{(aq)}^{+n}}^m \right]_{(actual)} \cdot \left[a_{B_{(aq)}^{-n}}^n \right]_{(actual)} \tag{13-27}$$

At saturation, Eq. 13-27 yields the saturation ion activity product given by:

$$K_{sp} = \left[a_{A(aq)}^m \right]_{(eq)} \cdot \left[a_{B(aq)}^n \right]_{(eq)} \quad (13-28)$$

Thus, a saturation index can be defined as:

$$SI = \log_{10} \left(\frac{K_{ap}}{K_{sp}} \right) \quad (13-29)$$

and is used to determine the state of saturation of an aqueous solution by a mineral as follows:

$$SI \begin{cases} < 0, & \text{undersaturated} \\ = 0, & \text{saturated} \\ > 0, & \text{supersaturated} \end{cases} \quad (13-30)$$

The composition of the various species in aqueous solutions undergoing dissolution/precipitation processes depends on various factors including pressure, temperature, and *pH*. For example, Figure 13-4, generated by Schneider (1997) using SOLMINEQ.88 (Kharaka et al., 1988) depicts the

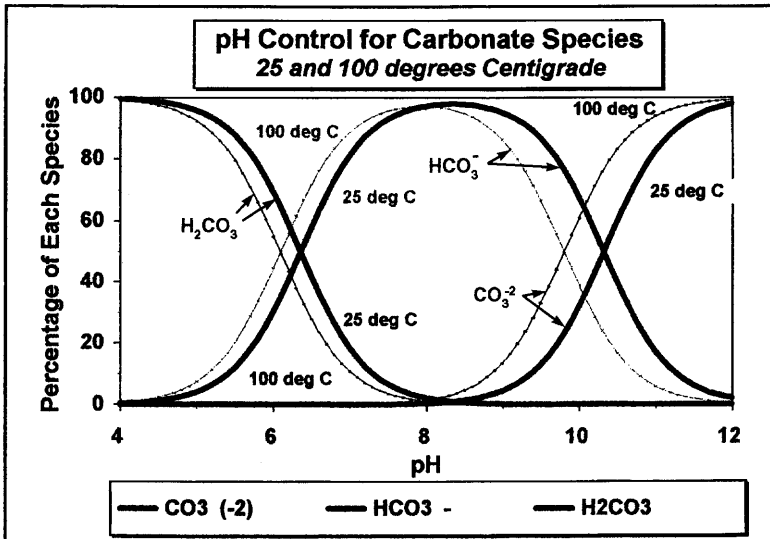


Figure 13-4. Effect of pH on distribution of carbonate species (after Schneider, ©1997; reprinted by permission of G. W. Schneider).

affect of pH on the composition of the typical carbonate species, namely $H_2CO_3^0$, HCO_3^- , and CO_3^{-2} .

Similarly Figure 13–5 indicates the affect of pH on the composition of typical aqueous aluminum species, namely Al^{+3} , $Al(OH)_2^+$, $Al(OH)_4^-$, and $Al(OH)^{+2}$, generated by Schneider (1997) using the SOLMINEQ.88 software.

Activity-Activity Charts

The Activity-Activity charts depict the regions of precipitation of various solid mineral phases. The equations of the lines separating these regions are obtained by rearranging the logarithmic expression of the equilibrium constant in a linear form to relate the saturation products of the various mineral phases. For example, the equilibrium constant for Eq. 13–25 is given by (Schneider, 1997):

$$K_{eq} = \frac{a_{H_4SiO_4^0}^{0.1} \cdot a_{H^+}^{8.8}}{a_{Mg^{+2}}^{2.15} \cdot a_{Fe^{+2}}^{2.25}} \equiv \frac{K_{sp_{chlorite}}}{K_{sp_{kaolinite}}} \quad (13-31)$$

in which the activities of the water and the solid kaolinite and chlorite phases were taken unity. A logarithm of Eq. 13–31 yields the linear equation for the kaolinite-chlorite phase boundary as:

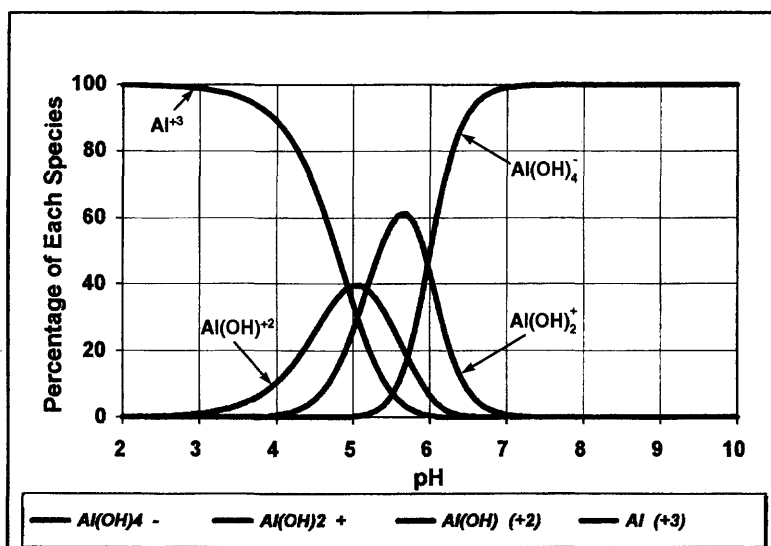


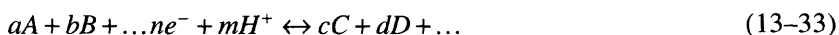
Figure 13–5. Effect of pH on distribution of aluminum species (after Schneider, ©1997; reprinted by permission of G. W. Schneider).

$$\log_{10} K_{sp_{kaolinite}} = \log_{10} K_{sp_{chlorite}} - \log_{10} K_{eq} \quad (13-32)$$

A plot of $K_{sp_{chlorite}}$ versus $K_{sp_{kaolinite}}$ according to Eq. 13-32 yields the kaolinite-chlorite stability chart (Schneider, 1997) using the SOLMINEQ.88 program (Kharaka et al., 1988). Schneider (1997) points out that the determination of the aqueous species activities is particularly complicated in highly concentrated oilfield brines because of the complexing of cations with inorganic and organic anions, and can be better accomplished by means of a simulator such as the SOLMINEQ.88 program by Kharaka et al. (1988).

pe– pH Charts

The *pe* – *pH* charts are constructed to describe the redox state of reservoirs (Stumm and Morgan, 1996; Schneider, 1997). Considering the electrons, e^- , and protons, H^+ , involved, chemical equilibrium reactions, such as oxidation-reduction (redox) and acid-base reactions, are represented by



The electron activity (*pe*) and potentiometric acidity (*pH*) can be conveniently expressed by the following equations, respectively:

$$pe = -\log_{10}[e^-] \quad (13-34)$$

and

$$pH = -\log_{10}[H^+] \quad (13-35)$$

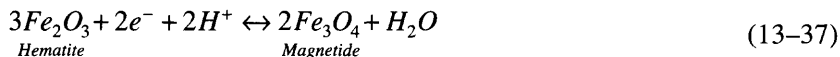
The electrode potential (*Eh*) and electron activity (*pe*) are related by (Schneider, 1997)

$$Eh = \frac{2.30259RT}{F} pe \quad (13-36)$$

in which T denotes the absolute temperature in K , $R = 8.31441 \text{ J} \cdot \text{K}^{-1} \cdot \text{mol}^{-1}$ is the universal gas constant and $F = 9.64846 \times 10^4 \text{ Coloumb/mol}$ is the Faraday constant. The electrode potential can be measured directly. Eqs. 13-34 through 36 form the convenient mathematical bases for constructing the *pe– pH* or *Eh–pH* charts. However, the *pe* – *pH* charts are preferred over the *Eh–pH* charts because, while the sign of *pH* does not change and the slopes of the stability boundaries are independent of temperature, the sign of the *Eh* potential depends on the direction of

the reaction and the slopes of the stability boundaries are temperature dependent (Schneider, 1997).

For example, consider (Schneider, 1997):



Assigning unity for the activities of the water and solid mineral phases, the equilibrium constant expression reads as (Schneider, 1997):

$$K_{eq} = \frac{1}{a_{e^-}^2 \cdot a_{H^+}^2} \quad (13-38)$$

Hence, a logarithm of Eq. 13-38 yields the equation for the hematite-magnetite boundary as:

$$pe = \frac{1}{2} \log K_{eq} - pH \quad (13-39)$$

which can be used to construct a $pe - pH$ chart (Schneider, 1997).

Geochemical Model Assisted Analysis of Solid Mineral—Aqueous Phase Interactions and Construction of Charts

Because of the highly complicated nature of the interactions of solid minerals and aqueous solution in geological porous media, it is most convenient to facilitate appropriate geochemical models for the analysis of the potential chemical interactions and formation damage affects. A typical example of such studies has been carried out by Schneider (1997) in an effort to quantify the potential formation damage problems, which would result from the invasion of incompatible foreign water, such as by drilling and workover fluids and water flooding, into the Lower Spraberry sandstone reservoir formation of Texaco's Jo Mill Unit (JMU) field.

Mineral Characterization and Analyses

Based on the analyses using a scanning electron microscope, electron microprobe, and x-ray diffraction, Schneider (1997) determined the properties of the sandstone as: "Fine-grained, immature sandstones that

contain considerable detrital clay minerals and carbonate clasts, along with quartz, plagioclase, and minor volcanic rock fragments and *K*-feldspar grains. Observed accessory minerals were muscovite, glauconite, hornblende, zircon, and pyrite. Authigenic minerals are dominated by carbonate cements and filamentous lathes of pore-lining and pore-filling illite. Some authigenic chlorite and overgrowths of quartz and feldspar are also present." He reports that the formation porosities and permeabilities are in the ranges of 10–20% and 0.5 to several *mD*, having considerable natural fracture permeability in certain regions and possibly some systematic fractures. He reports that this sandstone formation contains 6–10 volume % illite, 1–2 volume % chlorite, and negligible amounts of kaolinite (Scott, 1988).

Typical minerals present in porous rocks and subject to dissolution in contact with aqueous phase include the various types of carbonates such as calcite, $CaCO_3$, magnesite, $MgCO_3$, dolomite, $CaMg(CO_3)_2$, strontianite, $SrCO_3$, witherite, $BaCO_3$, and siderite, $FeCO_3$, and various types of sulfates such as anhydrite, $CaSO_4$, gypsum, $CaSO_4 \cdot 2H_2O$, celestine, $SrSO_4$, and barite, $BaSO_4$ (Schneider, 1997).

Schneider (1997) points out that the kaolinite compositions remain close to the $Al_2Si_2O_5(OH)_4$ formula, but the illite and chlorite formulae may vary as indicated by Aja et al. (1991a,b). He considered the typical mean compositions of the Bothamsall (Pennsylvanian), Rotliegendes (Permian), and Gulf Coast illites given, respectively, by (Warren and Curtis, 1989; Kaiser, 1984):

$$K_{0.80}(Mg_{0.13}Fe_{0.07}Al_{1.80})(Al_{0.60}Si_{3.40})O_{10}(OH)_2 \quad (13-40)$$

$$K(Mg_{0.15}Fe_{0.15}Al_{1.70})(Al_{0.70}Si_{3.30})O_{10}(OH)_2 \quad (13-41)$$

$$K_{0.6}(Mg_{0.25}Al_{1.80})(Al_{0.5}Si_{3.5})O_{10}(OH)_2 \quad (13-42)$$

Schneider considered the typical mean compositions of the Gulf Coast (Kaiser, 1984) and the North Sea (Curtis et al., 1984, 1985) chlorites given, respectively, by

$$Mg_{2.3}Fe_{2.3}Al_{1.4}(Al_{1.4}Si_{2.6})O_{10}(OH)_8 \quad (13-43)$$

$$Mg_{2.15}Fe_{2.25}Al_{1.5}(Al_{1.30}Si_{2.70})O_{10}(OH)_8 \quad (13-44)$$

Water Analyses

Although the analyses of the various Jo Mill Unit produced waters were available from the Inorganic Laboratory of Texaco EPTD, Schneider (1997) considered only the analyses of waters from the wells at five locations that did not make any appreciable amount of water. Therefore, for all practical purposes, these locations preserved their original water compositions. He also considered the analyses of the Mule Shoe Ranch and Canyon Reef waters that can be used for drilling and waterflooding operations. The analyses of these waters are presented in Table 13–1 by Schneider (1997).

Schneider (1997) used the SOLMINEQ.88 software to simulate the potential interactions and adverse affects of the formation minerals and aqueous phase. He assumed equilibrium conditions for conservative predictions of the rock-fluid interactions and water compatibility.

Saturation Index Charts

The compatibility of foreign water with the JMU reservoir connate water is investigated in this section using the saturation index charts.

Saturation Indices of the JMU Reservoir Waters

Schneider (1997) determined the saturation indices of the carbonates and sulfates, given in Table 13–2 for the JMU #7231 water using the SOLMINEQ.88 program. The saturation index values reported with positive and negative signs in Table 13–2 indicate conditions of super-saturation and under-saturation, respectively, for various minerals. The only unexpected result is the unusually low predicted siderite under-saturation of the water. However, in general, the saturation indices of the various minerals calculated by the SOLMINEQ.88 program is consistent with the mineralogy of the JMU sandstone formation. This is a further confirmation of the accuracy of the geochemical model (Schneider, 1997).

Mixing Paths on the Mineral Stability Charts

Effects of mixing foreign and reservoir waters on mineral stability are best realized by constructing mixing paths on the mineral stability charts.

Schneider (1997) investigated the compatibility of the JMU #7231 well connate water with the Mule Shoe Ranch and Canyon Reef waters considered for potential use in drilling and/or water flooding operations. The analyses of these waters are given by Schneider (1997) in Table 13–1. It is apparent that the Mule Shoe water has a higher CO_2^{-2} and

Table 13–1
Ionic Species Concentrations (mg/L) of the
Jo Mill Unit Reservoir Waters*

Ionic Species	JMU #7234	JMU #7231	JMU #6234	JMU #1333	JMU #2433	Mule Shoe Ranch Water	Canyon Reef Water
Na ⁺	58650	60430	57340	58140	54950	1862	52600
Ca ⁺²	2847	3037	2864	2890	2854	42	4617
Mg ⁺²	663	753	693	779	736	19	980
K ⁺	962	412	994	300	964	14	538
Ba ⁺²	2.41	2.18	2.2	3.5	1.95	0.03	0.75
Sr ⁺²	780	812	788	828	761	1.7	301
Total Fe	10.3	0.16	20.7	<0.03	1.14	<0.03	11.6
Total Al	0.5	0.6	0.5	0.6	.05	0.07	0.7
Cl ⁻	106400	110000	99500	105500	94000	1450	94500
Br ⁻	835	892	788	902	793	5.3	4.52
SO ₄ ⁻²	283	246	364	161	265	1669	689
CO ₃ ⁻²	0	0	0	0	0	16	0
HCO ₃	240	240	73	220	293	484	134
H ₄ SiO ₄ ⁰	2.2	4.3	1.7	3.7	2.4	3.6	2.8
pH	6.83	7.23	6.97	7.56	7.21	8.41	7.09
TDS	170837	175932	162639	168822	154826	5559	154370
Tartarate	ND	ND	ND	ND	ND	ND	ND
Malonate	ND	ND	ND	ND	ND	ND	ND
Succinate	24.6	26.2	21.5	22.1	19.3	ND	15.1
Glycolate	ND	ND	ND	ND	ND	ND	ND
Formate	23.3	8.3	28.9	5.5	7.7	ND	8.4
Acetate	304	290	313	195	326	ND	36.1
Propionate	22	8.9	18.6	ND	22.5	ND	ND
Butyrate	5.7	5.4	ND	ND	6.3	ND	<3.0
Oxalate	ND	<3.0	<3.0	ND	ND	<3.0	ND

* After Schneider, ©1997; reprinted by permission of G. W. Schneider.

ND: Not determined

HCO_3^- content and, therefore, higher alkalinity than the other waters reported in Table 13–1. He used the SOLMINEQ.88 program and simulated the consequences of mixing the JMU #7231 connate water with 10% volume increments of the Mule Shoe Ranch and Canyon Reef waters. Schneider (1997) constructed an illite-chlorite mineral stability chart based on the following reaction equation with proper stoichiometric coefficients for the Rotliegendes illite formula:

Table 13–2
Saturation Indices of Various Minerals*

Mineral Phase	Formula	Calculated Saturation Index
Illite	$K (Mg_{.15} Fe^{2+}_{.15} Al_{1.7}) (Si_{3.3} Al_{.7}) O_{10} (OH)_2$	+3.58
Chlorite	$(Al_{1.5} Fe^{2+}_{2.25} Mg_{2.15}) Al_{1.3} Si_{2.7} O_{10} (OH)_8$	+2.57
Kaolinite	$Al_2 (Si_2O_5) (OH)_4$	+4.11
Calcite	$CaCO_3$	+1.84
Dolomite	$CaMg(CO_3)_2$	+4.24
Siderite	$FeCO_3$	–33.11
Magnesite	$MgCO_3$	+1.88
Strontianite	$SrCO_3$	+1.23
Witherite	$BaCO_3$	–2.73
Anhydrite	$CaSO_4$	–1.77
Gypsum	$CaSO_4 \cdot 2H_2O$	–1.85
Barite	$BaSO_4$	–0.45
Celestine	$SrSO_4$	–0.68

* After Schneider, ©1997; reprinted by permission of G. W. Schneider.

$$\begin{aligned}
 &KMg_{0.15}Fe_{0.15}Al_{2.4}Si_{3.3}O_{10}(OH)_2 + 1.6929Mg^{+2} + 1.7786Fe^{+2} \\
 &+ 7.3714H_2O \leftrightarrow Mg_{2.15}Fe_{2.25}Al_{2.8}Si_{2.7}O_{10}(OH)_8 + K^+ \\
 &+ 0.9857H_4SiO_4^0 + 5.9429H^+
 \end{aligned}
 \tag{13–45}$$

He then plotted the curves for mixing the JMU connate water with the Mule Shoe water on this chart for the 8.4, 9.5, and 10.5 *pH* values, as shown in Figure 13–6-A, B, and C, respectively. Figure 13–6 indicates that illite becomes less stable at higher *pH*. He also investigated the effect of the K^+ activity on the illite stability. The mixing curves for 0, 2 and 5 weight % *KCl* solutions at the 10.5 *pH* level are shown in Figures 13–7-A, B, and C, respectively. Clearly, adding *KCl* increases the illite stability. However, K^+ activity has a relatively smaller effect than *pH*, in view of the comparison of Figures 13–6 and 13–7.

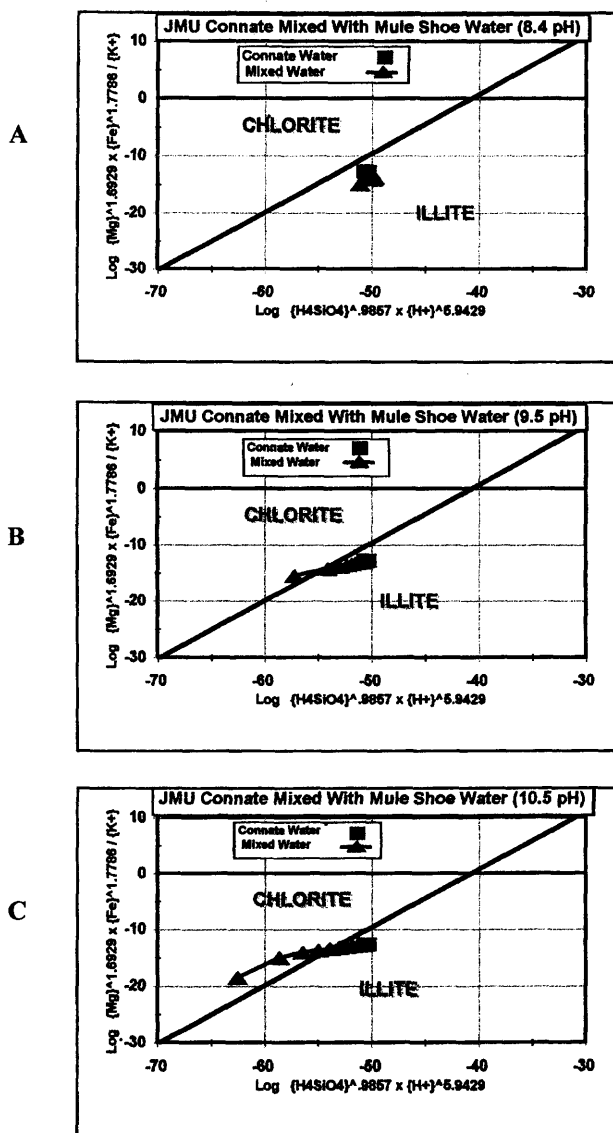


Figure 13-6. Effect of pH on mixtures of connate and Mule Shoe waters (after Schneider, ©1997; reprinted by permission of G. W. Schneider).

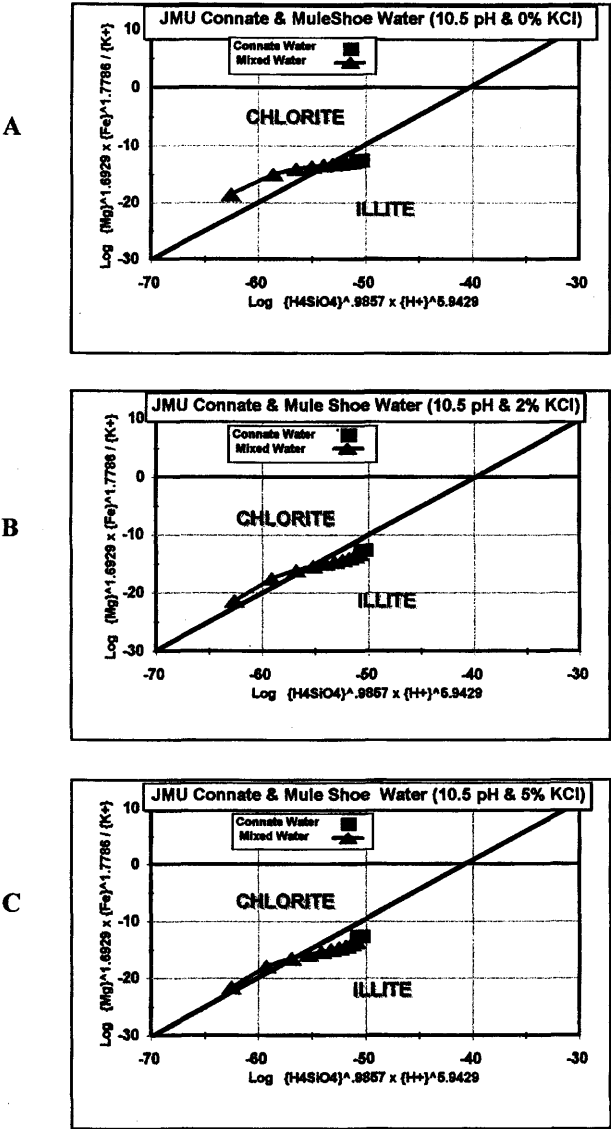
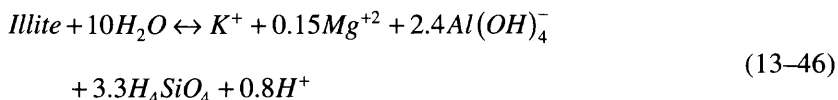


Figure 13–7. Effect of KCl on illite stability (after Schneider, ©1997; reprinted by permission of G. W. Schneider).

Saturation Index Charts for Clay Minerals

Schneider (1997) constructed the illite saturation index curves for mixing the Mule Shoe water with the JMU connate water as a function of the volume percent Mule Shoe water in the mixture. For this purpose, he considered the following dissolution/precipitation reaction for the Rotliegendes illite formula:



He explains that the Mule Shoe Ranch water is usually treated with lime and therefore its *pH* is above 10. A comparison of Figures 13–8A and B reveals that injecting a high *pH* Mule Shoe Ranch water into the reservoir reduces the illite stability of the JMU connate water upon mixing. The saturation index curves shown in Figures 13–9A and B by Schneider (1997) indicate that adding *KCl* into the Mule Shoe Ranch water improves the illite stability.

In Figures 13–10A and B, the illite stability curves obtained by Schneider (1997) are given for the Santa Rosa and Canyon Reef waters, respectively. Figure 13–10A indicates that injecting large volumes of the Mule Shoe Ranch water into the JMU reservoir reduces the illite stability. In contrast, the Canyon Reef water is compatible with the JMU connate water and should not create any illite unstability problems as indicated by Figure 13–10B.

Schneider (1997) constructed the chlorite saturation index curves shown in Figures 13–11A and B based on the following dissolution/precipitation reaction for the North Sea chlorite formula:

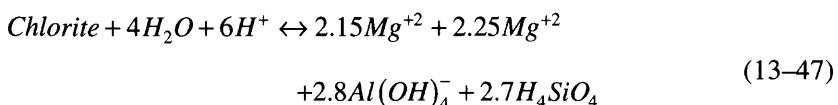
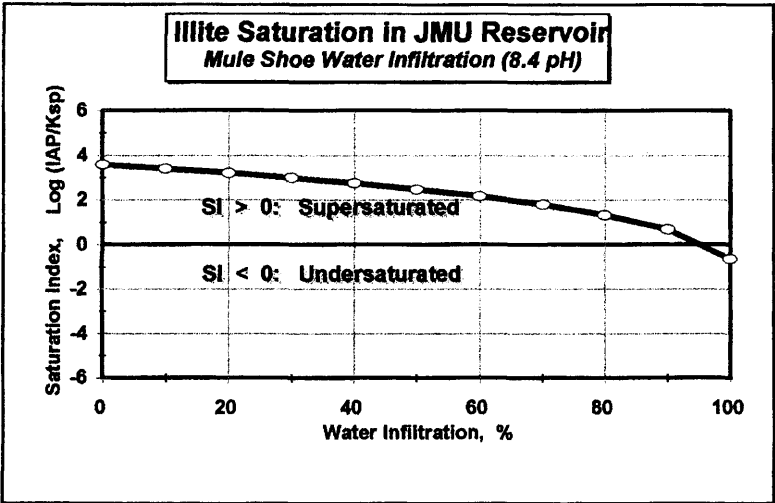


Figure 13–11A reveals that the Mule Shoe Ranch water becomes incompatible with the JMU Connate water with respect to the chlorite stability upon large volumes of water injection. Whereas, the Canyon Reef water is compatible, as indicated by Figure 13–11B.

Schneider (1997) constructed the kaolinite saturation index curves shown in Figures 13–12A and B based on the following dissolution/precipitation reaction:

(text continued on page 357)

A



B

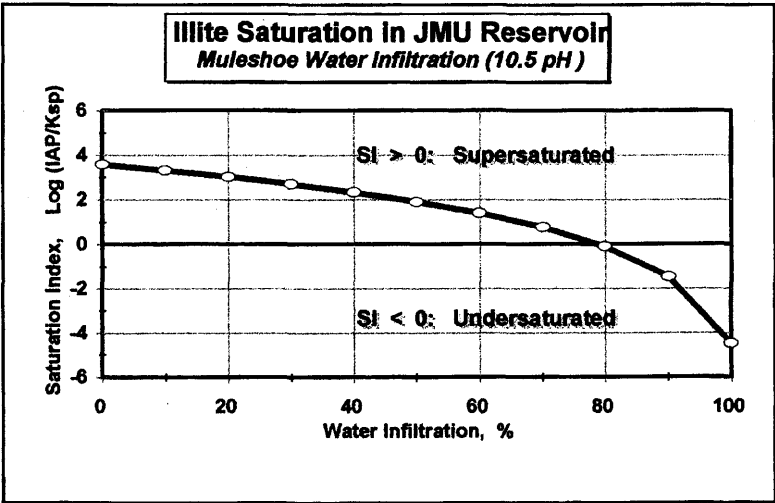
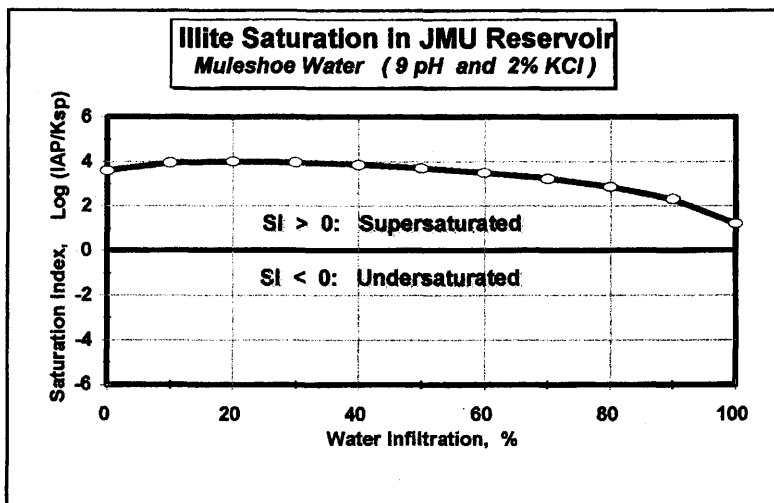


Figure 13–8. Effect of pH on illite saturation (after Schneider, ©1997; reprinted by permission of G. W. Schneider).

A



B

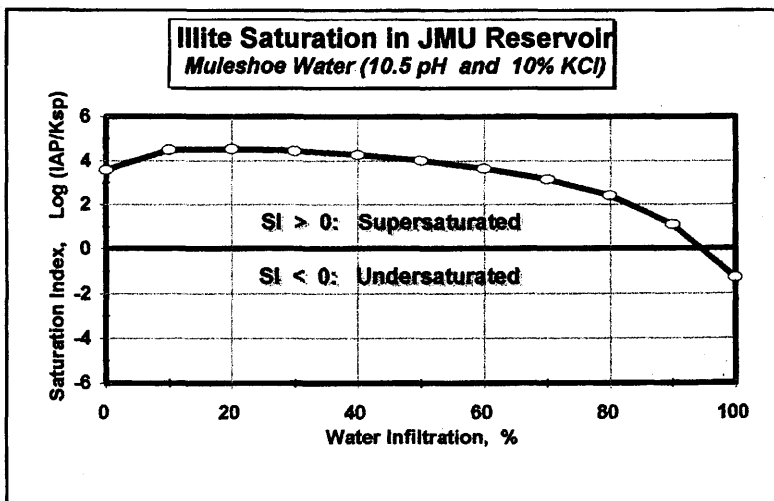
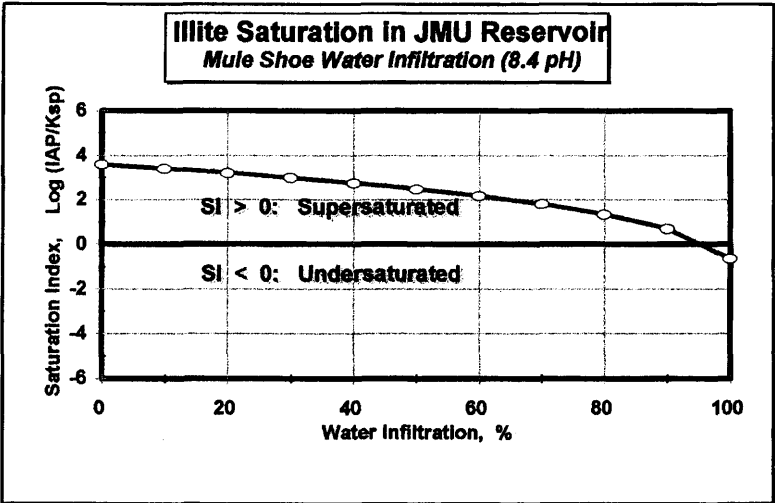


Figure 13-9. Effect of pH and K^+ activity on illite saturation (after Schneider, ©1997; reprinted by permission of G. W. Schneider).

A



B

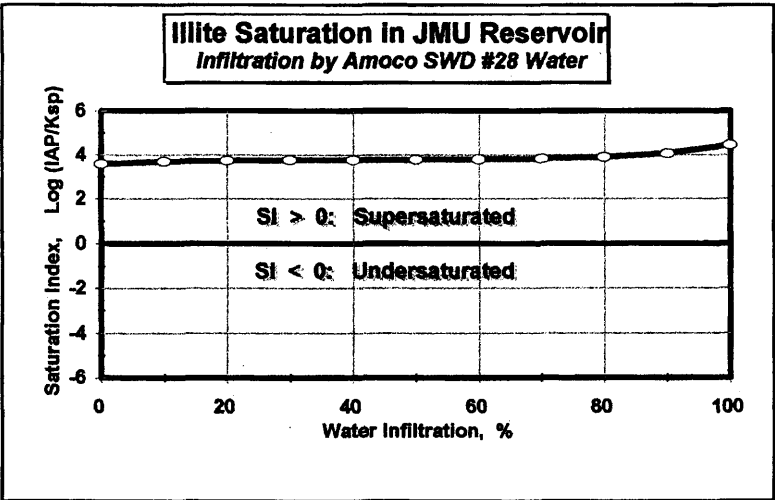
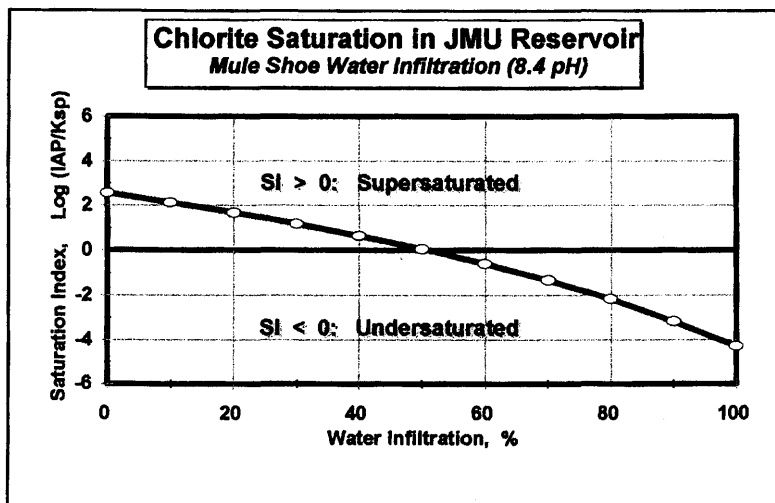


Figure 13–10. Illite saturation for mixtures of connate and invasion waters (after Schneider, ©1997; reprinted by permission of G. W. Schneider).

A



B

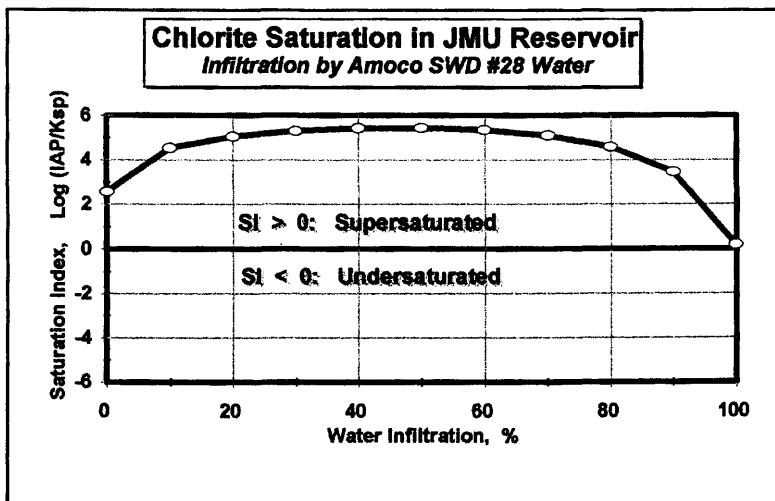
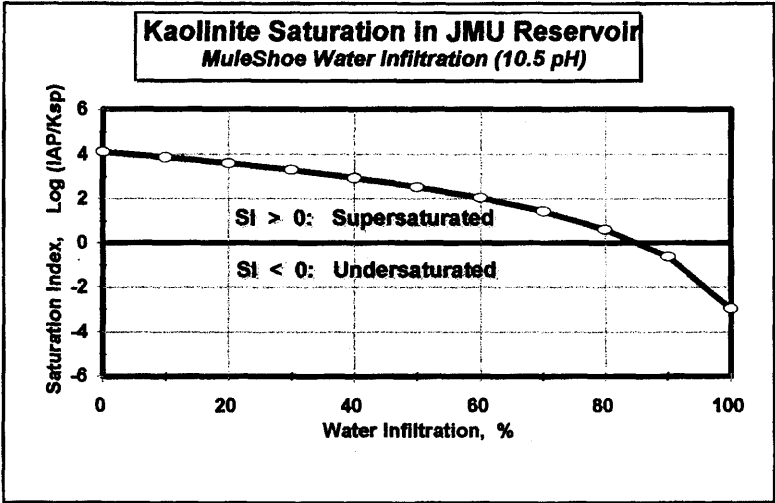


Figure 13-11. Chlorite saturation for mixtures of connate and invasion waters (after Schneider, ©1997; reprinted by permission of G. W. Schneider).

A



B

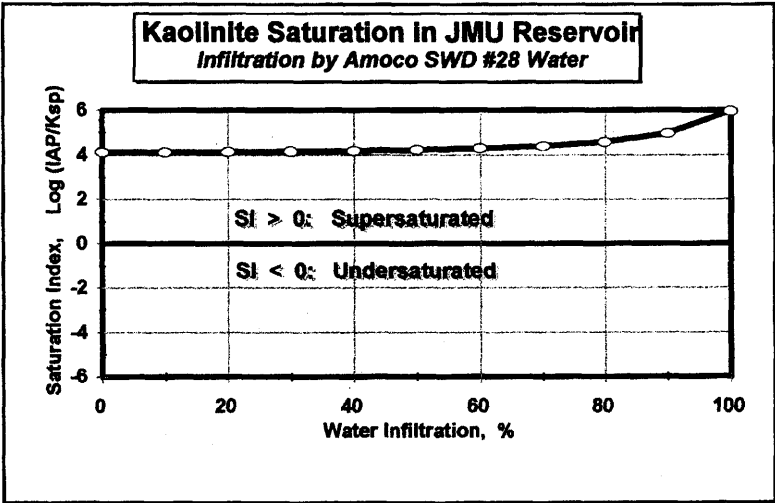
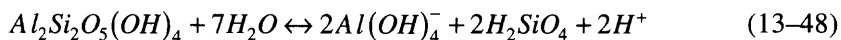


Figure 13–12. Kaolinite saturation for mixtures of connate and invasion waters (after Schneider, ©1997; reprinted by permission of G. W. Schneider).

(text continued from page 351)



A comparison of Figures 13–12A and B reveals that the Canyon Reef water is compatible with the JMU connate water with respect to kaolinite, whereas the Mule Shoe water becomes incompatible upon large volumes of water injection into the reservoir.

Saturation Index Charts for Carbonates and Sulfates

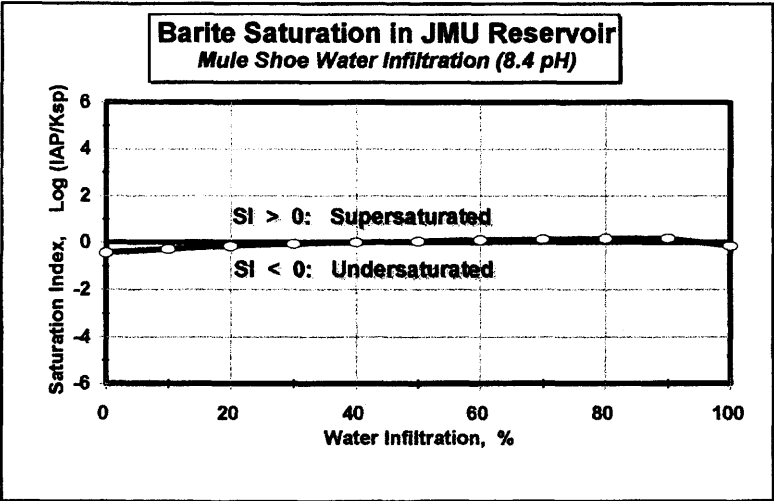
Using the SOLMINEQ.88 program, Schneider (1997) generated the saturation index curves for the mixing of waters for calcite, $CaCO_3$, magnesite, $MgCO_3$, dolomite, $CaMg(CO_3)_2$, witherite, $BaCO_3$, strontianite, $SrCO_3$, anhydrite, $CaSO_4$, gypsum, $CaSO_4 \cdot 2H_2O$, barite, $BaSO_4$, and celestine, $SrSO_4$ given in Figures 13–13 through 16, respectively. Figures 13–13A and B show the barite saturation index charts for mixing the JMU connate water with the Mule Shoe Ranch and Canyon Reef waters, respectively. It is apparent that mixing sufficient volumes of the Mule Shoe Ranch water with the JMU connate water will induce barite precipitation. But, the mixtures of the Canyon Reef and JMU connate waters will not lead to any precipitation. Figures 13–14A and B show the celestine saturation index charts for mixing the JMU connate water with the Mule Shoe Ranch and Canyon Reef waters. Figure 13–14A shows that around 80% volume Mule Shoe Ranch water content, the water mixture is nearly saturated with celestine. However, the mixtures of the Canyon Reef and the JMU connate waters do not yield any precipitation.

As indicated by the water analysis presented in Table 13–1, the JMU connate water is undersaturated by anhydrite and gypsum. Therefore, the saturation index charts shown in Figures 13–15A and B indicate no possibility of anhydrite or gypsum precipitation as a result of mixing JMU connate water with any portions of the Canyon Reef water.

The water analysis given in Table 13–1 indicate that the JMU connate water is supersaturated by calcite and dolomite and undersaturated by witherite. Consequently, as indicated by Figures 13–16A, B, and C, mixing of this water with any portions of the Mule Shoe Ranch and Canyon Reef waters will not result in appreciable calcite and dolomite dissolution and any witherite precipitation.

(text continued on page 362)

A



B

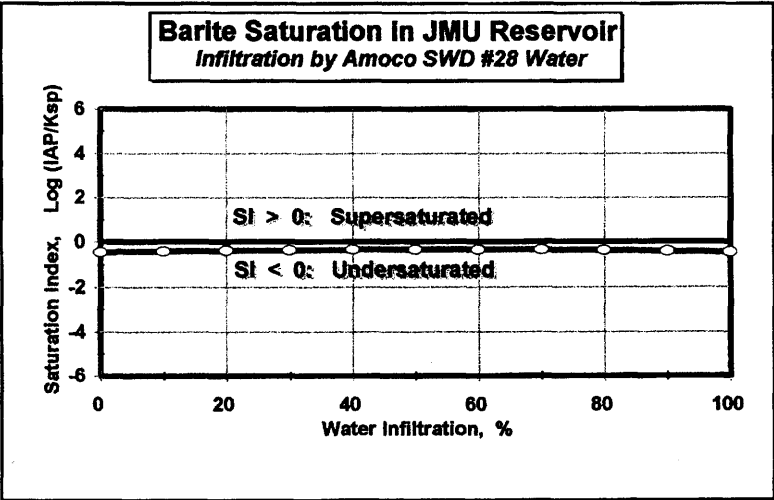
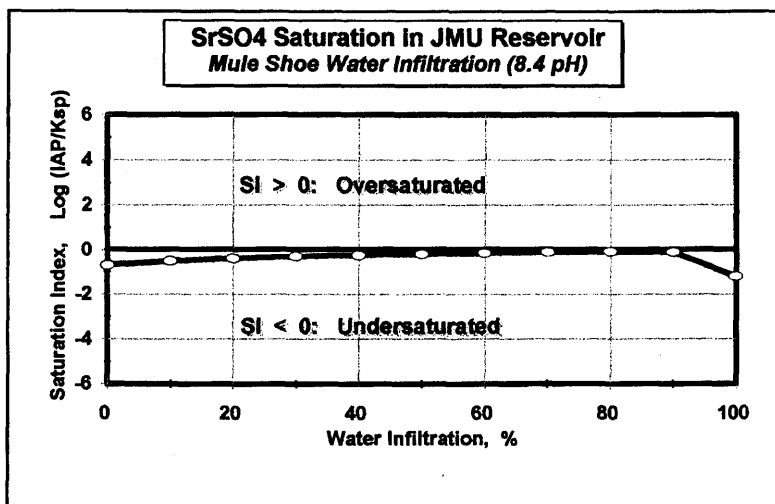


Figure 13–13. Barite saturation for mixtures of connate and invasion waters (after Schneider, ©1997; reprinted by permission of G. W. Schneider).

A



B

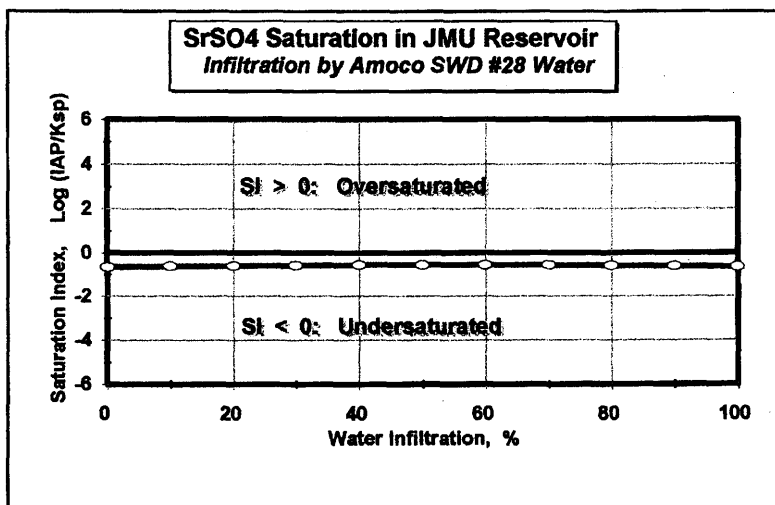
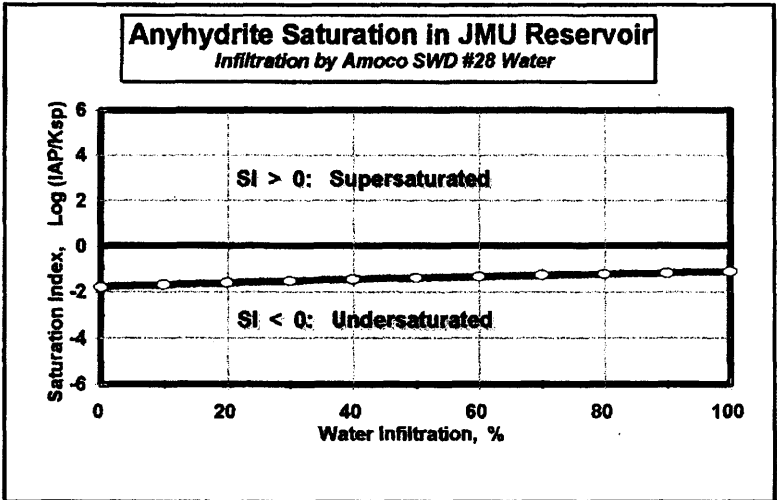


Figure 13-14. Celestine saturation for mixtures of connate and invasion waters (after Schneider, ©1997; reprinted by permission of G. W. Schneider).

A



B

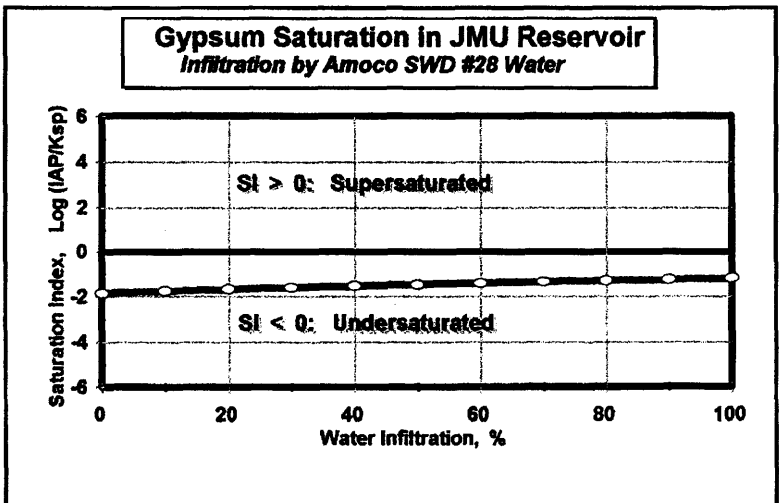
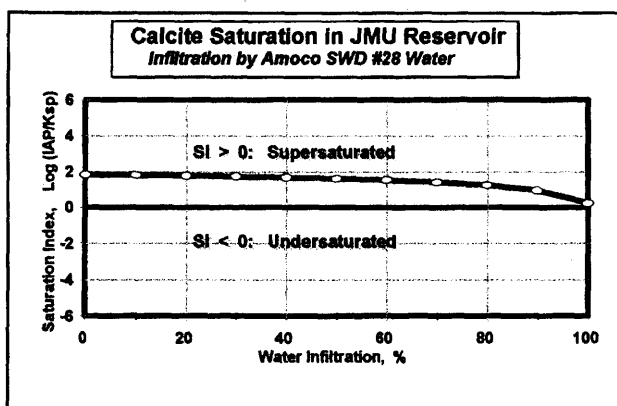
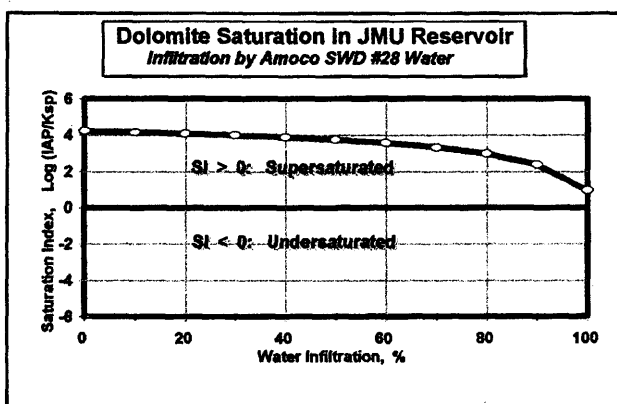


Figure 13-15. Saturation of various sulfate minerals for mixtures of connate and invasion waters (after Schneider, ©1997; reprinted by permission of G. W. Schneider).

A



B



C

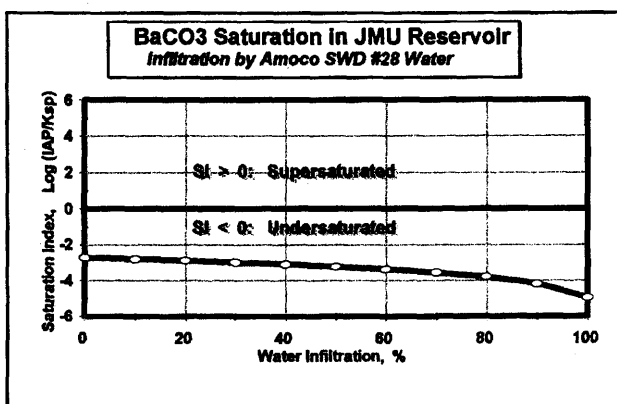


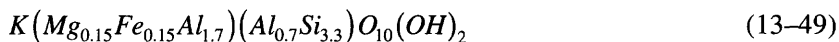
Figure 13-16. Saturation of various carbonate minerals for mixtures of connate and invasion waters (after Schneider, ©1997; reprinted by permission of G. W. Schneider).

(text continued from page 357)

Activity-Activity Charts

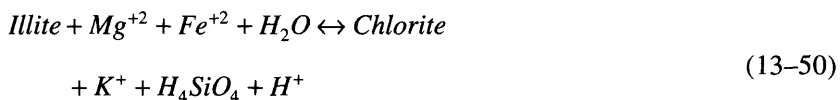
Schneider (1997) equilibrated the activities of the five connate water compositions given in Table 13-1 to the 135°F temperature of the Jo Mill Unit reservoir using the SOLMINEQ.88 program. He then plotted these activity values on the activity-activity charts. As can be seen in Figures 13-17 through 13-20, all points appear inside the mineral stability fields of the types of clay minerals present in the sandstone formation of the Jo Mill Unit reservoir. Hence, this confirmed the validity of the geo-chemical model and the accuracy of the mineral stability field charts generated by the SOLMINEQ.88 program.

Schneider (1997) explains that the formula



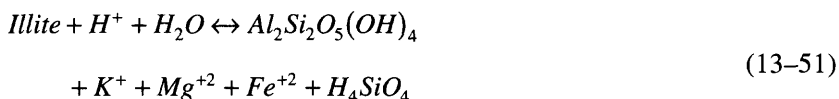
of the Rotliegendes illite is somewhat similar to the formula $KAl_2(AlSi_3)O_{10}(OH)_2$ of the muscovite, which is an end-member composition illite. Because the JMU reservoir contains a high amount of illite (6-10 volume %), the JMU reservoir connate water compositions should appear within the muscovite stability region as indicated by Figure 13-17 by Schneider (1997).

Schneider (1997) constructed the illite-chlorite mineral stability charts shown in Figure 13-18 based on the following illite to chlorite incongruent reactions using the proper stoichiometric coefficients according to the compositional formulae of the illites and chlorites mentioned above:



Again, as indicated by the mineral stability charts shown in Figure 13-18 by Schneider (1997), all the JMU reservoir connate water composition appear inside the mineral stability regions of the illites.

Schneider (1997) constructed the illite-kaolinite mineral stability charts shown in Figure 13-19 based on the following illite to kaolinite incongruent reactions using a proper set of stoichiometric coefficients according to the compositional formulae of the illites and kaolinites considered for the study:



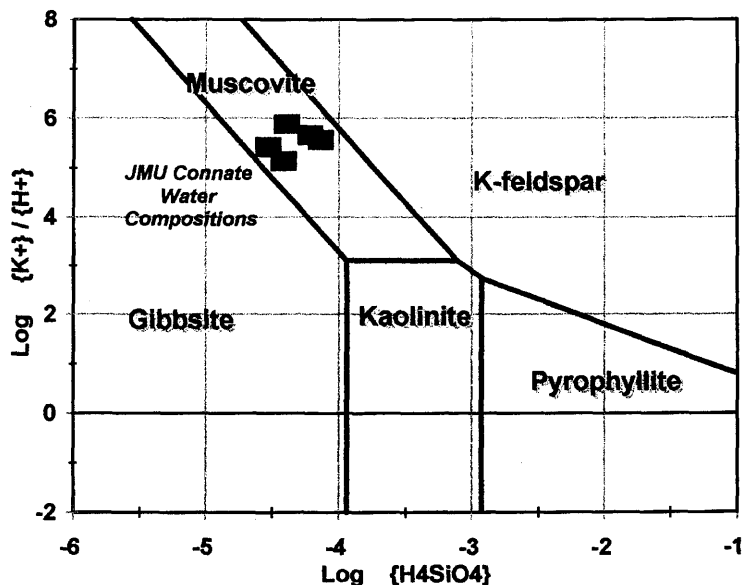
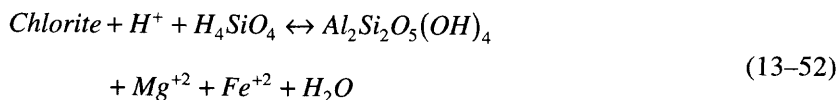


Figure 13-17. Stability chart for aluminosilicate minerals (after Schneider, ©1997; reprinted by permission of G. W. Schneider).

Because of the existence of a large quantity of illite (6–10 volume %) and a negligible amount of kaolinite in the JMU sandstone reservoir formations, all the JMU connate waters appear inside the illite stability region.

Schneider (1997) constructed the chlorite-kaolinite mineral stability charts shown in Figure 13-20 based on the following chlorite to kaolinite incongruent reactions using the proper set of stoichiometric coefficients according to the compositional formulae of the chlorites considered for the study



Because of a relatively larger quantity of the chlorite (1–2 volume %) compared to the negligible amount of kaolinite present in the JMU sandstone formation, all the JMU connate waters appear inside the chlorite stability region.

(text continued on page 367)

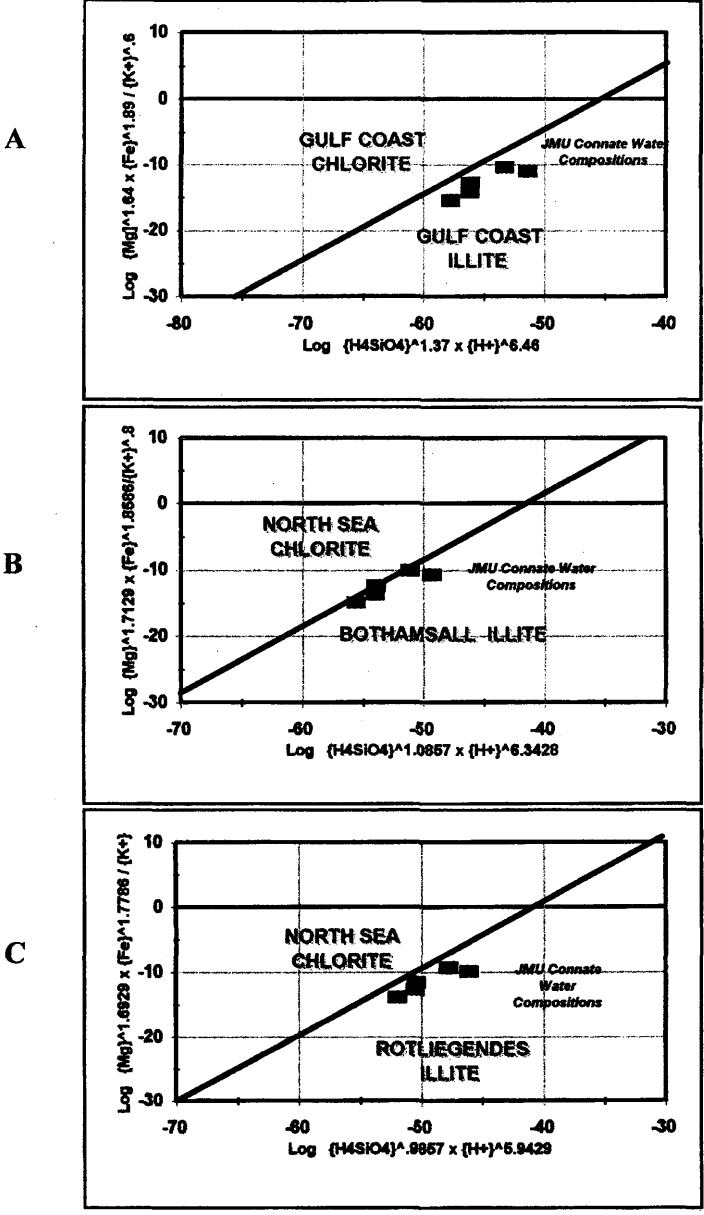


Figure 13-18. Illite-chlorite mineral stability chart (after Schneider, ©1997; reprinted by permission of G. W. Schneider).

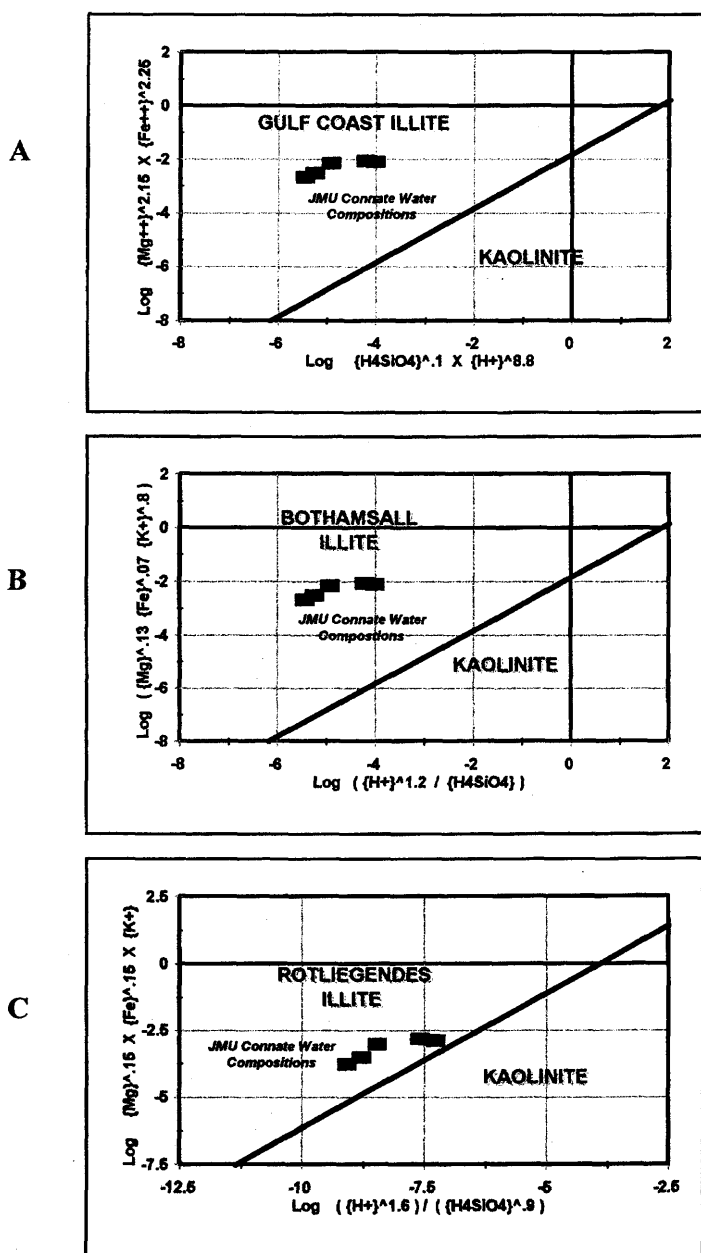
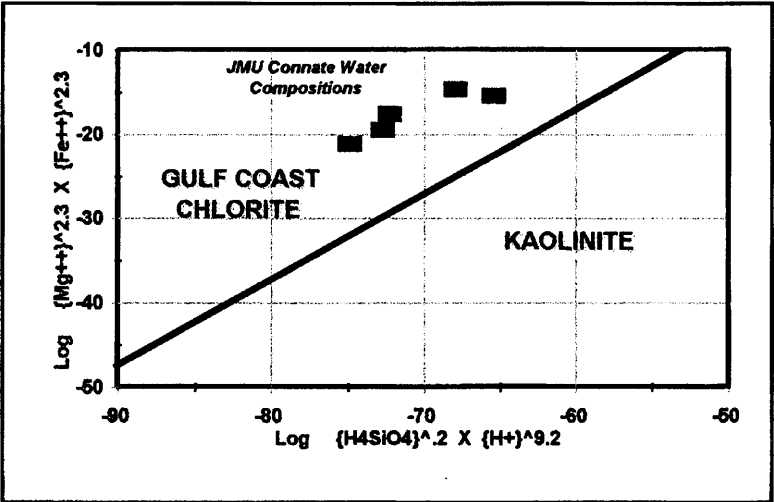


Figure 13–19. Illite-kaolinite mineral stability chart (after Schneider, ©1997; reprinted by permission of G. W. Schneider).

A



B

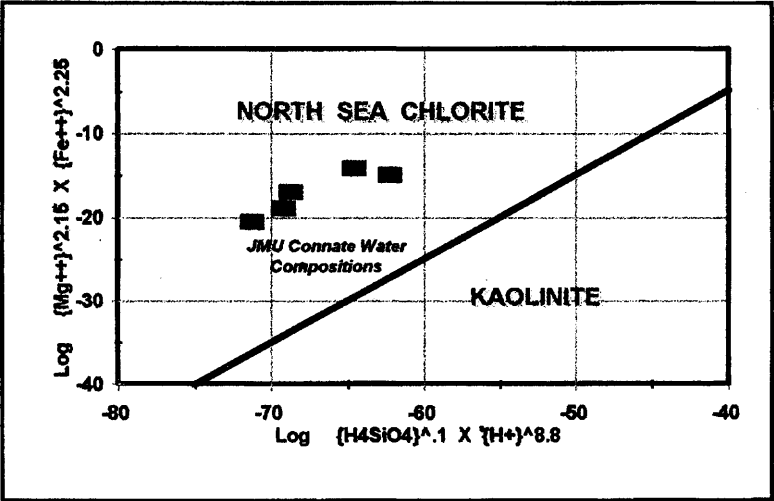


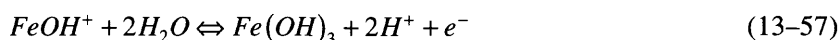
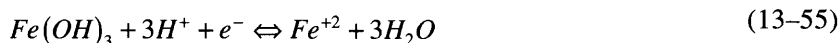
Figure 13–20. Chlorite-kaolinite mineral stability chart (after Schneider, ©1997; reprinted by permission of G. W. Schneider).

(text continued from page 362)

pe – pH Charts

Aqueous Species of the Fe – O – H₂O System

Schneider (1997) constructed the *pe* – *pH* charts for the aqueous species involving the following half-reactions of the *Fe – O – H₂O* system:



for which he wrote the following *pe* – *pH* relationships:

$$pe = \log K_{eq} - \log \left(\frac{\{Fe^{+2}\}}{\{Fe^{+3}\}} \right) \quad (13-58)$$

$$pH = \frac{1}{3} \log K_{eq} - \frac{1}{3} \log \{Fe^{+3}\} \quad (13-59)$$

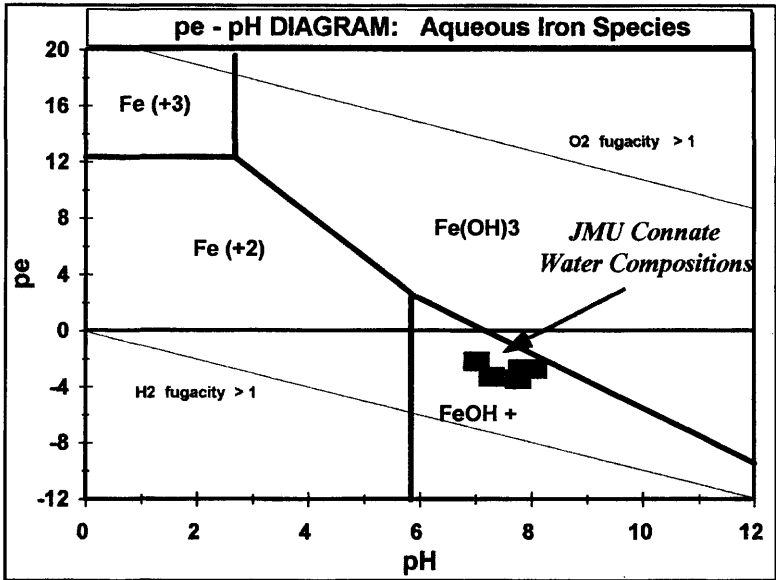
$$pe = \log K_{eq} - \log \{Fe^{+2}\} - 3pH \quad (13-60)$$

$$pH = \log K_{eq} - \log \left(\frac{\{Fe^{+2}\}}{\{FeOH^+\}} \right) \quad (13-61)$$

$$pe = -\log K_{eq} - 2pH - \log \{FeOH^+\} \quad (13-62)$$

Schneider (1997) then applied the SOLMINEQ.88 program and constructed the charts shown in Figure 13-21A by plotting Eqs. 13-58

A



B

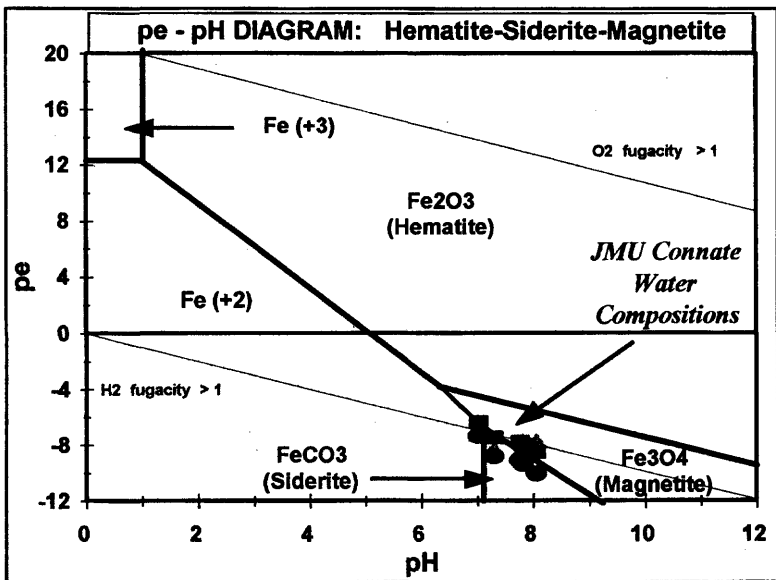
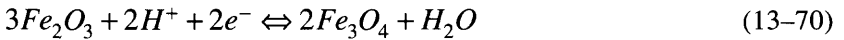
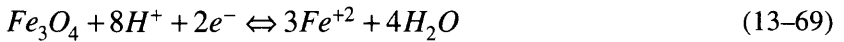
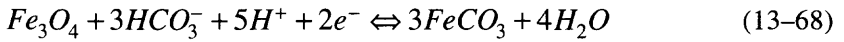
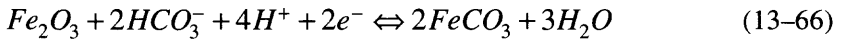
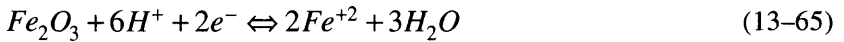


Figure 13-21. $pe - pH$ chart for $\text{Fe} - \text{O} - \text{H}_2\text{O}$ system (after Schneider, ©1997; reprinted by permission of G. W. Schneider).

through 62 to represent the stability boundaries. For this purpose, he used a mean activity value of $10^{-5.6}$ m for Fe^{+2} , even though the actual activity values for Fe^{+2} in the JMU connate waters vary between $10^{-4.3}$ and $10^{-6.4}$ m. All JMU connate water compositions appear in the $FeOH^+$ solution region. But, $Fe(OH)_3$ can precipitate if the pe or pH is varied to move into the $Fe(OH)_3$ stability region.

Mineral Species of the $Fe - O - H_2O$ System

Schneider (1997) also constructed the $pe - pH$ charts for the minerals involving the half-reactions of the $Fe - O - H_2O$ system:



from which he wrote the following $pe - pH$ relationships:

$$pe = \frac{1}{2} \log K_{eq} - \log \{Fe^{+2}\} - 3pH \quad (13-71)$$

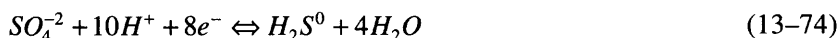
$$pe = \frac{1}{2} \log K_{eq} + \log \{HCO_3^-\} - 2pH \quad (13-72)$$

$$pe = \frac{1}{2} \log K_{eq} + \frac{3}{2} \log \{HCO_3^-\} - \frac{5}{2} pH \quad (13-73)$$

Schneider (1997) then applied the SOLMINEQ.88 program and constructed the charts shown in Figure 13–21B by plotting Eqs. 13–71 through 73 to represent the stability boundaries. The JMU connate water compositions yield somewhat different pE values for the redox reaction couples of $Fe_2O_3 - Fe^{+2}$, $Fe_2O_3 - FeCO_3$, and $Fe_3O_4 - FeCO_3$, as indicated by triangles, squares and circles, respectively, in Figure 13–21B by Schneider (1997). Overall, Schneider concludes, based on Figures 13–21A and B, that “the JMU reservoir is a highly-reduced environment.”

Aqueous Species of the Fe – O – H₂O – S System

Schneider (1997) considered the following half-reactions for the sulfate and sulfide species present in an aqueous system:



Of the relationships that could be written for the half-reactions given by Eqs. 13–74 through 78, Schneider (1997) considered only the following relationship for the $SO_4^{-2} - S_{(solid)}$ redox reaction couple:

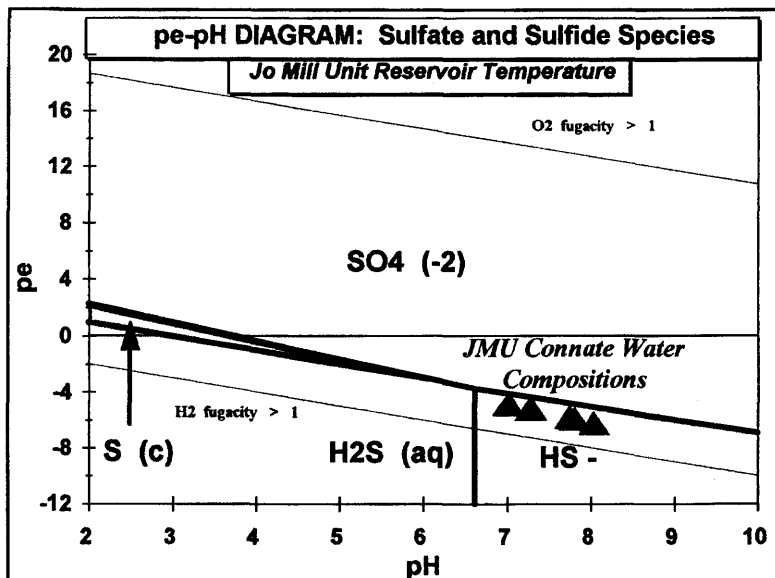
$$pe = \frac{1}{6} \log K_{eq} - \frac{4}{3} pH + \frac{1}{6} \log \{SO_4^{-2}\} \quad (13-79)$$

because only the sulfate concentrations were determined as indicated by the water analyses given in Table 13–1 and the H_2S^0 and HS^- species activities determined by the SOLMINEQ.88 program are dependent on the SO_4^{-2} activities. Figure 13–22A shows that all the JMU connate water compositions appear in the reduced stability region.

Mineral Species of the Fe – O – H₂O – S System

Schneider (1997) also considered the following half-reactions for the minerals involving the $Fe - O - H_2O - S$ system:

A



B

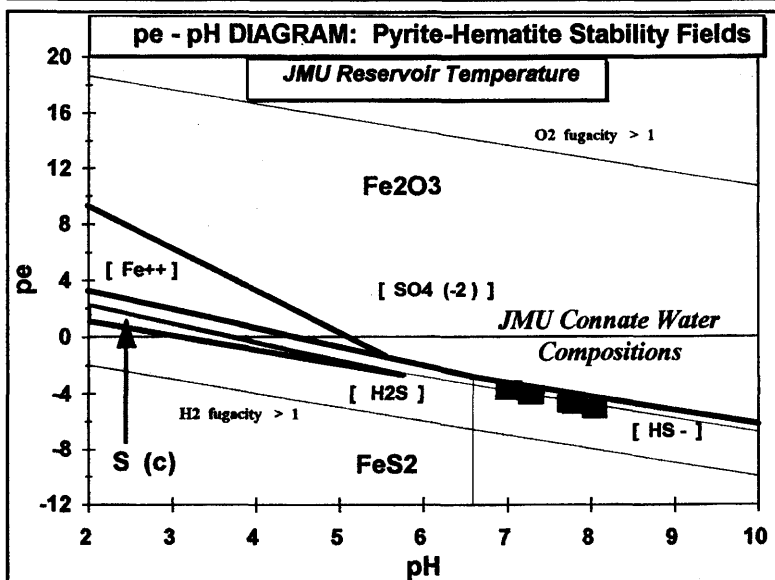
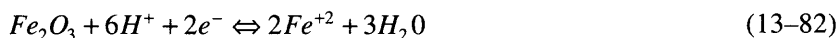
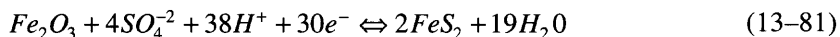
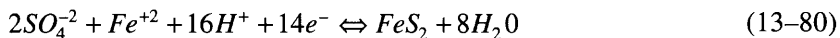


Figure 13-22. *pe* - *pH* chart for $\text{Fe} - \text{O} - \text{H}_2\text{O} - \text{S}$ system (after Schneider, ©1997; reprinted by permission of G. W. Schneider).



from which he wrote the following relationships

$$pe = \frac{1}{14} \log K_{eq} + \frac{1}{7} \log \{SO_4^{-2}\} + \frac{1}{14} \log \{Fe^{+2}\} - \frac{8}{7} pH \quad (13-83)$$

$$pe = \frac{1}{30} \log K_{eq} + \frac{4}{30} \log \{SO_4^{-2}\} - \frac{38}{30} pH \quad (13-84)$$

These equations were used to construct the hematite and pyrite stability regions shown in Figure 13-22B for the $SO_4^{-2} - FeS_{2(solid)}$ redox reaction couple. The JMU connate water compositions appear in the reduced stability region.

The Aqueous O – H₂O System

Schneider (1997) points out that the waters pumped from the surface to the JMU reservoir are likely to contain some dissolved oxygen gas. Therefore, Schneider (1997) constructed a $pe - pH$ chart for the oxygenated waters at the JMU reservoir temperature as shown in Figure 13-23, based on the stability boundaries developed for the reduction of oxygen according to the following reactions given by Drever (1988):



Figure 13-23 shows the range of the pe values for the oxygenated waters at the JMU reservoir temperature.

References

- Aja, S. U., Rosenberg, P. E., & Kittrick, J. A., "Illite Equilibria in Solutions: I. Phase Relationships in the System $K_2O-Al_2O_3-SiO_2-H_2O$ between 25 and 250°C," *Geochimica et Cosmochimica Acta*, Vol. 55, 1991a, pp. 1353-1364.

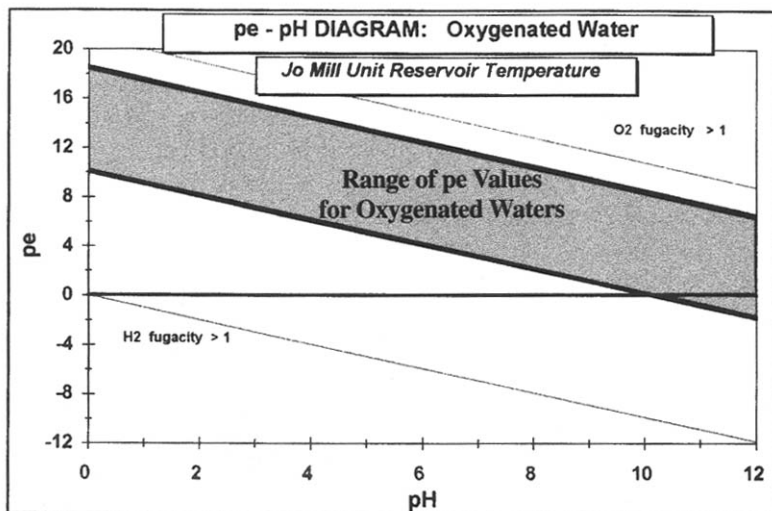


Figure 13-23. *pe* range for oxygenated waters determined by the reaction model of Drever (1988) (after Schneider, ©1997; reprinted by permission of G. W. Schneider).

- Aja, S. U., Rosenberg, P. E., & Kittrick, J. A., "Illite Equilibria in Solutions: II. Phase Relationships in the System K_2O - MgO - Al_2O_3 - SiO_2 - H_2O ," *Geochimica et Cosmochimica Acta*, Vol. 55, 1991b, pp. 1365-1374.
- Amaefule, J. O., Kersey, D. G., Norman, D. L., & Shannon, P. M., "Advances in Formation Damage Assessment and Control Strategies," CIM Paper No. 88-39-65, Proceedings of the 39th Annual Technical Meeting of Petroleum Society of CIM and Canadian Gas Processors Association, June 12-16, 1988, Calgary, Alberta, 16 p.
- Basset, R. L., & Melchior, D. C., "Chemical Modeling of Aqueous Systems—An Overview," Chapter 1, pp. 1-14, in *Chemical Modeling of Aqueous Systems II*, Melchoir, D. C. & Basset, R. L. (Eds.), ACS Symposium Series 416, ACS, Washington, 1990.
- Bertero, L., Chierici, G. L., Gottardi, G., Mesini, E., & Mormino, G., "Chemical Equilibrium Models: Their Use in Simulating the Injection of Incompatible Waters," *SPE Reservoir Engineering Journal*, February 1988, pp. 288-294.
- Bethke, C. M., *Geochemical Reaction Modeling, Concepts and Application*, Oxford University Press, New York, 1996, 397 p.
- Bjørkum, P. A., & Gjelsvik, N., "An Isochemical Model for Formation of Authigenic Kaolinite, K-feldspar, and Illite in Sediments," *Journal of Sedimentary Petrology*, Vol. 58, No. 3, 1988, pp. 506-511.

- Carnahan, C. L., "Coupling of Precipitation-Dissolution Reactions to Mass Diffusion via Porosity Changes," *Chemical Modeling of Aqueous Systems II*, Chapter 18, pp. 234–242, D.C. Melchior & R. L. Basset (Eds.), ACS Symposium Series 416, American Chemical Society, Washington, DC, 1990.
- Chang, F. F., and Civan, F., "Modeling of Formation Damage due to Physical and Chemical Interactions between Fluids and Reservoir Rocks," SPE 22856 paper, Proceedings of the 66th Annual Technical Conference and Exhibition of the Society of Petroleum Engineers, October 6–9, 1991, Dallas, Texas.
- Chang, F. F., & Civan, F., "Predictability of Formation Damage by Modeling Chemical and Mechanical Processes," SPE 23793 paper, Proceedings of the SPE International Symposium on Formation Damage Control, February 26–27, 1992, Lafayette, Louisiana, pp. 293–312.
- Chang, F. F., & Civan, F., "Practical Model for Chemically Induced Formation Damage," *Journal of Petroleum Science and Engineering*, Vol. 17, No. 1/2, February 1997, pp. 123–137.
- Curtis, C. D., Ireland, B. J., Whiteman, J. A., Mulvaney, R., & Whittle, C. K., "Authigenic Chlorites: Problems with Chemical Analysis and Structural Formula Calculation," *Clay Minerals*, Vol. 19, 1984, pp. 471–481.
- Curtis, C. D., Hughes, C. R., Whiteman, J. A., & Whittle, C. K., "Compositional Variation Within Some Sedimentary Chlorites and Some Comments on their Origin," *Mineralogical Magazine*, Vol. 49, 1985, pp. 375–386.
- Demir, I., "Formation Water Chemistry and Modeling of Fluid-Rock Interaction for Improved Oil Recovery in Aux Vases and Cypress Formations," Department of Natural Resources, Illinois State Geological Survey, Illinois Petroleum Series 148, 1995, 60 p.
- Dewers, T., Civan, F., and Atkinson, G., "Formation Damage and Carbonate Scale During Sub-Salt Petroleum Production," research proposal funded by the Interdisciplinary Research Incentive Program at the University of Oklahoma, 2000, 20 p. unpublished.
- Drever, J. I., *The Geochemistry of Natural Waters, Second Edition*, Prentice Hall, New York City, 1988.
- Dullien, F. A. L., *Porous Media Fluid Transport and Pore Structure*, 2nd ed., Academic Press, Inc., San Diego, 1992, 574 p.
- ESTSC/COSMIC, "Geochemical Modeling of Aqueous Systems, EQ3NR," *Software Technology Transfer*, Energy Science and Technology Software Center (ESTSC), Oak Ridge, TN, and NASA Computer Software Technology Transfer Center (COSMIC), the University of Georgia, Athens, GA, Vol. 1, No. 1, Winter 1993, p. 17.
- Fletcher, P., *Chemical Thermodynamics for Earth Scientists*, Longman Group UK Ltd., London, 1993.

- Glover, M. C., & Guin, J. A., "Dissolution of a Homogeneous Porous Medium by Surface Reaction," *AIChE Journal*, Vol. 19, No. 6, November 1973, pp. 1190–1195.
- Haggerty, D. J., & Seyler, B., "Investigation of Formation Damage from Mud Cleanout Acids and Injection Waters in Aux Vases Sandstone Reservoirs," Department of Natural Resources, Illinois State Geological Survey, Illinois Petroleum Series 152, 1997, 40 p.
- Hayes, M. J., & Boles, J. R., "Volumetric Relations Between Dissolved Plagioclase and Kaolinite in Sandstones: Implications for Aluminum Mass Transfer in San Joaquin Basin, California," *Origin, Diagenesis, and Petrophysics of Clay Minerals in Sandstones*, SEPM Special Publication No. 47, 1992, pp. 111–123.
- Helgeson, H. C., Brown, T. H., Nigrini, A., & Jones, T. A., "Calculation of Mass Transfer in Geochemical Processes Involving Aqueous Solutions," *Geochimica Cosmochimica Acta*, Vol. 34, 1970, pp. 569–592.
- Holstad, A., "Mathematical Modeling of Diagenetic Processes in Sedimentary Basins," *Mathematical Modelling of Flow Through Porous Media*, Bourgeat, A. P., Carasso, C., Luckhaus, S., & Mikelić, A., (Eds.), World Scientific Publ. Co. Pte. Ltd., 1995, pp. 418–428.
- Israelachvili, J., *Intermolecular and Surface Forces*, 2nd ed., Academic Press, San Diego, 1992, 450 p.
- James, R. O., & Parks, G. A., "Characterization of Aqueous Colloids by their Electrical Double-Layer and Intrinsic Surface Chemical Properties," in *Surface and Colloid Science*, Vol. 12, Matijevic, E. (ed.), Plenum Press, New York, pp. 119–216.
- Jennings, A. A., & Kirkner, D. J., "Instantaneous Equilibrium Approximation Analysis," *J. of Hydraulic Eng.*, Vol. 110, No. 12, 1984, pp. 1700–1717.
- Kaiser, W. R., "Predicting Reservoir Quality and Diagenetic History in the Frio Formation (Oligocene) of Texas," *Clastic Diagenesis: AAPG Memoir 37*, McDonald, D. A. & Surdam, R. C. (Eds.), American Association of Petroleum Geologists, 1984, pp. 195–215.
- Kandiner, H. J., & Brinkley, S. R., "Calculation of Complex Equilibrium Relations," *Ind. Eng. Chem.*, Vol. 42, 1950, pp. 850–855.
- Kharaka, Y. K., & Barnes, I., "SOLMINEQ: Solution-mineral-equilibrium Computations: U.S. Geological Survey Computer Contributions," NTIS No. PB215-899, 1973, 81 p.
- Kharaka, Y. K., Gunter, W. D., Aggarwal, P. K., Perkins, E. H., & DeBraul, J. D., "SOLMINEQ.88: A Computer Program for Geochemical Modeling of Water-Rock Interactions," U.S. Geological Survey Water-Resources Investigations Report 88-4227, Menlo Park, CA, 1988, 429 p.
- Labrid, J., & Bazin, B., "Flow Modeling of Alkaline Dissolution by a Thermodynamic or by a Kinetic Approach," *SPE Reservoir Engineering*, May 1993, pp. 151–159.

- Li, Y-H., Crane, S. D., Scott, E. M., Braden, J. C., & McLelland, W. G., "Waterflood Geochemical Modeling and a Prudhoe Bay Zone 4 Case Study," *SPE Journal*, Vol. 2, March 1997, pp. 58-69.
- Li, Y-H., Fambrough, J. D., & Montgomery, C. T., "Mathematical Modeling of Secondary Precipitation from Sandstone Acidizing," *SPE Journal*, December 1998, pp. 393-401.
- Lichtner, P. C., "Continuum Model for Simultaneous Chemical Reactions and Mass Transport in Hydrothermal Systems," *Geochimica et Cosmochimica Acta*, Vol. 49, 1985, pp. 779-800.
- Lichtner, P. C., "The Quasi-Stationary State Approximation to Coupled Mass Transport and Fluid-Rock Interaction in a Porous Medium," *Geochimica et Cosmochimica Acta*, Vol. 52, 1988, pp. 143-165.
- Lichtner, P. C., "Time-Space Continuum Description of Fluid/Rock Interaction in Permeable Media," *Water Resources Research*, Vol. 28, No. 12, December 1992, pp. 3135-3155.
- Liu, X., Ormond, A., Bartko, K., Li, Y., & Ortoleva, P., "A Geochemical Reaction-Transport Simulator for Matrix Acidizing Analysis and Design," *J. of Petroleum Science and Engineering*, Vol. 17, No. 1/2, February 1997, pp. 181-196.
- Liu, X., & Ortoleva, P., "A Coupled Reaction and Transport Model for Assessing the Injection, Migration, and Fate of Waste Fluids," SPE 36640 paper, Proceedings of the 1996 SPE Annual Technical Conference and Exhibition, Denver, Colorado, October 6-9, 1996, pp. 661-673.
- Liu, X., & Ortoleva, P., "A General-Purpose, Geochemical Reservoir Simulator," SPE 36700 paper, Proceedings of the 1996 SPE Annual Technical Conference and Exhibition, Denver, Colorado, October 6-9, 1996, pp. 211-222.
- Melchior, D. C., & Bassett, R. L. (Eds.), "Chemical Modeling of Aqueous Systems II," ACS Symposium Series 416, American Chemical Society, Washington, DC, 1990, 556 p.
- Nordstrom, D. K., & Munoz, J. L., *Geochemical Thermodynamics*, 2nd ed., Blackwell Scientific Publications, Boston, 1994.
- Ortoleva, P., *Geochemical Self-Organization*, Oxford University Press, New York, 1994.
- Plummer, L. N., *Geochemical Modeling of Water-Rock Interaction: Past, Present, Future*," in Water-Rock Interaction, Vol. 1, Kharaka, Y. K. & Maest, A. S. (Eds.), 1992, Balkema, Rotterdam, Brookfield, 858 p.
- Prigogine, I., & DeFay, R., *Chemical Thermodynamics*, D.H. Everett (trans.), Longmans Green and Co., London, 1954, 543 p.
- Rege, S. D., & Fogler, H. S., "Competition Among Flow, Dissolution and Precipitation in Porous Media," *AIChE J.*, Vol. 35, No. 7, 1989, pp. 1177-1185.

- Sahai, N., & Sverjensky, D. A., "GEOSURF: A Computer Program for Modeling Adsorption on Mineral Surfaces from Aqueous Solution," *Computers and Geosciences*, Vol. 24, No. 9, 1998, pp. 853–873.
- Schechter, R. S., & Gidley, J. L., "The Change in Pore Size Distribution from Surface Reactions in Porous Media," *AIChE Journal*, Vol. 15, No. 3, May 1969, pp. 339–350.
- Schneider, G. W., "A Geochemical Model of the Solution-Mineral Equilibria Within a Sandstone Reservoir," M.S. Thesis, The University of Oklahoma, 1997, 157 p.
- Scott, A. R., "Organic and Inorganic Geochemistry, Oil-Source Rock Correlation, and Diagenetic History of the Permian Spraberry Formation, Jo Mill Field, Northern Midland Basin, West Texas," M.S. Thesis, Sul Ross State University, Alpine, Texas, 1988.
- Sears, S. O., & Langmuir, D., "Sorption and Mineral Equilibria Controls on Moisture Chemistry in a C-Horizon Soil," *Journal of Hydrology*, Vol. 56, 1982, pp. 287–308.
- Shaughnessy, C. M., & Kline, W. E., "EDTA Removes Formation Damage at Prudhoe Bay," SPE 11188 paper, presented at the SPE Annual Technical Conference and Exhibition, New Orleans, Louisiana, September 26–29, 1982.
- Shaughnessy, C. M., & Kline, W. E., "EDTA Removes Formation Damage at Prudhoe Bay," *Journal of Petroleum Technology*, October 1983, pp. 1783–1792.
- Steefel, C. I., & Lasaga, A. C., "Evolution of Dissolution Patterns-Permeability Change Due to Coupled Flow and Reaction," *Chemical Modeling of Aqueous Systems II*, Chapter 16, pp. 212–225, D.C. Melchior & R. L. Basset (Eds.), ACS Symposium Series 416, American Chemical Society, Washington, DC, 1990.
- Stumm, W., & Morgan, J. J., *Aquatic Chemistry: Chemical Equilibria and Rates in Natural Waters*, John Wiley and Sons, New York, New York, 1996.
- Todd, A. C., & Yuan, M. D., "Barium and Strontium Sulfate Solid Solution Formation in Relation to North Sea Scaling Problems," SPE 18200 paper, Proceedings of the Society of Petroleum Engineers 63rd Annual Technical Conference and Exhibition, Houston, Texas, October 2–5, 1988, pp. 193–198.
- Walsh, M. P., Lake, L. W., & Schechter, R. S., "A Description of Chemical Precipitation Mechanisms and Their Role in Formation Damage During Stimulation by Hydrofluoric Acid," *Journal of Petroleum Technology*, September 1982, pp. 2097–2112.
- Warren, E. A., & Curtis, C. D., "The Chemical Composition of Authigenic Illite Within Two Sandstone Reservoirs as Analysed by TEM," *Clay Minerals*, Vol. 24, 1989, pp. 137–156.

- Westall, J. C., "Reactions at the Oxide-Solution Interface: Chemical and Electrostatic Models," in *Geochemical Processes at Mineral Surfaces*, Davis, J. A. & Hayes, K. F. (Eds.), ACS, Washington, 1986, pp. 54–78.
- Yates, D. E., Levine, S., & Healy, T. W., "Site-Binding Model of the Electrical Double Layer at the Oxide/Water Interface," *Journal of the Chemical Society Faraday Transactions I*, Vol. 70, 1974, pp. 1807–1818.
- Yeboah, Y. D., Somuah, S. K., & Saeed, M. R., "A New and Reliable Model for Predicting Oilfield Scale Formation," SPE 25166 paper, Proceedings of the SPE International Symposium on Oilfield Chemistry, New Orleans, Louisiana, March 2–5, 1993, pp. 167–176.

Chapter 14

Formation Damage by Organic Deposition

Summary

Paraffins, asphaltenes, and resins are the typical sources of organic deposition in wells, pipelines, and reservoir formation, during petroleum production. As a generic term, wax refers to deposits of paraffins, asphaltenes, and resins, mixed with some inorganic matter, such as clays, sand, and other debris. Organic deposition can occur both on the surfaces of well tubing and formation pores to reduce the flow efficiency and eventually to clog the flow paths completely.

This chapter presents a review of the thermodynamic and physico-chemical foundations of organic precipitation and scale formation as well as the governing phase behavior and rate equations. The criteria for precipitation is derived. The multi-phase formation damage model developed in a previous chapter is modified to accommodate organic precipitation at below and above bubble point conditions. The models available in the literature for prediction of formation damage by organic deposition are reviewed. Applications are presented for the formation damage in reservoirs.

Introduction

Organic scaling can be classified in two groups: (1) natural and (2) induced (Houchin and Hudson, 1986; Amaefule et al., 1988). Invasion of the near-wellbore formation by high pH filtrates, and injecting low surface tension fluids, such as light paraffins including pentane, hexane, diesel, gasoline, and naphta, and gas condensates into reservoirs can cause asphaltene precipitation (Amaefule et al., 1988). Asphaltenic/paraffinic sludges can be formed with the spent acid at low pH conditions that can be created during acidizing (Amaefule et al., 1988). Whereas, paraffins deposit primarily by cooling.

Generally, the organic deposits encountered along the production string and surface facilities contain larger proportions of paraffins, some asphaltenes and resins co-precipitated with the paraffins, some oil trapped within the deposits, and various inorganic substances, including clays, sand, and other materials (Khalil et al., 1997). The paraffin deposition primarily occurs by temperature decrease, whereas asphaltene and resin deposition occur because of a number of complicated phenomena, including the polydispersivity, steric colloid formation, aggregation, and electrokinetic deposition processes (Mansoori, 1997).

Leontaritis et al. (1992) state: "Probable causes of asphaltene flocculation are: (1) Drop in the reservoir pressure below the pressure at which asphaltenes flocculate and begin to drop out; (2) Mixing of solvents CH_4 , CO_2 with reservoir oil during EOR. . . . After flocculation asphaltenes exhibit an intrinsic change, which is usually positive. As a result, they show a strong tendency to attach to negatively charged surface, such as clays and sand."

As the wells in asphaltenic reservoirs are produced, the organic deposition begins within the upper section of the wells over which the pressure drops to below the asphaltene flocculation pressure, and then the organic deposition zone gradually progresses toward the bottom hole and eventually enters the near wellbore formation (Minssieux, 1997). Especially, the reservoir formations containing clays of large specific surfaces, such as Kaolinite, can initially adsorb and retain the polar asphaltenes and resins rapidly (Minssieux, 1997). As a result, multi-layer molecular deposits are formed over the pore surface (Acevedo, 1995). However, as the asphaltene precipitates suspended in the oil phase combine and form sufficiently large aggregates, these particles cannot pass through and are captured at the pore throats (Minssieux, 1997). The pore throat plugging causes the severest permeability loss because the gates connecting the pores are closed and/or an in-situ cake is formed by pore filling if the plugged pore throat still allows some flow through the jammed particles. Simultaneously, the flow is diverted toward larger flow paths (Wojtanowicz et al., 1987, 1988; Civan, 1995; Chang and Civan, 1997; Minssieux, 1997). "Organic deposits usually seal the flow constrictions because they are sticky and deformable. Therefore, the conductivity of a flow path may diminish without filling the pore space completely" (Civan, 1994, 1995).

Leontaritis (1998) stresses that the organic damage in oil reservoirs is primarily caused by asphaltene deposition and the region of asphaltene deposition may actually extend over large distances from the wellbore, especially during miscible recovery. Whereas, the organic damage caused by wax deposition is rather limited to a short distance (0 to 1 feet) from the wellbore, because wax deposition in the near wellbore region usually

occurs by the cooling of the oil caused either by high perforation pressure losses during oil production or by invasion and cooling of the hot oil saturated with the wax dissolved from the well walls as a result of the overbalanced, hot oiling treatments of the wells.

The decline of productivity of wells in asphaltenic reservoirs is usually attributed to the reduction of the effective mobility of oil by various factors (Amaefule et al., 1988; Leontaritis et al., 1992; Leontaritis, 1998). The effective mobility of oil is a convenient measure of oil flow capability because it combines the three relevant properties in one group as:

$$\lambda_0 = kk_{r0}/\mu_0 \quad (14-1)$$

where k is the permeability of the reservoir formation and k_{r0} and μ_0 are the relative permeability and viscosity of the oil, respectively. Hence, Leontaritis (1998) states that the asphaltene induced damage can be explained by three mechanisms. The first is the increase of the reservoir fluid viscosity by formation of a water-in-oil emulsion if the well is producing oil and water simultaneously. The oil viscosity may also increase by the increase of the asphaltene particle concentration in the near wellbore region as the oil converges radially toward the wellbore. But, experimental measurements indicate that the viscosity increase by asphaltene flocculation is negligible. The second mechanism is the change of the wettability of the reservoir formation from water-wet to oil-wet by the adsorption of asphaltene over the pore surface in the reservoir formation. However, this phenomenon is less likely because, usually, the asphaltenic reservoir formations are already mixed-wet or oil-wet, due to the fact that asphaltenes have already been adsorbed over the pore surface during the long periods of geological times prior to opening the wells for production. The third and most probable mechanism is the impairment of the reservoir formation permeability by the plugging of the pore throats by asphaltene particles.

The problems associated with organic deposition from the crude oil can be avoided or minimized by choosing operating conditions such that the reservoir oil follows a thermodynamic path outside the deposition envelope and, therefore, the deposition envelope concept can provide some guidance in this respect (Leontaritis et al., 1992). However, mathematical models implementing the deposition phase charts are also necessary in developing optimal strategies for optimal mitigation of the deposition problems during the exploitation of the petroleum reservoirs.

In the following sections, the characteristics, adsorption and phase behavior, and deposition and formation damage modeling of organic precipitates are presented.

Characteristics of Asphaltenic Oils

As indicated by Figure 14–1 by Philp et al. (1995), the boiling and melting points of hydrocarbons increase by the carbon number. Heavy crude oils contain large quantities of higher boiling components, which create problems during oil production (Speight, 1996). Speight and Long (1996) point out that chemical and physical alteration of oils may affect the dispersibility and compatibility of their higher molecular weight fractions and create various problems, such as phase separation, precipitation and sludge formation during the various phases of petroleum production, transportation, and processing.

Speight (1996) classified the constituents of the crude oil into four hydrocarbon groups: (1) volatile saturates (paraffins) and aromatics, (2) nonvolatile saturates (waxes) and aromatics, (3) resins, and (4) asphaltenes. Speight (1996) explains that the nomenclature of the petroleum fractions, such as given in Figure 14–2, is based on the techniques of separation of the crude oil into its fractions. Figure 14–3 by Leontaritis (1997) describes the various steps and techniques involved

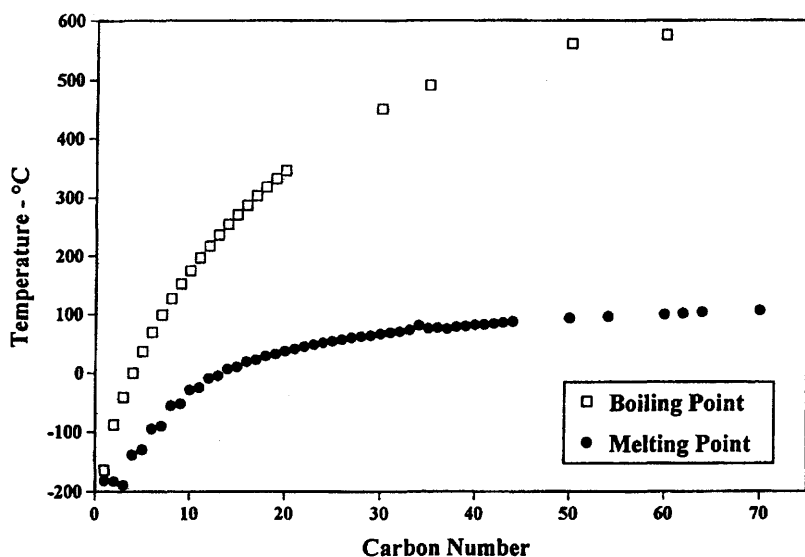


Figure 14–1. Effect of *n*-alkane carbon number on boiling and melting point temperatures (after Philp, R. P., Bishop, A. N., Del Rio, J.-C., and Allen, J., Cubitt, J. M., and England, W. A. (eds.), Geological Society Special Publication No. 86, pp. 71–85, ©1995; reprinted by permission of R. P. Philp and the Geological Society Publishing House).

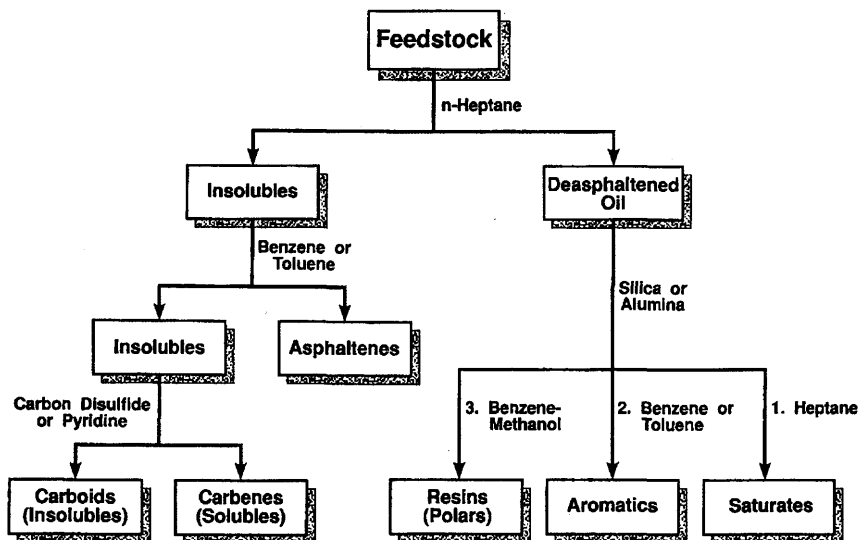


Figure 14–2. Classification of petroleum constituents based on laboratory fractionation (reprinted from *Journal of Petroleum Science and Engineering*, Vol. 22, Speight, J. G., “The Chemical and Physical Structure of Petroleum: Effects on Recovery Operations,” pp. 3–15, ©1999, with permission from Elsevier Science).

in the analysis of the crude oil, including cryoscopic distillation (CD), solvent extraction (SE), gas chromatography (GC), high performance liquid chromatography (HPLC), and gel permeation chromatography (GPC). Table 14–1 by Srivastava and Huang (1997) presents data on the chemical and physical properties of typical oil samples taken from Weyburn wells.

Leontaritis (1996, p. 14)* described the heavy fractions of petroleum as following:

Asphaltenes:

Highly condensed polyaromatic structures or molecules, containing heteroatoms (i.e., S, O, N) and metals (e.g., Va, Ni), that exist in petroleum in an aggregated state in the form of suspension and are surrounded and stabilized by resins (i.e., peptizing agents). They are known to carry an electrical charge, and thought to be polydisperse. Asphaltenes are a solubility class, hence, they are not pure, identical molecules. Pentane and Heptane are the two most frequently used solvents for separating asphaltenes from crude oil. The prefix *n*-Pentane or *n*-Heptane asphaltenes refers to the solvent used for

* Reprinted from Leontaritis ©1996, p. 14, by courtesy of Marcel Dekker, Inc.

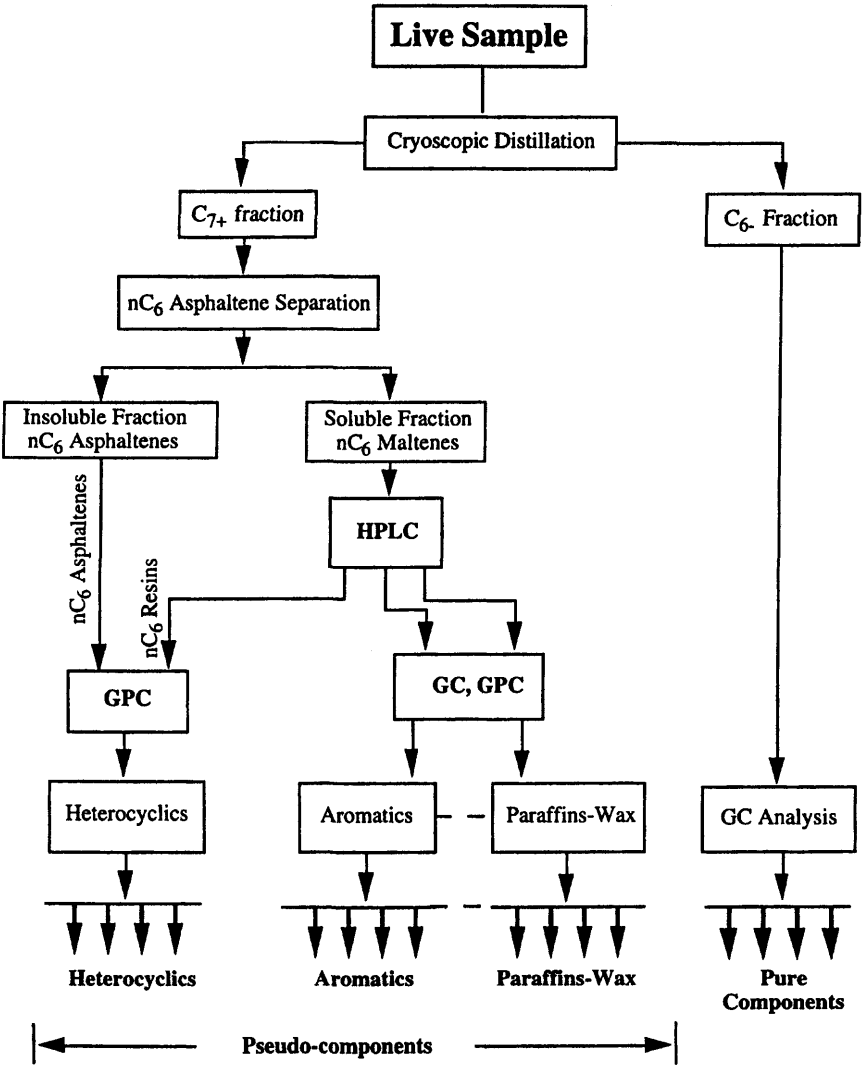


Figure 14-3. Steps of oil analysis and characterization for paraffin, aromatic, resin, and asphaltene (after Leontaritis, ©1997 SPE; reprinted by permission of the Society of Petroleum Engineers).

Table 14-1
Chemical and Physical Properties of Weyburn Dead Oils*

Temperature °C	Oil W1 ^a		Oil W2 ^b		Oil W3 ^c	
	Density kg/m ³	Viscosity mPa·s	Density kg/m ³	Viscosity mPa·s	Density kg/m ³	Viscosity mPa·s
15	878.9	-	854.9	-	869.2	11.76
20	875.9	12.8	842.4	4.60	864.4	9.40
59	846.1	4.2	-	-	-	-
61	-	-	813.1	2.35	-	-
63	-	-	-	-	839.4	3.15
Pressure MPa	Density @59°C ^d	Viscosity @59°C ^d	Density @61°C ^d	Viscosity @61°C ^d	Density @63°C ^d	Viscosity @63°C ^d
0.1	846.1	4.2	813.1	2.35	839.4	3.15
3.54	849.2	-	816.4	2.49	842.4	3.26
6.99	852.4	-	819.6	2.62	845.2	3.37
10.44	858.0	-	822.9	2.76	848.4	3.49
17.33	860.9	-	829.3	3.04	854.7	3.71
BS&W, vol %		0.1	0.2		0.5%	
Molecular Weight, g/g-mol		230	203		215	
Component	wt. %		wt. %		wt. %	
Saturates	48.5		55.3		48.4	
Aromatics	33.5		31.1		33.5	
Resins	13.2		9.6		13.2	
Asphaltenes	4.8		4.0		4.9	

^a Collected from Weyburn well 14-17-6-13 W2M

^b Collected from Weyburn well 3-11-7-13 W2M

^c Collected from Weyburn well Hz 12-18-6-13 W2M

^d Reservoir temperature for the oil samples

* Srivastava and Huang, ©1997 SPE; reprinted by permission of the Society of Petroleum Engineers.

their separation. The composition of *n*-Pentane asphaltenes is different from that of *n*-Heptane asphaltenes.

Resins:

Aromatic and polar molecules, also often containing heteroatoms and metals, that surround the asphaltene structures and are dissolved in the oil and help keep the asphaltenes in suspension. They are surface active and, at some thermodynamic states, form their own reversible micelles. They are polydisperse and have a range of polarity and aromaticity. Resins are considered to be pre-cursors to asphaltenes.

Paraffin Waxes:

Primarily aliphatic hydrocarbons (both straight and branched chain) that change state from liquid to solid during conventional oil production and processing operations. In addition to aliphatics, field deposits usually contain aromatic, naphthenic, resin, and asphaltenic molecules as well. The combined mass is called *wax*. Paraffin waxes usually melt at about 110°–160°F. Field waxes contain molecules that can have melting points in excess of 200°F.

Asphalt:

The residual (non-distillable) fraction of crude oil that contains suspended asphaltenes, resins, and the heaviest aromatic and paraffinic components of oils. Propane has been traditionally a very efficient and convenient solvent for separating asphalt from petroleum. Although, the latest commercial processes use other more efficient solvents for asphalt separation.

Leontaritis (1997) describes that: “Since waxes, asphaltenes and most resins are solid in their pure form and the other oil molecules are in liquid form, the overall crude oil mixture is a liquid solution of waxes, asphaltenes, and resins in the remaining liquid oil. . . . In general, the waxes and resins are dissolved in the overall crude oil. Whereas the asphaltenes are mostly undissolved in colloidal state.”

Anderson et al. (1997) state: “Petroleum asphaltenes are defined as the solids precipitating from a crude oil upon addition of an excess of a light hydrocarbon solvent, in general *n*-heptane or *n*-pentane.” Therefore, for practical purposes, the crude oil is considered in two parts. The first part consists of the high boiling-point and polar asphaltic components. This fraction of the crude oil creates various deposition problems during the exploitation of petroleum reservoirs. The second part is the rest of the crude oil, referred to as the deasphalted oil or the maltenes. This fraction of the crude oil acts as a solvent and maintains a suspension of the asphaltenes in oil as illustrated in Figure 14–4 by Leontaritis (1996). However, ordinarily, the asphaltenes do not actually disperse in the maltene unless some resins are also present in the crude oil. The resins help asphaltenes to disperse in oil as a suspension by means of the hydrogen-bonding process and the irreversible acid-base reactions of the asphaltene and resin molecules (Speight, 1996; Speight and Long, 1996; Chang and Fogler, 1994, 1996). Therefore, Leontaritis et al. (1992) point out that: “An oil that contains asphaltenes will not necessarily cause asphaltene problems during recovery and processing.” Leontaritis et al. (1992) draw attention to the fact that the Boscan crude of Venezuela has not created any asphaltene problems, although it has a large fraction (over

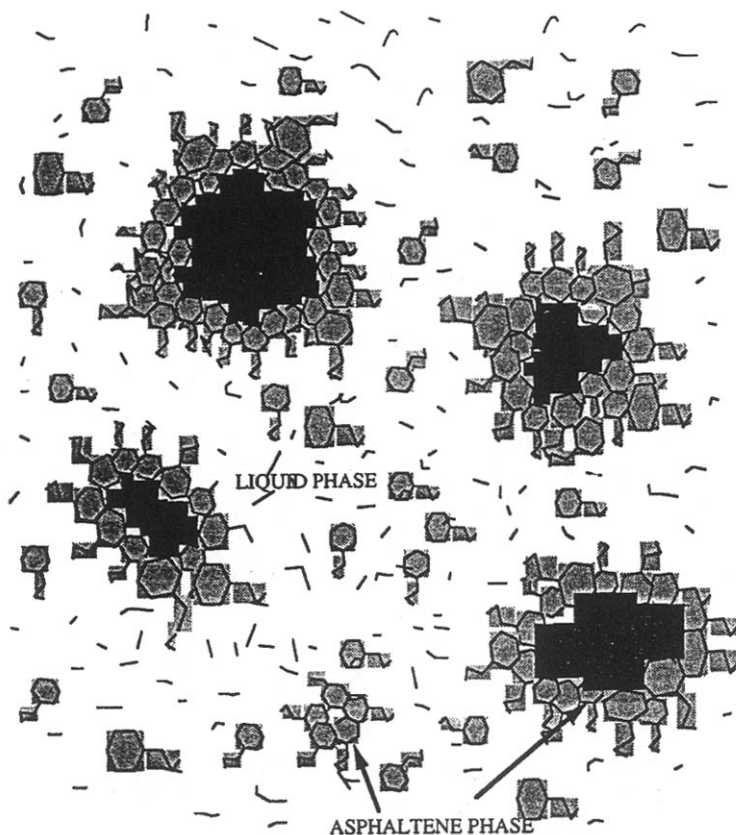


Figure 14-4. A proposed model for asphaltenic oils (after Leontaritis, ©1996; reprinted by courtesy of Marcel Dekker, Inc.).

17% by weight) of asphaltenes (Lichaa, 1977). Whereas, the Hassi-Messaoud oil has created severe asphaltene problems, although it has only a small fraction (0.1% by weight) of asphaltenes (Haskett and Tartera, 1965). In fact, de Boer et al. (1995) have concluded that light to medium crudes containing small amounts of asphaltenes may create more asphaltene precipitation problems during primary production. Nghiem and Coombe (1997) explain: "Heavier crudes that contain a larger amount of asphaltene have very little asphaltene precipitation problems as they can dissolve more asphaltene." Leontaritis et al. (1992) state that: "Asphaltene flocculation can be prevented by addition of resins and aromatics." The investigations of Chang and Fogler (1994, 1997) using model chemicals for resins have verified this statement.

Leontaritis (1996, p. 13) describes that “. . . asphaltene particles or micelles aggregate or flocculate into larger aggregates or flocs. . . . Asphaltene flocculation can be both reversible and irreversible. . . . Paraffin waxes, on the other the hand, . . . exhibit the phenomenon of crystallization. . . . Wax crystallization is generally a reversible process. However, paraffin waxes more than often precipitate together with resins and asphaltenes (which are said to be responsible for the observed irreversible thermodynamic phenomena). Hence, some wax precipitation is occasionally reported as irreversible.” Leontaritis (1996) points out that temperature and composition have a large affect and pressure has a small affect on the solubility of wax in oil. Leontaritis (1996) explains that the behavior of wax in oils can be determined by means of the cloud and pour points.

Ring et al. (1994) defined the cloud point as “the equilibrium temperature and pressure at which solid paraffin crystals begin to form in the liquid phase.” Leontaritis (1996) states: The “pour point is defined as the lowest temperature at which the fuel will pour and is a function of the composition of the fuel.”

Mechanisms of the Heavy Organic Deposition

In this section, the mechanisms of the heavy organic deposition according to Mansoori (1997) are described. Mansoori (1997) states that organic deposition during petroleum production and transportation may occur by one or several of the following four mechanisms:

1. *Polydispersivity effect.* As depicted in Figure 14–5 by Mansoori (1997), a stable state of a polydispersed oil mixture can be attained for a certain proper ratio of the polar to nonpolar and the light to heavy constituents in the crude oil at given temperature and pressure conditions. Thus, when the composition, temperature, or pressure are varied, the system may become unstable and undergo several processes. Figure 14–6 by Mansoori (1997) depicts the formation of micelle-type aggregates of asphaltene when polar miscible compounds are added into the system. Figure 14–7 by Mansoori (1997) describes the separation of the asphaltenes as a solid aggregate phase when more paraffinic hydrocarbons are added into the system.
2. *Steric colloidal effects.* At high concentrations, asphaltenes tend to associate in the form of large particles, as depicted in Figure 14–8 by Mansoori (1997). In the presence of some peptizing agents, such as resins, these particles can adsorb the peptizing agents and become suspended in the oil.



Figure 14-5. Heavy organics in petroleum crude (straight/curved line = paraffin molecules, solid ellipse = aromatic molecules, open ellipse = resin molecules, and solid blocky forms = asphaltene molecules) (reprinted from *Journal of Petroleum Science and Engineering*, Vol. 17, Mansoori, G. A., "Modeling of Asphaltene and Other Heavy Organic Depositions, pp. 101–111, ©1997, with permission from Elsevier Science; after Mansoori ©1994 SPE; reprinted by permission of the Society of Petroleum Engineers).

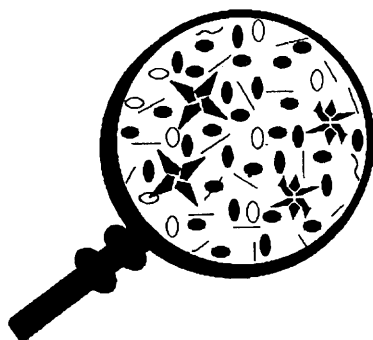


Figure 14-6. Colloidal phenomenon activated by addition of a polar miscible solvent (solid ellipse = an aromatic hydrocarbon) (reprinted from *Journal of Petroleum Science and Engineering*, Vol. 17, Mansoori, G. A., "Modeling of Asphaltene and Other Heavy Organic Depositions, pp. 101–111, ©1997, with permission from Elsevier Science).

3. *Aggregation effect.* When the concentration of the peptizing agent is low and its adsorbed quantity is not sufficient to occupy the particle surface completely, several particles can combine to form bigger particles as depicted in Figure 14-9 by Mansoori (1997). This phenomenon is called flocculation. When the particles become



Figure 14-7. Flocculation and precipitation of heavy components by addition of a non-polar miscible solvent (dashed line = a paraffin hydrocarbon) (reprinted from *Journal of Petroleum Science and Engineering*, Vol. 17, Mansoori, G. A., "Modeling of Asphaltene and Other Heavy Organic Depositions, pp. 101–111, ©1997, with permission from Elsevier Science; after Mansouri ©1994 SPE; reprinted by permission of the Society of Petroleum Engineers).



Figure 14-8. Steric colloidal phenomenon activated by addition of paraffin hydrocarbons (reprinted from *Journal of Petroleum Science and Engineering*, Vol. 17, Mansoori, G. A., "Modeling of Asphaltene and Other Heavy Organic Depositions, pp. 101–111, ©1997, with permission from Elsevier Science; after Mansouri ©1994 SPE; reprinted by permission of the Society of Petroleum Engineers).

sufficiently large and heavy, they tend to deposit out of the solution as depicted in Figure 14-10 by Mansoori (1997).

4. *Electrokinetic effect.* As explained by Mansoori (1997), during the flow of oil through porous media and pipes, a "streaming current" and a potential difference are generated because of the migration

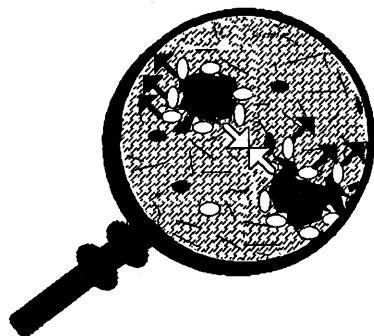


Figure 14-9. Migration of peptizing molecules (solid arrows) by change of chemical potential balance (reprinted from *Journal of Petroleum Science and Engineering*, Vol. 17, Mansoori, G. A., "Modeling of Asphaltene and Other Heavy Organic Depositions, pp. 101–111, ©1997, with permission from Elsevier Science; after Mansouri ©1994 SPE; reprinted by permission of the Society of Petroleum Engineers).



Figure 14-10. Flocculation and deposition (big arrow) of large heavy organic particles (reprinted from *Journal of Petroleum Science and Engineering*, Vol. 17, Mansoori, G. A., "Modeling of Asphaltene and Other Heavy Organic Depositions, pp. 101–111, ©1997, with permission from Elsevier Science; after Mansouri ©1994 SPE; reprinted by permission of the Society of Petroleum Engineers).

of the charged particles of the asphaltene colloids. The asphaltene particles are positively charged but the oil phase is negatively charged, as depicted in Figure 14-11 by Mansoori (1997). Therefore, the negative upstream and positive downstream potentials are generated along the pipe to resist the flow of the colloidal particles, as

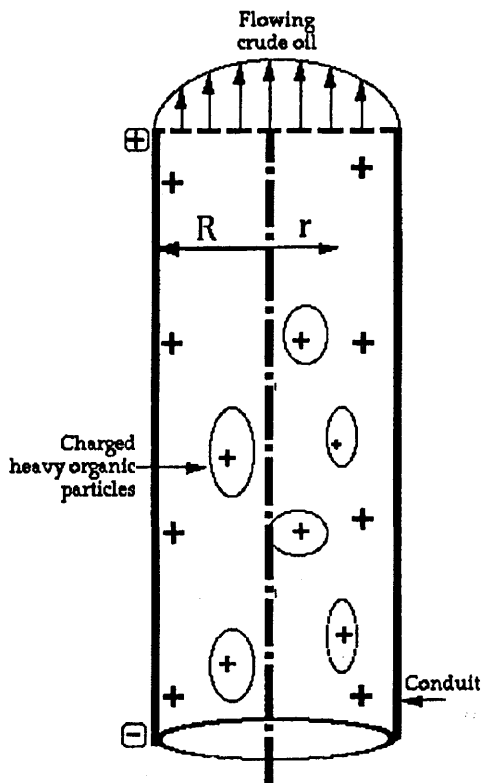


Figure 14-11. Streaming potential generated by oil flow in a pipe (reprinted from *Journal of Petroleum Science and Engineering*, Vol. 17, Mansoori, G. A., "Modeling of Asphaltene and Other Heavy Organic Depositions, pp. 101-111, ©1997, with permission from Elsevier Science; after Mansoori ©1994 SPE; reprinted by permission of the Society of Petroleum Engineers).

depicted in Figure 14-12 by Mansoori (1997). This, in turn, induces a back diffusion of the colloidal asphaltene particles. Mansoori (1997) points out that the deposition of the polar, asphaltene by the electrokinetic effect and the non-polar paraffins by the dynamic pour point crystallization effect, could occur simultaneously when the oil contains both asphaltenes and paraffins.

Asphaltene and Wax Phase Behavior and Deposition Envelopes

In this section, a brief summary of the review of the asphaltene and wax phase behavior by Leontaritis (1996) is presented.

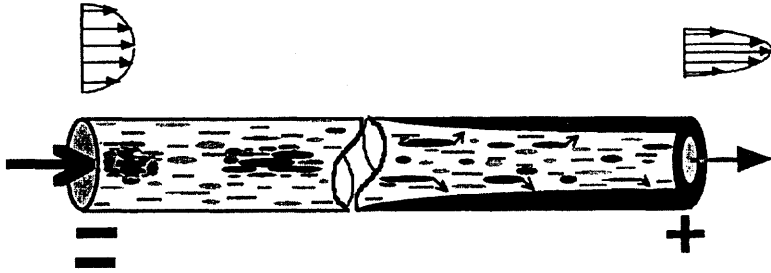


Figure 14-12. Electrokinetic deposition in a pipeline (reprinted from *Journal of Petroleum Science and Engineering*, Vol. 17, Mansoori, G. A., "Modeling of Asphaltene and Other Heavy Organic Depositions, pp. 101–111, ©1997, with permission from Elsevier Science).

Accurate measurement of the asphaltene and wax phase behavior is expensive and requires sophisticated techniques for proper handling of the reservoir fluid samples and laboratory testing of the recombined reservoir fluids. Therefore, Leontaritis (1996) suggests that phase diagrams can be more economically and rapidly developed by simulation with a limited number of actual data required for tuning and calibration. Leontaritis (1996) demonstrated this exercise by applying the Thermodynamic-Colloidal model by Leontaritis (1993). Nghiem and Coombe (1997) state: "Above the saturation pressure, the precipitation is solely due to pressure, while below the saturation both pressure and composition affect the precipitation behavior." However, more research is needed in this area.

Leontaritis (1996) points out that wax crystallization and asphaltene flocculation phenomena occur at low and high temperatures, respectively. Then, he hypothesizes that these two phenomena should, therefore, represent the two extreme cases of the phase behavior and there should be continuously varying intermediate phase behavior in between these two extremes depending on the composition of the heavy fractions of the crude oils, as schematically shown in Figure 14-13 by Leontaritis (1996). Although it sounds reasonable and there is some evidence of support for this hypothesis, more research is obviously needed to verify this hypothesis.

The schematic Figures 14-14 and 14-15 by Leontaritis (1996) depict the features of typical asphaltene and wax deposition envelopes, respectively. As explained by Leontaritis (1996), the phase diagrams of the asphaltenic fluids typically do not have a critical point, because the asphaltenic fluids can only have bubble-point lines and no dew-point lines, as they cannot vaporize. Leontaritis (1996, 1998) refers to the locus of the thermodynamic conditions for asphaltene flocculation as the

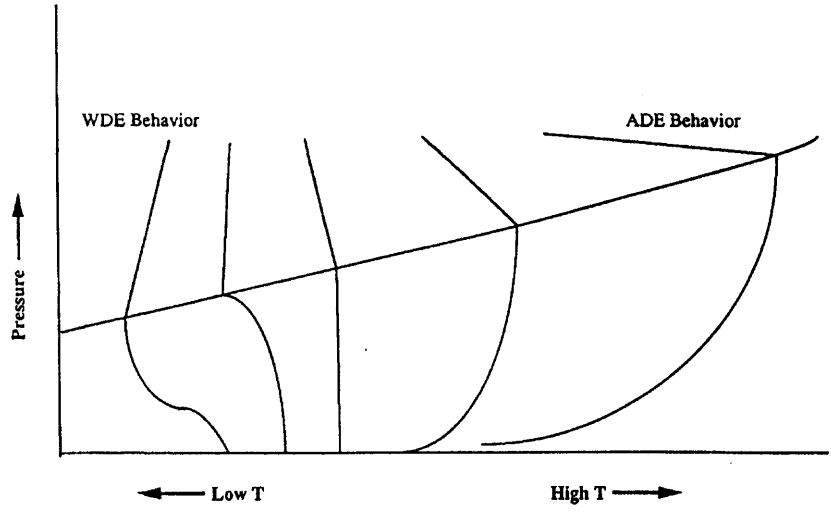


Figure 14-13. Unification of the wax deposition envelope (WDE) and the asphaltene deposition envelope (ADE) (after Leontaritis, ©1996; reprinted by courtesy of Marcel Dekker, Inc.).

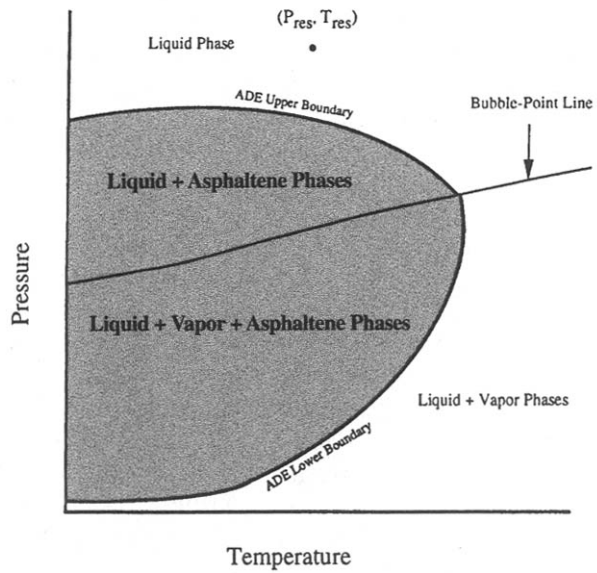


Figure 14-14. Typical asphaltene deposition envelope (ADE) (after Leontaritis, ©1996; reprinted by courtesy of Marcel Dekker, Inc.).

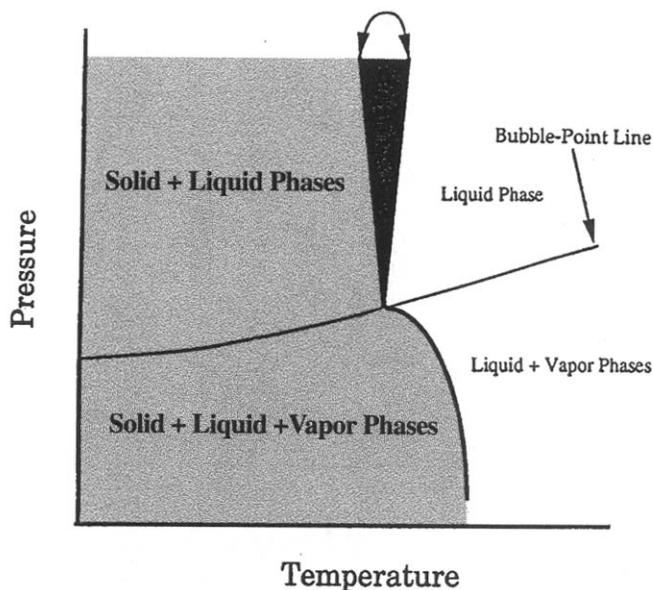
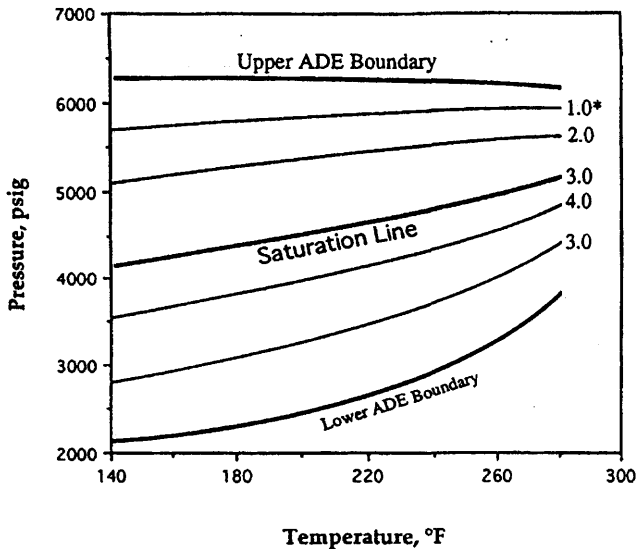


Figure 14-15. Typical wax deposition envelope (WDE) (after Leontaritis, ©1996; reprinted by courtesy of Marcel Dekker, Inc.).

Asphaltene-Deposition-Envelope (ADE), as shown in Figure 14-14. Typically, the pressure-temperature phase diagrams of the asphaltenic oils are characterized by several phase quality lines and a saturation (bubble-point) line in between the upper and lower boundaries of the asphaltene deposition envelope as indicated on Figure 14-16 by Leontaritis (1996) for a South-American oil. Leontaritis (1996) estimated the intersection of the upper ADE with the bubble-point line at around 370°F for this oil. Figures 14-17 through 14-19 by Leontaritis (1996) are typical simulated charts showing the asphaltene deposition envelope, the asphaltene phase volume versus temperature, and the asphaltene phase volume versus pressure for a North-American oil, respectively.

Leontaritis (1996) refers to the locus of the thermodynamic conditions for wax crystallization as the Wax-Deposition-Envelope (WDE). The sketch of a typical Wax-Deposition-Envelope is given in Figure 14-15 by Leontaritis (1996). Figures 14-20 and 14-21 by Leontaritis (1996) depict the affect of the light-ends and the pressure-temperature relationship on the onset of wax crystallization (cloud point) of oils. The affect of the pressure on the onset of wax crystallization is demonstrated for

(text continued on page 399)



* Mls of asphaltene phase per mole of reservoir fluid.

Figure 14-16. Asphaltene deposition envelope (ADE) for a South American reservoir oil (after Leontaritis, ©1996; reprinted by courtesy of Marcel Dekker, Inc.).

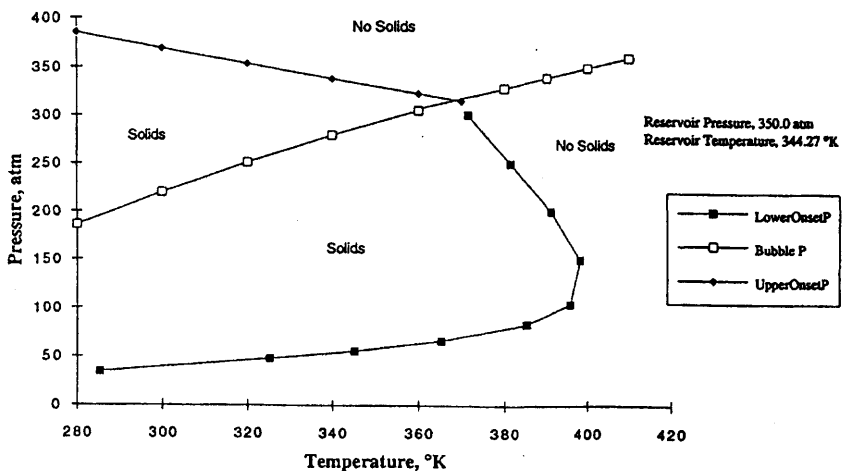


Figure 14-17. Asphaltene deposition envelope (ADE) for Asph Wax Oil Company live oil (after Leontaritis, ©1996; reprinted by courtesy of Marcel Dekker, Inc.).

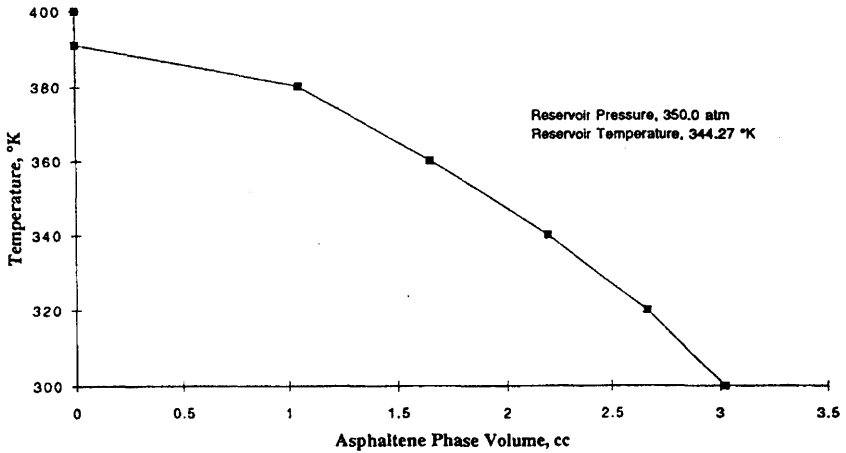


Figure 14-18. Asphaltene phase volume vs. temperature for an Asph Wax Oil Company live oil at 200 atm pressure (after Leontaritis, ©1996; reprinted by courtesy of Marcel Dekker, Inc.).

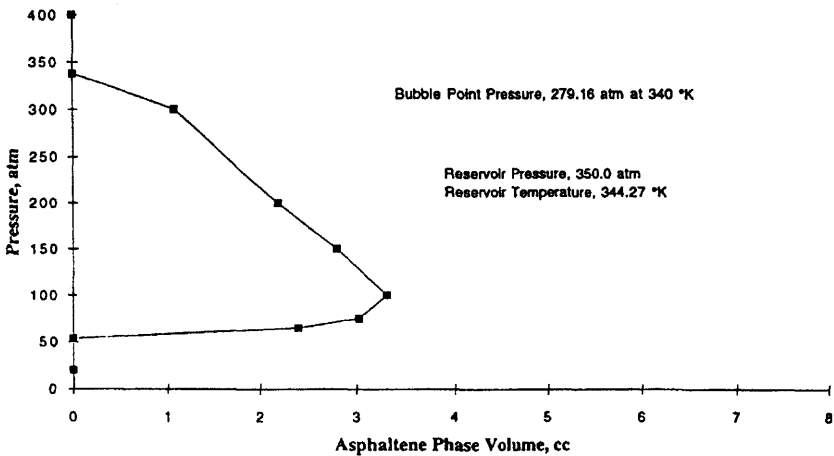


Figure 14-19. Asphaltene phase volume vs. pressure for Asph Wax Oil Company live oil at 340°K temperature (after Leontaritis, ©1996; reprinted by courtesy of Marcel Dekker, Inc.).

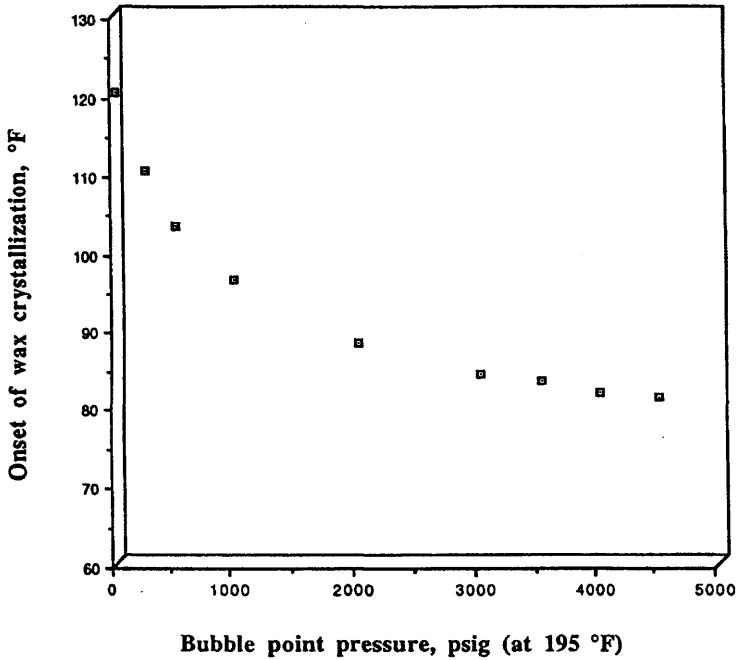


Figure 14-20. Onset of wax crystallization vs. the bubble point temperature (after Leontaritis, ©1996; reprinted by courtesy of Marcel Dekker, Inc.).

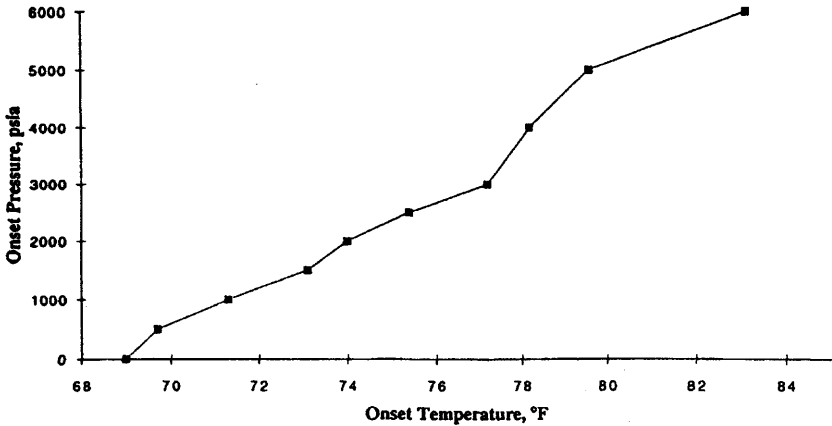


Figure 14-21. Pressure-temperature effects on onset of wax crystallization in a synthetic mixture of kerosene and candle wax (after Leontaritis, ©1996; reprinted by courtesy of Marcel Dekker, Inc.).

(text continued from page 395)

three live-oils in Figure 14-22 by Leontaritis (1996). The typical Wax-Deposition-Envelope of a North American recombined live oil constructed by laboratory measurements is given in Figure 14-23 by Leontaritis (1996). He also developed the Wax-Deposition-Envelope given in Figure 14-24 for a North Sea live oil by using a Wax Model. Using the same Wax Model, Leontaritis (1996) has predicted the affect of temperature on the fraction of the wax crystallized at 200, 50, and 1 atm pressures as shown in Figures 14-25, 14-26, and 14-27, respectively, as well as the affect of the pressure on the fraction of the wax crystallized at 280°K as shown in Figure 14-28.

Mansoori (1997) mentions that experimental measurement of the pressure-composition phase diagrams involving heavy organic deposition by miscible gas injection, at reservoir temperatures, is very costly. Therefore, he suggested generating these charts by simulation. Figure 14-29 produced by Mansoori (1997) is an example of a typical chart for asphaltenic oils dissolving carbon dioxide. Figures 14-30 and 14-31 by Mansoori (1997) indicate the electrokinetics affect on asphaltene deposition in pipelines from typical asphaltenic oils dissolving a miscible component at various temperatures. These figures contain two charts. The upper chart shows the static onset of deposition of asphaltene on a

(text continued on page 404)

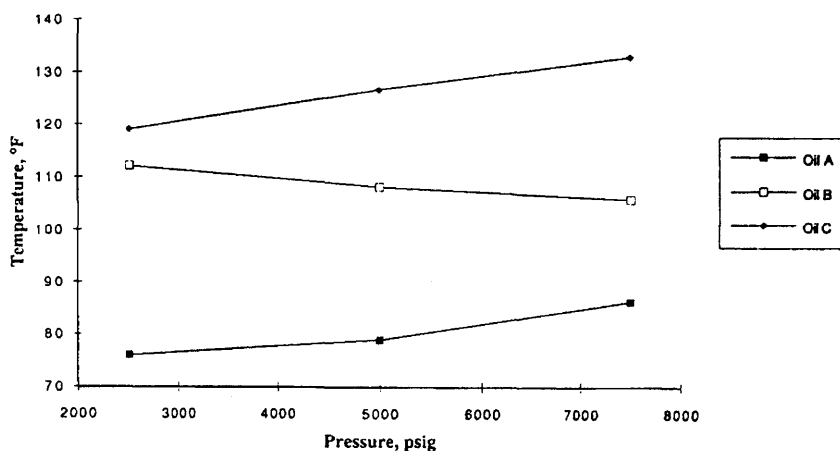


Figure 14-22. Upper wax deposition envelope boundaries for three different reservoir oils (after Leontaritis, ©1996; reprinted by courtesy of Marcel Dekker, Inc.).

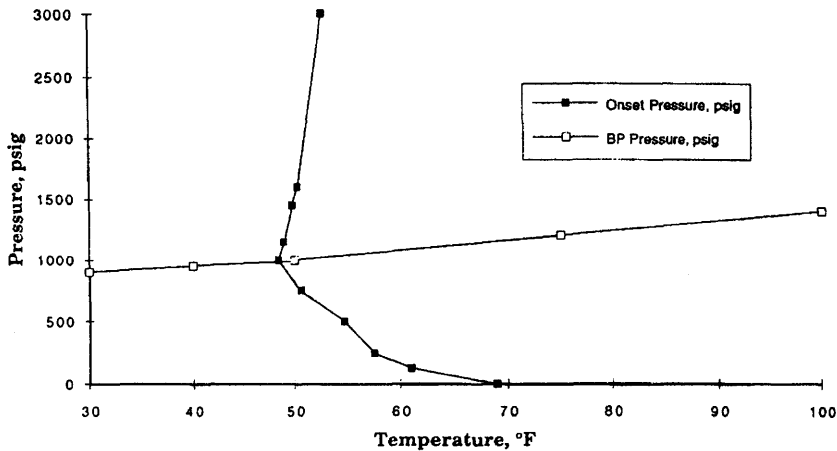


Figure 14-23. Wax deposition envelope for a North American recombined reservoir oil (after Leontaritis, ©1996; reprinted by courtesy of Marcel Dekker, Inc.).

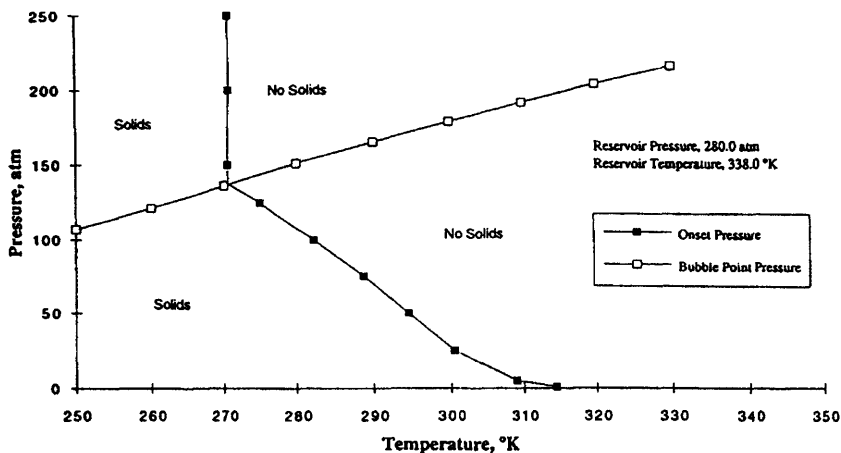


Figure 14-24. Wax deposition envelope for an Asph Wax Oil Company live oil (after Leontaritis, ©1996; reprinted by courtesy of Marcel Dekker, Inc.).

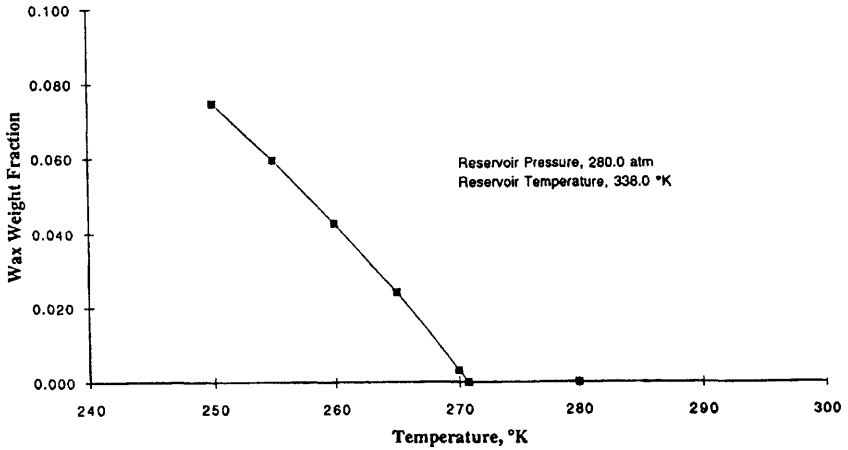


Figure 14-25. Wax weight fraction vs. temperature for an Asph Wax Oil Company live oil at 200 atm pressure (after Leontaritis, ©1996; reprinted by courtesy of Marcel Dekker, Inc.).

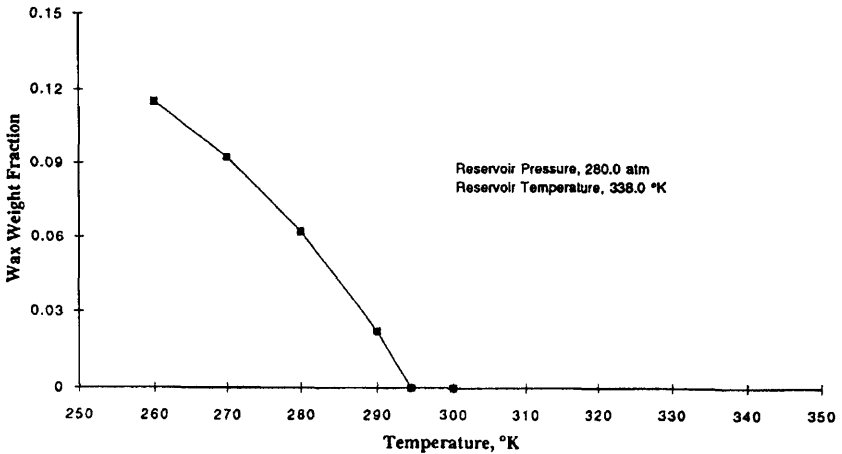


Figure 14-26. Wax weight fraction vs. temperature for an Asph Wax Oil Company live oil at 50 atm pressure (after Leontaritis, ©1996; reprinted by courtesy of Marcel Dekker, Inc.).

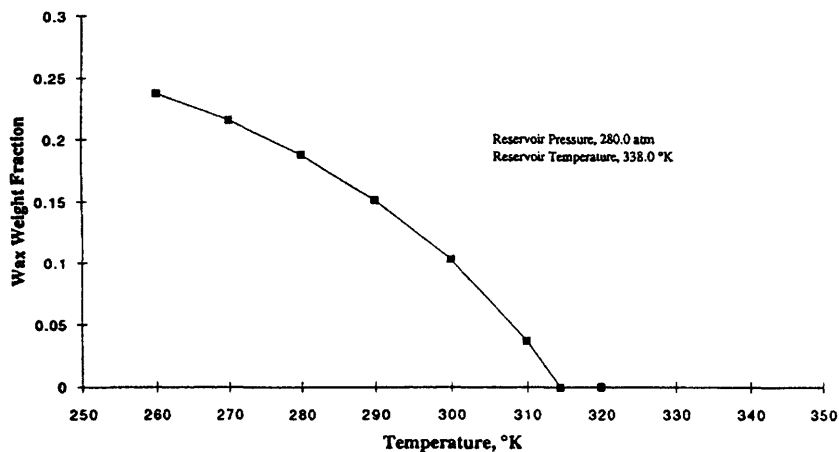


Figure 14-27. Wax weight fraction vs. temperature for an Asph Wax Oil Company stock tank oil at 1 atm pressure (after Leontaritis, ©1996; reprinted by courtesy of Marcel Dekker, Inc.).

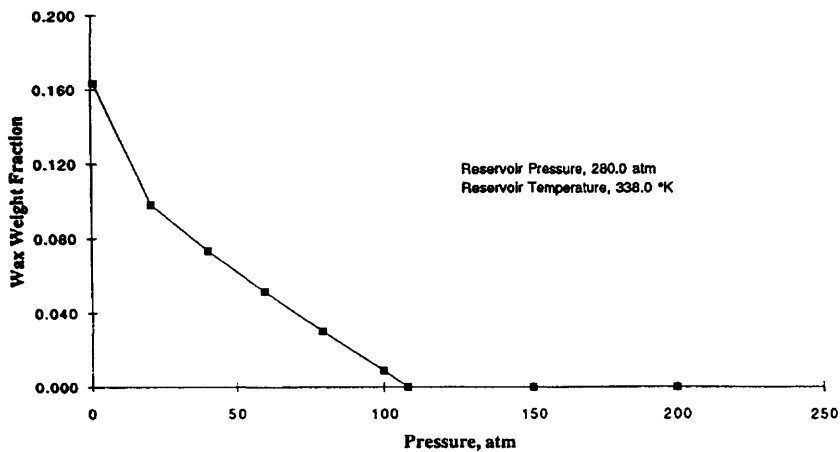


Figure 14-28. Wax weight fraction vs. pressure for an Asph Wax Oil Company live oil at 280°K temperature (after Leontaritis, ©1996; reprinted by courtesy of Marcel Dekker, Inc.).

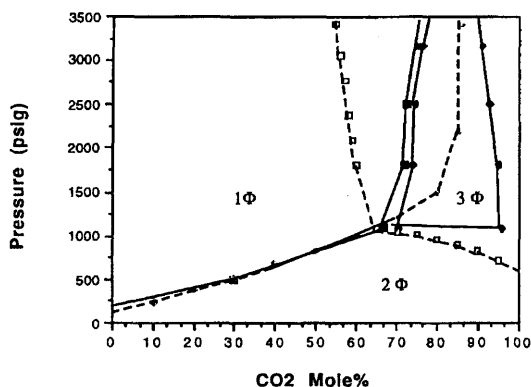


Figure 14-29. Static ($P - x$) phase diagram of a crude oil mixed with a miscible injectant (MI) at 60°F (reprinted from *Journal of Petroleum Science and Engineering*, Vol. 17, Mansoori, G. A., "Modeling of Asphaltene and Other Heavy Organic Depositions, pp. 101-111, ©1997, with permission from Elsevier Science, after Mansoori ©1994 SPE, reprinted by permission of the Society of Petroleum Engineers).

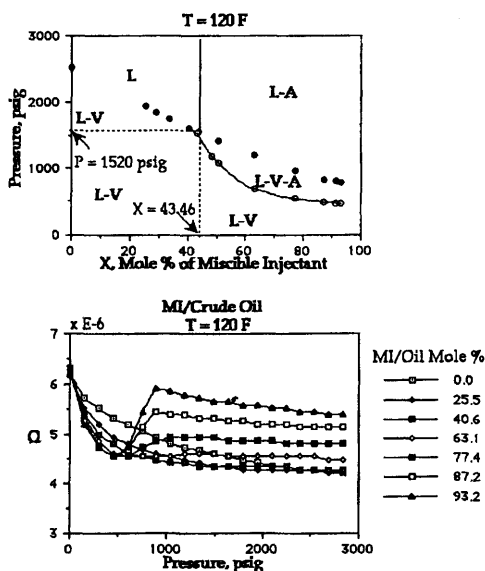


Figure 14-30. Static ($P - x$) and dynamic ($P - Q$) phase diagrams of the same crude oil in Figure 14-29, mixed with the same miscible injectant (MI) at 120°F (reprinted from *Journal of Petroleum Science and Engineering*, Vol. 17, Mansoori, G. A., "Modeling of Asphaltene and Other Heavy Organic Depositions, pp. 101-111, ©1997, with permission from Elsevier Science, after Mansoori ©1994 SPE, reprinted by permission of the Society of Petroleum Engineers).

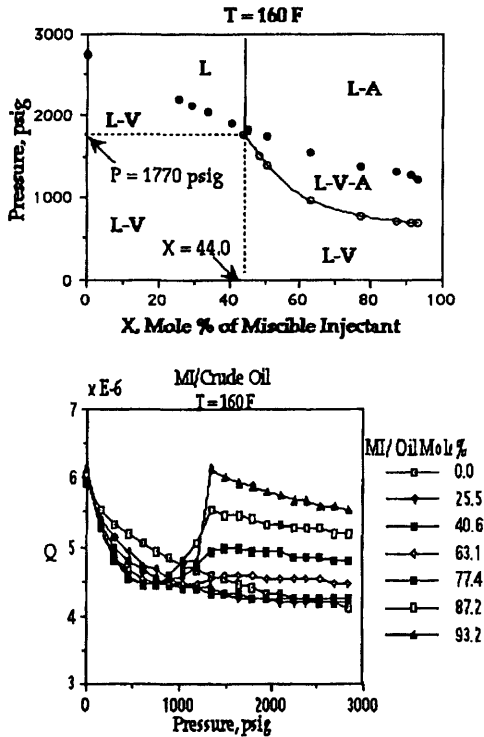


Figure 14-31. Static ($P - x$) and dynamic ($P - Q$) phase diagrams of the same crude oil in Figure 14-29, mixed with the same miscible injectant (MI) at 160°F (reprinted from *Journal of Petroleum Science and Engineering*, Vol. 17, Mansoori, G. A., "Modeling of Asphaltene and Other Heavy Organic Depositions, pp. 101-111, ©1997, with permission from Elsevier Science, after Mansoori ©1994 SPE, reprinted by permission of the Society of Petroleum Engineers).

(text continued from page 399)

pressure vs. composition relationship. The lower chart shows the dynamic, Q (defined below) versus pressure relationship for asphaltenic oils flowing in wells or pipelines for different miscible component and oil ratio. The Q function is given by (Mansoori, 1997):

$$Q = U^{1.75} d^{0.75} / k \quad (14-2)$$

in which U is the average oil velocity in the pipe, d is the pipe diameter, and k is the conductivity of the oil. The regions above and below these curves express the flow conditions leading to deposition and no deposition

of asphaltenes, respectively. Hence, these charts help determine the operating conditions of pipes to avoid precipitation.

Asphaltene Adsorption

Nonequilibrium adsorption in porous media may be described by a bilinear adsorption model according to Gupta and Greenkorn (1973), given by:

$$\frac{\partial \Gamma}{\partial t} = k_1 + k_2 c + k_3 \Gamma + k_4 c \Gamma = k_1 + k_2 c \left(1 + \frac{\Gamma}{k_2/k_4} \right) + k_3 \Gamma \quad (14-3)$$

subject to the initial condition that $\Gamma = \Gamma_0, t = 0$

At equilibrium, Eq. 14-3 becomes:

$$\frac{1}{\Gamma} \left(c - \frac{k_1}{k_2} \right) = -\frac{k_3}{k_2} - \frac{k_4}{k_2} c \quad (14-4)$$

In Eqs. 14-3 and 4, t is time, Γ is the concentration of species adsorbed in porous media, c is the concentration of the species in solution, and k_1, k_2, k_3 , and k_4 are some empirical coefficients.

Manoranjana and Stauffer (1996) used simplified forms of Eqs. 14-3 and 4. The first is referred to as the nonequilibrium sorption equation given by:

$$\frac{\partial \Gamma}{\partial t} = k_f c (\Gamma_s - \Gamma) - k_b \Gamma_s \quad (14-5)$$

subject to $\Gamma = \Gamma_0, t = 0$

The second is the Langmuir isotherm, which applies at local equilibrium,

$$\frac{c}{\Gamma} = \frac{c}{\Gamma_s} + \frac{1}{\Gamma_s K} \quad (14-6)$$

where k_f and k_b denote the rate constants for the forward, sorption and backward, desorption rate processes, $K = k_f/k_b$ denotes the equilibrium constant, Γ_s is the saturation concentration of the adsorbed species at complete monolayer coverage of the pore surface. Dubey and Waxman (1991) have shown that the adsorption of asphaltene from anhydrous

nonpolar solvents and toluene on common minerals followed the monolayer, Langmuir Type I adsorption mechanism according to Eq. 14-6. However, the adsorption of asphaltene from nitrobenzene solution followed a multilayer, Langmuir Type II adsorption mechanism. See Figures 14-32 and 14-33 given by Dubey and Waxman (1991). They have also shown that there is an adsorption/desorption hysteresis for asphaltene as indicated by Figure 14-34. Figures 14-35 and 14-36 reported by Acevedo et al. (1995) also indicate monolayer and multilayer adsorption mechanisms, respectively.

Ali and Islam (1997, 1999) used the following model for adsorption of asphaltene according to the application of the surface excess theory by Sircar et al. (1972). The asphaltenic oil is considered to have an asphaltene and an oil (maltene) pseudo-species, denoted respectively by the indices $i=1$ and $i=2$. Let x_i and x'_i denote the mass fractions of species i dissolved in the oil phase and adsorbed in the porous medium, respectively. n'_i is the mass of species i adsorbed per unit mass of porous media. n' is the total mass of species (oil plus asphaltene) adsorbed per unit mass of porous media given by:

$$n' = \sum_{i=1}^2 n'_i \quad (14-7)$$

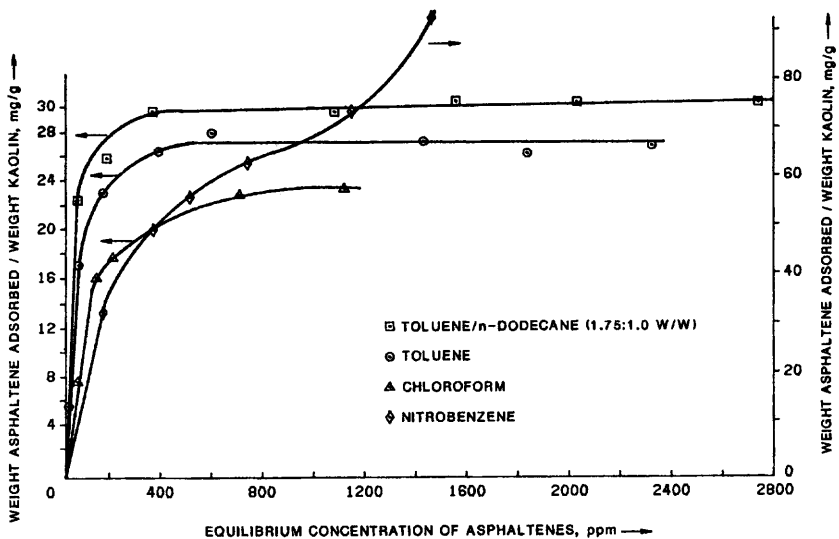


Figure 14-32. Adsorption isotherms for asphaltenes on kaolin from various solvents (Dubey and Waxman, ©1991 SPE; reprinted by permission of the Society of Petroleum Engineers).

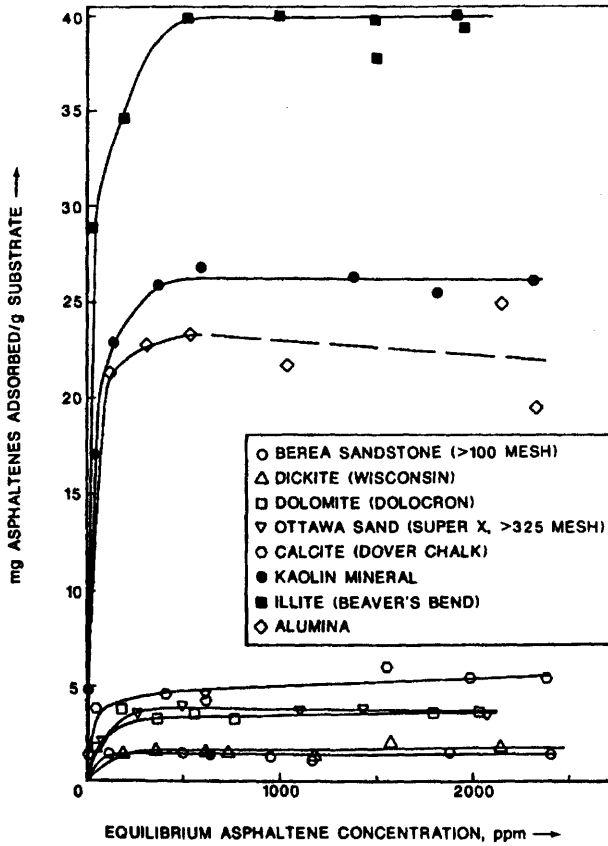


Figure 14-33. Adsorption isotherms for asphaltenes on clay and mineral surfaces from toluene (Dubey and Waxman, ©1991 SPE; reprinted by permission of the Society of Petroleum Engineers).

Then, assuming that all oil is in contact with the porous media, the surface excess of species i can be expressed as:

$$n_i^e = n'(x_i' - x_i) : i = \text{asphaltene or oil} \quad (14-8)$$

They assume that the theory is applicable for both mono- and multi-layer adsorption.

A balance of the oil and asphaltene adsorbed over the pore surface yields:

$$\frac{1}{n'} = \frac{x_1'}{m_1} + \frac{x_2'}{m_2} \quad (14-9)$$

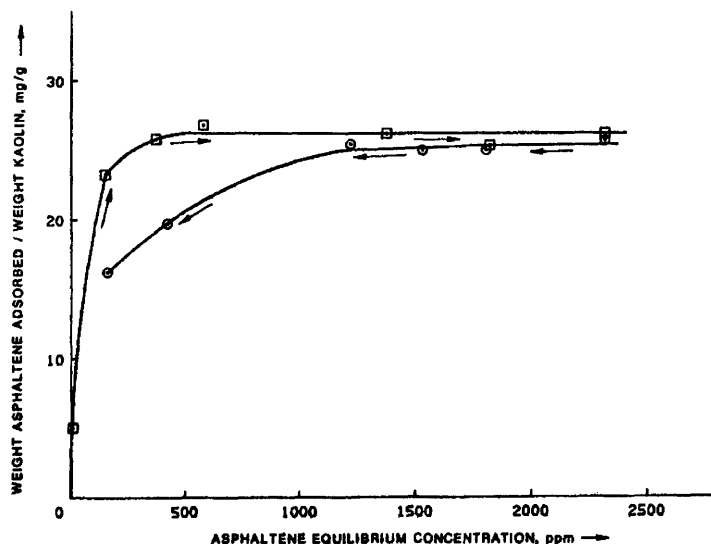


Figure 14-34. Hysteresis of adsorption/desorption isotherms for asphaltenes on kaolin from toluene (Dubey and Waxman, ©1991 SPE; reprinted by permission of the Society of Petroleum Engineers).

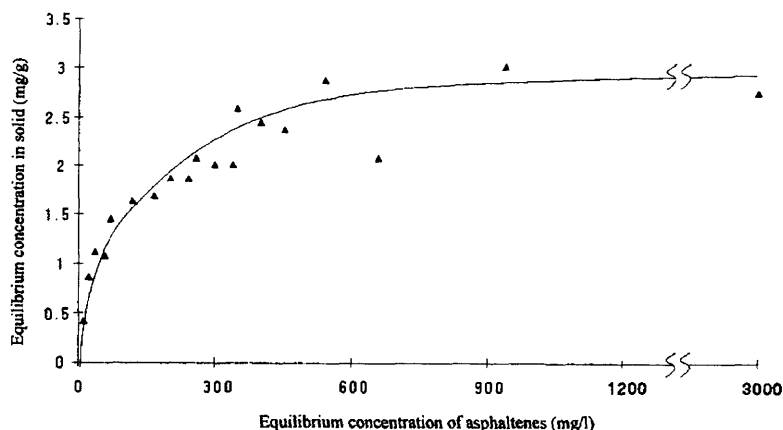


Figure 14-35. Adsorption isotherm for Cerro Negro asphaltenes on inorganic material surface from toluene at 26°C (reprinted from *Journal of Fuel*, Vol. 74, Acevedo, S., Ranaudo, M. A., Escobar, G., Gutiérrez, L., & Ortega, P., "Adsorption of Asphaltenes and Resins on Organic and Inorganic Substrates and Their Correlation with Precipitation Problems in Production Well Tubing," pp. 595–598, ©1995, with permission from Elsevier Science).

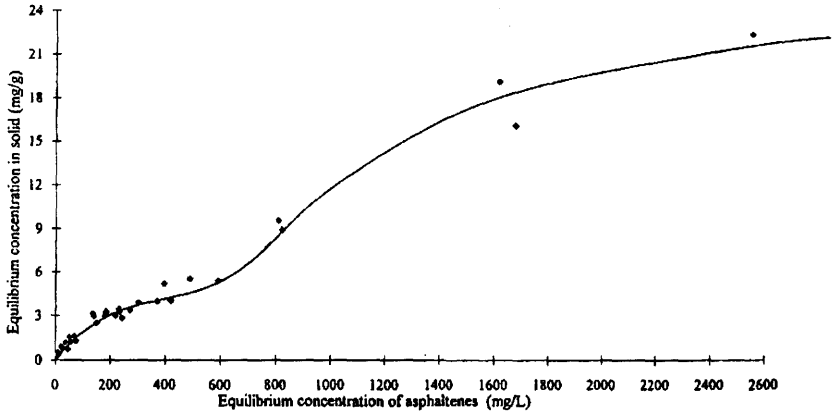


Figure 14-36. Adsorption isotherm for Ceuta asphaltenes on inorganic material surface from toluene at 26°C (reprinted from *Journal of Fuel*, Vol. 74, Acevedo, S., Ranaudo, M. A., Escobar, G., Gutiérrez, L., & Ortega, P., "Adsorption of Asphaltenes and Resins on Organic and Inorganic Substrates and Their Correlation with Precipitation Problems in Production Well Tubing," pp. 595-598, ©1995, with permission from Elsevier Science).

In Eq. 14-9, m_1 and m_2 denote the monolayer coverage of asphaltene and carrier oil, respectively, expressed as mass of species adsorbed per unit mass of porous solid. Then, a selectivity parameter, as defined below, is introduced:

$$S = \frac{x'_1/x'_2}{x_1/x_2} \quad (14-10)$$

Therefore, from Eqs. 14-9 and 10, they obtained the following expression for the amount of asphaltene adsorbed:

$$n_1^e = n'_1 x'_1 = \frac{m_1 x_1 S}{S x_1 + (m_1/m_2) x_2} \quad (14-11)$$

Using Eqs. 14-8 and 10, they derived the following expression for the surface excess amount of the asphaltene:

$$n_1^{ea} = \frac{m_1 x_1 x_2 (S-1)}{S x_1 + (m_1/m_2) x_2} \quad (14-12)$$

As a result, the rates of adsorption or desorption are expressed according to:

$$\frac{\partial n_1^{ea}}{\partial t} = k_j (n_1^e - n_1^{ea}) : j = \text{adsorption, desorption} \quad (14-13)$$

where n_1^e and n_1^{ea} denote the amount of species 1 (asphaltene) adsorbed/desorbed and the actual surface excess of species 1 per unit mass of porous formation. The initial condition is given as:

$$n_1^{ea} = n_{10}^{ea}, t = 0 \quad (14-14)$$

Empirical Algebraic Model for Formation Damage by Asphaltene Precipitation in Single Phase

Minssieux (1997) has demonstrated that the predominant mechanisms of the asphaltene deposition can be identified by means of the Wojtanowicz et al. (1987, 1988) analytic models. He also observed that the asphaltene precipitates existing in the injected oil can pass into porous media without forming an external filtercake.

The characteristics of the oils used are given in Tables 14-2 and 14-3, and the conditions and results of the coreflood experiments are given in Tables 14-4 and 14-5 by Minssieux (1997). The analyses of typical data according to Wojtanowicz et al. (1987, 1988) formulae are given in Figures 14-37 and 14-38 by Minssieux (1997). Figure 14-37

Table 14-2
Characteristics of Stock Tank Oils*

Field	Reservoir temperature (°C)	SARA ANALYSIS				Res/Asph ratio	Viscosity (cP 20°)	°API
		Sat	Ar	Resins	Asph.			
Weyburn	50	40.1	46.1	8.5	5.3	1.6	13	29
Lagrove	80	65.7	22.8	7.5	4	1.9	7.7	43
Hassi-Messaoud	119	70.5	25.5	3.3	0.15	22	1.5 (80°)	43
Boscan (Reference)	81	15	37	34	14	2.4		10

* Minssieux, ©1997 SPE; reprinted by permission of the Society of Petroleum Engineers.

Table 14-3
Characteristics of Crude and Asphaltenes*

Crude origin (°API)	% Asphaltene (weight)	Average MW (vpo/toluene)	Asphaltenes analysis			Tmax (°C) pyrolysis
			H/C	O/C	% S	
Weyburn 29	5.3	6000	1.00	0.025		416
Lagrange 43	4	"7000 à 8700"	1.00	0.010	3.80	416
H. Messaoud 45	0.15	1120 "well scales"	0.88	0.034	0.80	420
Boscan (10°) "as a reference"	10.7	8000	1.14	0.039	6.70	406

* Minssieux, ©1997 SPE; reprinted by permission of the Society of Petroleum Engineers.

Table 14-4
Conditions of Core Floods*

Test ref.	Type of rock	T (°C)	Crude used	Petrophysical data		Injection rate (cm ³ /hour)
				ø %	K _H (mD)	
GF 1	Fontainebleau sandstone	50	Weyburn	13.1	107	50 80
GF 2	id.	id.	id.	13.6	87	10
GF 3	id.	id.	id.	13.7	77.4	10 20 50 80
GF 12	id.	80	H. Messaoud	8	6	10
GVM 5	Vosges sandstone	50	Weyburn	24.7	29	10
GVM 10	id.	50	Weyburn	24.3	12.2	10 5
GVM 13	id.	80	Lagrange	26	73	10
GVR 8	id.	50	Weyburn	22.6	15.2	10
GVR 11	id.	80	Lagrange			
GP 9	Palatinat sandstone	80	H. Messaoud	22.6	1.1	10 5
GP 14	id.	id.	id.	23	2	5
HMD 11	Res. rock from HMD	id.	id.			
HMD 26	id.	id.	id.	7.1	0.67	8

* Minssieux, ©1997 SPE; reprinted by permission of the Society of Petroleum Engineers.

Table 14-5
Conditions of Core Flood Tests*

Test ref.	Crude used	Average amount of deposits (mg/g rock)	Deposition profile inlet → outlet	K reduction (%) after 50 PV	Observations
GF 1	Weyburn			20	Model type of porous medium (pure silica)
GF 2	W.	0.30	Uniform	42.5	
GF 3	W.	0.21	Uniform	58.5	
GF 12	H.MD	0.34	Decreasing	0 47 after 150 PV	
GVM 5	W.	1.0	Decreasing	88	Vosges clayey sandstone (illite)
GVM 10	W.	0.48	Decreasing	89	
GVM 13	Lagrange	-	-	<10	
GVR 8	W.	0.11	Decreasing	87	Vosges sandstone II
GVR 11	Lagrange	<0.10	Near core inlet accumulation		Final K_H difficult to measure
GP 9	H.MD	0.33	Decreasing	60	Palatinat sandstone (Kaolinite)
GP 14	H.MD	No plugging		-	crude injected with additive
HMD 11	H.MD	0.58 ("Resins")	Uniform		Reservoir-rock core samples from H.MD field
HMD 26	H.MD	0.41 ("Resins")	Uniform	6 (50 after 700 PV)	

* Minssieux, ©1997 SPE; reprinted by permission of the Society of Petroleum Engineers.

shows the results of the analysis of the GF3 test data considering the possibility of the gradual surface deposition, single pore plugging, and in-situ cake formation by pore filling mechanisms in formation damage. As can be seen, only the $\sqrt{K/K_0}$ vs. PV (pore volume) data yields a straight line plot, indicating that the damage mechanism is the gradual surface deposition. In the case of the GV5 data, Figure 14-38 indicates that the damage mechanism is the in-situ cake formation by pore filling, because K_0/K vs. PV data yields a straight line plot for this case (see Table 10-1).

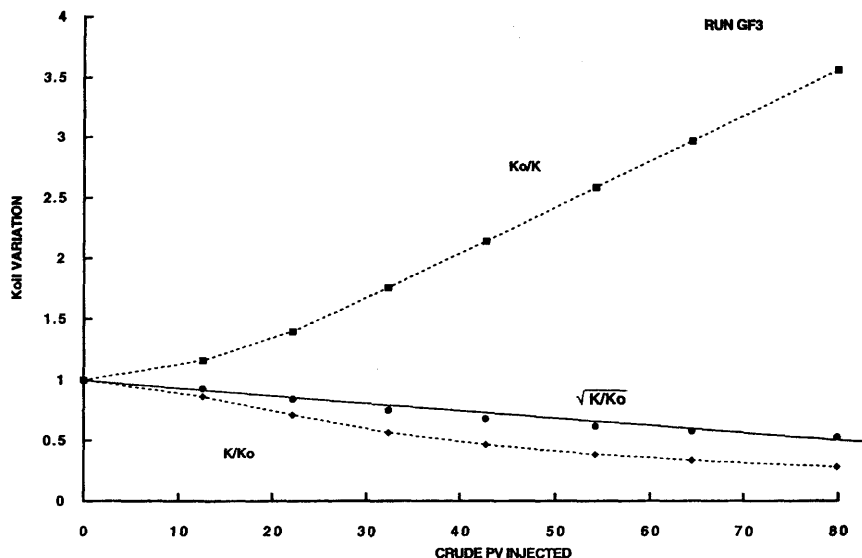


Figure 14-37. Correlation of the experimental permeability reduction data reveals a uniform surface deposition mechanism (Minssieux, ©1997 SPE; reprinted by permission of the Society of Petroleum Engineers).

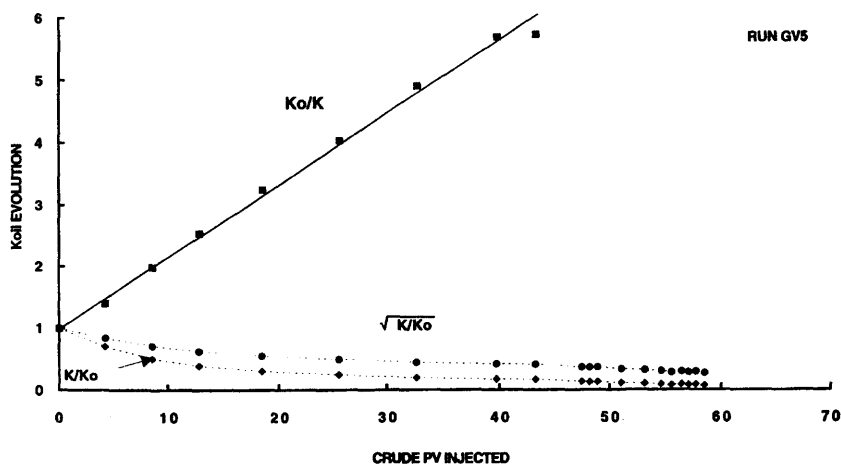


Figure 14-38. Correlation of the experimental permeability reduction data reveals a pore blocking deposition mechanism (Minssieux, ©1997 SPE; reprinted by permission of the Society of Petroleum Engineers).

Simplified Analytic Model for Asphaltene-Induced Formation Damage in Single-Phase

Leontaritis (1998) developed a simplified model for prediction of formation damage and productivity decline by asphaltene deposition in under-saturated (above bubble-point pressure) asphaltenic oil reservoirs. This model consists of a set of algebraic equations. In this section, the Leontaritis model is presented with some modifications for consistency with the rest of the presentation of this chapter.

As schematically shown in Figure 14–39, for analysis, Leontaritis (1998) considers the portion of the reservoir defined by the radius of drainage of a production well. In this region, the flow is assumed radial.

Figure 14–40 schematically depicts the variation of the flowing bottom hole pressure during constant rate production, while the external reservoir pressure and the onset of the asphaltene flocculation pressure remain constant.

The calculational steps of this model are described briefly in the following.

Step 1. The initiation time for asphaltene precipitation is referred to as zero (i.e., $t = 0$). Given the well productivity index, PI , the flowing bottom hole pressure, $p_w|_{t=0}$, prior to asphaltene damage is calculated from the definition of the productivity index:

$$PI = \frac{q}{p_e - p_w} = \frac{2\pi kh}{\mu \ell n(r_e/r_w)} \quad (14-15)$$

Then, the steady-state radial pressure profile prior to damage is calculated by:

$$p_o(r) = p_{w_o} + \frac{q\mu}{2\pi kh} \ell n\left(\frac{r}{r_w}\right) \quad (14-16)$$

The asphaltene deposition is assumed to occur within the near wellbore region, $r_w < r < r_{AF}$, where the pressure is below the asphaltene flocculation pressure, p_{AF} . The radius of this region, r_{AF} , is determined by Eq. 14–16 for $p = p_{AF}$, according to Figure 14–41. Leontaritis (1998) assumes that the pressure beyond this region (i.e., $r_{AF} \leq r \leq r_e$) is not influenced by asphaltene deposition in the near wellbore region.

The region $r_w \leq r \leq r_{AF}$ is divided into a number of sections of finite width Δr . Steps 2 and 3 calculations are carried out over each Δr segment for a time increment by Δt , consecutively, as described in the following.

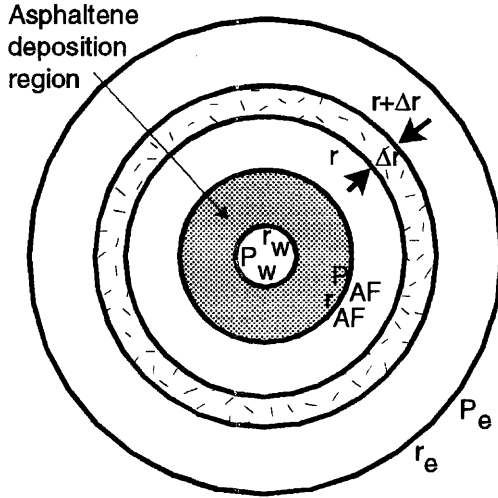


Figure 14-39. Producing reservoir drainage area (modified after Leontaritis, 1998).

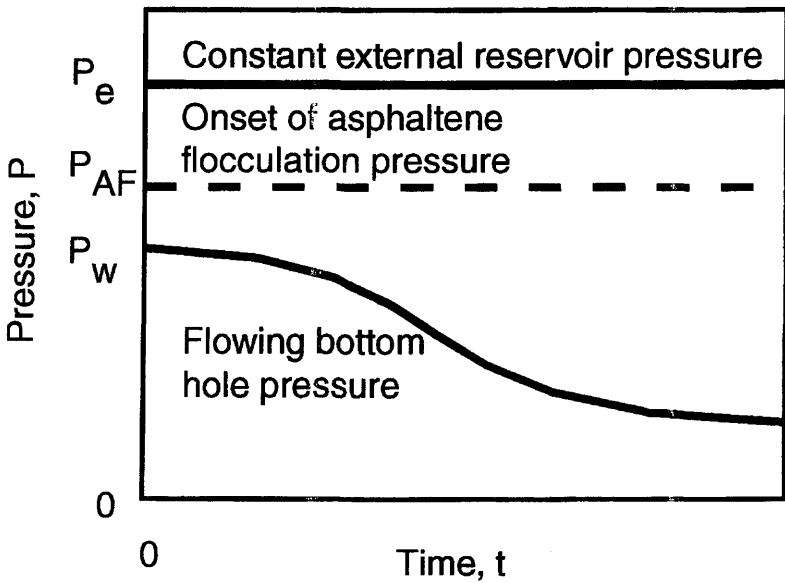


Figure 14-40. Variation of the flowing bottom hole pressure during constant rate production (modified after Leontaritis, 1998).

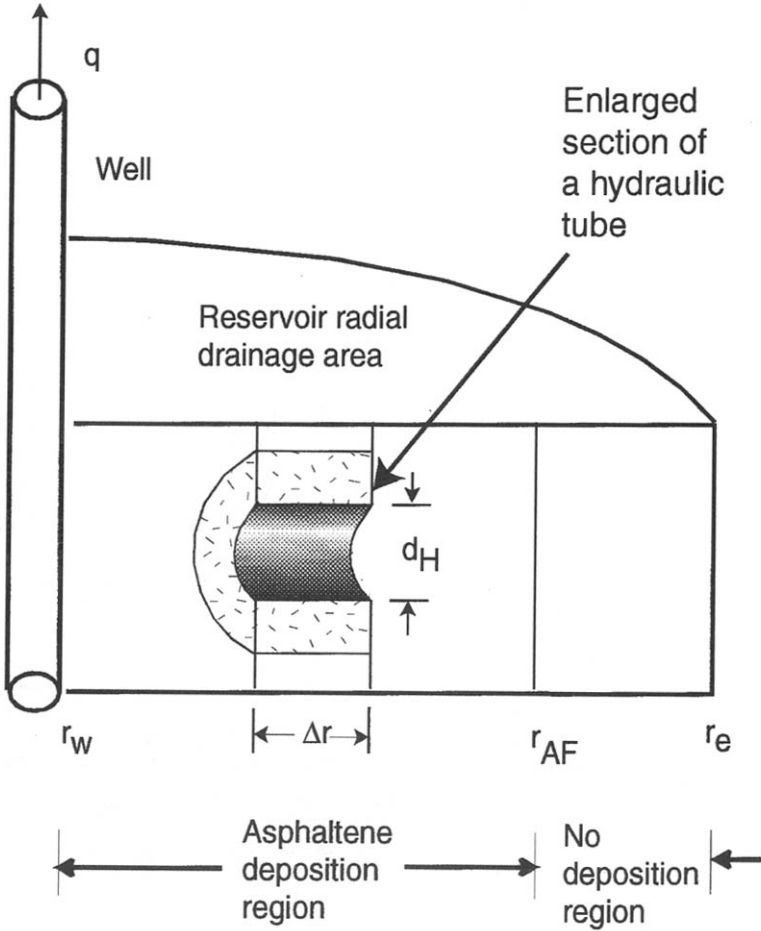


Figure 14-41. Asphaltene deposition induced formation damage in the near-wellbore region (modified after Leontaritis, 1998).

Step 2. Similar to Wojtanowicz et al. (1987, 1988), Leontaritis considers the porous media as a bundle of tortuous flow tubes. Thus, the mean hydraulic diameter is estimated by the ratio of the total pore volume to the total pore surface area of the flow channels according to:

$$\frac{d_H}{2} = \frac{AL\phi}{AL(1-\phi)A_g/V_g} = \frac{\phi V_g}{(1-\phi)A_g} \quad (14-17)$$

where A , L , and ϕ denote the cross-sectional area, length, and porosity of a core plug, and A_g and V_g are the mean surface area and the mean volume of the porous media grains. If the mean, spherical grain diameter is denoted by d_g , then Eq. 14–17 can be expressed as:

$$d_H = \frac{d_g}{3} \left(\frac{\phi}{1-\phi} \right) \quad (14-18)$$

Next, the tube size distribution function, $f(D_A)$, the mole fraction, x_A , and molar volume, v_A , of the flocculated asphaltenes, and the moles of reservoir fluid, m_{RF} , at the prevailing pressure and temperature conditions within the near wellbore region are determined according to Leontaritis (1997). Figure 14–42 shows a typical asphaltene particle size distribution.

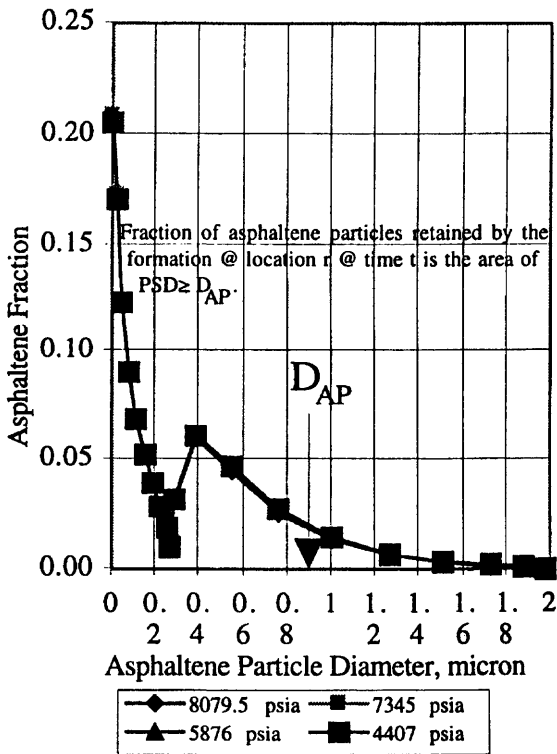


Figure 14–42. Asphaltene particle size distribution (after Leontaritis, ©1998 SPE, reprinted by permission of the Society of Petroleum Engineers).

Leontaritis (1998) assumes that permeability impairment primarily occurs by pore throat plugging and generalizes the one-third rule-of-thumb of filtration as the particles larger than a certain fraction of the pore size cannot penetrate a filter, and determines the fraction of the particles, f_{trap} , which are captured and deposited at the pore throats. Thus, the rule-of-thumb for trapment of particles at the pore throats is generalized to estimate the critical particle diameter for plugging as a fraction of the hydraulic tube diameter as:

$$D_{Acr} = \alpha D_H \quad (14-19)$$

in which α is as an empirical factor accounting for the smallest particle that can be filtered. Its value is determined to match the model predictions to measured data, instead of setting it to a prescribed value, like 1/3. Then, the fraction of the asphaltene particles that cannot pass through the pore throats and, therefore, are captured at the pore throats is determined by:

$$f_t = \int_{D_{Acr}}^{\infty} f(D_A) dD_A \quad (14-20)$$

Step 3. The incremental moles of asphaltene particles trapped and the incremental flow area closed within the Δt time interval are estimated, respectively, by:

$$\Delta m_t = m_{RF} x_A f_{trap} \quad (14-21)$$

and

$$\Delta A_t = \Delta m_{trap} v_A a_A \beta \quad (14-22)$$

where a_A is the specific surface of the asphaltene particles retained in porous media, estimated as:

$$a_A = \frac{4\pi(D_A/2)^2}{\frac{4}{3}\pi\left(\frac{D_A}{2}\right)^3} = \frac{6}{D_A} \quad (14-23)$$

where D_A is the mean diameter of the asphaltene particles retained. β is an empirical factor accounting for the plugging by asphaltene particles.

Therefore, combining Eqs. 14–20 through 23 over a number of N consecutive, discrete time steps, Δt , the cumulative flow area closed to flow by pore throat plugging is estimated by:

$$A_t = \sum_{j=1}^N \Delta A_{tj} = \sum_{j=1}^N (m_{RF} x_A f_t v_A \gamma / D_H)_j \quad (14-24)$$

where $\gamma = 6\beta/\alpha$ is a combined constant.

Hence, the area open to flow during damage is given by:

$$A = A_o - A_t \quad (14-25)$$

where the area open to flow is determined by:

$$A = 2\pi r h \phi \quad (14-26)$$

and the initial area of flow is given by:

$$A_o = 2\pi r h \phi_o \quad (14-27)$$

Based on Eqs. 14–25 through 27, the instantaneous porosity is given by:

$$\phi = \phi_o (1 - A_t / A_o) \quad (14-28)$$

According to Wojtanowicz et al. (1987, 1988), the area open to flow during formation damage by pore throat plugging is linearly related to permeability (see Chapter 10):

$$A \sim K \quad (14-29)$$

Therefore, the instantaneous permeability is given by:

$$K = K_o (1 - A_t / A_o) \quad (14-30)$$

The productivity ratio is calculated by:

$$\alpha = PI / PI_o \quad (14-31)$$

in which the productivity index is defined by:

$$PI = \frac{q}{\Delta p} = \frac{KA}{\mu \Delta r} \quad (14-32)$$

Hence, combining Eqs. 14–25 and 30–32 yields the following expression for the productivity ratio:

$$\alpha = (1 - A_t/A_o)^2 \quad (14-33)$$

Note that Eq. 14–33 is different than the equation given by Leontaritis (1998) because Eq. 14–33 is squared.

The pressure loss by damage is calculated by Eqs. 14–31 through 33 as:

$$\Delta p = \Delta p_o / (1 - A_t/A_o)^2 \quad (14-34)$$

Next, calculate the new pressure value by:

$$p = p_o - \Delta p \quad (14-35)$$

Step 4. When Steps 2 and 3 over all the Δr segments are completed, the pressure loss by skin and the skin factor are calculated as following. Note that the drawdown pressure is given during damage as:

$$p_e - p_w = \frac{q\mu}{2\pi k_o h} \left[\ell n \left(\frac{r_e}{r_w} \right) + s \right] \quad (14-36)$$

where s is the van Everdingen-Hurst skin factor. Thus, the loss of the pressure by the skin effect is given by:

$$\Delta p_s = \frac{q\mu s}{2\pi k_o h} \quad (14-37)$$

Consequently, comparing Eqs. 14–16 and 36 in view of Eq. 14–37 yields:

$$\Delta p_s = p_w - p_{wo} \quad (14-38)$$

Once the pressure loss by skin is calculated by Eq. 14–38, the skin factor can then be calculated by Eq. 14–37.

Step 5. Another time increment, Δt , is taken and Steps 2–4 are repeated until either the final time considered for the calculation is reached or the flow rate of production can no longer be kept constant, which is the condition imposed for the above described model.

Leontaritis considers that a steady-state is attained when the deposition and erosion rates equal. Then, the asphaltene deposition stops and the area open to flow attains a certain minimum limit value. Because of the lack of a better asphaltene erosion theory, Leontaritis assumes that the area of flow can be empirically expressed as some fraction of the initial area. His equation can be expressed in terms of Eq. 14–31 as:

$$A \cong A_o(a\alpha + b) \quad (14-39)$$

which, in the limit, yields the final area to be reached at the steady-state as:

$$A_f = \lim_{\alpha \rightarrow 0} A = A_o b \quad (14-40)$$

Because, initially, $\alpha = 1$ and $A = A_o$, Eq. 14–39 yields:

$$a + b = 1 \quad (14-41)$$

Based on Eqs. 14–40 and 41, it can be concluded that $0 \leq a \leq 1$ and $0 \leq b \leq 1$. However, there is no clear evidence of the use of Eqs. 14–39 through 41 in his calculational procedure.

Using the data given in Figures 14–42 and 14–43 with this model, Leontaritis (1998) obtained the results presented in Figures 14–44 through 14–47.

Plugging–Nonplugging Pathways Model for Asphaltene Deposition in Single-Phase

Ali and Islam (1997, 1998) considered only asphaltene deposition and resorted to a simplified, single phase formation damage modeling approach according to Gruesbeck and Collins (1982). Here, their model is presented in a manner consistent with the rest of the presentation of this chapter. Also, a few missing equations are supplied. Note that this model applies for undersaturated oils.

The rate of deposition in the plugging paths is given by:

$$\partial \epsilon_p / \partial t = k_p u_p \sigma_p (\phi_{p_o} - \epsilon_p) \quad (14-42)$$

(text continued on page 424)

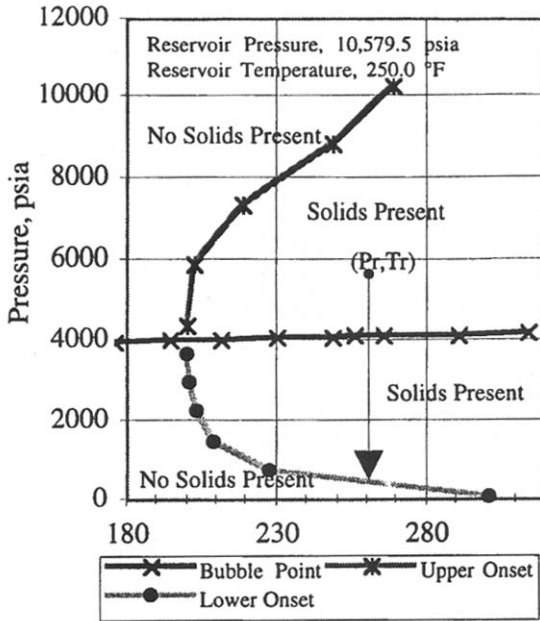


Figure 14-43. Asphaltene deposition envelope for an AsphWax Oil Company reservoir oil (after Leontaritis, ©1998 SPE; reprinted by permission of the Society of Petroleum Engineers).

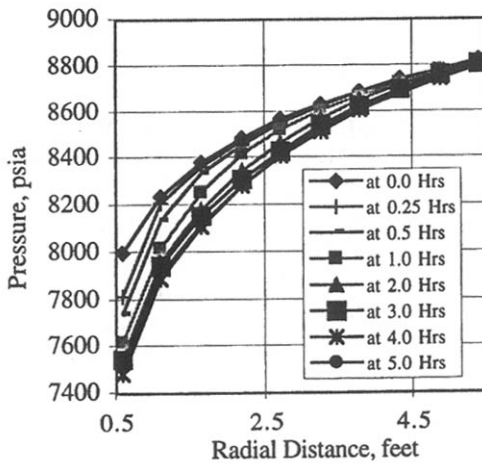


Figure 14-44. Variation of pressure profile in the asphaltene-damaged region (after Leontaritis, ©1998 SPE; reprinted by permission of the Society of Petroleum Engineers).

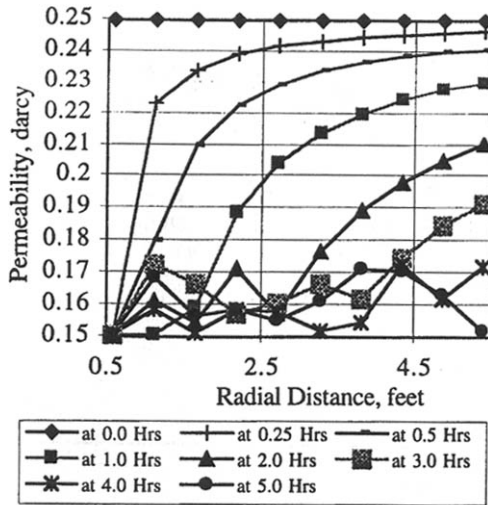


Figure 14-45. Variation of permeability profile in the asphaltene-damaged region (after Leontaritis, ©1998 SPE; reprinted by permission of the Society of Petroleum Engineers).

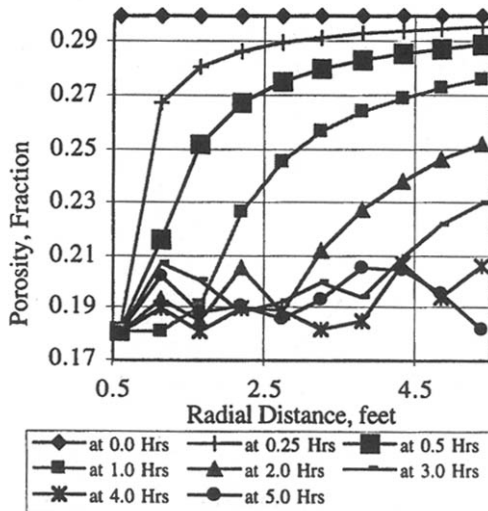


Figure 14-46. Variation of porosity profile in the asphaltene-damaged region (after Leontaritis, ©1998 SPE; reprinted by permission of the Society of Petroleum Engineers).

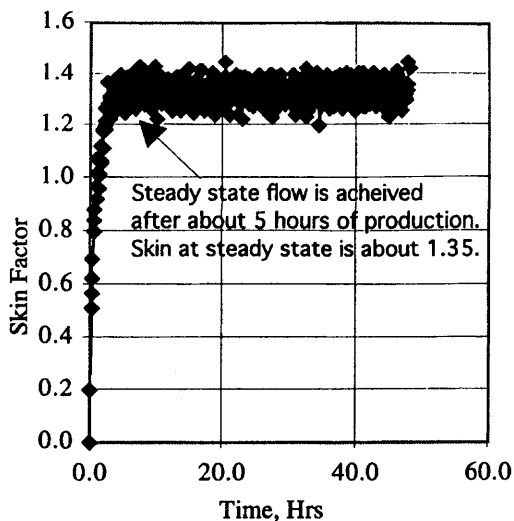


Figure 14-47. Variation of skin factor by asphaltene-induced damaged (after Leontaritis, ©1998 SPE; reprinted by permission of the Society of Petroleum Engineers).

(text continued from page 421)

$$\varepsilon_p = 0, \quad t = 0 \quad (14-43)$$

The deposition in the nonplugging paths is expressed by:

$$\partial \varepsilon_{np} / \partial t = k_d w_{p,L} - k_e \varepsilon_{np} (u_{np} - u_c) \quad (14-44)$$

$$\varepsilon_{np} = 0, \quad t = 0 \quad (14-45)$$

Note

$$k_e \neq 0, \quad u_{np} \geq u_c \quad (14-46)$$

$$k_e = 0, \quad u_{np} < u_c \quad (14-47)$$

The fluid flux in the plugging pathways is given by:

$$u_p = u \frac{K_p}{f_p K_p + f_{np} K_{np}} \quad (14-48)$$

Note that Ali and Islam (1997, 1998) used the original Gruesbeck and Collins (1982) equation, which misses the f_p and f_{np} terms in Eq. 14-48 instead of the corrected Eq. 14-48 given independently by Civan (1992) and Schechter (1992).

The flow in the nonplugging pathways is given by:

$$u_{np} = u \frac{K_{np}}{f_p K_p + f_{np} K_{np}} \quad (14-49)$$

$$f_p + f_{np} = 1 \quad (14-50)$$

Following Gruesbeck and Collins (1982), Ali and Islam (1997) assumed f_p and f_{np} as some characteristic values of the porous medium and determined them to match the model predictions to experimental data.

The permeability impairments in the plugging and nonplugging pathways were represented by the Gruesbeck and Collins (1982) empirical expressions, given, respectively, by:

$$K_p \cong K_{po} \exp(-\alpha \varepsilon_p^4) \quad (14-51)$$

$$K_{np} \cong K_{npo} / (1 + \beta \varepsilon_{np}) \quad (14-52)$$

where K_{po} and K_{npo} denote the permeabilities of the plugging and nonplugging pathways before damage, and α and β are some adjustable constants.

Ali and Islam (1997) assumed the same concentrations in the plugging and nonplugging pathways. Thus, the mass balance of the suspended particles of asphaltene in the flowing fluid can be expressed as (Civan, 1995, 1996):

$$\begin{aligned} \phi \rho_L \frac{\partial w_{p,L}}{\partial t} + \rho_L u_L \frac{\partial w_{p,L}}{\partial x} = \frac{\partial}{\partial x} \left(\phi \rho_L D_{p,L} \frac{\partial w_{p,L}}{\partial x} \right) \\ + \phi (\dot{m}_p - \dot{m}_L w_{p,L}) \end{aligned} \quad (14-53)$$

In laboratory core tests, the mass rate of phase L added per unit volume of phase L is zero:

$$\dot{m}_L = 0 \quad (14-54)$$

The mass rate of asphaltene particles added to phase L is given by:

$$\phi \dot{m}_p = -\rho_p \left(\frac{\partial \epsilon_p}{\partial t} + \frac{\partial \epsilon_p^{ea}}{\partial t} \right) \quad (14-55)$$

where ϵ_p and ϵ_p^{ea} denote the retention by filtration and adsorption, respectively. The formulation by Ali and Islam (1997) implies that they expressed the dispersion coefficient as a linear function of the interstitial velocity of the fluid:

$$D_{p,L} = \lambda v_L \quad (14-56)$$

where λ is an empirically determined coefficient and v_L is the interstitial velocity, given by:

$$v_L = u_L / \phi \quad (14-57)$$

Assuming a constant rate injection of oil into a core plug and constant oil density and applying Eqs. 14-54 through 57, Eq. 14-53 can be written as:

$$\phi \rho_L \frac{\partial w_{p,L}}{\partial t} + \rho_L u_L \frac{\partial w_{p,L}}{\partial x} = \lambda \rho_L u_L \frac{\partial^2 w_{p,L}}{\partial x^2} - \rho_p \left(\frac{\partial \epsilon_p}{\partial t} + \frac{\partial \epsilon_p^{ea}}{\partial t} \right) \quad (14-58)$$

It can be shown that Eq. 14-58 can be reformulated in the form given by Ali and Islam (1997). However, the last term in their equation appears to probably have a typographical error, because σ in their equation should be replaced by $\partial \sigma / \partial t$. The same error has been repeated by Ali and Islam (1998).

The initial and boundary conditions for Eq. 14-58 are given by:

$$w_{p,L} = 0, \quad 0 \leq x \leq L, \quad t = 0 \quad (14-59)$$

$$w_{p,L}^o = w_{p,L} - \lambda \frac{\partial w_{p,L}}{\partial x}, \quad x = 0, \quad t > 0 \quad (14-60)$$

$$\frac{\partial w_{p,L}}{\partial x} = 0, \quad x = L, \quad t > 0 \quad (14-61)$$

Using the input data given in Table 14–6, Ali and Islam (1998) obtained the results presented in Figures 14–48 through 14–50.

Table 14–6
Model Parameters*

Experimental Parameters	
C_0 , wt%	3
k , md	11.3
n_0 , mg/g	200
q , mL/min	0.5, 1, 2, 3
ϕ	0.35
ρ_1 , °API	29.29
ρ_r , g/mL	2.71
Pore volume, cm ³	136
Run 1 mL/min	0.5
Run 2, mL/min	1
Run 3, mL/min	2
Run 4, mL/min	3
Adjustable Parameters	
λ , cm	0.1
m_a/m_o	15
S	100
m_a	$0.05 n_0$
K_1 , hour ⁻¹	20
K_2 , hour ⁻¹	0.008
α , cm ⁻¹	6.3
β , second ⁻¹	0.00085 through 0.01
u_{c1} , cm · second ⁻¹	0.032
δ , cm ⁻¹	0.2
ρ , cm ⁻¹	10
ε	10
f	0.82
a	10
k_{pi} , md	11.3
k_{npi}/k_{pi}	10

* After Ali and Islam, ©1998 SPE; reprinted by permission of the Society of Petroleum Engineers.

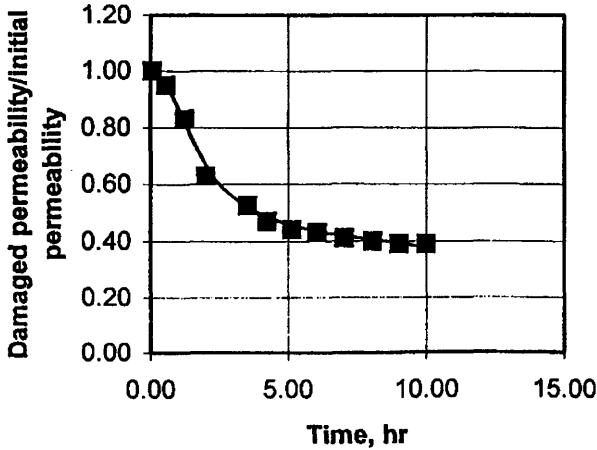


Figure 14-48. Permeability reduction for injection at 0.5 mL/min rate (after Ali and Islam, ©1998 SPE; reprinted by permission of the Society of Petroleum Engineers).

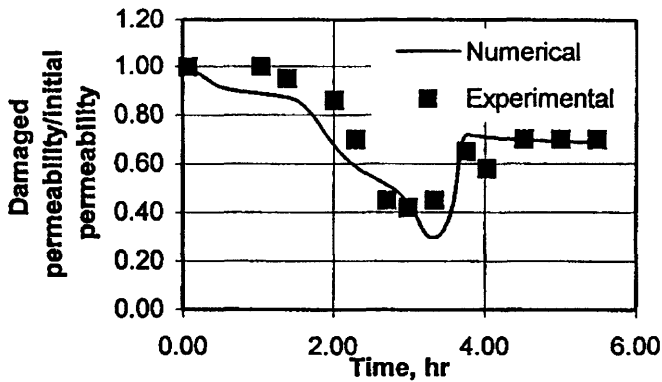


Figure 14-49. Permeability reduction for injection at 2 mL/min rate (after Ali and Islam, ©1998 SPE; reprinted by permission of the Society of Petroleum Engineers).

Two-Phase and Dual-Porosity Model for Simultaneous Asphaltene-Paraffin Deposition

Considerations of the Model

Here, the formulation of Civan's (1995) model is presented. The reservoir fluid system can be single phase or multiphase depending on

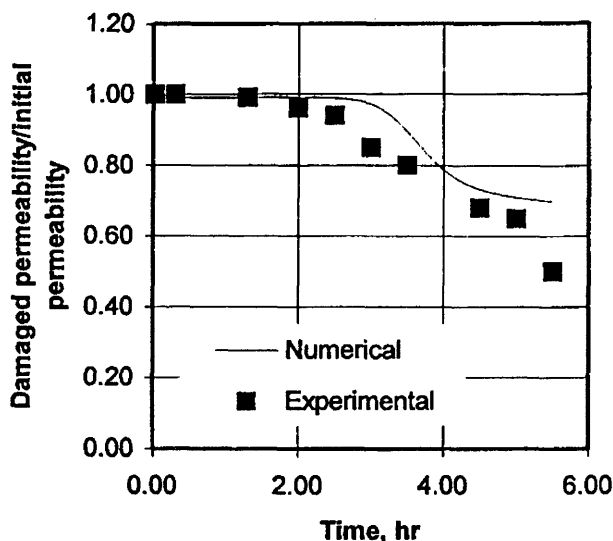


Figure 14–50. Permeability reduction for injection at 3 mL/min rate (after Ali and Islam, ©1998 SPE; reprinted by permission of the Society of Petroleum Engineers).

the prevailing reservoir conditions. Above the bubble-point pressure conditions, the oil is undersaturated and single phase. Below the bubble-point pressure conditions, the oil is saturated and can be two-phase. Civan (1995) developed a model that is applicable for both conditions. His model also considered the possibility of simultaneous deposition of asphaltenes and paraffins. As stated by Civan (1995), “Although they are a mixture of different molecular weight components, the paraffins and asphaltenes are lumped into two groups as the paraffin, p , and the asphaltene, a , pseudo-components. The other components of the oil are grouped as the oil pseudo-component, o , which acts as a solvent. The mixture of the various gases are grouped as the gas pseudo-component, g .”

Thus, Civan’s (1995) model considers four pseudo-components: (a) paraffin, par , (b) asphaltene, asp , (c) oil, o , and (d) gas, g . The system of the fluids and the porous formation is considered in three phases as the vapor, V , liquid, L , and solid, S , following Ring et al. (1994). The solid phase is considered in two parts: (1) porous matrix (unchanged), and (2) organic deposits (varying).

Civan (1995) considers that the paraffin and asphaltene transport may occur both in dissolved and precipitate forms depending on the state of saturation of the oil phase. This assumption is supported by Mansoori

(1997) who points out that: “. . . asphaltenes are partly dissolved and partly in colloidal state (in suspension) in oil peptized (or stabilized) primarily by resin molecules that are adsorbed on asphaltene surface.” The permeability impairment may occur by (a) gradual pore size reduction, and (b) pore throat plugging and sealing. The ratio of the plugging and nonplugging paths vary by organic deposition. Single- or two-phase fluid conditions may exist depending on whether the condition is above or below the bubble-point pressure. The various phases are assumed at thermal equilibrium within the bulk volume. Non-Newtonian fluid behavior is considered for high concentrations of organic precipitates and solutes. Non-Darcy flow behavior is assumed for flow through passages narrowing due to precipitation.

Porosity and Permeability Relationships

The porosity and permeability alterations are predicted based on a modified version of the plugging and nonplugging pathways concept of Gruesbeck and Collins (1982). Relatively smooth and large diameter flowpaths are assumed to mainly undergo a surface deposition and are called nonplugging. Highly tortuous and variable diameter flowpaths are called plugging. The retainment of organic deposits in the plugging pathways occurs by jamming and pore throat blocking.

Consider that ϕ_{p_o} and ϕ_{np_o} denote the pore volume fractions and ϵ_p and ϵ_{np} are the fractions of the bulk volume occupied by organic deposits of the plugging and nonplugging pathways of the porous media. Thus, the instantaneous porosities in the plugging and nonplugging flow paths are given, respectively, by:

$$\phi_p = \phi_{p_o} - \epsilon_p \quad (14-62)$$

$$\phi_{np} = \phi_{np_o} - \epsilon_{np} \quad (14-63)$$

Although, Gruesbeck and Collins (1982) assume characteristic constant values, it is reasonable to consider that the fractions of the bulk volume containing the plugging and nonplugging pathways vary during deposition and are estimated by, because of the lack of a better theory:

$$f_p = \phi_p / \phi \quad (14-64)$$

$$f_{np} = \phi_{np} / \phi \quad (14-65)$$

The instantaneous and initial porosities of the porous medium are given, respectively, by:

$$\phi = \phi_p + \phi_{np} \quad (14-66)$$

$$\phi_o = \phi_{po} + \phi_{np_o} \quad (14-67)$$

The total organic deposit volume fraction and the instantaneous porosity are given, respectively, by:

$$\varepsilon = \varepsilon_p + \varepsilon_{np} \quad (14-68)$$

$$\phi = \phi_o - \varepsilon \quad (14-69)$$

The rate of deposition in the plugging pathways can be expressed by:

$$\partial \varepsilon_p / \partial t = k_p u_p \sigma_p \phi_p \quad (14-70)$$

subject to the initial condition

$$\varepsilon_p = \varepsilon_{p_o}, t = 0 \quad (14-71)$$

for which

$$k_d \neq 0 \quad \text{when} \quad t \geq t_p \quad (14-72)$$

$$k_d = 0, \quad t < t_p \quad (14-73)$$

Here, t_p is the time of initiation of the particle bridges and jamming. This is the time at which the pore throat-to-particle diameter ratio drops to below its critical value determined by the following empirical correlation (Civan, 1990, 1996):

$$D_t / D_p < (D_t / D_p)_{cr}, \quad (D_t / D_p)_{cr} = A [1 - \exp(-B \text{Re}_p)] + C \quad (14-74)$$

in which the particle Reynolds number is given by:

$$\text{Re}_p = \rho_p \sigma_p u D_p / (\mu \phi) \quad (14-75)$$

The rate of deposition in the nonplugging tubes can be expressed by (Civan, 1994, 1995, 1996):

$$\partial \varepsilon_{np} / \partial t = k_d u_{np} \sigma_{np} \phi_{np}^{2/3} - k_e \varepsilon_{np} \eta_e (\tau_w - \tau_{cr}) \quad (14-76)$$

subject to the initial condition

$$\varepsilon_{np} = \varepsilon_{np_0}, \quad t = 0 \quad (14-77)$$

Here,

$$k_e \neq 0, \quad \tau_w \geq \tau_{cr} \quad (14-78)$$

$$k_e = 0, \quad \tau_w < \tau_{cr} \quad (14-79)$$

For simplification purposes, Civan (1995) assumed that organic deposits are sticky and, therefore, once deposited they cannot be removed. Consequently, the second term in Eq. 14-76 can be dropped. Mansoori (1997) tends to support this argument. Although Leontaritis (1998) considered the possibility of erosion of deposits, it is not apparent if he actually implemented this possibility in his calculational steps. k_d and k_e are the surface deposition and mobilization rate constants. η_e is the fraction of the uncovered deposits estimated by:

$$\eta_e = \exp(-k\varepsilon) \quad (14-80)$$

τ_{cr} is the minimum shear stress necessary to mobilize the surface deposits. τ_w is the wall shear-stress given by the Rabinowitsch-Mooney equation (Metzner and Reed, 1995):

$$\tau_w = k'(8v/D)^{n'} \quad (14-81)$$

in which the interstitial velocity, v , is related to the superficial velocity, u , by:

$$v = u/\phi \quad (14-82)$$

and the mean pore diameter is given by:

$$D \sim (K_{np}/\phi_{np})^{1/2} \quad (14-83)$$

The permeabilities of the plugging and nonplugging pathways are given by the following empirical relationships (Civan, 1994):

$$K_p = K_{p_o} \exp \left[-\alpha (\phi_{p_o} - \phi_p)^{n_1} \right] = K_{p_o} \exp (-\alpha \epsilon_p^{n_1}) \quad (14-84)$$

and

$$K_{np} = K_{np_o} (\phi_{np} / \phi_{np_o})^{n_2} = K_{np_o} (1 - \epsilon_{np} / \phi_{np_o})^{n_2} \quad (14-85)$$

Then, the average permeability of the porous medium is given by:

$$K = f_p K_p + f_{np} K_{np} \quad (14-86)$$

The superficial flows in the plugging and nonplugging pathways are given respectively, by:

$$u_p = u K_p / K \quad (14-87)$$

$$u_{np} = u K_{np} / K \quad (14-88)$$

The total superficial flow is given by (Gruesbeck and Collins, 1982):

$$u = f_p u_p + f_{np} u_{np} \quad (14-89)$$

Considering the simultaneous deposition of paraffins and asphaltenes, ϵ_p and ϵ_{np} in Eqs. 14-62 through 69 denote the sum of the paraffins and asphaltenes, that is,

$$\epsilon_p = \epsilon_{p, par} + \epsilon_{p, asp} \quad (14-90)$$

$$\epsilon_{np} = \epsilon_{np, par} + \epsilon_{np, asp} \quad (14-91)$$

Description of Fluid and Species Transport

The preceding treatment of the porous media impairment phenomena implies that the suspended particle and dissolved species concentrations may be different in the plugging and nonplugging pathways. Then, separate sets of balance equations are required for the plugging and

nonplugging pathways. Consequently, the numerical solution would require highly intensive computational effort. However, this problem can be conveniently circumvented by assuming that there is hydraulic interaction between these pathways (i.e., they are not isolated from each other).

1. The mass balances are considered for the following four pseudo-components
 - a. Gas
 - b. Oil
 - c. Suspended paraffins and asphaltenes
 - d. Dissolved paraffins and asphaltenes
2. Total thermal equilibrium energy balance is considered
3. Non-Newtonian fluid description using the Rabinowitsch-Mooney equation is resorted
4. The Forchheimer equation for the non-Darcy flow description is used
5. The average flow is defined as a volume fraction weighted linear sum of the flow through the plugging and nonplugging paths according to Gruesbeck and Collins (1982)
6. The average permeability is defined as a volume weighted linear sum of the permeabilities of the plugging and nonplugging paths according to Gruesbeck and Collins (1982)
 - a. In the plugging paths, a snowball deposition effect is represented by an exponential decay function
 - b. In the nonplugging paths, a gradual pore size reduction, represented by the power law function, is considered
7. The precipitation of the asphaltene and paraffin is predicted, applying Chung's (1992) thermodynamic model for non-ideal solutions to determine the cloud point and the quantity of the precipitates to be formed.

The total mass balance of the gas component is given by:

$$\begin{aligned} \frac{\partial}{\partial t}(\phi S_V \rho_V + \phi S_L \rho_L w_{g,L}) + \frac{\partial}{\partial x}(\rho_V u_V + \rho_L u_L w_{g,L}) \\ + \phi(S_V \dot{m}_{g,V} + S_L \dot{m}_{g,L}) = 0 \end{aligned} \quad (14-92)$$

The first, second, and third terms respectively represent the accumulation, transport, and well production.

Assuming that the oil component exists only in the liquid phase and does not vaporize into the gas phase, the oil component mass balance is given by:

$$\frac{\partial}{\partial t}(\phi S_L \rho_L w_{oL}) + \frac{\partial}{\partial x}(\rho_L u_L w_{oL}) + \phi S_L \dot{m}_{o,L} = 0 \quad (14-93)$$

for which Ring et al. (1994) assumed $w_{oL} \cong 1.0$. Considering that organic precipitates only exist in the liquid phase, because it is the wetting phase for these particles, the suspended paraffin and asphaltene particle mass balances are expressed by:

$$\begin{aligned} & \frac{\partial}{\partial t}(\phi S_L \rho_L w_{p,L} + \epsilon_p \rho_p) + \frac{\partial}{\partial x}(u_L \rho_L w_{p,L}) + \phi S_L \dot{m}_{p,L} \\ &= \frac{\partial}{\partial x} \left[\phi S_L D_{pL} \frac{\partial w_{p,L}}{\partial x} \right]; \quad p = \text{asphaltene, paraffin} \end{aligned} \quad (14-94)$$

Note that

$$\rho_L w_{p,L} = \rho_{p,L} = \rho_p \sigma_{p,L} \quad (14-95)$$

If the particle density, ρ_p , is assumed constant, and the suspended particle content is expressed by the volume fraction of organic substance (paraffin or asphaltene), $\sigma_{p,L}$, according to Eq. 14-95, then Eq. 14-94 can be simplified as:

$$\begin{aligned} & \frac{\partial}{\partial t}(\phi S_L \sigma_{p,L}) + \frac{\partial}{\partial x}(u_L \sigma_{p,L}) + \frac{\partial \epsilon_p}{\partial t} + \frac{\phi S_L \dot{m}_{pL}}{\rho_p} \\ &= \frac{\partial}{\partial x} \left[\phi S_L D_{pL} \frac{\partial \sigma_{p,L}}{\partial x} \right]; \quad p = \text{asphaltene or paraffin} \end{aligned} \quad (14-96)$$

Note that both Ring et al. (1994) and Civan (1996) neglected the term on the right, representing the dispersion of particles.

The mass balances of the paraffin and asphaltene dissolved in oil is given by:

$$\begin{aligned} & \partial/\partial t(\phi S_L \rho_L x_{iL}) + \partial/\partial x(\rho_L u_L x_{iL}) + \phi S_L \dot{m}_{iL}/M_i \\ &= \partial/\partial x[\phi S_L D_{iL} \partial/\partial x(\rho_L x_{iL})]; \quad i = \text{asphaltene or paraffin} \end{aligned} \quad (14-97)$$

S is the saturation, ρ is the density, t is the time, x is distance, u is the volume flux, $\sigma_{p,L}$ is the volume fraction of the organic precipitates in

the liquid phase, $w_{p,L}$ denotes the mass fraction, x_{iL} is the mole fraction of organic dissolved in the oil, M_i is the molecular weight and D_{iL} is the dispersion coefficient. $\partial \epsilon_i / \partial t$ represents the volume rate of retention of organic deposits in porous media determined according to Eqs. 14–68, 69, and 76.

Assuming that the various phases are at thermal equilibrium at a temperature of $T_V = T_L = T_S = T$, the total porous media energy balance is given by:

$$\begin{aligned}
 & \partial / \partial t \left[\phi S_V \rho_V U_V + \phi S_L \rho_L U_L + \epsilon_{par} \rho_{par} U_{par} \right. \\
 & \left. + \epsilon_{asp} \rho_{asp} U_{asp} + (1 - \phi - \epsilon_{par} - \epsilon_{asp}) \rho_s U_s \right] + \\
 & \partial / \partial x \left(\rho_V u_V H_V + \rho_L u_L H_L \right) + \phi S_V \dot{q}_V + \phi S_L \dot{q}_L = \\
 & u_v \partial P_v / \partial x + u_L \partial P_L / \partial x + \\
 & \partial / \partial x \left\{ \left[\phi S_V k_V + \phi S_L k_L + \epsilon_{par} k_{par} + \epsilon_{asp} k_{asp} + \right. \right. \\
 & \left. \left. (1 - \phi - \epsilon_{par} - \epsilon_{asp}) k_s \right] \partial T / \partial x \right\}
 \end{aligned} \tag{14-98}$$

where U and H are the internal energy and enthalpy, respectively, \dot{q} is the energy loss, p is pressure, k denotes the thermal conductivity, and T is temperature.

Ring et al. (1994) simplified Eq. 14–98 as:

$$\begin{aligned}
 & \frac{\partial}{\partial t} \left[\phi S_V \rho_V U_V + \phi S_L \rho_L U_L + \phi S_p \rho_p U_p + (1 - \phi) \rho_s U_s \right] \\
 & + \frac{\partial}{\partial x} (\rho_V H_V u_V + \rho_L H_L u_L) + Q_L + Q_H + Q_E = \frac{\partial}{\partial x} \left(\phi k \frac{\partial T}{\partial x} \right)
 \end{aligned} \tag{14-99}$$

The first, second, and third terms represent the accumulation, convection, and conduction heat transfer. The last terms represent the heat carried away by production at wells, heat losses into formation surrounding the reservoir and the external heat losses.

The deposition of organic precipitates in porous media reduces the flow passages causing the fluids to accelerate. Therefore, Darcy's law is modified as following, considering the inertial effects, according to the Forchheimer equation (Civan, 1996):

$$u_J = -\mu_J^{-1} N_{nd_J} K \partial p_J / \partial x : J = V \text{ or } L \quad (14-100)$$

where K is the permeability, p_J is the fluid pressure, and the non-Darcy number is given by:

$$N_{nd_J} = (1 + \text{Re}_J)^{-1} \quad (14-101)$$

in which the porous media Reynolds number is given by:

$$\text{Re}_J = \rho_J u_J K \beta / \mu_J \quad (14-102)$$

where β is the inertial flow coefficient, and ρ_J and μ_J denote the density and viscosity of a fluid phase J .

Note that the formulations presented here are applicable for multi-dimensional cases encountered in the field if $\partial/\partial x$ is replaced by $\vec{\nabla} \cdot$ and a vector-tensor notation is applied.

Phase Transition

The source terms appearing on the right of Eqs. 14–92 through 99 are considered a sum of the internal (rock-fluid and fluid-fluid interactions) and external (wells) sources. When the oil is supersaturated, the internal contribution to the source terms in Eq. 14–94 is determined as the excess quantity of organic content of oil above the organic solubility at saturation conditions determined by Chung's (1992) thermodynamic model:

$$\dot{m}_{p,L} = \partial/\partial t (x_{p,L} - x_{p,L}^s), x_{p,L} > x_{p,L}^s \quad (14-103)$$

$$\dot{m}_{p,L} = 0, x_{p,L} < x_{p,L}^s ; \quad p = \text{asphaltene or paraffin} \quad (14-104)$$

where $x_{p,L}^s$ represents the mole-fraction of dissolved organic at saturation.

Civan (1995) carried out case studies similar to Ring et al. (1994) using the Sutton and Roberts data (1974). Figure 14–51 shows a comparison of the predicted and measured permeability impairments by paraffin deposition for below and above bubble point pressure cases.

Note that, above the bubble point pressure, only the liquid phase exists and there is more severe formation damage. Whereas, below the bubble point pressure, both the liquid and vapor phases exist and there is less severe formation damage.

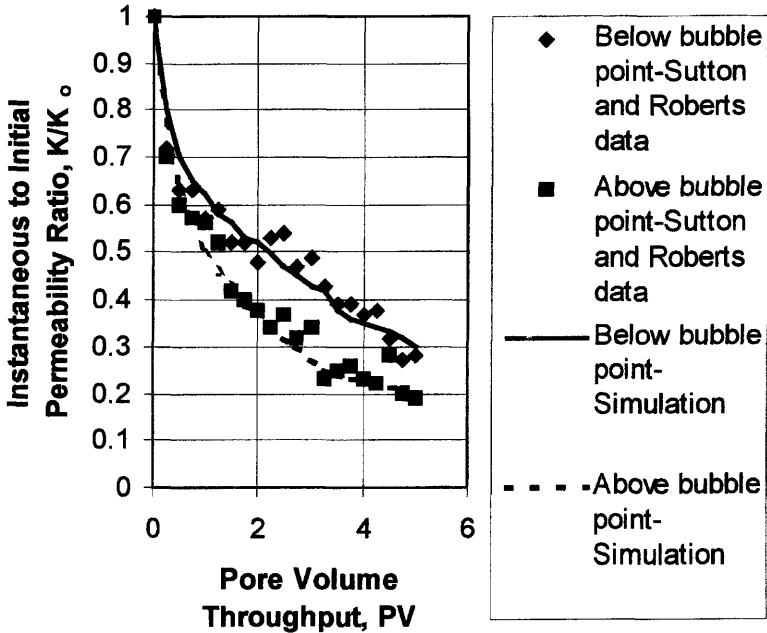


Figure 14-51. Comparison of the Sutton and Roberts (1974) experimental data and simulation results for permeability reduction by organic deposition below and above bubble point pressure.

Single-Porosity and Two-Phase Model for Organic Deposition

Ring et al. (1994) developed a two-phase model considering only the paraffin precipitation. They assumed that (1) oil is always saturated with the paraffin, (2) the solution is ideal, (3) paraffin deposition obeys a first order kinetics, (4) pores undergo an irreversible continuous plugging, and (5) permeability reduction obeys a power law:

$$\frac{K}{K_o} = \left(\frac{\phi}{\phi_o} \right)^m \quad (14-105)$$

Ring et al. (1994) determined that $m \cong 8$ for paraffin deposition.

Wang et al. (1999) developed an improved model considering the simultaneous deposition of asphaltenes and paraffins. Wang et al. (1999)

model incorporates the features of Civan's (1995) dual-porosity model for a single-porosity treatment. The formulation of the Wang et al. (1999) model and its experimental verification are described in the following.

Formulation*

Wang et al. (1999) used the ideal-solution theory to predict the solubility and precipitation of paraffin and asphaltene in crude oil; an improved one-dimensional, three-phase, and four-pseudo-component model to represent the transport of paraffin and asphaltene precipitates; and a deposition model including the static and dynamic pore surface depositions and pore throat plugging to describe the deposition of the paraffin and asphaltene. The model was developed for analysis of the laboratory core flow tests. The gravity effects and the capillary pressure effects between vapor and liquid phases have been neglected. The oil, gas, and solid phases were assumed at thermal equilibrium.

The oil, gas, paraffin, and asphaltene pseudo-components are denoted by O , G , P , and A , respectively. The vapor and the liquid phases are denoted by V and L , respectively. Considering both the free and dissolved gases, the gas component mass balance equation is given by:

$$\frac{\partial}{\partial t}(\phi S_V \rho_V + \phi S_L \rho_L w_{GL}) + \frac{\partial}{\partial x}(\rho_V u_V + \rho_L u_L w_{GL}) = 0 \quad (14-106)$$

where ϕ represents the porosity of the porous media, S_V, ρ_V, u_V are the saturation, density and flux of the vapor phase, respectively, and S_L, ρ_L, u_L are the saturation, density and flux of the liquid phase, respectively. w_{GL} represents the mass fraction of the dissolved gas in the liquid phase.

Considering that the oil component exists only in the liquid phase, its mass balance is given by:

$$\frac{\partial}{\partial t}(\phi S_L \rho_L w_{OL}) + \frac{\partial}{\partial x}(\rho_L u_L w_{OL}) = 0 \quad (14-107)$$

where w_{OL} is the mass fraction of the oil component in the liquid phase.

The paraffin mass balance equation is expressed by considering that it may be partly dissolved and/or suspended as particles in the liquid phase and deposited in porous media:

* Reprinted by permission of the Society of Petroleum Engineers from Wang et al., ©1999 SPE, SPE 50746 paper.

$$\begin{aligned} \frac{\partial}{\partial t}(\phi S_p \rho_p + \phi S_L \rho_L w_{PL}) + \frac{\partial}{\partial x}(\rho_L u_L w_{SPL} + \rho_L u_L w_{PL}) = \\ -\rho_p \frac{\partial \varepsilon_p}{\partial t} \end{aligned} \quad (14-108)$$

where S_p is the saturation of the suspended paraffin in the oil phase and ρ_p is the density of the paraffin. w_{PL} represents the mass fraction of the dissolved paraffin in the liquid phase. w_{SPL} is the mass ratio of the paraffin precipitates suspended in the liquid phase to the liquid phase. ε_p is the volume fraction of the deposited paraffin in the bulk porous media.

The asphaltene mass balance equation is written similarly as:

$$\begin{aligned} \frac{\partial}{\partial t}(\phi S_A \rho_A + \phi S_L \rho_L w_{AL}) + \frac{\partial}{\partial x}(\rho_L u_L w_{SAL} + \rho_L u_L w_{AL}) = \\ -\rho_A \frac{\partial \varepsilon_A}{\partial t} \end{aligned} \quad (14-109)$$

in which S_A is the saturation of the suspended asphaltene and ρ_A is the density of asphaltene. w_{AL} represents the mass fraction of the dissolved asphaltene in the liquid phase. w_{SAL} is the mass ratio of the asphaltene precipitates suspended in the liquid phase to the liquid phase. ε_A is the volume fraction of the deposited asphaltene in the bulk porous media.

The vapor and liquid phase volumetric fluxes are given by Darcy's equation, respectively, as:

$$u_v = -\frac{K k_{RV}}{\mu_v} \frac{\partial P}{\partial x} \quad (14-110)$$

$$u_L = -\frac{K k_{RL}}{\mu_L} \frac{\partial P}{\partial x} \quad (14-111)$$

where K is the absolute permeability of the porous media, and k_{RV} and μ_v are the relative permeability and viscosity of the vapor phase, respectively. k_{RL} and μ_L are the relative permeability and viscosity of the liquid phase, respectively. Neglecting the capillary pressure between the vapor and liquid phases, P represents the pressure of the pore fluids.

The total thermal equilibrium energy balance equation is expressed as:

$$\begin{aligned}
& \frac{\partial}{\partial t} [\phi S_V \rho_V H_V + \phi S_L \rho_L H_L + (\phi S_P + \epsilon_P) \rho_P H_P + \\
& (\phi S_A + \epsilon_A) \rho_A H_A + (1 - \phi - \epsilon_P - \epsilon_A) \rho_F H_F] \\
& + \frac{\partial}{\partial x} (\rho_V u_V H_V + \rho_L u_L H_L) = \\
& \frac{\partial}{\partial x} \left\{ [\phi S_V K_V + \phi S_L K_L + (\phi S_P + \epsilon_P) K_P + \right. \\
& \left. (\phi S_A + \epsilon_A) K_A + (1 - \phi - \epsilon_P - \epsilon_A) K_F] \frac{\partial T}{\partial x} \right\}
\end{aligned} \tag{14-112}$$

where H_V, H_L, H_P, H_A and H_F are the enthalpies of the vapor, liquid, paraffin, asphaltene, and porous media, respectively. K_V, K_L, K_P, K_A and K_F are the thermal conductivities of the vapor, liquid, paraffin, asphaltene, and porous media, respectively. T is the equilibrium temperature of the system.

The saturations of the vapor and liquid phases, and the paraffin and asphaltene precipitates suspended in the liquid phase, add up to 1:

$$S_V + S_L + S_P + S_A = 1 \tag{14-113}$$

The ideal-solution theory (Weingarten and Euchner, 1988; Chung, 1992) is applied for the paraffin and asphaltene solubility predictions, respectively, as:

$$X_{PL} = X_{Ps} \exp \left[-\frac{\Delta H_P}{R} \left(\frac{1}{T} - \frac{1}{T_{pm}} \right) \right] \tag{14-114}$$

$$X_{AL} = X_{As} \exp \left[-\frac{\Delta H_A}{R} \left(\frac{1}{T} - \frac{1}{T_{Am}} \right) \right] \tag{14-115}$$

where X_{PL} and X_{AL} indicate the mole fractions of the paraffin and asphaltene dissolved in the oil, respectively, and X_{Ps} and X_{As} are the mole fractions of the paraffin and asphaltene at saturation. ΔH_P and ΔH_A are the latent heats of fusion of the paraffin and asphaltene, respectively.

R is the universal gas constant. T_{Pm} and T_{Am} are the melting point temperatures of the paraffin and asphaltene, respectively. However, improved models are available by Lira-Galeana and Firoozabadi (1996), Yarranton and Masliyah (1996), and Zhou et al. (1996).

Applying Civan's model (1996), the paraffin and asphaltene deposition rates are given, respectively, by:

$$\frac{\partial \epsilon_P}{\partial t} = \lambda_P S_P \phi^{2/3} + \sigma_P S_P \phi^{2/3} u_L + \gamma_P S_P \phi u_L \quad (14-116)$$

$$\frac{\partial \epsilon_A}{\partial t} = \lambda_A S_A \phi^{2/3} + \sigma_A S_A \phi^{2/3} u_L + \gamma_A S_A \phi u_L \quad (14-117)$$

in which the first term represents the static surface deposition and λ is the static surface deposition rate constant. The second term represents the dynamic surface deposition and σ is the dynamic surface deposition rate constant. The third term represents the pore throat plugging deposition and γ is the plugging deposition rate constant.

The static surface deposition is assumed to occur irrespective of the fluid flow. However, the dynamic surface deposition is dominant during flow. The plugging deposition is considered based on the following criteria:

$$\gamma_j = \gamma_{ji} [1 + \alpha_j (\epsilon_P + \epsilon_A)], D_{pcr} < D_p, j = P, A \quad (14-118)$$

$$\gamma_j \equiv 0 \text{ otherwise, } j = P, A \quad (14-119)$$

γ_{ji} is the initial value of the plugging deposition rate constant. α_j represents empirically determined constants. D_p is the mean particles diameter. D_{pcr} is the critical, mean pore throats diameter below which pore throat plugging occurs, determined by Civan (1996):

$$D_{pcr} = D_{pt} A [1 - \exp(-BC_p u / \phi)] \quad (14-120)$$

where D_{pt} is the mean pore throat diameter and A and B are empirical constants. C_p is the suspended particle mass concentration in the oil.

The instantaneous porosity is given by:

$$\phi = \phi_i - \epsilon_P - \epsilon_A \quad (14-121)$$

and the instantaneous permeability is estimated by (Civan et al., 1989):

$$k = k_i \left(\frac{\phi}{\phi_i} \right)^3 \quad (14-122)$$

where ϕ_i and k_i are the initial porosity and permeability of the porous media, respectively.

Model Assisted Analysis of Laboratory Data

Wang et al. (1999) solved the model equations using an implicit finite difference method. They determined the best estimates of the parameters by history matching. The data used in six test cases and the best estimates of the model parameters are presented in Tables 14-7 and 14-8 by Wang et al. (1999).

Case 1

Sutton and Roberts (1974) first heated a Berea sandstone core saturated with a Shannon Sand crude oil to 54.4°C and then cooled the outlet of the core to 21.1°C for 2 hours without any flow. The cloud point of the oil used in their experiment was 37.8°C. The paraffin and asphaltene contents of the crude oil were 4.1 and 0.7 weight percents, respectively. Then, they conducted a flow experiment by injecting the Shannon Sand crude oil. The temperature of the outlet of the core was kept at 21.1°C. Figure 14-52 shows that the simulated results are satisfactory. They first simulated the static surface deposition during 2 hours of cooling without fluid flow. Then, they simulated the damage during flow. The pore throat plugging did not take place as indicated by the estimated values of rate constants given in Table 14-7.

Case 2

Sutton and Roberts (1974) have injected a Muddy formation crude oil into a Berea sandstone core. The outlet temperature of the core was kept at 21.1°C. The cloud point temperature of the oil sample is 35°C. The paraffin and asphaltene contents of the crude oil were 6.1 and 0.1 weight percents, respectively. Figure 14-53 shows the satisfactory simulated results. The static and dynamic surface depositions occurred, but the pore throat plugging did not occur as indicated by the values of the rate constants given in Table 14-7. Because the oil and core properties are very close for Cases 1 and 2, the permeability damage is also similar, as shown in Figures 14-52 and 14-53.

Table 14-7
Parameters for Cases 1 and 2*

CASE	1	2
Temperature		
T_m , °C	54.4	54.4
T_{cm} , °C	21.1	21.1
Gas pseudo-component		
M_g , g/gmole	16.0	16.0
ρ_{pg} , g/cm ³	0.00083	0.00083
Oil pseudo-component		
M_o , g/gmole	104.11	122.51
ρ_{og} , g/cm ³	0.72	0.75
Paraffin pseudo-component		
M_p , g/gmol	522.4	478.7
w_{ps} (%)	4.1	6.1
ρ_{pzc} , g/cm ³	0.83	0.98
T_{pm} , °C	75.7	71.7
ΔH_p , cal/g-mole	26,000	23,600
Asphaltene pseudo-component		
M_A , g/gmol	5,000.0	5,000.0
w_A (%)	0.7	0.1
ρ_{Azc} , g/cm ³	1.1	1.1
T_{Am} , °C	178.7	178.7
ΔH_A , cal/g-mole	44,400	44,400
Core Properties		
L , cm	30.5	30.5
D , cm	2.5	2.5
ϕ_i , fraction	0.25	0.25
k_i , darcy	0.405	0.314
Data for Simulation		
Δx , cm	2.54	2.54
Δt , sec	40.0	40.0
Number of blocks	12	12
Δp , atm	0.68	0.68
Deposition Parameters^①		
$\lambda_p = \lambda_A$, 1/sec	0.0001	0.000123
$\sigma_p = \sigma_A$, 1/cm	0.0245	0.0185
$\gamma_{pi} = \gamma_{Ai}$, 1/cm	0.0	0.0
$\alpha_p = \alpha_A$	0.0	0.0
A	0.0	0.0
B	0.0	0.0

① Obtained by history matching

* After Wang et al., ©1999 SPE; reprinted by permission of the Society of Petroleum Engineers.

Table 14–8
Parameters for Cases 3 through 6*

CASE	3	4	5	6
Oil Properties				
T, °C	50	50	-	-
μ (at 20 °C), cp	13	13	5.27	5.27
API	29	29	29.29	29.29
w_A (%)	5.3	5.3	53①	53①
M_A , g/gmol	6,000	6,000	6,000	6,000
Core Properties				
L, cm	5.08	5.08	26.5	26.5
D, cm	2.3	2.3	2.56	2.56
k_i , darcy	0.107	0.0122	0.011	0.011
ϕ_i	0.131	0.243	0.35	0.35
Data for Simulation				
Δx , cm	0.42	0.42	2.21	2.21
Δt , sec	100.0	7200.0	500.0	500.0
Number of blocks	12	12	12	12
Flow rate, ml/min	-	-	0.5	3.0
Deposition Parameters②				
λ_p , l/sec	0.0	0.0	0.0	0.0
σ_p , l/cm	0.0	0.0	0.0	0.0
γ_{Pi} , l/cm	0.0	0.0	0.0	0.0
α_p	0.0	0.0	0.0	0.0
λ_A , l/sec	0.0	0.0	0.0	0.0
σ_A , l/cm	0.0008	0.0039	0.75	0.7
γ_{Ai} , l/cm	0.0	0.0005	0.0	0.9
α_A	0.0	0.0	0.0	1600
A	0.0	180	0.0	200
B	0.0	100	0.0	95

① The asphaltene content of the injected oil obtained by mixing an oil containing 3% (weight) asphaltene with asphaltene at the 60 to 40 volume ratio.

② Obtained by history matching

* After Wang et al., ©1999 SPE; reprinted by permission of the Society of Petroleum Engineers.

Case 3

Wang et al. (1997) simulated Minssieux's (1997) RUN GF 1 experiments where the Weyburn oil (Canadian oil) was injected into the Fontainebleau sandstone at the reservoir temperature. The asphaltene and resin contents are 5.3% and 8.5% by weight. Only the dynamic surface deposition occurred as indicated by the rate constants given in Table 14–8. Figure 14–54 shows satisfactory results.

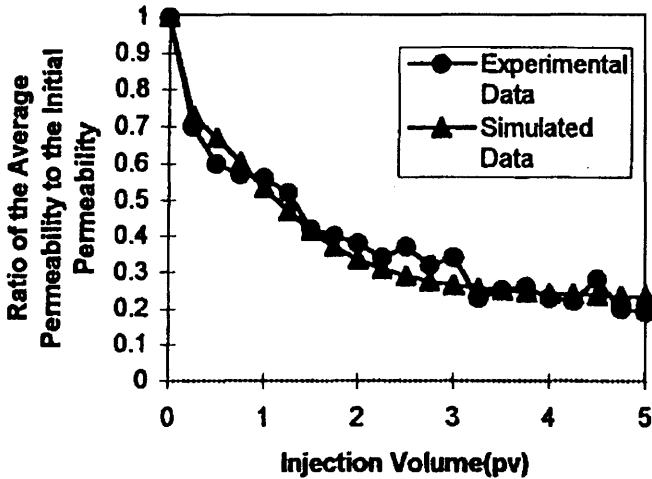


Figure 14-52. Simulation of the Sutton and Roberts (1974) experimental data for Case 1 (after Wang et al., ©1999 SPE; reprinted by permission of the Society of Petroleum Engineers).

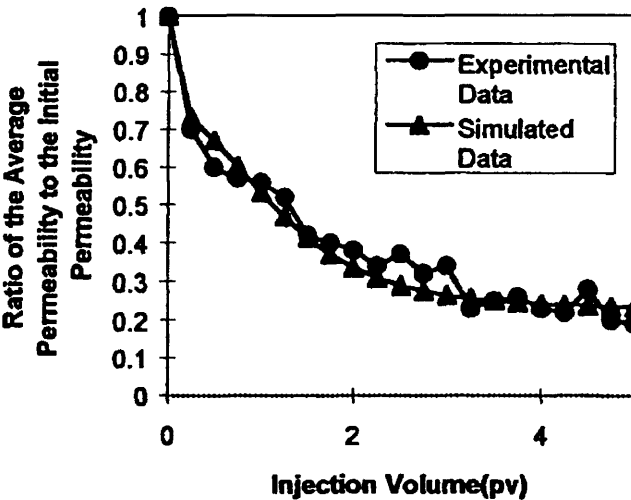


Figure 14-53. Simulation of the Sutton and Roberts (1974) experimental data for Case 2 (after Wang et al., ©1999 SPE; reprinted by permission of the Society of Petroleum Engineers).

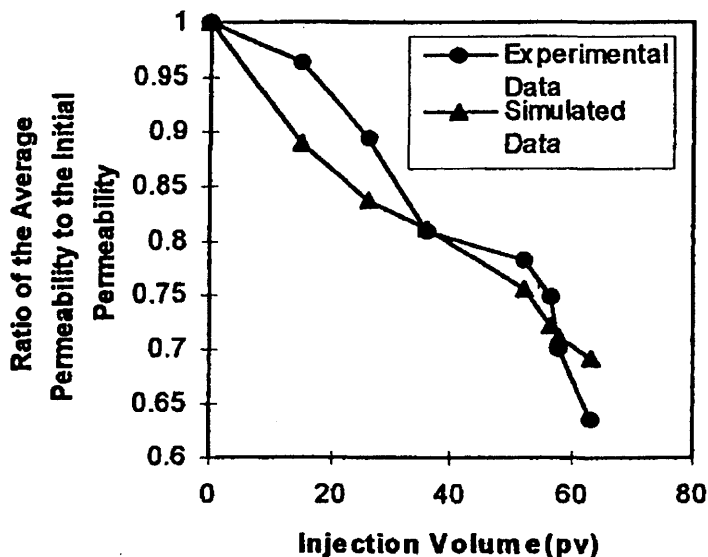


Figure 14-54. Simulation of the Minssieux (1997) experimental data for Case 3 (after Wang et al., ©1999 SPE; reprinted by permission of the Society of Petroleum Engineers).

Case 4

Wang et al. (1999) simulated the RUN GVM 10 data of Minssieux (1997). The oil sample is the same as Case 3, but the Vosges sandstone was used instead. The porosity of this sandstone, 0.243, is much higher than the Fontainebleau sandstone. The permeability of the sandstone, 12.2 md, is much lower than the Fontainebleau sandstone. Figure 14-55 shows the simulated results. The dynamic surface deposition and pore throat plugging took place as indicated by the estimated values of rate constants, given in Table 14-8.

Case 5

Wang et al. (1999) used the data by Ali and Islam (1997). A 60 to 40 volumetric mixture of a crude oil containing 3% of asphaltene by weight and extra asphaltene was injected into a core at a constant rate of 0.5 ml/min. The experiment was carried out at the reservoir temperature and pressure. The simulated results are shown in Figure 14-56. Only the surface deposition occurred as indicated by values of the rate constants given in Table 14-8.

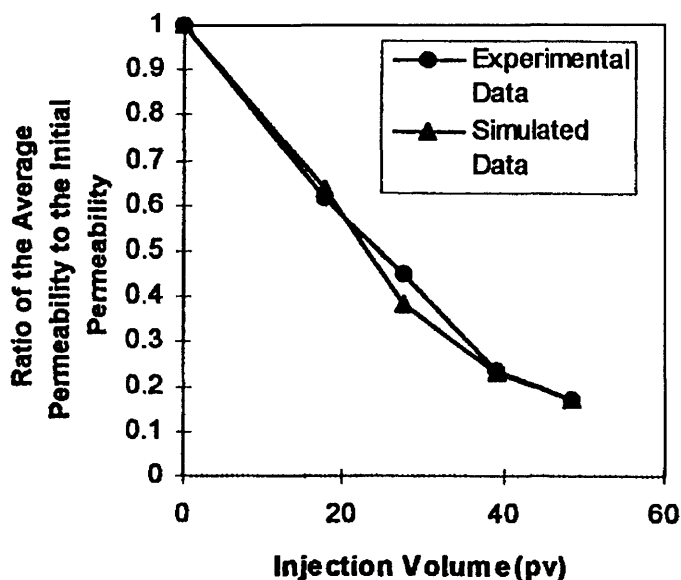


Figure 14-55. Simulation of the Minssieux (1997) experimental data for Case 4 (after Wang et al., ©1999 SPE; reprinted by permission of the Society of Petroleum Engineers).

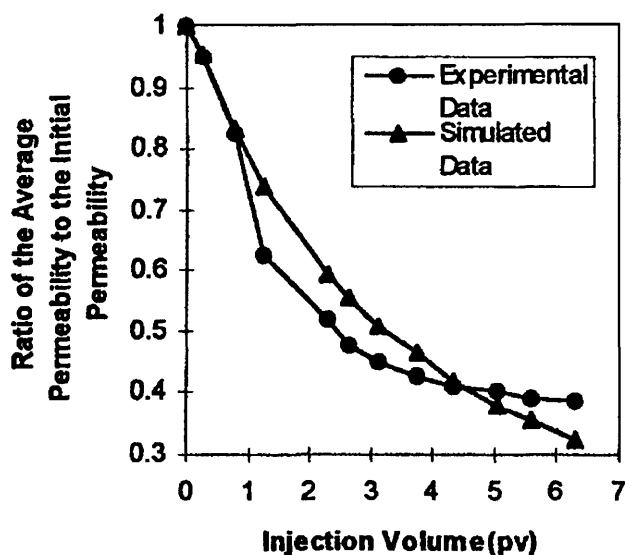


Figure 14-56. Simulation of the Ali and Islam (1998) experimental data for Case 5 (after Wang et al., ©1999 SPE; reprinted by permission of the Society of Petroleum Engineers).

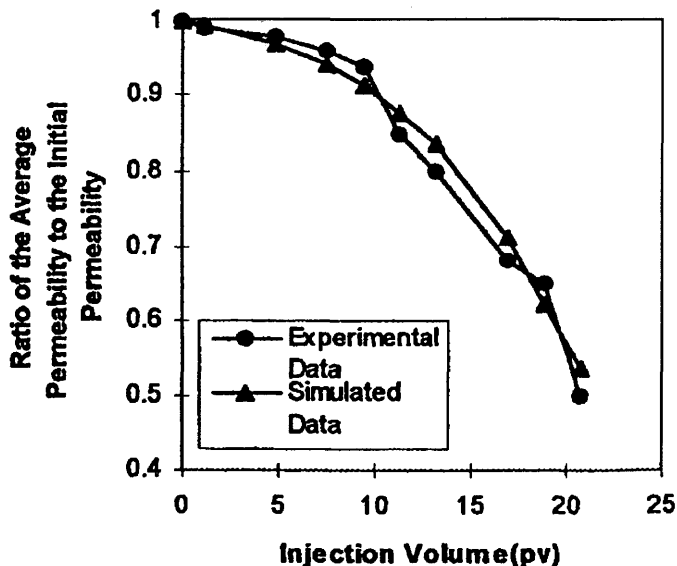


Figure 14-57. Simulation of the Ali and Islam (1998) experimental data for Case 6 (after Wang et al., ©1999 SPE; reprinted by permission of the Society of Petroleum Engineers).

Case 6

Next, Wang et al. (1999) simulated another data of Ali and Islam (1997). The core and oil are the same as in Case 5, but the injection rate is 3 ml/min. Both the dynamic surface deposition and pore throat plugging occurred. Figure 14-57 indicates that the simulated result satisfactorily match the experimental data.

References

- Acevedo, S., Ranaudo, M. A., Escobar, G., Gutiérrez, L., & Ortega, P., "Adsorption of Asphaltenes and Resins on Organic and Inorganic Substrates and Their Correlation with Precipitation Problems in Production Well Tubing," *Fuel*, Vol. 74, No. 4, 1995, pp. 595-598.
- Ali, M. A., & Islam, M. R., "The Effect of Asphaltene Precipitation on Carbonate-Rock Permeability: An Experimental and Numerical Approach," SPE Paper No. 38856, Proceedings of the 1997 SPE Annual Conference and Exhibition, held in San Antonio, Texas, October 1997, pp. 139-146.

- Ali, M. A., & Islam, M. R., "The Effect of Asphaltene Precipitation on Carbonate-Rock Permeability: An Experimental and Numerical Approach," *SPE Production and Facilities Journal*, August 1998, pp. 178–183.
- Amaefule, J. O., Kersey, D. G., Norman, D. L., & Shannon, P. M., "Advances in Formation Damage Assessment and Control Strategies," CIM Paper No. 88-39-65, Proceedings of the 39th Annual Technical Meeting of Petroleum Society of CIM and Canadian Gas Processors Association, June 12–16, 1988, Calgary, Alberta, 16 p.
- Andersen, S. I., Keul, A., & Stenby, E., "Variation in Composition of Subfractions of Petroleum Asphaltenes," *Petroleum Science and Technology*, Vol. 15, No. 7 & 8, 1997, pp. 611–645.
- Chang, F. F., & Civan, F., "Practical Model for Chemically Induced Formation Damage," *J. of Petroleum Science and Engineering*, Vol. 17, 1997, pp. 123–137.
- Chang, C.-L., & Fogler, H. S., "Peptization and Coagulation of Asphaltenes in Apolar Media Using Oil-Soluble Polymers," *Fuel Science and Technology International*, Vol. 14, No. 1 & 2, 1996, pp. 75–100.
- Chang, C.-L., & Fogler, H. S., *Langmuir*, Vol. 10, 1994, pp. 1749–1758.
- Chung, T.-H., "Thermodynamic Modeling for Organic Solid Precipitation," SPE 24851, Proceedings of the 67th Annual technical Conference and Exhibition of the SPE held in Washington, D.C., October 4–7, 1992, pp. 869–878,
- Civan, F., "A Generalized Model for Formation Damage by Rock-Fluid Interactions and Particulate processes," SPE 21183 paper, Proceedings of the SPE 1990 Latin American Petroleum Engineering Conference, October 14–19, 1990, Rio de Janeiro, Brazil, 11 p.
- Civan, F., "Evaluation and Comparison of the Formation Damage Models," SPE 23787 paper, Proceedings of the SPE International Symposium on Formation Damage Control, February 26–27, 1992, Lafayette, Louisiana, pp. 219–236.
- Civan, F., Predictability of Formation Damage: An Assessment Study and Generalized Models, Final Report, U.S. DOE Contract No. DE-AC22-90BC14658, April 1994.
- Civan, F., "A Multi-Phase Mud Filtrate Invasion and Well Bore Filter Cake Formation Model," SPE 28709 paper, Proceedings of the SPE International Petroleum Conference & Exhibition of Mexico, October 10–13, 1994, Veracruz, Mexico, pp. 399–412.
- Civan, F., "Modeling and Simulation of Formation Damage by Organic Deposition," Proceedings of the First International Symposium on Colloid Chemistry in Oil Production: Asphaltene and Wax Deposition, ISCOP '95, Rio de Janeiro, Brazil, November 26–29, 1995, pp. 102–107.

- Civan, F. "A Multi-Purpose Formation Damage Model" SPE 31101 paper, the SPE Formation Damage Control Symposium, Lafayette, Louisiana, February 14–15, 1996, pp. 311–326.
- Civan, F., "Interactions of the Horizontal Wellbore Hydraulics and Formation Damage," SPE 35213 paper, Proceedings of the SPE Permian Basin Oil & Gas Recovery Conf., March 27–29, 1996, Midland, Texas, pp. 561–569.
- Civan, F., Knapp, R. M., & Ohen, H. A., "Alteration of Permeability by Fine Particle Processes," *Journal of Petroleum Science and Engineering*, Vol. 3, Nos. 1/2, October 1989, pp. 65–79.
- DeBoer, R. B., Leerlooyer, K., Eigner, M. R. P., & van Bergen, A. R. D., "Screening of Crude Oils for Asphalt Precipitation: Theory, Practice, and the Selection of Inhibitors," SPEPF, February 1995, pp. 55–61.
- Dubey, S. T., & Waxman, M. H., "Asphaltene Adsorption and Desorption From Mineral Surfaces," *SPE Reservoir Engineering*, August 1991, pp. 389–395.
- Gruesbeck, C. and R. E. Collins, "Entrainment and Deposition of Fine Particles in Porous Media," *SPEJ*, pp. 847–856, December 1982.
- Gruesbeck, C. and Collins, R. E., "Particle Transport Through Perforations," *SPEJ*, December 1982, pp. 857–865.
- Gupta, S. P., & Greenkorn, R. A., "Dispersion During Flow in Porous Media with Bilinear Adsorption," *Water Resources Research*, Vol. 9, 1973, pp. 1357–1368.
- Haskett, C. E., & Tartera, M., "A Practical Solution to the Problem of Asphaltene Deposits-Hassi Messaoud Field, Algeria," *JPT*, April 1965, pp. 387–391.
- Houchin, L. R., & Hudson, L. M., "The Prediction, Evaluation and Treatment of Organic Damage Caused by Organic Deposition," SPE 14818 paper, Proceedings of the Seventh SPE Symposium on Formation Damage Control, February 26–27, 1986, Lafayette, Louisiana, pp. 83–90.
- Khalil, C. N., Rocha, N. O., & Silva, E. B., "Detection of Formation Damage Associated to Paraffin in Reservoirs of the Recôncavo Baiano, Brazil," Proceedings of the 1997 SPE International Symposium on Oil Field Chemistry held in Houston, Texas, February 18–21, pp. 277–281.
- Leontaritis, K. J., "Application of a Thermodynamic-Colloidal Model of Asphaltene Flocculation," presented at the Symposium of Solids Deposition, Area 16C of Fuels and Petrochemical Division, AIChE Spring National Meeting and Petroleum Exposition, March 28–April 1, 1993, Houston, Texas.
- Leontaritis, K. J., "The Asphaltene and Wax Deposition Envelopes," *Fuel Science and Technology International*, Vol. 14, No. 1 & 2, Marcel Dekker, Inc., New York, 1996, pp. 13–39.

- Leontaritis, K. J., "PARA-Based (Paraffin-Aromatic-Resin-Asphaltene) Reservoir Oil Characterizations," SPE Paper 37252, Proceedings of the 1997 SPE International Symposium on Oilfield Chemistry held in Houston, Texas, February 18–21, 1997, pp. 421–440.
- Leontaritis, K. J., "Asphaltene Near-Wellbore Formation Damage Modeling," SPE Paper 39446, Proceedings of the 1998 SPE Formation Damage Control Conference held in Lafayette, Louisiana, February 18–19, 1998, pp. 277–288.
- Leontaritis, K. J., & Mansoori, G. A., "Asphaltene Flocculation During Oil Production and Processing: A Thermodynamic-Colloidal Model," SPE Paper 16258, Proceedings of the SPE International Symposium on Oil Field Chemistry, San Antonio, Texas, January 1987, pp. 149–158.
- Leontaritis, K. J., Amaefule, J. O., and Charles, R. E., "A Systematic Approach for the Prevention and Treatment of Formation Damage Caused by Asphaltene Deposition," SPE Paper 23810, Proceedings of the SPE International Symposium on Formation Damage Control, Lafayette, LA, February 26–27, 1992, pp. 383–395.
- Lichaa, P. M., "Asphaltene Deposition Problem in Venezuela Crudes, Usage of Asphaltenes in Emulsion Stability," *Oil Sands*, June 1997, pp. 609–624.
- Lira-Galeana, C., & Firoozabadi, A., "Thermodynamics of Wax Precipitation in Petroleum Mixtures," *AIChE Journal*, Vol. 42, No. 1, January 1996, pp. 239–248.
- Manoranjana, V. S., & Stauffer, T. B., "Exact Solution for Contaminant Transport with Kinetic Langmuir Sorption," *Water Resources Research*, Vol. 32, No. 3, 1996, pp. 749–752.
- Mansoori, G. A., "Modeling of Asphaltene and Other Heavy Organic Depositions," *Journal of Petroleum Science and Engineering*, Vol. 17, 1997, pp. 101–111.
- Mansoori, G. A., "Modeling and Prevention of Asphaltene and Other Heavy Organic Deposition in Oil Wells," Paper SPE 27070, proceedings of the International Symposium on Formation Damage Control held in Lafayette, Louisiana, 9–10 February 1994, pp. 9–18.
- Mansoori, G. A., "Modeling and Prevention of Asphaltene and Other Heavy Organic Deposition in Oil Wells," SPE 27070 paper, presented at the Third Latin American/Caribbean Petroleum Engineering Conference, April 27–29, 1994, Buenos Aires, Argentina.
- Marquardt, D. W., "An Algorithm for Least-squares Estimation of Nonlinear Parameters," *J. Soc. Indust. Appl. Math.*, Vol. 11, 1963, p. 431.
- Metzner, A. B., & Reed, J. C., "Flow of Non-Newtonian Fluids—Correlation of the Laminar, Transition, and Turbulent Flow Regions," *AIChE J.*, Vol. 1, No. 4, 1955, pp. 434–440.

- Minssieux, L., "Core Damage From Crude Asphaltene Deposition" SPE 37250 paper, 1997 SPE International Symposium on Oilfield Chemistry, February 18–21, 1997, Houston, Texas.
- Nghiem, L. X., & Coombe, D. A., "Modeling Asphaltene Precipitation During Primary Depletion," *SPE Journal*, Vol. 2, June 1997, pp. 170–176.
- Philp, R. P., Bishop, A. N., Del Rio, J.-C., and Allen, J., "Characterization of High Molecular Weight Hydrocarbons (>C₄₀) in Oils and Reservoir Rocks," in *The Geochemistry of Reservoirs*, Cubitt, J. M. and England, W. A. (Eds.), Geological Society Special Publication No. 86, 1995, pp. 71–85.
- Ring, J. N., Wattenbarger, R. A., Keating, J. F., and Peddibhotla, S., "Simulation of Paraffin Deposition in Reservoirs," *SPE Production & Facilities*, February 1994, pp. 36–42.
- Schechter, R. S., *Oil Well Stimulation*, Prentice Hall, Englewood Cliffs, New Jersey, 1992, 602 p.
- Sircar, S., Novosad, J., & Myers, A. L., "Adsorption from Liquid Mixtures on Solids, Thermodynamics of Excess Properties and Their Temperature Coefficients," *I&EC Fund.*, Vol. 11, 1972, p. 249.
- Speight, J. G., "Asphaltenes in Crude Oil and Bitumen: Structure and Dispersion," Chapter 8, pp. 377–401, in *Suspensions: Fundamentals and Applications in the Petroleum Industry*, Schramm, L. L. (Ed.), Advances in Chemistry Series 251, American Chemical Society, 1996, Washington, DC, 800 p.
- Speight, J. G., "The Chemical and Physical Structure of Petroleum: Effects on Recovery Operations," *J. of Petroleum Science and Engineering*, Vol. 22, Nos. 1–3, 1999, pp. 3–15.
- Speight, J. G., "Solvent Effects in the Molecular Weights of Petroleum Asphaltenes," Preprints ACS, Div. Pet. Chem., pp. 825–832.
- Speight, J. G., & Long, R. B., "The Concept of Asphaltenes Revisited," *Fuel Science and Technology International*, Vol. 14, No. 1 & 2, 1996, pp. 1–12.
- Srivastava, R. K., & Huang, S. S., "Asphaltene Deposition During CO₂ Flooding: A Laboratory Assessment," Paper SPE 37468, Proceedings of the 1997 SPE Productions Operations Symposium, held in Oklahoma City, Oklahoma, March 9–11, 1997, pp. 617–635.
- Sutton, G. D., & Roberts, L. D., "Paraffin Precipitation During Fracture Stimulation," *JPT*, September 1974, pp. 997–1004.
- Wang, S., Civan, F., & Strycker, A. R., "Simulation of Paraffin and Asphaltene Deposition in Porous Media," SPE 50746 paper, SPE International Symposium on Oilfield Chemistry, February 16–16, 1999, Houston, Texas, pp. 449–458.
- Weingarten, J. S., & Euchner, J. A., "Methods for Predicting Wax Precipitation and Deposition," *SPE*, February 1988, pp. 121–132.

- Wojtanowicz, A. K., Krilov, Z., & Langlinais, J. P., "Experimental Determination of Formation Damage Pore Blocking Mechanisms," Trans. of the ASME, *Journal of Energy Resources Technology*, Vol. 110, 1988, pp. 34–42.
- Wojtanowicz, A. K., Krilov, Z. and Langlinais, J. P.: "Study on the Effect of Pore Blocking Mechanisms on Formation Damage," Paper SPE 16233, presented at Society of Petroleum Engineers Symposium, March 8–10, 1987, Oklahoma City, Oklahoma, pp. 449–463.
- Yarranton, H. W., & Masliyah, J. H., "Molar Mass Distribution and Solubility Modeling of Asphaltenes," *AIChE Journal*, Vol. 42, No. 12, December 1996, pp. 3533–3543.
- Zhou, X., Thomas, F. B., & Moore, R. G., "Modeling of Solid Precipitation from Reservoir Fluid," *Journal of Canadian Petroleum Technology*, Vol. 35, No. 10, December 1996, pp. 37–45.

Part V

Assessment of the Formation Damage Potential

**Testing, Simulation,
Analysis, and
Interpretation**

Chapter 15

Laboratory Evaluation of Formation Damage

Summary

Frequently, the formation damage potential of petroleum bearing formations and methods of circumventing and remediation of formation damage are investigated by subjecting the reservoir core samples to flow at near-in situ conditions in the laboratory. The scenarios planned for field applications are simulated in the laboratory under controlled conditions and the response of the core samples under these conditions are measured. The tests carried out over a range of variables yield valuable data and insight into the reaction of the core samples to fluid conditions and its effect on the alteration of the core properties. These data can be used for model assisted analysis of the processes leading to formation damage. This exercise yields important information about the relative contributions of the various mechanisms to formation damage and help determine the values of the relevant process parameters. This information can be used to simulate the formation damage processes at the field scale. This, then, provides a valuable tool for quickly reviewing and screening the various alternative scenarios and optimizing the field applications to avoid or minimize the formation damage problems in the field.

In this chapter, a brief description of the commonly practiced laboratory procedures and measurement techniques is presented. The presentation is made in three parts: (1) evaluation of the core samples, (2) preparation and characterization of the fluid samples, and (3) experimental design, instrumentation, and measurement techniques.

Introduction

Development of meaningful laboratory testing and data interpretation techniques for assessment of the formation damage potential of petroleum-

bearing formations under actual scenarios of field operations, and for evaluation of techniques for restoration and stimulation of damaged formations are essential for efficient exploitation of petroleum reservoirs. Experimental systems and procedures should be designed to extract meaningful and accurate experimental data. The data should be suitable for use with the available analytical interpretation methods. This is important to develop reliable empirical correlations, verify mathematical models, identify the governing mechanisms, and determine the relevant parameters. These are then used to develop optimal strategies to mitigate the adverse processes leading to formation damage during reservoir exploitation. As expressed by Thomas et al. (1998):

Laboratory testing is a critical component of the diagnostic procedure followed to characterize the damage. To properly characterize the formation damage, a complete history of the well is necessary. Every phase, from drilling to production and injection, must be evaluated. Sources of damage include drilling, cementing, perforating, completion and workover, gravel packing, production, stimulation, and injection operations. A knowledge of each source is essential. For example, oil-based drilling mud may cause emulsion or wettability changes, and cementing may result in scale formation in the immediate wellbore area from pH changes. Drilling damage in horizontal wells can be very high because of the long exposure time during drilling (mud damage and the mechanical action of the drill pipe on the formation face); thus, the well's history may indicate several potential sources and types of damage.

For meaningful formation damage characterization, laboratory core flow tests should be conducted under certain conditions (Porter, 1989; Mungan, 1989):

1. Samples of actual fluids and formation rocks and all potential rock-fluid interactions should be considered.
2. Laboratory tests should be designed in view of the conditions of all field operations, including drilling, completion, stimulation, and present and future oil and gas recovery strategies and techniques.
3. The ionic compositions of the brines used in laboratory tests should be the same as the formation brines and injection brines involving the field operations.
4. Cores from oil reservoir should be unextracted to preserve their native residual oil states.

This is important because Mungan (1989) says that "Crude oils, especially heavy and asphaltenic crudes, provide a built-in stabilizing

effect for clays and fines in the reservoir, an effect that would be removed by extraction.”

Fundamental Processes of Formation Damage in Petroleum Reservoirs

Formation damage in petroleum-bearing formation occurs by various mechanisms and/or processes, depending on the nature of the rock and fluids involved, and the in-situ conditions. The commonly occurring processes involving rock-fluid and fluid-fluid interactions and their affects on formation damage by various mechanisms have been reviewed by numerous studies, including Mungan (1989), Gruesbeck and Collins (1982), Khilar and Fogler (1983), Sharma and Yortsos (1987), Civan (1992, 1994, 1996), Wojtanowicz et al. (1987, 1988), Masikewich and Bennion (1999), and Doane et al. (1999).

The fundamental processes causing formation damage can be classified as following:

1. Physico-chemical
2. Chemical
3. Hydrodynamic
4. Mechanical
5. Thermal
6. Biological

Laboratory tests are designed to determine, understand and quantify the governing processes, their parameters, and dependency on the in-situ and various operational conditions, and their effect on formation damage. Laboratory tests help determine the relative contributions of various mechanisms to formation damage. For convenience, the frequently encountered formation damage mechanisms can be classified into two groups (Amaefule et al., 1988; Masikewich and Bennion, 1999): (1) fluid-fluid interactions and (2) fluid-rock interactions. The fluid-fluid interactions include: (a) emulsion blocking, (b) inorganic deposition, and (c) organic deposition. The fluid-rock interactions include: (a) mobilization, migration and deposition of in-situ fine particles, (b) invasion, migration and deposition of externally introduced fine particles, (c) alteration of particle and porous media properties by surface processes such as absorption, adsorption, wettability change, swelling, and (d) damage by other processes, such as counter-current imbibition, grinding and mashing of solids, and surface glazing that might occur during drilling of wells (Bennion and Thomas, 1994).

Selection of Reservoir Compatible Fluids

Figure 15–1 by Masikewich and Bennion (1999) outlines the typical information, tests and processes necessary for laboratory testing and optimal design, and selection of fluids for reservoir compatibility. Hence, Masikewich and Bennion (1999) classify the effort necessary for fluid testing and design into six steps:

1. Identification of the fluid and rock characteristics
2. Speculation of the potential formation damage mechanisms
3. Verification and quantification of the pertinent formation damage mechanisms by various tests
4. Investigation of the potential formation damage mitigation techniques
5. Development of the effective bridging systems to minimize and/or avoid fluids and fines invasion into porous media
6. Testing of candidate fluids for optimal selection

Experimental Set-up for Formation Damage Testing

The design of apparatus for testing of reservoir core samples with fluids varies with specific objectives and applications. Typical testing systems include core holders, fluid reservoirs, pumps, flow meters, sample collectors, control systems for temperature, pressure or flow, and data acquisition systems. The degree of sophistication of the design of the core testing apparatus depends on the requirements of particular testing conditions and expectations. Figures 15–2, 15–3, and 15–4 by Doane et al. (1999) describe, respectively, the typical designs of a primitive system that operates at ambient laboratory temperature, and overbalanced and underbalanced core testing apparatus that operate at reservoir temperature.

High quality and specific purpose laboratory core testing facilities can be designed, constructed, and operated for various research, development, and service activities. Ready-made systems are also available in the market.

The schematic drawing given in Figure 15–2 indicates that primitive core testing systems consist of a core holder, a pressure transducer controlling the pressure difference across the core, an annulus pump to apply an overburden pressure over the rubber sleeve containing the core plug, a reservoir containing the testing fluid such as a drilling mud or filtrate, a displacement pump to pump the testing fluid into the core plug, and an effluent fluid collection container, such as a test tube. There is no temperature control on this system. It operates at ambient laboratory conditions.

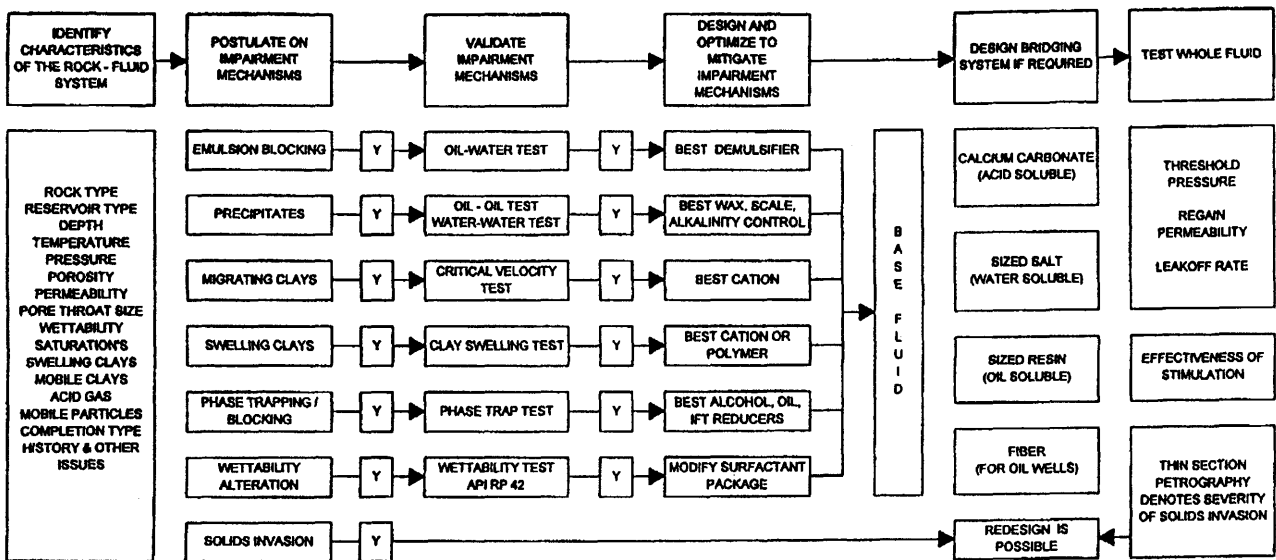


Figure 15-1. Outline of fluid design and development strategies and the process to circumvent reservoir issues (after Masikevich and Bennion, ©1999; reprinted by permission of the Canadian Institute of Mining, Metallurgy and Petroleum).

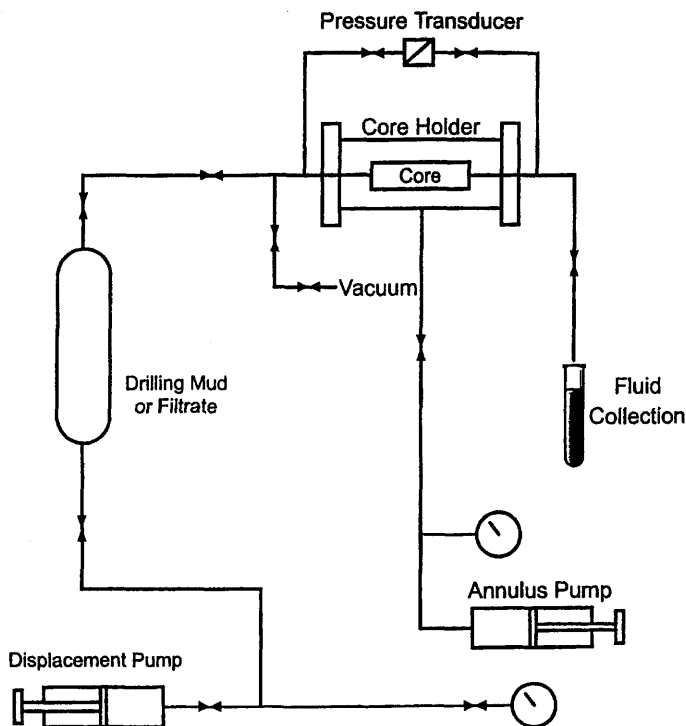


Figure 15-2. Primitive drilling fluid evaluation system (after Doane et al., ©1999; reprinted by permission of the Canadian Institute of Mining, Metallurgy and Petroleum).

The schematic drawing given in Figure 15-3 shows the elements of a typical overbalanced core testing apparatus. This system has been designed for core testing at near-in-situ temperature and stress conditions, although other features are similar to that of the primitive system shown in Figure 15-2. The schematic given in Figure 15-4 shows the elements of a typical underbalanced core testing apparatus, which also operates at near-in situ temperature and stress conditions.

Special Purpose Core Holders

Core flood tests can be conducted in one-dimensional linear (Figures 15-2, 15-3, and 15-4) and radial modes. Figures 15-5a-d by Saleh et al. (1997) show a schematic of typical radial flow models. Radial models

(text continued on page 466)

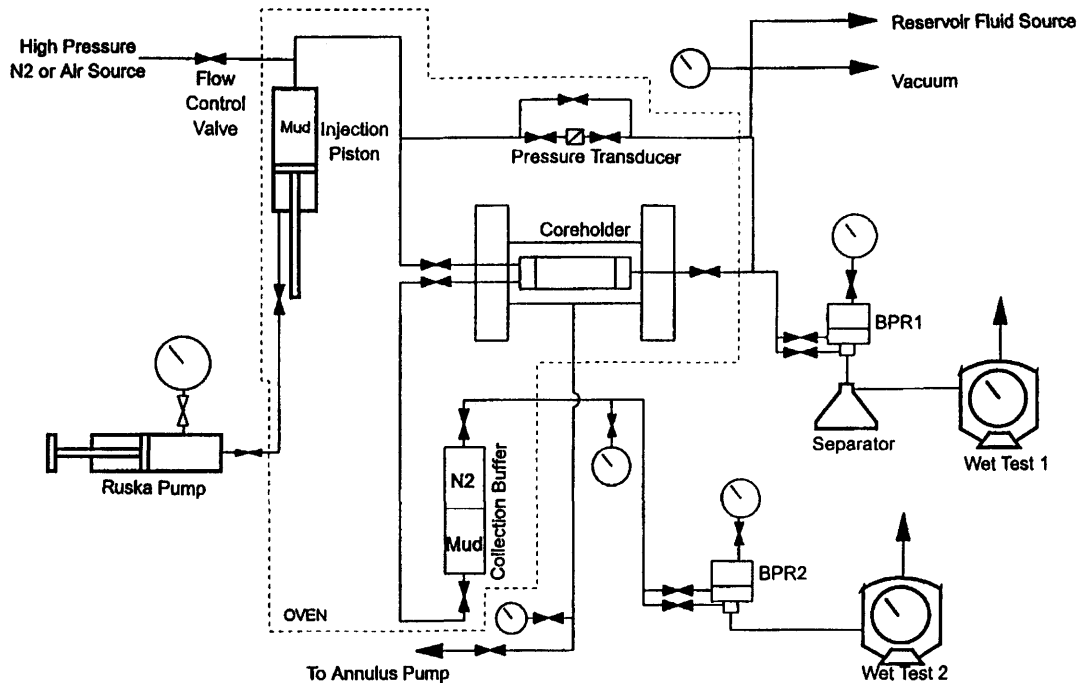


Figure 15–3. Current reservoir condition fluid leak-off evaluation system (after Doane et al., ©1999; reprinted by permission of the Canadian Institute of Mining, Metallurgy and Petroleum).

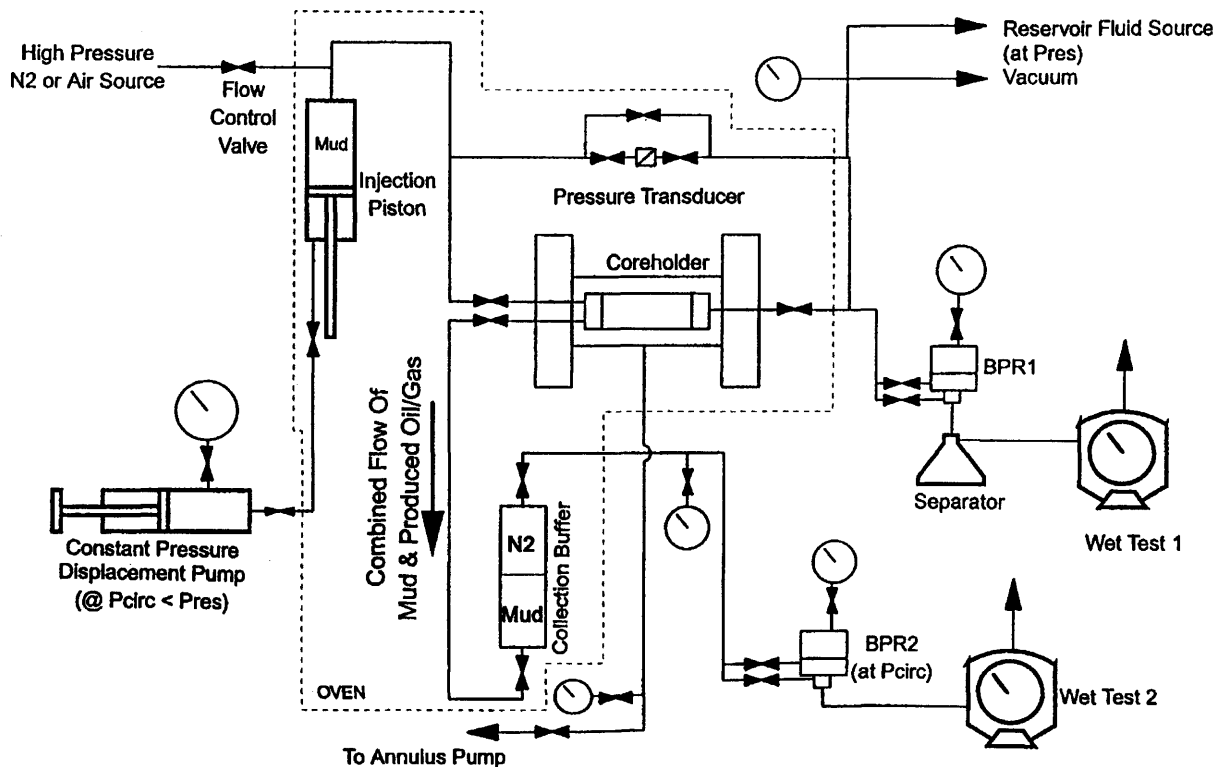


Figure 15-4. Underbalanced reservoir condition fluid leak-off evaluation system (after Doane et al., ©1999; reprinted by permission of the Canadian Institute of Mining, Metallurgy and Petroleum).

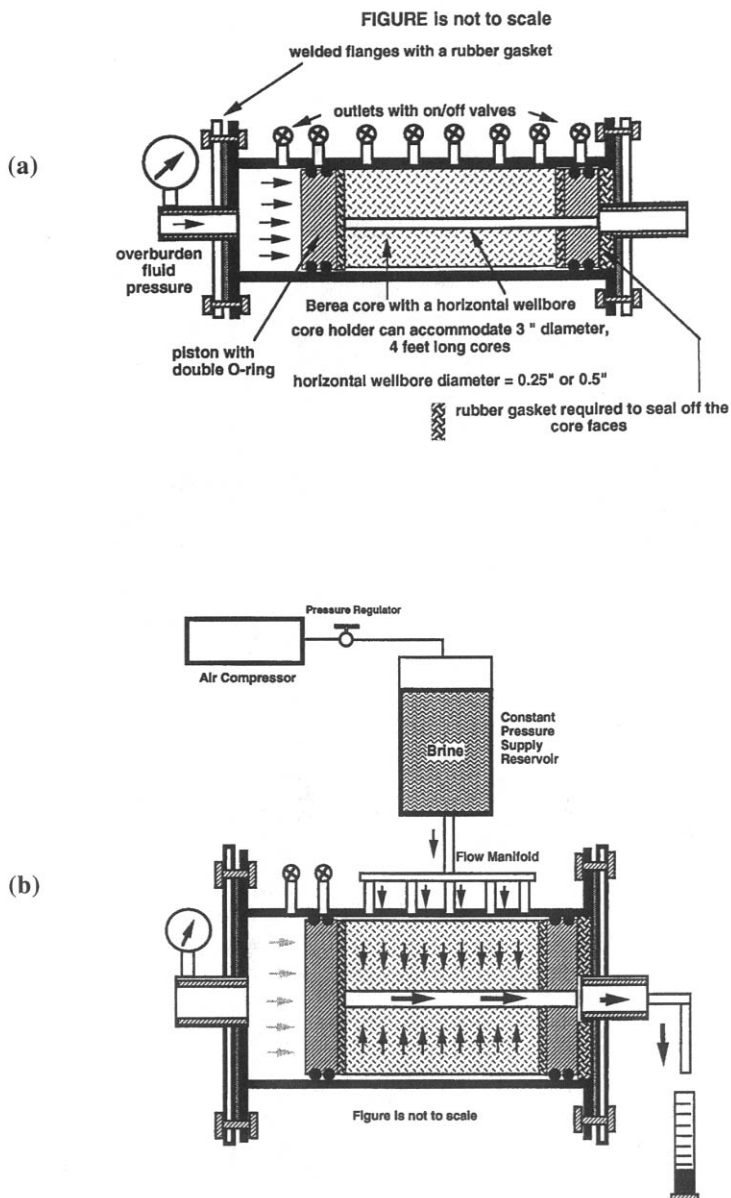


Figure 15-5. Systems for horizontal wellbore studies: (a) core holder design, (b) overall productivity evaluation, (c) overall injectivity evaluation, and (d) drilling fluid evaluation (reprinted from *Journal of Petroleum Science and Engineering*, Vol. 17, Saleh, S. T., Rostam, R., El-Rabaa, W., and Islam, M. R., "Formation Damage Study with a Horizontal Wellbore Model, pp. 87-99, ©1997; reprinted with permission from Elsevier Science).

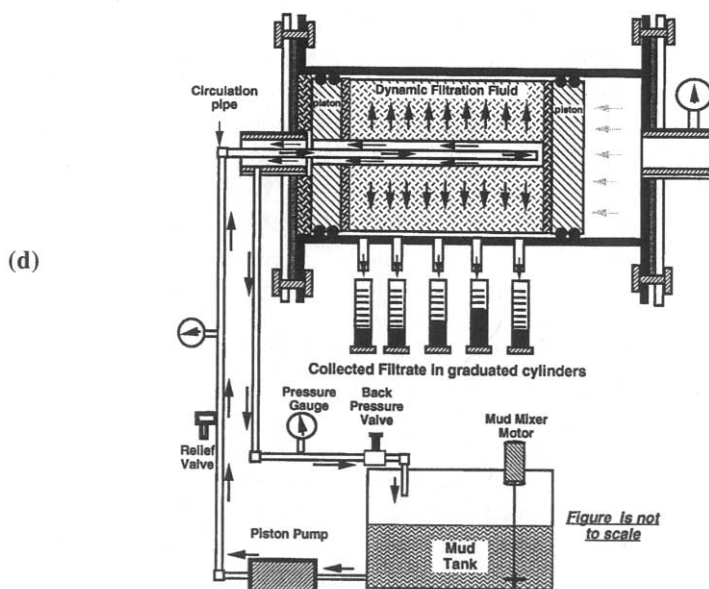
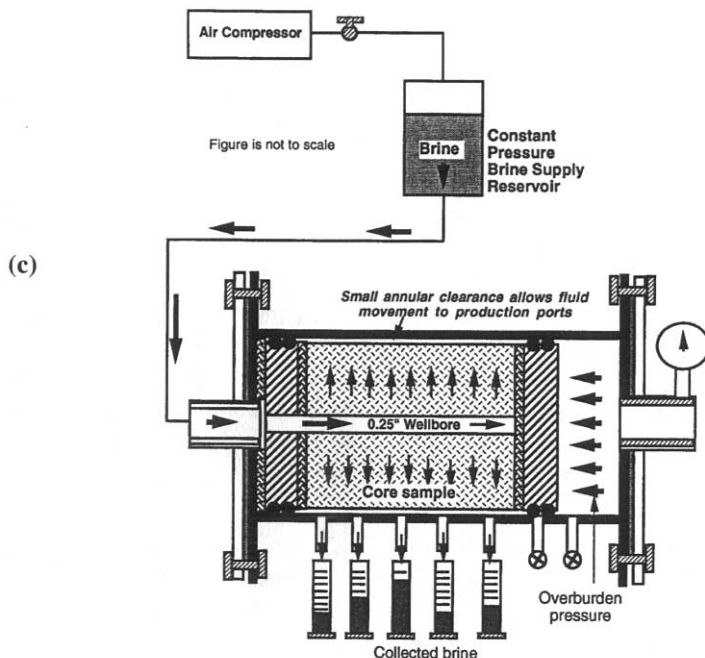


Figure 15-5 continued

(text continued from page 461)

better represent the effect of the converging or diverging flows in the near-wellbore formation. However, linear models are preferred for convenience in testing and preparation of core samples.

The majority of the core flow tests facilitate horizontal core plugs because the application of Darcy's law for horizontal flow does not include the gravity term and the analytical derivations used for interpretation of the experimental data is simplified. This approach provides reasonable accuracy for single-phase fluids flowing through small diameter core plugs. However, when multi-phase fluid systems with significantly different properties and particulate suspensions are flown through the core plugs, an uneven distribution of fluids and/or suspended particles can occur over the cross-sectional areas of cores. This phenomenon complicates the solution of the equations necessary for interpretation of the experimental data. In particular, errors arise because, frequently, the transport phenomena occurring in core plugs are described as being one-dimensional along the cores. In order to alleviate this problem, it is more convenient to conduct core flow tests using vertical core plugs. Consequently, the gravity term is included in Darcy's law, but errors associated with uneven distribution of fluid properties over the cross-sectional area of the core plugs are avoided. Therefore, Čerňanský and Široký (1985) used a vertical core holder.

The dimensions of the core plugs are important parameters and should be carefully selected to extract meaningful data. Typically 1 to 2 in (2.54 to 5.08 cm) diameter and 1 to 4 in (2.54 to 10.58 cm) long cores are used. The aspect ratio of a core plug is defined by the diameter-to-length ratio. Small diameter cores introduce more boundary effects near the cylindrical surface covered by the rubber sleeve. This, in turn, introduces errors in model-assisted data interpretation and analysis when one-dimensional models are used, as frequently practiced in many applications for computational convenience and simplification purposes. On the other hand, short cores do not allow for sufficient distance for investigation of the effect of the precipitation and dissolution processes and depth of invasion (Fambrough and Newhouse, 1993; Gadiyar and Civan, 1992; Doane et al., 1999). Longer cores are required for measurement of sectional or spatial porosity and permeability alteration.

As described by Doane et al. (1999), a number of special purpose core holders have been designed. Figure 15–6 shows a single core for which only the pressures at inlet and outlet ports can be measured. This type of system is usually used with small core plugs. It only yields core response, integrated over the core length. As shown in Figure 15–7, long cores equipped with intermediate pressure taps can provide information

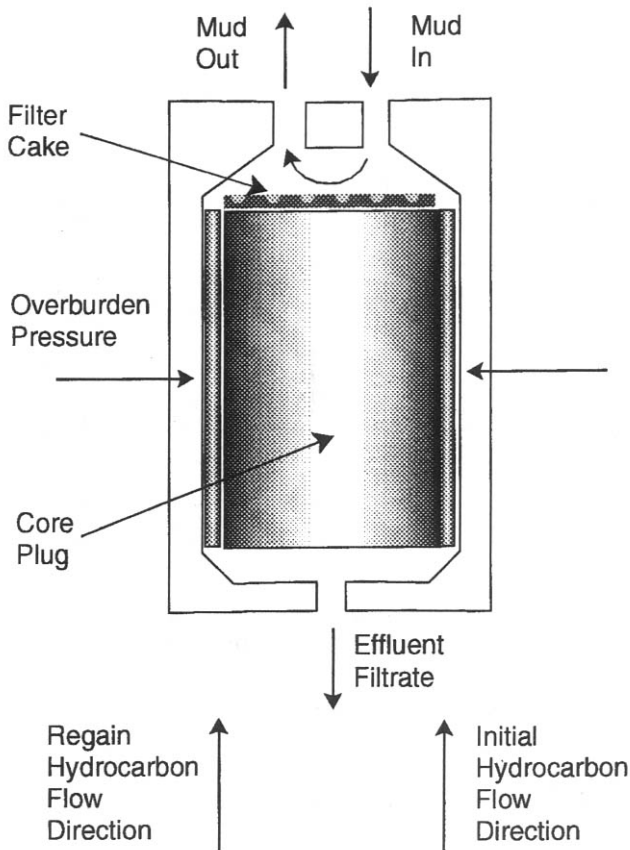


Figure 15–6. Core holder design for drilling fluid leak-off evaluation systems (modified after Doane et al., ©1999; reprinted by permission of the Canadian Institute of Mining, Metallurgy and Petroleum).

on sectional permeability alteration over the core length. Especially, core holders designed for tomographic analysis using sophisticated techniques, such as NMR, Cat-scan, etc., may provide additional internal data. However, it is not always possible to obtain sufficiently long core plugs. In this case, several core plugs of the same diameter can be placed into a long core holder to construct a long core (20–40 cm long) and capillary contact membranes are placed between the core plugs to maintain capillary continuity (Doane et al., 1999).

As emphasized by Doane et al. (1999), small diameter core plugs are not sufficient for testing of heterogeneous porous rocks. Therefore, full

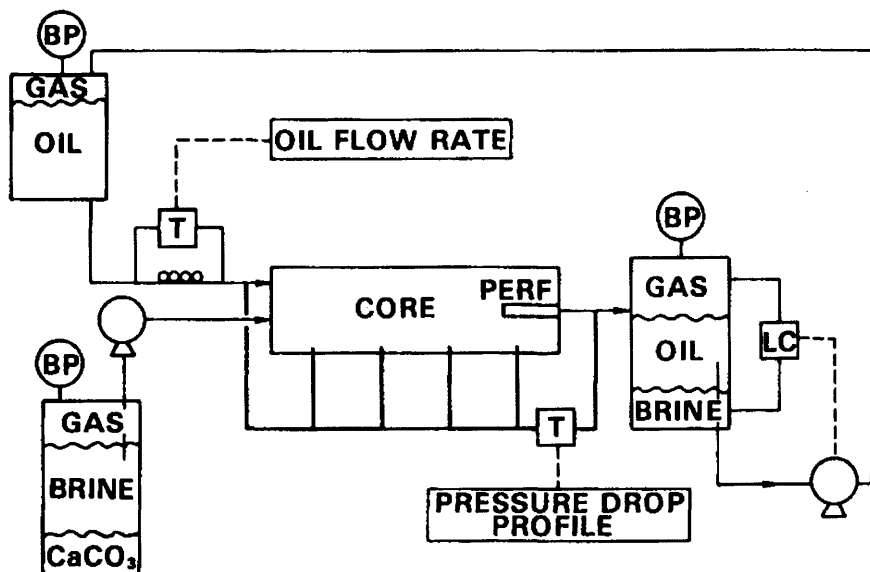


Figure 15-7. Scale damage evaluation system allowing for measurement of sectional pressure drops (after Shaughnessy and Kline, ©1983 SPE; reprinted by permission of the Society of Petroleum Engineers).

diameter core plugs have been used to alleviate this problem. But, Doane et al. (1999) warn, full diameter core plugs would not be representative when significant anisotropy exists between the horizontal and vertical permeability, such as in typical carbonate formations. For the latter case, they recommend the core holder arrangement shown in Figure 15-8. In this system, the two opposing side surfaces of the core plugs are flattened by facing off and the fluid is flown over the side surface by means of a specially designed sleeve. This provides larger surfaces exposed to fluid to include the effect of the heterogeneous features of the core plugs.

Obtaining and testing representative samples of fractured formations are difficult (Doane et al., 1999). Actual core samples containing natural fractures are preferred, but they are often difficult to obtain because core samples are usually poorly consolidated and may not include natural fractures (Doane et al., 1999). Then, a hydraulic fracturing apparatus can be used to prepare artificially fractured core plugs, as shown in Figure 15-9 by Doane et al. (1999).

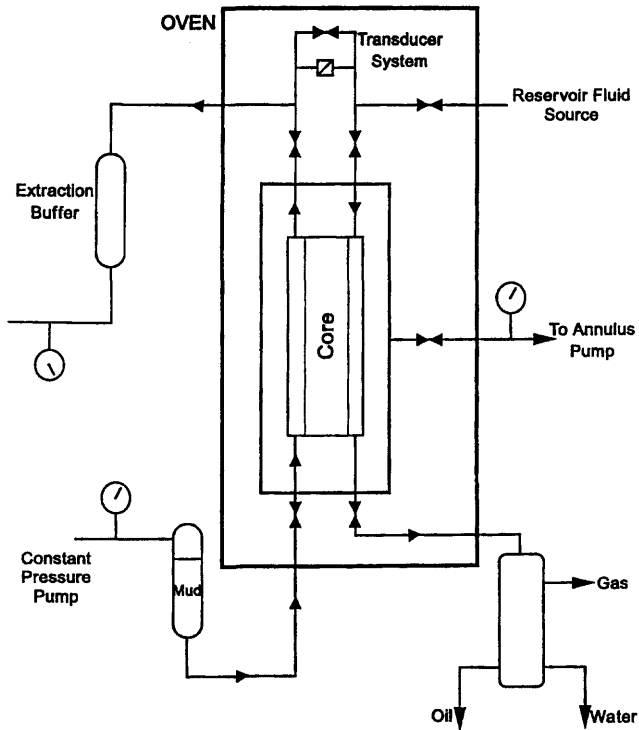


Figure 15-8. Cross-flow fluid leak-off evaluation system for heterogeneous full diameter cores (after Doane et al., ©1999; reprinted by permission of the Canadian Institute of Mining, Metallurgy and Petroleum).

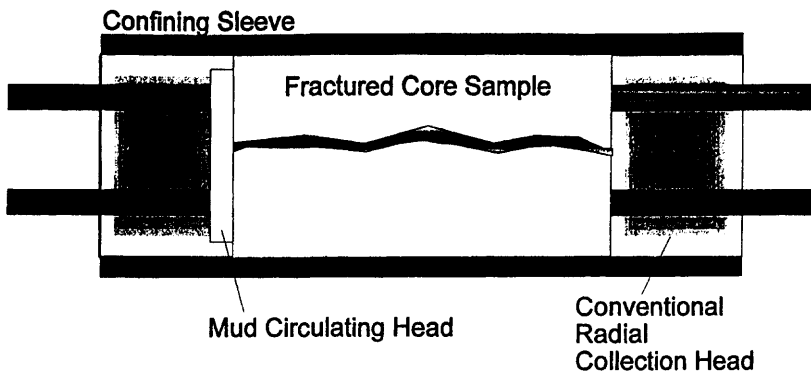


Figure 15-9. Core holder design for fractured core flow evaluation systems (after Doane et al., ©1999; reprinted by permission of the Canadian Institute of Mining, Metallurgy and Petroleum).

Guidelines and Program for Laboratory Formation Damage Testing

Recommended Practice for Laboratory Formation Damage Tests*

Introduction

The following procedure has been designed to provide a methodology for assessing formation damage in a variety of testing situations. Consequently, it is not rigorous in all areas and operator selection of the precise method or technique used is necessary at several points in the procedure. This procedure will however serve to minimize variability in test results if it is accurately followed and, if departures from this procedure are documented, it will help in the comparison of data derived from different tests.

This procedure is not meant to provide detailed instructions on the use of the various pieces of equipment referred to. It is assumed that the reader will have a good working knowledge of the principles and practices involved in formation damage testing.

When reporting results obtained using this procedure, details of all departures from these recommendations should be recorded in the final report along with details of methods used where more than one option is provided.

Core Preparation and Characterization

Cutting and Trimming the Plugs. Plugs should be cut to give a minimum diameter of 1 inch (2.54 cm). Larger plugs, sized to fit particular core holders are preferable. The samples should have a minimum length of 1 inch (2.54 cm) and should be taken from the center of the core to minimize the impact of any coring fluid invasion. The plugging method and drill bit lubricant used during plugging will be determined by the state of preservation of the sample and the reservoir type.

Cutting Consolidated Core. A standard core analysis rotary core plunger should be used with lubricant selected as below:

- a. Well preserved core. If the core is well preserved then the appropriate fluid for the zone from which it is derived should be used; i.e. formation brine or crude oil for an oil well and formation brine

* Reproduced with permission of the Society of Petroleum Engineers from SPE 38154 paper by Marshall et al., 1997 SPE.

for a gas well (using gas as a lubricant may cause precipitation from formation brine inside the core).

- b. Poorly preserved core. If the core is poorly preserved and will require cleaning prior to testing, then the plugging fluid should be inert mineral oil—fluids such as crude oil or formation brine should not be used in this case as they may cause precipitation within the core.

Cutting Unconsolidated Core. One of the following two methods should be used depending on the state of the sample:

- a. Homogeneous sample. Plunge plugging, where a sharp-edged metallic cylinder is pushed into the soft rock, should be used.
- b. Inhomogeneous sample. If the sample contains hard nodules, cement patches or lamination then a rotary plugger should be used with either compressed air (sample at ambient temperature) or liquid nitrogen (frozen sample) as a lubricant.

Trimming the Plugs. After plugging, the samples should be trimmed (lubricant as for plugging) to give flat end faces perpendicular to the plug sides. The samples should be stored under the plugging fluid prior to cleaning or testing. The end faces of all plug samples should be cleaned of fines/rock flour generated during trimming.

Mounting and Labeling the Plugs. At this stage the samples should be encased in inert material leaving the end faces exposed, using PTFE tape, together with heat shrink tubing. For poorly consolidated samples it may also be necessary to apply restraining grids to the plug end faces. The samples should be assigned a wellbore and a formation end face which are annotated on the side of the plug and not on the end faces.

Cleaning and Drying. Once a cleaning and drying method has been selected, it should be identical for all samples in a particular study. See notes in the accompanying text for definitions of the terms Native State, Cleaned Sample and Restored State.

Native State Cores. Native State samples should not be cleaned and should be prepared to S_{wi} (irreducible water saturation) with the appropriate single phase fluid using one of the methods described in Section “Preparation to Base Saturation” given below.

Non-Native State Cores. For core samples not in their Native State, cleaning is required. Cleaned samples may be obtained in one of the following ways:

- a. Samples which do not contain delicate or sensitive minerals can be cleaned in standard core analysis soxhlets using solvents or solvent

mixtures and dried in a high temperature (90°C) oven. Samples containing delicate or sensitive minerals such as illite or smectite should be cleaned by continuous immersion in cold static solvents and dried by critical point drying. If the equipment required is not available or if a faster technique is required the samples can be cleaned using continuous immersion soxhlets and dried in a low temperature (60°C) oven. Cleaned and dried samples should be stored in a desiccator prior to measurement of base parameters.

Note: Commonly used solvents for cleaning include toluene, xylene, methanol, chloroform and acetone. There is no general agreement over which solvent is best in a given situation.

- b. Samples can be cleaned in core holders by flowing miscible solvents (or solvent mixtures).
- c. Samples can be “cleaned” by flowing alternatively light mineral oil (or crude oil if sufficient quantities are available) and formation brine until complete displacement of original fluids is achieved. The cleaning is ended by flowing oil to S_{wi} and if necessary replacing the mineral oil with crude oil by miscible flooding at S_{wi} . Reservoir temperature should be used.

Restored State Samples. If a Restored State sample is required, this can be achieved by first of all following the procedures outlined in Section “Non-Native State Cores” above, saturating the sample as described in Section “Plug Saturation” given below, and then aging at reservoir conditions for an extended period of time (3–6 weeks).

Plug Selection—Selection of Duplicates. Prior to the flood tests, a sufficient number of duplicate plugs should be selected so that the entire test program can be conducted using essentially the same sample of rock. The following criteria are to be used during plug selection:

- a. Similar permeability (preferably within 20% as determined by K_a (or K_o for native state samples) measurement)
- b. Similar grain size/pore throat size distribution (determined by SEM, thin section and possibly mercury injection of plug trims or carcass material)
- c. Similar composition/lithology (determined by XRD, SEM, thin sections of trims/carcass or CT scans of plugs)

It is difficult to quantify the parameters in b) and c) and the comparative suitability of duplicates must be made using expert judgement.

Plug Saturation. 100% saturation is defined as being within 2% of base saturation.

Saturation With Formation Brine. Cleaned samples should initially be saturated with formation brine. This may be achieved using one of the following methods as determined by the cleaning process previously employed:

- a. If the samples have been cleaned using immersion methods then the dry samples are placed in a saturating vessel. A vacuum is applied and then formation brine is introduced and sufficient pressure is applied to ensure 100% formation brine saturation (as determined by weighing).
- b. If the samples have been cleaned by flowing solvents in a core holder ending with 100% methanol saturation (as determined by effluent composition) then the methanol can be exchanged by miscible flooding with formation brine to 100% water saturation (as determined by effluent composition). Gas phase should be eliminated by applying back pressure.

Preparation to Base Saturation. Prior to the flood test, for both Native State and Restored State, the samples should be prepared to a defined saturation/capillary pressure. For both oil and gas wells, irreducible formation brine saturation should be used. There are various methods which can be used to achieve this saturation. These include porous plate, dynamic core holder and ultracentrifuge. Due to the wide variety of core sample characteristics and test objectives, no one method can be recommended as being the most applicable for all situations. After preparation to base saturation, samples should be stored under the appropriate fluid and conditions prior to return permeability testing.

Fluid Preparation

Simulated Formation Water. Simulated formation water (SFW) should be prepared using analytical grade inorganic salts to obtain the appropriate levels of the ions, as determined by elemental analysis, and then degassed. The SFW should be filtered to 0.45 micron.

Fluids Used for Initial and Final Permeabilities—Kerosene or Inert Mineral Oil. Kerosene or inert mineral oil should be filtered to 0.45 micron.

Formation Brine. Formation brine, if available, should be filtered to 0.45 micron at reservoir temperature. Alternatively, simulated formation water (SFW) should be freshly prepared as discussed in Section “Simulated Formation Water,” given above.

Crude Oil. It is usual to use dead crude but since it may contain a certain amount of produced water, this should be removed. The crude oil should be filtered using a 0.45 micron filter at a temperature above the wax appearance temperature.

Gases. Oxygen-free nitrogen, filtered through a 0.45 micron filter, should be used. After filtration, the nitrogen should be humidified at inlet pressure conditions to prevent the sample from drying out during testing.

Wellbore Fluids—Drilling Fluid (Whole Mud). Drilling fluids to be used in return permeability testing should be as representative as possible. In the case of laboratory prepared muds, they should contain all the components of the proposed formulation including weighting agents and contaminants and should be mixed according to standard API procedures where available.

Laboratory muds should be artificially aged by hot rolling for 16 hours at the relevant bottom hole temperature, prior to testing. These should also be passed through a mesh sieve to simulate mud conditioning where relevant (mesh size to reflect shale shaker screen sizes used in the field).

In the case of field muds, the mud should be sheared on a Silverson mixer with the appropriate head (square hole emulsor screen for invert muds, 0-polymer head for water-based muds) for 5 minutes per laboratory barrel (350 ml) prior to use to ensure that the mud is in a representative state. Again, the mud should be passed through a mesh sieve to simulate mud conditioning where relevant.

Drilling Fluid (Filtrate). Drilling fluid should be prepared as above, then filtered such that the filtrate obtained is representative of the filtrate lost to the formation through the filter cake.

Filtrate should be obtained either by centrifuging the sample or by using a High Temperature High Pressure fluid loss cell. The filtrate collected is then further filtered to approximately one third of the average pore throat diameter of the reservoir core and should be used within 16 hours of filtering.

Solids Free Completion Fluid. Solids free completion fluids (e.g., brine, acid) should be prepared including all additives planned for the well. They should be filtered to the appropriate specification for that formation and/or field practice.

Completion Fluid Containing Solids. This section refers mainly to Loss Control Material (LCM). These fluids should be prepared such that the particle size distribution is representative of that expected downhole. Filtering of the prepared fluid is optional, depending on the type of effects to be measured.

Test Procedures

Wellbore Fluid Placement. The prepared sample for evaluation should be loaded into a core holder capable of attaining reservoir net confining pressure and temperature ratings for the matching of reservoir in situ conditions. Pressures and flow rates should be continuously logged as functions of time.

The core sample should be mounted in the horizontal position for analysis. The confining stress on the sample should be gradually increased while at the same time the pore pressure of the fluid in place is also increased to maintain a net confining stress ratio equivalent to the in situ reservoir stress conditions. The rate of increase of net stress on the sample should not exceed 1000 psi (68 bar) per hour.

The test apparatus and sample should be heated to an equivalent reservoir temperature. During heating, the pore pressure and confining stress should be adjusted to maintain initial conditions. Monitoring of the sample temperature and applied pore and confining pressures during this process is required to determine when reservoir conditions have been attained.

The sample should be allowed to stabilize at the test temperature and pressure for at least 4 hours before testing begins.

Note: In order to prevent damage in the sample due to fines mobilization during flow testing it is recommended that a separate critical velocity test be performed to determine the flow rates which can be applied without causing permeability reductions due to fines migration. Preparation of the critical velocity sample should be the same as the preparation technique used for the test samples.

Initial Permeability. Formation fluid should be flowed in the production direction (from "formation to wellbore") by injection at constant rate. Where the critical velocity is not known, the flow rate should be as low as possible yet sufficient to generate a measurable pressure drop. Where the critical velocity is known for the test material, then the flow rate should be $\leq 50\%$ of the critical rate. The differential pressure across the sample should be recorded. Particular regard should be paid to anomalies caused by mobilization of fine material within the test sample. The flow should be maintained until the pressure drop has stabilized and does not vary by more than 5% for a minimum of 10 pore volumes. Fluid flow is ceased once initial permeability is established.

Drilling Fluid Placement—Whole Mud. To simulate well conditions, drilling fluid should be flowed over the 'wellbore' face of the sample.

The drilling fluid should be pre-heated prior to placement to match the bottom hole temperature. The drilling fluid should be applied to the sample face at the same overbalance pressure as in the reservoir and should be dynamically circulated over the face of the test sample for a minimum of 4 hours. Where comparative testing of mud on the formation is required the mud flow rate will be a constant for each mud type. During circulation the drilling fluid pressure and pore pressure should be recorded to ensure the values remain stable (less than 5% variation).

During dynamic drilling fluid circulation the amount of fluid invasion into the test sample should be monitored at the "formation" end of the sample. The method of monitoring should be recorded. Invasion volume as a function of time should be recorded to allow the evaluation of spurt loss as the mud cake builds up and the effectiveness of the cake to prevent filtrate invasion into the test sample (leak off).

Static drilling fluid placement should follow the dynamic placement. During the static placement the mud pressure should be maintained without flowing fluid over the "wellbore" face of the sample. The static placement should be for a minimum of 16 hours. As in the dynamic placement, recording of invasion volume as function of time measured at the "formation" face of the sample during the static placement is required to monitor mud cake performance. Following the static placement the mud should be dynamically circulated for a minimum of 1 hour.

A fluid system that requires a wash or breaker fluid, will need to have a step included into the test sequence in which placement and contact with this fluid are simulated.

Mud Filtrate. 10 pore volumes of the mud filtrate should be injected at the reservoir temperature through the core in the "wellbore to formation" direction at 1 ml/min and the pressure differential measured.

Completion Fluid Placement—Solids-Free Completion Fluid. 10 pore volumes of the solids-free completion fluid should be injected through the core in the wellbore to formation direction at the static reservoir temperature. The fluid should be injected at a rate similar to that used when establishing initial permeability (Section "Initial Permeability," given above).

Fluid Loss Control Pill. Fluid loss control pills should be exposed to the wellbore face at the appropriate overbalance. This should be carried out at static reservoir temperature for a representative amount of time as determined by the operation being simulated, but a 16 hour minimum is recommended. Fluid loss over time and differential pressure during the exposure period should be recorded as well as the filter cake thickness.

Clean-up Treatments. Any clean-up treatment should be flowed over the wellbore face of the sample at a pressure differential appropriate to the

reservoir conditions. Fluid should be allowed to flow through the core once breakthrough is achieved and the pressure differential should be maintained until a representative amount of fluid has been lost. A shut in period either before or after circulating the fluid may be utilized if appropriate to simulate field practice. The amount of fluid lost into the core over time and the differential pressure should be recorded.

Production Simulation. After the placement of drilling fluid (and possibly other fluids) it is important to simulate a return to production in the “formation to wellbore” direction. This can be performed under conditions of constant pressure or constant flow rate. The permeability is determined after either of these methods.

- a. **Determination of flow rate at constant pressure (drawdown).** Drawdown should be performed by decreasing the pressure at the wellbore end of the plug and maintaining the formation end pressure at pore pressure allowing flow through the plug, mud cake and mud. The pressure drop should simulate that to be used in the reservoir. Drawdown should be continued until constant flow rate is achieved. If this is not achieved, the fact should be included in the report. Pressure and flow rate should be measured throughout this procedure.

Note: Where permitted by the core holder design, flow regimes incorporating flow across the face of the core should be used.

- b. **Determination of differential pressure at constant flow rate.** This procedure differs from a) above by using a constant flow rate and measuring the corresponding differential pressures across the core. The flow rate should be representative of the flux at the wellbore face. Flow should be continued until constant pressure is achieved. The pressure required for the initiation of flow should be recorded.

Determination of Return Permeability. The final or return permeability measurement (or measurements) can be made at two different stages:

- a. Immediately after Section “Production Simulation,” given above, and when a stable flow rate/pressure drop has been achieved, the permeability of the tested core plug can be measured.
- b. After preparation of the core plug in the same way as for the initial permeability (Section “Core Preparation and Characterization,” given above), the permeability can be measured.

To determine the return permeability, repeat the procedure used in Section “Initial Permeability,” given above, to measure the initial permeability, ensuring that identical fluids and flow rates are used.

Reporting

A written report should be produced using Table 15–1 as a guide to composition.

The report should contain all the section headings listed in the left hand column of Table 15–1. The content of each section cannot be specified to cover all situations but suggested elements, which should be included to facilitate interpretation and use of the results obtained, are included in the right hand column of the table.

Core Flood Tests

Core flood tests can be conducted in various ways depending on the convenience and requirements of specific applications and/or the interpretation methods available.

Core floods are usually accomplished under the conditions of constant pressure difference across the core plugs or constant flow through the core plugs. This provides convenience for interpretation of the experimental data by means of a mathematical model. However, maintaining constant pressure difference and constant flow conditions in actual test conditions may be difficult and may not be truly accomplished, in spite of the use of high-quality equipment. Therefore, interpretation methods that can allow for variable flow conditions are preferred.

Core flood tests can be conducted using single or multiple core holders. Multiple core holders may be run in series or parallel depending on the specific reasons. Parallel core holders may be required for various reasons. Similar core plugs in parallel may be flown simultaneously and certain formation damage effects, such as filter cake thickness, porosity, or precipitate quantity, can be measured separately and over different time periods for each core plug. Tests to establish the effect of the permeability contrast, such as for conformance control studies, require floods using parallel core plugs with different permeabilities (Prada et al., 2000). Core plugs may be run in series to simulate the effect of formation damage over long distances.

Core flood tests can be conducted in two ways: (1) interrupted core floods and (2) continuous corefloods (Haggerty and Seyler, 1997). In interrupted core flood tests, the fluid injection is interrupted at certain time intervals and permeability is measured. In continuous core flood tests, the effective permeabilities are measured during the injection process.

Laboratory Procedures for Evaluation of Formation Damage Problems

The laboratory procedures required for evaluation of common formation damage problems are described in this section according to Keelan

Table 15–1
List of Elements to be Included in Report*

Section Headings	Suggested Elements to be Included
Date of issue	
Reporting authors	
Type of formation material used in tests	<ul style="list-style-type: none"> • e.g., core/outcrop/synthetic
Objectives of the test and background	<ul style="list-style-type: none"> • Requesting party • Well/formation to be investigated • Origin of formation material • Origin of brines/crudes/fluids • Project history
Mineralogy of material used in test	<ul style="list-style-type: none"> • Pore throat size and method of determination used • Results of XRD, SEM and thin section analyses before and after treatment(s)
Characteristics of core plug	<ul style="list-style-type: none"> • Preserved or restored; if restored, method used for core restoration • Cutting method and lubricants used • Water saturation, S_{wi} • Method of preparation to base saturation • Aging time (restoration) • Cleaning methods (detail to include equipment, solvents and procedures used)
Fluids used in test	<ul style="list-style-type: none"> • Muds: full compositional information and preparation methods, field or laboratory source, details of additional solids/contaminants • Brines: chemical analysis • Oil: crude (live/dead), synthetic • Gas: type, humidified or not
Test conditions	<ul style="list-style-type: none"> • Plug dimensions and orientation relative to bedding • Surface area of plug face exposed to fluids • Core holder dimensions and rig schematic (including diagram) • Core and fluid temperatures (e.g., if lower than core temperature during dynamic phase) • Pore pressure • Overburden pressure • Overbalance pressure • Drawdown pressure/flow rate

* Reproduced with permission of the Society of Petroleum Engineers from SPE 38154 paper by Marshall et al., 1997 SPE.

(table continues)

Table 15–1 continued

Section Headings	Suggested Elements to be Included
	<ul style="list-style-type: none">• Volume of fluid produced during drawdown• Exposure period (including dynamic/static periods)• Flow rate during dynamic period (if applicable)• Shear rates at core face during dynamic period (if applicable)
Results	<ul style="list-style-type: none">• Core plug reference• Depth taken (if known/applicable)• Fluids used in test• Test sequence (e.g., flood/drawdown/breaker drawdown)• Permeability, initial and final• Pressure drop across core with time• Flow rate with time• Cumulative volume flowed with time• Viscosity of fluids• Fluid loss vs. time• Temperature and pressure at which fluid collected• Break-through pressure (if applicable)• Comments on test by investigator
Deviations from recommended practice	
Interpretation	

and Koepf (1977). They classified the frequently encountered formation damage problems into four groups:

1. The blocking of pore channels by solids introduced by drilling or by completion, workover, or injection fluids,
2. Clay-water reaction that yields clay hydration and swelling, or clay particle dispersion and pore plugging by movement with produced or injected water,
3. Liquid block that normally is caused by extraneous water introduced into the formation at the wellbore during drilling, coring, completion, or workover, and
4. The caving and subsequent flow of unconsolidated sands into the wellbore.

The Liquid Block Problem

As explained in Figure 15-10 by Keelan and Koepf (1977), "liquid block reduces effective permeability to the hydrocarbon." Before damage, the original mobile water saturation range in $0.20 < S_w < 0.80$. After extraneous water incompatible with the formation invades the porous media, the irreducible water saturation raises to about 34% from its original value of 0.20. Hence, the line AA' shifts to the line DD' . Consequently, the relative permeability of the oil at the irreducible water saturation decreases from the original 0.9 value to about 0.3, which amounts to a three-fold reduction of permeability to the hydrocarbon. On the other hand, damage by clay hydration and fine particles plugging caused by incompatible extraneous fluid invasion increases the residual oil from its original 0.2 ($S_w = 0.8$) to about 0.26 ($S_w = 0.74$). Hence, the line BB' shifts to the line CC' . The permeability to water also decreases.

As a remedial action, Keelan and Koepf (1977) recommend treatments inferred by the capillary pressure equation:

$$p_c = \frac{2\sigma \cos \theta}{r} \quad (15-1)$$

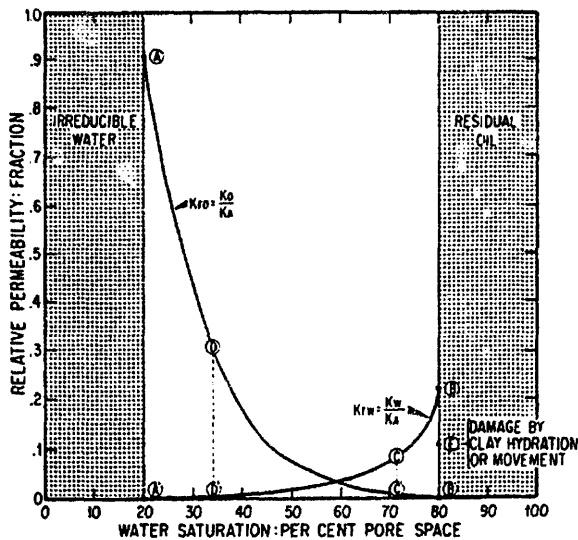


Figure 15-10. Effect of water block on relative permeability (after Keelan and Koepf, ©1977 SPE; reprinted by permission of the Society of Petroleum Engineers).

where p_c denotes the capillary pressure necessary for water retention, σ is the surface tension between water and hydrocarbon, θ is the contact angle between the water and hydrocarbon, and r is the pore radius. Eq. 15-1 indicates that water retention can be reduced by workover schemes reducing the surface tension and/or increasing the contact angle to favor a less water-wet condition.

The Mud Damage Problem

Keelan and Koepf (1977) explain that drilling muds contain solid particles that form a filter cake over the wellbore wall, the filter cake restricts the mud flow into the near well bore formation, but some filtrate and fine particle invasion are unavoidable and usually occurs. The filtrate may react with the resident formation clays causing clay swelling, mobilization, and migration. The released particles and the fine particles carried into the formation by the filtrate can plug the pores and reduce permeability of the formation. The water-based filtrates increase the irreducible water saturation and create water block and hydrocarbon permeability reduction.

Evaluation of Drilling Muds— Damage Potential and Removal

As depicted in Figure 15-11 by Amaefule et al. (1988), the face of a core sample is exposed to mud under a pressure difference across the core. As described by Keelan and Koepf (1977), test sequences can be conducted with and without the presence of mobile hydrocarbons in core plugs. Figure 15-12 by Keelan and Koepf (1977) delineates the test sequence without the presence of mobile hydrocarbons and shows the equations used to determine the magnitude of formation damage or remediation. Keelan and Koepf (1977) explain that "This test indicates impairment of productivity by clay hydration and movement of fines into the formation during the drilling operation, and any benefit of the fines' removal when the well flow in a reverse direction into the wellbore." The core plug is saturated with the brine to be tested and may or may not contain irreducible, immobile oil. Hence, the water-block effect is eliminated because the water saturation is constant. During these tests, the filtrate volume or rate versus the filtration time is measured until mud-off. If the experimental design permits, the filter cake properties, such as porosity, permeability, and thickness, and the effluent fines and liquid volumes should also be measured. The pressure difference applied to the core plug should be determined by scaling from the planned drilling over balance pressure (Keelan and Koepf, 1977).

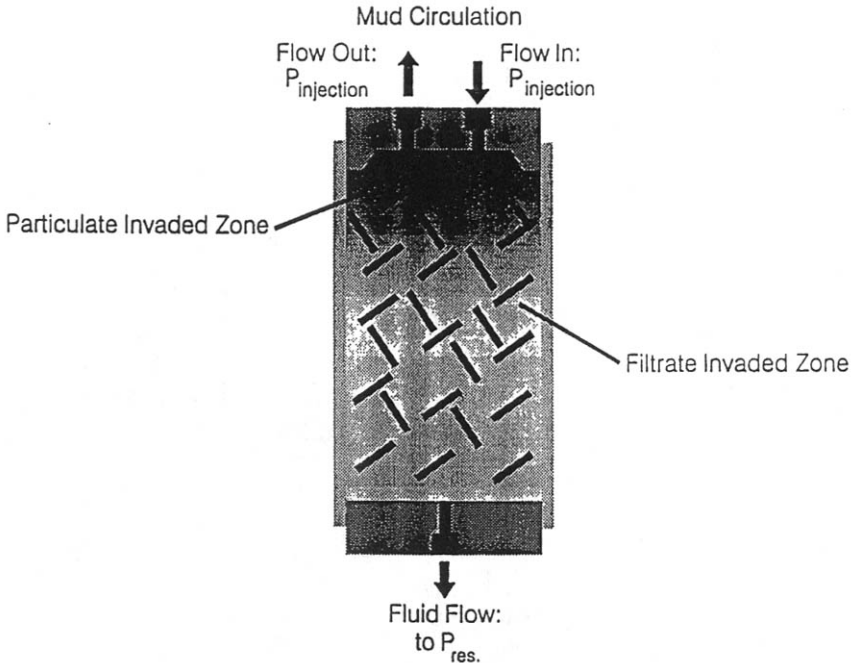


Figure 15–11. Core holder design for drilling mud evaluation systems (after Amaefule et al., ©1988; reprinted by permission of the Canadian Institute of Mining, Metallurgy and Petroleum).

Figure 15–13 by Keelan and Koepf (1977) delineates the test sequence with the presence of mobile hydrocarbons and shows the equations used to determine the magnitude of formation damage or remediation. They explain that this test indicates “the water-block potential of a formation.” In this test, the water saturation varies and is calculated by measuring the effluent filtrate volume. Any permeability reduction remaining, after the production of all the injected, extraneous filtrate water, is attributed to clay hydration and/or mud-solids invasion (Keelan and Koepf, 1977).

Figure 15–14 by Keelan and Koepf (1977) depicts the results of the evaluation tests of two muds, referred to as Muds A and B. Figure 15–14 indicates that Mud A causes more damage than Mud B. In the case of Mud A, the return permeability is only 6% of the initial permeability, while it is 54% for Mud B.

Keelan and Koepf (1977) conducted evaluation tests for two different drilling mud fluids, specially prepared for stabilizing the formation to

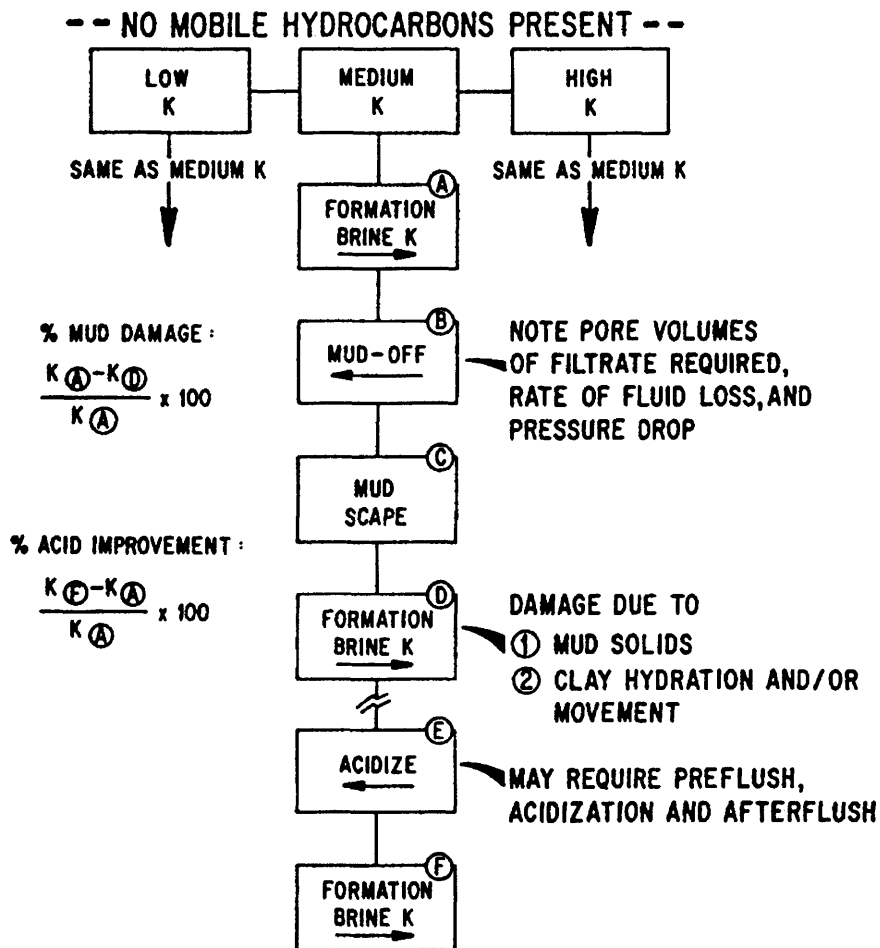


Figure 15-12. Test sequence without the presence of mobile hydrocarbons (after Keelan and Koepf, ©1977 SPE; reprinted by permission of the Society of Petroleum Engineers).

avoid formation damage during water flooding. Keelan and Koepf (1977) used fresh cores containing irreducible oil. They recommend running tests with the presence of irreducible oil because they explain that "The presence of residual oil, or associated organic compounds, sometimes protects clay surfaces, making them less sensitive to alteration when contacted by incompatible brines." They injected coarsely filtered mud

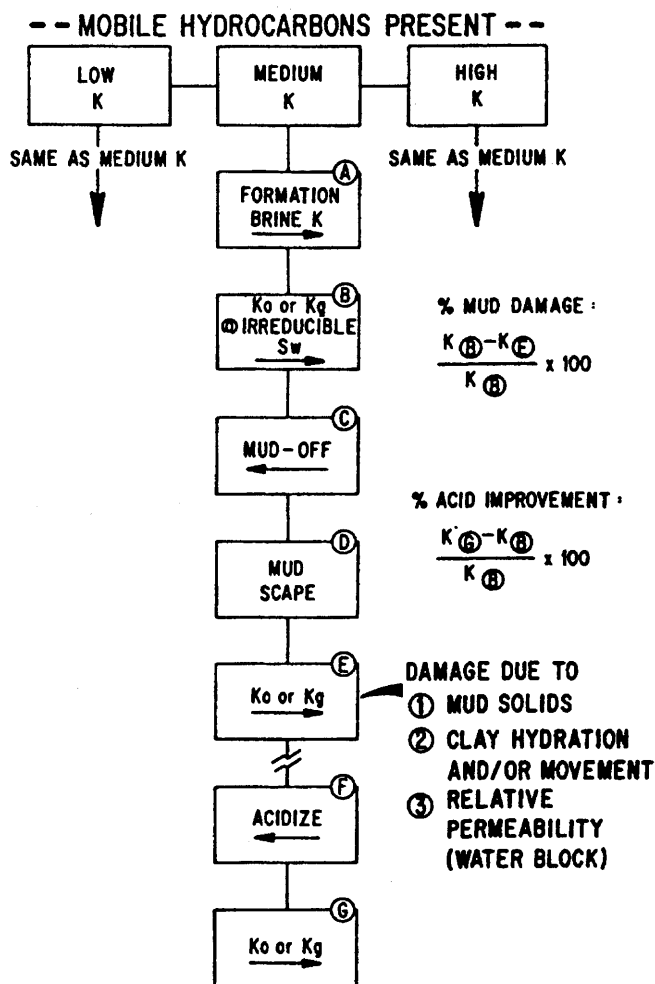


Figure 15-13. Test sequence with the presence of mobile hydrocarbons (after Keelan and Koepf, ©1977 SPE; reprinted by permission of the Society of Petroleum Engineers).

filtrates (thus containing fine particles) into core plugs and measured the permeability impairment. Figure 15-15 by Keelan and Koepf (1977) presents the results of injecting formation brine, filtrate, and injection brine samples into the core plugs. As can be seen, the effective permeability is 30% higher for KCl mud filtrate compared to that of lignosulfonate mud filtrate.

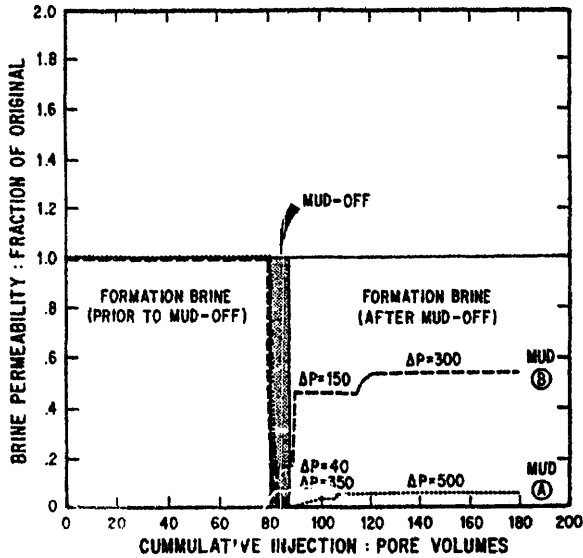


Figure 15-14. Mud damage evaluation (after Keelan and Koepf, ©1977 SPE; reprinted by permission of the Society of Petroleum Engineers).

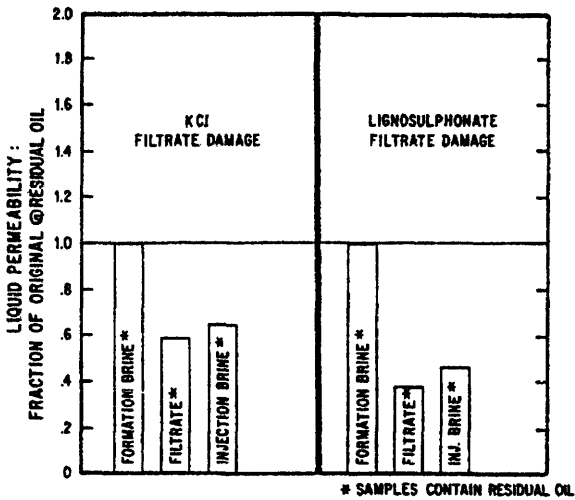


Figure 15-15. Permeability to injection brine following exposure to KCl and lignosulfonate mud filtrate (after Keelan and Koepf, ©1977 SPE; reprinted by permission of the Society of Petroleum Engineers).

For purposes of remediation treatment after damage, Keelan and Koepf (1977) evaluated two types of acids: (1) "a regular mud acid containing about 7½% inhibited HCl and a low surface-tension agent," and (2) a mud acid "composed of 3% HF and 12% HCl." They explain that "Recommended use of the HF acid required a preflush with 15% HCl, injection of the HF acid, and an after flush with diesel oil containing 20% of a mutual solvent." Based on the results presented in Figure 15–16, Keelan and Koepf (1977) summarized their interpretation of the acid treatment results as following:

1. Similar permeability reduction to each filtrate was noted in these test cores.
2. In the cores contacted with KCl filtrate, HF acid yielded 136% higher permeability to injection brine than did the regular mud acid, and resulted in a net permeability enhancement above initial. The regular mud acid was not effective, and final permeability to injection brine was no higher than when the acid wash was not used.
3. In the lignosulfonate-contacted cores, the regular mud acid and the HF acid were equally effective, and each yielded a permeability greater than the original.

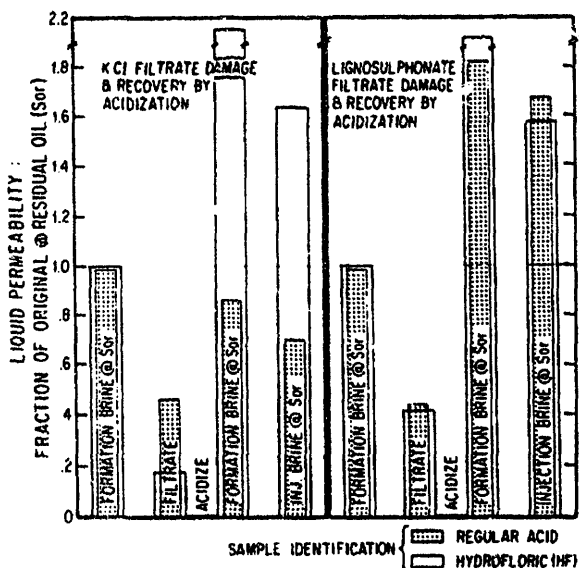


Figure 15–16. Permeability improvement by HF and HCl acid treatment following exposure to KCl and lignosulfonate mud filtrate (after Keelan and Koepf, ©1977 SPE; reprinted by permission of the Society of Petroleum Engineers).

4. In summary, either mud was suitable if HF acid was used for remedial treatment. If the regular mud acid was to be used, the most suitable drilling mud would be lignosulfonate.

Evaluation of Hydraulic Fracturing Fluids

As explained by Keelan and Koepf (1977) fracturing fluids cause formation damage by water-block, solids invasion associated with fluid leak-off, and clay hydration in the near-fracture formation. Therefore, it is important to use compatible fluids and fluid-loss additives. Hence, they recommend performing tests on core samples extracted from the reservoir formation, in which fractures will be created. In these tests, the spurt loss, fluid-loss coefficient, effect of additives, acid solubility of formation, fines release with the acid reaction, are typically determined (Keelan and Koepf, 1977).

Evaluation of Workover and Injection Fluids

These tests indicate the incompatibility of clays with the extraneously introduced water, including filtered formation brine and filtered mud filtrate (Keelan and Koepf, 1977). Such tests can also be used to evaluate the effectiveness of clay stabilizers added to workover and injection fluids (Keelan and Koepf, 1977). Keelan and Koepf (1977) state that "Use of filtered workover fluids removes plugging solids and results in evaluation of damage resulting from clay swelling and/or clay-particle movement." The rock-water system is considered compatible when the formation permeability does not decrease by fluid injection. Keelan and Koepf (1977) state that

The clays damage productivity either by swelling in place or by release from their anchor point and subsequent movement to block pore channels. The inclusion of certain ions in workover and injection fluids often offers a relatively inexpensive and effective stabilization of the clays and prevention of productivity impairment.

Figure 15–17 by Keelan and Koepf (1977) presents the test sequence and the equations necessary for determining formation damage for evaluation of the compatibility of the injection and workover fluids with the formation clays. Figure 15–18 by Keelan and Koepf (1977) shows the results of injecting brines with and without KCl and CaCl_2 added. Injecting a brine, rather than the formation brine, into a core sample A reduced the permeability to 50% of its formation brine permeability. Injecting a brine containing 100 ppm KCl into a core sample B doubled

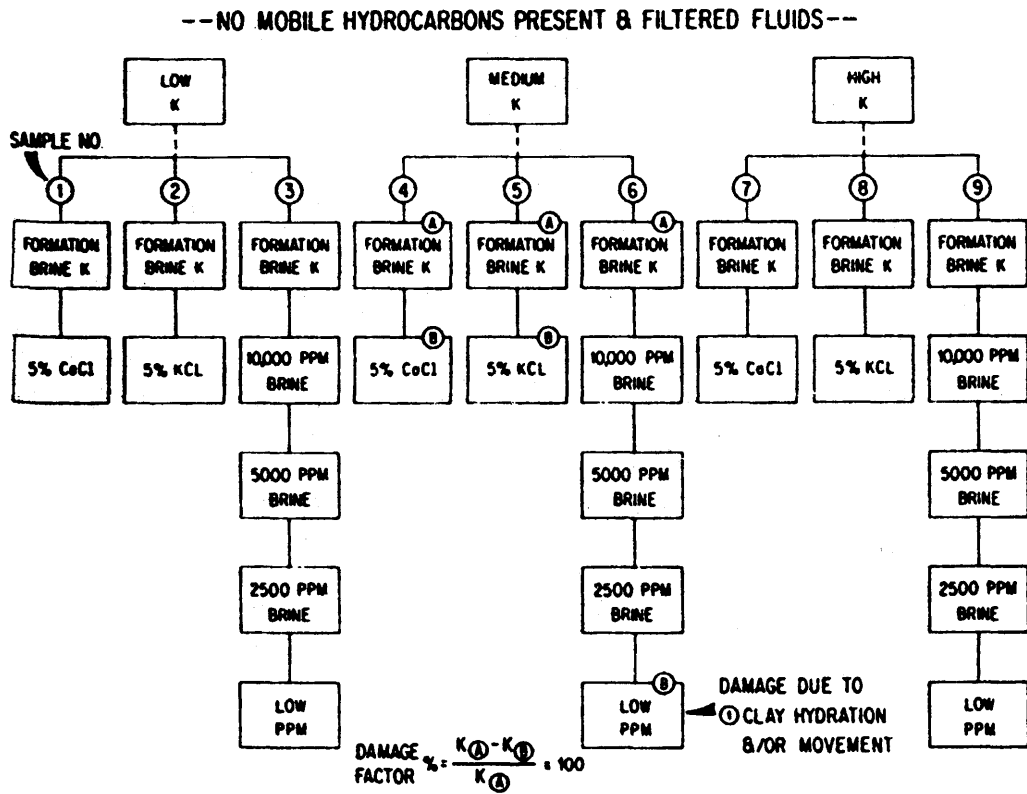


Figure 15-17. Test sequence for evaluation of injection and workover fluids (after Keelan and Koepf, ©1977 SPE; reprinted by permission of the Society of Petroleum Engineers).

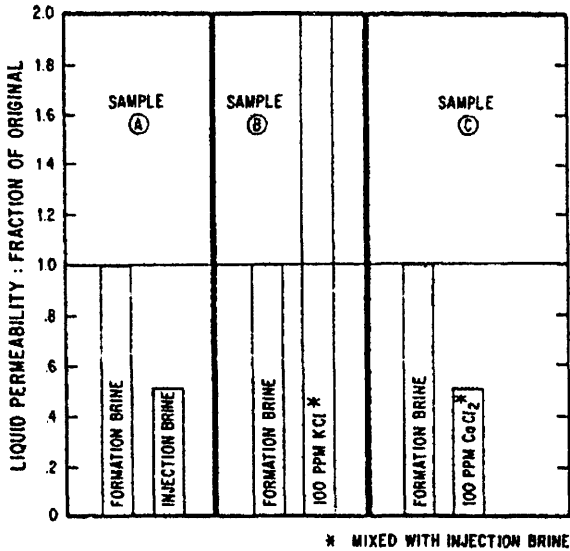


Figure 15-18. Permeability to injection brine with and without KCl and CaCl_2 addition (after Keelan and Koepf, ©1977 SPE; reprinted by permission of the Society of Petroleum Engineers).

its formation brine permeability. However, injecting a brine containing 100 ppm CaCl_2 reduced the permeability to 50% of its formation brine permeability. Figure 15-19 by Keelan and Koepf (1977) shows that consecutively decreasing concentrations of KCl and CaCl_2 in the injected brines yields permeabilities above the initial formation brine permeability. Keelan and Koepf (1977) concluded that KCl treatment is favorable even though the data appear unusual.

Keelan and Koepf (1977) recommend the water-oil relative permeability measurements as a practical approach to damage assessment in core plugs. Keelan and Koepf (1977) express that the fluids compatible with the core material should typically yield the relative permeability curves similar to those shown between the $\overline{AA'}$ and $\overline{BB'}$ lines in Figure 15-10. However, Keelan and Koepf (1977) explain that, when a filtered injection brine is injected into a core containing irreducible oil, a specific value of the water relative permeability, denoted by Point E in Figure 15-10, is obtained. This particular value represents the water relative permeability at the injection-wellbore formation face. Whereas, the water relative permeability at a sufficiently long distance from the well bore is represented by Point B.

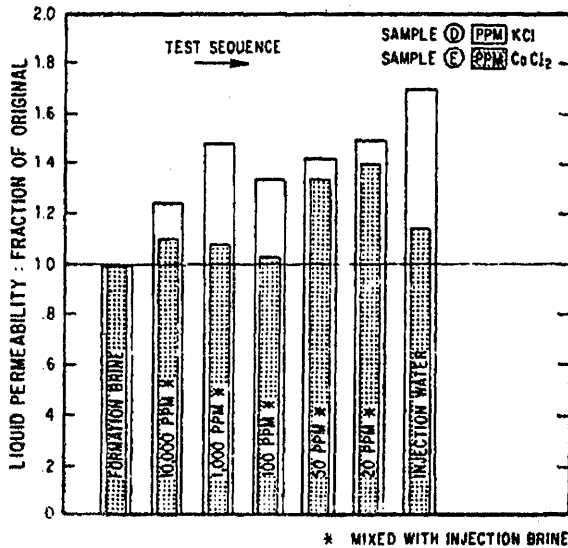


Figure 15-19. Permeability with reduced concentrations of KCl and CaCl_2 solutions (after Keelan and Koepf, ©1977 SPE; reprinted by permission of the Society of Petroleum Engineers).

Evaluation of Workover Damage and Remedial Chemicals

Figure 15-20 by Keelan and Koepf (1977) describes the testing schemes and equations necessary for determining the damage and evaluation of remedial chemical treatment of water block. Keelan and Koepf (1977) facilitate surface tension reducing chemicals to remove the water forming the water-block.

Critical Interstitial Fluid Velocity and pH for Hydrodynamic Detachment of Fines in Porous Media

The drag force acting upon a fine particle attached to the pore surface is proportional to the interstitial velocity and viscosity of the fluid and the surface area of the particle, as discussed in Chapter 8. As the fluid velocity is increased gradually, a critical velocity necessary for detachment of fine particles from the pore surface can be reached. Amaefule et al. (1987) state that "The critical velocity is dependent on the ionic strength and pH of the carrier fluid, interfacial tension, pore geometry

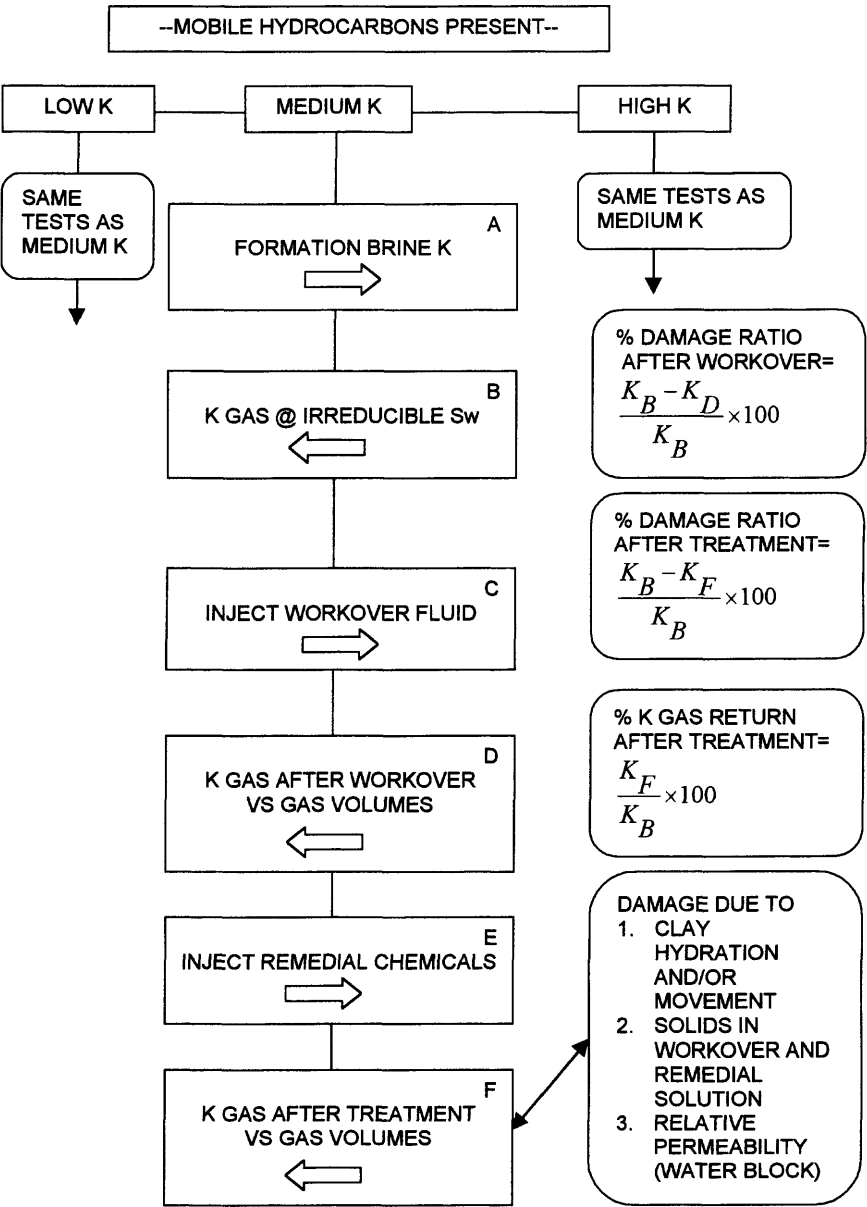


Figure 15-20. Test sequence for evaluation of workover fluid damage and remedial chemicals (after Keelan and Koepf, ©1977 SPE; reprinted by permission of the Society of Petroleum Engineers).

and morphology, and the wettability of the rock and fine particles.” Then, the particles are hydrodynamically removed from the pore surface and entrained by the fluid flowing through porous media. Fine particles migrating downstream with the fluid may encounter and plug narrow pore throats by a jamming process. This causes the pressure difference across the core to increase and the permeability to decrease. Therefore, from a practical point of view, the critical interstitial velocity is characterized as the interstitial velocity at which permeability reduction and pressure differential increase begin as the fluid velocity is increased gradually from a sufficiently low value (Gruesbeck and Collins, 1982; Gabriel and Inamdar, 1983; Egbogah, 1984; Amaefule et al., 1987, 1988; Miranda and Underdown, 1993).

The theory of the critical velocity determination is based on Forchheimer’s (1914) equation, given below, which describes flow through porous media for conditions ranging from laminar to inertial flow:

$$-\left[\frac{dp}{dx} + \rho g \sin \theta\right] = \frac{\mu}{K} u + \rho \beta u^2 \quad (15-2)$$

The interstitial velocity is given by:

$$v = u/\phi = q/(A\phi) \quad (15-3)$$

Considering horizontal flow, and constant fluid and core properties averaged over the core length, Eq. 15-2 can be integrated over the core length for applications to laboratory core tests. In view of Eq. 15-3, the resultant expression can be given in terms of the interstitial fluid velocity as

$$\frac{\Delta p}{v} = \frac{\phi \mu L}{K} + (\phi^2 \rho \beta L) v \quad (15-4)$$

or in terms of the flow rate as

$$\frac{\Delta p}{q} = \frac{\mu L}{KA} + \frac{\rho \beta L}{A^2} q \quad (15-5)$$

At sufficiently low fluid velocities, the fine particles remain attached to the pore surface and, therefore, there is no formation damage by fines migration and $\Delta p/v$ remains constant as depicted schematically in Figure 15-21a by

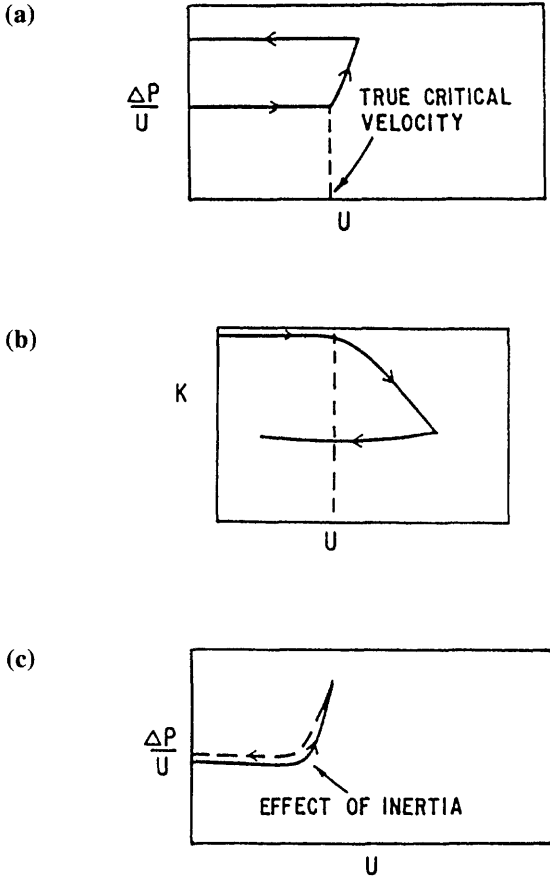


Figure 15-21. Method for laboratory determination of critical velocity for particle mobilization (after Amaefule et al., ©1988; reprinted by permission of the Canadian Institute of Mining, Metallurgy and Petroleum).

Amaefule et al. (1988). However, when the fluid velocity is gradually increased, first a critical velocity at which particle detachment by hydrodynamic forces begins, is reached, and then the value of $\Delta p/v$ or $\Delta p/q$ continuously increases (Figure 15-21a) and permeability continuously decreases (Figure 15-21b) by fines migration and deposition in porous media. As emphasized by Amaefule et al. (1987, 1988), the increase in $\Delta p/v$ or $\Delta p/q$ at high flow rates may be due to both fines migration and inertial flow effects (Figure 15-21c). For decoupling these two effects, Amaefule et al. (1987) propose a subsequent velocity reducing

test. When the flow rate is reduced gradually, the $\Delta p/q$ value should reach its original value measured during the velocity increasing test, if the critical velocity has not been reached during the previous velocity increasing test. However, if the critical velocity has been exceeded during the velocity increasing tests, a permeability impairment by fines mobilization and deposition would have occurred. Therefore, a subsequent velocity decreasing test will yield a value of $\Delta p/q$ different than the previous value measured during the velocity increasing test. Figure 15–22a by Amaefule et al. (1987) presents a schematic illustration of their approach to decoupling the fines migration and inertial effects using KCl saturated brine (55 kppm KCl) and kerosene oil at different saturation levels: (1) 100% water, (2) saturated with oil in the presence of irreducible water, and (3) 100% oil. They determined that the critical velocity is zero for oil flowing through cores at irreducible water saturation. Figure 15–23 based on experiments conducted with Berea core samples by Amaefule et al. (1988), shows that critical velocity is higher for KCl brines than NaCl/CaCl₂ brines.

Amaefule et al. (1987) verified their proposed approach by a series of tests: they injected a SOP (standard operating brine containing 50 kppm NaCl and 5 kppm CaCl₂) brine into a field core sample (2.54 cm diameter and 12.2% porosity) and measured $\Delta p/q$. During the increasing flow cycle, they determined the critical velocity to be 0.0674 cm/s based on their plot of data shown in Figure 15–24. They also measured the effluent brine pH during the flow tests, as it may provide some evidence of the physico-chemical interactions of the aqueous solution with the formation (Amaefule et al., 1987; Millan-Arcia and Civan, 1992). As shown in Figure 15–24, during the flow test, with increasing SOP brine velocity, the pH first decreased from the initial value of 8.45, reached a minimum value of 6.74, and then increased to a value of 7.5. As can be seen from Figure 15–24, the minimum pH coincides with the critical interstitial velocity. This finding is particularly significant. Therefore, Keelan and Amaefule (1993) recommend monitoring injection and produced water pH as an integral part of critical interstitial velocity determination. Amaefule et al. (1987) explain the change of pH to attain a minimum at the critical velocity due to the increase of the K^+ ion in the aqueous phase by exchange of the K^+ cations of the formation minerals with the Na^+ and Ca^{2+} cations of the aqueous phase.

Following the velocity increasing cycle, Amaefule et al. (1987) conducted a velocity reducing cycle until a velocity of 0.027 cm/s was reached. As can be seen in Figure 15–24b, the permeability first reduced to 66% of its initial value and then to 55% after an additional one pore

(text continued on page 499)

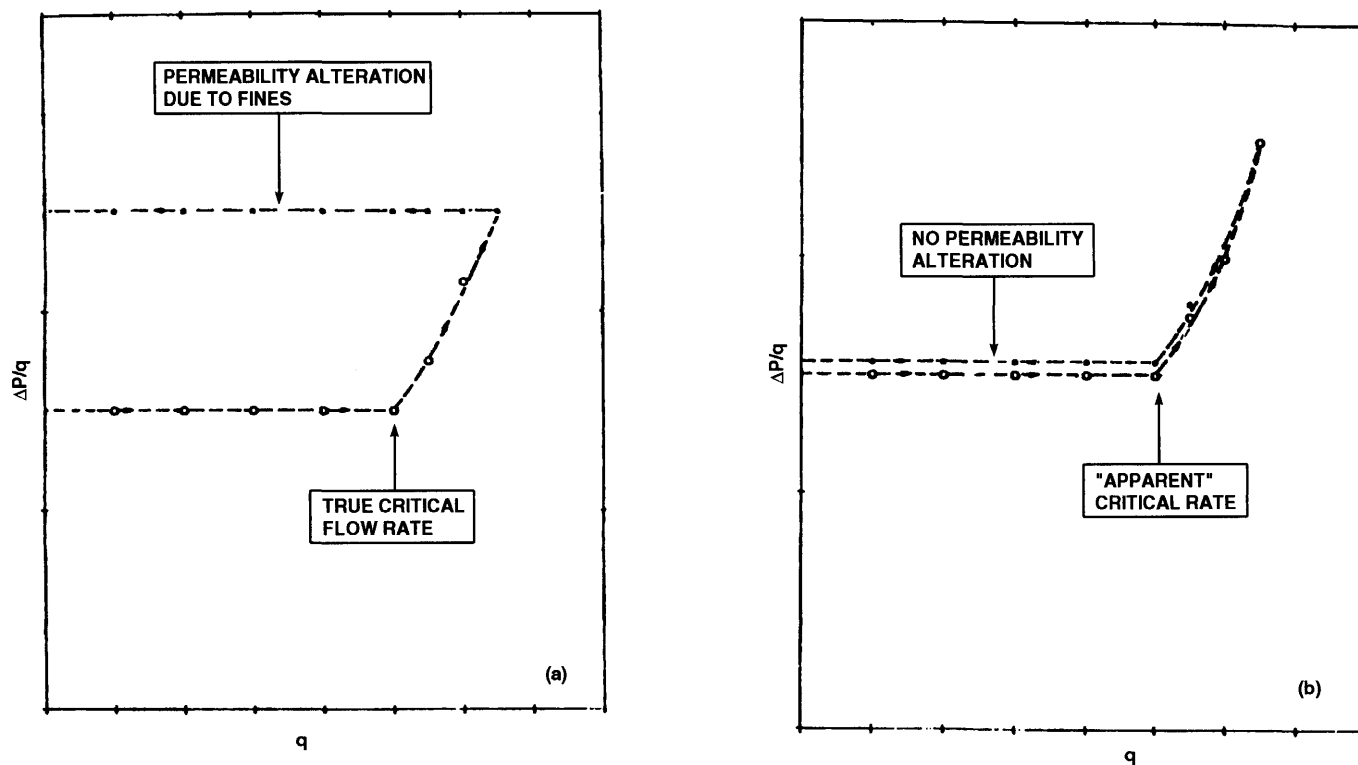


Figure 15-22. Effect of flow regime: (a) permeability alteration by mobilized particles during Darcy flow, and (b) apparent permeability alteration by mobilized particles during non-Darcy flow (after Amaefule et al., ©1987 SPE; reprinted by permission of the Society of Petroleum Engineers).

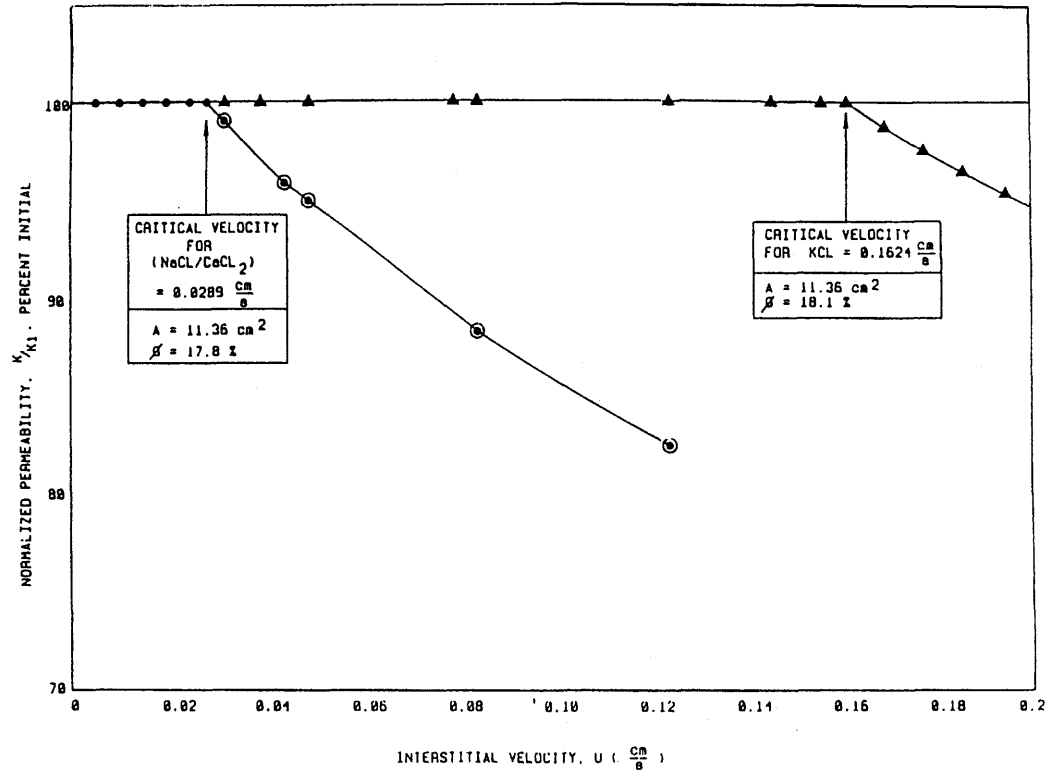


Figure 15-23. Normalized permeability vs. interstitial fluid velocity for two brines (after Amaefule et al., ©1988; reprinted by permission of the Canadian Institute of Mining, Metallurgy and Petroleum).

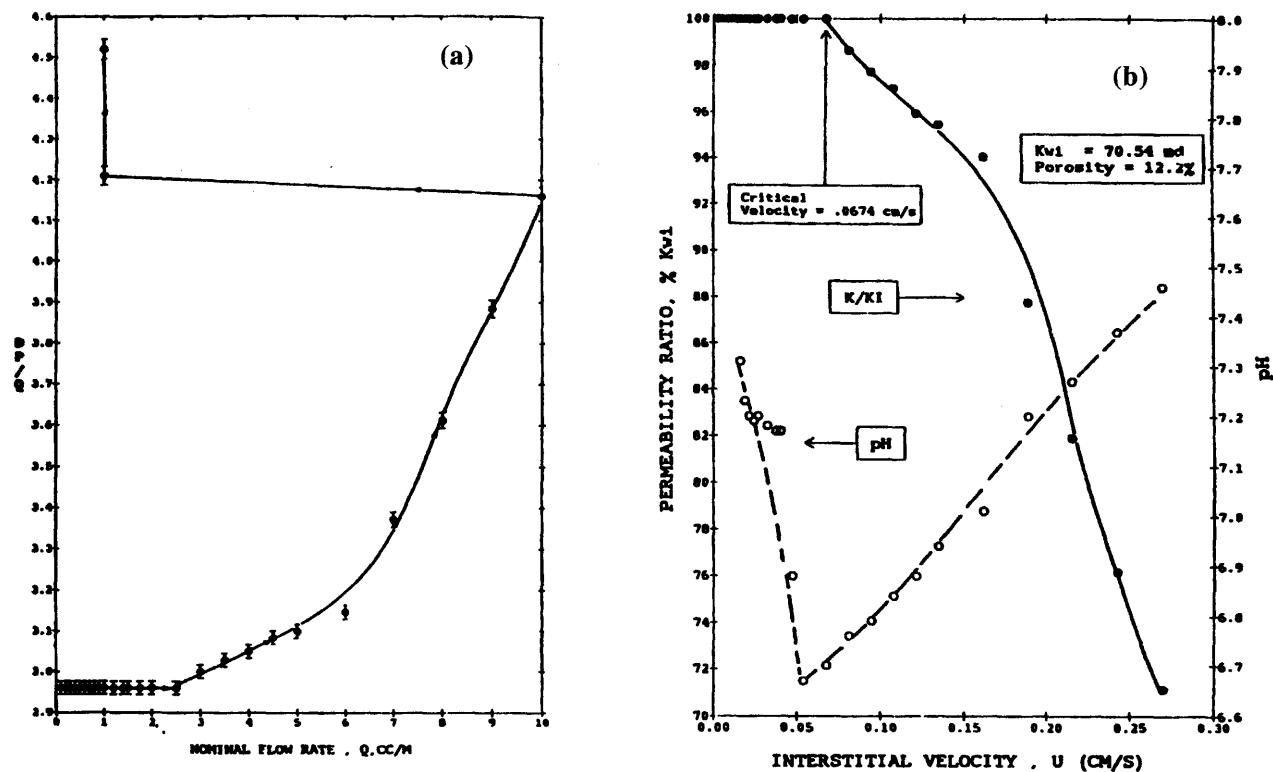


Figure 15-24. Injection of SOP brine into a field core at 3,000 psi pressure: (a) pressure drop per flow rate vs. flow rate and (b) instantaneous to initial permeability ratio and pH vs. interstitial fluid velocity (after Amaefule et al., ©1987 SPE; reprinted by permission of the Society of Petroleum Engineers).

(text continued from page 495)

volume of the SOP brine injection at the same rate of 0.027 cm/s, indicating the dependency of the permeability reduction to the brine throughput as a result of simultaneous entrainment, migration, and redeposition of fine particles in porous media.

When Amaefule et al. (1987) reversed the flow, they observed a rebound of permeability to 90% of the initial permeability because of dislodging of clogged pores, but the permeability decreased to 87% of initial after a one pore volume brine injection. Amaefule et al. (1987) explain this affect due to the fines entrainment and then migration and redeposition phenomena. They observed a similar affect on the effluent brine pH variation.

Scaling from Laboratory to Bottom Hole

Miranda and Underdown (1993) developed a method for scaling laboratory data to the bottom hole dimensions based on the schematic given in Figure 15–25. For this purpose, the interstitial fluid velocities expressed in terms of the parameters of the core plug and perforated wellbore are equated as:

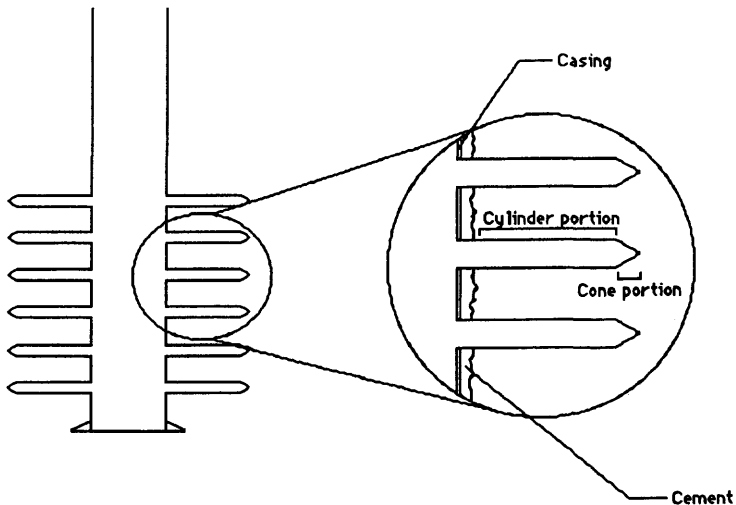


Figure 15–25. Perforation tunnel model for scaling laboratory core tests (after Miranda and Underdown, ©1993 SPE; reprinted by permission of the Society of Petroleum Engineers).

$$v_c = \left(\frac{q}{A\phi} \right)_{core} = \left(\frac{q}{A\phi} \right)_{wellbore} \quad (15-6)$$

The cross-sectional area of the core plug is known. They expressed the total inflow area of the perforated wellbore interval by:

$$A = E_s N_s L_i \left[0.7\pi dh + 0.3\pi r \sqrt{r^2 + h'^2} \right] \quad (15-7)$$

where E_s denotes the shot efficiency in percent, N_s is the perforation density expressed as the number of shots per foot, L_i is the interval length in ft, d is the diameter of perforations in ft, and h and h' denote the lengths of the cylindrical and conical portions of the perforation tunnel, respectively. The factors 0.7 and 0.3 represent the fractions of flow entering the cylindrical and conical sections of the perforation tunnel, determined as inferred by the studies of Deo et al. (1987).

Determination of the Formation Damage Potential by Laboratory Testing

Haggerty and Seyler (1997) conducted an extensive laboratory investigation of formation damage by mud cleanout acids and injection waters in Aux Vases sandstone reservoirs. They determined that typical Aux Vases reservoir formation is "a poorly cemented, soft, friable, fine-grained sandstone with pores lined with diagenetic clay minerals (Figure 15-26). The diagenetic clay mineral suite in Aux Vases reservoirs is a closely intergrown mixture of mixed-layered illite/smectite, chlorite, and illite. No kaolinite was found in the Aux Vases reservoir rocks sampled." They recommended that injection waters should be as saline as the formation brines and a properly formulated mud cleanout acid should be used to reduce formation damage.

Petrographic Analyses

Seyler (1998) conducted an extensive petrographical analyses of the core samples obtained from Aux Vases reservoirs. Seyler (1998) examined over 150 thin sections.

The petrographical analyses conducted included:

1. Standard optical microscopy using thin sections. For this purpose, they stained the thin sections with potassium ferricyanide and alizarine red to distinguish and detect the carbonate phases. Petro-

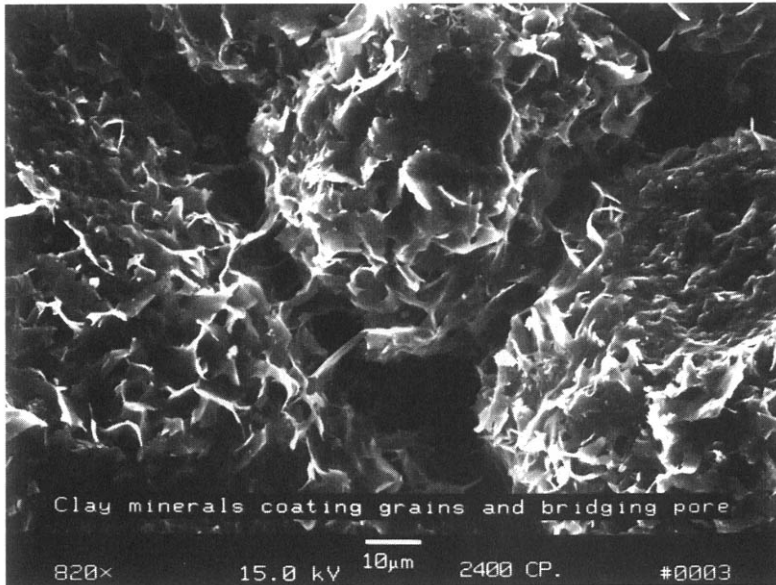


Figure 15-26. SEM of a critical-point-dried sample from a typical Aux Vases reservoir (2,400-ft depth, Budmark 3 Burr Oak, Energy Field) shows pore-lining and -bridging diagenetic clay minerals (closely intergrown mixed-layered illite/smectite, chlorite, and illite) and no quartz overgrowths (after Haggerty and Seyler, 1997; reprinted by permission of the Illinois State Geological Survey).

graphical characteristics and attributes, such as grain composition and size, cementing agents, porosity types, and reservoir quality were determined.

2. X-ray diffraction analysis (XRD). The XRD analyses determined the type and semi-quantitative composition of the minerals present in the samples.
3. Scanning electron microscopy (SEM) with energy dispersive x-ray microbeam (EDX) analysis, referred to as the SEM/EDX analysis. For this purpose, the samples were sputter-coated with gold and palladium. The SEM analyses identified the pore-lining minerals and the EDX analysis determined the elemental composition.

The analyses of the individual core samples are presented in Table 15-2 by Haggerty and Seyler (1997). They concluded that Aux Vases formation core samples contained 65–90% quartz, 3–15% feldspar, 0–15% calcite and 2–7% clay minerals.

Table 15-2
Aux Vases Samples: Bulk Weight Percentage of Clay Minerals
(absolute percentage of other minerals)

Depth ft	Perm. md	Porosity %	I %	I/S %	C %	BC %	Q %	Kf %	Pf %	Cc %	D %
Farrar 1 McCreery, Dale Consolidated Field — API 1205523456											
3,190.5	49.0	20.4	3.2	1.4	0.7	5.3	84.5	1.3	2.5	6.4	0.0
3,191.5	81.5	23.4	2.8	1.5	0.7	5	81.6	1.7	3.2	8.6	0.0
3,192.7	106.0	25.6	2.5	1.1	0.6	4.3	84.9	1.5	3.7	5.6	0.0
3,194.0	116.0	23.6	3.4	2.5	0.9	6.8	79.5	1.2	4.3	8.1	0.0
3,195.7	55.8	19.8	2.6	1.5	0.7	4.8	88.0	0.0	1.9	3.2	2.0
3,197.9	56.8	24.8	3.1	1.7	0.8	5.6	80.7	2.6	2.6	8.5	0.0
3,199.4	41.9	24.3	2.1	1.5	0.6	4.2	82.5	2.7	3.7	6.8	0.0
3,201.0	35.5	21.4	3.1	2.3	0.9	6.3	82.3	2.6	3.3	5.5	0.0
3,203.3	27.9	18.6	2.1	2.1	0.4	4.6	77.8	1.5	1.9	14.2	0.0
3,205.8	15.8	21.4	2.4	2.1	0.5	5.1	83.7	1.2	2.4	7.6	0.0
3,207.1	1.8	14.6	3.1	4.2	0.7	8	67.8	0.8	1.5	21.8	0.0
3,208.4	2.5	13.1	1.7	1.9	0.5	4.1	82.9	1.7	2.8	8.4	0.0
3,209.9	-0.1	0.7	5.2	4.7	1.9	11.8	68.4	1.2	1.8	16.8	0.0
3,212.7	NA	NA	2.7	3.7	0.0	6.4	2.4	0.0	0.0	91.2	0.0
3,216.7	NA	NA	1.5	2.0	0.0	3.5	2.9	0.0	0.0	93.6	0.0
3,219.2	NA	NA	4.6	4.4	0.1	9.1	3.4	0.0	0.0	71.8	15.6
Gallagher Drilling Company 2 Mack, Zeigler Field — API 1205523750											
2,605.5	24.9	14.4	5.5	2.7	1.1	9.4	69.2	0.0	2.9	18.5	0.0
2,606.5	216.0	25.1	3.7	2.7	2.2	8.7	64.2	3.0	7.4	16.7	0.0
2,608.5	49.0	22.1	2.9	1.2	1.9	6	85.0	1.1	3.9	3.9	0.1
2,610.5	64.0	22.1	2.4	1.4	2.2	6	86.4	0.6	4.0	2.9	0.0
2,611.5	124.0	24.1	1.7	0.8	1.9	4.3	86.2	0.4	4.9	3.9	0.3
2,612.5	152.0	25.5	4.2	1.9	3.3	9.4	72.1	8.9	6.1	3.4	0.0
2,614.5	35.6	23.6	2.3	1.2	3.7	7.1	77.9	2.3	9.0	3.7	0.0
2,617.5	89.5	24.5	0.5	0.3	1.5	2.3	91.4	0.0	4.4	1.9	0.0
2,618.5	47.8	24.8	1.2	0.6	4.3	6.2	82.7	0.2	7.1	3.8	0.0
2,620.5	47.8	23.5	2.0	2.1	6.0	10.1	61.8	20.5	4.3	3.3	0.0
2,621.5	56.0	23.8	2.2	0.7	7.2	10.1	78.8	0.6	6.4	4.2	0.0
2,623.7	NA	NA	2.4	2.1	5.2	9.7	72.7	0.2	2.2	15.2	0.0
2,623.8	-0.1	8.8	2.5	1.9	5.3	9.7	80.3	5.0	3.1	1.9	0.0
2,625.5	-0.1	17.0	2.5	2.5	4.9	9.9	84.5	0.5	3.7	1.5	0.0
2,629	-0.1	11.0	1.0	1.1	3.0	5.1	90.6	0.4	3.9	0.0	0.0
Budmark 2 Morgan Coal, Energy Field — API 1219923465											
2,387.6	184.0	21.3	1.6	0.9	2.4	5	80.8	0.0	8.2	6.0	0.0
2,388.4	246.0	21.7	1.2	1.1	1.9	4.2	56.5	0.2	8.2	30.9	0.0
2,390.1	69.0	23.6	1.4	0.7	2.5	4.7	85.4	0.6	2.6	6.7	0.0
2,392.7	85.0	23.3	0.8	0.3	1.7	2.7	72.7	0.2	7.8	16.6	0.0
2,394.7	69.0	20.6	1.0	0.5	3.0	4.5	76.3	0.4	6.3	12.5	0.0
2,395.2	4.3	13.6	1.6	0.9	4.1	6.6	63.5	0.0	2.5	27.5	0.0
Superior Oil Company 1 Price, Boyd Field — API 1208101972											
2,129.0	0.0	7.3	1.2	0.9	0.5	2.6	93.7	2.0	1.0	0.5	0.2
2,131.0	1.7	17.7	0.8	0.6	1.5	2.9	90.7	3.3	2.3	0.5	0.3
2,133.0	118.0	15.1	0.5	0.3	0.7	1.5	88.3	1.3	0.5	8.1	0.2
2,134.0	81.0	11.4	3.7	2.6	2.5	8.8	80.6	1.2	0.8	8.4	0.2
2,135.0	0.0	7.0	0.4	0.3	1.1	1.8	67.6	1.2	0.8	28.5	0.1
Superior Oil Company 7 Sanders, Boyd Field — API 1208101950											
2,141.0	42.0	21.6	1.1	0.8	0.7	2.6	80.9	2.5	0.7	12.9	0.5
2,144.0	362.0	24.2	0.4	0.3	0.7	1.5	84.2	2.6	1.3	10.1	0.4
2,151.0	140.0	21.5	1.4	1.0	1.6	4.1	84.9	3.2	1.6	6.0	0.3
2,155.0	58.0	19.5	0.6	0.5	1.3	2.4	88.3	2.9	1.1	4.7	0.5

Perm. = permeability, D = dolomite, Cc = calcite, C = chlorite, I = illite, I/S = illite/smectite, BC = bulk content, Kf = K-feldspar (microcline or orthoclase), Pf = plagioclase feldspar, Q = quartz

After Haggerty and Seyler, 1997; reprinted by permission of the Illinois State Geological Survey.

Haggerty and Seyler (1997) determined that calcite is the primary pore-filling mineral. They described the observed three types of pore filling calcite as: "In relative order of abundance, they are (1) patchy cement filling intergranular porosity (Figure 15-27c); (2) framework grains such as marine fossil fragments, ooids, and peloids; and (3) minute, late-stage euhedral crystals (Figure 15-27a) on diagenetic clay minerals that coat framework grains and line pores." Haggerty and Seyler (1997) describe the pore-lining minerals to be, "in descending order of abundance, dominantly diagenetic clay minerals, calcite, partially dissolved feldspars, solid hydrocarbons, anatase, barium-rich celestite, and traces of dolomite."

Haggerty and Seyler (1997) observed that "Pores in Aux Vases sandstone reservoirs are lined with, and may be bridged by, diagenetic clay minerals that consist of an intimately intergrown mixture of mixed-layered illite/smectite, chlorite, and illite (Figure 15-28). Although clay minerals constitute only 2-7% of the bulk mineral content, SEM analysis indicates that clay minerals coat more than 95% of pore surfaces. Therefore, an understanding of the composition and response of these diagenetic clay minerals to injected fluids is of utmost importance when selecting drilling muds and stimulation methods." "Chlorite identified by XRD and SEM/EDX analyses in Aux Vases samples is typically not iron-rich, but contains approximately equal amounts of iron and magnesium." "Reservoirs containing chlorite rich in iron may be more susceptible to formation damage than those containing other varieties of chlorite because they may form insoluble iron oxides or iron hydroxides."

Haggerty and Seyler (1997) report that the mixed-layered illite/montmorillonite (smectite) varieties are the only water sensitive, expandable clay minerals they found in the Aux Vases core samples.

Focus and Design of Experimental Studies

The primary objective of the studies by Haggerty and Seyler (1997) is the Experimental Investigation of Formation Damage by (1) mud cleanout acids and (2) injection waters in Aux Vases sandstone reservoirs.

Haggerty and Seyler (1997) describe that: "Development of sandstone reservoirs in the Illinois Basin typically includes these steps:

1. Drilling with freshwater mud;
2. Perforating the potential reservoir zone, if casing is used, or open hole completions with casing cemented above the producing zone;
3. Preflushing with 15% hydrochloric acid (HCL) or mud cleanout acid (MCA) to remove drilling mud;

(text continued on page 506)

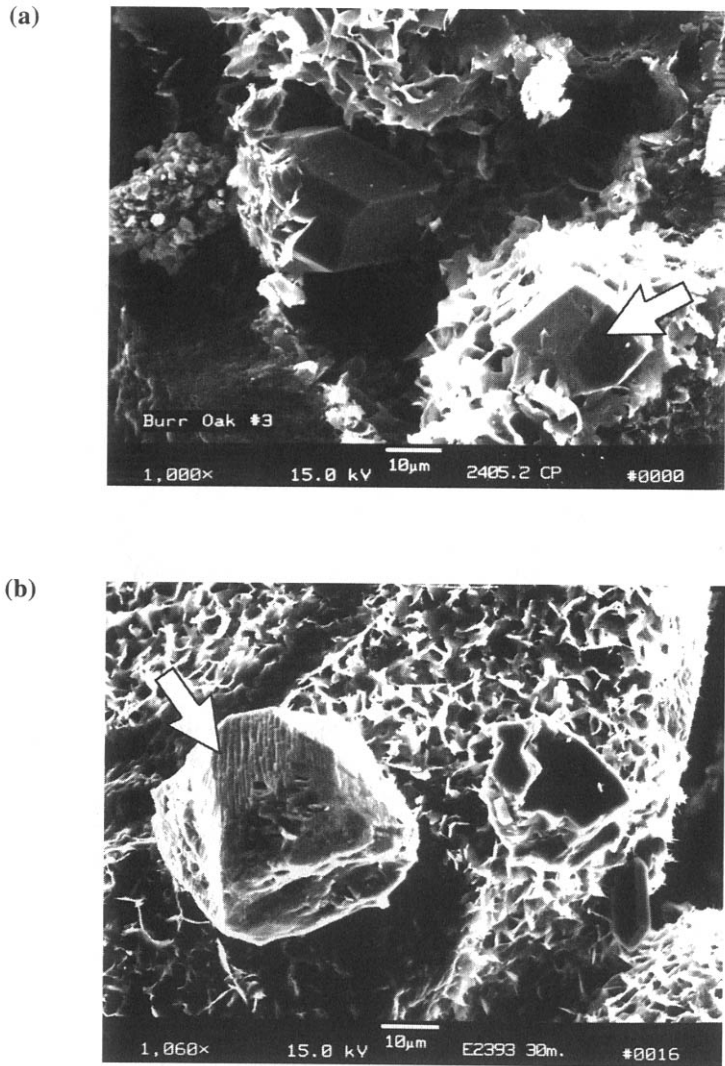
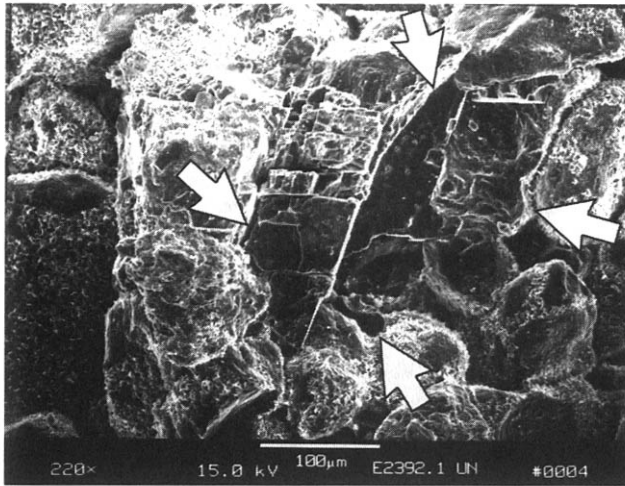
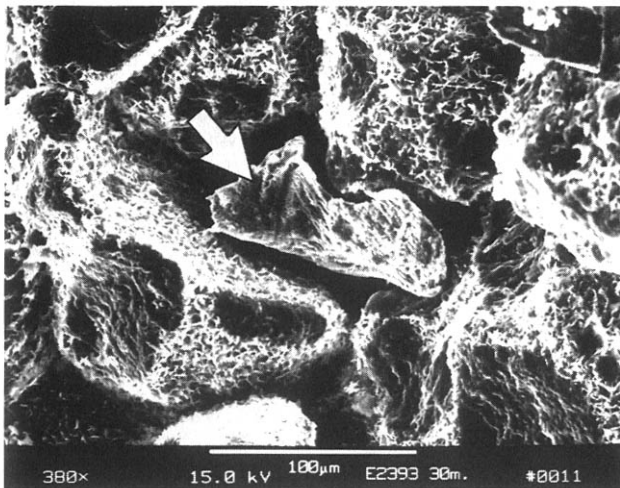


Figure 15–27. SEMS comparing acid-soaked with untreated wafers sliced from 1-inch-diameter core plugs from two wells in Energy Field: (a) An untreated, critical-point-dried sample (2,405.2-ft depth, Budmark 3 Burr Oak) shows a late-stage, minute calcite crystal with sharp euhedral edges (arrow) on top of diagenetic clay minerals; its position indicates that it precipitated after the clay minerals. This type of calcite is the first to be affected by exposure to MCA or 15% HCl; (b) A minute calcite crystal (arrow) was etched on this sample (2,393.5-ft-depth, Budmark 2 Morgan Coal) after 30 minutes of soaking in MCA. Compare the etched faces with the straight euhedral crystal faces shown in Figure 15–27a; clay minerals do not appear to have been affected; (c) An untreated sample (2,393.5-ft-depth, Budmark 2 Morgan Coal)

(c)



(d)



shows patchy calcite cement filling pores (arrows). This type of calcite is much more extensive than the minute late-stage crystals shown in Figure 15-27a. Dissolution of this type of calcite would improve porosity and permeability of reservoirs; (d) Partial dissolution of pore-filling calcite cement (arrow) after 30 minutes of soaking the sample (depth 2,393.5-ft, Budmark 2 Morgan Coal) in MCA. Compare this example with the untreated calcite cement shown in Figure 15-27c. The edges of the calcite are etched and contrast sharply with the flat, smooth cleavage surfaces in the untreated sample. Note that the clay minerals appear to have been unaffected (after Haggerty and Seyler, 1997; reprinted by permission of the Illinois State Geological Survey).

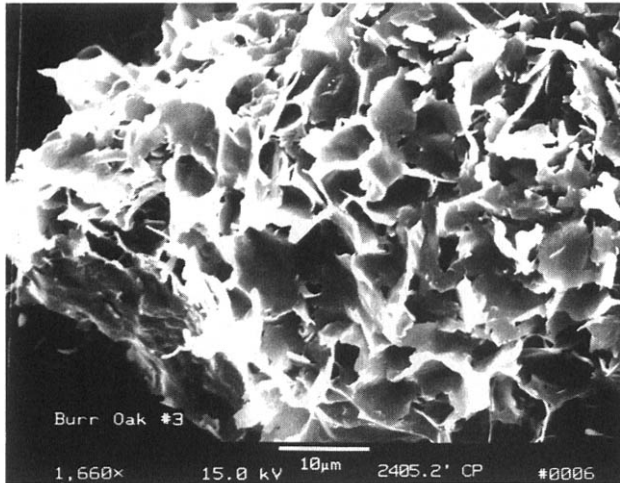


Figure 15–28. SEM shows a close-up of typical intergrown diagenetic clay minerals coating grains and lining pores in Aux Vases reservoirs. This sample was critical-point-dried to preserve the morphology of hydrated clay minerals composed of intimately intergrown mixed-layered illite/smectite, chlorite, and illite. Fresh cores with preserved fluids needed for critical point drying were available from only two wells. This sample (2,405-ft depth, Budmark 3 Burr Oak, Energy Field) was chosen because the well is near the Budmark 2 Morgan Coal well sampled for this study (after Haggerty and Seyler, 1997; reprinted by permission of the Illinois State Geological Survey).

(text continued from page 503)

4. Cleaning out perforations or the well bore with MCA;
5. Initial swabbing to retrieve stimulation fluids and induce oil flow toward the wellbore;
6. Hydraulic fracturing using a freshwater gelled pad and sand proppant;
7. Final swabbing during the production test.

Table 15–3 (adapted from Piot and Perthuis, 1989) clearly indicates that exposure of Aux Vases formation to acid solution can activate some reactions with the resident minerals.

In an effort to simulate the field practice in the laboratory investigations, Haggerty and Seyler (1997) state that: “The experiments focused on five objectives:

1. Determine how MCA containing 15% HCL with additives, typically used during completion and/or stimulation, affects pore-lining

Table 15-3
Reactions of Aux Vases Sandstone Minerals with Well Fluids*

Mineral	Exposure to fluids	Solubility in 15% HCl	Chemical composition	Released
Quartz	Low	Insoluble	SiO ₂	None
K-feldspar	Low to med	Low	K(AlSi ₃ O ₈)	K ⁺ , Al ³⁺ , Si ⁴⁺
Na-feldspar	Low to med	Insoluble	Na(AlSi ₃ O ₈)	None
Illite	High	Low	(Fe,Mg)K _x Al ₂ (Si _{4-x} Al _x)O ₁₀ (OH) ₂	K ⁺ , Al ³⁺ , Si ⁴⁺
Mixed-layered illite/smectite	High	Low	(Fe,Mg)K _x Al ₂ (Si _{4-x} Al _x)O ₁₀ (OH) ₂	K ⁺ , Al ³⁺ , Si ⁴⁺
		Low	(½Ca,Na)·7(Al,Mg,Fe) ₄ ·(Si,Al) ₈ O ₂₀ (OH) ₄ ·nH ₂ O	Ca ²⁺ , Na ⁺ , Fe ²⁺ , Mg ²⁺ , Al ³⁺ , Si ⁴⁺
Chlorite	High	Low to med	(Mg,Fe) ₅ (Al,Fe)(Al,Si ₃ O ₁₀)(OH) ₈	Mg ²⁺ , Fe ²⁺ , Al ³⁺ , Si ⁴⁺
Calcite	Low to high	High	CaCO ₃	Ca ²⁺ , CO ₃ ⁻
Fe-dolomite	Low	High	(Ca,Mg,Fe)CO ₃	Mg ²⁺ , Fe ²⁺ , Ca ²⁺ , CO ₃ ⁻
Anatase	Low	Insoluble	TiO ₂	None
Barite-celestite	Low	Insoluble	(Ba,Sr)SO ₄	None
Solid H-carbon	Low to med	Med	C, OH, H, S, N	C ⁺ , S ⁺
Pyrite	Low	Insoluble	Fe ₂ S	None

* Adapted from Piot and Pertuis (1989).

After Haggerty and Seyler, 1997; reprinted by permission of the Illinois State Geological Survey.

- minerals and the permeability of Aux Vases reservoir rocks by conducting dynamic, constant rate injection coreflood experiments;
- Investigate how 15% HCL and MCA affects crude oil from Aux Vases reservoirs by conducting compatibility experiments;
 - Examine how exposure to fluids of various salinities affects permeability in samples of Aux Vases reservoirs by conducting coreflood experiments;
 - Investigate the effects of long-term contact of 15% HCL and MCA with pore-lining minerals in reservoir samples by conducting static soak experiments;
 - Compare XRD analyses of the bulk mineralogy and SEM/EDX analyses of pore-lining minerals with flood results to identify minerals that would be most affected by fluids commonly used during drilling, completion, and stimulation of Aux Vases reservoirs.

Therefore, Haggerty and Seyler (1997) carried out five sets of bench experiments, with the specific objectives described in Table 15-4. The direct contact experiments have been conducted to determine the effect of the acids on the physical properties of crude oil. In the coreflood tests, they continuously injected excessive amounts (25 to 50 pore volumes) of fluid during coreflood experiments. Therefore, Haggerty and Seyler (1997) state that their coreflood experiments most closely represent the

Table 15–4
Experimental Overview

Type of experiment	Fluids	Field, well	Depth ft	To determine
Direct contact: crude oil and acids	Crude oils	Boyd, Baldrige B5 Bizot	2,170	Compatibility of 15% HCl vs MCA
		Dale, Farrar 2 McCullum Community	3,158–3,176	
		Energy, Budmark 2 Morgan Coal	2,385–2,395	
		Zeigler, Gallagher Drilling 1 Alex	2,615–2,630	
Coreflood: continuous injection at a constant rate	MCA	Energy, Budmark 2 Morgan Coal	2,392.1	Effects on permeability and pore-lining minerals
	MCA	Zeigler, Gallagher Drilling 2 Mack	2,627	
	15% HCl	Energy, Budmark 2 Morgan Coal	2,393.5	
Coreflood: interrupted injection, constant rate	MCA	Dale Cons, Farrar 1 McCreery	3,198.7	Effects of interrupting injection and soaking sample in MCA; simulates potential damage after injection and before swabbing
	MCA	Energy, Budmark 2 Morgan Coal	2,391.1	
Core waterflood: interrupted injection, constant rate	Waters, various salinities	Boyd, Superior Oil 9 Sanders	2,163	Sensitivity of rock to injected water of varying salinities; note permeability changes
		Energy, Budmark 2 Morgan Coal	2,390	
		Energy, Budmark 2 Morgan Coal	2,388	
		Zeigler, Gallagher Drilling 2 Mack	2,611	
		Dale Cons., Farrar 1 McCreery	3,200.6	
		Energy, Budmark 2 Morgan Coal	2,388.3	
Acid soak	15% HCl	Energy, Budmark 2 Morgan Coal	2,392.8	Long-term reaction of reservoir rock to MCA and 15% HCl
	MCA	Energy, Budmark 2 Morgan Coal	2,393	

After Haggerty and Seyler, 1997; reprinted by permission of the Illinois State Geological Survey.

completely flushed reservoir zones and, under these conditions, the precipitates cannot deposit and cause formation damage in porous media, within the time scale of the convective flow. The acid soak experiments served for the purpose of observing the long-term effects of reactions in unflushed and incompletely flushed zones.

Description and Preparation of Materials

Core Plugs. Table 15–5 shows the sources and available data of the Aux Vases reservoir core samples used by Haggerty and Seyler (1997). One-inch-diameter (2.54 cm) core plugs were extracted out of 4-inch-diameter

Table 15-5
Samples Used for the Experiments and Methods Used to Describe Them

Field, well and well ID	Depth <i>ft</i>	SEM/EDX	XRD	Thin section
Energy	2,393.5	Yes	No	No
2 Morgan Coal	2,388.3	Yes	Yes	Yes
1219923465	2,391.1	Yes	No	No
	2,390	No	Yes	Yes
	2,388	No	No	No
	2,393	Yes	No	No
	2,392.8	Yes	Yes	Yes
Dale	3,198.7	Yes	No	Yes
1 McCreery	3,200.6	No	No	No
1205523456				
Zeigler	2,611	Yes	Yes	Yes
2 Mack	2,627	Yes	Yes	Yes
1205523750				
Boyd	2,163	No	No	No
9 Sanders				
1208102628				

After Haggerty and Seyler, 1997; reprinted by permission of the Illinois State Geological Survey.

whole cores with maximum possible lengths permitted by drilling. In the coreflood experiments, they used core plugs of 1-inch (2.54 cm) to 2.5-inch (6.35 cm) long. In the MCA and HCL soak experiments, they used 1-inch-diameter (2.54 cm) and 0.25-inch-thick (0.635 cm) core plug wafers.

Fluids. Halliburton, Inc. provided the MCA solution containing “15% HCL in a proprietary formulation of surfactants, suspending agents, anti-sludge agents, clay mineral stabilizers, iron-sequestering agents, and corrosion inhibitors,” as stated by Haggerty and Seyler (1997).

The characteristics of the waters used by Haggerty and Seyler (1997) are described in Table 15-6. The Aux Vases formation brine was obtained from the Budmark No. 3 Morgan Coal lease in Energy Field, filtered, and then used in coreflood tests with a 13.7% TDS (total dissolved solids) content.

A fresh water mixture containing 1.2% TDS and its mixtures with the formation brine at various proportions, as described in Table 15-6, were synthetically prepared and used in the coreflood tests. Haggerty and Seyler (1997) measured the resistivities of these mixtures and then

Table 15–6
Characteristics of Water Mixtures

Type	Ca ²⁺	Na ⁺	Ionic composition meq/l			Cl ⁻	SO ₄ ²⁻	HCO ₃ ⁻	pH	R _w	TDS %
			Ba ²⁺	Fe ³⁺	Mg ²⁺					Ω-m	
Formation brine	341	1883	0.0	0.4	173	2394	1.0	1.7	6.1	0.063	13.7
Supply water	16	14	0.1	0.0	13	28.2	13.5	1.5	5.3	0.433	1.2
95%(1) – 5%*										0.064	13.5
90%(1) – 10%										0.068	12.4
75%(1) – 25%										0.076	10.5
50%(1) – 50%										0.124	5.95

* 95% (by volume) of formation brine and 5% (by volume) of the supply water.
meq/l = mole wt/charge per liter

After Haggerty and Seyler, 1997; reprinted by permission of the Illinois State Geological Survey.

estimated their TDS using the TDS-resistivity correlation developed by Demir (1995):

$$TDS(ppm) = \frac{6,786.09}{R_w^{1.2853} 1.022^T} \quad (15-8)$$

where R_w denotes the resistivity of water in Ω-m and T denotes the water temperature in °F.

Equipment

Haggerty and Seyler (1997) performed their coreflood tests using a TEMCO™ integrated coreflood apparatus. This system is described schematically in Figure 15–29. A conventional Hassler-type coreholder is placed in an oven for temperature control. The core is placed inside a rubber sleeve between metal end pieces. Spacers are attached to adjust for different core lengths. The space between the coreholder and rubber sleeve is filled with a pressurized hydraulic fluid. A confining pressure pump and gauge system applies pressure to the rubber sleeve containing the core sample. The confining pressure applied over the core plugs prevents the bypassing of the injected fluids around core plugs and the mixing of the injected and hydraulic fluids. The coreholder is connected to oil and water reservoirs and the oil and water recycling cylinders. The coreholder is equipped with an inlet pressure transducer and gauge and a back pressure regulator and gauge. The other auxiliary equipment

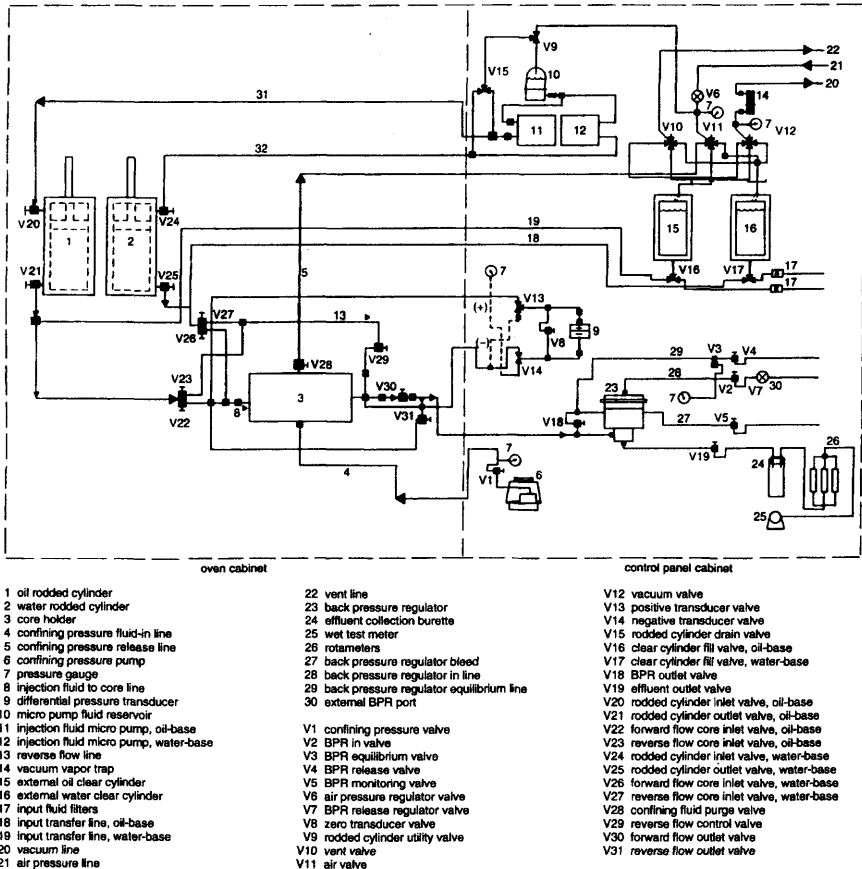


Figure 15–29. Temco integrated coreflood apparatus (after Haggerty and Seyler, 1997; reprinted by permission of the Illinois State Geological Survey).

includes a nitrogen gas cylinder, rotameters, pressure valves, and a wet test meter (Oil and Gas Section—ISGS, 1993).

Coreflood Tests

Haggerty and Seyler (1997) report that the core plugs were cleaned in a CO_2 /solvent core cleaner and vacuum-dried. Then the porosity and permeability to nitrogen gas were measured. The baseline liquid permeability was measured by injecting $1.5 \text{ cm}^3/\text{min}$ brine continuously into the core plugs. They determined the $1.5 \text{ cm}^3/\text{min}$ rate by scaling the typical reservoir fluid velocity of 14 ft/day and 68.6 bbl/day in a 10-foot-thick pay zone, using the scaling coefficient of unity ($LV\mu_w = 1$) for 65%

oil recovery at water breakthrough (Kyte and Rapoport, 1958; Delclaud, 1991). This corresponds to 0.296 cm/min or 1.5 cc/min flow through 1-inch-diameter core plugs. They measured the pressure difference between the inlet and outlet of the core plugs and calculated the effective liquid permeability of the core plugs using Darcy's law.

Haggerty and Seyler (1997) estimated the overburden pressure of the Aux Vases formations located at 2,100 to 3,200-ft depths to be in the range of 2,100 to 3,200 psi by assuming a gradient of 1 psi/ft for typical sedimentary basins (Levenson, 1967). Assuming the reservoir fluid is normally pressured and using a hydrostatic pore pressure gradient of 0.45 psi/ft, they estimated the pore fluid pressure to be 1,200 psi. The bottom hole temperatures of wells in the Aux Vases formations vary from 75° to 98°F (24° to 36°C). However, they performed the coreflood tests at 1,000 psig (6,895 KPa) confining pressure and 75°F (24°C) temperature. They assumed that the effects of the differences between the test and field conditions are negligible based on the arguments by Amyx et al. (1960) and Eickmeier and Ramey (1970). They conducted the flow tests at constant injection rates. The pressure difference across the core plugs typically varied between 10–50 psi (69.8–345 KPa) for injection at a 14 ft/day rate. A 50–75 psi (345–517 KPa) back pressure was sufficient to maintain single phase and avoid CO_2 gas bubbles.

As stated by Haggerty and Seyler (1997) tests conducted using core plugs have certain, inherent limitations:

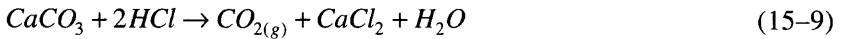
1. Their small size represents a very small percentage of the total reservoir; therefore the entire range of effects that introduced fluid may have on reservoir behavior cannot be fully determined, and
2. Each experiment represents a discrete phase of the drilling, completion, or stimulation process.

However, coreflood tests conducted at near in-situ conditions can help explain the reactions between pore-lining minerals and extraneous fluids introduced by drilling, completion and stimulation operations (Haggerty and Seyler, 1997). Then, the cumulative effects of the rock-fluid interactions on formation damage can be determined by simulation or other means.

Experimental Results

Haggerty and Seyler (1997) conducted a number of tests with 15% HCL and 15% HCL-MCA to determine the effect of the clay stabilizing agents present in the mud cleaning acid (MCP) provided by Halliburton, Inc.

Calcite Dissolution with the MCA. The HCL in the MCA dissolves calcite by the reaction:



The produced carbon dioxide (CO_2) gas dissolves in the aqueous phase at elevated pressures, but separates as the effluent solution comes out of the core. Haggerty and Seyler (1997) conducted four types of tests. These tests and their results are summarized in the following.

Coreflood Tests with MCA. They conducted interrupted and continuous acid corefloods using a 15% HCL-MCA on samples described in Tables 15-3 and 15-4. They injected ten pore volumes of the acid solution into the core plugs for complete flushing of the cores to simulate the total flushing of the near-wellbore formation during acid stimulation.

The primary objective of the interrupted corefloods was to investigate the effects of the MCA solution on the formation without the presence of other reservoir fluids (i.e., oil and brine). Therefore, Haggerty and Seyler (1997) injected MCA into a dry core sample. The acid injection was interrupted at certain time intervals and the permeability of the core was measured. Figures 15-30 and 15-31 show the measured permeabilities of two different core plugs. The acid dissolved the calcite cement and permeability increased. Although some fine particles may have been unleashed by calcite dissolution, damage by fine particles migration and deposition was not observed because the fine particles were flushed out of the core plugs by an excessive amount of acid injection (ten pore volumes). In fact, after 24 hours of exposure, Haggerty and Seyler (1997) detected fine-grained sand, silt-sized grains of nonclay minerals, and diagenetic clay particles in the effluent.

The continuous acid corefloods were conducted to simulate the flushing of the near wellbore formation in the presence of formation fluids. For this purpose, the cores were restored to their reservoir conditions by a series of displacement processes. First, the cores were saturated with brine, the brine was displaced by oil up to irreducible water saturation, and the cores were allowed to establish oil-water equilibrium by soaking them in oil for 48 hours. The oil present in the cores, prepared in this way, was displaced with brine and then MCA was injected to displace the brine and effective permeabilities were measured during continuous acid injection. As indicated in Figure 15-32 by Haggerty and Seyler (1997), the permeability first decreased rapidly and then increased continuously. Haggerty and Seyler (1997) attribute the initial decreasing of permeability to carbon dioxide (CO_2) gas production.

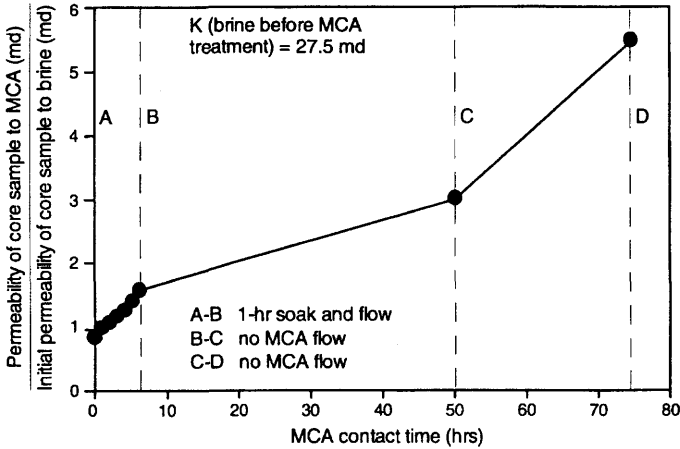


Figure 15-30. An interrupted, constant flow rate, acid coreflood exposed a core plug (3,198.7-ft depth, Farrar 1 McCreery, Dale Cons. Field) to MCA for 74 hours. Permeability increased with MCA-rock contact time as calcite cement dissolved, dislodging some fine grains that were flushed out of the core sample (after Haggerty and Seyler, 1997; reprinted by permission of the Illinois State Geological Survey).

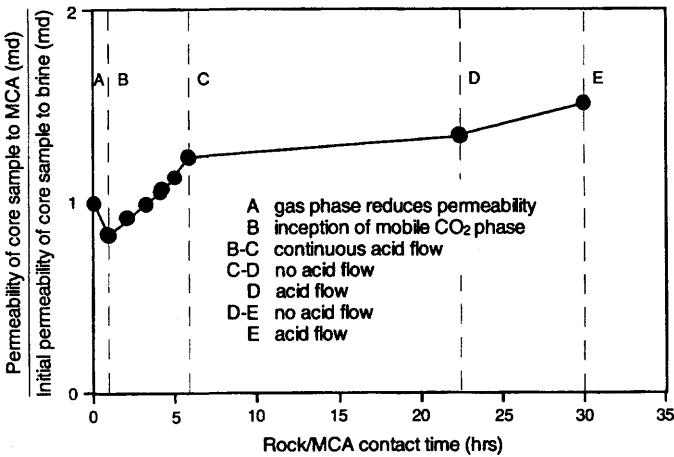


Figure 15-31. Permeability changes during a 30-hour, interrupted, constant flow rate (1.5 cm³/min) coreflood test using a 1-inch-diameter core plug (2,392.1-ft depth, Budmark 2 Morgan Coal, Energy Field). Permeability increased with MCA-rock sample contact (no flow) and flow times. The increase is more pronounced in the McCreery core plug (Figure 15-30) because of the dissolution of large amounts of calcite cement aligned along crossbedding laminae; the Budmark 2 Morgan Coal sample did not have as much calcite cement (after Haggerty and Seyler, 1997; reprinted by permission of the Illinois State Geological Survey).

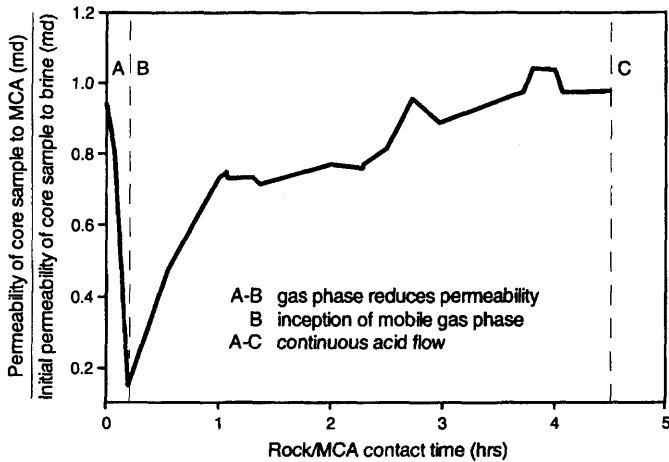


Figure 15-32. Permeability of a sample (2,627.5-ft depth, Gallagher Drilling Co. 2 Mack, Zeigler Field) varied significantly during a 4.5-hour continuous, constant rate coreflood test using MCA (after Haggerty and Seyler, 1997; reprinted by permission of the Illinois State Geological Survey).

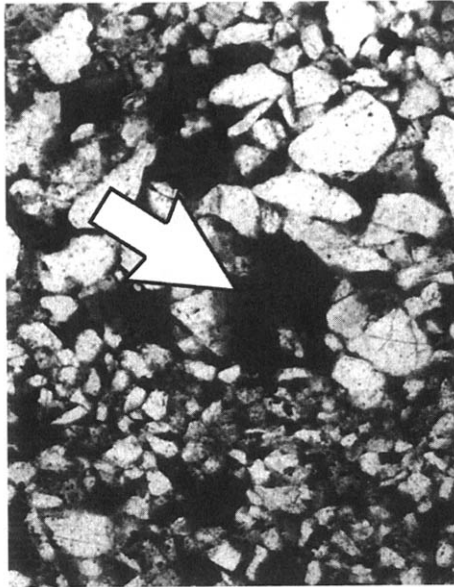
Figures 15-33a and b are the photomicrograph and SEM photomicrograph, respectively, of a thin section taken from a core plug exposed to MCA for 75 hours. These photomicrographs clearly show that calcite cement was dissolved and the pores were enlarged.

Calcite Dissolution in MCA Soak Tests. The MCA soak tests were conducted statically (without flow) at ambient room conditions to observe the effect of acid on pore-lining minerals. These tests determine the effect of the acid remaining in locations far away from the well bore after acid stimulation.

Figures 15-27a and 15-26 by Haggerty and Seyler (1997) show that untreated core samples are loosely cemented and friable sandstone with grains coated with diagenetic clay minerals. Figure 15-27c shows pores filled with patchy calcite cement in an untreated sample. Figures 15-27c and d show the pores of 30 minute acid-treated cores. Comparison of Figure 15-27a to Figure 15-27b and Figures 15-27c to Figure 15-27d indicate that some crystals and patches of calcite cement were partially dissolved after 30 minutes, but the diagenetic clay minerals were not affected. Haggerty and Seyler (1997) attribute this to the function of clay-stabilizing additives present in the MCA.

Coreflood Tests With 15% HCL without Additives. In order to determine the effect of acid treatment without the clay stabilizers, Haggerty and

(a)



(b)

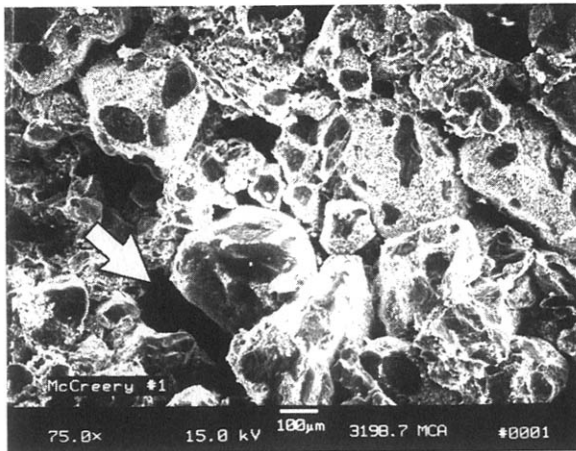


Figure 15–33. (a) Photomicrograph of a thin section made from the core plug after 74 hours of exposure to MCA shows that coarse grained laminae, filled with calcite cement prior to the coreflood, developed a channelized pore system due to total dissolution of calcite cement along the laminae. As a result, large oversize pores formed (arrow); (b) SEM photomicrograph of the same sample after coreflood also shows enlarged pores (arrow) and diagenetic clay minerals coating siliciclastic framework grains. The framework grains have bimodal size distribution and are either very fine grained (100 µm) or medium grained at 250 µm or greater (after Haggerty and Seyler, 1997; reprinted by permission of the Illinois State Geological Survey).

Seyler (1997) conducted a number of tests using an aqueous solution containing 15% HCL only. As shown in Figure 15–34, the permeability of the core plug increased. They attributed the permeability increase to calcite dissolution and concluded that the aluminum- or magnesium-rich chlorites in the Aux Vases formations do not produce iron gels that could cause permeability reduction.

The effluent ion analyses presented in Table 15–7 by Haggerty and Seyler (1997) clearly indicate leaching, dissolution and disintegration of the pore-lining diagenetic clay minerals and the pore-filling cements by the 15% HCL solution coreflood tests. The SEMs shown in Figures 15–35a through c by Haggerty and Seyler indicate the deposition of various precipitates in treatment with 15% HCL without the presence of the stabilizing agents, as a result of the reaction of the acid with the pore minerals and brine. Figure 15–35d shows the remaining quartz minerals stripped off the clay mineral coatings by the 15% HCL acid solution.

Soak Tests With 15% HCL without Additives. Haggerty and Seyler (1997) observed significantly more mineral precipitation, as shown in Figures 15–35a-d, with samples soaked with 15% HCL compared to those soaked in MCA.

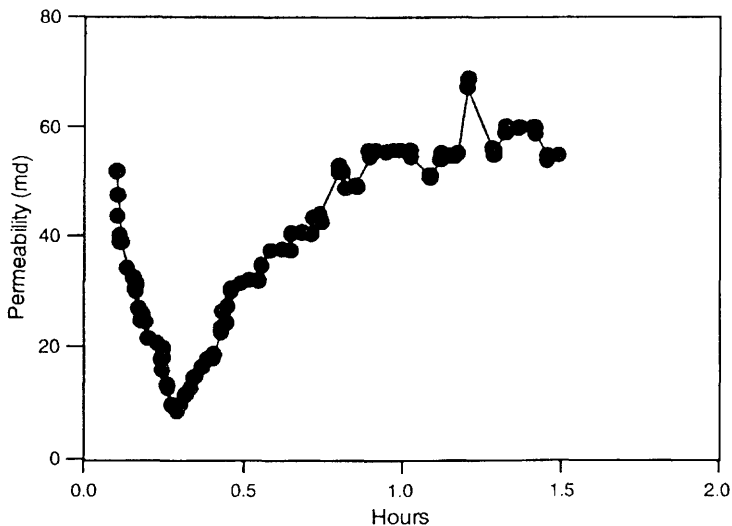


Figure 15–34. Permeability of a core plug (2,393.5-ft depth, Budmark 2 Morgan Coal, Energy Field) changed as the HCL-rock contact time increased during a continuous, constant rate acid flood test using 15% HCL (after Haggerty and Seyler, 1997; reprinted by permission of the Illinois State Geological Survey).

Table 15-7
Composition of Effluent from HCl Coreflow: Energy Field Sample,
2,392.6-foot depth, Budmark 2 Morgan Coal Well

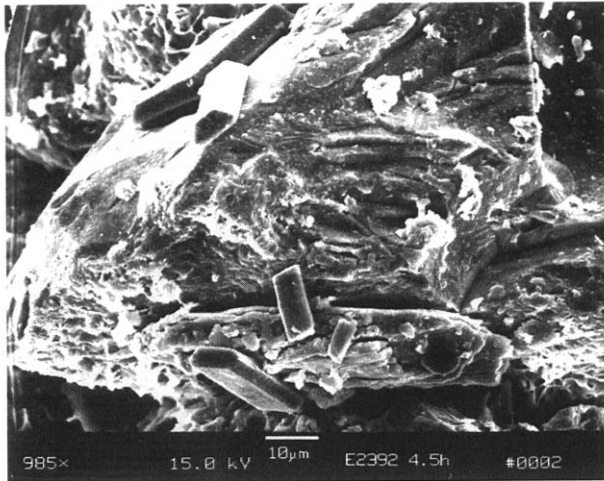
Effluent sampled at	mg/l					
	Al	As	B	Ba	Be	Ca
1 hour	26.5	0.2	0.26	2.18	0.004	8250
2 hours	250	.1	0.11	0.68	.001	1550
2 days	56.4	.1	0.1	0.83	0.002	3130
	Cd	Co	Cr	Cu	Fe	
1 hour	0.04	0.40	8.1	19.4	109	
2 hours	0.46	0.46	11.1	10.6	409	
2 days	.01	0.34	15.1	9.21	158	
	K	La	Li	Mg	Mn	Mo
1 hour	9	0.52	0.19	92.6	15.4	40.8
2 hours	7	0.19	0.47	177	4.09	21.2
2 days	6	0.28	0.12	48.5	7.49	15.4
	Na	Ni	Li	Mg	Mn	Mo
1 hour	895	131	08	0.010	.1	17.8
2 hours	168	57.4	0.14	0.009	.1	15.7
2 days	154	49.4	0.04	0.022	.1	19.2
	Sr	Ti	Tl	V	Zn	Zr
1 hour	17.1	0.10	.1	0.02	1.64	0.07
2 hours	1.63	0.13	.1	0.70	1.74	0.07
2 days	2.35	0.11	.1	0.20	0.80	0.10

After Haggerty and Seyler, 1997; reprinted by permission of the Illinois State Geological Survey.

Coreflood Tests for Water Sensitivity. Haggerty and Seyler (1997) injected different salinity brines into Aux Vases core plugs and conducted two types of water sensitivity tests: (1) determination of the critical salt concentration and (2) permeability impairment and restoration.

In the first type test, permeability of the core plugs were monitored while injecting brines with slowly reduced salinities. For this purpose, they begin injecting first the formation brine (TDS = 120,000 ppm), and then brines progressively diluted with deionized water. Figure 15-36 by Haggerty and Seyler (1997) show that Aux Vases formation is sensitive to waters having salinities below the salinity of the formation water and the water sensitivity is more pronounced at lower salinities.

(a)



(b)

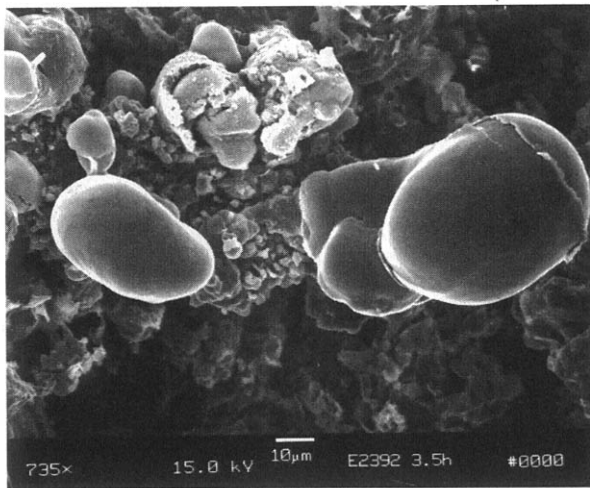
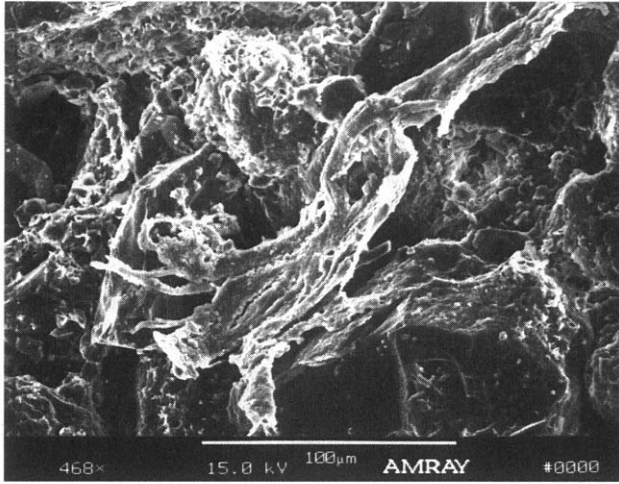


Figure 15–35. SEMs illustrate the effects of soaking Aux Vases core plug wafers (2,392.4-ft depth, Budmark 2 Morgan Coal, Energy Field) in a 15% HCl solution without any of the additives found in MCA. The most common precipitates in these samples are shown in Figures 15–35a–c. (a) Gypsum crystals precipitated because of the reaction of pore minerals and formation brine with 15% HCl. EDX analysis shows that S and Ca are the predominant detectable elements in these crystals. (b) Blebs that do not display any crystalline structure and appear to be an amorphous or gel-like substance containing Fe and Cl, as identified by EDX analysis. (The EDX unit used in this study detects elements with atomic numbers of 6 or greater.)

(c)



(d)

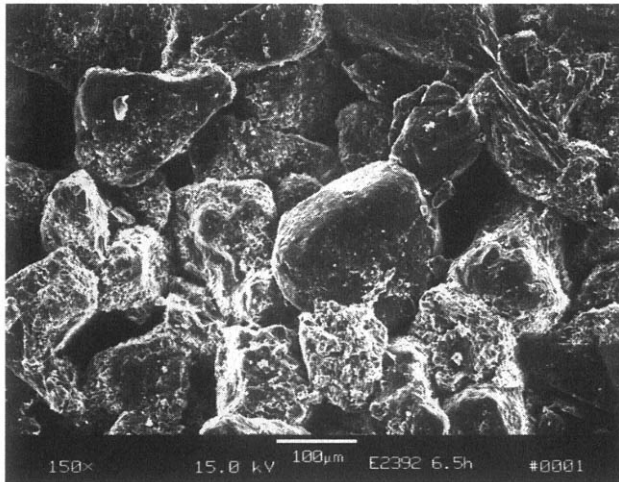


Figure 15–35 continued. (c) In another amorphous material, EDX analysis has identified Ca, Cl, Al, Si, and Fe. All these precipitates are attributed to the reaction of pore minerals and formation brine with 15% HCl because they have not been observed in any untreated samples; (d) The smooth quartz grains without their original clay mineral coatings (Figure 15–26) indicates widespread removal, disintegration, or dissolution of diagenetic clay minerals—the effects of long-term soaking in 15% HCl (after Haggerty and Seyler, 1997; reprinted by permission of the Illinois State Geological Survey).

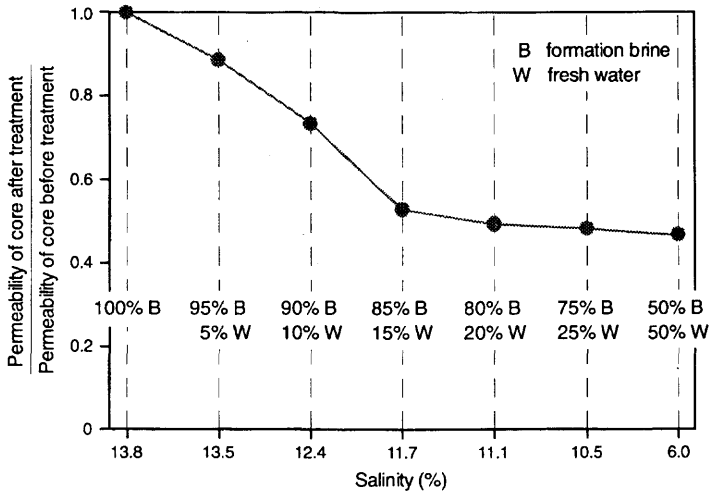


Figure 15-36. Various mixtures of produced brine and deionized water were injected into a core plug (2,388-ft depth, Budmark 2 Morgan Coal, Energy Field). Decreasing salinity corresponded with decreasing permeability, which suggests that injection of fluids less saline than formation brine can cause formation damage (after Haggerty and Seyler, 1997; reprinted by permission of the Illinois State Geological Survey).

In the second type tests, the formation, fresh water, and formation brines progressively diluted by fresh water were injected in separate tests until equilibrium and the permeability variations were measured. Figure 15-37 by Haggerty and Seyler (1997) shows that permeability decreased in all cases, even though halite precipitation from formation brine and dissolution in fresh water later caused temporary increase of permeability. They could not restore the permeability by injecting a brine of higher salinity into a core, exposed to fresh water, possibly because the clay minerals permanently swelled and/or migrated to and plugged the pore throats.

Haggerty and Seyler (1997) concluded that permeability impairment by water flooding of Aux Vases reservoirs can only be avoided by injecting waters as saline as the formation brines.

Oil-Acid Compatibility. Haggerty and Seyler (1997) investigated the compatibility of oil with 15% HCL acid without additives and with 15% HCL-MCA containing proprietary additives. They mention that the typical additives used in MCA solutions include demulsifying and/or antisludging agents. As depicted in Figure 15-38 by Haggerty and Seyler (1997), 15% HCL without any additives formed an emulsified sludge with

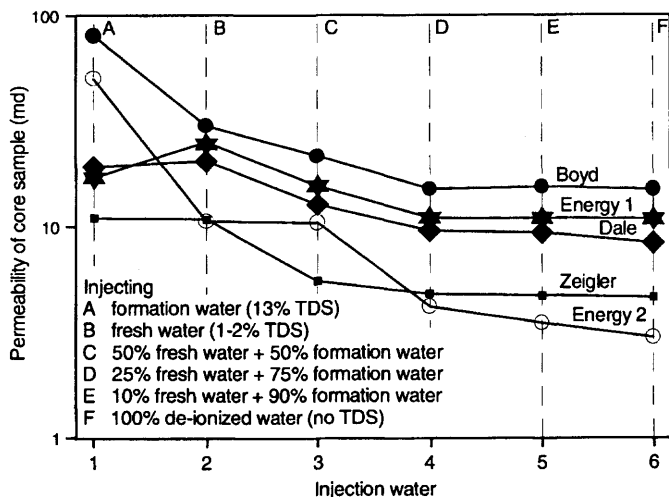


Figure 15-37. Changes in permeability of core plugs tested with water of varying salinities. The most pronounced decrease occurred in high permeability samples from Energy and Boyd Fields. An early but brief increase in permeability in a low permeability sample from Energy Field was probably due to dissolution of halite precipitated when brine evaporated during air drying (after Haggerty and Seyler, 1997; reprinted by permission of the Illinois State Geological Survey).

the oil and, therefore, it has the potential of reducing the fluid mobility in the reservoir. Whereas, the MCA used in their tests did not form any sludge, indicating that the antisludging agents were effective for preventing the emulsification process.

Summary of Results. Haggerty and Seyler (1997) summarized the findings of their experimental investigations in Table 15-8. Presentation of results in concise forms, similar to Table 15-8, provides a convenient means of translating the results of extensive and lengthy work to practical recipes for the field operators and decision makers.

References

- Amaefule, J. O., Ajufo, A., Peterson, E., & Durst, K., "Understanding Formation Damage Processes," SPE 16232 paper, SPE Production Operations Symposium, Oklahoma City, Oklahoma, 1987.
- Amaefule, J. O., Kersey, D. G., Norman, D. L., & Shannon, P. M., "Advances in Formation Damage Assessment and Control Strategies,"

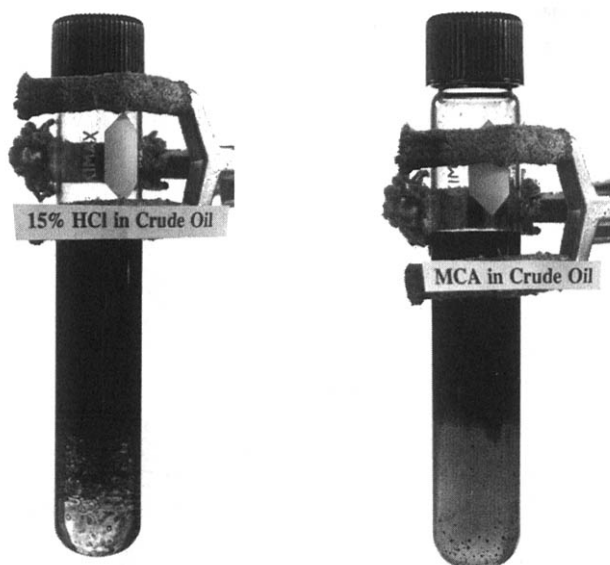


Figure 15-38. (a) Emulsified sludge formed immediately upon contact of Aux Vases oil with 15% HCl; (b) When MCA was added to Aux Vases oil, sludge did not form, presumably because of the surfactant in the MCA (after Haggerty and Seyler, 1997; reprinted by permission of the Illinois State Geological Survey).

Table 15-8
Summary of Experimental Results

Experiment	Figures	Change in permeability
Crude oil/15% HCl	15-38	(Decrease)*
Crude oil/MCA	15-38	(No change)*
Continuous corefloods with MCA	15-31 and 32	Increase 0–60%
Continuous coreflood with HCl	15-34	Increase up to 30%
Discontinuous coreflood with MCA	15-30	Increase up to 600%
HCl soak	15-35a–d	Could not measure
MCA soak	15-27b and 15-27d	Could not measure
Water sensitivity		
Gradual increase in freshwater	15-36	Decrease 15–56%
Boyd (2,163-ft depth)	15-37	-60.0% to -76.0%
Energy (2,388-ft depth)	15-37	-74.5% to -93.6%
Energy (2,190-ft depth)	15-37	+34.6% to -23.5%
Dale (3,200.6-ft depth)	15-37	+5.3% to -53.7%
Zeigler (2,611-ft depth)	15-37	0 to -58.4%

* Inferred from experiment results, not directly measured.

After Haggerty and Seyler, 1997; reprinted by permission of the Illinois State Geological Survey.

- CIM 88-39-65 paper, 39th Annual Technical Meeting of Petroleum Society of CIM and Canadian Gas Processors Association, June 12–16, 1988, Calgary, Alberta, 16 p.
- Amyx, J. W., Bass Jr., D. M., & Whiting, R. L., *Petroleum Reservoir Engineering, Physical Properties*, R.L. McGraw-Hill, 1960, New York, 610 p.
- Bennion, D. B., & Thomas, F. B., “Underbalanced Drilling of Horizontal Wells: Does it Really Eliminate Formation Damage?,” SPE 27352 paper, SPE Formation Damage Control Symposium, February 1994, Lafayette, LA.
- Čerňanský, A., & Široký, R., “Deep-bed Filtration on Filament Layers on Particle polydispersed in Liquids,” *Int. Chem. Eng.*, Vol. 25, No. 2, 1985, pp. 364–375.
- Civan, F., “A Generalized Model for Formation Damage by Rock-Fluid Interactions and Particulate Processes,” SPE 21183 paper, SPE 1990 Latin American Petroleum Engineering Conference, October 14–19, 1990, Rio de Janeiro, Brazil, 11 p.
- Civan, F., “Evaluation and Comparison of the Formation Damage Models,” SPE 23787 paper, SPE International Symposium on Formation Damage Control, February 26–27, 1992, Lafayette, Louisiana, pp. 219–236.
- Civan, F., Predictability of Formation Damage: An Assessment Study and Generalized Models, Final Report, U.S. DOE Contract No. DE-AC22-90-BC14658, April 1994.
- Civan, F., “A Multi-Phase Mud Filtrate Invasion and Well Bore Filter Cake Formation Model,” SPE 28709 paper, SPE International Petroleum Conference & Exhibition of Mexico, October 10–13, 1994, Veracruz, Mexico, pp. 399–412.
- Civan, F., “A Multi-Purpose Formation Damage Model,” SPE 31101 paper, SPE Formation Damage Symposium, Lafayette, Louisiana, February 14–15, 1996, pp. 311–326.
- Delclaud, J., “Laboratory Measurement of the Residual Gas Saturation,” in Worthington, P. F. & Longeron, D. (Eds.), *Advances in Core Evaluation II*, Proceedings of the Second Society of Core Analysts, European Core Analysis Symposium, London, UK, pp. 431–451, 1991.
- Demir, I., “Formation Water Chemistry and Modeling Fluid-Rock Interaction for Improved Oil Recovery in Aux Vases and Cypress Formations,” Illinois Basin, Illinois Petroleum Series 148, Department of Natural Resources, Illinois State Geological Survey, 1995, 60 p.
- Deo, M., Tariq, S., & Halleck, P. J., “Linear and Radial Flow Targets for Characterizing Downhole Flow in Perforations,” SPE 16896 paper, 62nd Annual Technical Conference and Exhibition of the Society of Petroleum Engineers, September 27–30, 1987, Dallas, Texas, pp. 181–188.

- Doane, R. D., Bennion, D. B., Thomas, F. B., Bietz, R., & Bennion, D. W., "Special Core Analysis Designed to Minimize Formation Damage Associated with Vertical/Horizontal Drilling Applications," *J. Canadian Petroleum Technology*, Vol. 38, No. 5, May 1999, pp. 35–45.
- Egbogah, E. O., "An Effective Mechanism for Fines Movement Control in Petroleum Reservoirs," CIM 84-35-16 paper, 35th Annual Technical Meeting of the Petroleum Society of CIM, June 10–13, 1984, Calgary, Canada.
- Eickmeier, J. R., & Raimey Jr., H. J., "Wellbore Temperature and Heat Losses During Production or Injection Operations," 7016 paper, Proceedings of the 21st Annual Technical Meeting, Calgary, Canada, May 1970, Canadian Institute of Mining.
- Fambrough, J. D., & Newhouse, D. P., "A Comparison of Short-Core and Long-Core Acid Flow Testing for Matrix Acidizing Design," SPE 26186 paper, SPE Gas Technology Symposium, June 28–30, 1993, Calgary, Canada, pp. 491–502.
- Forchheimer, P., *Hydraulik*, L. Ed. Teubner, Leipzig and Berlin, Ch. 15, 1914, pp. 116–118.
- Gabriel, G. A., & Inamdar, G. R., "An Experimental Investigation of Fines Migration in Porous Media," SPE 12168 paper, SPE Annual Technical Conference and Exhibition, September 5–8, 1983, San Francisco, California.
- Gadiyar, B., & Civan, F., "Acidization Induced Formation Damage—Experimental and Modeling Studies," SPE 27400 paper, SPE Formation Damage Control Symposium, February 9–10, 1994, Lafayette, Louisiana, pp. 549–560.
- Gruesbeck, C., & Collins, R. E., "Entrainment and Deposition of Fine Particles in Porous Media," *SPEJ*, December 1982, pp. 847–856.
- Haggerty, D. J., & Seyler, B., "Investigation of Formation Damage from Mud Cleanout Acids and Injection Waters in Aux Vases Sandstone Reservoirs," Illinois Petroleum Series 152, Department of Natural Resources, Illinois State Geological Survey, 1997, 40 p.
- ISGS Oil and Gas Section, "Improved and Enhanced Oil Recovery Through Reservoir Characterization: Standard Operating and QA/QC Procedures," Illinois State Geological Survey, Open File Series 1993–13, 184 p.
- Keelan, D., & Amaefule, J. O., "Rock-Water Reaction: Formation Damage," *Laboratory Methods*, Part 5, pp. 249–257, in *Development Geology Reference Manual*, Methods 10, 1993, edited by D. Morton-Thompson and A. M. Woods, 548 p. AAPG Publication, Tulsa, Oklahoma.
- Keelan, D. K., & Koepf, E. H., "The Role of Cores and Core Analysis in Evaluation of Formation Damage," *JPT*, May 1977, pp. 482–490.

- Kersey, D. G., "The Role of Petrographic Analysis in the Design of Non-damaging Drilling, Completion, and Stimulation Programs," SPE 14089 paper, SPE International Meeting on Petroleum Engineering, Beijing, March 17–20, 1986.
- Khilar, K. C., & Fogler, H. S., "Water Sensitivity of Sandstones," *SPEJ*, February 1983, pp. 55–64.
- Kia, S. F., Fogler, H. S., & Reed, M. G., "Effect of Salt Composition on Clay Release in Berea Sandstones," SPE 16254, February 1987.
- Kyte, J. R., & Rapoport, L. A., "Linear Waterflood Behavior and End Effects in Water-Wet Porous Media," *Transactions of the American Institute of Mining, Metallurgy and Petroleum Engineers*, Vol. 213, 1958, pp. 423–426.
- Levorsen, A. I., *Geology of Petroleum* (2nd ed.), W.H. Freeman & Company, 1967, San Francisco, California, 409 p.
- Marshall, D. S., Gray, R., & Byrne, M., "Development of a Recommended Practice for Formation Damage Testing," SPE 38154 paper, SPE European Formation Damage Conference, June 2–3, 1997, The Hague, The Netherlands, pp. 103–113.
- Masikevich, J., & Bennion, D. B., "Fluid Design to Meet Reservoir Issues—A Process," *J. Canadian Petroleum Technology*, Vol. 38, No. 5, May 1999, pp. 61–71.
- Miranda, R. M., & Underdown, D. R., "Laboratory Measurement of Critical Rate: A Novel Approach for Quantifying Fines Migration Problems," SPE 25432 paper, SPE Production Operations Symposium, March 21–23, 1993, Oklahoma City, Oklahoma, pp. 271–286.
- Mungan, N., "Discussion of An Overview of Formation Damage," *JPT*, Vol. 41, No. 11, November 1989, p. 1224.
- Piot, B. M., & Perthuis, H. G., "Matrix Acidizing of Sandstones," in M. J. Economides & K. G. Nolte (eds.), *Reservoir Stimulation* (2nd ed.), Prentice-Hall, Englewood Cliffs, New Jersey, 1989, pp. 14.1–6.
- Porter, K. E., "An Overview of Formation Damage," *JPT*, Vol. 41, No. 88, 1989, pp. 780–786.
- Prada, A., Civan, F., & Dalrymple, E. D., "Evaluation of Gelation Systems for Conformance Control," Paper SPE 59322, SPE Permian Basin Oil & Gas Recovery Conference held in Midland, TX, March 21–23, 2000, 15 p.
- Saleh, S. T., Rustam, R., El-Rabaa, W., & Islam, M. R., "Formation Damage Study with a Horizontal Wellbore Model," *J. of Petroleum Science and Engineering*, Vol. 17, No. 1/2, 1997, pp. 87–99.
- Selby, R. J., "Flow of Fines and Sand Production in Unconsolidated Porous Media," Masters thesis, The University of Alberta, 1987, 212 p.
- Seyler, B., "Geologic and Engineering Controls on Aux Vases Sandstone Reservoirs in ⁷ Field, Illinois—A Comprehensive Study of a

- Well-Managed Oil Field," Illinois Petroleum Series 153, 1998, Department of Natural Resources, Illinois State Geological Survey, 79 p.
- Sharma, M. M., & Yortsos, Y. C., "Fines Migration in Porous Media," *AIChE J.*, Vol. 33, No. 10, 1987, pp. 1654–1662.
- Thomas, R. L., Saxon, A., & Milne, A. W., "The Use of Coiled Tubing During Matrix Acidizing of Carbonate Reservoirs Completed in Horizontal Deviated, and Vertical Wells," *SPE Production & Facilities*, August 1998, pp. 147–162.
- Wojtanowicz, A. K., Krilov, Z., & Langlinais, J. P., "Experimental Determination of Formation Damage Pore Blocking Mechanisms," Trans. of the ASME, *Journal of Energy Resources Technology*, Vol. 110, 1988, pp. 34–42.
- Wojtanowicz, A. K., Krilov, Z., & Langlinais, J. P., "Study on the Effect of Pore Blocking Mechanisms on Formation Damage," SPE 16233 paper, Society of Petroleum Engineers Symposium, March 8–10, 1987, Oklahoma City, Oklahoma, pp. 449–463.

Chapter 16

Simulator Development*

Summary

An overview of the formation damage models pointing out their common bases and special features have been presented in previous chapters. In this chapter, the methodology for development of a formation damage simulator and applications for typical cases are presented. The equations forming the various models are classified into several groups: algebraic equations, ordinary differential equations, partial differential equations, initial and boundary conditions, and constraints. The numerical calculation schemes are developed for computer programming.

Introduction

In spite of many experimental studies of the formation damage of oil and gas bearing formations, there have been only a few reported attempts to mathematically model the relevant processes and develop formation damage simulators (Civan, 1990, 1992, 1994, 1996). The use of these models in actual reservoir analysis and management has been rather limited because of the difficulties in understanding and implementing these models, as well as due to the limitations in the applicability of these models. Most present formation damage models consider a single fluid phase and the dominant formation damage mechanism is assumed to be the mobilization, migration, and retention of fine particles in porous matrix. Although, these models have been validated using experimental data obtained from reservoir core samples under controlled laboratory conditions, their applicability is rather limited in the field conditions. Most formation damage cases

* Parts of this chapter have been reprinted with permission of the U.S. Department of Energy and the Society of Petroleum Engineers from Civan (1994).

encountered in actual reservoirs are associated with multi-phase flow and other factors which are not considered in the present single phase formation damage models. In addition, determination of the model parameters have not been well addressed.

Formation damage refers to permeability impairment by alteration of porous media due to rock-fluid and fluid-fluid interactions in geological porous formations. The phenomena leading to formation damage is a rather complicated process involving mechanical, physical, thermal, biological, and chemical factors. A formation damage model is a mathematical expression of the permeability impairment due to the alteration of the porous media texture and surface characteristics. This must be a dynamic model, which is coupled with a porous media fluid flow model to predict the mutual effects of formation damage and flow conditions in oil and gas reservoirs. Therefore, although the main emphasis and objective are to develop a formation damage model, we must also address the modeling of fluid flow in porous media. Thus, the basic constituents of the overall modeling effort involve: (1) porous media realization, (2) formation damage model, (3) fluid and species transport model, (4) numerical solution, (5) parameter estimation, and (6) model validation and application. In reality, porous matrix and the fluids contained within pore volume display a discrete structure. For convenience, however, a continuum approach using average properties over representative elemental porous media volume is preferred.

Porous media is considered in two parts: (1) the flowing phase, denoted by the subscript f , consisting of a suspension of fine particles flowing through and (2) the stationary phase, denoted by the subscript s , consisting of the porous matrix and the particles retained (see Figure 8–3 in Chapter 8).

Model development begins with the realization of porous media. Figure 3–5 depicts a conceptual view of the various levels of analysis and modeling to represent the processes occurring in a real system (the reservoir). The steps from microscopic to macroscopic are required for integration from local to global representation. Although it would be more rigorous to proceed through these steps, we resort to a continuum modeling approach using the average properties over representative elemental porous media for simplification purposes. The loss of information on the process details are then compensated by empirical formulations. Empiricism cannot be avoided because of the irregular structure of geological porous media and the disposition of various fluid phases and particulate matter.

Description of Fundamental Model Equations

The basic model equations are the mathematical expressions for the following (Civan, 1994):

1. Mass balance
 - a. Fluid phases (convection)
 - Gas/Liquid 1/Liquid 2
 - b. Species (convection/dispersion)
 - Solid (indigenous/external, water wet/oil wet/intermediately wet, swelling/non-swelling)
 - Ionic (anions/cations)
 - Molecular
2. Momentum balance
 - Fluid phases (Gas/Liquid 1/Liquid 2) (Forchheimer/Darcy)
3. Porosity-Permeability-Texture relationship
4. Particle transport efficiency factor
5. Swelling rate
 - a. Formation
 - b. Particle
6. Pore throat plugging criteria and rate
7. Particle mobilization rate
8. Internal and external filter cake formation
9. Plug-type deposition rate
10. Pore surface deposition rate
11. External fluid infiltration rate
 - a. Oil-based
 - b. Water-based
 - c. Emulsion
12. Effective porosity
13. Interphase particle and species exchange rates
14. Critical salt concentration
15. Critical velocity
16. Wettability index (water wet, oil wet, intermediately wet)
17. Phase equilibrium conditions
18. Non-Darcy coefficient correlation
19. Dynamic pore size distribution
20. Dynamic pore throat distribution
21. Chemical equilibrium
22. Particle size growth

The simulation input file requires the following information (Gruesbeck and Collins, 1982; Amaefule et al., 1988; Baghdikian et al., 1989; Civan et al., 1989; Chang and Civan, 1992; Civan, 1994):

1. Phenomena considered:
 - Dissolution/precipitation of mineral salts
 - Mobilization/retention of particles

- Cation exchange between rock and fluids
- Liquid absorption by porous matrix
- Particle size variation
- Crystallization processes
- 2. Injection fluid conditions:
 - Rate or pressure specified
 - Particle free or particle containing
- 3. Rock properties:
 - Core length
 - Core diameter
 - Initial porosity
 - Initial permeability
 - Dispersion coefficient in porous media
 - Diffusion coefficient for liquid in porous matrix
- 4. Properties of the fluid and suspended particles:
 - Viscosity of liquid
 - Density of porous matrix material
 - Density of mineral salts
 - Density of clay particles
 - Density of externally injected particles
 - Critical velocity for particle mobilization
 - Critical salt concentration
- 5. Stoichiometric coefficients for chemical reactions in liquid media
 - Aqueous Phase
- 6. Conditions of the problem:
 - Initial conditions in porous media
 - Concentration of ionic, molecular, and particulate species
 - Boundary conditions
 - Injection end
 - Constant pressure or flux
 - Species concentration or flux
 - Outlet end
 - Constant pressure
 - Species flux
- 7. Model parameters:
 - Delete the parameters of the mechanisms neglected for a specific problem
 - Assign the measured values for the parameters that are directly measurable by laboratory procedures
 - Identify the parameters for which the best estimates will be obtained by history matching
- 8. Laboratory core flow test data that will be used for history matching:
 - Input-Output pressure differential or input volume flux versus pore volume injected

- Effluent species concentrations versus pore volume injected
9. Output that can be requested:
- Best estimates of the unknown parameters
 - Predicted versus measured data
 - Simulation of pressure; various species concentrations in the flowing fluid and the pore surface; porosity and permeability as functions of pore volume injected or time

Numerical Solution of Formation Damage Models

Depending on the level of sophistication of the considerations, theoretical approaches, mathematical formulations, and due applications, formation damage models may be formed from algebraic and ordinary and partial differential equations, or a combination of such equations. Numerical solutions are sought under certain conditions, defined by specific applications. The conditions of solution can be grouped into two classes: (1) initial conditions, defining the state of the system prior to any or further formation damage, and (2) boundary conditions, expressing the interactions of the system with its surrounding during formation damage. Typically, boundary conditions are required at the surfaces of the system, through which fluids enter or leave, such as the injection and production wells or ports, or that undergo surface processes, such as exchange or reaction processes.

Algebraic formation damage models are either empirical correlations and/or obtained by analytical solution of differential equation models for certain simplified cases. Numerical solution methods for linear and nonlinear algebraic equations are well developed.

Ordinary differential equation models describe processes in a single variable, such as either time or one space variable. However, as demonstrated in the following sections, in some special cases, special mathematical techniques can be used to transform multi-variable partial differential equations into single-variable ordinary differential equations. Amongst these special techniques are the methods of combination of variables and separation of variables, and the method of characteristics. The numerical solution methods for ordinary differential equations are well developed.

Partial differential equation models contain two or more independent variables. There are many numerical methods available for solution of partial differential equations, such as the finite difference method (Thomas, 1982), finite element method (Burnett, 1987), finite analytic method (Civan, 1995), and the method of weighted sums (the quadrature and cubature methods) (Civan, 1994, 1994, 1995, 1996, 1998; Malik and Civan, 1995; Escobar et al., 1997). In general, implementation of

numerical methods for solution of partial differential equations is a challenging task.

In the following sections, several representative examples are presented for instructional purposes. They are intended to provide some insight into the numerical solution process. Interested readers can resort to many excellent references available in the literature for details and sophisticated methods. For most applications, however, the information presented in this chapter is sufficient and a good start for those interested in specializing in the development of formation damage simulators.

Although numerical simulators can be developed from scratch as demonstrated by the examples given in the following sections, we can save a lot of time and effort by taking advantage of ready-made softwares available from various sources. For this purpose, the spreadsheet programs are particularly convenient and popular. Various softwares for solving algebraic, ordinary, and partial differential equations are available. Commercially available reservoir simulators can be manipulated to simulate formation damage, such as by paraffin deposition as demonstrated by Ring et al. (1994).

Ordinary Differential Equations

In this section, several examples are given to illustrate the numerical solution of ordinary differential equation models. Specifically, the simplified formation damage and filtration models, developed in previous chapters, are solved.

Example 1: Wojtanowicz et al. Fines Migration Model

- a. Derive a numerical solution for the following modified Wojtanowicz et al. (1987, 1988) fines migration model

$$\frac{d}{dt} [AL(\phi c + \sigma)] = q(c_{in} - c), \quad t > 0 \quad (16-1)$$

$$\frac{d\sigma}{dt} = k_r c - k_e \sigma, \quad t > 0 \quad (16-2)$$

$$\phi = \phi_o - \frac{\sigma}{\rho}, \quad t > 0 \quad (16-3)$$

subject to

$$c = 0, \sigma = 0, t = 0 \quad (16-4)$$

- b. Plot c and σ versus t using the following data until $\phi = 0$: $A = 1 \text{ cm}^2$, $L = 1 \text{ cm}$, $\phi_o = 0.20$, $q = 0.5 \text{ cm}^3/\text{min}$, $c_{in} = 0.85 \text{ gr/cm}^3$, $\rho = 1.00 \text{ gr/cm}^3$, $k_r = 0.7 \text{ min}^{-1}$, $k_e = 0.2 \text{ min}^{-1}$

Expanding Eq. 16-1 and then substituting Eqs. 16-2 and 3 and rearranging yields

$$\frac{dc}{dt} = \frac{\frac{q}{AL}(c_{in} - c) - \left[1 - \frac{c}{\rho}\right](k_r c - k_e \sigma)}{\phi_o - \frac{\sigma}{\rho}} \quad (16-5)$$

A simultaneous solution of Eqs. 16-2 and 5 as a function of time, subject to the initial conditions given by Eq. 16-4, can be readily obtained using an appropriate method, such as by the Runge-Kutta-Fehlberg four (five) method available in many ordinary differential equation solving software (IMSL, 1987, for example). Then, the porosity variation is calculated by Eq. 16-3. A typical numerical solution is presented in Figure 16-1.

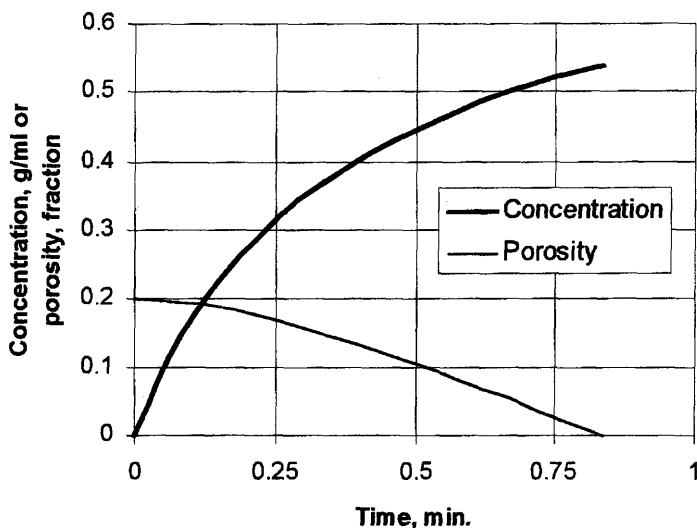


Figure 16-1. Particle concentration and porosity vs. time.

Example 2: Čerňanský and Šíroký Fines Migration Model

The numerical solution is carried out for $\tau'_{\mathcal{C}} = 0$. Here, the numerical solution approach presented by Čerňanský and Šíroký (1985) is described. Define the dimensionless time and distance, respectively, by:

$$T = t/(L/u) \quad (16-6)$$

$$X = x/L \quad (16-7)$$

Thus, invoking Eqs. 16-6 and 7, Eqs. 10-84 and 91 of Chapter 10, respectively, become:

$$\frac{\partial \varepsilon}{\partial T} + \frac{\partial \sigma}{\partial X} = 0 \quad (16-8)$$

$$\frac{\partial \varepsilon}{\partial T} = k_p L \sigma (\phi_o - \varepsilon) - k'_e L \varepsilon u \mu / K \quad (16-9)$$

Eqs. 16-8 and 9 are a system of hyperbolic partial differential equations, which can be transformed into a system of ordinary differential equations by means of the method of characteristics as:

$$\frac{d\sigma}{dX} = -f(\sigma, \varepsilon) \quad (16-10)$$

$$\frac{d\varepsilon}{dT} = f(\sigma, \varepsilon) \quad (16-11)$$

in which

$$f(\sigma, \varepsilon) = k_p L \sigma (\phi_o - \varepsilon) - k'_e L \varepsilon u \mu / K \quad (16-12)$$

The characteristics are given by:

$$\frac{dT}{dX} = 0, \text{ or } T = \text{constant} \quad (16-13)$$

$$\frac{dX}{dT} = 0, \text{ or } X = \text{constant} \quad (16-14)$$

The conditions of solution for Eqs. 16-8 and 9 are:

$$\varepsilon = 0, \quad 0 \leq X \leq 1, \quad T = 0 \quad (16-15)$$

$$\sigma = \sigma_{in}, \quad X = 0, \quad T \geq 0 \quad (16-16)$$

Applying the condition given by Eq. 16-15, Eq. 16-10 becomes:

$$\frac{d\sigma}{dX} = -k_p L \sigma \phi_o \quad (16-17)$$

for which the analytic solution is given by:

$$\sigma = \sigma_{in} \exp(-k_p L \phi_o X) \quad (16-18)$$

The system of ordinary differential equations given by Eqs. 16-10 and 11 are solved by means of the fourth-order Runge-Kutta method, subject to the conditions given by Eqs. 16-15 and 16 along the characteristic represented by Eq. 16-14.

Figure 16-2 shows the dimensionless effluent particles concentration as a function of the cumulative volume injected per unit area. Figures 16-3 and 16-4 show typical suspended particle concentration and the particles retained in porous media as a function of distance along the porous media at different times.

Example 3: Civan's Incompressive Cake Filtration without Fines Invasion Model

The equations of Civan's (1998, 1999) incompressive cake filtration model are given in Chapter 12. As described in Chapter 12, the ordinary differential equations of this model have been solved by the Runge-Kutta-Fehlberg four (five) numerical scheme (Fehlberg, 1969), subject to the initial condition given by Eq. 12-14.

Example 4: Civan's Compressive Cake Filtration Including Fines Invasion Model

The equations of Civan's (1998, 1999) compressive cake filtration including fines invasion model are given in Chapter 12. As described in

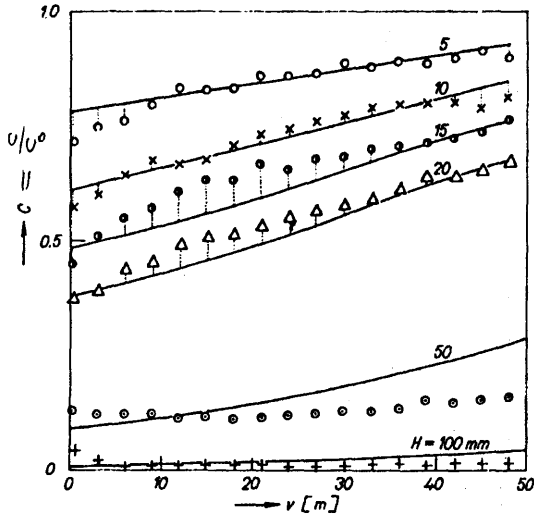


Figure 16-2. Experimental and simulated dimensionless concentrations vs. filtrate volume for the POP 1 material, using $c_o = 0.1 \text{ kg/m}^3$, $H = 5, 10, 15, 20, 50$, and 100 mm , and $u = 0.5 \text{ cm/s}$ (Čerňanský, A., & Šíroky, R., 1985; reprinted by permission of the AIChE, ©1985 AIChE, all rights reserved; and after Čerňanský and Šíroky, 1982, reprinted by permission).

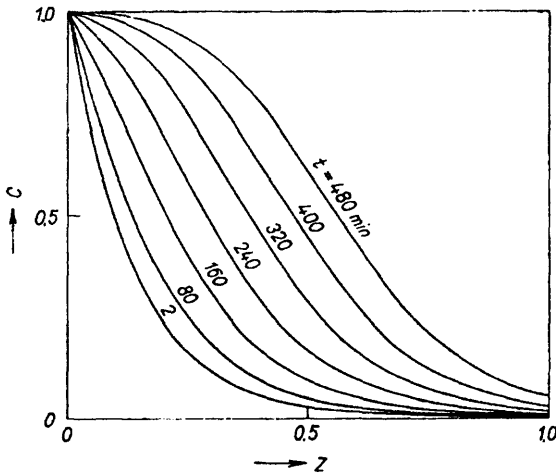


Figure 16-3. Simulated dimensionless concentration vs. dimensionless distance at different times for the FINET-PES 1 material, using $c_o = 0.1 \text{ kg/m}^3$, $H = 100 \text{ mm}$, and $u = 0.5 \text{ cm/s}$ (Čerňanský, A., & Šíroky, R., 1985; reprinted by permission of the AIChE, ©1985 AIChE, all rights reserved; and after Čerňanský and Šíroky, 1982, reprinted by permission).

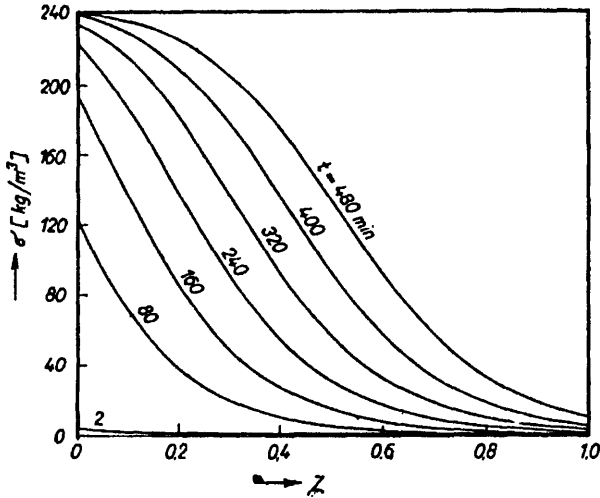


Figure 16-4. Simulated mass of particles retained per unit volume of porous material vs. dimensionless distance at different times for the FINET-PES 1 material, using $c_o = 0.1 \text{ kg/m}^3$, $H = 100 \text{ mm}$, and $u = 0.5 \text{ cm/s}$ (Čerňanský, A., & Šíroky, R., 1985; reprinted by permission of the AIChE, ©1985 AIChE, all rights reserved; and after Čerňanský and Šíroky, 1982, reprinted by permission).

Chapter 12, the ordinary differential equations of this model have been solved by the Runge-Kutta-Fehlberg four (five) numerical scheme (Fehlberg, 1969), subject to the initial condition given by Eq. 12-14.

Partial Differential Equations

In this section, the application of the finite difference method for solution of partial differential type models is illustrated by several examples.

The Method of Finite Differences

The method of finite differences is one of many methods available for numerical solution of partial differential equations. Because of its simplicity and convenience, the method of finite differences is the most frequently used numerical method for solution of differential equations. This method provides algebraic approximations to derivatives so that differential equations can be transformed into a set of algebraic equations, which can be solved by appropriate numerical procedures. Although the finite difference approximations can be derived by various methods, a

simple method based on the power series approach is presented here to avoid complicated mathematical derivation. Interested readers may resort to many excellent textbooks and literature available on the finite difference method. The information provided in this chapter is sufficient for many applications and for the purpose of this book. Most transport phenomenological models involve first and second order derivatives. Therefore, the following derivation is limited to the development of the first and second order derivative formulae. However, the higher order derivative formulae can be readily derived by the same approach presented in this chapter.

First Order Derivatives

In general, a function can be approximated by a power series as:

$$f(x) = \sum_{i=0}^{\infty} a_i x^i = a_0 + a_1 x + a_2 x^2 + \dots \quad (16-19)$$

in which a_0, a_1, a_2, \dots are some fitting coefficients. To determine the fitting coefficients, consider any set of three discrete function values f_{i-1}, f_i , and f_{i+1} located at the sample points x_{i-1}, x_i , and x_{i+1} , respectively, as shown in Figure 16-5.

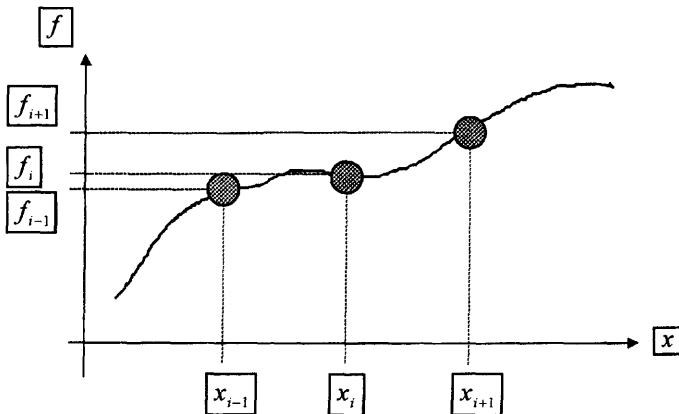


Figure 16-5. Sample points considered for the finite difference method.

More points could be considered for better accuracy. Higher order finite difference formulae can be derived easily using the quadrature method as described by Civan (1994). With three points, we can write the following three quadratic approximations at $i-1, i, i+1$:

$$f_{i-1} = a_0 + a_1 x_{i-1} + a_2 x_{i-1}^2 \quad (16-20)$$

$$f_i = a_0 + a_1 x_i + a_2 x_i^2 \quad (16-21)$$

$$f_{i+1} = a_0 + a_1 x_{i+1} + a_2 x_{i+1}^2 \quad (16-22)$$

If the middle point is considered as a reference point, then the locations of the three points are given by:

$$x_{i-1} = -\Delta x, x_i = 0, x_{i+1} = \Delta x \quad (16-23)$$

Thus, substituting Eq. 16-23 into Eqs. 16-20 through 22, and then solving the resultant three algebraic equations simultaneously yields the following expressions for the fitting coefficients of the quadratic expression:

$$a_0 = f_i \quad (16-24)$$

$$a_1 = \frac{f_{i+1} - f_{i-1}}{2\Delta x} \quad (16-25)$$

$$a_2 = \frac{f_{i-1} - 2f_i + f_{i+1}}{2(\Delta x)^2} \quad (16-26)$$

On the other hand, the derivative of Eq. 16-19 for quadratic approximation is given by:

$$\frac{df}{dx} = a_1 + 2a_2 x \quad (16-27)$$

Thus, the following forward difference formula is obtained by substituting Eqs. 16-25 and 26 into Eq. 16-27 for a_1, a_2 at $x = x_{i-1} = -\Delta x$:

$$\frac{df_{i-1}}{dx} = \frac{-3f_{i-1} + 4f_i - f_{i+1}}{2\Delta x} \quad (16-28)$$

The central difference formula is obtained as, by substituting Eqs. 16–25 and 26 for a_1, a_2 into Eq. 16–27 at $x = x_i = 0$:

$$\frac{df_i}{dx} = \frac{f_{i+1} - f_{i-1}}{2\Delta x} \quad (16-29)$$

The backward difference formula is obtained as, by substituting Eqs. 16–25 and 26 for a_1, a_2 into Eq. 16–27 at $x = x_{i+1} = \Delta x$:

$$\frac{df_{i+1}}{dx} = \frac{f_{i-1} - 4f_i + 3f_{i+1}}{2\Delta x} \quad (16-30)$$

Second Order Derivatives

A similar procedure can be applied to derive the second (and higher) order derivative approximations. Thus, consider a power series expansion as:

$$f'(x) = \frac{df}{dx} = \sum_{i=0}^{\infty} b_i x^i = b_0 + b_1 x + b_2 x^2 + \dots \quad (16-31)$$

Expressions similar to Eqs. 16–24 through 26 are obtained for the fitting coefficients, given by:

$$b_0 = f'_i \quad (16-32)$$

$$b_1 = \frac{f'_{i+1} - f'_{i-1}}{2\Delta x} \quad (16-33)$$

$$b_2 = \frac{f'_{i-1} - 2f'_i + f'_{i+1}}{2(\Delta x)^2} \quad (16-34)$$

The derivative of the quadratic equation is obtained from Eq. 16–31 as:

$$f'' = b_1 + 2b_2 x \quad (16-35)$$

Thus, the forward difference formula is obtained as, by substituting Eqs. 16–33 and 34 for b_1, b_2 at $x = x_{i-1} = -\Delta x$ into Eq. 16–35:

$$\frac{d^2 f_{i-1}}{dx^2} = \frac{-3f'_{i-1} + 4f'_i - f'_{i+1}}{2\Delta x} \quad (16-36)$$

The central difference formula is obtained as, by substituting Eqs. 16-33 and 34 for b_1, b_2 at $x = x_i = 0$ into Eq. 16-35:

$$\frac{d^2 f_i}{dx^2} = \frac{f'_{i+1} - f'_{i-1}}{2\Delta x} \quad (16-37)$$

The backward difference formula is obtained as, by substituting Eqs. 16-33 and 34 for b_1, b_2 into Eq. 16-35 for $x = x_{i+1} = \Delta x$:

$$\frac{d^2 f_{i+1}}{dx^2} = \frac{f'_{i-1} - 4f'_i + 3f'_{i+1}}{2\Delta x} \quad (16-38)$$

However, only the central second order derivative formula is used in our models. Thus, substituting the first order forward and backward difference formulae given by Eqs. 16-28 and 30 into Eq. 16-37, the central second order difference formula is obtained as:

$$\begin{aligned} \frac{d^2 f_i}{dx^2} &= \frac{f'_{i+1} - f'_{i-1}}{2\Delta x} = \frac{\frac{f_{i-1} - 4f_i + 3f_{i+1}}{2\Delta x} - \frac{-3f_{i-1} + 4f_i - f_{i+1}}{2\Delta x}}{2\Delta x} \\ &= \frac{f_{i-1} - 2f_i + f_{i+1}}{(\Delta x)^2} \end{aligned} \quad (16-39)$$

Example 5: Civan and Engler Mud Filtrate Invasion Model

The normalized equations of the Civan and Engler (1994) model (see Eqs. 18-27 through 30, Chapter 18) are given by the transport equation:

$$\beta \frac{\partial^2 c}{\partial r^2} - \alpha \frac{\partial c}{\partial r} = \frac{\partial c}{\partial t} \quad (16-40)$$

subject to the initial condition

$$c = 0, 0 \leq r \leq 1, t = 0 \quad (16-41)$$

and the inlet and outlet boundary conditions

$$uc - \frac{1}{Pe} \mathcal{D} \frac{\partial c}{\partial r} = (uc)_{in}, r = 0, t > 0 \quad (16-42)$$

$$\frac{\partial c}{\partial r} = 0, r = 1, t > 0 \quad (16-43)$$

For numerical solution purposes, the time-space solution domain is discretized as shown in Figure 16-6, by separating the time and space into a number of equally spaced discrete points. Δr and Δt denote the grid point spacing and time increment, respectively. Accurate solution with

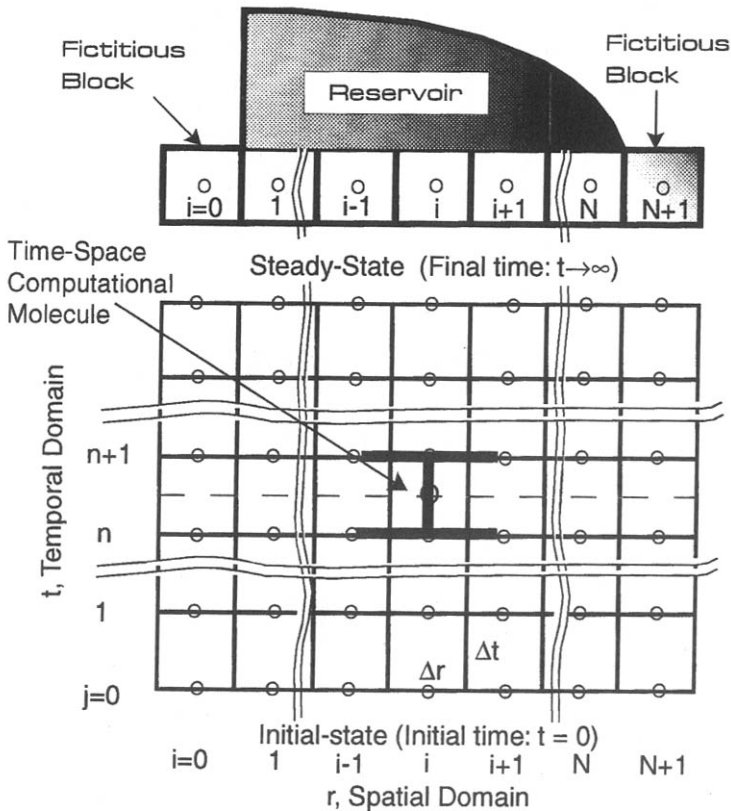


Figure 16-6. Discretization of the time-space computational domain and the grid system.

a uniform grid requires sufficiently small Δr and Δt , and therefore a high level of computational effort. This approach is selected here for simplicity. Computationally efficient schemes can be developed by varying the grid size in space and time. This is beyond the scope of this book.

The grid system depicted in Figure 16-6 is implemented here by central finite difference formulae, derived in the previous section. The spatial grid points are denoted by the subscript indices $i = 0, 1, 2, \dots, N, N+1$. Because the spatial grid points were placed in the center of the grid blocks, the points identified by $i = 0$ and $i = N+1$ are outside the inlet and outlet boundaries and, therefore, called fictitious points. The points designated by $i = 1, 2, \dots, N$ are the real points, called interior points. The discrete times are denoted by the superscript indices $n = 0, 1, 2, \dots, \infty$. $n = 0$ denotes the initial condition, at which time the concentrations at various discrete spatial points are prescribed by Eq. 16-41.

The central difference formulae necessary to develop a numerical solution are given as following:

$$\frac{\partial c_i}{\partial r} = \frac{c_{i+1} - c_{i-1}}{2\Delta r} \quad (16-44)$$

$$\frac{\partial^2 c_i}{\partial r^2} = \frac{c_{i+1} - 2c_i + c_{i-1}}{(\Delta r)^2} \quad (16-45)$$

$$\frac{\partial c_{i-1/2}}{\partial r} = \frac{c_i - c_{i-1}}{\Delta r} \quad (16-46)$$

$$\frac{\partial c_{i+1/2}}{\partial r} = \frac{c_{i+1} - c_i}{\Delta r} \quad (16-47)$$

$$\frac{\partial c^{n+1}}{\partial t} = \frac{c^{n+1} - c^n}{\Delta t} \quad (16-48)$$

The concentration values at the inlet and outlet boundaries are estimated by the following arithmetic averages:

$$\bar{c}_{i-1/2} = \frac{c_{i-1} + c_i}{2} \quad (16-49)$$

$$\bar{c}_{i+1/2} = \frac{c_i + c_{i+1}}{2} \quad (16-50)$$

Applying the Crank-Nicolson formulation (see Thomas, 1982), the central difference discretization of Eq. 16–40 in time and space yields:

$$\begin{aligned} & \frac{1}{2} \left[\beta_i^n \frac{c_{i+1}^n - 2c_i^n + c_{i-1}^n}{(\Delta r)^2} - \alpha_i^n \frac{c_{i+1}^n - c_{i-1}^n}{2\Delta r} \right. \\ & \left. + \beta_i^{n+1} \frac{c_{i+1}^{n+1} - 2c_i^{n+1} + c_{i-1}^{n+1}}{(\Delta r)^2} - \alpha_i^{n+1} \frac{c_{i+1}^{n+1} - c_{i-1}^{n+1}}{2\Delta r} \right] \\ & = \frac{c_i^{n+1} - c_i^n}{\Delta t}, i = 1, 2, \dots, N \text{ and } n = 1, 2, \dots, \infty \end{aligned} \quad (16-51)$$

The initial condition given by Eq. 16–41 can be expressed as:

$$c_i = 0: i = 1, 2, \dots, N, n = 0 \quad (16-52)$$

The inlet boundary condition given by Eq. 16–42 can be discretized as:

$$u_{i=1/2} c_{i=1/2} - \frac{\mathcal{D}_{i=1/2}}{Pe} \frac{c_{i=1} - c_{i=0}}{\Delta r} = (uc)_{in}, i = 1/2 \quad (16-53)$$

in which

$$c_{i=1/2} = \frac{1}{2} (c_{i=0} + c_{i=1}) \quad (16-54)$$

Thus, substituting Eq. 16–54 into 53, the fictitious point value is determined as:

$$c_0 = \left((uc)_{in} - \tilde{B} c_1 \right) / \tilde{A} \quad (16-55)$$

where

$$\tilde{A} = \frac{u_{i=1/2}}{2} + \frac{\mathcal{D}_{i=1/2}}{Pe\Delta r} \quad (16-56)$$

$$\tilde{B} = \frac{u_{i=1/2}}{2} - \frac{\mathcal{D}_{i=1/2}}{Pe\Delta r} \quad (16-57)$$

The outlet boundary condition given by Eq. 16-43 is discretized as:

$$\frac{c_{N+1} - c_N}{\Delta r} = 0 \quad (16-58)$$

from which the fictitious point value is obtained as:

$$c_{N+1} = c_N \quad (16-59)$$

For convenience in numerical solution, first we rearrange Eq. 16-51 as:

$$\begin{aligned} A_i^{n+1} c_{i-1}^{n+1} + B_i^{n+1} c_i^{n+1} + C_i^{n+1} c_{i+1}^{n+1} &= D_i^n, i = 1, 2, \dots, N \text{ and} \\ n &= 1, 2, \dots, \infty \end{aligned} \quad (16-60)$$

in which

$$A_i = \frac{\beta_i}{(\Delta r)^2} + \frac{\alpha_i}{2\Delta r} \quad (16-61)$$

$$B_i = -2 \left[\frac{\beta_i}{(\Delta r)^2} + \frac{1}{\Delta t} \right] \quad (16-62)$$

$$C_i = \frac{\beta_i}{(\Delta r)^2} - \frac{\alpha_i}{2\Delta r} \quad (16-63)$$

$$D_i^n = -[A_i^n c_{i-1}^n + B_i^n c_i^n + C_i^n c_{i+1}^n] \quad (16-64)$$

Next, we incorporate the fictitious point values near the inlet and outlet boundaries into Eq. 16-60. For this purpose, applying Eq. 16-60 at the inlet and outlet grid blocks by substituting $i = 1$ and $i = N$, respectively, yields:

$$A_1^{n+1} c_0^{n+1} + B_1^{n+1} c_1^{n+1} + C_1^{n+1} c_2^{n+1} = D_1^n, i = 1 \quad (16-65)$$

$$A_N^{n+1} c_{N-1}^{n+1} + B_N^{n+1} c_N^{n+1} + C_N^{n+1} c_{N+1}^{n+1} = D_N^n, i = N \quad (16-66)$$

Substituting Eqs. 16–55 and 59 into Eqs. 16–65 and 66, respectively, yields:

$$\tilde{B}_1^{n+1} c_1^{n+1} + C_1^{n+1} c_2^{n+1} = \tilde{D}_1^n, i = 1 \quad (16-67)$$

$$A_N^{n+1} c_{N-1}^{n+1} + \tilde{B}_N^{n+1} c_N^{n+1} = D_N^n, i = N \quad (16-68)$$

in which

$$\tilde{B}_1 = B_1 - \frac{A_1 \tilde{B}}{\tilde{A}}, \quad \tilde{D}_1 = D_1 - \frac{A_1}{\tilde{A}} (uc)_{in} \quad (16-69)$$

$$\tilde{B}_N = B_N + C_N \quad (16-70)$$

Eq. 16–67 for $i = 1$, Eq. 16–60 for $i = 2, 3, \dots, N-1, N$, and Eq. 16–68 for $i = N$ can be compiled in a form of a tri-diagonal coefficient linear matrix equation as:

$$\begin{bmatrix} \tilde{B}_1 & C_1 & & 0 \\ A_2 & B_2 & C_2 & \\ \dots & \dots & \dots & \dots \\ A_i & B_i & C_i & \\ \dots & \dots & \dots & \dots \\ 0 & & A_N & \tilde{B}_N \end{bmatrix}^{n+1} \begin{bmatrix} c_1^{n+1} \\ c_2^{n+1} \\ \vdots \\ \vdots \\ c_{N-1}^{n+1} \\ c_N^{n+1} \end{bmatrix} = \begin{bmatrix} \tilde{D}_1 \\ D_2 \\ \vdots \\ D_i \\ \vdots \\ D_{N-1} \\ D_N \end{bmatrix}^n \quad (16-71)$$

and solved by Thomas algorithm (see Thomas, 1982).

Figure 16–7 shows the typical concentration profiles calculated by Civan and Engler (1994) at different times using the parameter values $a = 0.08 m^3/h$, $b = 1.67 \times 10^{-5} h^{-1}$, $f = 51.7$, $g = 1.25$, $h = 0.5m$, $r_w = 0.05m$, and $r_e = 10m$.

Note that in this presentation, the dimensionless quantities were defined as following:

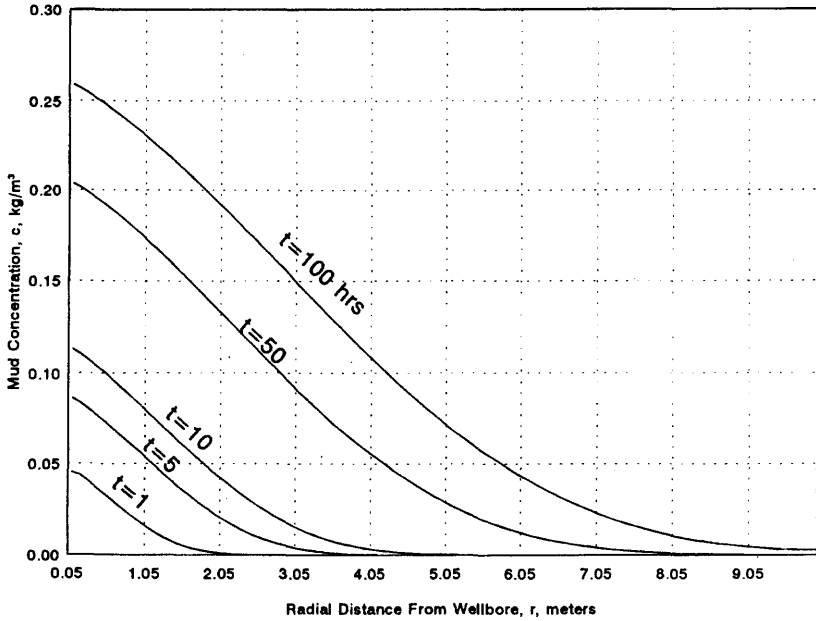


Figure 16-7. Mud filtrate concentration vs. radial distance from wellbore at different times (reprinted from *Journal of Petroleum Science and Engineering*, Vol. 11, Civan, F., & Engler, T., "Drilling Mud Filtrate Invasion—Improved Model and Solution," pp. 183–193, ©1994; reprinted with permission from Elsevier Science).

$$c = C/C_o \quad (16-72)$$

$$r = (R - r_w)/(r_e - r_w) \quad (16-73)$$

$$t = T/T_o \quad (16-74)$$

where C_o and C denote the initial and instantaneous filtrate concentrations, r_w and r_e are the wellbore and outlet boundary radii, and Eq. 16-73 is different than the dimensionless distance

$$r = R/r_w \quad (16-75)$$

used by Civan and Engler (1994). Eq. 16-73 is preferred because it maps the radial distance over a unit-size domain.

References

- Amaefule, J. O., Kersey, D. G., Norman, D. L., & Shannon, P. M., "Advances in Formation Damage Assessment and Control Strategies," CIM Paper No. 88-39-65, Proceedings of the 39th Annual Technical Meeting of Petroleum Society of CIM and Canadian Gas Processors Association, June 12–16, 1988, Calgary, Alberta, 16 p.
- Baghdikian, S. Y., Sharma, M. M., & Handy, L. L., Flow of Clay Suspensions Through Porous Media, *SPE Reservoir Engineering*, Vol. 4., No. 2., May 1989, pp. 213–220.
- Burnett, D. S., *Finite Element Analysis*, Addison-Wesley Publishing Company, Massachusetts, 1987, 844 p.
- Čerňanský, A., & Široký, R., "Hlbkova Filtracia Polydisperznych Castic z Kvapalin na Vrstvach z Vlakistan," *Chemicky Prumysl*, Vol. 32 (57), No. 8, 1982, pp. 397–405.
- Čerňanský, A., & Široký, R., "Deep-bed Filtration on Filament Layers on Particle Polydispersed in Liquids," *Int. Chem. Eng.*, Vol. 25, No. 2, 1985, pp. 364–375.
- Chang, F. F., & Civan, F., Predictability of Formation Damage by Modeling Chemical and Mechanical Processes, SPE 23793 paper, Proceedings of the SPE International Symposium on Formation Damage Control, February 26–27, 1992, Lafayette, Louisiana, pp. 293–312.
- Civan, F., A Generalized Model for Formation Damage by Rock-Fluid Interactions and Particulate Processes, SPE 21183, Proceedings of SPE 1990 Latin American Petroleum Engineering Conference, Rio de Janeiro, Brazil, October 14–19, 1990, 11 p.
- Civan, F. "Evaluation and Comparison of the Formation Damage Models," SPE 23787 paper, Proceedings of the SPE International Symposium on Formation Damage Control, February 26–27, 1992, Lafayette, Louisiana, pp. 219–236.
- Civan, F., "Numerical Simulation by the Quadrature and Cubature Methods," SPE 28703 paper, Proceedings of the SPE International Petroleum Conference and Exhibition of Mexico, October 10–13, 1994, Veracruz, Mexico, pp. 353–363.
- Civan, F., "Solving Multivariable Mathematical Models by the Quadrature and Cubature Methods," *Journal of Numerical Methods for Partial Differential Equations*, Vol. 10, 1994, pp. 545–567.
- Civan, F., "Rapid and Accurate Solution of Reactor Models by the Quadrature Method," *Computers & Chemical Engineering*, Vol. 18. No. 10, 1994, pp. 1005–1009.
- Civan, F., Predictability of Formation Damage: An Assessment Study and Generalized Models, Final Report, U.S. DOE Contract No. DE-AC22-90-BC14658, April 1994.

- Civan, F., "Practical Implementation of the Finite Analytic Method," *Applied Mathematical Modeling*, Vol. 19, No. 5, 1995, pp. 298–306.
- Civan, F., "A Multi-Purpose Formation Damage Model," SPE 31101 paper, Proceedings of the SPE Formation Damage Symposium, February 14–15, 1996, Lafayette, Louisiana, pp. 311–326.
- Civan, F., "A Time-Space Solution Approach for Simulation of Flow in Subsurface Reservoirs," *Turkish Oil and Gas Journal*, Vol. 2, No. 2, June 1996, pp. 13–19.
- Civan, F., "Incompressible Cake Filtration: Mechanism, Parameters, and Modeling," *AIChE J.*, Vol. 44, No. 11, November 1998, pp. 2379–2387.
- Civan, F., "Practical Model for Compressive Cake Filtration Including Fine Particle Invasion," *AIChE J.*, Vol. 44, No. 11, November 1998, pp. 2388–2398.
- Civan, F., "Quadrature Solution for Waterflooding of Naturally Fractured Reservoirs," *SPE Reservoir Evaluation & Engineering J.*, April 1998, pp. 141–147.
- Civan, F., "Phenomenological Filtration Model for Highly Compressible Filter Cakes Involving Non-Darcy Flow," SPE 52147 paper, Proceedings of the 1999 SPE Mid-Continent Operations Symposium, March 28–31, 1999, Oklahoma City, Oklahoma, pp. 195–201.
- Civan, F., "Predictive Model for Filter Cake Buildup and Filtrate Invasion with Non-Darcy Effects," SPE 52149 paper, Proceedings of the 1999 SPE Mid-Continent Operations Symposium, March 28–31, 1999, Oklahoma City, Oklahoma, pp. 203–210.
- Civan, F., & Engler, T., "Drilling Mud Filtrate Invasion—Improved Model and Solution," *J. of Petroleum Science and Engineering*, Vol. 11, 1994, pp. 183–193.
- Civan, F., Knapp, R. M., & Ohen, H. A., Alteration of Permeability Due to Fine Particle Processes, *J. Petroleum Science and Engineering*, Vol. 3, Nos. 1/2, Oct. 1989, pp. 65–79.
- Escobar, F. H., Jongkittinarukorn, K., & Civan, F., "Cubature Solution of the Poisson Equation," *Communications in Numerical Methods in Engineering*, Vol. 13, 1997, pp. 453–465.
- Fehlberg, E., "Low-Order Classical Runge-Kutta Formulas with Stepsize Control and their Application to Some Heat Transfer Problems," NASA TR R-315, Huntsville, Alabama, July 1969.
- Gruesbeck, C., & Collins, R. E., Entrainment and Deposition of Fine Particles in Porous Media, *SPEJ*, December 1982, pp. 847–856.
- IMSL—FORTRAN Subroutines for Mathematical Applications IMSL Inc., Houston, Texas, Version 1.0, April 1987.
- Malik, M., & Civan, F., "A Comparative Study of Differential Quadrature and Cubature Methods Vis-A-Vis Some Conventional Techniques

- in Context of Convection-Diffusion-Reaction Problems,” *Chemical Engineering Science*, Vol. 50, No. 3, 1995, pp. 531–547.
- Ohen, H. A., & Civan, F., Simulation of Formation Damage in Petroleum Reservoirs, SPE 19420 paper, Proceedings of the SPE 1990 Symposium on Formation Damage Control, February 22–23, 1990, Lafayette, Louisiana.
- Ring, J. N., Wattenbarger, R. A., Keating, J. F., & Peddibhotla, S., “Simulation of Paraffin Deposition in Reservoirs,” *SPE Production & Facilities*, February 1994, pp. 36–42.
- Thomas, G. W., *Principles of Hydrocarbon Reservoir Simulation*, International Human Resources Development Corporation, Publishers, Boston, 1982, 207 p.
- Wojtanowicz, A. K., Krilov, Z., & Langlinais, J. P., “Experimental Determination of Formation Damage Pore Blocking Mechanisms,” *Trans. of the ASME, Journal of Energy Resources Technology*, Vol. 110, 1988, pp. 34–42.
- Wojtanowicz, A. K., Krilov, Z., & Langlinais, J.P., “Study on the Effect of Pore Blocking Mechanisms on Formation Damage,” SPE 16233 paper, Presented at the Society of Petroleum Engineers Symposium, Oklahoma City, Oklahoma, March 8–10, 1987, pp. 449–463.

Chapter 17

Model Assisted Analysis and Interpretation of Laboratory and Field Tests

Summary

A review of the typical laboratory and field data is presented. The model parameters are classified in groups with respect to the methods available to determine their values. The techniques available for directly measurable parameters are described. The parameters that can be determined by the history matching method described in the previous chapter are identified. For this purpose, an objective function is formulated in terms of the directly measurable formation damage indicators such as injectivity or productivity loss, permeability impairment and effluent fluid conditions, including fines concentration, pH, and species content.

The methodology for the model assisted analysis and interpretation of laboratory and field data using formation damage simulators is presented. The criteria for scaling from laboratory to field are developed based on the method of dimensional analysis. The optimal strategies are presented for the identification of the governing formation damage mechanisms and their relative contributions and importance, estimation and correlation of the model parameters, model calibration by history matching, validation and improvement, and sensitivity and simulation studies.

Introduction

J. Willard Gibbs stated that “The purpose of a theory is to find that viewpoint from which experimental observations appear to fit the pattern” (Duda, 1990). Toward this end, we carry out theoretical analysis and

modeling, and experiments under controlled conditions in an effort to predict the behavior of the interactions of the reservoir rock and fluid systems. However, model predictions usually involve uncertainties because of the approximations in systems description and uncertainties in the parameters and measurements. Luckert (1994) draws attention to the fact that "the models often contain only differential values while the experimental values are integrals." Thus, for direct comparison with experimental data, the models must be transformed into integral forms either by analytical or numerical solution methods.

As explained by Frenklach and Miller (1985), the predictive equations of natural phenomena, frequently called mathematical models, are usually derived in the form of differential and/or integral equations, and often solutions can only be obtained by numerical methods. Frenklach and Miller (1985) stress that the dynamic model building process has to deal with several important issues: (1) adequacy, (2) statistical reliability of the proposed model, and (3) determination of its parameters. Frenklach and Miller (1985) describe the usual approach taken to determine the model parameters as an iterative adjustment of the parameter values until the numerical solution of the model, called the model response or prediction, fits the experimental data. They add that frequently the adjustment of the parameter values is guided by the sensitivity analysis based on the partial derivatives of the predictions of the model with respect to its parameters. Frenklach and Miller (1985) draw attention to several problems associated with this approach: (1) in the statistical sense, the sensitivity is physically meaningful only if the model is adequate, (2) sensitivity varies during a dynamic process and, therefore, point estimates of sensitivities in the parameter space are not adequate, and (3) correlating sensitivities independently of each other complicates the interpretation of the sensitivities. Frenklach and Miller (1985) circumvent these problems by incorporating the parameter estimation, adequacy test, and sensitivity analysis tasks into mathematical modeling. Their parameter estimation approach is based on developing an analytically or numerically determined functional relationship between the response and parameters of the model. For this purpose the individual responses of the dynamic model for different prescribed values of the parameters are obtained by means of the numerical solution of the model. Then a functional relationship between the model responses and prescribed parameter values is developed by applying a statistical analysis. They recommend the application of the experimental design techniques to improve the efficiency of this method.

The objectives of model assisted analysis and interpretation include the identification of the governing formation damage mechanisms and their relative contributions and importance; estimation and correlation of the

model parameters; model calibration via history matching; model verification and improvement; and sensitivity and simulation studies (Civan, 1996). Direct measurement of all the model parameters is usually not feasible when the model involves many parameters. Therefore, many researchers (Civan et al., 1989; Ohen and Civan, 1990, 1993; Millan-Arcia and Civan, 1992; Chang and Civan, 1991, 1992, 1997; and Liu and Civan, 1995, 1996; Civan, 1994, 1996; Wilhite et al., 1991; Vittal et al., 1988) have resorted to indirect methods of inferring the values of such parameters by history matching of some experimental data. Although others (Gruesbeck and Collins, 1982; Amaefele et al., 1988; Sharma and Yortsos, 1987; Khilar and Fogler, 1987; Civan, 1998) offer some analytical expressions and/or direct measurement methods, these apply only to extremely simplified models having only a few model parameters. For complicated models, history matching appears the best choice in lack of a better method. However, some parameters may be measured and the remainder can be estimated by an optimal history matching method to minimize an objective function expressing the weighted sum of the squares of the deviations between the directly measured and model predicted formation damage indicators such as pressure loss, permeability impairment, and effluent conditions (Civan, 1996). For this purpose, simulated annealing is appealing as a practical optimization method (Szucs and Civan, 1996) because it does not require any derivative evaluations and it leads to global minimum without being trapped in one of the local minimal. However, the achievability of the uniqueness of the estimated parameter values depends on and increases by the amount of the measured data. Ucan et al. (1997) have demonstrated that uniqueness can be achieved if both the external and internal core fluid data are used simultaneously. Typical internal data include the sectional pressure difference and fluid saturations along the core plug. Typical external data includes the pressures at the core inlet and outlet, and the effluent solution properties.

Measurement Error*

Measurements are uncertain numbers that are random and independent variables (Reilly, 1992). As stated by Cook (1980):

Error is the uncertainty in a measured quantity. An opposite expression is accuracy which is the reliability of the measurement. Precision, on the other hand, is the repeatability or reproducibility of a

* Reproduced by permission of the Society of Petroleum Engineers from Civan, ©1989, SPE, Paper 19073.

measurement. Hence, the measurements can be precise but not accurate; meaning that there is a systematic error.

There are three main sources of errors that affect the accuracy of measurements (Civan, 1989). The first is the human errors resulting from improper handling of instruments and incorrect readings of indicators such as the manometer, clock, pressure gauge, etc. The second source of error is the systematic errors in the instruments themselves. Errors involving various elements of instruments can accumulate and lead to pronounced errors in the value of the measurements. The third source of errors is the statistical errors, which are not predictable. Fluctuations in ambient pressure and temperature, and in electric power supply are examples of statistical errors. Statistical and human errors can be referred conveniently to as random errors. Human errors can be minimized by using the instruments carefully and maintaining them in good condition, but errors in instruments are systematic and often are undetected. Statistical errors are unavoidable. Thus, repeated measurements of variables should be taken to obtain statistically good results (although this will not change the systematic errors).

Random Error

In the following, first the relations for the error estimate referring only to the random error are discussed.

The values of variables, x_i , measured at $i = 1, 2, \dots, n$, repeated tests differ somewhat from each other. Thus, an arithmetic mean value of the measured values should be used, defined by

$$\bar{x} = \sum_{i=1}^n x_i / n \quad (17-1)$$

However, the mean value alone does not indicate the extent of reproducibility of the measurements. Therefore, an estimate of the confidence limits should also be given. In this respect, one of the following forms of random error estimates can be used, assuming the random errors are normally distributed:

a. Standard deviation

$$\sigma_x = (\overline{x^2} - \bar{x}^2)^{1/2} \quad (17-2)$$

in which

$$\overline{x^2} = \sum_{i=1}^n x^2 / n \quad (17-3)$$

b. Average random error

$$A_x = 0.7979\sigma_x \quad (17-4)$$

c. Probable error

$$P_x = 0.6745\sigma_x \quad (17-5)$$

Hence, the measured value is reported in terms of its mean value and the random error or confidence limits as $x \pm E$, where E can be represented by one of the random error expressions (i.e., σ_x , A_x , or p_x). See Mickley et al. (1957), Spiegel (1961), and Schenck, Jr. (1961) for details.

Composite random error in a calculated value obtained by a series of calculational steps can be estimated analytically based on the accuracy of various quantities involving these calculation steps. For this purpose, the upper bounds of the overall random error can be determined by applying the rules given in the next section.

Systematic Error

As stated by Ku (1969) "systematic error is a fixed deviation that is inherent in each and every measurement." Hence, the measurements can be corrected for the systematic error if the magnitude and direction of the systematic error are known. Complex devices make it difficult to predict their accuracy. Leaks, variation of temperature, and pressure also influence the accuracy. Large volume flow-type tests suffer from sudden variation of species composition due to their larger residence times. All of these are sources of errors.

The mechanical design parameters and dimensions of experimental systems immensely effect the accuracy of measurements. Careful analysis of their design and innovative improvements to increase their accuracy are vital for measurement with better accuracy.

Error Analysis—Propagation, Impact, Estimation

Although the phenomenological descriptions of processes are generally accomplished in terms of differential equations, called mathematical models, solutions can be obtained analytically for simplified cases and numerically for complicated cases. Accuracy of model predictions is

dependent on various factors, including (1) the adequacy of the model, (2) the accuracy of the input data, and (3) the accuracy of the solution technique. Various sources of uncertainties affect the reliability of the predictions of models, as described in Figure 17-1 by Bu and Damsleth (1996). Experimental measurements taken under controlled test conditions to determine the input-output (or cause-and-affect or the parity relationship) response of systems (such as core plugs undergoing a flow test) also involve uncertainties.

In general, solutions of models, called model predictions, and the response of the test systems under prescribed conditions can be represented numerically or analytically by functional relationships, mathematically expressed as:

$$f = f(x_1, x_2, \dots, x_n) \quad (17-6)$$

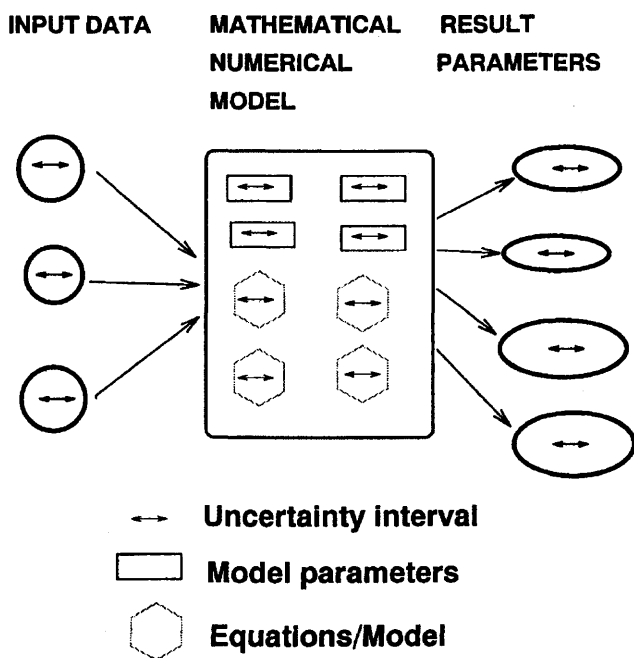


Figure 17-1. Sources of errors and uncertainty associated with mathematical modeling (after Bu and Damsleth, ©1996 SPE; reprinted by permission of the Society of Petroleum Engineers).

in which f is a system response and x_1, x_2, x_3, \dots denote the various input variables and parameters. Uncertainties involved in actual calculations (predictions) or measurements (experimental testing) lead to estimated or approximate results, the accuracy of which depend on the errors involved. Therefore, the actual values are the sum of the estimates and the errors. Thus, if $\tilde{f}, \tilde{x}_1, \tilde{x}_2, \dots, \tilde{x}_n$ indicate the estimated values of the function and its variables, and $\Delta f, \Delta \tilde{x}_1, \Delta \tilde{x}_2, \dots, \Delta \tilde{x}_n$ represent the errors or uncertainties associated with these quantities, the following equations, expressing the actual quantities as a sum of the estimated values and the errors associated with them, can be written:

$$x_1 = \tilde{x}_1 \pm \Delta \tilde{x}_1 \quad (17-7)$$

$$x_2 = \tilde{x}_2 \pm \Delta \tilde{x}_2 \quad (17-8)$$

.....

$$x_n = \tilde{x}_n \pm \Delta \tilde{x}_n \quad (17-9)$$

$$f = \tilde{f} \pm \Delta \tilde{f} \quad (17-10)$$

The estimation of the propagation and impact of errors is usually based on a Taylor series expansion (Chapra and Canale, 1998):

$$\begin{aligned} f(x_1, x_2, \dots, x_n) = f(\tilde{x}_1, \tilde{x}_2, \dots, \tilde{x}_n) &+ \frac{1}{1!} \left[(x_1 - \tilde{x}_1) \frac{\partial f(\tilde{x}_1, \tilde{x}_2, \dots, \tilde{x}_n)}{\partial x_1} \right. \\ &+ (x_2 - \tilde{x}_2) \frac{\partial f(\tilde{x}_1, \tilde{x}_2, \dots, \tilde{x}_n)}{\partial x_2} + \dots \Big] \\ &+ \text{higher order terms} \end{aligned} \quad (17-11)$$

Neglecting the higher order terms for relatively small errors, Eq. 17-11 can be written in a compact form as:

$$f \cong \tilde{f} + \sum_{i=1}^n (x_i - \tilde{x}_i) \frac{\partial \tilde{f}}{\partial x_i} \quad (17-12)$$

Then, applying Eqs. 17-7-10 into Eq. 17-12, the error or the uncertainty in the function value can be estimated by (Chapra and Canale, 1998):

$$\Delta \tilde{f} = \sum_{i=1}^n \Delta \tilde{x}_i \left| \frac{\partial \tilde{f}_i}{\partial x_i} \right| \quad (17-13)$$

or by a norm as (Reilly, 1992)

$$\Delta \tilde{f} = \left[\sum_{i=1}^n \left(\Delta \tilde{x}_i \frac{\partial \tilde{f}_i}{\partial x_i} \right)^2 \right]^{1/2} \quad (17-14)$$

The uncertainty associated with summation and/or subtraction of numbers, defined by Eqs. 17-7 through 9, is the square root of the squares of the uncertainties in these numbers (Reilly, 1992). Thus, if

$$f = \pm x_1 \pm x_2 \pm \dots \pm x_n \quad (17-15)$$

then

$$\Delta \tilde{f} = \left[(\Delta x_1)^2 + (\Delta x_2)^2 + \dots + (\Delta x_n)^2 \right]^{1/2} \quad (17-16)$$

The relative uncertainty in a multiplication or division of numbers is the square root of the sum of the squares of the relative uncertainties in these numbers (Reilly, 1992). Thus, if

$$f = x_1 \times x_2 \times \dots \times x_n \quad (17-17)$$

$$\text{then } \Delta \tilde{f} = \tilde{f} \left[\left(\frac{\Delta \tilde{x}_1}{\tilde{x}_1} \right)^2 + \left(\frac{\Delta \tilde{x}_2}{\tilde{x}_2} \right)^2 + \dots + \left(\frac{\Delta \tilde{x}_n}{\tilde{x}_n} \right)^2 \right]^{1/2} \quad (17-18)$$

and

$$f = \tilde{f} \pm \Delta \tilde{f} = \tilde{f} \left\{ 1 \pm \left[\sum_{i=1}^n \left(\frac{\Delta \tilde{x}_i}{\tilde{x}_i} \right)^2 \right]^{1/2} \right\} \quad (17-19)$$

For example, given a function like

$$f(x) = e^{-2x^2} \quad (17-20)$$

the error in the function value as a result of using an erroneous measured value of $x = 0.5 \pm 0.1$ can be estimated by applying Eq. 17-13 as:

$$\Delta \tilde{f} = \Delta \tilde{x} \left| -4\tilde{x}e^{-2\tilde{x}^2} \right| \quad (17-21)$$

Thus, substituting $\tilde{x} = 0.5$ and $\Delta\tilde{x} = 0.1$ into Eqs. 17–20 and 21 yields $\tilde{f} = 0.6$ and $\Delta\tilde{f} = 0.1$. Therefore, the calculated value is expressed according to Eq. 17–10 as:

$$f = 0.6 \pm 0.1 \quad (17-22)$$

As another example, consider

$$f = f(x, y) = x/y \quad (17-23)$$

Thus

$$\partial f / \partial x = 1/y \text{ and } \partial f / \partial y = -x/y^2 \quad (17-24)$$

Eq. 17–13 can be applied as:

$$\Delta\tilde{f} = \Delta\tilde{x} \left| \frac{\partial \tilde{f}}{\partial x} \right| + \Delta\tilde{y} \left| \frac{\partial \tilde{f}}{\partial y} \right| \quad (17-25)$$

Thus, Eqs. 17–23 through 25 lead to the following relative error expression:

$$\frac{\Delta\tilde{f}}{\tilde{f}} = \frac{\Delta\tilde{x}}{|\tilde{x}|} + \frac{\Delta\tilde{y}}{|\tilde{y}|} \quad (17-26)$$

A similar result is obtained for $f = f(x, y) = xy$.

It can be shown for $f = f(x, y) = x + y$ that

$$\frac{\Delta\tilde{f}}{\tilde{f}} = \frac{\Delta\tilde{x} + \Delta\tilde{y}}{|\tilde{x}| + |\tilde{y}|} \quad (17-27)$$

For $f = f(x) = x^n$, we can derive

$$\frac{\Delta\tilde{f}}{\tilde{f}} = n \frac{\Delta\tilde{x}}{|\tilde{x}|} \quad (17-28)$$

For $f = f(x) = \ln x$, we obtain

$$\frac{\Delta\tilde{f}}{\tilde{f}} = \frac{\Delta\tilde{x}}{|\tilde{x} \ln \tilde{x}|} \quad (17-29)$$

Applying Eq. 17–14 for Eq. 17–23 results in

$$\frac{\Delta \tilde{f}}{\tilde{f}} = \left[\left(\frac{\Delta \tilde{x}}{\tilde{x}} \right)^2 + \left(\frac{\Delta \tilde{y}}{\tilde{y}} \right)^2 \right]^{1/2} \quad (17-30)$$

A similar result for $f = xy$ is obtained.

Bu and Damsleth (1996) consider Darcy's law as an example

$$K = \frac{\mu L}{A} \frac{q}{\Delta p} \quad (17-31)$$

Let

$$b \equiv q/\Delta p \quad (17-32)$$

Thus, they express relative error in the calculated K value as a function of the measurements involving errors as (apply Eq. 17–14):

$$\frac{\Delta \tilde{K}}{\tilde{K}} = \left[\left(\frac{\Delta \tilde{\mu}}{\tilde{\mu}} \right)^2 + \left(\frac{\Delta \tilde{L}}{\tilde{L}} \right)^2 + \left(\frac{\Delta \tilde{A}}{\tilde{A}} \right)^2 + \left(\frac{\Delta \tilde{b}}{\tilde{b}} \right)^2 \right]^{1/2} \quad (17-33)$$

Sensitivity Analysis—Stability and Conditionality

Sensitivity analysis is an important tool for systematic evaluation of mathematical models (Lehr et al., 1994). Sensitivity analysis can be used for various purposes, including model validation, evaluating model behavior, estimating model uncertainties, decision making using uncertain models, and determining potential areas of research (Lehr et al., 1994).

Sensitivity analysis provides information about the effect of the errors and/or variations in the variables and/or parameters and models on the predicted behavior. Sensitivity of a model to changes in its input data determines the condition of the model (Chapra and Canale, 1998).

The sensitivity of a system's outcome or response to changes in a variable is defined by the partial derivative (Lehr et al., 1994):

$$S_x = \frac{\partial \tilde{f}}{\partial x} \equiv \tilde{f}' \quad (17-34)$$

Relative sensitivity (Lehr et al., 1994) or the condition number (Chapra and Canale, 1998) is defined as the ratio of the relative change or error in the function to the relative change or error in the variable or parameter value. Thus, for a single parameter function, the relative sensitivity can be expressed by means of Eq. 17-12 as (Lehr et al., 1994; Chapra and Canale, 1998):

$$\Delta_x = \frac{\frac{\Delta \tilde{f}}{\tilde{f}}}{\frac{\Delta \tilde{x}}{\tilde{x}}} = \frac{\tilde{x} \tilde{f}'}{\tilde{f}} = \frac{\tilde{x} S_x}{\tilde{f}} \quad (17-35)$$

Thus, the condition number or relative sensitivity can be used as a criteria to evaluate the effect of an uncertainty in the x variable on the condition of a system as (Chapra and Canale, 1998):

$$|\Delta_x| \begin{cases} < 1, \text{ effect in the function is attenuated} \\ = 1, \text{ effect in the function is same as the variation in the variable} \\ > 1, \text{ effect in the function is amplified} \end{cases} \quad (17-36)$$

Given the differential equations of a model, the sensitivity equations can be formulated for determining the sensitivity trajectory. The following example by Lehr et al. (1994) illustrates the process.

Consider a mathematical model given by an ordinary differential equation as:

$$\frac{df(x, t)}{dt} = g(f, x, t) \quad (17-37)$$

A differentiation of the $g(f, x, t)$ function with respect to the variable (or parameters) x leads to:

$$\frac{dg}{dx} = \frac{\partial g}{\partial f} \frac{\partial f}{\partial x} + \frac{\partial g}{\partial x} \quad (17-38)$$

Substituting Eqs. 17-34 and 37 into Eq. 17-38 and rearranging yield the following sensitivity trajectory equation:

$$\frac{d}{dt} \left(\frac{df}{dx} \right) \equiv \frac{dS_x}{dt} = \frac{\partial g}{\partial f} S_x + \frac{\partial g}{\partial x} \quad (17-39)$$

One of the practical applications of the sensitivity analysis is to determine the critical parameters, which strongly effect the predictions of models (Lehr et al., 1994). Lehr et al. (1994) studied the sensitivity of an oil spill evaporation model. Figures 17-2 and 17-3 by Lehr et al. (1994) depict the sensitivity of the fractional oil evaporation, f , from an oil spill with respect to the initial bubble point, T_B , and the rate of bubble point variation by the fraction of oil evaporated (the slope of the evaporation curve), $T_G \equiv \partial^2 T_B / \partial t \partial f$, respectively. Examination of Figures 17-2 and 17-3 reveals that the initial bubble point T_B is the critical parameter, influencing the sensitivity of the oil spill evaporation model. Figure 17-2 clearly indicates that there is a strong correlation between the sensitivity with respect to the slope of the evaporation curve and the bubble point. Whereas, Figure 17-3 shows that the sensitivity with respect to the slope of the evaporation curve cannot be correlated with the slope of the evaporation curve.

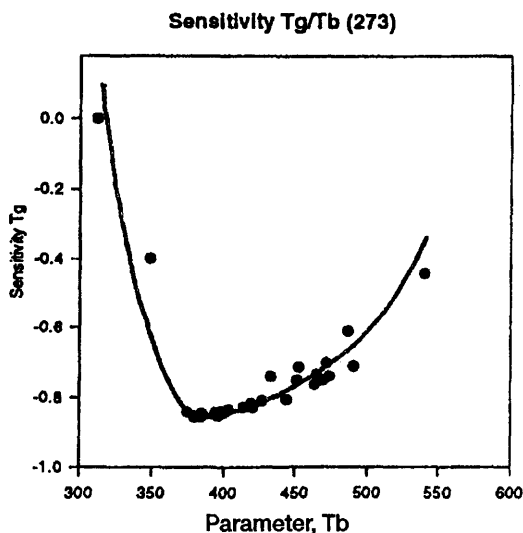


Figure 17-2. Dependence of the sensitivity with respect to T_G on the initial bubble point T_B (modified after Lehr, W., Calhoun, D., Jones, R., Lewandowski, A., and Overstreet, R., "Model Sensitivity Analysis in Environmental Emergency Management: A Case Study in Oil Spill Modeling," Proceedings of the 1994 Winter Simulation Conference, J. D. Tew, S. Manivannan, D. A. Sadowski, and A. F. Seila (eds.), pp. 1198-1205, ©1994 IEEE; reprinted by permission).

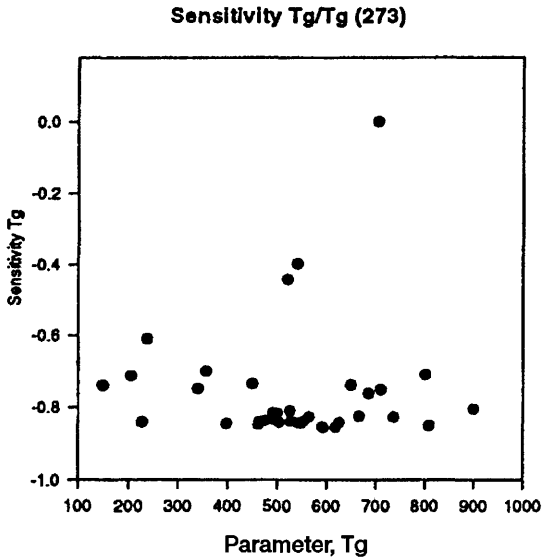


Figure 17-3. Dependence of the sensitivity with respect to T_G on T_G (after Lehr, W., Calhoun, D., Jones, R., Lewandowski, A., and Overstreet, R., "Model Sensitivity Analysis in Environmental Emergency Management: A Case Study in Oil Spill Modeling," Proceedings of the 1994 Winter Simulation Conference, J. D. Tew, S. Manivannan, D. A. Sadowski, and A. F. Seila (eds.), pp. 1198–1205, ©1994 IEEE; reprinted by permission).

Model Validation, Refinement, and Parameter Estimation

As stated by Civan (1994), confidence in the model cannot be established without validating it by experimental data. However, the microscopic phenomena is too complex to study each detail individually. Thus, a practical method is to test the system for various conditions to generate its input-output response data. Then, determine the model parameters such that model predictions match the actual measurements within an acceptable tolerance. However, some parameters may be directly measurable. A general block diagram for parameter identification and model development and verification is given in Figure 17-4 (Civan, 1994).

Experimental System

The experimental system is a reservoir core sample subjected to fluid flow. The input variables are injection flow rate or pressure differential and its particles concentration, temperature, pressure, pH, etc. The output

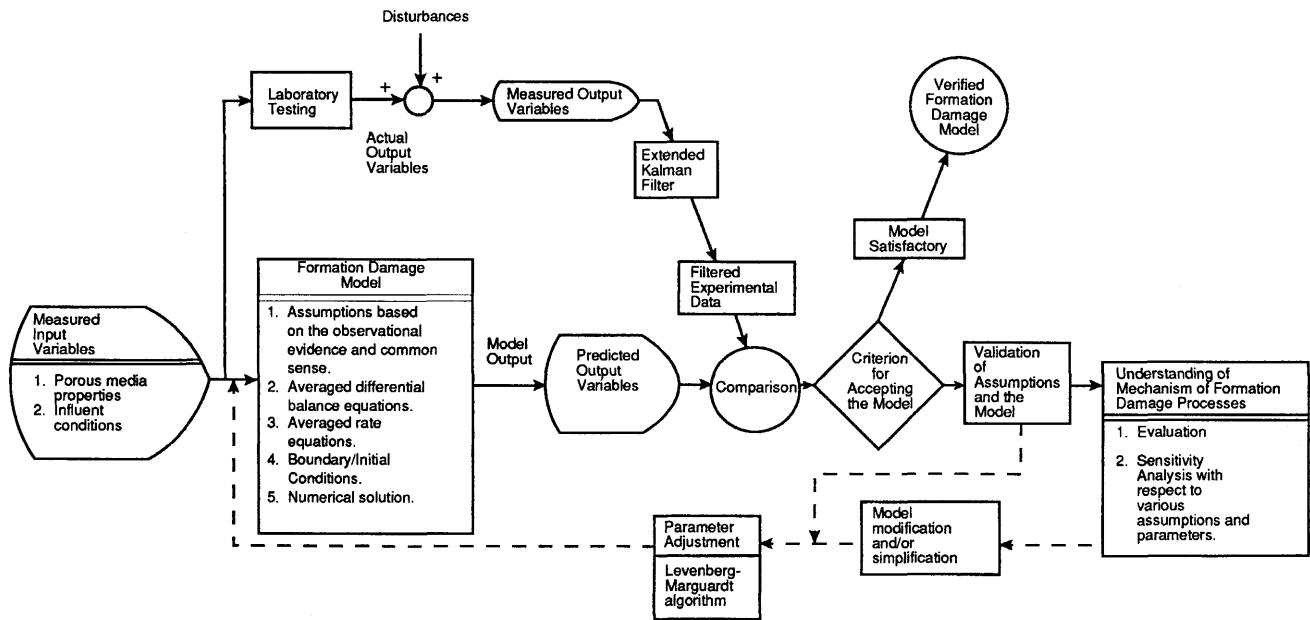


Figure 17–4. Steps for formation damage process identification and model development (after Civan, 1994; reprinted by permission of the U.S. Department of Energy).

variables are the measured pressure differential, pH, and species concentration of the effluent. Frequently, data filtering and smoothing are required to remove noise from the data as indicated in Figure 17-4. However, some important information may be lost in the process. Millan-Arcia and Civan (1990) reported that frequent breakage of particle bridges at the pore throat may cause temporary permeability improvements, which are real and not just a noise. Baghdikian et al. (1989) reported that accumulation and flushing of particle flocs can cause an oscillatory behavior during permeability damage.

Parity Equations

An integration of the model equations over the length of core yields the equations of a macroscopic model called the "parity equations." However, for a complicated model of rock-fluid-particle interactions in geological porous formations it is impractical to carry out such an integration analytically. Hence, an appropriate numerical method, such as described in Chapter 16, is facilitated to generate the model response (pressure differential across the core or sectional pressure differentials, and the effluent conditions) for a range of input conditions (i.e., the conditions of the influent, confining stress, temperature, pressure, pH, etc.).

Parameter Estimation with Linearized Models

Luckert (1994) points out that estimating parameters using linearized model equations obtained by transformation is subject to uncertainties and errors because of the errors introduced by numerical transformation of the experimental data. Especially, numerical differentiation is prone to larger errors than numerical integration. Luckert (1994) explains this problem on the determination of the parameters K and q of the following filtration model:

$$\frac{d^2t}{dV^2} = K \left(\frac{dt}{dV} \right)^q \quad (17-40)$$

where t and V denote the filtration time and the filtrate volume, respectively. This equation can be linearized by taking a logarithm as

$$\log \left(\frac{d^2t}{dV^2} \right) = \log K + q \log \left(\frac{dt}{dV} \right) \quad (17-41)$$

Thus, a straightline plot of Eq. 17–41 using a least-squares fit provides the values of $\log K$ and q as the intercept and slope of this line, respectively. Luckert (1994) points out, however, this approach leads to highly uncertain results because numerical differentiation of the experimental data involves some errors, second differentiation involves more errors than the first derivative, and numerical calculation of logarithms of the second numerical derivatives introduce further errors. Therefore, Luckert (1994) recommends linearization only for preliminary parameter estimation, when the linearization requires numerical processing of experimental data for differentiation. Luckert (1994) states that “From a statistical point of view, experimental values should not be transformed in order that the error distribution remains unchanged.”

In Chapter 12, detailed examples of constructing diagnostic charts for determining the parameters of the incompressible cake filtration model by Civan (1998) have been presented. It has been demonstrated that the model parameters can be determined from the slopes and intercepts of the straight line plots of the experimental data according to the linearized forms of the various equations, describing the linear and radial filtration processes. Using the parameter values determined this way, Civan (1998) has shown that the model predictions compared well with the measured filtrate volumes and cake thicknesses. The advantage of this type of direct method is the uniqueness of the parameter values as described in Chapter 12. As described in Chapter 10, Wojtanowicz et al. (1987, 1988) also used linearized diagnostic equations given in Table 10–1 for determining the parameters of their single-phase fines migration models.

History Matching for Parameter Identification

The model equations contain various parameters dealing with the rate equations. They are determined by a procedure similar to history matching commonly used in reservoir simulation. In this method, an objective function is defined as

$$J(X) = (Y_m - Y_c)^T W (Y_m - Y_c) = \sum_{i=1}^n w_i (y_m - y_c)_i^2 \quad (17-42)$$

where Y_m is the measured values, Y_c is the calculated values, W is the weighting matrix, $W = V^{-1}$, V is the variance-covariance matrix of the measurement error, and n is the number of data points. Szucs and Civan (1996) facilitated an alternative formulation of the objective function, called the p -form, which lessens the effect of the outliers in the measured data points.

Then, a suitable method is used for minimizing the objective function to obtain the best estimates of the unknown model parameters (Ohen and Civan, 1990, 1993).

Note that the number of measurements should be equal or greater than the number of unknown parameters. When there are less measurements than the unknown parameters, additional data can be generated by interpolation between the existing data points. However, for meaningful estimates of the model parameters the range of the data points should cover a sufficiently long test period to reflect the effect of the governing formation damage mechanisms.

The above described method has difficulties. First, it may require a lot of effort to converge on the best estimates of the parameter values. Second, there is no guarantee concerning the uniqueness of the parameter values determined with nonlinear models. However, some parameters can be eliminated for less important mechanisms for a given formation and fluid system. The remaining parameters are determined by a history matching procedure. In this method, the best estimates of the unknown parameters are determined in such a way that the model predictions match the measurements obtained by laboratory testing of cores within a reasonable accuracy (Civan, 1994).

Frequently used optimization methods are: (1) trial-and-error [tedious and time consuming]; (2) Levenberg-Marquardt (Marquardt, 1963) method [requires derivative evaluation, computationally intensive]; (3) simulated annealing [algebraic and practical (Szucs and Civan, 1996; Ucan et al., 1997)].

Detailed examples of the history matching method by Ohen and Civan (1990, 1993) have been presented in Chapter 10.

Sensitivity Analysis

Once the model is developed and verified with experimental data, studies of the sensitivity of the model predictions with respect to the assumptions, considerations, and parameters of the model can be conducted. Consequently, the factors having negligible effects can be determined and the model can be simplified accordingly. Models simplified this way are preferred for routine, specific applications. For example, Figure 17–5 by Ziauddin et al. (1999) shows the effect of including tertiary reactions on the predicted alimuna and silica concentrations during gel precipitation by sandstone acidizing at different temperatures. Figure 17–6 by Gadiyar and Civan (1994) shows the effect of the acidizing reaction rate constants on permeability alteration. The solid line represents the best fit of the experimental data using the best estimates of the model parameters obtained by history matching. When the parameter values were

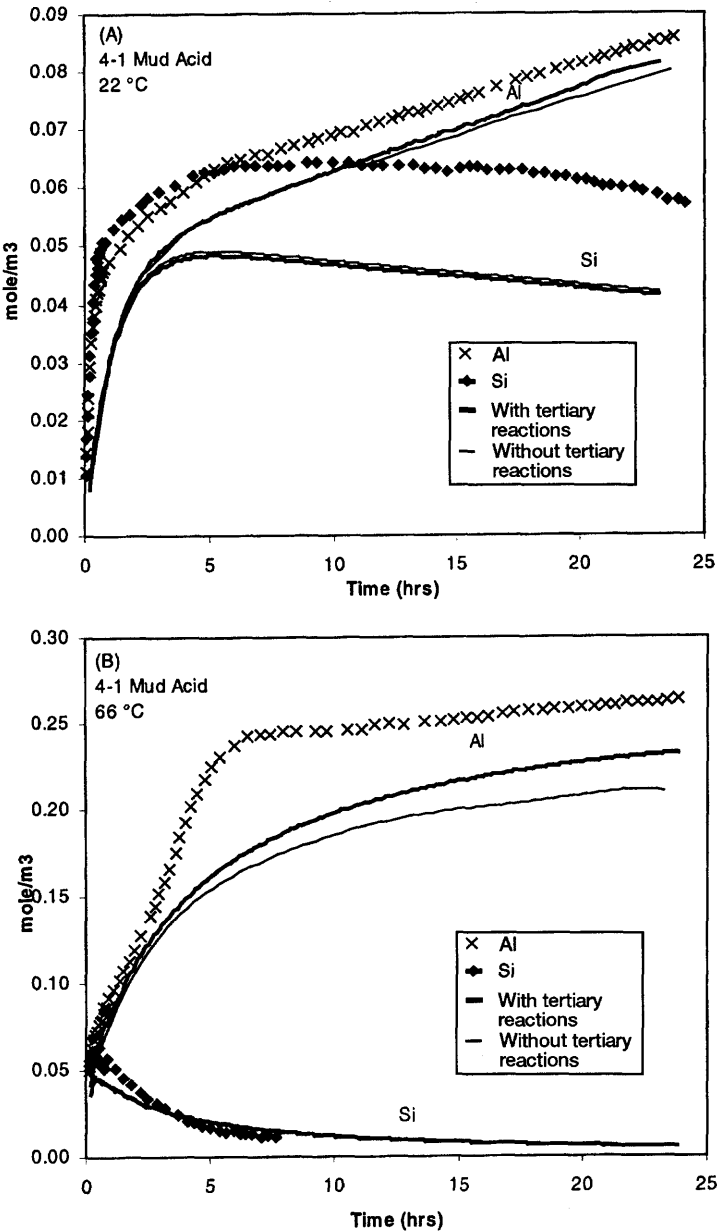


Figure 17-5. Sensitivity analysis for the tertiary reaction at different temperatures: (a) 22°C and (b) 66°C (after Ziauddin et al., ©1999; reprinted by permission of the Society of Petroleum Engineers).

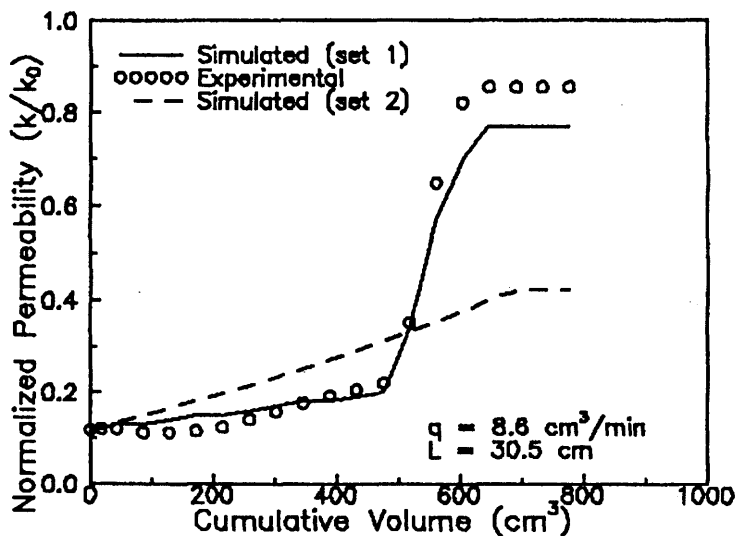


Figure 17-6. Dependence of the sensitivity with respect to the model parameters (after Gadiyar and Civan, ©1994 SPE; reprinted by permission of the Society of Petroleum Engineers).

perturbed in a random manner, a significantly different trend, represented by the dashed line, was obtained.

Determination of the Formation Damage Potential by Simulation

Reservoir exploitation processes frequently cause pressure, temperature and concentration changes, and rock-fluid and fluid-fluid interactions, which often adversely effect the performance of these processes. Prior to any reservoir exploitation applications, extensive laboratory, field and simulation studies should be conducted for assessment of the formation brine and mineral chemistry and the formation damage potential of the reservoir. Consequently, optimal strategies can be designed to effectively mitigate the adverse effects and improve the oil and gas recovery.

Typical examples of such detailed studies have been presented in a series of reports by Demir (1995), Haggerty and Seyler (1997), and Seyler (1998) for characterization of the brine and mineral compositions and the investigation of the formation damage potential in the Mississippian Aux Vases and Cypress formations in the Illinois Basin. Demir (1995) used the chemical data on the formation brines and minerals to interpret the

geology, determine the properties (porosity, permeability, water saturation), and estimate the formation damage potential of these reservoirs.

Formation Minerals and Brines

The stratigraphic dispositions of the Aux Vases and Cypress formations are shown in Figure 17-7 by Leetaru (1990) given by Demir (1995).

Formation Brines

Demir (1995) reports that brine samples were gathered from the oil producing wells in the Aux Vases and Cypress formations. Also, the samples of the brines of the Cypress and Waltersburg formations, which

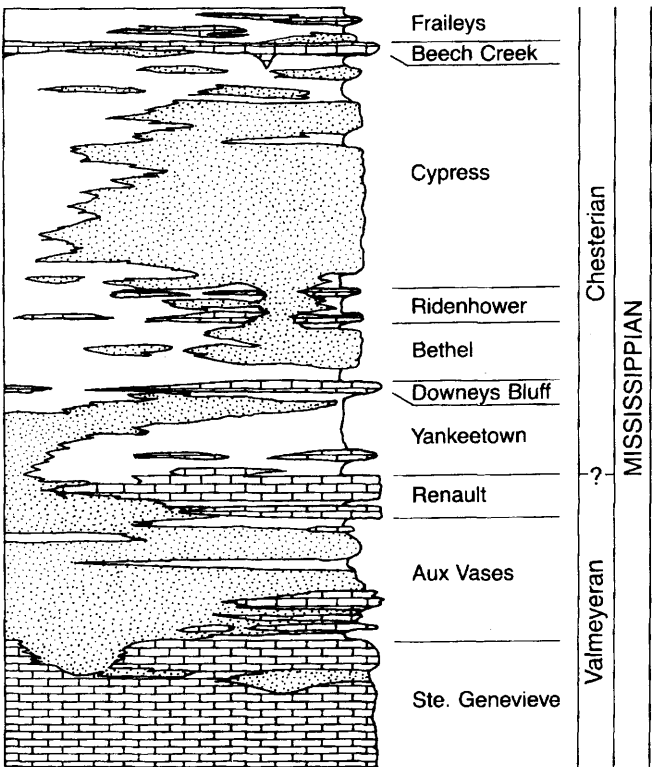


Figure 17-7. Generalized upper Valmeyeran and Chesterian geologic column (Mississippian system) of southern Illinois (from Leetaru, 1990; after Demir, 1995; reprinted by permission of the Illinois State Geological Survey).

are used for water flooding in the Aux Vases and Cypress reservoirs, were collected from the separation tanks. Prior to sample collection, chemical treatments, such as acidizing and corrosion inhibitor applications in the wells, were ceased usually for 24 hours, but at least for 4 hours. The brine samples were collected using the USGS method, described in Figure 17–8, and isolated from exposure to the atmosphere to avoid oxidation and degassing. The samples were identified by the well API numbers and field names, and the pH, Eh resistivity, total dissolved solids (TDS), and laboratory chemical analysis of these samples were determined. The results are summarized in Table 17–1 by Demir (1995). The methods used to analyze the formation brine samples are described in Table 17–2 according to ISGS (1993).

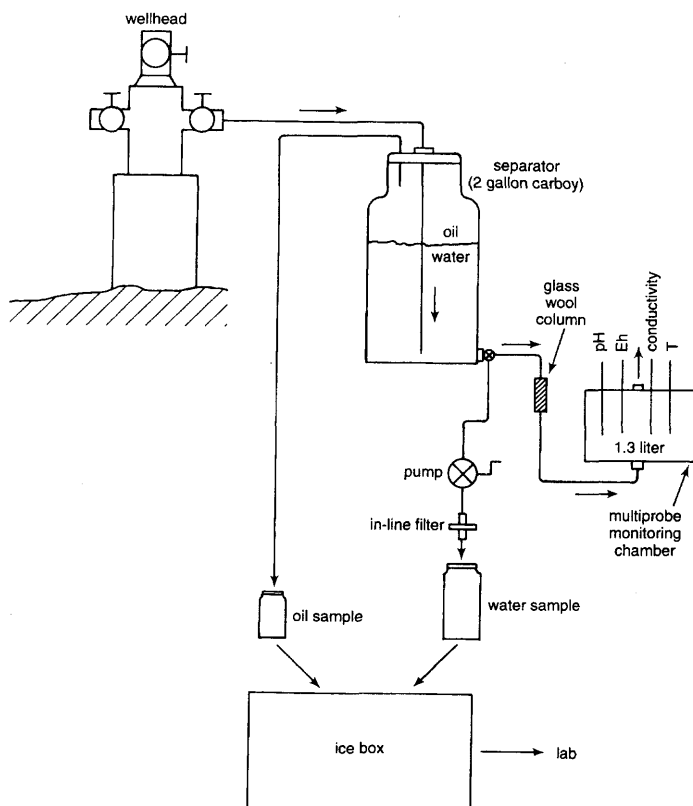


Figure 17–8. Schematic of the setup for collecting formation fluids in the field (after Demir, 1995; reprinted by permission of the Illinois State Geological Survey).

Table 17–1
Well identification and Chemical Composition of Formation Waters for Selected Locations

Sample no.	API no.	Field name	Strat. Unit	Average depth (ft.)	Resis. (ohm-m)	Eh (mV)	pH	TDS (mg/l)	Anions and Major Cations (mg/L)									
									Cl	Br	I	SO ₄	NO ₃	CO ₃	HCO ₃	Na	Ca	Mg
EOR-B115	120552391900	AKIN	Cypr.	2825	0.0601	–186	6.44	145333	87000	160	3.50	270	0.62	0.04	140	52100	4010	1370
EOR-B92	121913194800	BARNHILL	Aux V.	3360	0.0639	–234	6.89	132780	78000	110	13.00	1300	0.08	0.10	110	46400	5170	1310
EOR-B17	120270314300	BARTELSON	Cyp.	967	0.1382	–318	7.01	49667	29000	84	5.60	2.5	0.10	0.86	460	18160	892	601
EOR-B70	121932941500	CARM NORTH	Aux. V.	3236	0.0676	–150	5.92	125460	74000	180	7.00	304	0.60	0.05	60	43830	5340	1210
EOR-B51	121913099200	CLAY CITY C.	Aux V.	3234	0.0782	–335	7.24	100768	59000	130		690	<0.04	1.00	170	35560	3770	1040
EOR-B93	121910790600	CLAY CITY C.	Aux V.	3102	0.0692	–287	6.56	116926	68000	140	7.70	1200	<0.01	0.13	180	42100	3750	1180
EOR-B52	121913114900	CLAY CITY C.	Cyp.	2940	0.0670	–285	7.24	124254	72000	140		990	0.27	0.34	230	45940	3490	1140
EOR-B107	120552347200	DALE CONS.	Aux. V.	3172	0.0615	–134	5.34	137444	84000	160	9.90	9.5	0.41	0.00	64	44850	5820	1950
EOR-B101	120552272100	DALE CONS.	Cyp.	2959	0.0621	–270	6.24	140537	83000	150	2.40	930	0.36	0.05	90	50700	4050	1270
EOR-B99	121652490500	ELDORADO W.	Aux V.	2864	0.0746	–213	6.56	108598	65000	180	10.20	430	0.24	0.39	210	36200	4030	1960
EOR-B60	121992347700	ENERGY	Aux V.	2364	0.0632	–102	6.63	132040	79000	180	10.00	1.8	0.25	0.01	60	44210	5370	2510
EOR-B9	120810016700	KING	Aux V.	2744	0.0621	–287	6.81	141529	85000	180	3.90	720	0.06	0.11	120	48540	4710	1720
EOR-B36	120292340200	MATTOON	Cyp.	1820	0.0692	–276	6.85	117069	69000	140	4.70	600	0.10	0.26	140	41050	4490	1330
EOR-B35	120290127300	MATTOON	Aux V.	1808	0.1252	–314	7.36	56100	33000	71	2.00	31	<0.02	1.30	170	20450	1580	564
EOR-B73	121932575700	NEW HARMONY C.	Cyp.	2611	0.0707	–156	5.92	116603	67000	190	8.20	30	0.29	0.45	120	42990	4340	1310
EOR-B41	120472399500	PARKERSBURGH	L. Cyp.	2804	0.0723	–284	6.74	116429	71000	140	7.00	510	0.90	0.21	110	37810	5200	1340
EOR-B83	120252742400	SAILOR SPRING C.	Aux V.	2909	0.0613	–144	6.13	146456	85000		7.00	660	0.38	0.03	79	53780	5120	1360
EOR-B113	Injc. Water	STORMS C.	Wallerbrg		0.1406	–59	7.22	44320	25000	64	3.50	36	0.51	0.36	300	17450	892	468
EOR-B22	121450227300	TAMAROA	Cyp.	1159	0.0877	–178	6.47	87529	52000	140	6.30	18	0.10	0.07	180	30910	2450	1430
EOR-B23	Injec. Water	TAMAROA	Cyp.	NA	0.0877	–73	6.68	85236	51276+					<1	156	30220	2058	1164
EOR-B59	120552387700	ZEIGLER	Aux V.	2629	0.0610	–111	6.24	137329	82000	190	10.00	490	0.29	0.03	120	45950	6020	1900

After Demir, 1995; reprinted by permission of the Illinois State Geological Survey.

Table 17–1 continued

Sample no.	Minor and Trace Constituents (mg/L)																								
	K	Sr	NH ₄	Ba	Li	Fe	Mn	B	Si	Al	Pb	Ti	V	Co	Ni	Cu	Zn	Zr	Cd	Be	Cr	As	Se	Mo	Sb
EOR-B115	105	130	31	0.66	3.90	3.00	0.43	2.89	1.60	0.2	<0.4	<0.04	<0.08	<0.07	<0.1	<0.06	<0.02	<0.08	<0.05	<0.003	<0.07	<0.5	<0.7	<0.08	<0.3
EOR-B92	182	145	23	0.22	6.86	0.40	0.73	4.10	4.80	0.1	<0.4	0.03	<0.07	<0.07	<0.1	<0.05	<0.02	<0.07	<0.05	<0.003	<0.07	<0.5	<0.7	<0.08	<0.3
EOR-B17	69	101	23	252.00	4.90	0.10	1.07	2.60	4.90	<0.4	<0.4	0.02	<0.08	0.15	<0.1	<0.05	<0.02	0.08	<0.05	<0.003	<0.07	<0.5	0.7	<0.08	1.2
EOR-B70	170	313	21	2.19	7.10	6.10	1.25	3.70	3.20	<0.1	<0.4	<0.04	<0.07	<0.07	<0.1	0.04	<0.02	<0.07	<0.05	<0.003	<0.07	<0.5	0.6	<0.08	<0.3
EOR-B51	173	192	26	0.51	6.27	<0.06	0.34	3.00	5.70	0.2	<0.4	0.03	<0.08	<0.07	<0.1	<0.05	<0.02	<0.08	<0.05	<0.003	<0.07	<0.5	<0.7	<0.08	<0.3
EOR-B93	187	133	30	0.77	5.93	0.60	0.52	5.40	5.20	0.1	<0.4	0.04	<0.07	<0.07	<0.1	<0.05	<0.02	<0.07	<0.05	<0.003	<0.07	<0.5	<0.7	<0.08	<0.3
EOR-B52	174	106	28	0.26	6.77	0.17	0.87	2.20	5.20	0.2	<0.4	0.03	<0.08	<0.07	<0.1	<0.05	<0.02	<0.08	<0.05	0.009	<0.07	<0.5	<0.7	<0.08	<0.3
EOR-B107	175	322	26	2.77	7.10	34.90	1.43	3.94	6.70	0.3	<0.4	<0.04	<0.08	<0.07	<0.1	<0.05	<0.02	<0.08	<0.05	<0.003	<0.07	<0.5	<0.7	<0.08	<0.3
EOR-B101	149	149	26	0.29	5.82	5.00	1.20	2.30	4.00	0.1	<0.4	0.03	<0.07	<0.07	<0.1	<0.05	<0.02	<0.07	<0.05	<0.003	<0.07	<0.5	<0.7	<0.08	1.6
EOR-B99	210	321	23	0.81	12.90	1.40	0.52	2.80	4.40	0.1	<0.4	0.03	<0.07	<0.07	<0.1	<0.05	<0.02	<0.07	<0.05	<0.003	<0.07	<0.5	<0.7	0.08	<0.3
EOR-B-60	190	441	31	12.50	12.00	6.00	0.74	1.80	3.30	<0.2	<0.4	0.04	<0.08	<0.07	<0.15	<0.05	<0.02	<0.08	<0.05	<0.003	<0.07	<0.5	<0.8	<0.08	<0.3
EOR-B9	280	199	36	0.75	10.70	<0.06	0.56	3.40	4.40	0.3	<0.4	0.04	<0.08	<0.07	<0.1	<0.05	<0.02	<0.02	<0.05	<0.003	<0.07	<0.5	<0.7	<0.08	<0.3
EOR-B36	102	175	25	0.52	5.20	0.19	0.89	1.67	3.50	0.1	<0.4	0.03	<0.07	<0.07	<0.15	<0.05	<0.02	<0.08	<0.05	<0.003	<0.07	<0.5	<0.7	<0.08	<0.3
EOR-B35	61	132	17	10.90	1.90	<0.06	0.15	1.95	5.70	0.1	<0.4	<0.04	<0.07	<0.07	<0.15	0.03	<0.02	<0.08	<0.05	<0.003	<0.07	<0.5	<0.7	<0.08	<0.3
EOR-B73	80	315	16	183.00	3.70	5.40	2.63	2.90	5.20	<0.1	<0.4	<0.04	<0.07	0.11	<0.1	0.06	<0.02	<0.07	<0.05	<0.003	<0.07	<0.5	<0.7	<0.08	<0.3
EOR-B41	131	147	17	1.15	5.00	<0.06	1.89	2.76	4.20	0.2	<0.4	0.03	<0.07	<0.07	<0.15	0.02	<0.02	<0.07	<0.05	<0.003	<0.07	<0.5	0.8	<0.08	<0.3
EOR-B83	216	180	27	1.90	7.10	7.00	0.89	3.80	5.60	0.1	<0.4	<0.04	<0.07	<0.07	<0.1	<0.06	<0.02	<0.07	<0.05	<0.003	0.05	<0.5	<0.7	<0.08	<0.3
EOR-B113	41	39	9	6.60	1.70	1.50	0.38	3.42	2.30	0.1	<0.4	<0.04	<0.08	<0.07	<0.1	<0.06	<0.02	<0.07	<0.05	0.003	<0.07	<0.5	<0.7	<0.08	<0.3
EOR-B22	128	204	29	6.42	5.51	15.30	0.44	1.20	3.70	0.2	<0.4	0.03	<0.08	<0.07	<0.1	<0.05	<0.02	<0.08	<0.05	0.003	<0.07	<0.5	<0.7	<0.08	0.8
EOR-B23	134	195		7.10		18.00	0.72	2.79	3.19		<0.4	0.12		<0.07	<0.15	<0.06	<0.02	0.07	<0.05	0.014			<0.08	0.7	
EOR-B59	196	381	35	0.44	10.60	17.20	1.04	2.19	3.40	0.2	<0.4	0.05	<0.08	<0.07	<0.15	<0.05	0.49	<0.08	<0.05	<0.003	<0.07	<0.5	<0.8	<0.08	1.2

Table 17-2
Methods for Analyses of Formation Brines

Analytic Method	Chemical Elements and Ions
Inductively coupled plasma spectrometer	sodium (<i>Na</i>), calcium (<i>Ca</i>), magnesium (<i>Mg</i>), potassium (<i>K</i>), strontium (<i>Sr</i>), barium (<i>Ba</i>), lithium (<i>Li</i>), iron (<i>Fe</i>), manganese (<i>Mn</i>), boron (<i>B</i>), silicon (<i>Si</i>), aluminum (<i>Al</i>), lead (<i>Pb</i>), titanium (<i>Ti</i>), vanadium (<i>V</i>), cobalt (<i>Co</i>), nickel (<i>Ni</i>), copper (<i>Cu</i>), zinc (<i>Zn</i>), zirconium (<i>Zr</i>), cadmium (<i>Cd</i>), beryllium (<i>Be</i>), chromium (<i>Cr</i>), arsenic (<i>As</i>), selenium (<i>Se</i>), molybdenum (<i>Mo</i>), antimony (<i>Sb</i>)
Standard ASTM-EPA procedures (ASTM 1976, U.S. EPA, 1975, 1985)	Anions and ammonium (NH_4^+)
Titrimetric-mercuric nitrate method	chloride (Cl^-)
Titrimetric method	bromide (Br^-) and iodide (I^-)
Turbidimetric method	sulfate (SO_4^{2-})
Spectro-photometric-cadmium reduction method	nitrate (NO_3^-)
Titrimetric method	carbonate (CO_3^{2-}) and bicarbonate (HCO_3^-)
Potentiometric-ion selective electrode method	ammonium (NH_4^+)

After Demir, 1995.

Formation Minerals

The core samples used for mineralogical analyses are described in Table 17-3 by Demir (1995). The mineralogical compositions of these samples were determined by means of the x-ray diffraction techniques according to ISGS (1993). The mean concentrations of minerals in Aux Vases and Cypress formation cores are given in Figure 17-9 by Demir (1995).

Formation Heterogeneity

The maps of the areal distributions of the total dissolved solids (TDS) of the Aux Vases and Cypress formation brines are shown in Figures 17-10

Table 17-3
Identification of Core Samples for which Mineralogical
Data Were Available

Sample API no.	Well name	Field name	Formation	Average depth (ft)
01120	Mattoon no. 1	Mattoon	Aux Vases	1902.0
00312	Bates no. 1	Mattoon	Aux Vases	1882.0
23465	Morgan Coal no. 2	Energy	Aux Vases	2391.4
23491	Burr Oak no. 3	Energy	Aux Vases	2406.3
00392	L. M. Compton no. 1	Mode	Aux Vases	1813.0
23456	McCreery no. 1	Dale Consol.	Aux Vases	3204.9
23744	Mack no. 1 (020*4)	Zeigler	Aux Vases	2623.0
23750	Mack no. 2	Zeigler	Aux Vases	2617.3
23753	Mack no. 3	Zeigler	Aux Vases	2642.5
23768	Mack no. 5	Zeigler	Aux Vases	2623.4
23769	Mack no. 6	Zeigler	Aux Vases	2625.6
	Misc. Mack Sample	Zeigler	Aux Vases	2626.0
01070	Novak no. 4	Oakdale	Aux Vases	2880.0
01543	Horrell no. 3	Oakdale	Aux Vases	2915.0
23499	Breeze no. 1	Oakdale	Aux Vases	2880.6
00078	G. D. Chaffee no. 1	Stewardson	Aux Vases	1954.0
01862	Chaffee no. 8	Stewardson	Aux Vases	1970.0
01972	Price no. 1	Boyd	Aux Vases	2133.0
01950	Sanders no. 7	Boyd	Aux Vases	2148.0
01935	F. High no. 2	Boyd	Aux Vases	2130.0
00496	E. W. Hale	King	Aux Vases	2740.0
00488	Ford no. 1	King	Aux Vases	2738.0
00490	L. Wallace no. 1	King	Aux Vases	2732.0
00090	I. W. Mace no. 1	King	Aux Vases	2752.0
00459	St. Game Farm no. 1	King	Aux Vases	2748.5
01301	Eugene Tnan no. 1	Mattoon	Cypress	1803.0
01131	Anna Strong no. 8	Mattoon	Cypress	1778.0
00795	Ruth Upholt no. 6	Mattoon	Cypress	1821.0
01319	Strong-Seamen no. 1	Mattoon	Cypress	1831.0
01169	Kuehne Mfg. no. 1	Mattoon	Cypress	1813.0
00291	Joshua Akers no. 1	Mattoon	Cypress	1860.0
01330	Elizabeth Strong no. 7	Mattoon	Cypress	1872.0
00788	N. D. Rick no. 9	Mattoon	Cypress	1866.0
00325	A. G. Camine no. 1	Mattoon	Cypress	1736.0
02187	Stockton Lease no. 1	Tamaroa	Cypress	1160.5
00551	Kampwerth no. 1	Bartelso	Cypress	1002.0
01266	Hempen no. 1	Bartelso	Cypress	1063.0
01812	Droege Unit no. 2	Richview	Cypress	1498.5
01165	Campbell Lease no. 3	Xenia East	Cypress	2538.0

After Demir, 1995; reprinted by permission of the Illinois State Geological Survey.

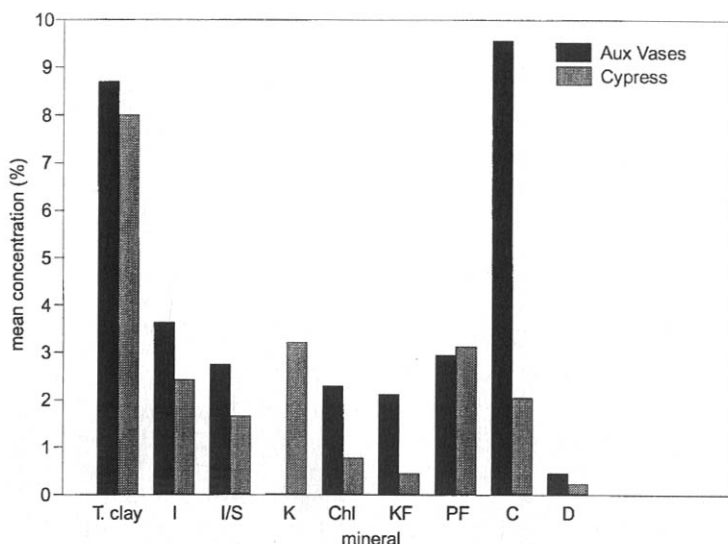


Figure 17–9. Mean concentrations of minerals (excluding quartz) in Aux Vases (25 cores) and Cypress (14 cores) formations core samples. T. clay = total clay; I = illite; I/S = illite/smectite; K = kaolinite; Chl = chlorite; KF = potassium feldspar; PF = plagioclase; C = calcite; D = dolomite (after Demir, 1995; reprinted by permission of the Illinois State Geological Survey).

and 17–11, respectively, by Demir (1995). Demir (1995) states that “variations in water chemistry in a given reservoir in the same field can indicate a lack of communication between different pools, or mineralogical heterogeneity within the reservoir.” Figure 17–12 by Demir (1995) indicates that the total dissolved solids (TDS) increase by depth. However, the data points are somewhat scattered. This indicates the presence of structural and stratigraphic irregularities in the basin (Demir, 1995).

Inferring Reservoir Properties from Resistivity versus TDS and Temperature Relationships

The brine resistivities and TDS of formation brines, measured before degassing and oxidation, can be used to estimate water saturations and permeabilities (Demir, 1995). The maps of the areal distributions of the resistivities in the Aux Vases and Cypress formations are given in Figures 17–13 and 17–14, respectively, by Demir (1995). Based on the linear plot shown in Figure 17–15, Demir (1995) developed the following empirical relation between the resistivity and the TDS content of the brine samples at 25°C temperature:

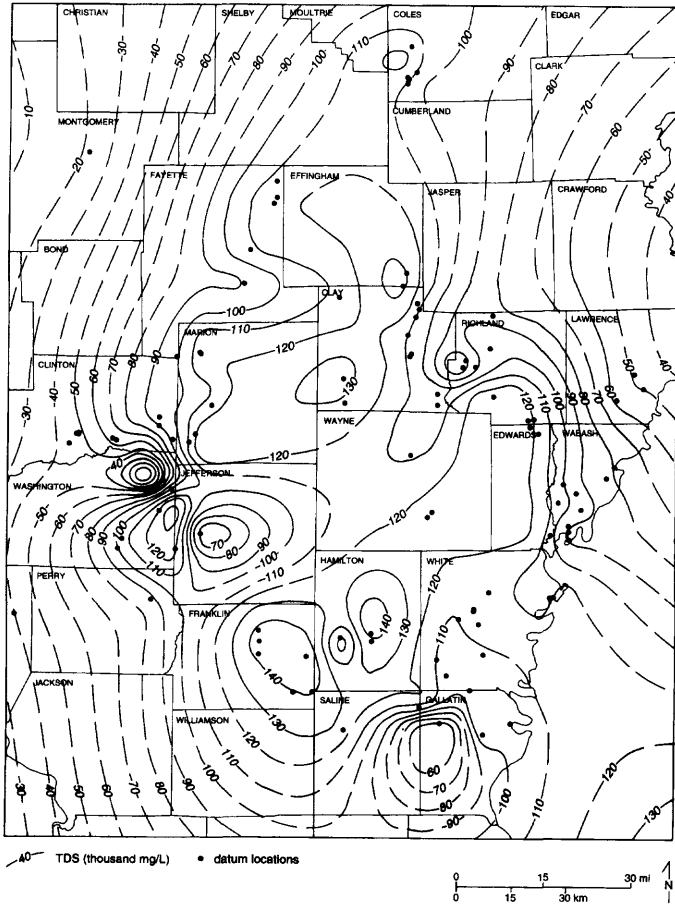


Figure 17-10. Areal distribution of TDS in Cypress formation waters (after Demir, 1995; reprinted by permission of the Illinois State Geological Survey).

$$\log R_{w(25)} = 2.841 - 0.788 \log(TDS) \quad (17-43)$$

In addition, Demir (1995) developed two more empirical relationships. The first equation predicts brine resistivities at temperatures, $T(^{\circ}\text{C})$, in the range of 18–60 $^{\circ}\text{C}$, given the brine resistivity at 25 $^{\circ}\text{C}$:

$$R_{w(T)} = 1.5 R_{w(25)}^{0.987} / 1.017^T \quad (17-44)$$

The second equation predicts brine resistivities at temperatures, $T(^{\circ}\text{C})$, in the range of 18–60 $^{\circ}\text{C}$, given the TDS value in the range of 48,697–148,028 mg/l:

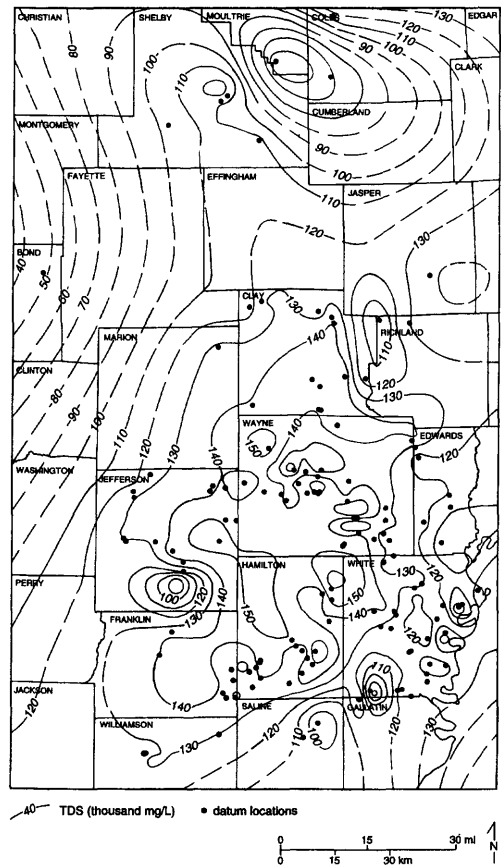


Figure 17–11. Areal distribution of TDS in Aux Vases formation waters (after Demir, 1995; reprinted by permission of the Illinois State Geological Survey).

$$R_{w(T)} = \frac{957}{TDS^{0.778} 1.017^T} \tag{17-45}$$

Once the resistivity is known, Demir (1995) explains that water saturation can be estimated by the Archie (1942) equation. Alternatively, Demir (1995) explains that saturation can also be estimated using the data of TDS and apparent water salinity (AWS) determined by the TDT-K Thermal Decay Timelog technique (Schlumberger, 1989, pp. 128–130). Then, the permeability can be estimated by means of the empirical relationships of porosity, permeability, and water saturation according to Schlumberger (1989, pp. 138–139).

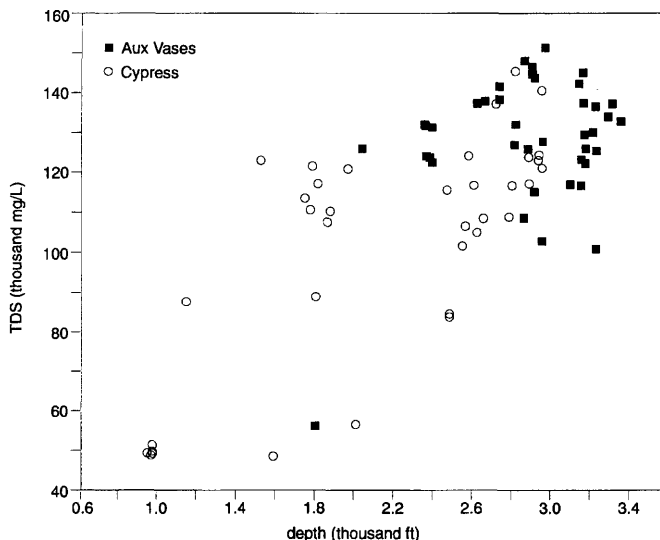


Figure 17-12. Relationship between total dissolved solids (TDS) content and depth of Aux Vases and Cypress formation waters in Illinois (after Demir, 1995; reprinted by permission of the Illinois State Geological Survey).

Formation Damage Potential

Demir (1995) points out that knowledge on formation brines is essential for diagnosis and handling of formation damage problems. Table 17-4 presents the saturation indices of the typical minerals that have potential of precipitating in reservoir formations and boreholes calculated by Demir (1995) at the Aux Vases and Cypress reservoir formation conditions using the Table 17-1 data in the geochemical model SOLMINEQ-88 (Kharaka et al., 1988). For this purpose, Demir (1995) estimated the reservoir fluid temperatures and pressures using a geothermal gradient of 0.67°C per 100 feet (Pollack and Watts, 1976) and a hydraulic potential gradient of 0.465 psi per foot (Dickinson, 1953), respectively.

Table 17-4 data indicate that the majority of the brines are saturated or supersaturated by calcite, barite, and Fe-sulfides. Demir (1995) explains the presence of supersaturation conditions because of the prevention of mineral precipitation by ion effects, ion pairs, and kinetic and activation energy barriers. However, Demir (1995) adds, minerals may precipitate and cause formation damage when temperature, pressure, chemical composition, pH, Eh, and ionic strength are varied during improved recovery processes.

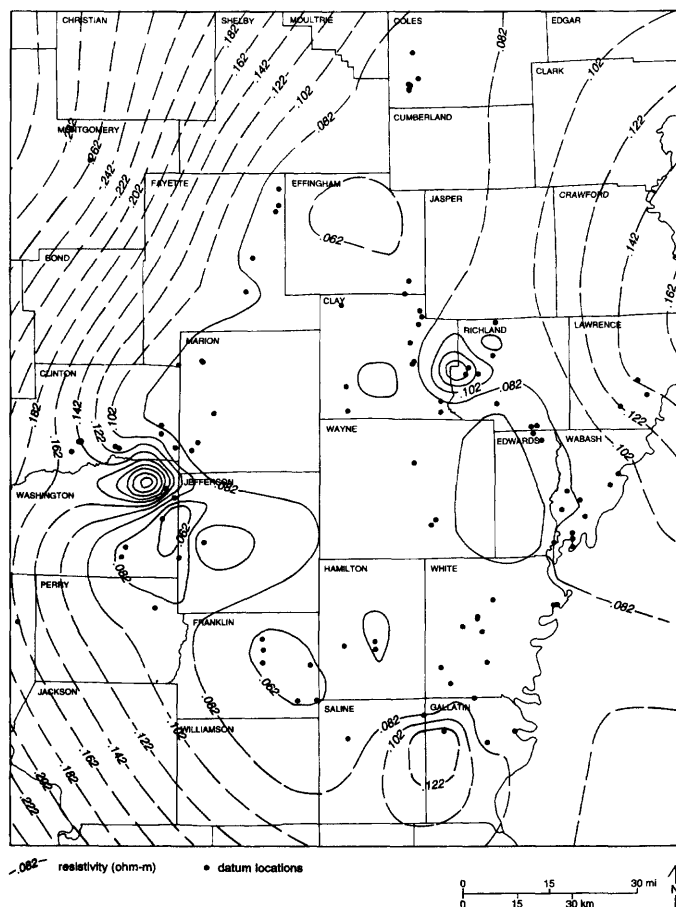


Figure 17-13. Areal distribution of Cypress formation waters resistivities (after Demir, 1995; reprinted by permission of the Illinois State Geological Survey).

Using the reaction path model REACT (Bethke, 1992), Demir (1995) simulated mineral precipitation and/or dissolution and porosity variation scenarios for potential improved oil recovery applications in the Aux Vases and Cypress reservoir formations. Because of incomplete measured data, Demir (1995) made several assumptions and estimations on the formation mineralogy and fluid chemistry, which introduced some uncertainties into the simulations. But, the results are still useful in understanding and estimating the potential formation damaging processes. Typical cases and results presented by Demir (1995) are summarized in the following.

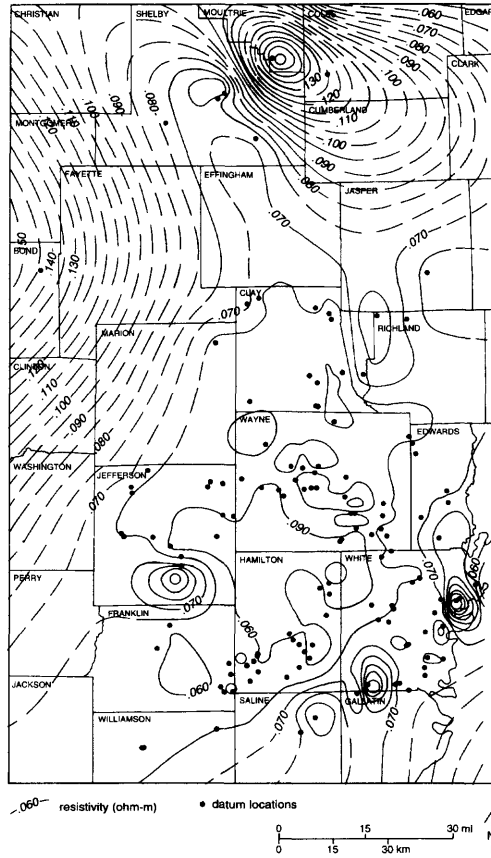


Figure 17-14. Areal distribution of Aux Vases formation waters resistivities (after Demir, 1995; reprinted by permission of the Illinois State Geological Survey).

Acid Treatment of Wells

Demir (1995) simulated the treatment of the Morgan Coal no. 3 well in Energy Field, Williamson County, Illinois using mud-cleaning acids (MCA). Table 17-5 presents the reservoir mineralogy data from a nearby well, the Morgan Coal no. 2 well, used by Demir (1995) for the Morgan Coal no. 3 well. Figure 17-16 by Demir (1995) describes the hypothetical zones around the well considered for simulation of the MCA treatment of the near wellbore formation. Considered for simulation were 7.5 and 15% HCL-MCA solutions containing 0.1 molal KCL (clay stabilizer) and

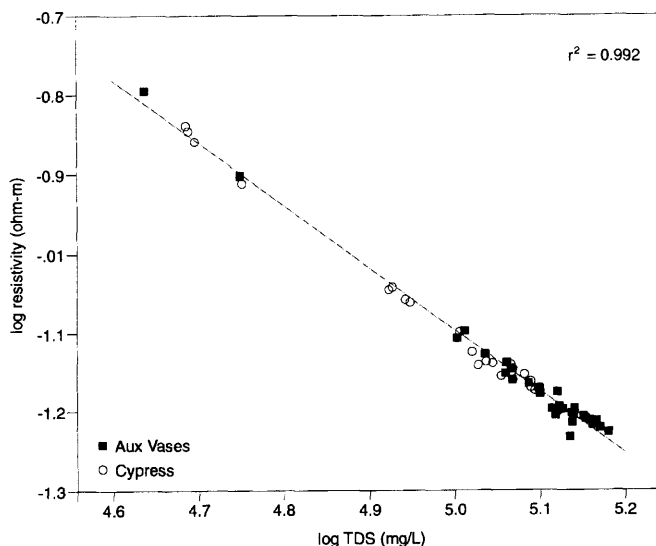


Figure 17-15. Relationship between Aux Vases and Cypress formation water resistivities and TDS. The r^2 is the square of the correlation coefficient (after Demir, 1995; reprinted by permission of the Illinois State Geological Survey).

Table 17-4

Saturation Indexes (SI)^a of Minerals that have the Potential for Formation Damage in Five Aux Vases and Five Cypress Formation Water Samples*

			Saturation indexes				
Sample	Formation	Field	Calcite	Gypsum	Celestite	Barite	Fe-sulfide ^b
EOR-B17	Cypress	Bartelso	0.4	-3.3	-2.8	0.8	2.1, 2.2, 11.0
EOR-B36		Mattoon	0.3	-0.5	-0.5	0.2	2.1, 2.2, 11.5
EOR-B52		Clay City	0.8	-0.3	-0.4	0.0	2.5, 2.6, 11.1
EOR-B73		New Harmony	-0.7	-1.8	-1.5	1.3	2.0, 2.1, 11.4
EOR-B101		Dale Cons.	-0.5	-0.3	-0.3	0.0	2.5, 2.7, 12.1
EOR-B9	Aux Vases	King	0.3	-0.4	-0.3	0.3	1.5, 1.6, 10.6
EOR-B35		Mattoon	0.5	-2.0	-1.6	0.4	2.2, 2.3, 10.7
EOR-B70		Carmi North	-1.0	-0.7	-0.5	0.3	2.0, 2.1, 11.5
EOR-B93		Clay City	0.1	-0.2	-0.3	0.5	2.1, 2.2, 11.3
EOR-B99		Eldorado	0.1	-0.7	-0.3	0.1	2.5, 2.6, 11.7

^a SI>0, supersaturated; SI=0, equilibrium; SI<0, undersaturated.

^b The first, second, and third numbers belong to pyrothite, troilite, and pyrite, respectively.

* See Table 17-1 for detailed information on the samples and text for computation of reservoir temperature and pressure.

After Demir, 1995; reprinted by permission of the Illinois State Geological Survey.

Table 17-5
Mineralogical Composition and Porosity of the Producing Sandstone
Interval in the Morgan Coal No. 2 Well, Energy Field

Depth (ft)	Minerals (wt. %, except the last row)								Porosity
	Illite	Illite/smectite	Chlorite	Quartz	K-feldspar	Plagioclase	Calcite	Other	(%)
-387.6	1.6	0.9	2.4	81	0.0	8.2	6.0	4.7	21.3
-388.4	1.2	1.1	1.9	57	0.2	8.2	31.0	5.7	21.7
-390.1	1.4	0.7	2.5	85	0.6	2.6	6.7	0.6	23.6
-392.7	0.8	0.3	1.7	73	0.2	7.8	17.0	0.4	23.3
-394.7	1.0	0.5	3.0	76	0.4	6.3	13.0	0.0	20.6
-395.2	1.6	0.9	4.1	63	0.0	2.5	27.0	tr	13.6
Average (wt.%)	1.3	0.7	2.6	73	0.2	5.9	16.8	1.9	—
Average (vol.%)	1.3	0.8	2.3	71	0.3	6.0	16.1	1.8	22.0 ^a

^a 22.1 was rounded to 22 in geochemical modeling computations.

tr = trace.

After Demir, 1995; reprinted by permission of the Illinois State Geological Survey.

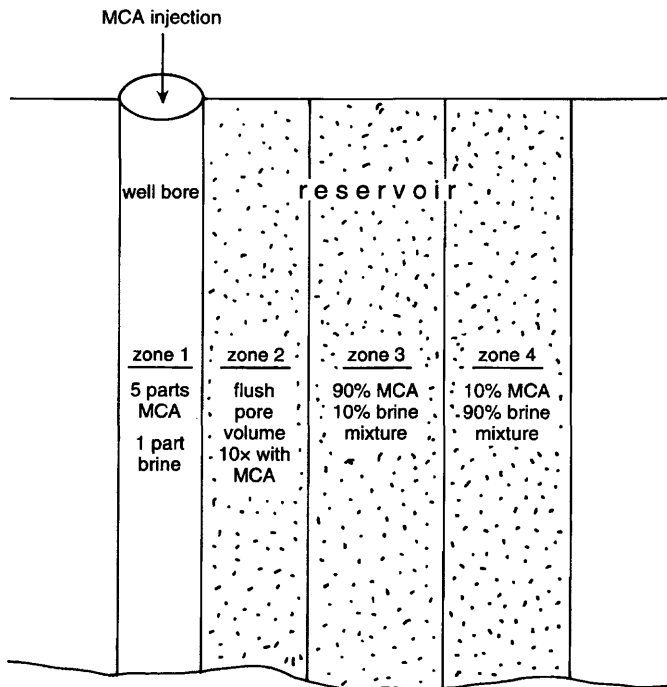


Figure 17-16. Hypothetical zones (not to scale) around an Energy Field well in which reactions were simulated (after Demir, 1995; reprinted by permission of the Illinois State Geological Survey).

the formation brine with the analysis given for sample EOR-B6 in Table 17-1. The reservoir temperature was taken as 36°C.

The simulated changes of the mineral contents in various zones after 2 days of exposure to the treatment fluids are presented in Tables 17-6 and 17-7 by Demir (1995), respectively, for 15 and 7.5% HCL-MCA treatments. Table 17-8 by Demir (1995) shows the predicted pH, and the CO_2 gas and dissolved iron species produced by 7.5 and 15% HCL-MCA treatments. Figures 17-17 and 17-18 by Demir (1995) show the predicted changes in mineral compositions and the fugacity of the produced CO_2 gas, which dissolves in aqueous phase readily at elevated reservoir fluid pressure conditions, for 15% HCL-MCA treatment.

The results of the simulations by Demir (1995) indicate an increase in porosity with either 15% or 7.5% HCL-MCA treatment. Demir (1995) concludes, however, that the probability of asphaltene precipitation is higher with 15% HCL-MCA treatment because of the higher acidity and dissolved iron concentrations in this case compared to 7.5% HCL-MCA treatment.

Waterflooding

Demir (1995) simulated the consequences of waterflooding operations in the Dale consolidated field. Demir (1995) considered the injection and the Aux Vases formation brines with the analyses of samples EOR-B101 and EOR-B107, respectively, given in Table 17-1. The Aux Vases reservoir formation mineralogical composition and porosity were approximated by data obtained from a McCreery no. 1 well core, given in Table 17-9 by Demir (1995). The Aux Vases formation brine pH had to be adjusted to 5.85 to achieve convergence in the simulation, although the actual field measured value was 5.34. The reservoir temperature taken was 37°C. Demir (1995) simulated two different scenarios: (1) replacement of pore water by flushing, and (2) mixing of pore and injection waters.

In the first case, a ten pore volume of injection water was injected to completely flush out the pore water and react with the formation minerals until thermodynamic equilibrium. As can be seen by the simulated results given in Table 17-10 by Demir (1995), the porosity is unaffected and remains constant at 20%, for all practical purposes, when compared with the values given in Table 17-9 by Demir (1995), in spite of the variation of the individual mineral constituents of the formation, as shown in Figure 17-19 by Demir (1995).

In the second case, Demir (1995) simulates the consequences of mixing the injection and pore waters at a ratio of 1:1 and the resultant reactions

(text continued on page 590)

Table 17-6
Mineral Volume Corresponding to Each kg (917 cm³) of
Pore Water (at a 50% water saturation), or 1834 cm³ Total
Pore Volume Before and After Treatment of a Production
Well in Energy Field with 15% HCl-MCA

Mineral	Original volume (cm ³)		Final volume (cm ³)	
	Measured	Predicted	Predicted	Net change ^a
Zone 2				
Quartz	4703	4703	4703	0
Albite	393	393	393	0
Calcite	1060	1057	147	-913
Chlorite	154	123	0	-154
Illite	112	68	0	-112
Smectite	26	67	0	-26
K-feldspar	17	17	0	-17
Kaolinite	0	49	161	+161
Mordenite-K	0	0	115	+115
Pyrite	0	tr	0.1	+0.1
Siderite	0	0	83	+83
Net change in total mineral volume				-863
% Change in total pore volume ^b				+47.1
Final porosity (%) ^c				32.4
Zone 3				
Quartz	4703	4703	4703	0
Albite	393	393	393	0
Calcite	1060	1057	239	-821
Chlorite	154	123	0	-154
Illite	112	68	0	-112
Smectite	26	67	0	-26
K-feldspar	17	17	0	-17
Kaolinite	0	49	161	+161
Mordenite-K	0	0	115	+115
Pyrite	0	tr	0.2	+0.2
Siderite	0	0	84	+84
Net change in total mineral volume				-770
% Change in total pore volume ^b				+42
Final porosity (%) ^c				31.2
Zone 4				
Quartz	4703	4703	4703	0
Albite	393	393	393	0
Calcite	1060	1057	1053	-7
Chlorite	154	123	102	-52
Illite	112	68	92 (muscovite) ^d	-20
Smectite	26	67	90	+64
K-feldspar	17	17	0	-17
Kaolinite	0	49	39	+39
Pyrite	0	tr	0.2	+0.2
Siderite	0	0	2	+2
Strontianite	0	0.3	0.3	+0.3
Net change in total mineral volume				+9.5
% Change in total pore volume ^b				-0.5
Final porosity (%) ^c				21.9

^a Difference between original measured values and values after reaction path ended.

^b (net change in total mineral volume/original total pore volume) x 100.

^c (1 + (% change in total pore volume/100)) x (original porosity).

^d Model assumes muscovite is a proxy for illite.

tr = trace.

After Demir, 1995; reprinted by permission of the Illinois State Geological Survey.

Table 17-7
Mineral Volume Corresponding to Each kg (917 cm³) of
Pore Water (at a 50% water saturation), or 1834 cm³ Total
Pore Volume Before and After Treatment of a Production
Well in Energy Field with 7.5% HCl-MCA

Mineral	Measured	Predicted	Predicted	Net change ^a
Zone 2				
Quartz	4703	4703	4703	0
Albite	393	393	393	0
Calcite	1060	1057	699	-361
Chlorite	154	123	0	-154
Illite	112	68	0	-112
Smectite	26	67	29	+3
K-feldspar	17	17	0	-17
Kaolinite	0	49	165	+165
Mordenite-K	0	0	86	+86
Siderite	0	0	80	+80
Net change in total mineral volume				-310
% Change in total pore volume ^b				+16.9
Final porosity (%) ^c				25.7
Zone 3				
Quartz	4703	4703	4703	0
Albite	393	393	393	0
Calcite	1060	1057	735	-325
Chlorite	154	123	0	-154
Illite	112	68	0	-112
Smectite	26	67	29	+3
K-feldspar	17	17	0	-17
Kaolinite	0	0	161	+161
Mordenite-K	0	0	115	+115
Pyrite	0	tr	0.2	+0.2
Siderite	0	0	90	+90
Net change in total mineral volume				-239
% Change in total pore volume ^b				+13
Final porosity (%) ^c				24.9
Zone 4				
Quartz	4703	4703	4703	0
Albite	393	393	393	0
Calcite	1060	1057	1056	-4
Chlorite	154	123	109	-45
Illite	112	68	90 (muscovite) ^d	-22
Smectite	26	67	87	+61
K-feldspar	17	17	0	-17
Pyrite	0	tr	0.2	+0.2
Kaolinite	0	0	37	+37
Strontianite	0	0.3	0.3	+0.3
Net change in total mineral volume				+10.5
% Change in total pore volume ^b				-0.6
Final porosity (%) ^c				21.9

^a Difference between original measured values and values after reaction path ended.

^b (net change in total mineral volume/original total pore volume) x 100.

^c $(1 + (\% \text{ change in total pore volume}/100)) \times (\text{original porosity})$.

^d Model assumes muscovite is a proxy for illite.

tr = trace.

After Demir, 1995; reprinted by permission of the Illinois State Geological Survey.

Table 17-8
Predicted pH, CO₂ Gas, and Dissolved Iron Species Generated when a Production Well in Energy Field was Treated with MCA

Treatment	Parameter	Concentration		
		Zone 2	Zone 3	Zone 4
15% HCl-MCA	CO ₂ gas fugacity	10 ^{1.9}	10 ^{1.8}	10 ^{-1.9}
	pH	4.21	4.29	6.51
	Fe ⁺⁺ (molal)	0.0072	0.0066	0.0012
	FeCl ₂ (molal)	0.0114	0.0100	0.0010
	FeCl ⁺ (molal)	0.0161	0.0144	0.0020
	Total Fe (molal)	0.0340	0.0310	0.0042
7.5% HCl-MCA	CO ₂ gas fugacity	10 ^{1.5}	10 ^{1.3}	10 ^{-2.0}
	pH	4.50	4.65	6.59
	Fe ⁺⁺ (molal)	0.0047	0.0041	0.0008
	FeCl ₂ (molal)	0.0015	0.0015	0.0006
	FeCl ⁺ (molal)	0.0049	0.0046	0.0012
	Total Fe (molal)	0.0110	0.0100	0.0026

After Demir, 1995; reprinted by permission of the Illinois State Geological Survey.

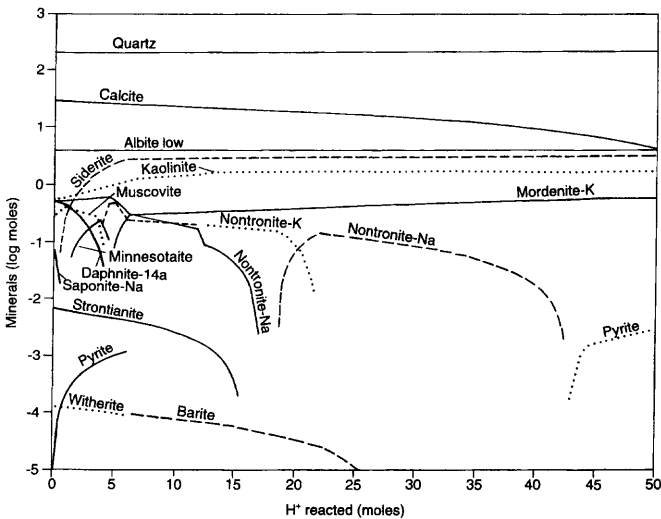


Figure 17-17. Predicted changes in mineralogical compositions along the reaction path when 1 part of pore water is flushed with 10 parts of 15% HCl-MCA in an Energy Field well (after Demir, 1995; reprinted by permission of the Illinois State Geological Survey).

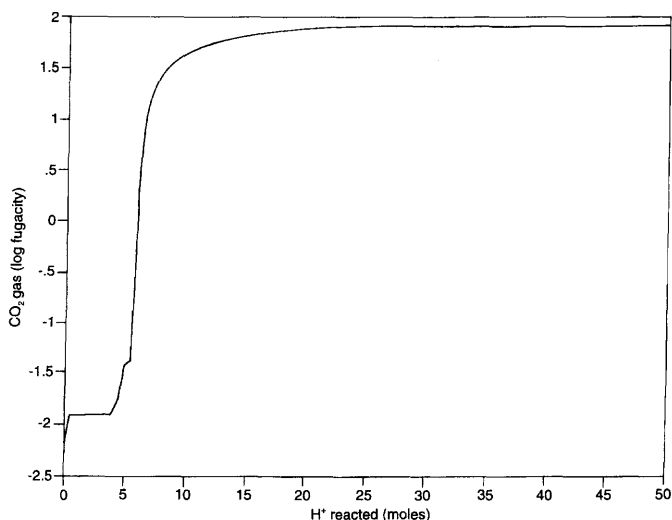


Figure 17-18. Predicted change in CO_2 fugacity along the reaction path when 1 part of pore water is flushed with 10 parts of 15% HCl-MCA in an Energy Field well (after Demir, 1995; reprinted by permission of the Illinois State Geological Survey).

Table 17-9
Mineralogical Composition and Porosity of the Producing Sandstone Interval in McCreery No. 1 Well, Dale Consolidated Field

Depth (ft)	Minerals (wt. %, except the last row)							Porosity
	Illite	Illite/smectite	Chlorite	Quartz	K-feldspar	Plagioclase	Calcite	(%)
-3190.5	3.2	1.4	0.7	84.5	1.3	2.5	6.4	20.4
-3191.5	2.8	1.5	0.7	81.6	1.7	3.2	8.6	23.4
-3192.7	2.5	1.1	0.6	84.9	1.5	3.7	5.6	25.6
-3194.0	3.4	2.5	0.9	79.5	1.2	4.3	8.1	23.6
-3195.7	2.6	1.5	0.7	88	1.9	3.2	2.0	19.8
-3197.9	3.1	1.7	0.8	80.7	2.6	2.6	8.5	24.8
-3199.4	2.1	1.5	0.6	82.5	2.7	3.7	6.8	24.3
-3201.0	3.1	2.3	0.9	82.3	2.6	3.3	5.5	21.4
-3203.0	2.1	2.1	0.4	77.8	1.5	1.9	14.2	18.6
-3205.8	2.4	2.1	0.5	83.7	1.2	2.4	7.6	21.4
-3207.1	3.1	4.2	0.7	67.8	0.8	1.5	21.8	14.5
-3208.4	1.7	1.9	0.5	82.9	1.7	2.8	8.4	13.1
-3209.9	5.2	4.7	1.9	68.4	1.2	1.8	16.8	11.5
Average (wt.%)	2.9	2.2	0.8	80.4	1.5	2.7	9.3	—
Average (vol.%)	2.9	2.1	0.8	80.8	1.6	2.7	9.1	20.0 ^a

^a 20.2 was rounded to 20 in geochemical modeling computations.

After Demir, 1995; reprinted by permission of the Illinois State Geological Survey.

Table 17-10
Mineral Volume Corresponding to Each kg (917 cm³) of Pore Water
(at a 50% water saturation), or 1834 cm³ Total Pore Volume,
Before and After Flushing the Pore Volume Ten Times with Injection
Water in Dale Consolidated Field

Minerals	Original mineral volume (cm ³)		Predicted mineral volume (cm ³) after reaction path	Net change ^a
	Measured	Predicted by model		
Quartz	5853	5894	5937	+84
Albite	193	193	167	-26
Calcite	657	657	656	-1
Chlorite	58	22 (daphnite)	0	-58
Illite	290	176 (muscovite) ^b	331 (muscovite) ^b	+41
Smectite	77	71 (nontronite + saponite)	111 (nontronite + saponite)	+34
K-feldspar	116	116	0	-116
Kaolinite	0	131	38	+ 38
Pyrite	0	tr	1	+1
Strontianite	0	0.1	1	+1
Witherite	0	tr	tr	nd
Net change in total mineral volume				-2
% Change in total pore volume ^c				+0.1
Final porosity (%) ^d				20.0

^a Difference between original measured values and values after reaction path ended.

^b Model assumes muscovite is a proxy for illite.

^c (net change in total mineral volume/original total pore volume) x 100.

^d $(1 + (\% \text{ change in total pore volume}/100)) \times (\text{original porosity})$.

tr = trace, nd = not detectable.

After Demir, 1995; reprinted by permission of the Illinois State Geological Survey.

(text continued from page 585)

until thermodynamic equilibrium. The results presented by Demir (1995) in Table 17-11 indicate a negligible change of porosity from 20 to 20.2%.

In both the 10 times pore volume flush and 1:1 mixture cases, the pH was predicted to remain approximately neutral (Figure 17-20 by Demir, 1995). Therefore, Demir (1995) concludes that asphaltene precipitation, which occurs in acidic media, is not likely during waterflooding, and clay swelling should not occur because the TDS and chemical compositions of the injection and formation brines are similar.

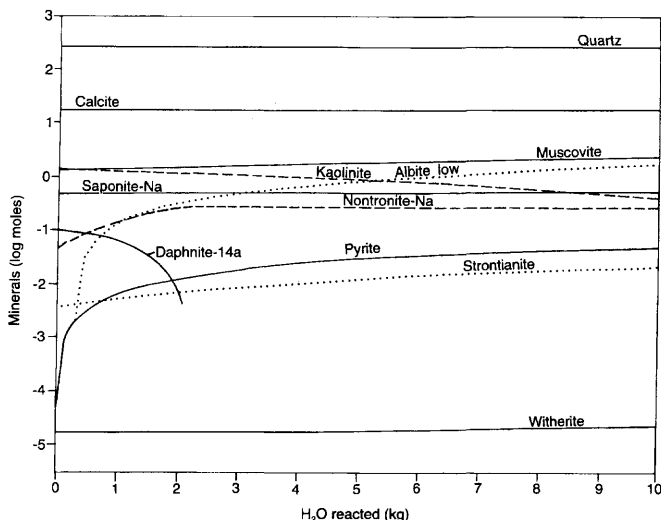


Figure 17-19. Predicted changes in mineral concentrations along the reaction path when 1 part pore water is flushed with 10 parts injection water in the Aux Vases reservoir, Dale Consolidated Field (after Demir, 1995; reprinted by permission of the Illinois State Geological Survey).

Carbon Dioxide Flooding

Demir (1995) simulated the consequences of carbon dioxide flooding in Tamaroa field. Demir (1995) compared the results of two scenarios: (1) reaction of 1 mole of carbon dioxide, and (2) reaction of 5 mole of carbon dioxide with the formation minerals and/or brine until thermodynamic equilibrium. The formation brine was assumed the same as sample EOR-B22 given in Table 17-1 and the average formation mineral composition and porosity were assumed as those given in Table 17-12 by Demir (1995). The reservoir temperature was taken as 32°C.

In the first case, the reaction of 1 mole of carbon dioxide within a formation containing 1 kg of brine was simulated. As can be seen from the results presented in Table 17-13 and Figure 17-21 by Demir (1995), the porosity remain approximately constant, in spite of the changes of the individual mineral constituents. Demir (1995) concludes that pH is above the original pH value of 6.5 (Figure 17-22) making the asphaltene precipitation unlikely and the relatively high TDS should prevent clay swelling.

In the second case, Demir (1995) simulates the reaction of 5 mole of carbon dioxide. The results presented in Table 17-14 and Figure 17-23

Table 17-11
Mineral Volume Corresponding to Each kg (917 cm³) of Pore Water
(at a 50% water saturation), or 1834 cm³ Total Pore Volume,
Before and After Mixing Injection and Formation Waters at a 1:1
Ratio in Dale Consolidated Field

Minerals	Original mineral volume (cm ³)		Predicted mineral volume (cm ³) after reaction path	Net change ^a
	Measured	Predicted by model		
Quartz	5853	5894	5948	+95
Albite	193	193	184	-9
Calcite	657	657	657	0
Chlorite	58	22 (daphnite)	26	-32
Illite	290	176 (muscovite) ^b	327 (muscovite) ^b	+37
Smectite	77	71 (nontronite + saponite)	65 (saponite)	-12
				-12
K-feldspar	116	116	0	-116
Kaolinite	0	131	28	+28
Pyrite	0	tr	0.4	+0.4
Strontianite	0	0.1	0.2	+0.2
Witherite	0	tr	tr	nd
Net change in total mineral volume				-20.4
% Change in total pore volume ^c				+1.1
Final porosity (%) ^d				20.2

^a Difference between original measured values and values after reaction path ended.

^b Model assumes muscovite is a proxy for illite.

^c (net change in total mineral volume/original total pore volume) x 100.

^d (1 + (% change in total pore volume/100)) x (original porosity).

tr = trace, nd = not detectable.

After Demir, 1995; reprinted by permission of the Illinois State Geological Survey.

by Demir (1995) indicate a reduction of porosity from 19 to 18.4%. Based on the simulated pH variation given in Figure 17-22, Demir (1995) concludes that decreased pH values may initiate asphaltene precipitation, but the peptizing effects of resins (about 10-18% present in the oil) minimizes the possibility of asphaltene precipitation.

Alkali Flooding

Demir (1995) simulated the consequences of alkali flooding in Tamaroa field. Demir (1995) considered the same formation minerals and brine information used in the carbon dioxide flooding. Three alkali solutions were considered: (1) 0.5 mole of $NaOH$, (2) 0.25 mole of Na_2CO_3 , and (3) 0.25 mole of Na_2SiO_3 . Simulations were carried out for 30 days

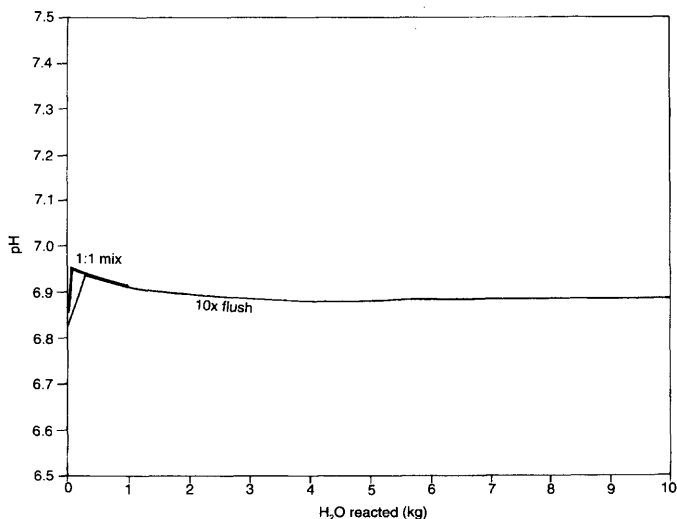


Figure 17-20. Predicted change in pH along the reaction path when 1 part of pore water is flushed with 10 parts of injection fluid and when pore and injection waters are mixed at a 1:1 ratio in the Aux Vases reservoir, Dale Consolidated Field (after Demir, 1995; reprinted by permission of the Illinois State Geological Survey).

Table 17-12
Mineralogical Composition and Porosity of Producing Sandstone
Interval in Stockton No. 1 Well, Tamaroa Field

Depth (ft)	Minerals (wt. %, except the last row)							Porosity
	Illite	Illite/smectite	Kaolinite	Chlorite	Quartz	Plagioclase	Calcite	(%)
-1155.5	tr	tr	0.6	0.2	98	0.5	0.4	21.5
-1160.5	0.3	0.2	3.5	1.6	90	4.1	0.1	20.7
-1163.5	0.5	0.8	3.7	3.1	77	9.8	4.6	15.8
-1165.5	tr	tr	0.5	0.3	97	1.8	0.2	19.3
Average (wt.%)	0.2	0.3	2.9	1.3	90.5	4.1	1.3	—
Average (vol.%)	0.3	0.3	2.9	1.1	90	4.2	1.3	19.0 ^a

^a In geochemical modeling computations 19.3 was rounded to 19.

tr = trace.

After Demir, 1995; reprinted by permission of the Illinois State Geological Survey.

Table 17-13
Mineral Volume Corresponding to Each kg (943 cm³) of Pore Water
(at a 40% water saturation), or a Total Pore Volume of 2358 cm³,
Before and After the Reaction of 1 mol CO₂ Gas with the Cypress
Reservoir in Tamaroa Field

Minerals	Original mineral volume (cm ³)		Predicted mineral volume (cm ³) after reaction path	Net change ^a
	Measured	Predicted by model		
Quartz	9045	9045	9045	0
Albite	423	423	423	0
Calcite	132	132	133	+1
Chlorite ^b	103	47 (daphnite)	4 (daphnite)	-99
Kaolinite	291	273	303	+12
Illite ^b	22	13 (muscovite) ^c	13 (muscovite) ^c	-9
Smectite ^b	9	67 (nontronite	64 (saponite) + saponite)	+55
Gibbsite	0	33	23	+23
Dawsonite	0	0	5	+5
Siderite	0	0	26	+26
Pyrite	0	tr	0.2	+0.2
Strontianite	0	0.1	0.1	+0.1
Witherite	0	tr	tr	nd
Net change in total mineral volume				+14.3
% Change in total pore volume ^d				-0.6
Final porosity (%) ^e				18.9

^a Difference between original measured values and values after reaction path ended.

^b The original measured volumes of these minerals were adjusted somewhat to make the simulation runs converge (compare the first and second columns of this table to those of table 11).

^c Model assumes muscovite is a proxy for illite.

^d (net change in total mineral volume/original total pore volume) x 100.

^e (1 + (% change in total pore volume/100)) x (original porosity).

tr = trace, nd = not detectable.

After Demir, 1995; reprinted by permission of the Illinois State Geological Survey.

following an injection of ten pore volumes of alkali solutions to flush out the pore water. The results are presented in Tables 17-15 through 17-17, and Figures 17-24 through 17-26 for the NaOH, Na₂SiO₃ and Na₂CO₃ alkaline floods, respectively. The average porosity decreased from 19% to 18.6, 17.7 and 17.7% for the NaOH, Na₂SiO₃ and Na₂CO₃ alkaline floods, respectively.

As shown in Figure 17-27 by Demir (1995), the aqueous phase Na⁺ activity available for improved oil recovery was reduced significantly

(text continued on page 603)

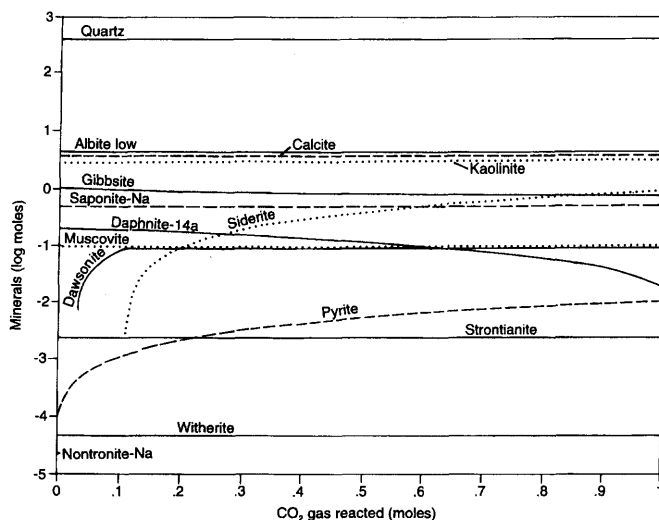


Figure 17-21. Predicted changes in mineral concentrations along the reaction path when the Cypress reservoir is flooded with 1 mol CO₂ solution in Tamaroa Field (after Demir, 1995; reprinted by permission of the Illinois State Geological Survey).

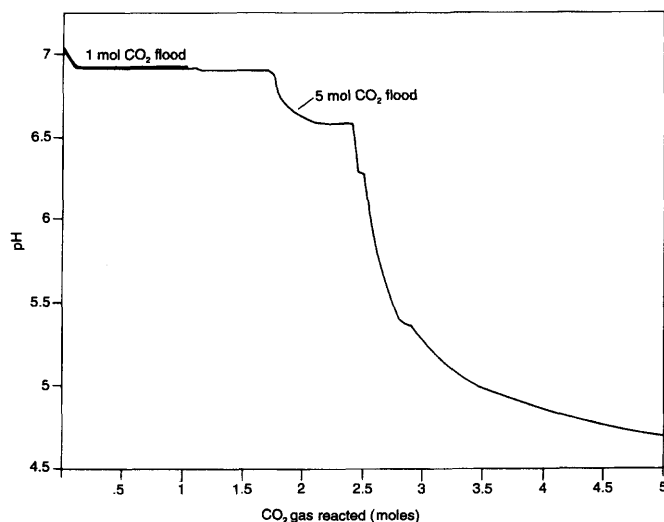


Figure 17-22. Predicted change in pH along the reaction path when the Cypress reservoir is flooded with 1 mol and 5 mol CO₂ solutions in Tamaroa Field (after Demir, 1995; reprinted by permission of the Illinois State Geological Survey).

Table 17-14
Mineral Volume Corresponding to Each kg (943 cm³) of Pore Water
(at a 40% water saturation), or a Total Pore Volume of 2358 cm³,
Before and After the Reaction of 5 mol CO₂ Gas with the Cypress
Reservoir in Tamaroa Field

Minerals	Original mineral volume (cm ³)		Predicted mineral volume (cm ³) after reaction path	Net change ^a
	Measured	Predicted by model		
Quartz	9045	9045	9045	0
Albite	423	423	423	0
Calcite	132	132	121	-11
Chlorite ^b	103	47 (daphnite)	0	-103
Kaolinite	291	273	293	+2
Illite ^b	22	13 (muscovite) ^c	0	-22
Smectite ^b	9	67 (nontronite + saponite)	0	-9
Gibbsite	0	33	0	
Clinoptilolite	0	0	76	+76
Dawsonite	0	0	61	+61
Siderite	0	0	28	+28
Magnesite	0	0	30	+30
Mordenite	0	0	20	+20
Pyrite	0	tr	0.2	+0.2
Strontianite	0	0.1	0.1	+0.1
Witherite	0	tr	tr	nd
Net change in total mineral volume				+72.3
% Change in total pore volume ^d				-3.1
Final porosity (%) ^e				18.4

^a Difference between original measured values and values after reaction path ended.

^b The original measured volumes of these minerals were adjusted somewhat to make the simulation runs converge (compare the first and second columns of this table to those of table 11).

^c Model assumes muscovite is a proxy for illite.

^d (net change in total mineral volume/original total pore volume) x 100.

^e (1 + (% change in total pore volume/100)) x (original porosity).

tr = trace, nd = not detectable.

After Demir, 1995; reprinted by permission of the Illinois State Geological Survey.

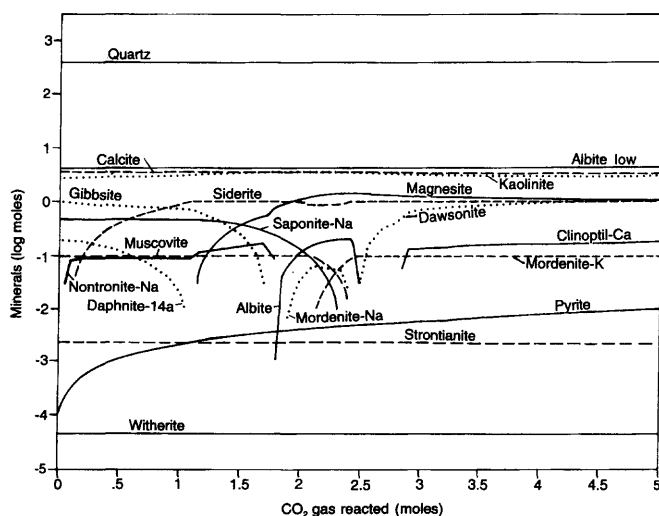


Figure 17-23. Predicted changes in mineral concentrations along the reaction path when the Cypress reservoir is flooded with 5 mol CO₂ solution in Tamaroa Field (after Demir, 1995; reprinted by permission of the Illinois State Geological Survey).

Table 17-15
Mineral Volume Corresponding to Each kg (943 cm³) of Pore Water
(at a 40% water saturation), or a Total Pore Volume of 2358 cm³,
Before and After the Reaction of 0.5 mol NaOH Solution with the
Cypress Reservoir in Tamaroa Field

Minerals	Original mineral volume (cm ³)		Predicted mineral volume (cm ³) after reaction path	Net change ^a
	Measured	Predicted by model		
Quartz	9045	9045	9045	0
Albite	423	423	423	0
Calcite	132	132	104	-28
Chlorite ^b	103	47 (daphnite)	93 (daphnite + ripidolite)	-10
Kaolinite	291	273	0	-291
Illite ^b	22	13 (muscovite) ^c	0	-22
Smectite ^b	9	67 (nontronite + saponite)	0	-9
Prehnite	0	0	53	+53
Analcime	0	0	261	+261
Phlogopite	0	0	14	+14
Gibbsite	0	33	82	+82
Pyrite	0	tr	0	
Strontianite	0	0.1	0.1	+0.1
Witherite	0	tr	tr	nd
Net change in total mineral volume				+50.1
% Change in total pore volume ^d				-2.1
Final porosity (%) ^e				18.6

^a Difference between original measured values and values after reaction path ended.

^b The original measured volumes of these minerals were adjusted somewhat to make the simulation runs converge (compare the first and second columns of this table to those of table 11).

^c Model assumes muscovite is a proxy for illite.

^d (net change in total mineral volume/original total pore volume) x 100.

^e (1 + (% change in total pore volume/100)) x (original porosity).

tr = trace, nd = not detectable.

After Demir, 1995; reprinted by permission of the Illinois State Geological Survey.

Table 17-16
Mineral Volume Corresponding to Each kg (943 cm³) of Pore Water
(at a 40% water saturation), or a Total Pore Volume of 2358 cm³,
Before and After the Reaction of 0.25 mol Na₂SiO₃ Solution with the
Cypress Reservoir in Tamaroa Field

Minerals	Original mineral volume (cm ³)		Predicted mineral volume (cm ³) after reaction path	Net change ^a
	Measured	Predicted by model		
Quartz	9045	9045	9045	0
Albite	423	423	423	0
Calcite	132	132	123	-9
Chlorite ^b	103	47 (daphnite)	93 (Ripidolite + clinocllore)	-10
Kaolinite	291	273	0	-291
Illite ^b	22	13 (muscovite) ^c	0	-22
Smectite ^b	9	67 (nontronite + saponite)	0	-9
Analcime	0	0	421	+421
Prehnite	0	0	17	+17
Phlogopite	0	0	14	+14
Gibbsite	0	33	54	+54
Pyrite	0	tr	0.2	+0.2
Strontianite	0	0.1	0.1	+0.1
Witherite	0	tr	tr	nd
Net change in total mineral volume				+165.3
% Change in total pore volume ^d				-7.0
Final porosity (%) ^e				17.7

^a Difference between original measured values and values after reaction path ended.

^b The original measured volumes of these minerals were adjusted somewhat to make the simulation runs converge (compare the first and second columns of this table to those of table 11).

^c Model assumes muscovite is a proxy for illite.

^d (net change in total mineral volume/original total pore volume) x 100.

^e (1 + (% change in total pore volume/100)) x (original porosity).

tr = trace, nd = not detectable.

After Demir, 1995; reprinted by permission of the Illinois State Geological Survey.

Table 17-17
Mineral Volume Corresponding to Each kg (943 cm³) of Pore Water
(at a 40% water saturation), or a Total Pore Volume of 2358 cm³,
Before and After the Reaction of 0.25 mol Na₂CO₃ Solution with the
Cypress Reservoir in Tamaroa Field

Minerals	Original mineral volume (cm ³)		Predicted mineral volume (cm ³) after reaction path	Net change ^a
	Measured	Predicted by model		
Quartz	9045	9045	9045	0
Albite	423	423	423	0
Calcite	132	132	134	+2
Chlorite ^b	103	47 (daphnite)	47 (daphnite)	-56
Kaolinite	291	273	38	-253
Illite ^b	2	13 (muscovite) ^c	13	+11
Smectite ^b	9	67 (nontronite + saponite)	69 (saponite)	+60
Dawsonite	0	0	130	+130
Analcime	0	0	226	+226
Gibbsite	0	33	39	+39
Rhodochrosite	0	0	tr	
Pyrite	0	tr	0.2	+0.2
Strontianite	0	0.1	0.1	+0.1
Witherite	0	tr	tr	tr
Net change in total mineral volume				+159.3
% Change in total pore volume ^d				-6.7
Final porosity (%) ^e				17.7

^a Difference between original measured values and values after reaction path ended.

^b The original measured volumes of these minerals were adjusted somewhat to make the simulation runs converge (compare the first and second columns of this table to those of table 11).

^c Model assumes muscovite is a proxy for illite.

^d (net change in total mineral volume/original total pore volume) x 100

^e (1 + (% change in total pore volume/100)) x (original porosity)

tr = trace.

After Demir, 1995; reprinted by permission of the Illinois State Geological Survey.

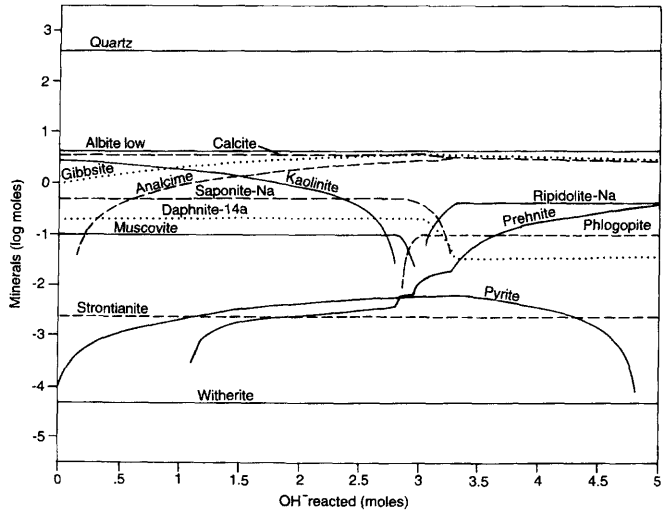


Figure 17-24. Predicted changes in mineral concentrations along the reaction path when the Cypress reservoir is flooded with 0.5 mol NaOH solution in Tamaroa Field (after Demir, 1995; reprinted by permission of the Illinois State Geological Survey).

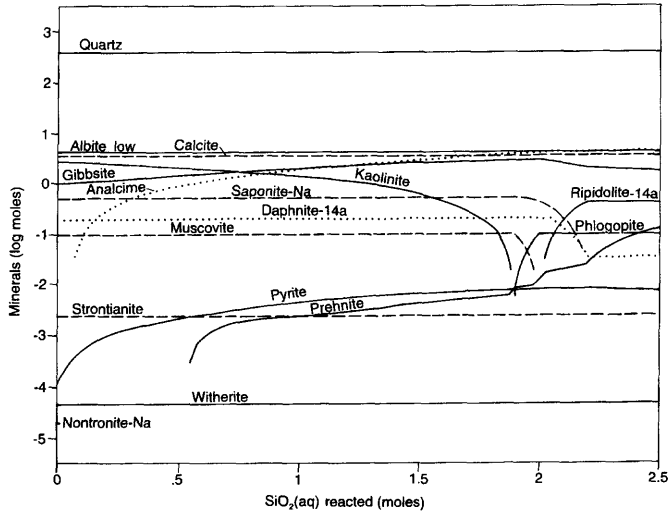


Figure 17-25. Predicted changes in mineral concentrations along the reaction path when the Cypress reservoir is flooded with 0.25 mol Na_2SiO_3 solution in Tamaroa Field (after Demir, 1995; reprinted by permission of the Illinois State Geological Survey).

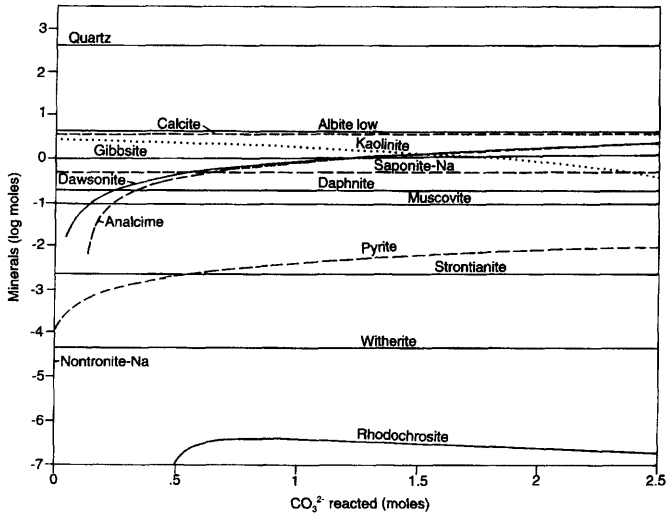


Figure 17-26. Predicted changes in mineral concentrations along the reaction path when the Cypress reservoir is flooded with 0.25 mol Na_2CO_3 solution in Tamaroa Field (after Demir, 1995; reprinted by permission of the Illinois State Geological Survey).

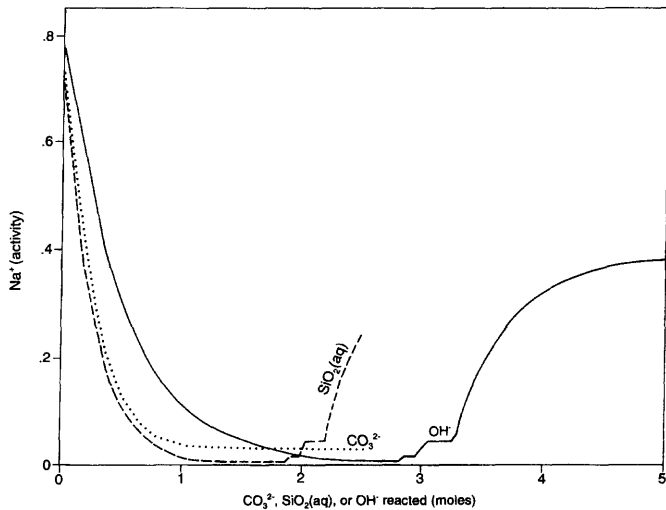


Figure 17-27. Predicted change in Na^+ activity along the reaction path when the Cypress reservoir is flooded with three types of alkali solutions (0.5 mol NaOH , 0.25 mol Na_2SiO_3 , or 0.25 mol Na_2CO_3) in Tamaroa Field (after Demir, 1995; reprinted by permission of the Illinois State Geological Survey).

(text continued from page 594)

by dissolution and/or precipitation reactions during alkaline flooding. However, more Na^+ activity remains during the $NaOH$ flooding. Therefore, Demir (1995) concludes that the $NaOH$ flooding is preferred over the Na_2SiO_3 and Na_2CO_3 flooding. Because of the increased pH, asphaltene precipitation is not likely. Clay swelling is not a concern for the $NaOH$ and Na_2SiO_3 flooding. However, clay swelling is likely for the Na_2CO_3 flooding because of the reduction of TDS to below the original TDS content of the formation water.

Demir (1995) warns that "because natural processes are complex, extreme caution should be taken when geochemical modeling is used for prediction purposes."

References

- Amaefule, J. O., Kersey, D. G., Norman, D. L., & Shannon, P. M., "Advances in Formation Damage Assessment and Control Strategies", CIM 88-39-65 paper, Proceedings of the 39th Annual Technical Meeting of Petroleum Society of CIM and Canadian Gas Processors Association, June 12-16, 1988, Calgary, Alberta, 16 p.
- Baghdikian, S. Y., Sharma, M. M., & Handy, L. L., Flow of Clay Suspensions Through Porous Media, *SPE Reservoir Engineering*, Vol. 4., No. 2., May 1989, pp. 213-220.
- Bethke, C. M., *Geochemical Reaction Modeling, Concepts and Application*, Oxford University Press, New York, 1996, 397 p.
- Bu, T., & Damsleth, E., "Errors and Uncertainties in Reservoir Performance Predictions," *SPE Formation Evaluation*, September 1996, pp. 194-200.
- Chang, F. F., & Civan, F., "Modeling of Formation Damage due to Physical and Chemical Interactions between Fluids and Reservoir Rocks," SPE 22856 paper, Proceedings of the 66th Annual Technical Conference and Exhibition of the Society of Petroleum Engineers, October 6-9, 1991, Dallas, Texas.
- Chang, F. F., & Civan, F., "Predictability of Formation Damage by Modeling Chemical and Mechanical Processes," SPE 23793 paper, Proceedings of the SPE International Symposium on Formation Damage Control, February 26-27, 1992, Lafayette, Louisiana, pp. 293-312.
- Chang, F. F., & Civan, F., "Practical Model for Chemically Induced Formation Damage," *J. of Petroleum Science and Engineering*, Vol. 17, No. 1/2, February 1997, pp. 123-137.
- Chapra, S. C., & Canale, R. P., *Numerical Methods for Engineers*, 3rd ed., McGraw-Hill, Inc., 1998, Boston, 924 p.

- Civan, F., "Review of Methods for Measurement of Natural Gas Specific Gravity," SPE 19073 paper, Proceedings of the SPE Gas Technology Symposium, June 7–9, 1989, Dallas, Texas, pp. 173–186.
- Civan, F., Knapp, R. M., & Ohen, H. A., "Alteration of Permeability by Fine Particle Processes," *J. Petroleum Science and Engineering*, Vol. 3, Nos. 1/2, October 1989, pp. 65–79.
- Civan, F., Predictability of Formation Damage: An Assessment Study and Generalized Models, Final Report, U.S. DOE Contract No. DE-AC22-90-BC14658, April 1994.
- Civan, F., "A Multi-Purpose Formation Damage Model," SPE 31101, Proceedings of the SPE Formation Damage Symposium, Lafayette, Louisiana, February 14–15, 1996, pp. 311–326.
- Civan, F., "Incompressible Cake Filtration: Mechanism, Parameters, and Modeling," *AIChE J.*, Vol. 44, No. 11, November 1998, pp. 2379–2387.
- Cook, A. R., *Introduction to Engineering*, ENGR 1113 Class Notes, Civil Engineering and Environmental Science, University of Oklahoma, 1980.
- Demir, I., "Formation Water Chemistry and Modeling of Fluid-Rock Interaction for Improved Oil Recovery in Aux Vases and Cypress Formations," Department of Natural Resources, Illinois State Geological Survey, Illinois Petroleum Series 148, 1995, 60 p.
- Demir, I. and Seyler, B., "Chemical Composition and Geological History of Saline Waters in Aux Vases and Cypress Formations, Illinois Basin," *Aquatic Geochemistry*, Vol. 5, pp. 281–311, 1999.
- Duda, J. L., "A Random Walk in Porous Media," *Chemical Engineering Education Journal*, Summer 1990, pp. 136–144.
- Frenklach, M., & Miller, D. L., "Statistically Rigorous Parameter Estimation in Dynamic Modeling Using Approximate Empirical Model," *AIChE Journal*, Vol. 31, No. 3, March 1985, pp. 498–500.
- Gadiyar, B., & Civan, F., "Acidization Induced Formation Damage—Experimental and Modeling Studies," SPE 27400 paper, Proceedings of the 1994 SPE Formation Damage Control Symposium, February 9–10, 1994, Lafayette, Louisiana, pp. 549–560.
- Gruesbeck, C., & Collins, R. E., "Entrainment and Deposition of Fine Particles in Porous Media," *SPEJ*, December 1982, pp. 847–856.
- Haggerty, D. J., & Seyler, B., "Investigation of Formation Damage from Mud Cleanout Acids and Injection Waters in Aux Vases Sandstone Reservoirs," Department of Natural Resources, Illinois State Geological Survey, Illinois Petroleum Series 152, 1997, 40 p.
- ISGS Oil and Gas Section, "Improved and Enhanced Oil Recovery Through Reservoir Characterization: Standard Operating and QA/QC Procedures," Illinois State Geological Survey, Open File Series 1993–13.

- Khilar, K. C., & Fogler, H. S., "Colloidally Induced Fines Migration in Porous Media," in Amundson, N. R. & Luss, D. (Eds.), *Reviews in Chemical Engineering*, Vol. 4, Nos. 1 and 2, Freund Publishing House LTD., London, England, January-June 1987, pp. 41-108.
- Ku, H. K., "Precision Measurement and Calibration," *National Bureau of Standards*, Special Publication 300, Vol. 1, 1969, Washington, pp. 331-341.
- Leetaru, H. E., "Application of Old Electrical Logs in the Analysis of Aux Vases Sandstone (Mississippian) Reservoirs in Illinois," Illinois State Geological Survey, Illinois Petroleum Series 134, 1990, 21 p.
- Lehr, W., Calhoun, D., Jones, R., Lewandowski, A., & Overstreet, R., "Model Sensitivity Analysis in Environmental Emergency Management: A Case Study in Oil Spill Modeling," Proceedings of the 1994 Winter Simulation Conference, J. D. Tew, S. Manivannan, D. A. Sadowski, and A. F. Seila (eds.), 1994, pp. 1198-1205.
- Liu, X., & Civan, F., "Formation Damage by Fines Migration Including Effects of Filter Cake, Pore Compressibility and Non-Darcy Flow—A Modeling Approach to Scaling from Core to Field," SPE 28980 paper, SPE International Symposium on Oilfield Chemistry, February 14-17, 1995, San Antonio, TX.
- Liu, X., & Civan, F., "Formation Damage and Filter Cake Buildup in Laboratory Core Tests: Modeling and Model-Assisted Analysis," *SPE Formation Evaluation J.*, Vol. 11, No. 1, March 1996, pp. 26-30.
- Luckert, K., "Model Selection Based on Analysis of Residue Dispersion, Using Solid-Liquid Filtration as an Example," *International Chemical Engineering*, Vol. 34, No. 2, April 1994, pp. 213-224.
- Marquardt, D. W., "An Algorithm for Least Squares Estimation of Nonlinear Parameters," *SIAM J. Appl. Math.*, Vol. 11, 1963, pp. 431-441.
- Mickley, H. S., Sherwood, T. K., & Reed, C. E., *Applied Mathematics in Chemical Engineering*, 1957, McGraw-Hill, New York, pp. 49-52.
- Millan-Arcia, E., & Civan, F., "Characterization of Formation Damage by Particulate Processes," *J. Canadian Petroleum Technology*, Vol. 31, No. 3, March 1992, pp. 27-33.
- Miller, D., & Frenklach, M., "Sensitivity Analysis and Parameter Estimation in Dynamic Modeling of Chemical Kinetics," *International Journal of Chemical Kinetics*, Vol. 15, 1983, pp. 677-696.
- Ohen, H. A., & Civan, F., "Simulation of Formation Damage in Petroleum Reservoirs," SPE 19420 paper, Proceedings of the 1990 SPE Symposium on Formation Damage Control, Lafayette, Louisiana, Feb. 22-23, 1990, pp. 185-200.
- Reilly, P. M., "A Statistical Look at Significant Figures," *Chemical Engineering Education*, Summer 1992, pp. 152-155.

- Schenck, H., Jr., *Theories of Engineering Experimentation*, 1961, McGraw-Hill, New York.
- Schlumberger Log Interpretation Charts for 1989*, Schlumberger Education Services, 1989, Houston, Texas, 150 p.
- Seyler, B., "Geologic and Engineering Controls on Aux Vases Sandstone Reservoirs in Zeigler Field, Illinois—A Comprehensive Study of a Well-Managed Oil Field," Illinois Petroleum Series 153, 1998, Department of Natural Resources, Illinois State Geological Survey, 79 p.
- Sharma, M. M., & Yortsos, Y. C., "Fines Migration in Porous Media," *AIChE J.*, Vol. 33, No. 10, 1987, pp. 1654–1662.
- Spiegel, M. R., *Theory and Problems of Statistics*, 1961, Schaum Publ. Co., New York, p. 71.
- Szucs, P., & Civan, F., "Multi-Layer Well Log Interpretation Using the Simulated Annealing Method," *J. Petroleum Science and Engineering*, Vol. 14, Nos. 3/4, May 1996.
- Ucan, S., Civan, F., & Evans, R. D., "Uniqueness and Simultaneous Predictability of Relative Permeability and Capillary Pressure by Discrete and Continuous Means," *J. of Canadian Petroleum Technology*, Vol. 36, No. 4, pp. 52–61, 1997.
- Vitthal, S., Sharma, M. M., & Sepehrnoori, K., "A One-Dimensional Formation Damage Simulator for Damage Due to Fines Migration," SPE 17146 paper, Proceedings of the SPE Formation Damage Control Symposium, Bakersfield, California, February 8–9, 1988, pp. 29–42.
- Willhite, G. P., Green, D. W., Thiele, J. L., McCool, C. S., & Mertes, K. B., "Gelled Polymer Systems for Permeability Modification in Petroleum Reservoirs, Final Report," Contract No. DE-FG07-89 ID12846, U.S. Department of Energy, Bartlesville, Oklahoma, September 1991.
- Ziauddin, M., Berndt, O., & Robert, J., "An Improved Sandstone Acidizing Model: The Importance of Secondary and Tertiary Reactions," SPE 54728 paper, Proceedings of the 1999 SPE European Formation Damage Conference, May 31–June 1, 1999, The Hague, The Netherlands, pp. 225–237.

Part VI

Formation Damage Models for Field Applications

**Fluids and Solids
Invasion, Sand
Production, and
Scale Formation**

Chapter 18

Drilling Mud Filtrate and Solids Invasion and Mudcake Formation

Summary

Near wellbore mud filtrate and fines invasion during drilling operations and the resulting formation damage and filtercake formation are amongst the most important problems involving the petroleum reservoir exploitation. This chapter reviews the fundamental processes and their mathematical formulation necessary to develop models that can be used for assessment of the damaged zone, filtrate and fines concentrations, fluid saturations, and the filtercake thickness and permeability alteration during drilling. The effects of under and over balance drilling on near wellbore formation damage are discussed. The models for simulation of the single and two-phase flow situations in the formation with water or oil based drilling mud cases are described. External particle invasion prior to filtercake buildup and its effect on the formation damage by particle invasion and retention and filtercake formation are described. These models are demonstrated by various applications. The models presented here can be used for accurate estimation of the near wellbore fluid saturations and resistivity profiles, which are necessary for accurate well-log interpretation.

Introduction

As illustrated in Figure 18–1 by Yao and Holditch (1993), drilling of wells into subsurface reservoirs is usually accompanied with mud circulation in order to remove the frictional heat generated as the drill bit penetrates the rock, to provide a lubrication for reduction of the frictional

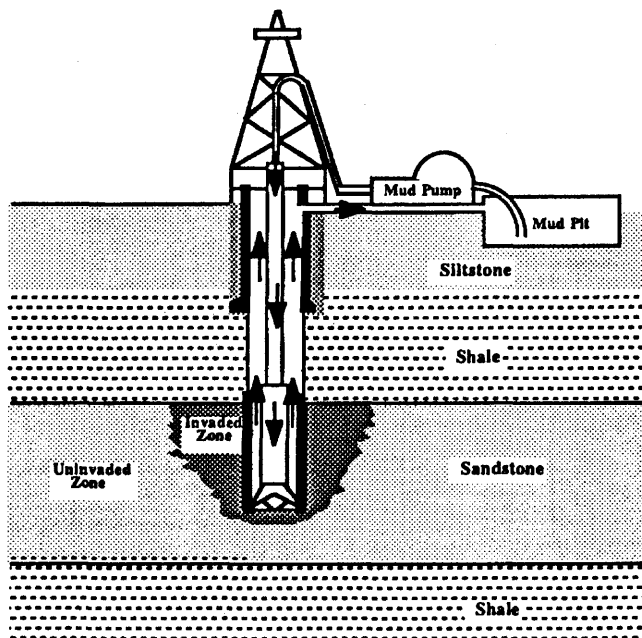


Figure 18–1. Mud filtrate invasion in the near-wellbore formation (after Yao and Holditch, ©1993 SPE; reprinted by permission of the Society of Petroleum Engineers).

effects, and to transport the cuttings of the rock produced during drilling. However, mud fines and filtrates can invade and damage the near wellbore formation as depicted in Figure 18–1. Typical drilling muds may be water-based, oil-based, or water-oil emulsion types. Usually, certain types of fine solid particles are added as weighting agents. Drilling muds are usually non-Newtonian fluids (Briscoe et al., 1994). As shown in Figure 18–2 using the data by Simpson (1974), the depth of filtrate invasion strongly depends on the type of muds. As can be seen, the depth of invasion is less with oil-based muds, more with water-based muds, and in between with emulsion muds applied to a water-wet formation.

Drilling of wells may be accomplished by overbalanced or underbalanced drilling techniques. As explained by Bennion et al. (1995), both techniques have certain advantages and disadvantages. In the overbalanced drilling, the downhole pressure of the circulating mud is maintained above the reservoir fluid pressure to prevent the reservoir fluids entering into the wellbore. Bennion et al. (1995) state that overbalanced drilling is more common because the downhole pressures of the conventional muds are usually higher than typical reservoir fluid pressures. Consequently, the

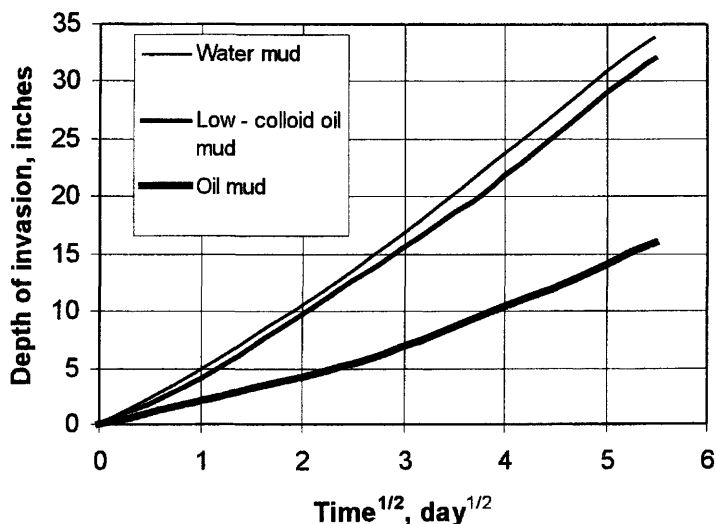


Figure 18–2. Depth of filtrate invasion data of Simpson (1974) plotted against the square root of time for different muds.

overbalance pressure forces the mud filtrate and solids to invade and damage the near wellbore formation and eventually form a protective sealing filtercake over the formation face. This problem can be alleviated by underbalanced drilling. Bennion et al. (1995) state that underbalanced drilling can be accomplished naturally using unweighted drilling muds in geostatically overpressured reservoirs or using oil-based muds, which are lighter than the water-based muds or foamed muds. As a result, forced invasion of mud filtrate and fines into the near wellbore formation is prevented. Bennion et al. (1995) explains that underbalanced drilling is particularly advantageous for high permeability, naturally fractured, and heterogeneous formations and for clayey formations that are sensitive to chemicals. However, they explain that underbalanced drilling does not completely eliminate the formation damage, because underbalanced conditions cannot be maintained at all times during drilling, some drilling fluids can still enter the near wellbore formation by spontaneous imbibition, and the formation face can be damaged due to insufficient lubrication and turbulence, and inefficient cooling. For these reasons, the protective sealing filtercake formed during overbalanced drilling is still beneficial.

As shown in Figure 18–3 by Yao and Holditch (1993), the mud filtrate invading the near wellbore formation mixes with and/or displaces the reservoir fluids (Civan, 1994, 1996; Phelps, 1995; Bilardo et al., 1996). As a result, a damaged zone is created around the wellbore (Liu and Civan, 1993, 1994, 1996; Civan and Engler, 1994).

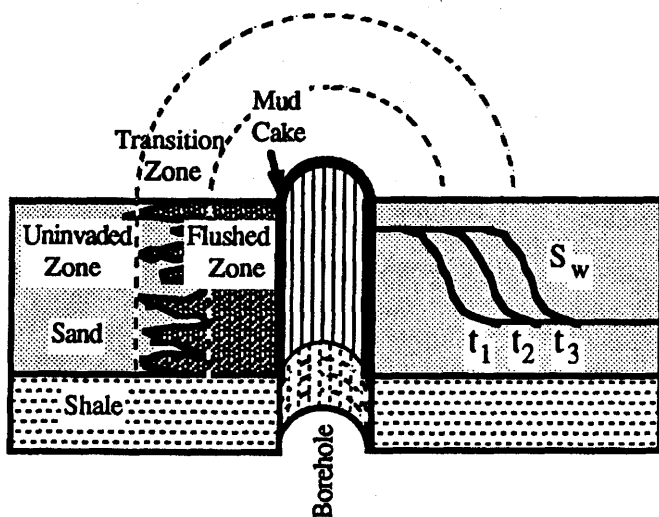


Figure 18-3. Detailed schematic of the various zones and the mud filtrate invasion profiles at different times in the near-wellbore formation (after Yao and Holditch, ©1993 SPE; reprinted by permission of the Society of Petroleum Engineers).

Prediction of the near wellbore conditions, such as mud filtrate and fines invasion and distribution, is important for accurate interpretation of the well-logs used for measurement and monitoring of the properties of the near wellbore formations and accurate estimation of the hydrocarbon content of the reservoirs (Civan and Engler, 1994; Phelps, 1995; Ramakrishnan and Wilkinson, 1997). Civan (1994) states: "This process is complicated by the formation of a mud filtercake and its effect on invasion by reducing the filtrate volume and the migration of fine particles into the porous formation. Simultaneously, the properties of the fluid phases in porous media, such as density and viscosity, vary as a result of mixing and interactions of reservoir fluids with the mud filtrate and fine particles." Therefore, for modeling purposes, the coupling of the external filtercake buildup and the near wellbore fluid invasion and formation damage is essential (see Figure 18-4).

Donaldson and Chernoglazov (1987) developed a "leaky-piston" filtrate invasion and convection-dispersion filtrate transport model applicable to cases involving drilling muds that can mix with the formation fluid. This model considers the dispersion of the mud filtrate within the formation fluid in a single-phase fluid system to estimate the salinity variation in the near wellbore region, but neglects the affect of mud fines invasion. This model was formulated for linear flow and the filtercake affect is

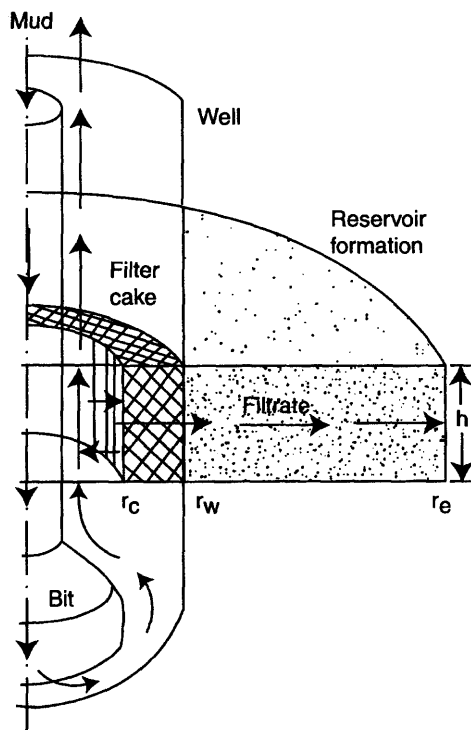


Figure 18–4. Mud-cake buildup over the wellbore sandface and filtrate invasion in the near-wellbore formation (after Civan, ©1999 SPE; reprinted by permission of the Society of Petroleum Engineers).

simulated by means of an empirically determined, decaying filter rate equation. Civan and Engler (1994) extended and improved this model for the radial filtrate invasion case applicable to actual openhole wells.

Yao and Holditch (1993) and Bilardo et al. (1996) have developed radial filtration models for reservoirs containing some formation water. They assumed that the mud filtrate mixes with the formation water as a single phase. Because their interest is in the development of models to estimate the water phase saturation, they do not consider a convection-dispersion transport equation for estimation of the brine salinity variation due to the mixing of the mud filtrate with the formation brine. However, the salinity would be required for the resistivity measurements. Phelps (1995) presents a model to determine the fluid saturations in layered formations during mud filtrate invasion. Civan (1994, 1998, 1999) presented an improved formulation of the multi-species and two-phase fluid transport in deforming

porous media; derivation of compressible and incompressible cake models with and without particle invasion; and an application for radial flow filtercake buildup and mud filtrate invasion. Olarewaju (1990) developed an analytical model for permeability alteration around wells due to drilling mud filtrate invasion and mudcake formation. Ramakrishnan and Wilkinson (1997) developed a radial model for water-based mud filtrate invasion. This model enables the determination of the saturations of the oil and water phases and the salt concentration in the water phase. They combine all the dissolved ions in brine into a single pseudo-component, called "salt." Chin (1995) presents numerical models for formation invasion for various applications including formation damage, measurement-while-drilling, and time lapse analysis.

In the following, single- and two-phase mud filtrate invasion models are presented.

Simplified Single Phase Mud Filtrate Invasion Model

Similar to Donaldson and Chernoglazov (1987), Civan and Engler (1994) assumed that the mud filtrate mixes with the reservoir fluid and the salt concentration varies. This model implicitly assumes a piston type immiscible displacement of oil similar to the formulations by Collins (1961) and Olarewaju (1990). Thus, the fluid zone can be viewed in two parts: the water phase and oil phase zones behind and ahead of the displacement front, located at a distance, $r_e(t)$. In this case, the front moves with time. The formulation is also applicable when the mud filtrate can mix with the reservoir fluid (i.e., of the same wetting type). The filtrate mixture is considered as a pseudo-component. The filtrate mass balance is given by:

$$\frac{\partial c}{\partial t} + \frac{u}{\phi} \frac{\partial c}{\partial r} = \frac{1}{r} \frac{\partial}{\partial r} \left(rD \frac{\partial c}{\partial r} \right); \quad r_w < r < r_e, \quad t > 0 \quad (18-1)$$

The initial condition is given by:

$$c = 0, \quad r_w \leq r \leq r_e, \quad t = 0 \quad (18-2)$$

The boundary conditions at the wellbore and the moving front are given, respectively, by:

$$uc - \phi D \frac{\partial c}{\partial r} = uc_0, \quad r = r_w, \quad t > 0 \quad (18-3)$$

$$\frac{\partial c}{\partial r} = 0, r = r_e, t > 0 \quad (18-4)$$

The volumetric flux is determined by:

$$u = \frac{q}{2\pi rh} \quad (18-5)$$

in which the filtrate invasion rate is assumed to follow an empirically determined exponential decay law according to Donaldson and Chernoglazov (1987):

$$q = ae^{-bt} \quad (18-6)$$

where a and b are empirical parameters.

The dispersion coefficient is expressed as power-law function of the volume flux (Donaldson and Chernoglazov, 1987):

$$D = fu^g \quad (18-7)$$

where f and g are empirical parameters.

Next, three dimensionless groups are defined for computational convenience and scaling purposes. The dimensionless concentration is defined as:

$$c_D = \frac{c}{c_0} \quad (18-8)$$

The dimensionless radial distance is given by:

$$r_D = \frac{r}{r_w} \quad (18-9)$$

The dimensionless time can be defined based on the dispersion or convection time scales, respectively, as (Civan, 1994):

$$t_D = \frac{t}{r_w^2/D_0} \quad (18-10)$$

$$t_D = \frac{t}{\phi r_w/u_0} \quad (18-11)$$

Because the process is mainly convection dominated, we use Eq. 18–11. The porous media pecllet number is expressed as:

$$Pe = \frac{u_0 r_w}{\phi D_0} \quad (18-12)$$

where u_0 and D_0 are some characteristic values that are the maximum values of u and D , determined as following.

Note that the filtration rate varies in a range of

$$0 \leq q \leq q_{\max} \quad (18-13)$$

where

$$q_{\max} = q|_{t=0} = a \quad (18-14)$$

according to Eq. 18–6. Thus, Eq. 18–5 yields:

$$u_0 \equiv u_{\max} = u|_{r_{\min}=r_w, t=0} = \frac{a}{2\pi r_w h} \quad (18-15)$$

Thus, the volume flux varies in the range of

$$0 \leq u \leq u_{\max} \equiv u_0 \quad (18-16)$$

or

$$0 \leq u_D = \frac{u}{u_0} \leq 1 \quad (18-17)$$

where it can be shown by means of Eqs. 18–5, 6, and 11 that:

$$u_D = \frac{u}{u_0} = \frac{1}{r_D} e^{-bt_0 t_D} \quad (18-18)$$

in which the convection time scale is given by:

$$t_0 = \phi r_w / u_0 \quad (18-19)$$

The dispersion coefficient varies in the range of:

$$0 \leq D \leq D_{\max} \equiv D_0 \quad (18-20)$$

or

$$0 \leq D_D = \frac{D}{D_0} \leq 1 \quad (18-21)$$

where it can be shown by means of Eqs. 18-7 and 18 that

$$D_D = u_D^g \quad (18-22)$$

Therefore, Eqs. 18-1 through 4 can be transformed into a set of dimensionless equations, respectively, as:

$$\frac{\partial c_D}{\partial t_D} + u_D \frac{\partial c_D}{\partial r_D} = \frac{1}{p_e} \frac{1}{r_D} \frac{\partial}{\partial r_D} \left[r_D D_D \frac{\partial c_D}{\partial r_D} \right] \quad (18-23)$$

$$c_D = 0, 1 \leq r_D \leq \frac{r_e}{r_w}, t_D = 0 \quad (18-24)$$

$$u_D c_D - \frac{1}{p_e} D_D \frac{\partial c_D}{\partial r_D} = u_D, r_D = 1, t_D > 0 \quad (18-25)$$

$$\frac{\partial c_D}{\partial r_D} = 0, r_D = \frac{r_e}{r_w}, t_D > 0 \quad (18-26)$$

Finally, substituting Eqs. 18-18 and 22 into Eqs. 18-23 through 26 and dropping the subscript "D" for dimensionless quantities, Eqs. 18-23 through 26, respectively, become:

$$\frac{\partial c}{\partial t} + \alpha \frac{\partial c}{\partial r} = \beta \frac{\partial^2 c}{\partial r^2} \quad (18-27)$$

$$c = 0, 1 \leq r \leq (r_e/r_w), t = 0 \quad (18-28)$$

$$uc - \frac{D}{p_e} \frac{\partial c}{\partial r} = u, r = 1, t > 0 \quad (18-29)$$

$$\frac{\partial c}{\partial r} = 0, r = (r_e/r_w), t > 0 \quad (18-30)$$

In Eq. 18–27, the parameters α and β are given by:

$$\alpha = \frac{1}{r_D} \left[\exp(-bt_0 t_D) - \frac{1}{p_e} \frac{(1-g)}{r_D^g} \exp(-gbt_0 t_D) \right] \quad (18-31)$$

$$\beta = \frac{1}{p_e} \left[\frac{1}{r_D^g} \exp(-gbt_0 t_D) \right] \quad (18-32)$$

Notice that Eq. 18–27 is linear, because α and β do not depend on the concentration, c .

The exterior radius, $r_e(t)$, of the invaded region can be determined from the following volumetric balance:

$$\pi [r_e^2(t) - r_w^2] h \phi = \int_0^t q dt = \frac{a}{b} (1 - e^{-bt}) \quad (18-33)$$

Civan and Engler (1994) considered the mixing of the mud filtrate with the resident fluid within a fixed, but sufficiently long, radial distance ($r_e = \text{constant}$) and obtained a numerical solution of the model using the Crank-Nicholson finite difference scheme as described in Chapter 16. Figure 16–8 shows the solution obtained using the parameter values given in Chapter 16. Based on Figure 16–8, the depth of filtrate invasion as a function of time is plotted in Figure 18–5. Note that Figure 18–5 resembles to the depth of invasion curves given by Simpson (1974).

Two-Phase Wellbore Mud Invasion and Filter Cake Formation Model

The following assumptions are made: (1) oil/water system, (2) aqueous phase density varies by the salt content, (3) radial and horizontal flow, and (4) homogeneous formation.

Civan (1994) and Ramakrishnan and Wilkinson (1997) modeled the radial invasion of water-based drilling muds into near-wellbore formation in oil reservoirs. Ramakrishnan and Wilkinson (1997) neglected the effects of the fluid compressibility, capillary pressure, gravity, salt dispersion, the porosity variation, and fine particle invasion. Therefore, the simplified model obtained under these conditions can be solved conveniently by the method of characteristics. Civan's (1994) model includes all of these effects. Therefore, it is much more complicated and requires a much more complicated numerical solution scheme. In the following, the formulation of the

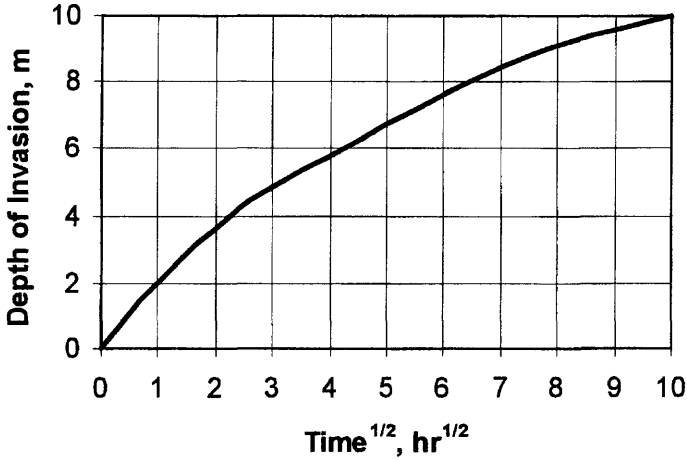


Figure 18–5. Plot of depth of filtrate invasion simulation data of Civan and Engler (1994) plotted against the square root of time for different muds.

filtrate invasion problem is presented by combining the features of the formulations given by Civan (1994) and Ramakrishnan and Wilkinson (1997).

Ramakrishnan and Wilkinson (1997) consider a two-phase fluid system in the near wellbore formation. The aqueous phase forms the wetting phase, denoted by W , and the oleic phase forms the nonwetting phase, denoted by N . Neglecting the change of volume by mixing, they express the density of the aqueous phase as a volumetrically weighted average of the densities of the aqueous phase at two extreme cases, namely, the density of the saturated solution, ρ_w^s , and the density of pure water, ρ_w^0 . Hence,

$$\rho_w = \rho_w^s \sigma + \rho_w^0 (1 - \sigma) \quad (18-34)$$

in which σ denotes the volume fraction of the saturated solution in the aqueous mixture.

All dissolved ions are lumped together into a “salt” pseudo-component. Then, the mass concentration of the salt in the aqueous phase is given by:

$$c = \rho_w^s \sigma \quad (18-35)$$

The salt mass balance is given by:

$$\frac{\partial}{\partial t} (\phi S_w c) + \frac{1}{r} \frac{\partial}{\partial r} \left[r \left(u_w c - \phi S_w D \frac{\partial c}{\partial r} \right) \right] = 0 \quad (18-36)$$

The initial condition is given by:

$$c = 0, r_w \leq r < \infty, t = 0 \quad (18-37)$$

The boundary conditions are given as:

$$(u_w c)_{in} = u_w c - \phi S_w D \frac{\partial c}{\partial r}, r = r_w, t > 0 \quad (18-38)$$

$$c = 0, r \rightarrow \infty, t > 0 \quad (18-39)$$

Neglecting the molecular diffusion, the dispersion coefficient is given by:

$$D = \alpha \left[\frac{u}{\phi(1 - S_{wc} - S_{Nr})} \right]^\beta \quad (18-40)$$

where α and β are some empirical constants, and S_{wc} and S_{Nr} denote the irreducible saturations of the aqueous and oleic phases, respectively.

Thus, assuming that ρ_w^s is constant at reservoir conditions and substituting Eq. 18-35 into Eq. 18-36 yields:

$$\frac{\partial}{\partial t}(\phi S_w \sigma) + \frac{1}{r} \frac{\partial}{\partial r}(r \sigma u_w) = \frac{1}{r} \frac{\partial}{\partial r} \left[r \phi S_w D \frac{\partial \sigma}{\partial r} \right] \quad (18-41)$$

Next, the mass balance of the aqueous phase is given by:

$$\frac{\partial}{\partial t}(\phi S_w \rho_w) + \frac{1}{r} \frac{\partial}{\partial r}(r \rho_w u_w) = 0 \quad (18-42)$$

Substituting Eq. 18-34 into 42 and applying Eq. 18-41 yields a volumetric water phase balance equation as:

$$\frac{\partial}{\partial t}(\phi S_w) + \frac{1}{r} \frac{\partial}{\partial r}(r u_w) = \left[1 - \frac{\rho_w^s}{\rho_w^0} \right] \frac{1}{r} \frac{\partial}{\partial r} \left[r \phi S_w D \frac{\partial \sigma}{\partial r} \right] \quad (18-43)$$

The initial condition is given by:

$$S_w = S_{wc}, r_w \leq r < \infty, t = 0 \quad (18-44)$$

The boundary conditions are given by:

$$S_w \cong 1 - S_{Nr}, r = r_w, t > 0 \quad (18-45)$$

$$\frac{\partial S_w}{\partial r} = 0 \text{ or } S_w = S_{wc}, r \rightarrow \infty, t > 0 \quad (18-46)$$

The mass balance equation of the oleic phase is given by:

$$\frac{\partial}{\partial t} [\phi(1 - S_w)\rho_N] + \frac{1}{r} \frac{\partial}{\partial r} (r\rho_N u_N) = 0 \quad (18-47)$$

Assuming the nonwetting phase density is constant, Eq. 18-47 is simplified and then added to Eq. 18-43 to obtain a total volumetric balance equation as:

$$\frac{\partial \phi}{\partial t} + \frac{1}{r} \frac{\partial}{\partial r} (ru) = \left(1 - \frac{\rho_w^s}{\rho_w^0}\right) \frac{1}{r} \frac{\partial}{\partial r} \left[r\phi S_w D \frac{\partial \sigma}{\partial r} \right] \quad (18-48)$$

in which u is the total volumetric flux given by:

$$u = u_w + u_N \quad (18-49)$$

which can be expressed in terms of the filtrate invasion rate q as:

$$u = \frac{q}{2\pi rh} \quad (18-50)$$

For convenience, the volumetric flux of the aqueous phase can be expressed in terms of the fractional flow function according to Buckley and Leverett as (Collins, 1961):

$$u_w = f_w u \quad (18-51)$$

where the fractional flow function of the aqueous phase is given by (Richardson, 1961), neglecting the gravity term for horizontal, radial flow:

$$f_w = F_w \left[1 + \frac{k_{rN}}{u\mu_N} \frac{dp_{cNW}}{dS_w} K \frac{\partial S_w}{\partial r} \right] \quad (18-52)$$

in which F_w is the zero capillary pressure and zero gravity fractional flow term, given by:

$$F_w = \left[1 + \frac{k_{rN} \mu_w}{k_{rW} \mu_N} \right]^{-1} \quad (18-53)$$

Substituting Eq. 18-49 for the total volumetric flux, and Darcy's equations for the aqueous and oleic phases into Eq. 18-48, results in the following equation for the pressure of the aqueous phase:

$$\begin{aligned} & \frac{\partial \phi}{\partial t} - \frac{1}{r} \frac{\partial}{\partial r} \left\{ rK \left[\left(\frac{k_{rW}}{\mu_w} + \frac{k_{rN}}{\mu_N} \right) \frac{\partial P_w}{\partial r} + \frac{k_{rN}}{\mu_N} \frac{dP_c}{dS_w} \frac{\partial S_w}{\partial r} \right] \right\} \\ & = \left(1 - \frac{\rho_w^s}{\rho_w^0} \right) \frac{1}{r} \frac{\partial}{\partial r} \left(r \phi S_w D \frac{\partial \sigma}{\partial r} \right), r_w \leq r < \infty, t > 0 \end{aligned} \quad (18-54)$$

The initial aqueous phase pressure is given by:

$$P_w = P_w^0(r), r_w \leq r < \infty, t = 0 \quad (18-55)$$

The pressure at a sufficiently long distance does not change. Thus

$$P_w = P_w^0(r), r \rightarrow \infty, t > 0 \quad (18-56)$$

The rate of invasion and the pressure of the filtrate at the formation face can be estimated as following using a filtercake buildup model according to Civan (1994, 1998, 1999).

Assuming an incompressible filtercake, the cake radius is given by (Civan, 1994, 1998, 1999):

$$-\frac{dr_c}{dt} = \frac{k_d u_f \big|_{r_c} \rho_{A\ell} - k_e (\tau - \tau_c)}{(1 - \phi_c) \rho_A} \quad (18-57)$$

The initial condition is given by:

$$r_c = 0, t = 0 \quad (18-58)$$

In the field, usually the mud pressure, P_{mud} , is maintained constant. Thus, the filtrate invasion rate varies. Note that Donaldson and Chernoglazov (1987) and Civan and Engler (1994) used empirical correlations for the filtrate invasion rate. Whereas, the filtrate invasion rate can be estimated by means of Darcy's law assuming incompressible filtercake and constant viscosity filtrate, as following:

$$\begin{aligned}
 u_f|_{r_w} &= u_f|_{r_c} \frac{r_c}{r_w} = \frac{q_f}{2\pi r_w h} = \frac{K_c (P_{mud}|_{r_c} - P_w|_{r_w})}{\mu_w r_w \ell n(r_w/r_c)} \\
 &= -\frac{K k_{rw}}{\mu_w} \frac{\partial p_w}{\partial r}, r = r_w, t > 0
 \end{aligned}
 \tag{18-59}$$

Application. Ramakrishnan and Wilkinson (1997) neglected the porosity variation and the capillary and gravity effects, and defined dimensionless distance and time, and normalized saturated solution volume fraction and saturation, respectively, as:

$$X = \left(\frac{r}{r_w} \right)^2 - 1 \tag{18-60}$$

$$T = \frac{\int_0^t q(t') dt'}{\pi r_w^2 \phi} = \frac{Q(t)}{\pi r_w^2 \phi} \tag{18-61}$$

$$C = \frac{\sigma - \sigma_c}{\sigma_f - \sigma_c} \tag{18-62}$$

where $Q(t)$ is the cumulative filtrate volume, r_w is the wellbore radius, and σ_c and σ_f denote the saturated solution volume fractions of the connate and filtrate aqueous phases. In addition, a normalized saturation can be defined as:

$$S = \frac{S_w - S_{wc}}{1 - S_{wc} - S_{nr}} \tag{18-63}$$

Therefore, neglecting the capillary and gravity terms in Eq. 18-52 and applying Eqs. 18-51 through 57 into Eqs. 18-43 and 41, respectively, yields the following aqueous phase saturation and saturated solution concentration equations:

$$\frac{\partial S}{\partial T} + \frac{dF_w}{dS_w} \frac{\partial S}{\partial X} = 0 \tag{18-64}$$

$$\frac{\partial C}{\partial T} + \frac{F_w}{S_w} \frac{\partial C}{\partial X} = 0 \tag{18-65}$$

The initial conditions are:

$$S = 0, C = 0, X > 0, T = 0 \quad (18-66)$$

The boundary conditions are:

$$S = 1, C = 1, X = 0, T > 0 \quad (18-67)$$

Ramakrishnan and Wilkinson (1997, 1999) have solved Eqs. 18–64 through 67 by applying the relative permeability functions given by Ramakrishnan and Wasan (1986). They considered that the filtrate invasion rate, $q(t)$, is an unknown function, but it can be uniquely determined by an inverse problem approach if the resistivity of the near wellbore formation is measured as a function of the radial distance. Figure 18–6 shows their solutions for low, medium, and high connate water saturations. However, the filtrate invasion rate can be directly predicted by applying Civan's (1994) formulation as following.

Applying the same simplifying assumptions used in deriving Eqs. 18–64 and 65 to Eq. 18–54 and Eq. 18–60 and $p_w = p_N = p$, yields the following simplified pressure equation:

$$\frac{\partial}{\partial X} \left\{ (1 + X) K \left[\frac{k_{rw}}{\mu_w} + \frac{k_{rN}}{\mu_N} \right] \frac{\partial P}{\partial X} \right\} = 0 \quad (18-68)$$

subject to the following initial and boundary conditions:

$$p = p^\circ(X), X > 0, T = 0 \quad (18-69)$$

$$\frac{q}{2\pi r_w h} = -\frac{2Kk_{rw}}{r_w \mu_w} \frac{\partial p}{\partial X} = \frac{K(p_c - p)}{\mu r_w \ell n(r_w/r_c)}, X = 0, T > 0 \quad (18-70)$$

$$p = p^\circ(X), X \rightarrow \infty, T > 0 \quad (18-71)$$

Eqs. 18–68 through 71 can be solved by the finite difference method to obtain the near wellbore pressure profile and the filtrate invasion rate.

References

- Bennion, D. B., Thomas, F. B., Bennion, D. W., & Bietz, R. F., "Underbalanced Drilling and Formation Damage—Is It a total solution?" *J. Canadian Petroleum Technology*, Vol. 34, No. 9, November 1995, pp. 34–41.

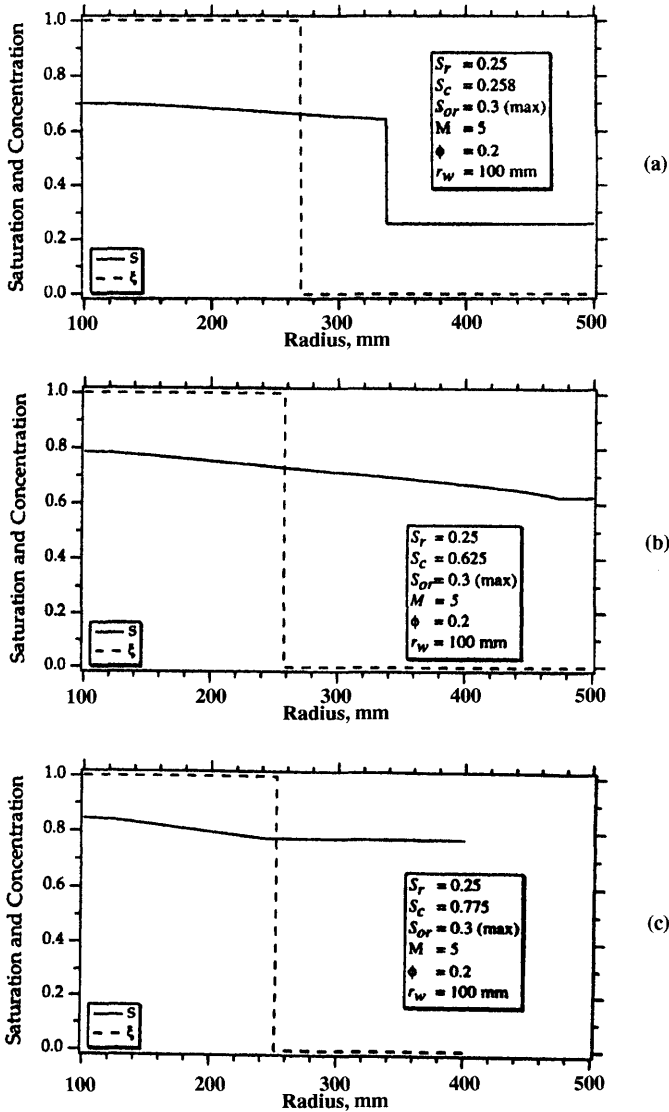


Figure 18-6. Saturation and concentration profiles for (a) low, (b) medium, and (c) high connate water saturations (after Ramakrishnan and Wilkinson, ©1997; reprinted with permission from Ramakrishnan, T. S., and Wilkinson, D. J., "Formation Productivity and Fractional Flow Curves from Radial Resistivity Variation Caused by Drilling Fluid Invasion," *Phys. Fluids*, Vol. 9, No. 4, April 1997, pp. 833-844, ©1997, the American Institute of Physics).

- Bilardo, U., Alimonti, C., Chiarabelli, A., & Caetani, F. C., "Formation Water Saturation from Drilling Fluid Filtrate Invasion: Comparison of Displacement Modelling and Induction Well Log Response," *J. Petroleum Science and Engineering*, Vol. 15, Nos. 2/4, August 1996, pp. 251–259.
- Briscoe, B. J., Luckham, P. F., & Ren, S. R., "The Properties of Drilling Muds at High Pressures and Temperatures," *Phil. Trans. R. Soc. London. A.*, Vol. 348, 1994, pp. 179–207.
- Chin, W. C., *Formation Invasion*, Gulf Publishing Co., Houston, TX, 1995, 240 p.
- Civan, F., & Engler, T., "Drilling Mud Filtrate Invasion—Improved Model and Solution," *J. of Petroleum Science and Engineering*, Vol. 11, pp. 183–193, 1994.
- Civan, F., "Rapid and Accurate Solution of Reactor Models by the Quadrature Method," *Computers & Chemical Engineering*, Vol. 18, No. 10, 1994, pp. 1005–1009.
- Civan, F., "A Multi-Phase Mud Filtrate Invasion and Well Bore Filter Cake Formation Model," SPE 28709 paper, Proceedings of the SPE International Petroleum Conference & Exhibition of Mexico, October 10–13, 1994, Veracruz, Mexico, pp. 399–412.
- Civan, F., "Interactions of the Horizontal Wellbore Hydraulics and Formation Damage," SPE 35213 paper, Proceedings of the SPE Permian Basin Oil & Gas Recovery Conf., March 27–29, 1996, Midland, Texas, pp. 561–569.
- Civan, F., "Practical Model for Compressive Cake Filtration Including Fine Particle Invasion," *AIChE J.*, Vol. 44, No. 11, November 1998, pp. 2388–2398.
- Civan, F., "Incompressive Cake Filtration: Mechanism, Parameters, and Modeling," *AIChE J.*, Vol. 44, No. 11, November 1998, pp. 2379–2387.
- Civan, F., "Phenomenological Filtration Model for Highly Compressible Filter Cakes Involving Non-Darcy Flow," SPE 52147 paper, Proceedings of the 1999 SPE Mid-Continent Operations Symposium, March 28–31, 1999, Oklahoma City, Oklahoma, pp. 195–201.
- Civan, F., "Predictive Model for Filter Cake Buildup and Filtrate Invasion with Non-Darcy Effects," SPE 52149 paper, Proceedings of the 1999 SPE Mid-Continent Operations Symposium, March 28–31, 1999, Oklahoma City, Oklahoma, pp. 203–210.
- Collins, E. R., *Flow of Fluids Through Porous Materials*, Penn Well Publishing Co., Tulsa, OK, 1961, 270 p.
- Donaldson, E. C., & V. Chernoglazov, "Drilling Mud Fluid Invasion Model," *J. Pet. Sci. Eng.*, Vol. 1, No. 1, 1987, pp. 3–13.
- Liu, X., & Civan, F., "A Multi-Phase Mud Fluid Infiltration and Filter Cake Formation Model," SPE 25215 paper, Proceedings, SPE

- International Symposium on Oilfield Chemistry, February 28–March 3, 1993, New Orleans, Louisiana, pp. 607–621.
- Liu, X., & Civan, F., “Formation Damage and Skin Factors Due to Filter Cake Formation and Fines Migration in the Near-Wellbore Region,” SPE 27364 paper, Proceedings of the 1994 SPE Formation Damage Control Symposium, Feb. 9–10, 1994, Lafayette, Louisiana, pp. 259–274.
- Liu, X., & Civan, F., “Formation Damage and Filter Cake Buildup in Laboratory Core Tests: Modeling and Model-Assisted Analysis,” *SPE Formation Evaluation J.*, Vol. 11, No. 1, March 1996, pp. 26–30.
- Olarewaju, J. S., “A Mathematical Model of Permeability Alteration Around Wells,” *Intl. J. for Numerical and Analytical Methods in Geomechanics*, Vol. 14, 1990, pp. 191–207.
- Phelps, G. D., “Computation of Mud Filtrate Invasion Profiles,” *J. Canadian Petroleum Technology*, Vol. 34, No. 1, January 1995, pp. 18–27.
- Ramakrishnan, T. S., & Wason, D. T., “Effect of Capillary Number on the Relative Permeability Function for Two-Phase Flow in Porous Media,” *Powder Technology Journal*, Vol. 48, 1986, pp. 99–124.
- Ramakrishnan, T. S., & Wilkinson, D. J., “Formation Producibility and Fractional Flow Curves from Radial Resistivity Variation Caused by Drilling Fluid Invasion,” *Phys. Fluids*, Vol. 9, No. 4, April 1997, pp. 833–844.
- Ramakrishnan, T. S., & Wilkinson, D. J., “Water-Cut and Fractional-Flow Logs from Array-Induction Measurements,” *SPE Reservoir Evaluation and Engineering Journal*, Vol. 2, No. 1, February 1999, pp. 85–94.
- Richardson, J. G., “Flow Through Porous Media,” in V. L. Streeter (Ed.), *Handbook of Fluid Dynamics*, Section 16, pp. 68–69, McGraw-Hill, New York, 1961.
- Simpson, J. P., “Drilling Fluid Filtration Under Simulated Downhole Conditions,” SPE Paper 4779, 1974.
- Yao, C. Y., & Holditch, S. A., “Reservoir Permeability Estimation from Time-Lapse Log Data,” SPE Paper 25513, Proceedings of the Production Operations Sym. Held in Oklahoma City, OK, March 21–23, 1993, pp. 963–975.
- Yao, C. Y., & Holditch, S. A., “Reservoir Permeability Estimation from Time-Lapse Log Data,” *SPE Formation Evaluation*, June 1996, pp. 69–74.

Chapter 19

Injectivity of the Waterflooding Wells

Summary

Waterflooding is one of the economically viable techniques for recovery of additional oil from mature fields. However, the brine used for waterflooding frequently contain suspended fine particles, which can deposit over the injection formation face and inside the near wellbore formation to reduce the injectivity of the waterflooding wells. Therefore, it is necessary to predict the economic life of the water injection wells and the treatment frequencies required for stimulation of the damaged wells. In this chapter, the models for prediction of the injectivity decline of the waterflooding wells are reviewed and demonstrated by typical applications.

Introduction

As stated by Civan (1998), "Waterflooding is one of the economically viable techniques for recovery of additional oil following the primary recovery." Among other factors, the efficiency of waterflooding depends on the performance of the water injection wells. Typical sources of water used for waterflooding are the brine produced from subsurface reservoirs for land-based reservoirs and the seawater for off-shore reservoirs. The reservoir brines usually contain suspended particles. When injected into a reservoir to drive the oil toward the production wells, the suspended particles are deposited within the near-wellbore formation by a deep-bed filtration process and formation of filter cakes over the injection well formation face, and reduce the permeability of the near-well bore formation and the performance of the injection wells. To maintain economic operations, the injection wells should be treated frequently to stimulate the impaired formation and replenish the injectivity of these wells. The injection water quality, injection conditions, the compatibility of the reservoir fluids and formation with the injected water, and the in-situ fluid

conditions are among the most important factors in determining the rate, extend and extent of damage, and the frequency of the stimulation treatments necessary for the water injection wells. Although the filtration of solids from the brine prior to injection can somewhat alleviate the well impairment, filtration of large quantities of brine is an economic detriment, as is the stimulation of the wells. Also, the foreign brines, such as sea water, are usually incompatible with the reservoir brine and cause inorganic precipitation in the near wellbore formation.

The experimental studies using laboratory core tests, including those by Barkman and Davidson (1972), Donaldson et al. (1977), Davidson (1979), Todd et al. (1979), Todd et al. (1984), Vetter et al. (1987), and Pang and Sharma (1994), have provided some insight into the mechanisms of the governing damage processes and yielded qualitative measures and rules-of-thumbs to predict the conditions leading to well impairment. However, application of such results in the field have often been unsatisfactory. For this reason, mathematical models are used to determine the performance and the economic life of the injection wells, injectivity decline, and the optimum conditions leading to extended economic operating life and optimum intervals required for well treatment. Mathematical models provide scientific guidance for accurate interpretation of the well performance and for developing optimal operating strategies.

As explained by Pang and Sharma (1994), Liu and Civan (1994, 1995, 1996), and Civan (1994), proper modeling of the well injectivity loss requires the coupling of the external cake buildup over the formation face and the particle retention in the near wellbore formation. Pang and Sharma (1994) point out that the models treating the internal and external filter cakes separately are, therefore, over simplified.

Pang and Sharma (1994, 1995) have derived the equations for evaluation of the performance of water injection into laboratory core plugs, and open-hole, perforated, and fractured wells, separately for the internal and external filtration phases. Their models apply for single-phase fluid because they assume that the near wellbore fluid system is water after a short period of the initial waterflooding. Liu and Civan (1994, 1995, 1996) developed a numerical model coupling the internal and external filtration processes. Liu and Civan models apply for both single- and two-phase fluids. Their model is especially suitable for interpretation of the laboratory core flow tests, for which the flow system is mostly two-phase.

Injectivity Ratio

Consider Figure 19–1 showing a typical near wellbore region. Here, we present a formulation according to Sharma et al. (1997) with slight modifications of the nomenclature. The injectivity ratio, $\alpha(t)$, is defined

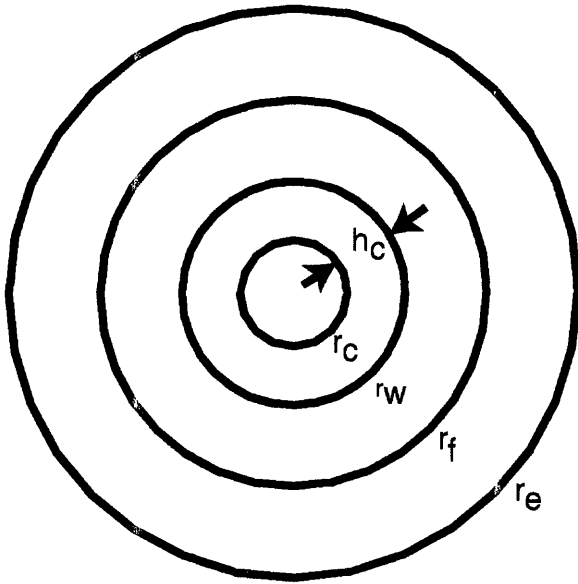


Figure 19-1. Schematic for analysis of open-hole radial filtration.

as the ratio of the instantaneous to the initial injectivity indices, I and I_o , as:

$$\alpha = I/I_o \quad (19-1)$$

Here, I_o is the initial, nondamaged injectivity index given in terms of the initial flow resistance R_o by:

$$I_o = \frac{q}{\Delta p_o} = \frac{1}{\mu R_o} \quad (19-2)$$

I is the instantaneous, damaged injectivity index given by:

$$I = \frac{q}{\Delta p} = \frac{1}{\mu(R_c + R_{NW} + R_R)} \quad (19-3)$$

In Eqs. 19-2 and 3, q is the constant water injection flow rate and Δp_o and Δp represent the difference of the fluid pressures at the wellbore,

r_w , and the external reservoir flooding radius, r_e , before and during damage, given respectively by:

$$\Delta p_o = (p_{wf} - p_e)_o \quad (19-4)$$

$$\Delta p = p_{wf} - p_e \quad (19-5)$$

The flow resistance before damage is given by:

$$R_o = \frac{1}{2\pi K_o h} \ln \left(\frac{r_e}{r_w} \right) \quad (19-6)$$

During damage, Sharma et al. (1997) estimate the flow resistance of the external filter cake of thickness, h_c , the damaged near wellbore formation extending from the wellbore radius of r_w to a radial distance of the damaged region, r_f , and the nondamaged formation beyond the radius, r_f , of the damage region extending to the reservoir radius, r_e , respectively, by:

$$R_c = \frac{1}{2\pi K_c h} \ln \left(\frac{r_w}{r_w - h_c} \right) \quad (19-7)$$

$$R_{NW} = \frac{1}{2\pi h} \int_{r_w}^{r_f} \frac{dr}{K(r)} = \frac{1}{2\pi \bar{K} h} \ln \left(\frac{r_f}{r_w} \right) \quad (19-8)$$

$$R_R = \frac{1}{2\pi K_o h} \ln \left(\frac{r_e}{r_f} \right) \quad (19-9)$$

\bar{K} is the average permeability of the damaged near wellbore region.

Laboratory damage tests are commonly conducted with core plugs. Therefore, the equations corresponding to Eqs. 19-6 through 9 for the linear case as given below according to Figure 19-2 are required:

$$R_o = \frac{L}{K_o} \quad (19-10)$$

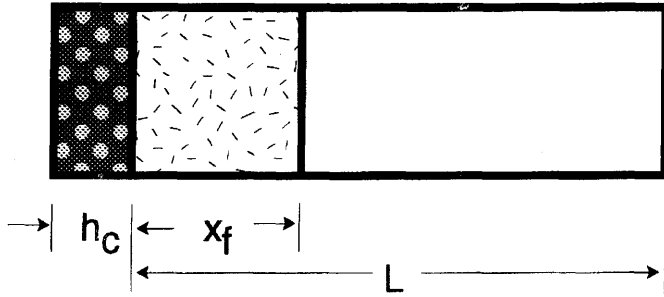


Figure 19–2. Schematic for analysis of linear core-plug filtration.

$$R_c = \frac{h_c}{K_c} \quad (19-11)$$

$$R_{NW} = \int_0^{x_f} \frac{dx}{K(x)} = \frac{x_f}{\bar{K}} \quad (19-12)$$

$$R_R = \frac{L - x_f}{K_o} \quad (19-13)$$

Half-Life of an Injector. Inferred by Fogler (1986), the half-life of an injector, $t_{1/2}$, can be defined as the time required for the injectivity to decline to half of its initial value. Hofsaess and Kleinitz (1998) expressed that:

The half-life is defined as the injection time (or volume) at which the rate declines to $\frac{1}{2}$ of its original value (for constant-pressure-injection) or the flowing pressure reaches twice its initial value (for constant-rate-injection).

Although many researchers, including Barkman and Davidson (1972), Pang and Sharma (1995), Sharma et al. (1997), have used “the half-life” extensively, Fogler (1986) states: “There is nothing special about using the time required for” the half-life. In fact, Fogler suggests that: “One could just as well use the time required to fall to $1/n$ of the initial value,” that is to the $t_{1/n}$ -life. Hence, there is no significance of the use of the injector well half-life.

Models Separating the Internal and External Filtration Processes

For convenience in the modeling, Pang and Sharma (1994) divide the entire filtration process into two phases: (1) the initial internal cake filtration, and (2) the later external cake filtration. They separate these two filtration phases by a “transition time” after which the particle migration into porous formation becomes negligible and an external filter cake begins forming over the injection well formation face. Sharma and Pang (1997) assumed that transition from the internal to the external cake filtration occurs when the porosity, ϕ , of the formation face decreases to a minimum critical value, ϕ^* , by particle deposition, below which particle invasion into porous media is not possible. Their models apply for single phase water flow in the near wellbore region. Hence, the effect of the oil-water two-phase flow during the initial water injection period is neglected because this initial period is relatively short.

Transition Time

Wennberg and Sharma (1997) estimate the transition time based on the expressions given by Iwasaki (1937) for particle deposition rate and the filtration coefficient, respectively, as:

$$d\sigma/dt = \lambda u c \quad (19-14)$$

and

$$\lambda/\lambda_o = 1 + b\sigma \quad (19-15)$$

where b is an empirical constant and λ_o is the filtration coefficient without particle deposition. Although more sophisticated expressions are available in the literature (See Chapter 8), they used Eq. 19-15 for simplicity. Thus, invoking Eq. 19-15 into Eq. 19-14 yields the following expression, similar to the rate equation for particle deposition in pluggable pathways given by Gruesbeck and Collins (1982):

$$d\sigma/dt = \lambda_o(1 + b\sigma)uc \quad (19-16)$$

They obtain the analytic solution of Eq. 19-16 for constant flow rate and suspension particle concentration for two cases as the following:

$$\sigma = \lambda_o u c t, \quad b = 0 \quad (19-17)$$

$$\sigma = (1/b) [\exp(\lambda_o b u c t) - 1] , \quad b \neq 0 \quad (19-18)$$

At the transition time, the porosity attains the minimum critical porosity, ϕ^* , and the maximum critical volume fraction of the deposited particles becomes $\sigma^* = \phi_o - \phi^*$. Under these conditions, Eqs. 19-17 and 18 can be used to obtain the following expressions, respectively, for the transition time:

$$t^* = (\phi_o - \phi^*) / (\lambda_o u c) , \quad b = 0 \quad (19-19)$$

$$t^* = \ln [b(\phi_o - \phi^*) + 1] / (\lambda_o b u c) , \quad b \neq 0 \quad (19-20)$$

Internal Filtration Models

Pang and Sharma (1994, 1995) and Sharma et al. (1997) have pursued their derivations in terms of the following variables:

$$v = u / \phi \quad (19-21)$$

$$\lambda' = \lambda v \quad (19-22)$$

$$n = \sigma / \phi \quad (19-23)$$

Here, v represents the interstitial velocity of the fluid phase and n denotes the fraction of the pore space occupied by the particle deposits in porous media. λ' is the product of the deposition rate constant, λ , and the interstitial velocity of the flowing suspension. In the following, their formulations are presented in a manner consistent with the rest of the presentation of this chapter.

The damage of a core plug by the injection of a dilute particulate suspension can be described by means of the volumetric balance equations of the suspended and deposited particles in porous media, given, respectively, by (Wennberg and Sharma, 1997):

$$\phi \frac{\partial c}{\partial t} + u \frac{\partial c}{\partial x} + \frac{\partial \sigma}{\partial t} = 0 \quad (19-24)$$

and

$$\frac{\partial \sigma}{\partial t} = \lambda u c \quad (19-25)$$

subject to the initial and boundary conditions given by (Pang and Sharma, 1994):

$$c = c_o(x), \sigma = \sigma_o(x), x > 0, t = 0 \quad (19-26)$$

$$c = c_f(t), x = 0, t > 0 \quad (19-27)$$

The instantaneous porosity is given by:

$$\phi = \phi_o - \sigma \quad (19-28)$$

The analytical solution of Eqs. 19–24 through 27 used by Pang and Sharma (1994) implies some simplifications. It applies for the injection of dilute suspension of particles. Therefore, the effect of small amount of particle deposition, σ , compared to the initial porosity can be neglected, the deposition rate coefficient is assumed constant, and a constant rate injection is considered. Thus, the analytic solution for constant $\phi \approx \phi_o$, $\lambda \approx \lambda_o$, and $u = u_o$ can be adopted from Rhee et al. (1986) as:

$$c(x, t) = c_o \left(x - \frac{ut}{\phi} \right) \exp \left(-\frac{\lambda ut}{\phi} \right), x > \frac{ut}{\phi} \quad (19-29)$$

$$c(x, t) = \left[c_f \left(t - \frac{\phi x}{u} \right) \right] \exp(-\lambda x), x < \frac{ut}{\phi} \quad (19-30)$$

where the term inside the square brackets expresses that c_f is a function of $(t - \phi x/u)$.

Considering that $c_f(t) = c_f$ is constant and $c_o(x) = 0$ and $\sigma_o(x) = 0$ in the laboratory core flow tests, Pang and Sharma (1994) simplify Eqs. 19–29 and 30, respectively, as:

$$c(x, t) = 0, x > ut/\phi \quad (19-31)$$

$$c(x, t) = c_f \exp(-\lambda x), x < ut/\phi \quad (19-32)$$

and using Eqs. 19–31 and 32, they obtain the solution of Eq. 19–25 as:

$$\sigma(x, t) = 0, x > ut/\phi \quad (19-33)$$

$$\sigma(x, t) = c_f \lambda u t \exp(-\lambda x), \quad x > ut/\phi \quad (19-34)$$

Pang and Sharma (1995) assumed that the permeability reduction primarily occurs by pore throat plugging. Therefore, they estimated the permeability of the porous formation as a harmonic average permeability of the combined plugged and unplugged regions as:

$$\frac{1}{K(x, t)} = \frac{f_p \sigma(x, t)}{K_p} + \frac{[1 - f_p \sigma(x, t)]}{K_m} \quad (19-35)$$

where f_p represents the volume fraction of the deposited particles contributing to pore throat plugging, K_p denotes the permeability of the plugged region near the pore throats, and K_m is the permeability of the formation matrix, assumed to remain constant, which is equal to the initial nondamaged permeability, K_o (i.e., $K_m \equiv K_o$). Therefore, Pang and Sharma (1995) rearranged Eq. 19-35 for the relative or fractional retained permeability of the porous formation undergoing particle deposition from dilute suspensions as, inferred by Payatakes et al. (1974):

$$\frac{K(x, t)}{K_o} = \frac{1}{1 + \beta \sigma(x, t)} \quad (19-36)$$

where β is an empirical damage factor given by:

$$\beta = f_p (K_o/K_p - 1) \quad (19-37)$$

Thus, they calculate the harmonic average permeability of the damaged portion of the core by:

$$\bar{K}(t) = \frac{x_f}{K_o} \bigg/ \int_0^{x_f} \frac{dx}{K(x, t)} \quad (19-38)$$

Substituting Eqs. 19-33, 34, and 36 into Eq. 19-38, and then integrating, they derive the following expression:

$$1/\bar{K}(t) = 1 + Nt \quad (19-39)$$

in which

$$N = \frac{\beta u c_f}{\phi x_f} [1 - \exp(-\lambda x_f)] \quad (19-40)$$

Note that Eq. 19-39 was previously derived by Wojtanowicz et al. (1987, 1988) as described in Chapter 10. Applying Eqs. 19-1 through 3, 10, 12, and 13, the injectivity ratio for the linear cases, applicable to laboratory core plugs without external cake formation ($R_c = 0$), is given by:

$$\alpha(t) = \frac{L}{\frac{x_f}{\bar{K}(x_f)} + \frac{(L - x_f)}{K_o}} \quad (19-41)$$

where

$$x_f = \frac{ut}{\phi}, \quad \frac{ut}{\phi} < L \quad (19-42)$$

$$x_f = L, \quad \frac{ut}{\phi} > L \quad (19-43)$$

Pang and Sharma (1994) simplify Eq. 19-41 by considering that the injection front reaches the outlet end of the core rapidly. Therefore, neglecting the damage during the short period of time until the front reaches the core outlet, Eqs. 19-39 and 41 yield for $x_f = L$ the following equation indicating that the reciprocal injectivity ratio is a linear function of time:

$$\frac{1}{\alpha(t)} \cong 1 + Nt \quad (19-44)$$

External Filtration Models

Considering the formation of an incompressible external cake without any particle invasion into the core plug, Pang and Sharma (1994) expressed the harmonic average permeability of the cake and the core system (Figure 19-2) as:

$$\frac{h_c + L}{K(t)} = \frac{h_c}{K_c(t)} + \frac{L}{K_o} \quad (19-45)$$

Sharma et al. (1997) determine the thickness of the external filter cake by means of a volumetric balance of the particles in the cake as:

$$h_c = 0, \quad t < t^* \quad (19-46)$$

$$h_c = \frac{\int_{t^*}^t q(t') c_f(t') dt'}{(1 - \phi_c) A}, \quad t > t^* \quad (19-47)$$

where A is the cross-sectional area of the core plug and c_f is the volume fraction of the fine particles in the water injected at a flow rate of q . For constant c_f and q , Eq. 19-47 simplifies as:

$$h_c = \frac{c_f q t}{(1 - \phi_c) A} \quad (19-48)$$

Thus, substituting Eq. 19-48 into 45 and considering that the filter cake thickness is much smaller than the length of the core plug (i.e., $h_c \ll L$), they obtained the following expression indicating that the reciprocal injectivity ratio is a linear function of time:

$$\frac{1}{\alpha(t)} \cong 1 + M t \quad (19-49)$$

where

$$M = \frac{K_o}{K_c} \left(\frac{c_f}{1 - \phi_c} \right) \frac{u}{\phi L} \quad (19-50)$$

Filtration Coefficient

Wennberg and Sharma (1997) point out that the filtration coefficient varies by particle deposition according to:

$$\lambda/\lambda_o = F(\sigma) \quad (19-51)$$

in which λ_o is the filtration coefficient with no deposited particles and $F(\sigma)$ is a function of the volume fraction of particles deposited. Their

review of the various expressions available for prediction of the filtration coefficient is summarized and presented in the following.

Ives (1967) proposed a general expression as:

$$\frac{\lambda}{\lambda_o} = \left(1 - \frac{\sigma}{\sigma_M}\right)^x \left(1 + \frac{\beta\sigma}{\phi_o}\right)^y \left(1 - \frac{\sigma}{\phi_o}\right)^z \quad (19-52)$$

in which x , y , z , and β are some empirical parameters and σ_M is the maximum of the volume fraction of the deposited particles necessary to make the filtration coefficient of porous media zero. This equation indicates that the filtration coefficient is equal to one when there is no deposited particles in porous media, and the filtration coefficient becomes zero when the volume fraction of deposited particles reaches a certain characteristic value of maximum σ_M .

Chiang and Tien (1985) developed an empirical correlation as:

$$\lambda/\lambda_o = 1 + \sigma^{0.755} (492 - 1.6 \times 10^4 N_r + 1.46 \times 10^5 N_r^2), \sigma < 10^{-2} \quad (19-53)$$

where N_r is the suspended particle to porous media grain diameter ratio:

$$N_r = D_p/D_g \quad (19-54)$$

Rajagopalan and Tien (1976) developed the following expression:

$$\begin{aligned} \lambda = & 0.72 A_s N_{Lo}^{1/8} N_r^{15/8} + 2.4 \times 10^{-3} A_s N_g^{1.2} N_r^{-0.4} \\ & + 4 A_s^{1/3} N_{pe}^{-2/3}, N_r < 0.18 \end{aligned} \quad (19-55)$$

in which the dimensionless groups are defined as following. A_s is Happel's dimensionless geometric parameter. N_{Lo} is the London parameter given by

$$N_{Lo} = 4H/(\pi\beta\mu D_p^2\nu) \quad (19-56)$$

where $H = 3.0 \times 10^{-13} \text{ erg}$ is Hamaker's constant. N_g is the gravity number given by:

$$N_g = (\rho_p - \rho_\ell) D_p^2 g / (18\mu\nu) \quad (19-57)$$

N_{pe} is the peclet number given by:

$$N_{pe} = vD_g / D \quad (19-58)$$

v is velocity, μ is viscosity, and ρ_p and ρ_f denote the particle and fluid densities, respectively.

β is a packing parameter given by

$$\beta = (1 - \phi)^{1/3} \quad (19-59)$$

where ϕ is the porosity in fraction. D is the coefficient of diffusion for the Brownian motion of particles.

Wennberg and Sharma (1997) analyzed the measurements of the filtration coefficient reported by various investigators and determined that these data mostly indicate power law-type relationships to the volumetric flux, the suspended particle size, and the porous media grain size as:

$$\lambda \sim u^{-\alpha}, D_p^\beta, D_g^{-\gamma} \quad (19-60)$$

where α , β , and γ are some empirical exponents. They determined that $0 \leq \alpha \leq 2$; $\beta > 0$ for $D_p > 1\mu m$ and $\beta < 0$ for $D_p < 1\mu m$; $0.6 < \beta < 1.2$ for Ottawa sand; and $\gamma \approx 0.9$ and 2.

Diagnostic-Type Curves for Water Injectivity Tests

Pang and Sharma (1994, 1997) identified four distinct type curves that can be used for interpretation of the water-quality tests. They justified these type curves with experimental data obtained from the literature as shown in Figure 19-3. Type curve 1 is a straight line indicating the formation of an incompressible external filter cake or a thin internal cake near the injection face of the core plug according to Eq. 19-49. The slope remains constant. Type curve 2 is for the similar case, but applies for compressible cakes. In this case, the porosity and permeability of the cake decrease by increasing filtration pressures. As a result, the slope of the curve increases with the filtration time or pore volume injected. Type curve 3 refers to a deep particle invasion and pore filling in the core plug, leading to a slower gradual permeability decrease. As a result, the slope of the curve decreases with the filtration time. Type curve 4 may be an S-shaped or other types of curves indicating a shift of the dominance of the different damage mechanisms during the filtration process.

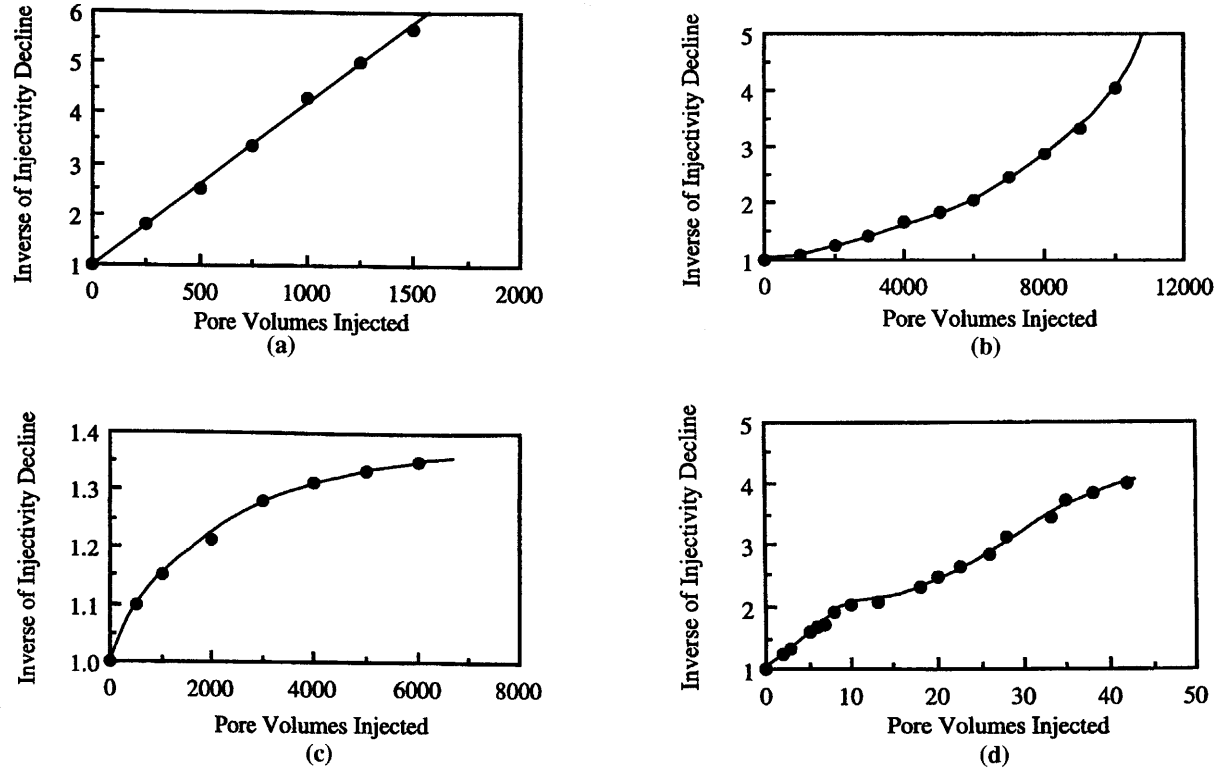


Figure 19-3. Diagnostic-type curves: (a) Type curve 1 (data from Todd et al., 1979), (b) Type curve 2 (data from Todd et al., 1984), (c) Type curve 3 (data from Todd et al., 1979), and (d) Type curve 4 (data from Pautz et al., 1989) (after Pang and Sharma, ©1997 SPE; reprinted by permission of the Society of Petroleum Engineers).

Models for Field Applications

Pang and Sharma (1994, 1995, 1997) have also applied the above methodology and derived the models for prediction of the injectivity ratio given in Table 19-1 for other cases. Specifically, the open-hole, perforated and fractured wells as depicted in Figures 19-1, 19-4 and 19-5 are considered separately in Table 19-1 for the internal and external filtration phases.

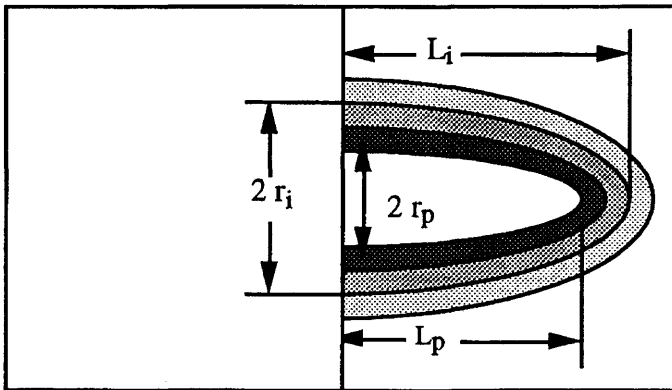


Figure 19-4. Details of perforation for analysis of internal filtration (after Pang and Sharma, ©1995 SPE; reprinted by permission of the Society of Petroleum Engineers).

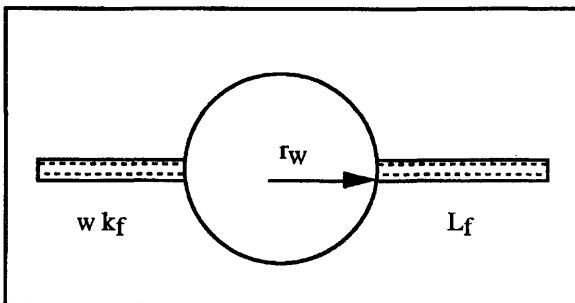


Figure 19-5. Details of vertical hydraulic fracture for analysis of internal filtration (after Pang and Sharma, ©1995 SPE; reprinted by permission of the Society of Petroleum Engineers).

Table 19-1
Models for Prediction of the Injectivity Ration

Open hole well	
$\frac{1}{\alpha} = \frac{1}{k_r(r_f)} \frac{\ln(r_f/r_w)}{\ln(r_e/r_w)} + \frac{\ln(r_e/r_f)}{\ln(r_e/r_w)}$	$\frac{1}{\alpha} = 1 + \frac{k_o}{k_c} \frac{\beta}{\ln(r_e/r_w)}$
$\frac{1}{k_r(t)} = 1 + Mt$	
$M = \delta f$	$\beta = \ln \frac{r_w}{r_w - h_c}$
$\delta = \frac{\beta C q}{2\pi r_w^2 h \phi_m \ln \frac{r_f}{r_w}}$	$h_c = \frac{C}{1 - \phi_c} \frac{qt}{2\pi r_w h}$
$f = \exp(a) [Ei(a) - Ei(ar_f^2/r_w^2)]$	
$Ei(x) = \int_x^\infty \frac{e^{-u}}{u} du$	
$r_f^2 = qt/(\pi h \phi_m) + r_w^2, \quad \text{for } qt/(\pi h \phi_m) < r_e^2 - r_w^2$	
$r_f^2 = r_e^2 - r_w^2, \quad \text{for } qt/(\pi h \phi_m) > r_e^2 - r_w^2$	
Perforated well	
$\frac{1}{\alpha} = \frac{\sum_{i=0}^{n-1} \frac{1}{k_r(r_i, t) H_i} \left(\ln \frac{\zeta_i + 1}{\zeta_i - 1} - \ln \frac{\zeta_{i+1} + 1}{\zeta_{i+1} - 1} \right) + \frac{1}{H_n} \ln \frac{\zeta_n + 1}{\zeta_n - 1}}{\frac{1}{H_p} \ln \frac{\zeta_p + 1}{\zeta_p - 1}}$	$\frac{1}{\alpha} = 1 + \frac{k_o}{k_c} \left(\frac{\ln \left(1 + \frac{2L_p}{r_p - h_c} \right)}{\ln \left(1 + \frac{2L_p}{r_p} \right)} - 1 \right)$
$k_r(r, t) = \frac{1}{1 + \beta n(r, t)}$	$h_c = \frac{C}{G h N_p} \int_0^t q dt$
$n(r, t) = \lambda C t \exp[-\lambda \pi (r^2 - r_p^2) L_p \phi_m / q_p]$	
$q_p = \frac{q}{N_p h}$	$G = (1 - \phi_c) \frac{4}{3} r_p L_p (2 + r_p / L_p)$
$\zeta_i = \exp(w_i)$	
$\tanh w_i = r_i / L_i$	
$H_i = r_i / \sinh w_i$	

Table 19-1 continued

Hydraulically fractured well

$$\frac{1}{\alpha} = \frac{1}{k_r(x_f)} + \left(1 - \frac{x_f}{r_e}\right)$$

$$\frac{1}{\alpha} = \frac{\ln\left(\frac{r_e}{L_f}\right) + \sum_{i=1}^{n-1} \ln\left(\frac{1 + CR_i}{r_{i-1}/r_i + CR_i}\right)}{\ln\left(\frac{r_e}{L}\right) + \ln\left(\frac{1 + CR}{r_w/L_f + CR}\right)}$$

$$x_f = Vt \quad \text{for } Vt < r_e$$

$$x_f = r_e \quad \text{for } Vt > r_e$$

$$\frac{1}{k_r(t)} = 1 + Mt$$

$$M = \delta f$$

$$\delta = \beta VC/r_e$$

$$f = 1 - \exp(-\lambda r_e/V)$$

$$CR = \frac{wk_f}{\pi L_f k_o}$$

$$CR_i = \frac{wk_{fi}}{\pi r_i k_o}$$

$$k_{fi} = \frac{k_f}{1 + \beta n(x, t)}$$

$$n(x, t) = 0 \quad \text{for } x > Vt$$

$$n(x, t) = \lambda Ct \exp(-\lambda x/V) \quad \text{for } x < Vt$$

(Fracture Damage)

After Pang and Sharma, ©1995 SPE; reprinted by permission of the Society of Petroleum Engineers.

Models Coupling the Internal and External Filtration Processes

Liu and Civan (1996) have developed a differential, phenomenological model that couples the external cake formation and the near wellbore invasion and deposition of fine particles. This model is applicable for the oil-water two-phase flow systems encountered during waterflooding of oil reservoirs. Whereas, the applicability of the models by Pang and Sharma (1994, 1995, 1997), Sharma et al. (1997), and Wennberg and Sharma (1997) is limited to the single-water phase system that occurs during late periods of the waterflooding in the near wellbore region because these models neglect the initial, two-phase flow in the near wellbore region. Although the initial near wellbore, two-phase flow period of waterflooding may be short and, therefore, negligible for the actual oil reservoirs, it is not negligible for the core plug flow tests. The description of the Liu and Civan (1996) model for impairment of the near wellbore region is given in Chapter 11. Therefore, this subject is not repeated here.

References

- Barkman, J. H., & Davidson, D. H., "Measuring Water Quality and Predicting Well Impairment," *JPT*, Trans., *AIME*, Vol. 253, July 1972, pp. 865-73.
- Chiang, H. W., & Tien, C., "Transient Behavior of Deep-Bed Filters," *Symp. Adv. in Solids-Liquid Separ.*, University College, London, 1983.
- Chiang, H. W., & Tien, C., "Dynamics of Deep Bed Filtration, Part I and II," *AIChE J.*, Vol. 31, August 1985, p. 1349.
- Civan, F., "Quadrature Solution for Waterflooding of Naturally Fractured Reservoirs," *SPE Reservoir Evaluation and Engineering*, April 1998, pp. 141-147.
- Davidson, D. H., "Invasion and Impairment of Formations by Particulates," SPE Paper 8210, Presented at the 54th Annual Fall Meeting of the SPE, Las Vegas, Nevada, September 23-26, 1979.
- Donaldson, E. C., Baker, B. A., & Carroll, H. B., Jr., "Particle Transport in Sandstone," SPE Paper 6905, Presented at the 52nd Annual Technical Conference of SPE, Denver, Colorado, October 9-12, 1977.
- Folger, H. S., *Elements of Chemical Reaction Engineering*, Prentice-Hall, Englewood Cliffs, New Jersey, 1986, pp. 197-198.
- Gruesbeck, C., & Collins, R. E., "Entrainment and Deposition of Fine Particles in Porous Media," *SPEJ*, December 1982, pp. 847-856.
- Hofsass, T., & Kleinitz, W., "Injectivity Decline in Wells with Non-uniform Perforation Properties," SPE 39586 paper, Proceedings of the 1998 SPE International Symposium on Formation Damage Control, February 18-19, 1998, Lafayette, Louisiana, pp. 631-640.
- Ives, K. J., *Deep Filters, Filtr. Sep.*, March/April 1967, pp. 125-135.
- Iwasaki, T., "Some Notes on Sand Filtration," *J. Am. Water Works Ass.*, Vol. 29, 1937, pp. 1591-1602.
- Liu, X., & Civan, F., "A Multi-Phase Mud Fluid Infiltration and Filter Cake Formation Model," SPE 25215 paper, Proceedings, SPE International Symposium on Oilfield Chemistry, February 28-March 3, 1993, New Orleans, Louisiana, pp. 607-621.
- Liu, X., & Civan, F., "Characterization and Prediction of Formation Damage in Two-Phase Flow Systems, SPE 25429 paper, proceedings of the SPE Production Operations Symposium, March 21-23, 1993, Oklahoma City, Oklahoma, pp. 231-248.
- Liu, X., & Civan, F., "Formation Damage and Skin Factors Due to Filter Cake Formation and Fines Migration in the Near-Wellbore Region," SPE 27364 paper, Proceedings of the 1994 SPE Formation Damage Control Symposium, Feb. 9-10, 1994, Lafayette, Louisiana, pp. 259-274.
- Liu, X., & Civan, F., "Formation Damage by Fines Migration Including Effects of Filter Cake, Pore Compressibility and Non-Darcy Flow—

- A Modeling Approach to Scaling from Core to Field," SPE Paper No. 28980, SPE International Symposium on Oilfield Chemistry, February 14–17, 1995, San Antonio, TX.
- Liu, X., & Civan, F., "Formation Damage and Filter Cake Buildup in Laboratory Core Tests: Modeling and Model-Assisted Analysis," *SPE Formation Evaluation J.* (March 1996) Vol. 11, No. 1, pp. 26–30.
- Pang, S., & Sharma, M. M., "A Model for Predicting Injectivity Decline in Water Injection Wells," SPE Paper 28489, presented at the SPE 69th Annual Technical Conference and Exhibition in New Orleans, September 25–28, 1994, pp. 275–284.
- Pang, S., & Sharma, M. M., "Evaluating the Performance of Open-Hole, Perforated and Fractured Water Injection Wells," SPE Paper 30127, presented at the SPE European Formation Damage Control Conference, the Hague, May 15–16, 1995.
- Pang, S., & Sharma, M. M., "A Model for Predicting Injectivity Decline in Water Injection Wells," *SPE Formation Evaluation*, September 1997, pp. 194–201.
- Pautz, J. F., et al., "Relating Water Quality and Formation Permeability to Loss of Injectivity," SPE Paper 18888, presented at the SPE Production Operations Symposium, Oklahoma City, Oklahoma, March 13–14, 1989.
- Payatakes, A. C., Rajagopalan, R., & Tien, C., "Application of Porous Media Models to the Study of Deep Bed Filtration," *The Canadian Journal of Chemical Engineering*, Vol. 52, December 1974.
- Rajagopalan, R., & Tien, C., "Trajectory Analysis of Deep-Bed Filtration with the Sphere-in-cell Porous Media Model," *AIChE J.*, Vol. 22, May 1976, pp. 523–533.
- Rhee, H. K., Aris, R., & Amundson, N. R., *First-order Partial Differential Equations: Volume I*, Prentice-Hall, 1986.
- Sharma, M. M., Pang, S., & Wennberg, K. E., "Injectivity Decline in Water Injection Wells: An Offshore Gulf of Mexico Case Study," SPE Paper 38180, Proceedings of the 1997 SPE European Formation Damage Conference held in the Hague, The Netherlands, June 2–3, 1997, pp. 341–351.
- Todd, A. C., et al., "Review of Permeability Damage Studies and Related North Sea Water Injection," SPE Paper 7883, presented at the SPE International Symposium on Oilfield and Geothermal Chemistry, Dallas, Texas, January 22–24, 1979.
- Todd, A. C., et al., "The Application of Depth of Formation Damage Measurements in Predicting Water Injectivity Decline," SPE Paper 12498, presented at the Formation Damage Control Symposium held in Bakersfield, California, February 13–14, 1984.
- Todd, A. C., et al., "The Value and Analysis of Core-Based Water Quality Experiments as Related to Water Injection Schemes," SPE Paper 17148,

- presented at the SPE Formation Damage Control Symposium held in Bakersfield, California, February 8–9, 1988.
- van Oort, E., van Velzen, J. F. G., & Leerlooijer, K., “Impairment by Suspended Solids Invasion: Testing and Prediction,” SPE Production & Facilities, August 1993, pp. 178–184.
- Vetter, O. J., et al., “Particle Invasion into Porous Medium and Related Injectivity Problems,” SPE Paper 16625, presented at the SPE International Symposium on Oilfield and Geothermal Chemistry in San Antonio, Texas, February 4–6, 1987.
- Wennberg, K. E., & Sharma, M. M., “Determination of the Filtration Coefficient and the Transition Time for Water Injection Wells,” SPE Paper 38181, Proceedings of the 1997 SPE European Formation Damage Conference held in the Hague, The Netherlands, June 2–3, 1997, pp. 353–364.
- Wojtanowicz, A. K., Krilov, Z., & Langlinais, J. P., “Study on the Effect of Pore Blocking Mechanisms on Formation Damage,” SPE 16233 paper, presented at Society of Petroleum Engineers Symposium, Oklahoma City, Oklahoma, March 8–10, 1987, pp. 449–463.
- Wojtanowicz, A. K., Krilov, Z., & Langlinais, J. P., “Experimental Determination of Formation Damage Pore Blocking Mechanisms,” Trans. of the ASME, *Journal of Energy Resources Technology*, Vol. 110, 1988, pp. 34–42.

Chapter 20

Reservoir Sand Migration and Gravel-Pack Damage: Stress-Induced Formation Damage, Sanding Tendency, Prediction, and Control

Summary

Characteristics of reservoir formations susceptible for sand production are reviewed. The mechanical and hydrodynamic processes causing sand production, migration, and retention in reservoir formations are described and modeled. Typical features of effective gravel pack designs are explained. The various parameters effecting the gravel-pack efficiency are discussed. A predictive model for sand filtration and retention in gravel-packs is presented and verified by means of typical test data.

Introduction

As stated by Geilikman and Dusseault (1997), "Sand production is a fluid-saturated granular flow." It has been observed that fines migration and well sanding tend to increase by rising water cuts beyond a certain threshold as a result of water-coning (or water cresting) induced by high rate production (Hayatdavoudi, 1999). Hayatdavoudi (1999) considers that five important parameters control the sand liquefaction process: (1) buoyancy of the fine particles, (2) variation of the effective density of sand, (3) pressure build-up in the near-wellbore region, (4) weak cohesive

cement between sand grains, and (5) low internal friction angle. Hayatdavoudi (1999) describes that the conditions inducing sand problems, include:

- (a) lack of grain to grain cement (2–5 percent carbonates, oxides of iron, and oxides of silica cement), (b) very small sand grain size usually less than 50–60 microns (very fine silt and clay sized material), (c) under consolidation/compaction due to the deposition of sediments in a viscous, low energy environment (i.e., turbidities), (d) rise of the water table, water encroachment, and water coning, and . . . (e) decreased submerged weight of the particle under variable saturation conditions.

Hayatdavoudi (1999) explains that high production rates induce sand production for several reasons. First, the pore pressure (net overburden stress) increases because of the lowering of the pore fluid pressure. Second, water invades the near-wellbore formation as a result of water coning (or cresting), which in turn alters the petrophysical parameters, including capillary pressure, osmotic pressure, and clay swelling pressure. Consequently, the effective shear resistance of the formation sand against the increasing pore pressure (or effective net overburden stress) diminishes and conditions favorable for sand liquefaction are created. Similar reasons were also suggested by Dusseault and Santarelli (1989).

Tremblay et al. (1998) report a communication being established between injection and production wells 500 meters apart in a reservoir through a wormhole because of sand production. In fact, Tremblay et al. (1998) point out that even in primary production, such as the cold production process for recovery of heavy oil from unconsolidated formations, essentially facilitates production for better access to heavy oil by forming wormholes and/or cavities. Sanding also explains the high sand cuts observed in some oil wells. Therefore, allowing sand production and not using sand exclusion techniques, such as gravel pack and screen, is essential for economic production of oil (Geilikman et al., 1994).

Sand Control

The need for sand control is determined by weakness of the formation and the maximum drawdown allowing flow without sand production (Weingarten, JPT, 1995). No measures for sand control may be necessary when drawdown allows production at desired rates, otherwise the well may be hydraulically fractured to obtain the desired rate without needing sand control (Weingarten, JPT, 1995). When the reservoir formation is highly weak, or the water influx due to reservoir pressure loss by

production induces sand production, proper sand control measures should be taken (Weingarten, JPT, 1995).

There are two conventional strategies available in dealing with sand production (Geilikman and Dusseault, 1997): (1) avoiding sand production problems by controlling pressure gradient and fluid flow rate, selective perforation of zones, resin injection and injecting resin-coated sand into formation, and (2) excluding sand production using gravel-packs, screens, and slotted liners in the wellbore.

For small zones, chemical sand consolidation treatments, such as resin applications, may be convenient (Weingarten, 1995). However, gravel-packing is preferred in many cases. Gravel packing (GP), conventional gel packs (CGP), high-rate water packs (HRWP), and frac-packing (FP) are the most frequently applied sand control methods (JPT, 1995). Weingarten (JPT, 1995) states that:

One obvious measure of performance is that the well should not produce sand. This requires proper gravel sizing and effective packing to prevent voids. Another key measure of success is productivity, both short and long term. The well should have a low skin, and productivity should not decline over time owing to fines infiltration of the pack or perforation tunnels.

King (JPT, 1995) states that "reservoirs with gas or water drive are better gravel-packing (GP) candidates." McLarty (JPT, 1995) explains that:

Laminated sands, severely damaged formations, and fines-migration problems should be considerations for frac-packing (FP) applications. FP's are not recommended in cases where poor cement has resulted or where nearby water or gas zones may also be stimulated. The wellbore's mechanical integrity must be able to accommodate higher treating pressures and the reservoir pressure should be sufficient to produce back the larger volume of fluids required. FP's would also be applicable in situations where a well has sanded up and it is suspected that the overburden pressure may have collapsed and pinched the reservoir off from the wellbore.

As explained by Gurley (JPT, 1995):

The primary objective of a frac-packing (FP) is to open and pack as many perforations as possible, and create a highly conductive flow path through a damaged zone or into a low-permeability formation . . . The fracture needs to extend only through the damaged zone

to be effective, but it is necessary to penetrate 50 to 100 ft and to achieve a tip screen out so as to achieve a wide fracture.

King (JPT, 1995) states that "reservoirs with high peak demands are good candidates for FP's."

Cornette (JPT, 1995) primarily recommends frac-packs (FP), especially for sand formations, which are prone to fines migration problems, or of low permeability or highly laminated types.

Cornette (JPT, 1995) points out that conventional gel packs (CGP) cause significant formation and perforation damage, and therefore are not favored, although they tend to lead to productive completions in formations less than 20 feet thick.

High-rate water packs (HRWP) are remedial short frac-packs, recommended for formations that are clean, homogeneous, and high permeability ($K > 50$ md for gas-bearing sands and $K > 100$ md for oil-bearing sands) (Cornette, JPT, 1995). They are less damaging than the conventional gel packs (CGP).

Gurley (JPT, 1995) explains that

The HRWP objective is to assure that the perforation tunnels are open and fully packed with gravel . . . Average fracture width will be very limited because the fractures do not extend very far into the reservoir.

McLarty (JPT, 1995) explains that

Water packs provide good grain-to-grain contact and would probably be the recommended GP fluid in situations where the interval is particularly hot ($> 280^{\circ}\text{F}$), excessively long (> 60 ft), or highly deviated ($> 60^{\circ}$ slope). They may not be economical or favorable from a formation-damage standpoint in situations where high-density brines must be applied.

When simultaneous water cut, fines migration, and well sanding problems are encountered, Hayatdavoudi (1999) recommends dropping the water level by a suitable completion technique, such as (a) horizontal drilling, (b) producing water from below the oil/water contact level and disposing it to another zone, and (c) suppressing the water-coning by choke adjustment.

Kanj et al. (1996) state that

In the final analysis, the decision on the sand control requirements has to be based on experience in the area with natural, perforated

completions. However, adjustments must be made for differences in completion method and efficiency, hole deviation, well depth, reservoir pressure, depletion and drawdown, water production expectancy, and development plans.

Frequently, sand production problems are alleviated by means of empirical rules-of-thumb, heuristic approaches, and know-how techniques (Kanj et al., 1996). Tables 20–1 and 20–2 by Kanj et al. (1996) compile the various heuristics and associated points available from some experts that can be used for predicting the sanding potential, and suitability of potential methods in sand control, respectively.

Gravel Design Criteria

In spite of the extensive reported work in the area of understanding and control of sand production, theoretical approaches and guidelines for predicting the sanding phenomena and techniques for sand control still need further research and development. As demonstrated by Bouhroum and Civan (1995), the majority of the available gravel sizing criteria, based on the gravel to sand grain size ratio do not actually agree with each other. Saucier (1969) and others developed gravel sizing criteria based on the gravel to mean size of the formation sand for similar percentile points of sieve analysis curves, solely from the geometrical point of view. Therefore, Bouhroum and Civan (1995) state:

A major problem with gravel-pack design criteria is the significant focus given by researchers to the geometrical retention criteria while neglecting the other aspects of the filtration process, such as clogging and hydrodynamics.

Table 20–3 by Tiffin et al. (1998) outlines typical sand sorting ratios that can be determined by sieve analyses. In this table, the cumulative % sieve size distributions are denoted by the letter “D”. For example, D50 indicates the sieve opening above which 50% of the sand particles are retained. Tiffin et al. (1998) report that typical moderate size, well sorted formation yields a D40/D90 value of 2.8, while a more poorly sorted sample yields a value of 10 for the D40/D90 ratio. Formations having different sizing may have the same sorting ratio. However, this does not matter because the focus of interest here is the ability of the formation sand particles to form bridges and plug screens or gravel pack

(text continued on page 654)

Table 20-1
Evaluation Criteria for Formation Assessment

FACTOR		CONDITIONS & VALUES		Pts	
Porosity (ϕ)	> 30%			+5	
	< 30%			+0	
Clay Content	> 15%			+5	
	< 15%			+0	
Original Pressure Gradient	> 0.6 psi/ft			+10	
	< 0.6 psi/ft			+0	
Current Pressure Gradient	> 0.3 psi/ft			+0	
	< 0.3 psi/ft			+5	
Formation Age	Young			+5	
	Old			+0	
	Age	TVD < 15,000ft.		+5	
	NotKnown	TVD > 15,000ft		+0	
Formation Depth	> 15,000 ft			+5	
	8,000 – 15,000 ft			+0	
	< 8,000 ft			+5	
Water Solubility	TRUE			+10	
	FALSE			+0	
Water Breakthrough	Water			+0	
	Oil/Gas	TRUE		+5	
		FALSE		+0	
Injector Well	TRUE			+15	
	FALSE			+0	
Formation Condition	Condition NotKnown	Old	ϕ > 30%	+5	
			ϕ < 30%	+0	
		Young	ϕ > 30%	+10	
			ϕ < 30%	+0	
		Age NotKnown	TVD < 15,000ft	ϕ > 30%	+10
				ϕ < 30%	+0
		TVD > 15,000ft	ϕ > 30%	+5	
			ϕ < 30%	+0	
		Friable		+5	
		Well Consolidated		+0	
Poorly Consolidated		+15			
API Gravity	Water/Gas			+0	
	Oil	< 15°		+0	
		15°–25°		+5	
		> 25°		+10	
Drawdown	Gas	< 750 psi		+0	
		> 750 psi		+15	
		< 400 psi		+0	
	Oil/Water	> 400 psi		+15	
Special Formation Conditions	(Well Consolidated) AND (Not Water Soluble)			-100	
	Otherwise			+0	

After Kanj, M., Zaman, M., & Roegiers, J.-C., ©1996; reprinted by permission of Computational Mechanics Inc.

Table 20-2
Heuristic Evaluation Criteria for Sand Control Methods

FACTOR	(1) Fine Sand	(2) Interval			(3) Multiple Packs		(4) Permeability Variation				(5) Fluid Produced		
		≤ 10 ft	10 - 50 ft	> 50 ft	Top	Bottom	Heterog.	Laminated	None	NotKnown	Gas	Oil	Water
WEIGHT	6	2	5	10	10	10	7	7	0	2	6	6	6
METHOD													
Auger Pack	A	B	B	A	N/A	A	A	B	A	B	A	A	A
Open Hole GP	B	A	A	B	N/A	A	B	A	A	B	A	A	A
Thru Tubing GP	C	C	C	E	N/A	A	C	D	A	D	B	C	C
Conventional GP	C	C	C	C	A	A	C	C	A	C	B	C	C
Consolidated Frac.	A	B	B	C	A	A	A	A	A	A	B	B	C
Frac Pack	A	A	A	B	A	A	A	A	A	A	A	A	A
Sand Consolidation	D	C	E	F	A	A	D	D	A	D	C	C	C
Drawdown Reduction	E	D	D	D	A	A	D	D	A	D	D	D	D
Hi Rate Water Pack	A	A	A	A	A	A	A	B	A	B	A	B	B
Resin Coated	D	C	C	D	A	A	D	D	A	D	D	D	D

FACTOR	(6) Productivity	(7) Old Well	(8) Permeability			(9) Longevity	(10) No Rig	(11) Trajectory			(12) Completion Type	
			≥ 50 md	< 50 md	NotKnown			> 45°	≤ 45°	Horiz.	Open	Cased
WEIGHT	10	2	7	7	2	9	10	7	4	7	10	10
METHOD												
Auger Pack	B	B	A	B	B	A	N/A	C	A	E	A	A
Open Hole GP	A	C	A	B	B	B	N/A	A	A	A	A	N/A
Thru Tubing GP	C	C	C	D	D	B	A	C	C	D	A	A
Conventional GP	C	C	C	D	D	B	N/A	C	C	D	A	A
Consolidated Frac.	A	B	B	A	B	B	A	C	A	C	A	A
Frac Pack	A	A	A	A	A	A	N/A	A	A	C	A	A
Sand Consolidation	D	F	C	D	D	C	C	E	D	F	N/A	A
Drawdown Reduction	E	E	D	C	D	D	B	D	D	D	A	A
Hi Rate Water Pack	B	A	B	B	B	A	N/A	A	A	A	A	A
Resin Coated	D	D	D	D	D	C	N/A	E	E	F	A	A

After Kanj, M., Zaman, M., & Roegiers, J-C., ©1996; reprinted by permission of Computational Mechanics Inc.

Table 20–3
Criteria for Formation Sand Sorting

Sorting or Comparison	Proposed Purpose
D50	Standard Saucier Criteria
D40/D90	Screen Damage Ratio from Pall
D10/D95	Size range between common min and max particle sizes
sub 325 mesh	Quantity of sub 44 micron particles

After Tiffin et al., ©1998 SPE; reprinted by permission of the Society of Petroleum Engineers.

(text continued from page 651)

(Tiffin et al., 1998). Based on their investigations, Tiffin et al. (1998) proposed the following sorting criteria and completion methods:

1. (D10/D95<10, D40/D90<3, sub 325 mesh<2%) the lowest sorting values with low fines content may be bare screen completion candidates. (Need >1 Darcy formation permeability for cased and perforated completion, with possible use of prepacked screens).
2. (D10/D95<10, D40/D90<5, sub 325 mesh<5%) low to medium sorting ranges, or with fines just out of range may best be served by bare screen completions with new technology, woven mesh screens. (Need >1 Darcy formation permeability for cased and perforated completion).
3. (D10/D95<20, D40/D90<5, sub 325 mesh<5%) medium ratio ranges may be served by larger gravel (7x or 8x 50%), placed in high rate water pack, particularly if the formation sand size is consistent over the zone (no laminations and minimum streaks).
4. (D10/D95<20, D40/D90<5, sub 325 mesh<10%) medium ratio ranges with too many fines may use a combination of larger gravel and a fines-passing screen.
5. (D10/D95<20, D40/D90<5, sub 325 mesh<10%) the highest ratios, particularly those coupled with large amounts of fines signal a critical need for enlarging the wellbore (move the gravel/formation sand interface away from the wellbore), through fracturing, horizontal or multi-lateral well technology underreaming, or large volume prepacking to minimize severe permeability damage at the gravel/sand interface due to flow.

Figure 20–1 by Skjærstein and Tronvoll (1997) indicate the in-situ stress conditions around a perforation cavity and replication of these

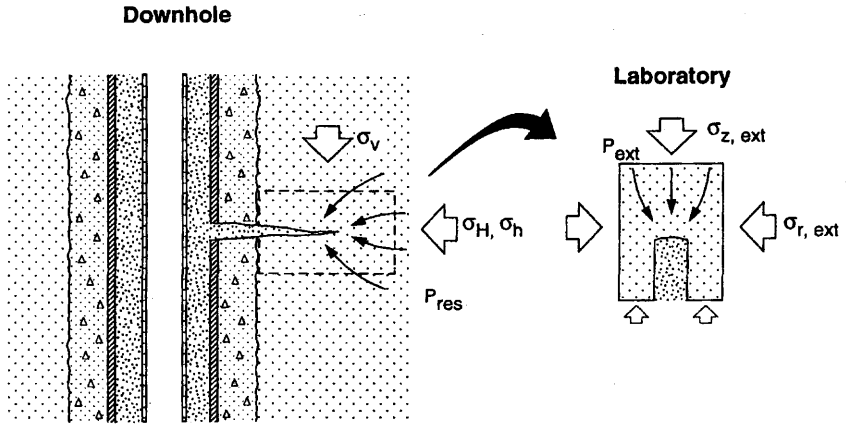


Figure 20-1. Representation of downhole perforation conditions in the laboratory (after Skjærstein and Tronvoll, ©1997 SPE; reprinted by permission of the Society of Petroleum Engineers).

conditions in a laboratory test sample. Figure 20-2 by Burton (1998) describes the typical flow pattern involving a perforated, cased-hole gravel-packed completion and delineates the location of various types of skin effect. As can be seen, completion pressure losses involve low- and high-velocity flow regions that can be classified as Darcy and non-Darcy flow regions, respectively.

Prediction of Sanding Conditions

Hayatdavoudi (1999) developed a simplified model by modifying the Spangler and Handy (1982) model.

The induced shear-stress, τ_i , in the direction of flow or its equivalent pressure drop and the induced acceleration, a_i , of the formation particles can be related by Newton's second law as (Spangler and Handy, 1982):

$$\tau_i = ma_i \quad (20-1)$$

where m is the mass of the sand particle. On the other hand, the maximum, critical, or threshold shear resistance of the sand, including the additional factors resulting from water invasion, is expressed as following by Hayatdavoudi (1999):

$$\tau_{cr} = \sigma_c + \left\{ \sigma_v - \left[P_p \pm (P_s + P_{os} + P_c) \right] \right\} \tan \theta_{cyc} \quad (20-2)$$

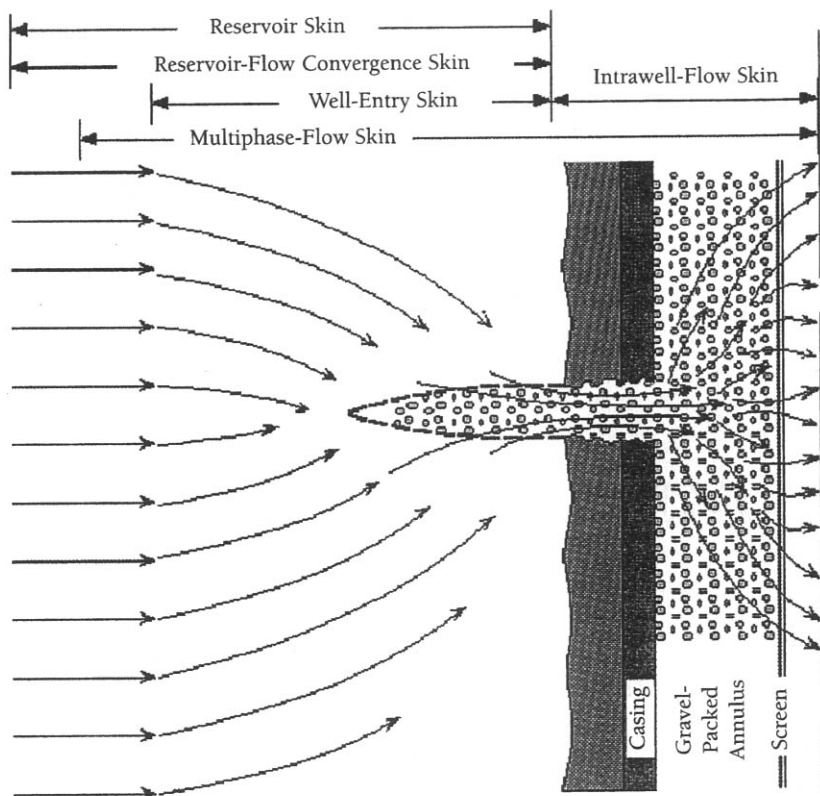


Figure 20–2. Flow field around a perforated, cased-hole gravel-packed completion (after Burton, ©1998 SPE; reprinted by permission of the Society of Petroleum Engineers).

where σ_c is the effective cohesive strength of the formation sand (lb/ft²) and σ_v is the effective vertical stress (lb/ft²). P_p , P_s , P_{os} , and P_c denote, respectively, the pore fluid, clay swelling, osmotic, and capillary pressures. θ_{cyc} denotes the cyclic angle of internal friction. Therefore, sand liquefaction occurs when the prevailing shear stress exceeds the threshold shear stress, that is,

$$\tau_i \geq \tau_{cr} \quad (20-3)$$

Neglecting the fluid acceleration effect, Hayatdavoudi (1999) expressed the induced acceleration of particles by

$$a_i = 2\pi f_{sw} v_{pv} \quad (20-4)$$

where v_{pv} is the induced velocity of particles and f_{sw} is the shear wave frequency. In case of the lack of information for Eq. 20-4, Hayatdavoudi (1999) recommends estimating a_i by:

$$a_i \cong 0.19g \quad (20-5)$$

where g denotes the gravitational acceleration.

Hayatdavoudi (1999) points out the importance of the buoyant unit weight of the in-situ particles when determining the particle mass, and estimates the in-situ particle mass by:

$$m = (\gamma_{ave}/g)z \quad (20-6)$$

where z represents the depth or height measured from a reference datum (ft) and γ_{ave} is the average specific weight of the formation sand (lb/ft³). The latter is expressed as:

$$\gamma_{avg} = \frac{1}{2} \left(\gamma_{in\ the\ oil\ zone} + \gamma_{in\ the\ water\ zone} \right) \quad (20-7)$$

in which the specific weights of the sand grains in the water and oil zones are given, respectively, by:

$$\gamma_{in\ the\ water\ zone} = \frac{\gamma_w G}{1 + e} \quad (20-8)$$

$$\gamma_{in\ the\ oil\ zone} = \frac{\gamma_o G}{1 + e} \quad (20-9)$$

where the void ratio, e , in terms of the fractional porosity, ϕ , is given by:

$$e = \frac{\phi}{1 - \phi} \quad (20-10)$$

and γ_w and γ_o are the specific weights of the water and oil phases, and G is the specific gravity of the sand grains.

As a fluid flows over the face of a cohesionless bed of particles, such as sand or gravel, the particles can be detached and lifted-off when the fluid shear-stress exceeds the minimum, critical shear-stress. Yalin and

Karahan (1979) developed a dimensionless correlation to predict the critical conditions for onset of particle mobilization (or scouring) by fluid shear. Following their approach, Tremblay et al. (1998) developed:

$$M_{cr} = 0.122 \text{Re}_{cr}^{-0.206} \quad (20-11)$$

in which Re_{cr} is the critical particle Reynolds number given by

$$\text{Re}_{cr} = \frac{\rho v_{cr} d}{\mu} \quad (20-12)$$

where v_{cr} is the critical shear velocity, d is the mean particle diameter, and ρ and μ are the density and viscosity of the fluid flowing over the particle bed.

M_{cr} is the critical mobility number given by

$$M_{cr} = \frac{\rho v_{cr}^2}{\gamma_s d} \quad (20-13)$$

where γ_s denotes the specific weight of the particles suspended in the fluid.

Applying Eq. 20-11, Tremblay et al. (1998) correlated their experimental data of laminar flow of various liquids over a loose bed of sand particles linearly on a full logarithmic scale and obtained the following expression for the critical shear velocity:

$$v_{cr} = 0.385 (\mu/\rho)^{0.0934} \gamma_s^{0.453} d^{0.36} \rho^{-0.453} \quad (20-14)$$

Then, they predict the critical shear-stress on the scouring face by:

$$\tau_{cr} = \rho v_{cr}^2 \quad (20-15)$$

Massive Sand Production Model

Many models with varying degrees of predictive capabilities are available for sand production. Here, the radial continuum model for massive sand production, coupling fluid, and granular matrix flows by Geilikman and Dusseault (1994, 1997) is presented for instructional purposes. This is a physics-based approach that includes the essential ingredients of a sand production model. However, applications to other

cases, such as horizontal and deviated wells, and different formations may require further developments.

The decline of pressure during production causes flow and stress-induced damage in the near-wellbore region. The increase in the deviatoric stress above the yield condition in unconsolidated sandstone formations cause instabilities and plastic flow leading to sand production.

As depicted in Figure 20–3, Geilikman and Dusseault (1997) considers two regions for modeling purposes: (1) a yielded-zone, initiating from the wellbore and extending to a propagating front radius, $R=R(t)$, and (2) an intact-zone, beyond the propagating front of the yielded-zone.

They consider a two-phase continuum medium: (1) a viscoplastic solid skeleton, and (2) an incompressible and viscous saturated fluid. The modeling is carried out per unit formation thickness.

The yield function, F , for granular matrix is defined as (Jackson, 1983; Collins, 1990; Pitman, 1990; Drescher, 1991):

$$F = \frac{\sigma_{\theta} - \sigma_r}{2} - c - \gamma \left(\frac{\sigma_r + \sigma_{\theta}}{2} - p \right) = 0 \quad (20-16)$$

where σ_r and σ_{θ} denote the radial and tangential stresses, respectively, (Pa), c is the cohesive strength (Pa), γ is a friction coefficient (dimensionless), and p is the fluid pressure (Pa).

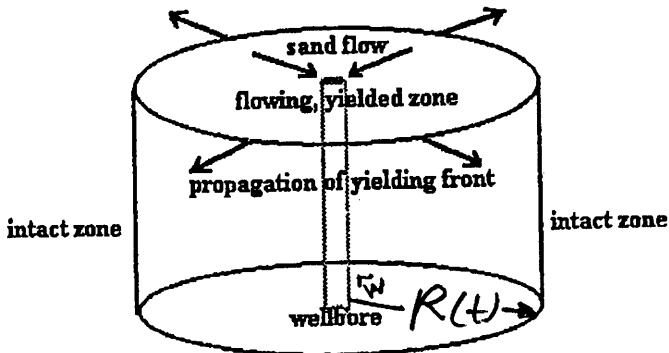


Figure 20–3. Growing yielded zone and the intact zone around a producing well (reprinted from *Journal of Petroleum Science and Engineering*, Vol. 17, Geilikman, M. B., and Dusseault, M. B., “Fluid Rate Enhancement from Massive Sand Production in Heavy-Oil Reservoirs,” pp. 5–18, ©1997, with permission from Elsevier Science).

The stress equilibrium condition for the solid skeleton is given by:

$$\frac{d\sigma_r}{dr} + \frac{\sigma_r - \sigma_\theta}{r} - b \frac{\mu}{K} (v_f - v_s) = 0 \quad (20-17)$$

in which b is the coefficient of the body force, approximated by:

$$b = \frac{\phi_i}{1 - \phi_i} \quad (20-18)$$

where ϕ_i is the porosity of the intact zone; K is permeability; μ is viscosity; v_f and v_s denote the fluid and solid phase velocities, respectively; and r is the radial distance.

The Darcy law is applied for the mobile fluid phase

$$\frac{dp}{dr} = -\frac{\mu}{K} (v_f - v_s) \quad (20-19)$$

Assuming that the fluid and solid phases are incompressible, the volumetric balance equations (equation of continuity) of the fluid and solid phases are given by:

$$\frac{\partial \phi}{\partial t} + \nabla \cdot (\phi v_f) = 0 \quad (20-20)$$

$$-\frac{\partial \phi}{\partial t} + \nabla \cdot [(1 - \phi) v_s] = 0 \quad (20-21)$$

In the intact zone, the porosity, ϕ_i , is assumed constant. Thus, Eqs. 20-20 and 21 simplify as:

$$\nabla \cdot (\phi v_f) = 0 \quad (20-22)$$

$$\nabla \cdot [(1 - \phi) v_s] = 0 \quad (20-23)$$

Thus, the fluid velocities in the yielded and intact zones can be expressed, respectively, by:

$$v_f = -\frac{q(t)}{2\pi\phi_y r} - \frac{1 - \phi_y}{\phi_y} v_s \quad (20-24)$$

$$v_f = -\frac{q_f(t)}{2\pi\phi_i r} \quad (20-25)$$

Similarly, the solid velocity is given by:

$$v_s = -\frac{q_s}{2\pi(1-\phi_y)r} \quad (20-26)$$

Therefore, substituting Eqs. 20-23 through 26 into Eq. 20-19 and integrating, yields the following fluid pressure profiles in the yielded and intact zones, respectively:

$$p_y(cr) = p_w + \frac{\mu}{2\pi\phi_y K_y} \left(q - \frac{q_s}{1-\phi_y} \right) \ell n \left(\frac{r}{r_w} \right), \quad r_w < r < R \quad (20-27)$$

and

$$p_i(r) = p_e - \frac{\mu q_f}{2\pi\phi_i K_i} \ell n \left(\frac{r_e}{r} \right), \quad R < r < r_e \quad (20-28)$$

The consistency and compatibility conditions for the fluid flow at the moving front are given, respectively, by:

$$\phi_i(v_i - V) = \phi_y(v_y - V), \quad r = R(t) \quad (20-29)$$

$$p_y = p_i, \quad r = R(t) \quad (20-30)$$

r_w and r_e denote the wellbore and reservoir radii, respectively, and p_w and p_e are the fluid pressures at these locations.

The consistency and compatibility conditions for the solid flow at the moving front between the yielded and intact zones are given, respectively, by:

$$(1-\phi_i)V = (1-\phi_y)(V - v_s) \quad (20-31)$$

where V is the front velocity, given by:

$$V \equiv dR/dt \quad (20-32)$$

in which $R=R(t)$ denotes the radial distance to the front. Substituting Eqs. 20–26 and 32 into Eq. 20–31, and solving the resulting expression for the cumulative volume of solids production, S_c , yields:

$$S_c(t) = \pi(\phi_y - \phi_i)(R^2 - r_w^2) \quad (20-33)$$

The volumetric rate of solid production is given by

$$q_s = dS_c/dt \quad (20-34)$$

In the yielded zone, eliminating the tangential stress, σ_θ , between Eqs. 20–16 and 17 leads to:

$$\frac{d\sigma_r}{dr} - \left(\frac{2}{1-\gamma} \right) \frac{1}{r} [\gamma(\sigma_r - p) + c] - \frac{b\mu}{K_y} (v_f - v_s) = 0 \quad (20-35)$$

subject to the conditions at the wellbore

$$\sigma_r = p_w, \quad r = r_w \quad (20-36)$$

and at the moving front

$$\sigma_r = p_y, \quad r = R(t) \quad (20-37)$$

Thus, substituting Eqs. 20–25 and 26 into Eq. 20–35 and solving, leads to the following expression for the radial stress in the yielded zone:

$$\left[\sigma_r(r) - p_y(r) \right] r^{-\lambda} - \frac{r_w^{-\lambda} - r^{-\lambda}}{\lambda} \left[\frac{2c}{1-\gamma} - \frac{(1+b)\mu}{2\pi\phi_y K_y} \left(q - \frac{q_s}{1-\phi_y} \right) \right] = 0 \quad (20-38)$$

where $\lambda = 2\gamma/(1-\gamma)$.

Substituting Eqs. 20–27 through 30 into Eq. 20–38, q_s can be calculated.

Incorporating some simplifying approximations, Geilikman and Dusseault (1997) obtain the following expression for sand production rate:

$$\begin{aligned}
& \frac{\mu(1+b)}{2\pi\phi_i K_i(1-\phi_y)} \frac{dS_c}{dt} \approx [P_c - P_w(t)] \frac{1+b}{\ell n(\rho_e/\rho)} \\
& + \frac{\left\{ (1-\gamma)(1+b)[P_c - P_w(t)] - \frac{2c(\rho^\lambda - 1)}{\lambda(1-\gamma)} \right\} \left[\frac{K_y\phi_y}{K_i\phi_i} + \frac{\ell n\rho}{\ell n(\rho_e/\rho)} \right]}{\frac{\rho^\lambda - 1}{\lambda} - (1-\gamma)\ell n\rho} \quad (20-39)
\end{aligned}$$

which can be numerically integrated assuming a wellbore fluid pressure history, represented by the following decay function:

$$p_w(t) = p_\infty + (p_c - p_\infty) \exp(-t/t_p) \quad (20-40)$$

where t_p is a characteristic time scale, p_c is some critical fluid pressure at which the yield criterion is met, and p_∞ is the limit value of the wellbore pressure for $t \gg t_p$.

The volumetric rates of fluid production is given by:

$$q_f(t) = \frac{q_o(t) \frac{K_y\phi_y}{K_i\phi_i} \ell n\left(\frac{r_e}{r_w}\right) + \frac{q_s(t)}{1-\phi_y} \ell n\left[\frac{R(t)}{r_w}\right]}{\ell n\left[\frac{R(t)}{r_w}\right] + \frac{K_y\phi_y}{K_i\phi_i} \ell n\left[\frac{r_e}{R(t)}\right]} \quad (20-41)$$

in which $q_o(t)$ is the rate of fluid production without any sand production, given by:

$$q_o(t) = \frac{2\pi K_i\phi_i}{\mu \ell n(r_e/r_w)} [p_e - p_w(t)] \quad (20-42)$$

Geilikman and Dusseault (1997) defined dimensionless sand production rate, time, characteristic time, and fluid production enhancement ratio, respectively as:

$$q_D = q_s \frac{\mu(1+b)}{2\pi K_i\phi_i(1-\phi_y)(p_c - p_\infty)} \quad (20-43)$$

$$\tau = t \frac{2K_i\phi_i(p_c - p_\infty)}{\mu(1+b)r_w^2} \quad (20-44)$$

$$\tau_p = t_p \frac{2K_i\phi_i(p_c - p_\infty)}{\mu(1+b)r_w^2} \quad (20-45)$$

$$E(t) = q_f(t)/q_o(t) \quad (20-46)$$

Figures 20–4 and 20–5 by Geilikman and Dusseault (1997) present typical solutions for the rate of sand production and enhancement of fluid production.

Sand Retention in Gravel-Packs

As stated by Bouhroum et al. (1994):

Sand production poses serious problems to tubular material, surface equipment and the stability of the well. . . . A popular method of

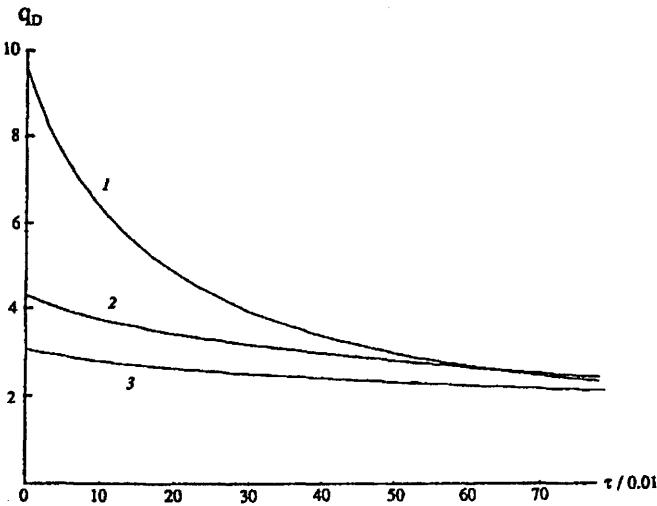


Figure 20–4. Dimensionless volumetric sand production rate vs. dimensionless time: Curves 1, 2, and 3 are for $T = 0.1, 0.5$, and 1.0 , respectively (reprinted from *Journal of Petroleum Science and Engineering*, Vol. 17, Geilikman, M. B., and Dusseault, M. B., “Fluid Rate Enhancement from Massive Sand Production in Heavy-Oil Reservoirs,” pp. 5–18, ©1997, with permission from Elsevier Science).

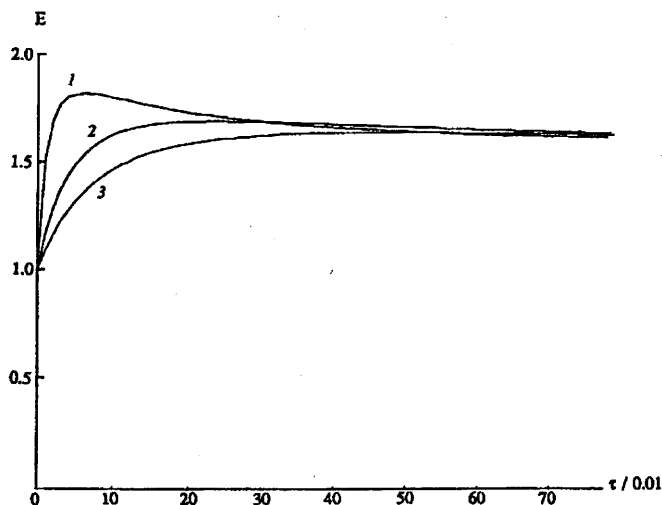


Figure 20-5. Short-term fluid production improvement vs. dimensionless time: Curves 1, 2, and, 3 are for $T = 0.1$, 0.5 , and, 1.0 , respectively (reprinted from *Journal of Petroleum Science and Engineering*, Vol. 17, Geilikman, M. B., and Dusseault, M. B., "Fluid Rate Enhancement from Massive Sand Production in Heavy-Oil Reservoirs," pp. 5–18, ©1997, with permission from Elsevier Science).

combating sand production is using gravel-packs. Gravel-packs have a protective function to inhibit the flow of sand particulates into the well.

Bouhroum et al. (1994) essentially applied the Ohen and Civan (1993) model, given in Chapter 10 with several simplifications for prediction of the gravel-pack permeability impairment by sand deposition. The important simplifying assumptions of this model are: (a) the sand particles are generated in the near-wellbore formation and deposited in the gravel-pack, and (b) the clay swelling effects are not considered. As attested by the results given in Figures 20-6 and 20-7, their predictions accurately match the experimental values.

References

- Bouhroum, A., Liu, X., & Civan, F., "Predictive Model and Verification for Sand Particulates Migration in Gravel-Packs," SPE 28534 paper, Proceedings of the SPE 69th Annual Technical Conference and Exhibition, September 25–28, 1994, New Orleans, Louisiana, pp. 179–191.

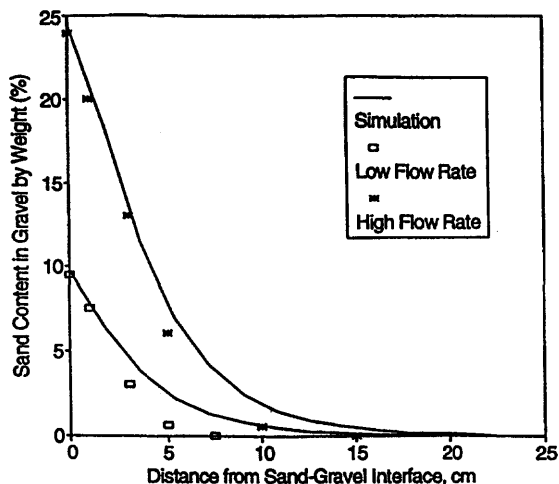


Figure 20-6. Simulation of experimental data for low and high flow rate profiles of migrated sand particles in a 7.5 gravel to sand ratio gravel-pack (after Bouhroum et al., ©1994 SPE; reprinted by permission of the Society of Petroleum Engineers).

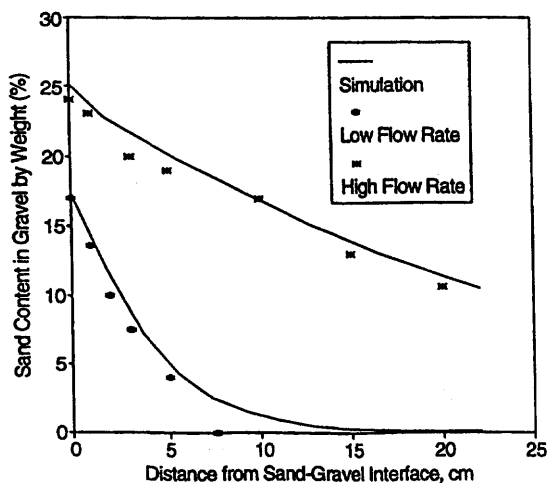


Figure 20-7. Simulation of experimental data for low and high flow rate profiles of migrated sand particles in a 6.3 gravel to sand ratio gravel-pack (after Bouhroum et al., ©1994 SPE; reprinted by permission of the Society of Petroleum Engineers).

- Bouhroum, A., & Civan, F., "A Critical Review of Existing Gravel-Pack Design Criteria," *Journal of Canadian Petroleum Technology*, Vol. 34, No. 1, 1995, pp. 35–40.
- Burton, R. C., "Perforation-Tunnel Permeability Can Assess Cased-Hole Gravel-Pack Performance," *J. of Petroleum Technology*, March 1998, pp. 86–87.
- Collins, I. F., "The Mathematical Structure of the Equations for Quasi-Static Plane Strain Deformations of Granular Material," in D. D. Joseph & D. G. Schaeffer (Eds.), *Two Phase Flow and Waves*, The IMA Volumes in Mathematics and its Applications Series 26, Springer, New York, p. 30, 1990.
- Drescher, A., "Analytical Methods in Bin-Load Analysis," *Developments in Civil Engineering Series 36*, Elsevier, Amsterdam, 255 p., 1991.
- Dusseault, M. B., & Santarelli, F. J., "A Conceptual Model for Massive Solids Production in Poorly-Consolidated Sandstones," *Rock at Great Depth*, Maury & Fourmantraux (Eds.), Balkema, Rotterdam, 1989, pp. 789–797.
- Geilikman, M. B., Dusseault, M. B., & Dullien, F. A. L., "Sand Production as a Viscoplastic Granular Flow," SPE 27343 paper, SPE International Symposium on Formation Damage Control, February 9–10, 1994, Lafayette, Louisiana, pp. 41–50.
- Geilikman, M. B., & Dusseault, M. B., "Fluid Rate Enhancement from Massive Sand Production in Heavy-Oil Reservoirs," *J. of Petroleum Science and Engineering*, Vol. 17, No. 1/2, 1997, pp. 5–18.
- Hayatdavoudi, A., "Formation Sand Liquefaction: A New Mechanism for Explaining Fines Migration and Well Sanding," SPE 52137 paper, SPE Mid-Continent Operations Symposium, March 28–31, 1999, Oklahoma City, Oklahoma, pp. 177–180.
- Jackson, R., "Some Mathematical and Physical Aspects of Continuum Models for the Motion of Granular Materials," in R.E. Meyer (Ed.), *Theory of Dispersed Multiphase Flow*, Academic Press, New York, New York, 1983.
- JPT, "Specialists Share Knowledge of Sand-Control Methods," *J. of Petroleum Technology*, July 1995, pp. 550–609.
- Kanj, M., Zaman, M., & Roegiers, J-C., "Highlights from the Knowledge-Base of a Sanding Advisor Called SITEX," *Computer Methods and Water Resources III*, Abousleiman, Y., Brebbia, C. A., Cheng, A.H.-D., & Ouazar, D. (Eds.), Computational Mechanics Publications, Southampton, Boston, 1996, pp. 391–398.
- Pitman, E. B., "Computations of Granular Flow in Hopper," in D. D. Joseph & D. G. Schaeffer (Eds.), *Two Phase Flow and Waves*, The IMA Volumes in Mathematics and its Applications Series 26, Springer, New York, 1990, p. 30.

- Saucier, R. J., "Successful Sand Control Design for High Rate Oil and Water Wells," *J. of Petroleum Technology*, Vol. 21, 1969, p. 1193.
- Saucier, R. J., "Considerations in Gravel-Pack Design," *J. of Petroleum Technology*, Vol. 26, 1974, p. 205.
- Skjærstein, A., & Tronvoll, J., "Gravel Packing: A Method of Wellbore Re-enforcement or Sand Filtering?," SPE 37506 paper, SPE Production Operations Symposium, March 9–11, 1997, Oklahoma City, Oklahoma, pp. 871–879.
- Spangler, M. G., & Handy, R. L., *Soil Engineering*, Harper & Row, New York City, New York, 1982.
- Tiffin, D. L., King, G. E., Larese, G. E., & Britt, R. E., "New Criteria for Gravel and Screen Selection for Sand Control," SPE 39437 paper, SPE Formation Damage Control Conference, February 18–19, 1998, Lafayette, Louisiana, pp. 201–214.
- Tremblay, B., Sedgwick, G., & Forshner, K., "Modeling of Sand Production from Wells on Primary Recovery," *Journal of Canadian Petroleum Technology*, Vol. 37, No. 3, March 1998, pp. 41–50.
- Yalin, M. S., & Karahan, E., "Inception of Sediment Transport," *Journal of the Hydraulics Division*, Vol. 105 (HY11), American Society of Civil Engineers, November 1979, pp. 1433–1443.

Chapter 21

Formation Damage by Scale Deposition

Summary

In this chapter, Roberts' (1997) simplified radial flow model for prediction of well flow performance during deposition of scales is presented. Its applications are presented for sulfur and calcite deposition problems according to Roberts (1997) and Satman et al. (1999), respectively.

Introduction

Scale deposition in porous media occurs when the fluid becomes supersaturated by changes of the in-situ pressure and/or temperature conditions (see Chapters 9, 13 and 14). Mathematical models are required for prediction of the effects of scale deposition on well flow performance and for development of strategies to mitigate the processes causing scale deposition. In this chapter, Roberts' (1997) simplified radial flow model is briefly described. Then, its applications and results for sulfur deposition by Roberts (1997) and for calcite deposition by Satman et al. (1999) are presented. These applications demonstrate the capabilities of Roberts' (1997) model. Leontaritis (1998) developed a radial flow model for organic deposition, which shares some common ground with Roberts' (1997) model (see Chapter 14).

Sulfur Deposition Model

The affect of sulfur deposition on the loss of well performance in some sour-gas reservoirs has been reported by Roberts (1997). As pointed out by Roberts (1997), sour-gas contains large quantities of elemental sulfur. Therefore, decrease of pressure and temperature during production of sour-gas can lead to the elemental sulfur dissolved in sour-gas to separate and deposit as solids and cause a decline of the well performance. Sulfur

deposition can occur both in the well and reservoir formation (Hyne, 1968, 1980, 1983; Kuo, 1972; Roberts, 1997). In this section, a brief discussion of the simplified analytical modeling effort by Roberts (1997) for prediction of the formation damage by sulfur deposition is presented.

Hyne (1968, 1980, 1983) has considered the possibility of formation of hydrogen polysulfides at high pressure and temperature conditions by reaction of the hydrogen sulfide and sulfur according to the following equation:



Roberts (1997) points out that two mechanisms may be considered for the solubility of sulfur in the sour-gas: (1) physical and (2) chemical. Hyne (1980, 1983) considered that sulfur may dissolve at high temperature and pressure conditions because of the production of hydrogen polysulfides by a reaction of the hydrogen sulfide with sulfur according to the following equation:



Thus, when the pressure and temperature are lowered, this reaction should reverse itself to form solid elemental sulfur. However, Roberts (1997) argues that its affect can be neglected because the reverse reaction is slow compared to the high flow rate conditions prevailing in the near-wellbore formation. Therefore, for all practical purposes, Roberts (1997) assumes and verifies that sulfur is physically dissolved in the sour-gas and separates instantaneously as solids when the pressure declines to below the saturation conditions.

Roberts (1997) draws attention to the field experience (Chernik and Williams, 1993) that sulfur deposition in liquid form does not create many problems, whereas sulfur deposition in solid form may cause severe formation damage problems.

Solubility of Sulfur in Natural Gas

Roberts (1997) states that elemental sulfur freezes at 119°C at atmospheric pressure, but the freezing point decreases by increasing H_2S concentration in the sour-gas. Because experimental measurement of the sulfur solubility is expensive and tedious, Roberts (1997) uses the simplified thermodynamic equation given by Chrastil (1982) based on the ideal solution theory for estimation of the sulfur solubility as:

$$c_r = \rho^k \exp(A/T + B) \quad (21-3)$$

In Eq. 21-3, c_r represents the concentration of the solid sulfur dissolved in the gas expressed as mass per unit reservoir gas volume

($g/reservoir\ m^3$), ρ is the density of the gas (kg/m^3), T is the reservoir gas temperature, and k , A , and B are some empirically determined parameters. As shown by Roberts (1997), using the data by Brunner and Woll (1980, 1988), the plots of Eq. 21-3 at given temperatures are fairly linear on the $\log c_r$ vs. $\log p$. Also, the plot of $\log c_r$ vs. $(1/T)$ given by Roberts (1997) shows a linear trend. Therefore, Roberts (1997) concludes that Eq. 21-3 can be used for prediction of the sulfur solubility in gas and presents the following correlation:

$$c_r = \rho^4 \exp\left(-\frac{4,666}{T} - 4.5711\right) \quad (21-4)$$

Note that Eq. 21-4 implicitly includes the affect of the reservoir gas pressure because the gas density is given by:

$$\rho = \frac{Mp}{ZRT} \quad (21-5)$$

Thus, invoking Eq. 21-5 and then differentiating Eq. 21-4 yields the following expression for the variation of the sulfur solubility by pressure at a prescribed reservoir temperature as:

$$\left(\frac{\partial c_r}{\partial p}\right)_T = 4c_r \left[1 - \frac{p}{Z} \left(\frac{\partial Z}{\partial p}\right)_T\right] \quad (21-6)$$

Modeling Near-Wellbore Sulfur Deposition

Consider the radial flow model of an areal drainage region around a well. Roberts (1997) considered a sour-gas reservoir operating under isothermal and semi-steady state radial flow conditions and expressed the pressure gradient as:

$$\frac{dp}{dr} = \frac{q\mu B}{2\pi r h k_a k_r} \quad (21-7)$$

where q is the constant gas production rate (m^3/s), μ is the gas viscosity ($Pa.s$), B is an empirical constant, the formation volume factor, h is the thickness of the net pay zone of the formation (m), r is the radial distance from the center of the well (m), k_a is the permeability of the formation at the initial water saturation (m^2), and k_r is the relative permeability

of the gas (dimensionless). Roberts (1997) assumes a relative permeability function as (Kuo, 1972):

$$\ell nk_r = aS_s \quad (21-8)$$

where “ a ” is an empirical constant.

The volume of the sulfur separating as solid precipitates for an infinitesimal reduction of pressure, dp , within an infinitesimally small time interval, dt , is given by:

$$dV_s = q \left(\frac{\partial c_r}{\partial p} \right)_T dp dt \quad (21-9)$$

and the volume fraction, S_s , of the hydrocarbon pore volume occupied by the sulfur deposits within an infinitesimally small cylindrical element of dr width is given by:

$$dS_s = \frac{dV_s}{2\pi r h dr \phi_i (1 - S_{wi})} \quad (21-10)$$

where ϕ_i and S_{wi} denote the initial porosity and irreducible water saturation, respectively.

Consequently, combining Eqs. 21-7 through 10 leads to the following expression for the rate of sulfur deposition:

$$\frac{dS_s}{dt} = \frac{q^2 (\partial c_r / \partial p)_T B \mu}{4\pi^2 k_a \exp(aS_s) h^2 \phi_i (1 - S_{wi}) r^2} \quad (21-11)$$

Eq. 21-11 can be numerically integrated subject to the initial condition that

$$S_s = 0 \quad (21-12)$$

Note that the amount of sulfur deposits can also be expressed as the fraction of the bulk volume occupied by the deposits as:

$$\epsilon_s = \phi_i (1 - S_{wi}) S_s \quad (21-13)$$

However, assuming constant μ , B , and $(\partial c_r / \partial p)_T$ values, Roberts (1997) integrates Eq. 21-11 analytically to obtain the following approximate expression:

$$S_s = \frac{1}{a} \ln \left\{ 1 + \left[\frac{aq^2 B \mu (\partial c_r / \partial p)_T}{4\pi^2 k_a h^2 \phi_i (1 - S_{wi})} \right] \frac{t}{r^2} \right\} \quad (21-14)$$

Figure 21-1 by Roberts (1997) shows the sulfur saturation of the pore volume determined by solving Eq. 21-14 using the assumed parameter values given as: $a = -6.22$, $B = 0.004583$, $\mu = 2.28 \times 10^{-5} \text{ Pa} \cdot \text{s}$, $k_a = 1.0 \text{ md}$, $h = 30 \text{ m}$, $\phi = 0.04$ in fraction, $S_{wi} = 0$, and $dc/dp = 4.0 \times 10^{-15} \text{ m}^3/\text{m}^3 - \text{Pa}$.

Prediction of Sulfur Deposition by Reservoir Simulation

Eq. 21-14 is only an approximate solution. Therefore, for realistic predictions, Roberts (1997) resorted to reservoir simulation. Roberts (1997) used a conventional black-oil reservoir simulator. For this purpose, Roberts (1997) considered that the oil phase with zero relative permeability can represent the sulfur deposits, and the condensate-to-gas ratio represents the partitioning of the elemental sulfur between the gas and oil phases. Roberts (1997) neglected the effect of the sulfur on the viscosity and formation volume factor of the sour-gas.

Figure 21-2 developed by Roberts (1997) shows a successful history matching of field data using the two-dimensional radial model for a layered formation. However, Roberts (1997) warns that, "The match obtained in Figure 21-2 is unlikely to be unique. Other reservoir descriptions

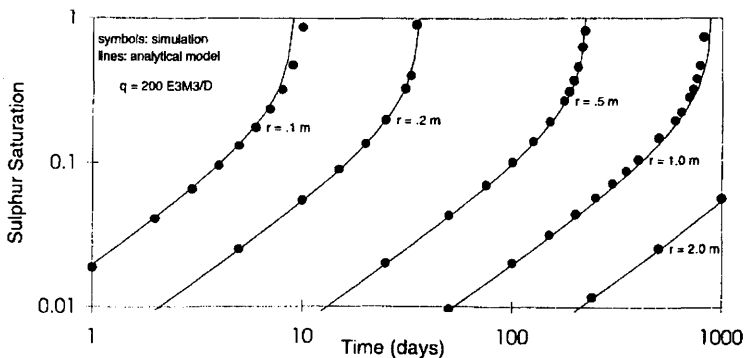


Figure 21-1. Simulation of sulfur saturations vs. time at various radial distances from the wellbore (after Roberts, ©1997 SPE; reprinted by permission of the Society of Petroleum Engineers).

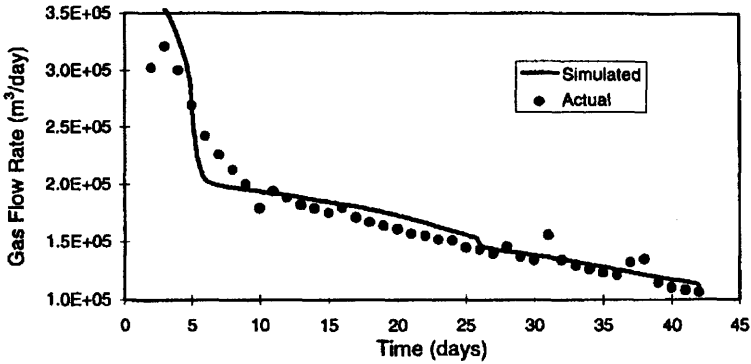


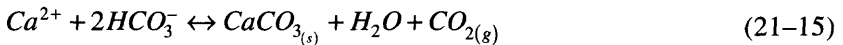
Figure 21–2. Simulation of production rate decline by sulfur deposition vs. time experimental data (after Roberts, ©1997 SPE; reprinted by permission of the Society of Petroleum Engineers).

(e.g., use of a layered model with different formation permeability) may yield equivalent results.”

Calcite Deposition Model

Adapting Roberts’ (1997) sulfur deposition model and the specific phase behavior of the CO_2 -brine systems, Satman et al. (1999) simulated the near-wellbore calcite deposition and the reduction of the geothermal well performance. The problem solved by Satman et al. (1999) and their results obtained using this model are presented in the following.

The operating chemical reaction relevant to this problem is given by



Satman et al. (1999) used the calcite solubility data available from Segnit et al. (1962). Using $q = 0.0642 \text{ m}^3/\text{s}$, $B = 1 \text{ rb/stb}$, $T = 200^\circ\text{C}$, $\mu = 1.4 \times 10^{-4} \text{ Pa} \cdot \text{s}$, $k_a = 9.869 \times 10^{-13} \text{ m}^2$, $h = 100 \text{ m}$, $a = -6.22$, $\phi = 0.1$ in fraction, and $dc/dp = 1.135 \times 10^{-12} \text{ m}^3/\text{m}^3 - \text{Pa}$ in the deposition model, they constructed Figure 21–3, showing the variation of the calcite saturation as a function of time at various radial distances from the well. Satman et al. (1999) carried out a number of case studies. The results are presented in Figures 21–4 through 21–7. Figure 21–4 shows the variation of the wellbore flowing pressure at constant flow rates during calcite deposition. Figure 21–5 shows the variation of the flow performance of wells at constant

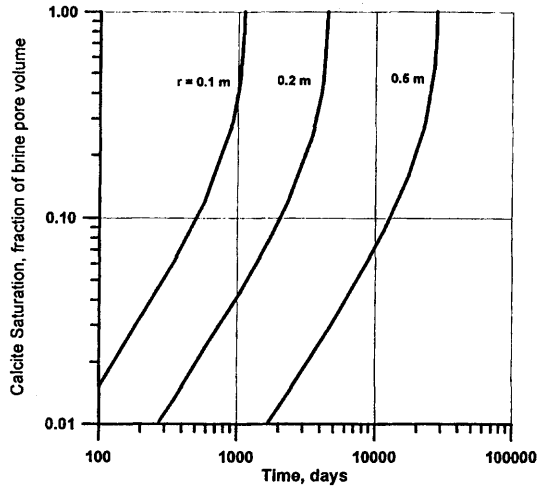


Figure 21-3. Simulation of calcite saturations vs. time at various radial distances from the wellbore (after Satman et al., ©1999; reprinted by permission of the Int. Institute for Geothermal Research, Italy).

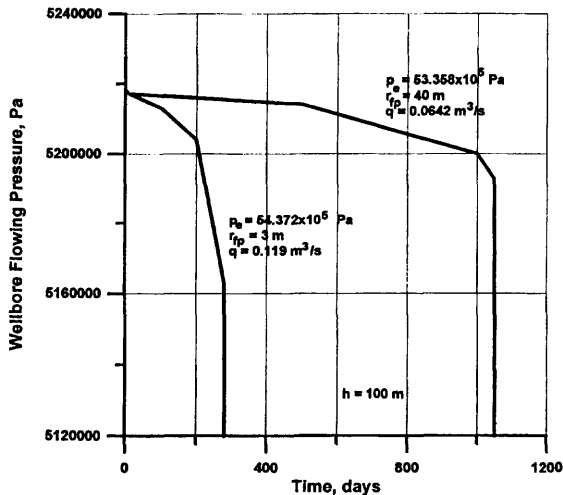


Figure 21-4. Simulation of the wellbore flowing pressure decline by plugging vs. time at 3 and 40 m radial distances to the flashing point from the wellbore, with 0.119 and 0.0642 m³/s brine flow rates, respectively, in a 100 m thick production zone (after Satman et al., ©1999; reprinted by permission of the Int. Institute for Geothermal Research, Italy).

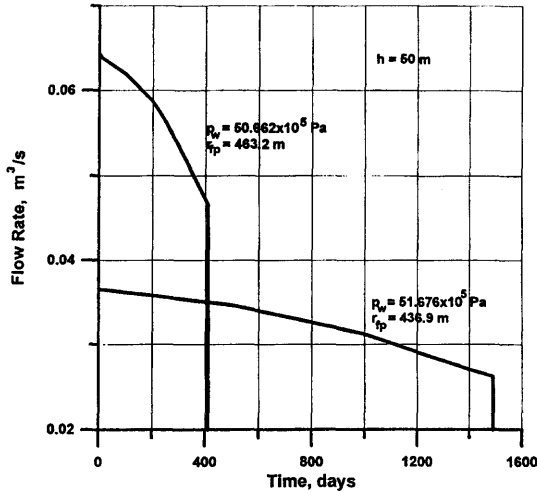


Figure 21–5. Simulation of the production rate decline by plugging vs. time at 436.9 and 463.2 m radial distances to the flashing point from the wellbore, for constant wellbore flowing pressure and a 50 m thick production zone (after Satman et al., ©1999; reprinted by permission of the Int. Institute for Geothermal Research, Italy).

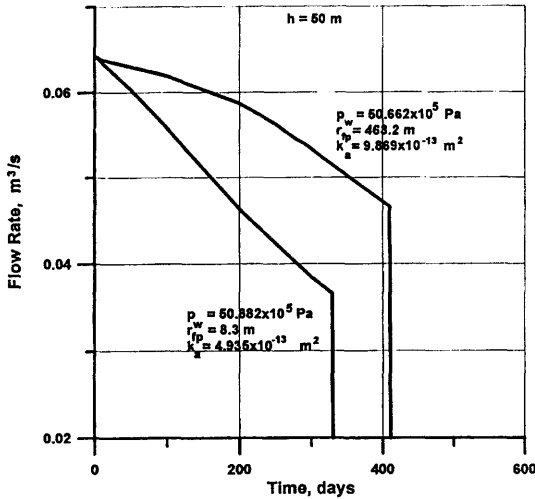


Figure 21–6. Simulation of the production rate decline by plugging vs. time at 8.3 and 463.2 m radial distances to the flashing point from the wellbore, with 0.119 and $0.0642 \text{ m}^3/\text{s}$ brine flow rates, in 50 m thick production zones of permeabilities of 4.935×10^{-13} and $9.869 \times 10^{-13} \text{ m}^2$, respectively (after Satman et al., ©1999; reprinted by permission of the Int. Institute for Geothermal Research, Italy).

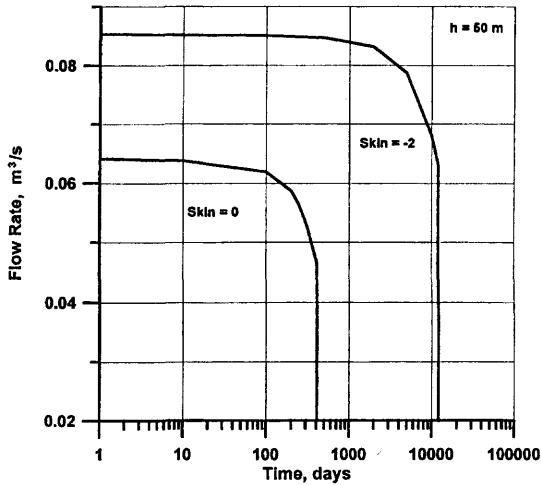


Figure 21-7. Simulation of the effect of skin development on the production rate decline vs. time in a 50 m thick production zone (after Satman et al., ©1999; reprinted by permission of the Int. Institute for Geothermal Research, Italy).

average reservoir fluid pressure during calcite deposition. Figure 21-6 shows the effect of the absolute permeability on the flow performance of wells during calcite deposition. Figure 21-7 shows the variation of the flow performance of wells during calcite deformation with different skin factors achieved by acid-stimulation of wells.

References

- Brunner, E., & Woll, W., "Solubility of Sulfur in Hydrogen Sulfide and Sour Gases," *SPEJ*, October 1980, p. 377.
- Brunner, E., Place, M. C. Jr., & Woll, W. H., "Sulfur Solubility in Sour Gas," *JPT*, December 1988, p. 1587.
- Chernik, P. S., & Williams, P. J., "Extended Production Testing of the Bearberry Ultra-Sour Gas Resource," Paper SPE 26190, presented at the 1993 SPE Gas Technology Symposium, Calgary, June 28-30.
- Chrastil, J., "Solubility of Solids and Liquids in Supercritical Gases," *J. Phys. Chem.*, No. 86, 1982, p. 3016.
- Hyne, J. B., "Study Aids Prediction of Sulfur Deposition in Sour Gas Wells," *Oil & Gas J.*, November 25, 1968, p. 107.
- Hyne, J. B., "Controlling Sulfur Deposition in Sour Gas Wells," *World Oil*, pp. 35, August 1983.

- Hyne, J. B., & Derdall, G., "Sulfur Deposition in Reservoirs and Production Equipment: Sources and Solutions," Paper presented at the 1980 Annual Gas Conditioning Conference, University of Oklahoma, Norman, Oklahoma, March 3–5.
- Kuo, C. H., "On the Production of Hydrogen Sulfide-Sulfur Mixtures from Deep Formations," *JPT*, September, 1972, p. 1142.
- Leontaritis, K. J., "Asphaltene Near-Wellbore Formation Damage Modeling," SPE 39446 paper, Proceedings of the 1998 SPE Formation Damage Control Conference, February 18–19, 1998, Lafayette, Louisiana, pp. 277–288.
- Roberts, B. E., "The Effect of Sulfur Deposition on Gaswell Inflow Performance," *SPE Reservoir Engineering*, May 1997, pp. 118–123.
- Satman, A., Ugur, Z., & Onur, M., "The Effect of Calcite Deposition on Geothermal Well Inflow Performance," *Geothermics*, Vol. 28, No. 3, 1999, pp. 425–444.
- Segnit, E. R., Holland, H. D., & Biscardi, C. J., "The Solubility of Calcite in Aqueous Solutions—I: The Solubility of Calcite in Water between 75° and 200°C at CO₂ Pressure up to 60 atm," *Geochimica et Cosmochimica Acta*, Vol. 26, 1962, pp. 1301–1331.
- Woll, W., "The Effect of Sour Gases on the Pressure-Melting Point Curve of Sulfur," *Erdoel, Erdgas Z.*, Vol. 9, 1983, p. 297.

Part VII

Diagnosis and Mitigation of Formation Damage

Measurement, Control, and Remediation

Chapter 22

Field Diagnosis and Measurement of Formation Damage

Summary

Methods for inferring formation damage in petroleum reservoirs and expressing formation damage and loss of well performance by various indicators are discussed. Skin factor, permeability variation index, viscosity variation index, damage ratio, flow efficiency, and depth of damage concepts are explained. Model-assisted analysis of the near-wellbore permeability alteration is demonstrated using pressure transient data. Monitoring formation damage effects by means of continuous real time series analysis and formation damage expert systems are reviewed.

Introduction

Field tests are regularly carried out for formation damage monitoring. Using appropriate precursors or signatures for detection of the imminent formation damage problems and their impact on oil production rates are important for two reasons, as stated by Hayatdavoudi (1999):

1. It would help us understand the reasons for a premature drop in oil production or formation damage.
2. It would give us adequate time to take the necessary, preventive remedial action(s) prior to the onset of a serious damage or an unusual drop in oil and gas production.

In this chapter, the loss of productivity or injectivity of wells by formation damage is expressed by alternative measures, and the various tests available for measurement and diagnosis of formation damage problems in the field are described.

Diagnosis and Evaluation of Formation Damage in the Field

As stated by Yeager et al. (1997), “No individual test or tool can provide the only information needed for damage mechanism identification and evaluation, and a historical perspective rather than an isolated perspective will result in a more complete diagnosis of the presence and type of damage.” Therefore, Yeager et al. (1997) further elaborate that “Damage mechanism identification requires a systematic approach to research, planning, and evaluation of all available information.”

For the most part, the diagnosis and measurement of formation damage in the field rely on well testing, well logging, history matching, and produced fluids analysis. The determination of the mechanisms responsible for loss of flow efficiency (productivity or injectivity) requires a number of studies. Yeager et al. (1997) recommend a three-stage approach consisting of:

1. Quantifying the degree of existing damage
2. Diagnosing the existing downhole damage mechanisms
3. Performing laboratory studies to increase knowledge about specific mechanisms

For this purpose, formation damage studies begin with the classification of the reservoir formation and review of the operational and engineering processes. The flow chart given by Yeager et al. (1997) in Figure 22–1 describes the information required on various aspects. The methodology for determination of the mechanisms responsible for flow efficiency is described in the flow chart given in Figure 22–2 by Yeager et al. (1997). Although, the Yeager et al. (1997) approach is intended for identification of damage in gas-storage wells, its applicability is extended here for general applications.

As stated by Yeager et al. (1997), the typical downhole diagnostic tests that can be conducted in the field include:

1. Well-test analysis to determine quantitatively if damage exists
2. Downhole video to observe the wellbore and formation areas
3. Physical sampling in the form of downhole liquids and solids
4. In the openhole completions, rotary sidewall core samples of the wellbore face as a “biopsy” of the storage formation

Yeager et al. (1997) recommend a downhole video run prior to the other downhole diagnostic tests and sampling for assessment of the presence, nature, and morphology of deposits on the wellbore surface and

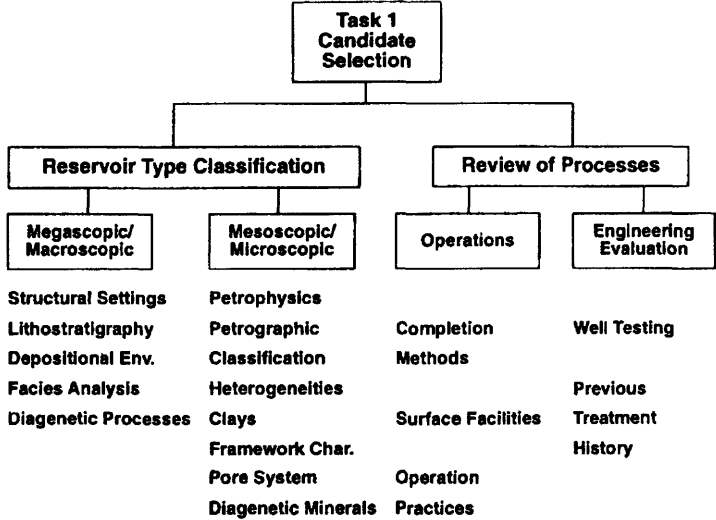


Figure 22–1. Issues involving candidate selection and reservoir formation damage studies (after Yeager et al., ©1997 SPE; reprinted by permission of the Society of Petroleum Engineers).

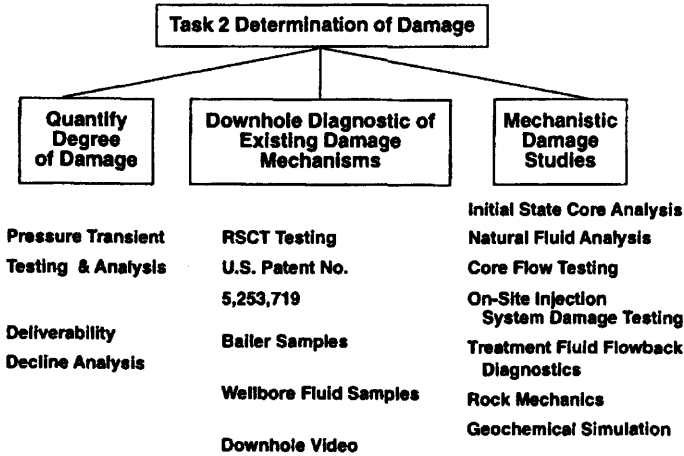


Figure 22–2. Issues involving reservoir formation damage determination (after Yeager et al., ©1997 SPE; reprinted by permission of the Society of Petroleum Engineers).

perforations. Figure 22-3 by Yeager et al. (1997) shows a schematic of a typical high-resolution video camera and a still image, indicating significant wellbore scaling, obtained using this camera. The video observations also provide valuable information necessary for determination of the flow distribution that can be used to improve the accuracy of the well-test interpretation and identification of the formation damage mechanisms (Yeager et al., 1997). Pressure transient tests yield information on the permeability and formation thickness product, (Kh), and skin factor, s . As pointed out by Yeager et al. (1997), pressure transient tests only provide information at a specific time, when the tests are conducted. Therefore, formation damage can be more effectively evaluated by conducting a series of tests over a length of time and also the true skin should be determined after corrections for other effects, such as non-Darcy or inertial effects (Yeager et al., 1997).

In openhole completed wells, core samples can be taken from the wells using a rotary sidewall coring tool (Yeager et al., 1997). The material on the face of the extracted cores should be carefully preserved during the transportation of the core for later analytical studies (Yeager et al., 1997).

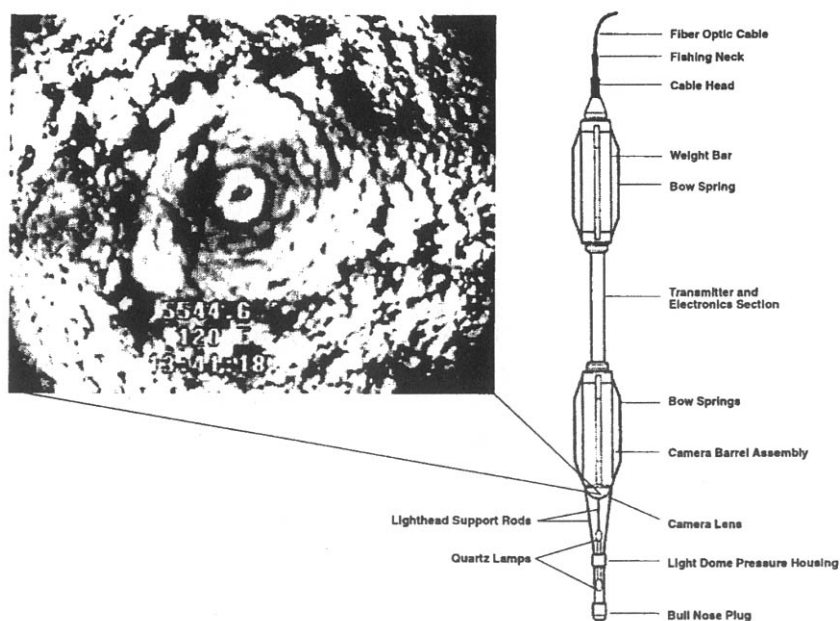


Figure 22-3. Typical downhole video image and elements of a downhole video camera (after Yeager et al., ©1997 SPE; reprinted by permission of the Society of Petroleum Engineers).

Pseudo-Damage Versus Formation Damage

Amaefule et al. (1988) plainly stated that "Formation damage is an expensive headache to the oil and gas industry." A number of factors cause formation damage in a complicated manner. Amaefule et al. (1988) grouped these factors in two categories:

1. Alteration of formation properties by various processes, including permeability reduction, wettability alteration, lithology change, release of mineral particles, precipitation of reaction-by products, and organic and inorganic scales formation
2. Alteration of fluid properties by various processes, including viscosity alteration by emulsion block and effective mobility change

The impact of formation damage can be observed in a variety of ways, including (1) abnormal decline in well productivity or injectivity, (2) misdiagnosis of potential pay zones as nonproductive, and (3) delay of pay-out on investment (Amaefule et al., 1988).

Hayatdavoudi (1999) points out that the analysis of production data is complicated because of:

1. Mechanical problems related to the tubing, safety valves, lift equipment, and wax, paraffin, and scale build-up in the tubing
2. Formation damage due to fines migration, development of skin, completion damage, and many other factors
3. Changes in reservoir conditions, like appearance of water-cut, changes in productivity index, and other related factors

Among other factors, the productivity or injectivity of wells depend on the pressure losses that occur along the flow path of produced or injected fluids. As schematically depicted in Figure 22-4, pressure losses may occur at various locations along the well and in the reservoir formation. Therefore, Piot and Lietard (1987) expressed the total skin of a well as a sum of the pseudoskin of flow lines from the formation face to the pipeline and the true skin due to formation damage. Here, the focus is on the near-wellbore formation damage problem. Figure 22-5 schematically depicts the damaged region around a well.

Measures of Formation Damage

Formation damage can be quantified by various terms, including (1) damage ratio, (2) skin factor, (3) permeability reduction index, (4) flow efficiency, and (5) depth of damage.

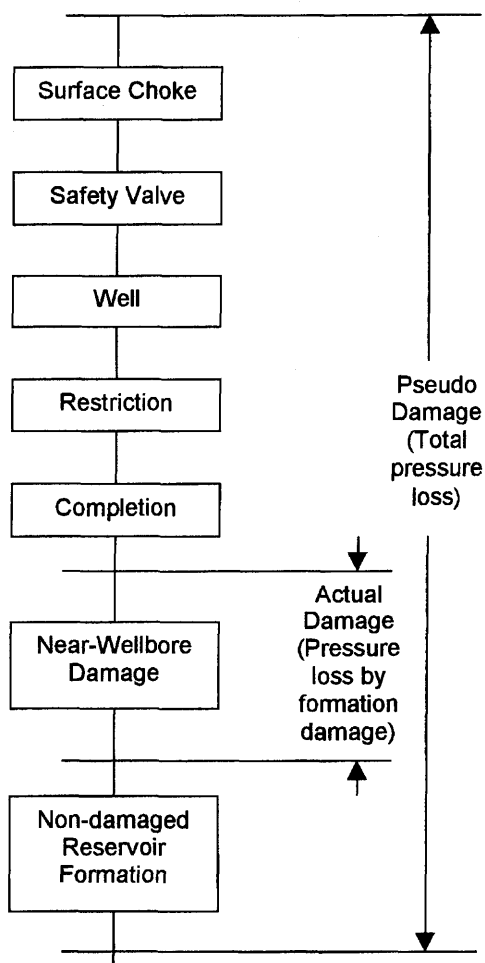


Figure 22-4. Pressure losses during production.

Skin Factor

The skin factor is a dimensionless parameter relating the apparent (or effective) and actual wellbore radii according to the parameters of the damaged region:

$$(r_w)_{\text{apparent}} = e^{-s} (r_w)_{\text{actual}} \quad (22-1)$$

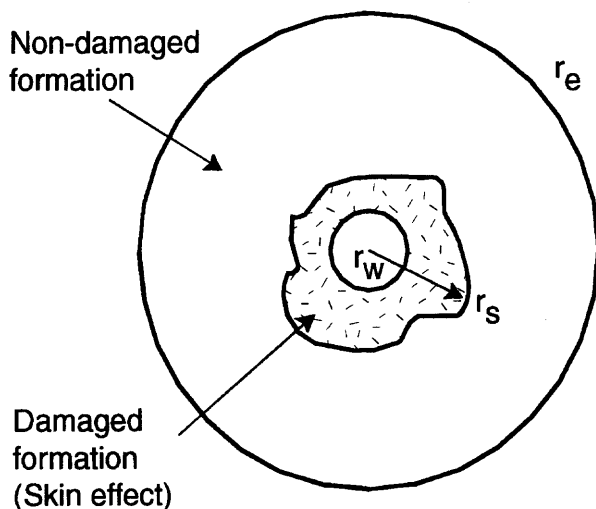


Figure 22-5. Schematic of a damaged zone in the near-wellbore (modified after Ohen and Civan, 1989).

where s is the skin factor. The skin factor is a lumped parameter incorporating the integral affect of the extend and extent of damage in the near-wellbore region. Frequently, in reservoir analysis and well test interpretation, the skin factor concept is preferred for convenience and simplicity, and for practical reasons. Therefore, many efforts have been made to express the skin factor based on the analytical solutions of simplified models relating well flow rate to formation and fluid conditions. In this respect, incompressible one-dimensional flow in a homogeneous porous media formulation approach has been popular.

Other cases, such as anisotropic elliptic and isotropic radial flow problems can be readily transformed into one-dimensional flow problems, using respectively

$$\frac{r^2}{K_x K_y K_z} = \frac{(x-a)^2}{K_x} + \frac{(y-b)^2}{K_y} + \frac{(z-c)^2}{K_z} \quad (22-2)$$

$$l = \ell n r$$

where K_x , K_y , and K_z are the permeabilities in the x , y , and z -principal directions in an anisotropic porous media; a , b and c denote the coordinates of the well; and r and ℓ denote the radial and linear distances in the flow direction.

The formation anisotropy ratio of permeability, β , is defined following Muskat (1937):

$$\beta_{x/y} = \sqrt{K_x/K_y}, \quad \beta_{x/z} = \sqrt{K_x/K_z} \quad (22-3)$$

Although this transformation distorts the wellbore shape from the cylindrical shape (Mukherjee and Economides, 1991), it can still be used for all practical purposes with sufficient accuracy.

Permeability Variation Index (PVI)

The permeability variation index expresses the change of formation permeability by near-wellbore damage as a fraction, given by

$$PVI = \frac{K - K_d}{K} = 1 - \frac{K_d}{K} \quad (22-4)$$

where K and K_d denote the formation permeabilities before and after damage, respectively.

Viscosity Variation Index (VVI)

The viscosity variation index expresses the change of fluid viscosity by various processes, such as emulsification, defined by:

$$VVI = \frac{\mu - \mu_d}{\mu} = 1 - \frac{\mu_d}{\mu} \quad (22-5)$$

where μ and μ_d denote the fluid viscosities before and after fluid damage, respectively.

Damage Ration (DR)

The damage ratio expresses the change of well flow rate by near-wellbore damage as a fraction, given by (Amaefule et al., 1988):

$$DR = \frac{q - q_d}{q} = 1 - \frac{q_d}{q} \quad (22-6)$$

where q and q_d denote the undamaged and damaged standard flow rates, respectively.

The production loss by alteration of formation properties can be formulated as following.

The theoretical undamaged and damaged flow rates for a steady-state incompressible radial flow in a homogeneous and isotropic porous media are given, respectively, by (Muskat, 1949; Amaefule et al., 1988):

$$q = \frac{2\pi Kh(p_e - p_w)}{\mu B \ell n(r_e/r_w)} \quad (22-7)$$

$$q_d = \frac{2\pi Kh(p_e - p_w)}{\mu B [\ell n(r_e/r_d) + (K/K_d) \ell n(r_d/r_w)]} \quad (22-8)$$

Therefore, substituting Eqs. 22-6 and 7, Eq. 22-8 yields the following expression for the damage ratio:

$$DR = \frac{(K/K_d - 1) \ell n(r_d/r_w)}{(K/K_d) \ell n(r_d/r_w) + \ell n(r_d/r_e)} \quad (22-9)$$

where μ and B are the fluid viscosity and formation volume factors. K and K_d are the undamaged and damaged effective permeabilities. h is the thickness of the effective pay zone, p_w and p_e are the wellbore and reservoir drainage boundary fluid pressures, r_w and r_e are the wellbore and reservoir drainage radii, and r_d is the radius of the damaged region.

The effective skin factor, s , is defined by (Craft and Hawkins, 1959):

$$s = (K/K_d - 1) \ell n(r_d/r_w) \quad (22-10)$$

Thus, substituting Eq. 22-10 into Eq. 22-9 yields the relationship between the damage ratio and the skin factor as:

$$DR = \frac{s}{s + \ell n(r_e/r_w)} \quad (22-11)$$

The economic impact of formation damage on reservoir productivity can be estimated in terms of the annual revenue loss by formation damage per well ($FD\$L$) at a given price of oil, p , according to Amaefule et al. (1988):

$$FD\$L = \left(365 \frac{\text{days}}{\text{year}} \right) \left(q \frac{\text{bbl}}{\text{day}} \right) \left(P \frac{\$}{\text{bbl}} \right) \left(DR \frac{\text{bbl unproduced}}{\text{bbl theoretical}} \right) \quad (22-12)$$

Figure 22-6 by Amaefule et al. (1988) shows the typical curves of the damage ratio and annual revenue loss per well as a function of the damage radius and degree determined by Eqs. 22-8 and 12, respectively.

Because the degree of damage varies in the near-wellbore region, it is more appropriate to express the total skin as a sum of the individual skins over consecutive segments of the formation as (Li et al., 1988; Lee and Kasap, 1998):

$$s = \sum_{i=1}^N s_i = \sum_{i=1}^N \left(K/K_{di} - 1 \right) \ell n(r_i/r_{i-1}) \quad (22-13)$$

where N represents the number of segments considered (see Figure 22-7).

The production loss by alteration of fluid properties can be formulated as following. Rapid flow of oil and water in the near-wellbore region promote mixing and emulsification. This causes a reduction in the hydrocarbon effective mobility, λ ($\lambda = K_e/\mu = Kk_r/\mu$) (Leontaritis, 1998), because emulsion viscosity is several fold greater than oil and water viscosities. High viscosity emulsion forms a stationary block which resists flow. It is called emulsion block. If μ and μ_d represent the viscosities of oil and emulsion, respectively, and a steady-state and incompressible radial flow is considered, the theoretical undamaged and damaged flow rates are given, respectively, by:

$$q = \frac{2\pi Kh(p_e - p_w)}{\mu B \ell n(r_e/r_w)} \quad (22-14)$$

$$q_d = \frac{2\pi Kh(p_e - p_w)}{\mu B \ell n(r_e/r_d) + \mu_d B_d \ell n(r_d/r_w)} \quad (22-15)$$

Thus, substituting Eqs. 22-14 and 15 into Eq. 22-6 Leads to the following expression for the damage ratio:

$$DR = \frac{[\mu_d B_d / (\mu B) - 1] \ell n(r_d/r_w)}{[\mu_d B_d / (\mu B)] \ell n(r_d/r_w) + \ell n(r_e/r_d)} \quad (22-16)$$

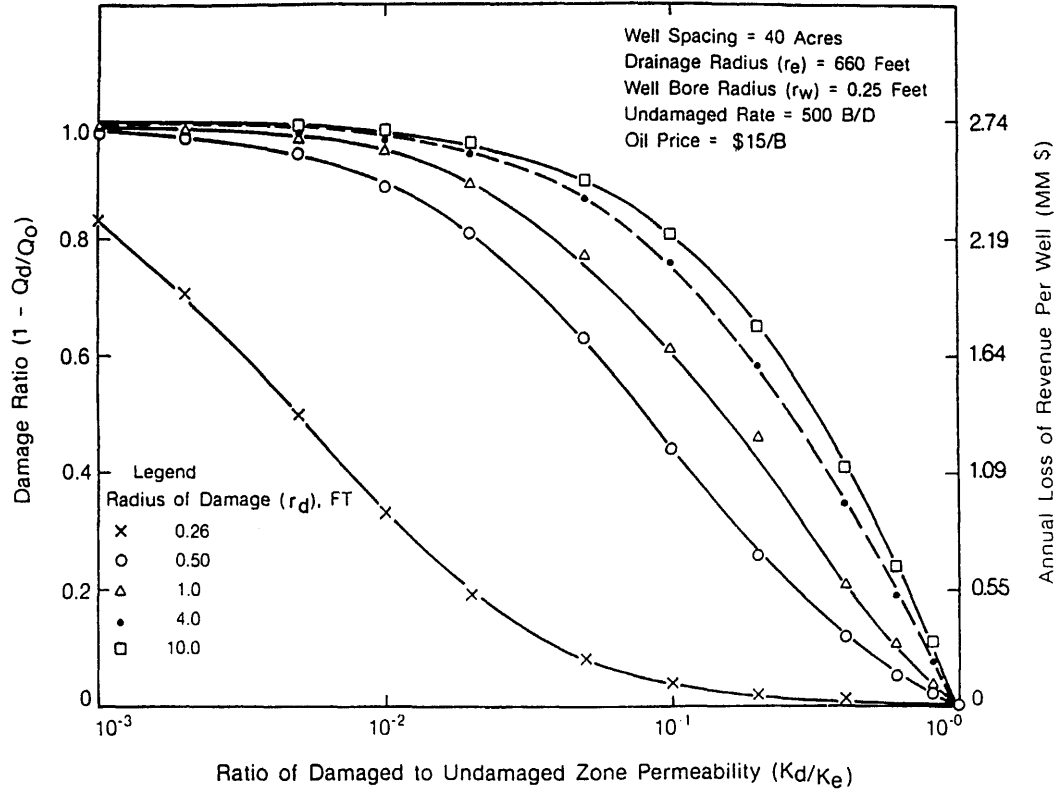


Figure 22-6. Effect of permeability impairment and damaged zone radius on damage ratio (after Amaefule et al., ©1988; reprinted by permission of the Canadian Institute of Mining, Metallurgy and Petroleum).

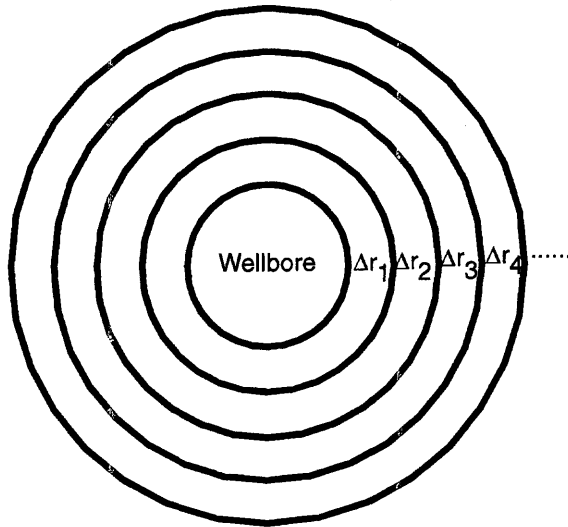


Figure 22–7. Near-wellbore damaged zone realized as a series of sectional damaged zones.

Figure 22–8 by Amaefule et al. (1988) shows the effect of emulsion block on oil production rate according to Eq. 22–16.

The viscous skin effect can be expressed similar to Zhu et al. (1999) as:

$$s_{\mu} = \left(\frac{\mu_d B_d}{\mu B} - 1 \right) \ell n \left(\frac{r_d}{r_w} \right) \quad (22-17)$$

Flow Efficiency

Flow efficiency is the ratio of the damaged to undamaged formation flow (production or injection) indices:

$$FE = \frac{FI_d}{FI} = \frac{\bar{p} - p_{wf} - \Delta p_s}{\bar{p} - p_{wf}} \quad (22-18)$$

where \bar{p} and p_{wf} denote the average reservoir fluid and flowing well bottom hole pressures, respectively, and Δp_s is the additional pressure loss by the skin effect. The flow efficiency of vertical wells for radial

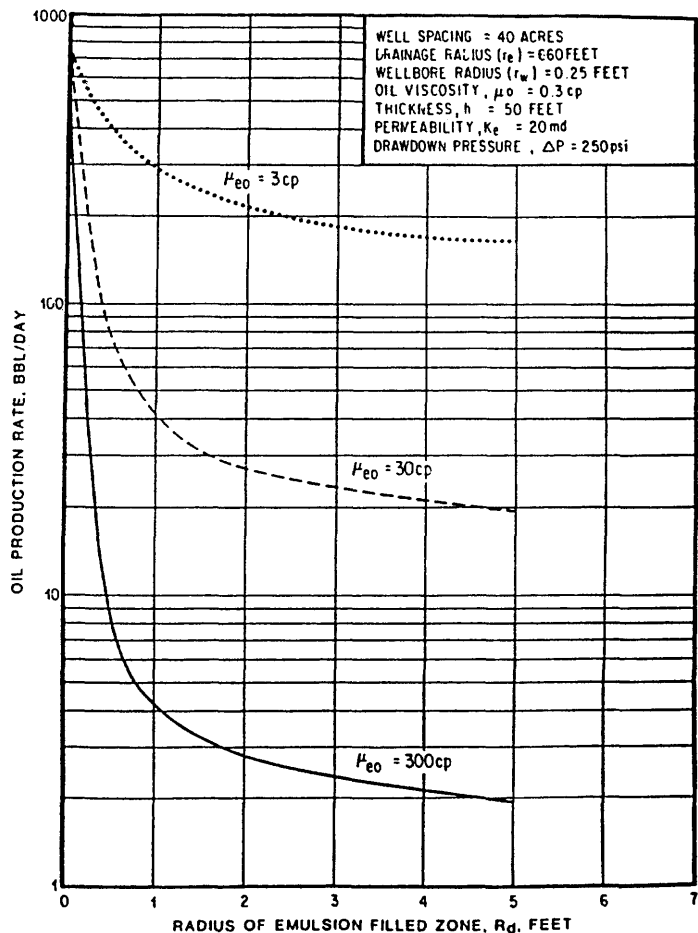


Figure 22-8. Effect of near-wellbore emulsion block on oil production rate decline (after Amaefule et al., ©1988; reprinted by permission of the Canadian Institute of Mining, Metallurgy and Petroleum).

and incompressible fluid flow at a steady-state condition is given by (Mukherjee and Economides, 1991):

$$FE_v = \frac{\ell n(r_e/r_w)}{s + \ell n(r_e/r_w)} \tag{22-19}$$

For practical purposes, flow efficiency of damaged wells has been correlated by means of the inflow performance relationship (IPR). For

example, Dias-Couto and Golan (1982) developed the following inflow performance relationship for wells producing oil with average reservoir fluid pressures at or below the bubble point pressure:

$$\frac{q_d}{q_{\max}} = (FE) \left(1 - \frac{p_{wf}}{\bar{p}} \right) \left[1.8 - 0.8(FE) \left(1 - \frac{p_{wf}}{\bar{p}} \right) \right] \quad (22-20)$$

Lekia and Evans (1990) extended this equation for wells producing oil with average reservoir fluid pressures above the bubble point pressure as:

$$\frac{q_d - q_{d,b}}{q_c} = (FE) \left(1 - \frac{p_{wf}}{p_b} \right) \left[1.8 - 0.8(FE) \left(1 - \frac{p_{wf}}{p_b} \right) \right] \quad (22-21)$$

where q_d is the oil flowrate of the damaged well, $q_{d,b}$ is the oil flow rate at the bubble point from a damaged well, q_{\max} is the maximum oil flow rate at $p_{wf} = 0$ from a non-damaged well, and q_c is the maximum oil flow rate of the Vogel (1968) part of the generalized IPR. Lekia and Evans (1990) express these by the following equations:

$$q_b = J(\bar{p} - p_b) \quad (22-22)$$

$$q_{d,b} = (FE) q_b \quad (22-23)$$

and

$$q_c = J p_b / 1.8 \quad (22-24)$$

J is the productivity index ($Bbl / d / psi$).

Depth of Damage

The depth of damage represents the distance of formation damage region measured from the wellbore.

Yan et al. (1997) correlated the depth of invasion of drilling and completion fluids by regression analysis of experimental data obtained by means of the slice cutting of damaged core plugs. Their empirical correlation is given by

$$d = 1.612 p^{0.521} (V_f / \phi)^{0.271} \exp(0.043K) \quad (22-25)$$

where d is the invasion depth in cm, p is the pressure in MPa, V_f is the cumulative filtrate loss in cm^3 , ϕ is porosity in percentage, and K is permeability in μm^2 (\sim Darcy).

Figure 18–5 given in Chapter 18 by Civan depicts the variation of the depth of damage during mud invasion as a function of the pore volume of filtrate invasion.

Model-Assisted Estimation of Skin Factor

As demonstrated by Ohen and Civan (1991, 1992, 1993), skin factor varies over time and can be predicted by means of a formation damage model. Figure 22–9 depicts the approach used by Ohen and Civan (1992) for prediction of the skin factor associated with formation damage resulting from fines migration and clay swelling effects in the near-wellbore formation.

Model-Assisted Analysis of the Near-Wellbore Permeability Alteration using Pressure Transient Data

The modeling and parameter estimation methods for determination of near-wellbore permeability alteration from pressure transient analysis data by Olarewaju (1990) are presented here.

Olarewaju (1990) considered a reservoir system, composed of two concentric zones, denoted as zones 1 and 2 in Figure 22–10. Zone 1 is located near the wellbore and its permeability has been altered by formation damage or stimulation processes. For example, zone 1 includes the near-wellbore formation, in which permeability impairment occurs by mud fluid and particle invasion and the mud cake formed over the sand face during drilling. Zone 2 represents the undamaged formation located beyond zone 1. The permeabilities of zones 1 and 2 are denoted by K_1 and K_2 and the radius of zone 1 of the skin effect region is r_1 . The external drainage radius of zone 2 is r_2 . The objective is to estimate the values of K_1 , K_2 , and r_1 using build-up pressure test data, such as by Olarewaju (1990) from a reservoir in which the permeability of a near-wellbore formation has been enhanced by acid stimulation. Ultimately, this information will be used to determine the skin factor as a measure of the effectiveness of the acid treatment.

For this purpose, Olarewaju (1990) developed a simplified mathematical model by considering (1) a slightly compressible single phase fluid, (2) constant thick-horizontal reservoir, (3) a constant rate producing well, and (4) a reservoir, as shown in Figure 22–10, with no-flow boundaries at the top, bottom, and external drainage radius.

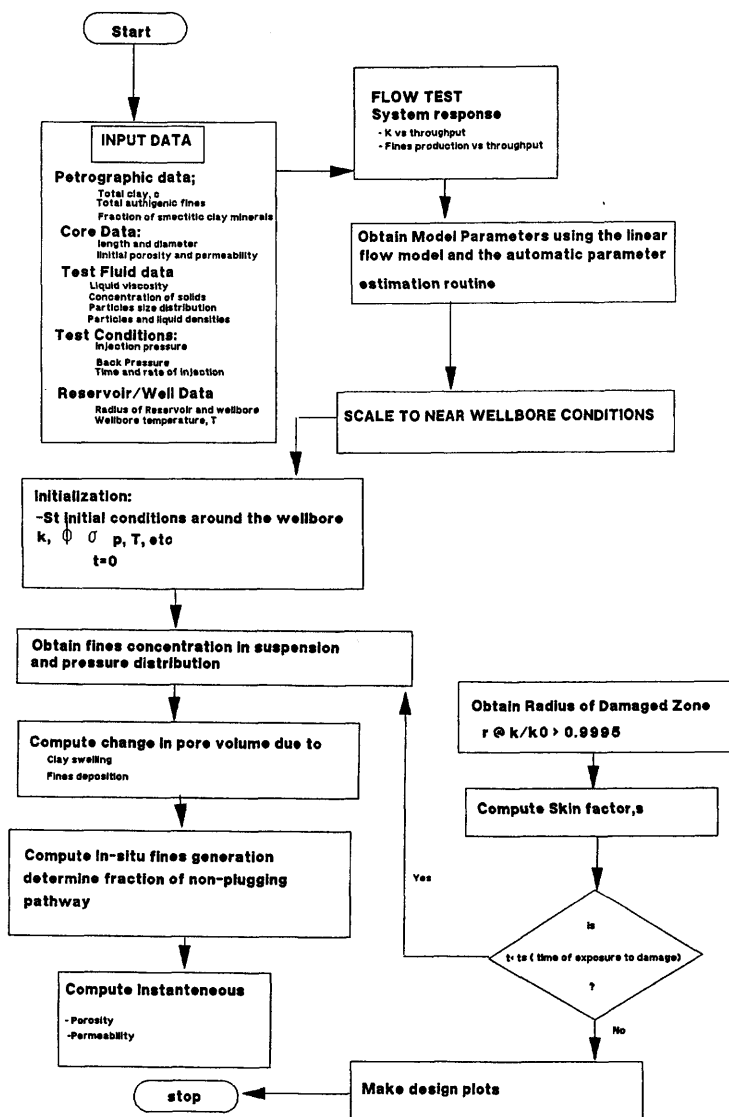


Figure 22-9. Steps of integrated near-wellbore formation damage analysis and prediction (after Ohen and Civan, ©1991 SPE; reprinted by permission of the Society of Petroleum Engineers).

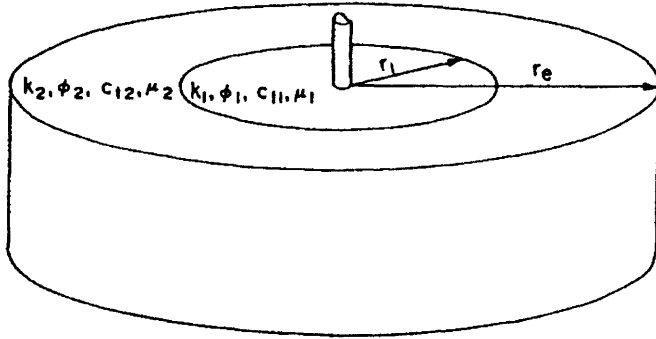


Figure 22-10. Composite of damaged and non-damaged regions realization of a reservoir (after Olarewaju, ©1990 John Wiley & Sons Limited; reproduced with permission).

The dimensionless partial differential equations of the Olarewaju (1990) model are given as following:

Zone 1 pressure equation:

$$\frac{1}{r_D} \frac{\partial}{\partial r_D} \left(r_D \frac{\partial P_{D1}}{\partial r_D} \right) = \frac{\partial P_{D1}}{\partial t_D}, 1 \leq r_D \leq a \quad (22-26)$$

Zone 2 pressure equation:

$$\frac{1}{r_D} \frac{\partial}{\partial r_D} \left(r_D \frac{\partial P_{D2}}{\partial r_D} \right) = \kappa \frac{\partial P_{D2}}{\partial t_D}, a \leq r_D \leq r_{De} \quad (22-27)$$

subject to the following conditions of solution:

Initial conditions (uniform initial pressure):

$$P_{D1}(r_D, 0) = P_{D2}(r_D, 0) = 0 \quad (22-28)$$

Inner boundary condition (constant rate):

$$\frac{\partial P_{D1}}{\partial r_D}(1, t_D) = -1 \quad (22-29)$$

Outer boundary condition (no-flow):

$$\frac{\partial P_{D2}}{\partial r_D}(r_{De}, t_D) = 0 \quad (22-30)$$

Interface boundary conditions (pressure and rate continuity):

$$P_{D1}(a, t_D) = P_{D2}(a, t_D) \quad (22-31)$$

$$\lambda \frac{\partial P_{D1}}{\partial r_D}(a, t_D) = \frac{\partial P_{D2}}{\partial r_D}(a, t_D) \quad (22-32)$$

The dimensionless variables and/or parameters are defined as following:

$$r_D = \frac{r}{r_w} \quad (22-33)$$

$$P_{D1} = \frac{\beta K_1 h (P_i - P_1)}{q \mu B} \quad (22-34)$$

$$t_D = \frac{\alpha K_1 t}{(\phi \mu c_t)_1 r_w^2} \quad (22-35)$$

$$\lambda = \left(\frac{K_1}{\mu_1} \right) \bigg/ \left(\frac{K_2}{\mu_2} \right) \quad (22-36)$$

$$\kappa = \frac{K_1}{(\phi \mu c_t)_1} \bigg/ \frac{K_2}{(\phi \mu c_t)_2} \quad (22-37)$$

$$a = \frac{r_1}{r_w} \quad (22-38)$$

$$r_{De} = \frac{r_e}{r_w} \quad (22-39)$$

In these equations, the indices 1 and 2 denote zones 1 and 2; r_w , r_e , and r represent the wellbore and drainage radii and radial distance from the center of the well, respectively; t is time, B is the formation volume factor, P_i and P_1 denote the initial reservoir and zone 1 radius pressures, μ is fluid viscosity, ϕ , K , and h represent the formation porosity, permeability, and thickness; c_t is the total compressibility, and $\alpha = 0.0002637$ and $\beta = 0.007082$ are some constant factors resulting from conversion from Darcy to field units.

The skin factor is calculated by

$$s = \left(\frac{K_2}{K_1} - 1 \right) \ln \left(\frac{r_1}{r_w} \right) \quad (22-40)$$

Eqs. 22–26 through 32 can be solved by an appropriate numerical method, such as by the finite difference method. However, Olarewaju (1990) obtained an analytical solution for the wellbore fluid pressure in the terms of the modified Bessel series I_o and K_o , in the Laplace domain, as:

$$P_{Dw}(s) = AI_o(\sqrt{s}) + BK_o(\sqrt{s}) \quad (22-41)$$

and then inverted it numerically using the Stehfest algorithm. Readers interested in details are referred to Olarewaju (1990).

Olarewaju (1990) presents the pressure and its derivative curves for different parameter values generated by the above model. Olarewaju (1990) also presented an application of this model to acidized well pressure build-up test data. Applying an automatic parameter estimation technique, similar to that described in Chapter 17, Olarewaju (1990) obtained an excellent history match of data as shown in Figure 22–11. For this purpose, Olarewaju (1990) used $r_w = 1$ ft, $h = 10$ ft, $\phi = 0.10$, $p_i = 4,000$ psia, $q = 8.27$ STB/D, $B = 1.21$ RB/STB, $\mu = 1$ cp, and $c_t = 9.8 \times 10^{-6}$ psi^{-1} . Olarewaju (1990) began the history matching process by the initial estimates of $K_1 = 1$ md, $K_2 = 0.1$ md, and $r_1 = 5$ ft and obtained the best match with $K_1 = 9.82$ md, $K_2 = 0.05$ md, and $r_1 = 51$ ft. Consequently, the skin factor was calculated as $s = -5.29$ using Eq. 22–40. However, Olarewaju (1990) warns that the solution is not unique because an infinite number of combinations of K_1 , K_2 , and r_1 may yield the same skin factor value.

Continuous Real Time Series Analysis for Detection and Monitoring Formation Damage Effects

Akaike (1999) explains that “Time series analysis intends to grasp the characteristics of the temporal movement or the dynamics of an object,

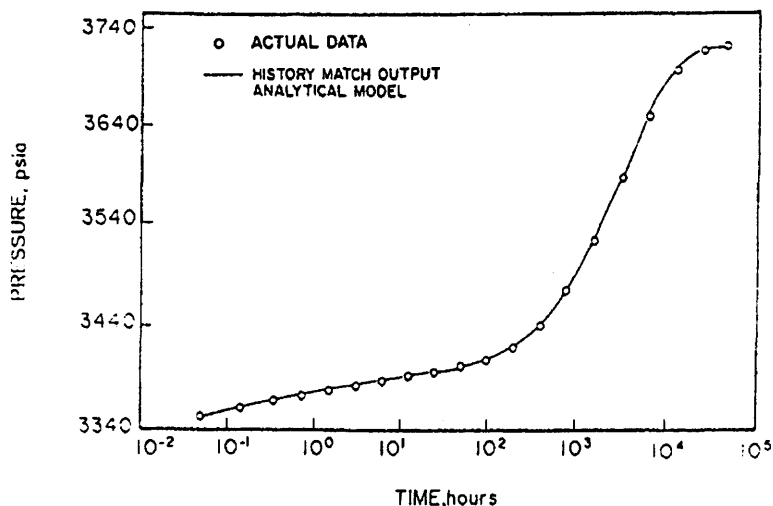


Figure 22-11. Simulation of pressure buildup data by history matching (after Olarewaju, ©1990 John Wiley & Sons Limited; reproduced with permission).

and its final purpose is the realization of an adequate prediction.” In this section, an innovative methodology introduced by Hayatdavoudi (1999) for interpretation of the production data by means of the Fourier series analysis is presented. Hayatdavoudi (1999) explains that “the Fourier periodogram coefficients, frequency, and phase changes of the gas-water ratio of the monthly production data indicate a certain predictable precursor (signature) to the drop in oil production and formation damage prior to the onset of the real production decline.” But, his applications have focused on the detection of the Fourier phase changes in the oil production data. However, he points out that such a precursor may indicate the total skin as an integral contribution of the loss of the reservoir drive energy during flow through formation, perforations, well, and surface equipment. The changes in the produced gas-water ratio, which depends on the solubility of light gases (CH_4 , CO_2 , etc.) in the reservoir brine, is an important precursor to changes in oil production because dissolved gas liberation provides a significant source of the reservoir drive energy (Hayatdavoudi, 1999).

Hayatdavoudi (1999) considers the produced oil and gas data as a time series signal, oscillating with certain frequency and phase, which signals certain specific characteristics of the production regime, with an amplitude measured as pressure or the pressure and rate product. Hayatdavoudi (1999) analyzed the well production signals using the Fourier transform method.

To demonstrate the applications of the time series analysis, Hayatdavoudi (1999) considered two different wells: Well No. 1 which could not be stimulated by acidizing, and Well No. 2 that could be successfully stimulated by acidizing.

Figure 22-12 by Hayatdavoudi (1999) shows the monthly production of the gas, oil and water, and the gas-water ratio for Well No. 1. As can be seen, the oil production decreased gradually, and the gas and water productions increased gradually. Although, the well was acidized at the end of Month 156, no appreciable production increase was observed. Therefore, it was concluded that the acidizing did not stimulate the well. Figure 22-13 by Hayatdavoudi (1999) shows the change of phase angle of the gas-water ratio, considered as a precursor to changes in oil production. As indicated by Figure 22-13, the phase angle (pc) began widening at Month 32. Therefore, Month 32 is considered the onset time of the formation damage. Hayatdavoudi (1999) recommends a low-cost preventive workover at Month 32 to delay or eliminate the need for acidizing of this well.

Figure 22-14 by Hayatdavoudi (1999) shows the production data for Well No. 2, for which the change in the phase angle and, therefore, the formation damage began at Month 33, as indicated by Figure 22-15 by Hayatdavoudi (1999). Notice the widening of the phase angle pattern

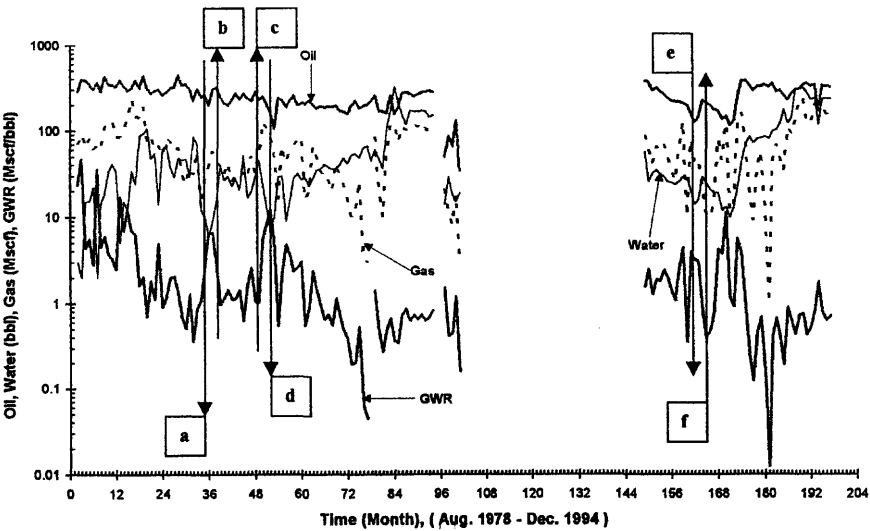


Figure 22-12. Well No. 1 production data (after Hayatdavoudi, 1999; reprinted by permission of A. Hayatdavoudi).

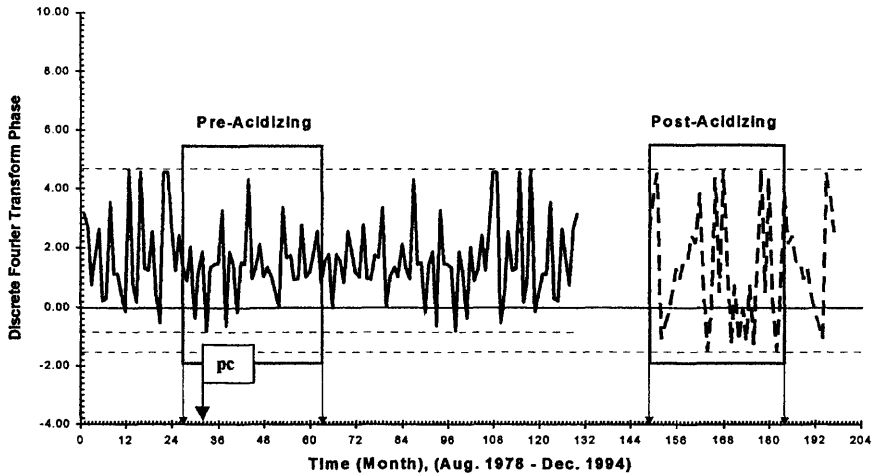


Figure 22-13. Discrete Fourier transform phase diagnostic analysis of Well No. 1 production data (after Hayatdavoudi, 1999; reprinted by permission of A. Hayatdavoudi).

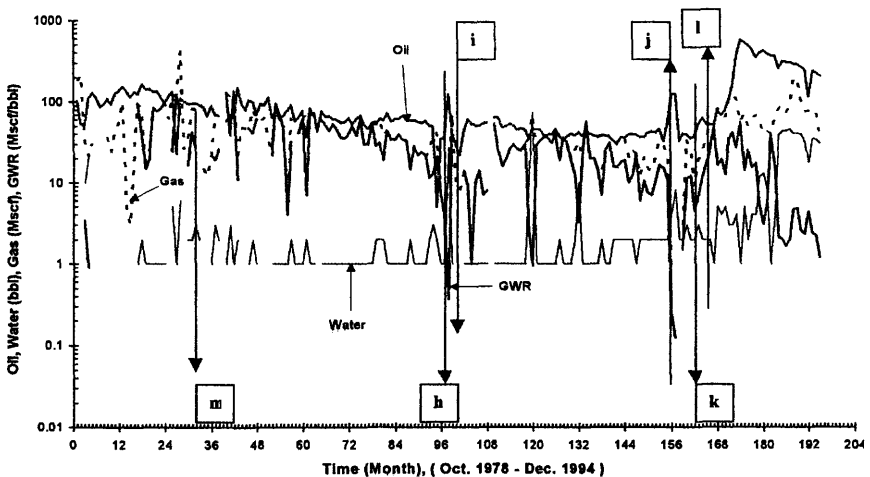


Figure 22-14. Well No. 2 production data (after Hayatdavoudi, 1999; reprinted by permission of A. Hayatdavoudi).

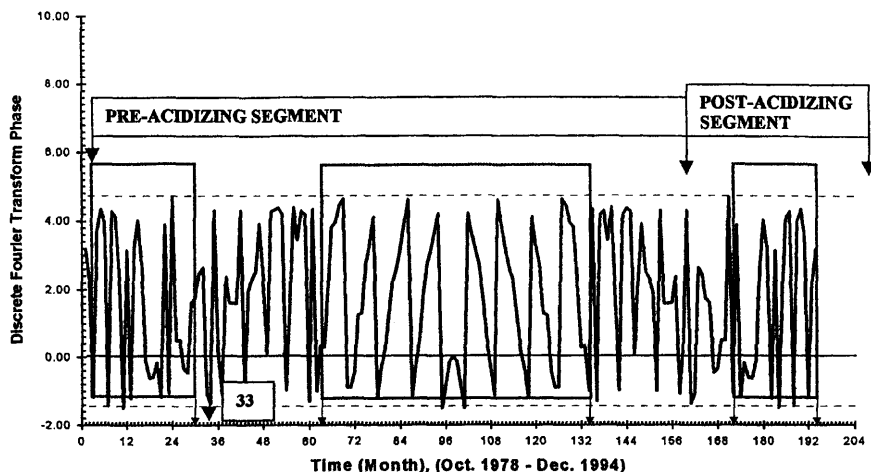


Figure 22-15. Discrete Fourier transform phase diagnostic analysis of Well No. 2 production data (after Hayatdavoudi, 1999; reprinted by permission of A. Hayatdavoudi).

beginning with Month 33 through Month 156, at which time the well was acidized. Therefore, Hayatdavoudi (1999) recommends a low cost preventive workover at Month 33 for Well No. 2. Because this preventive workover has not been made, Well No. 2 had to be acidized at the end of Month 156, which was more costly. Notice the significant tightening of the phase angle pattern following Month 156, indicating that the acidizing successfully stimulated Well No. 2.

The preceding exercises conducted by Hayatdavoudi (1999) indeed indicate that the change of the phase angle of the gas-water ratio is an effective precursor or signal for detection of the changes in the reservoir formation flow properties. This signal can be used to apply low-cost preventive measures at the onset of formation damage to avoid the need of costly stimulation treatments in the future.

Formation Damage Expert System

Development and application of knowledge and simulator-based expert systems for diagnosis, analysis, and mitigation of various formation damage and restoration processes are of continuing interest to the petroleum industry. Formation damage is a generic terminology, representing a large variety of adverse interactive processes causing flow impairment in petroleum reservoirs in a lumped manner. In a true sense, there is no fully

computerized and capable formation damage expert system available today. This is because formation damage occurs by many processes in a complicated manner that are not yet fully understood. Efforts are being made to understand and theoretically describe the governing processes. Quantitative determination of the various theoretical parameters at near in situ conditions will take a long time. As described in the previous chapters, modeling of various formation damage processes is an ongoing chore for the petroleum industry. Therefore, a truly useful formation damage advisor and expert program is a dream to accomplish in the future. However, companies and research institutions are developing proprietary expert systems with emphasis on certain specific applications. These systems capture the present state-of-the-knowledge in a systematic manner and make it available for analysis of specific types of formation damage problems. Such computerized systems integrate various pertinent knowledge, including the rule-of-thumbs, guidelines, recipes, and mathematical models generated in particular areas of formation damage to apply to similar problems rapidly. The accuracy and capability of such expert systems are limited to the amount and quality of information available, which continually improves with research growth and experience with similar problems. Simulators, dressed-up with colorful high-resolution graphics software, may lack the theoretical rigor of the phenomenological equations and/or accurate properties and rate data necessary for accurate history matching and prediction of the formation damage scenarios. Development of a truly useful formation damage expert requires an interdisciplinary effort and will take a long time.

References

- Akaike, H., "Mental Preparation for Time Series Analysis," *The Practice of Time Series Analysis*, Akaike, H., & Kitagawa, G. (eds.), Springer-Verlag New York, Inc., New York, New York, 1999, Chapter 23, pp. 367–371.
- Amaefule, J. O., Kersey, D. G., Norman, D. L., & Shannon, P. M., "Advances in Formation Damage Assessment and Control Strategies," CIM Paper No. 88-39-65, Proceedings of the 39th Annual Technical Meeting of Petroleum Society of CIM and Canadian Gas Processors Association, June 12–16, 1988, Calgary, Alberta, 16 p.
- Craft, B. C., & Hawkins, M. F., *Applied Petroleum Reservoir Engineering*, Prentice Hall, 1959.
- Dias-Couto, L. E., & Golan, M., "General Inflow Performance Relationship for Solution-Gas Reservoir Wells," *J. of Petroleum Technology*, February 1982, pp. 285–288.

- Hayatdavoudi, A., "Effect of Water-Soluble Gases on Production Decline, Production Stimulation, and Production Management, SPE 50781 paper, presented at the 1999 SPE International Symposium on Oilfield Chemistry, Houston, Texas, February 16–19, 1999.
- Lee, J., & Kasap, E., "Fluid Sampling from Damaged Formations," SPE 39817 paper, Proceedings of the 1998 SPE Permian Basin Oil and Gas Recovery Conference, March 25–27, 1998, Midland, Texas, pp. 565–570.
- Lekia, S., & Evans, R. D., "Generalized Inflow Performance Relationship for Stimulated Wells," *Journal of Canadian Petroleum Technology*, Vol. 29, No. 6, November–December 1990, pp. 71–75.
- Leontaritis, K. J., "Asphaltene Near-Wellbore Formation Damage Modeling," SPE 39446 paper, Proceedings of the 1998 SPE Formation Damage Control Conference, February 18–19, 1998, Lafayette, Louisiana, pp. 277–288.
- Li, Y-H., Fambrough, J. D., & Montgomery, C. T., "Mathematical Modeling of Secondary Precipitation from Sandstone Acidizing," *SPE Journal*, December 1998, pp. 393–401.
- Mukherjee, H., & Economides, M. J., "A Parametric Comparison of Horizontal and Vertical Well Performance," *SPE Formation Evaluation*, June 1991, pp. 209–216.
- Muskat, M., *The Flow of Homogeneous Fluids Through Porous Media*, McGraw-Hill Book Co., New York, New York, 1937.
- Muskat, M., *Physical Principles of Oil Production*, McGraw-Hill, Inc., New York, 1949.
- Ohen, H. A., & Civan, F., "Simulation of Formation Damage in Petroleum Reservoirs," SPE 19420 paper, Proceedings of the 1990 SPE Symposium on Formation Damage Control, Lafayette, Louisiana, February 22–23, 1990, pp. 185–200.
- Ohen, H. A., & Civan, F., "Predicting Skin Effects Due to Formation Damage by Fines Migration," SPE 21675 paper, Proceedings of the 1991 SPE Production Operations Symposium, Oklahoma City, Oklahoma, April 7–9, 1991, pp. 399–410.
- Ohen, H. A., & Civan, F., "Simulation of Formation Damage in Petroleum Reservoirs," *SPE Advanced Technology Series*, Vol. 1, No. 1, April 1993, pp. 27–35.
- Olarewaju, J. S., "A Mathematical Model of Permeability Alteration Around Wells," *Intl. J. for Numerical and Analytical Methods in Geomechanics*, Vol. 14, 1990, pp. 191–207.
- Piot, B. M., & Lietard, O. M., "Nature of Formation Damage in Reservoir Stimulation, in Economides," M. J. & K. S. Nolte (eds.), *Reservoir Stimulation*, Schlumberger Education Services, Houston, Texas, 1987.
- Vogel, J. V., "Inflow Performance Relationships for Solution-Gas Drive Wells," *J. of Petroleum Technology*, January 1968, pp. 83–92.

- Yan, J., Jiang, G., & Wu, X., "Evaluating of Formation Damage Caused by Drilling and Completion Fluids in Horizontal Wells," *Journal of Canadian Petroleum Technology*, Vol. 36, No. 5, 1997, pp. 36–42.
- Yeager, V. J., Blauch, M. E., Behenna, F. R., & Foh, S. E., "Damage Mechanisms in Gas-Storage Wells," SPE 38863 paper, Proceedings of the 1997 SPE Annual Technical Conference and Exhibition, October 5–8, 1997, San Antonio, Texas, pp. 477–486.
- Zhu, D., Hill, A. D., & Morgenthaler, L. N., "Assessment of Matrix Acidizing Treatment Responses in Gulf of Mexico Wells," Proceedings of the 1999 SPE Mid-Continent Operations Symposium held in Oklahoma City, Oklahoma, USA, March 28–31, 1999.

Chapter 23

Formation Damage Control and Remediation

Summary

Formation damage is an undesirable operational and economic problem that may occur during the various phases of oil and gas recovery from petroleum reservoirs. Control and remediation of formation damage are among the most important issues to be resolved for efficient exploitation of petroleum reservoirs and cost management. Designing certain chemicals and/or treatment procedures for damage control and remediation is a science as well as an art. Recipes that work for certain cases may not necessarily work for others. This chapter provides practicing engineers the understanding and tools available for prevention, control, and remediation of formation damage. A review of the commonly practiced methods is presented.

Introduction

Bennion (1999) defined formation damage as: “The impairment of the invisible, by the inevitable and uncontrollable, resulting in an indeterminate reduction of the unquantifiable,” and further, more formally as: “Any process that causes a reduction in the natural inherent productivity of an oil and gas producing formation, or a reduction in the injectivity of a water or gas injection well.” Bennion (1999) points out that the formation damage issue is often overlooked because of ignorance and apathy. In many cases, the operators are not seriously concerned with formation damage because of the belief that it can be circumvented later on, simply by acidizing and/or hydraulic fracturing. When the damage is limited to the region very close to the wellbore, this rationale makes sense, but the near wellbore damage may be an important issue in certain

cases, such as open hole completions (Bennion, 1999). Because formation damage is usually nonreversible, it is better to avoid formation damage rather than deal with it later on using expensive and complicated procedures (Porter, 1989; Mungan, 1986). In many cases, remedial treatments may also cause other types of damages, while the intent is to cure the present damage problems. When asked "Is it more cost effective to prevent formation damage or bypass it?" (JPT, ©1994 SPE; reprinted by permission of the Society of Petroleum Engineers), some experts replied as following:

McLeod: "There is no universal answer for this question. Often the formation quality determines whether it is more cost effective to prevent damage or to remove it or bypass it later by acidizing or hydraulic fracturing. Generally, damage prevention is more cost effective than removing or bypassing damage later."

Peden: "Prevention of damage must be cost effective but it requires a greater understanding of the physics of the processes, as well as an improvement both in our predictive and operational techniques. Bypassing damage can never be an attractive alternative to damage minimization."

Penberthy: "If it is more cost effective to prevent damage, then that is probably the best solution. If an effective, inexpensive acid job or a minifrac treatment is less expensive than the cost of the completion fluid, the post-treatment approach probably should be selected."

Some of the other comments of the experts are quoted in the following from JPT (1994):

Burnett: "If there is existing formation damage in a well, there are three choices: live with it; fracture or perforate past it; or use some means of removing it. The choice depends upon economics and technology.

The key to formation damage cleanup is understanding what has caused the damage. The damage may be caused by tenacious filter cakes, particle invasion into the rock, and/or fluid-filtrate chemical damage. Many of us believe that particulate damage extends only a few tenths of a foot into a zone. On the other hand, chemical damage (clay reactions, formation fines movement, rock/fluid incompatibility, and precipitation) can exist tens of feet into the pay zone. Near-well damage can be reduced (but not eliminated) with acids, oxidizers, and solvents. If you have deep damage, then sidetracking is nearly always the best option."

Peden: "The further we get away from the borehole, the less control we have over our ability to clean up or remove impairment . . . However, formation damage is largely characterized by a lack of understanding of the potential of the processes and the mechanisms involved . . . Greater understanding, training, and technology transfer is required between the service and operating-company sectors."

Penberthy: "One of the main causes for formation damage is using techniques, procedures, and fluid systems that are known to cause problems and risking the chance that somehow the operator will be able to "get by with it."

Whether a particular fluid is nondamaging depends on the particular site-specific application and formation in which the well is completed; i.e., there may be no such thing as a universal non-damaging completion fluid. Suggestions are to use clear brines that are compatible with the reservoir rock.

I will specify the guidelines for selecting an ideal fluid. While it may be rare that all properties can be achieved, compromising between fluid properties and characteristics should identify completion fluids that will provide acceptable results.

An ideal completion fluid should be compatible with the reservoir rock (nondamaging) and have low fluid loss, acceptable suspension and transport properties, thin filter cake, and low friction loss. The density should be easily controlled. The fluid should also be readily available, inexpensive, easily mixed and handled, and nontoxic."

Ali: "All brine systems are potentially formation damaging at high temperatures. In addition, unfavorable fluid/rock interaction at relatively low temperature can produce mobile fines with the added potential for the precipitation of carbonate, sulfide, sulfate, and sodium-chlorite scales. The need for thoroughly evaluating the compatibility of completion fluids with formation brine, formation mineralogy, and produced fluids cannot be overly stressed."

Burnett: "In fields we have studied, we've found that formation damage from water-based fluids was no worse than corresponding oil-based or synthetic fluids. The key is ensuring that the fluid, whatever it may be, is compatible with the formation fluids and the rock matrix."

McLeod: "In high-permeability formations, polymers and other fluid-loss control materials can cause severe damage if not mixed properly. Sometimes that damage may be removed by appropriate

acidizing. If fluid-loss pills are not used, sometimes fluid losses are so high that they pick up contaminants still attached to tubing and casing surfaces after incomplete cleaning of mud, rust, and other particles. Those particles are carried into the formation, where they are filtered out and reduce permeability.

Good filtration of compatible brines and shearing and filtering of polymers used for fluid-loss control are key to preventing or reducing damage. Even with good hydration techniques, microgels in polymer solutions can plug formations unless the microgels are reduced or removed by shearing and filtration before their placement in the well."

Peden: "To establish fluid-selection procedures, realize that formation damage is a result of either a solid/solid interaction between the drilling-mud particulates and the formation or a fluid/fluid interaction resulting from the base fluid interacting with the reservoir fluid. Or alternately, it is an interaction between the base fluid of the drilling mud and the rock constituents. To select appropriate fluids, devise testing programs that address those issues."

Ali: "By conducting core displacement tests with various drilling fluids on representative reservoir samples, the least damaging drilling fluid can be selected. In addition, fluid rheology, solids content and size distribution, overbalance pressure, formation permeability, and other parameters can be considered for selecting well-specific fluid systems."

Burnett: "We . . . recommend that our clients obtain certain basic information about the formation and about the fluids that contact the formation. Information such as mineral content, porosity, permeability, and formation pore-size distribution can be used to screen completion fluids."

Formation damage control and remediation is both a science and an art. There are no universally proven technologies that are panacea for all problems. Creative approaches, supported by science and laboratory and field tests yield the best solution. An examination of the reported studies reveals that numerous recipes and/or recommended procedures have been developed. However, their applicability and/or effectiveness have been validated for certain specific rock and fluid systems and, therefore generalization of these approaches is questionable. In this chapter, some of the more common treatment methods are reviewed. However, their applicability in specific fields should be investigated and

adapted by laboratory core testing. Here, they are only provided for instructional purposes, as our learning curve is still evolving, judging by the new techniques that are being introduced in the literature.

Selection of Treatment Fluids

As expressed by Thomas et al. (1998),*

The type and location of the damage must be determined to select the proper treating fluids . . . Additionally, precautions should be taken to avoid further damage. Damage can be from emulsions, wettability changes, a water block, scale, organic deposits (paraffin and asphaltenes), mix deposits (a mixture of scale and organic material), silt and clay, and bacterial deposits. In most cases, the type or types of damage cannot be precisely identified with 100% accuracy. However, the most probable type or types can be determined; therefore, most matrix treatments incorporate treating fluids to remove more than one type of damage.

The selection of the treatment fluids depends on the specific applications and purposes. The treatment fluid volumes are usually determined by means of laboratory core tests and mathematical models. Treatment fluids should contain various additives for various purposes. Thomas et al. (1998) explain the issue of additives as following:

Although proper fluid selection is critical to the success of a matrix treatment, the treatment may be a failure if the proper additives are not used. The major treating fluid is designed to remove the damage effectively. Additives are used to prevent excessive corrosion, sludging and emulsions, provide uniform fluid distribution, improve cleanup, and prevent precipitation of reaction products. Additionally, additives are used in preflushes and overflushes to stabilize clays, disperse paraffins and asphaltenes and inhibit scale and organic deposition. Additive selection is primarily dependent upon the treating fluid, the type of well, bottom-hole conditions, the type of tubulars, and the placement technique . . . Diverters are essential to obtain uniform fluid distribution in a horizontal well.

The volume of each additive used is dependent on the specific problem addressed. For example, surfactants are commonly used at 0.2 to 0.5% to lower surface and interfacial tension and provide water wetting. As a rule, the minimum amount of additive should be used. Normally, the recommended concentration is determined in the laboratory and is based on testing (i.e., nonemulsifiers, anti-sludge agents).

* Reproduced by permission of the Society of Petroleum Engineers, ©1998 SPE.

Clay Stabilization

When clays are exposed to low salinity solutions, two mechanisms cause formation damage (Himes et al., 1991). Swelling clays imbibe water into their crystalline structure and enlarge in size and plug the pore space. Mobilization, migration, and deposition of clays can plug the pore throats.

Himes et al. (1991) describe the desirable features of effective clay stabilizers, especially for applications in tight formation as following:

1. The product should have a low, uniform molecular weight to prevent bridging and plugging of pore channels.
2. The chemical should be nonwetting on sandstone surfaces to reduce water saturation.
3. It should have a strong affinity for silica (clay) surfaces to compete favorably with the gel polymers for adsorption sites when placed from gelled solutions and to resist wash-off by flowing hydrocarbons and brines.
4. The molecule must have a suitable cationic charge to neutralize the surface anionic charges of the clay effectively.

Inorganic Cations (IC)

Clay stabilization can be maintained by the aqueous solution salinity above that of the connate water (Himes et al., 1991). Figure 23–1 by Himes et al. (1991) shows the clay stabilizing effectiveness of various brines. The basal spacing versus the salt concentrations are shown as an indication of clay swelling, measured by x-ray diffraction (XRD). The clay will disperse when the basal spacing is greater than 21\AA (Himes et al., 1991). In this respect, Figure 23–1 indicates that the clays are stable even at very low concentrations of K^+ and NH_4^+ cations; whereas, a sufficiently high concentration of Na^+ cation is necessary to maintain clay stability. Therefore, K^+ and NH_4^+ are natural clay stabilizers, but are not permanent because they can be exchanged with Na^+ (Himes et al., 1991). Figure 23–1 shows that calcium ion can maintain clay stability, but it is not preferred as a clay stabilizing agent because it may react with formation brines and chemical additives (Himes et al., 1991). Cesium cation (Cs^+) is also very effective at low concentrations, but it is very rare and expensive (Khilar and Fogler, 1985; Himes et al., 1991). Damage resulting from clay swelling and mobilization, migration, and redeposition can be prevented by adding certain ions to stabilize the clays in workover and injection fluids (Keelan and Koepf, 1977). Five percent solutions of $CaCl_2$ and KCl , and hydroxy-aluminum ($OH-Al$) may be effective (Keelan and Koepf, 1977).

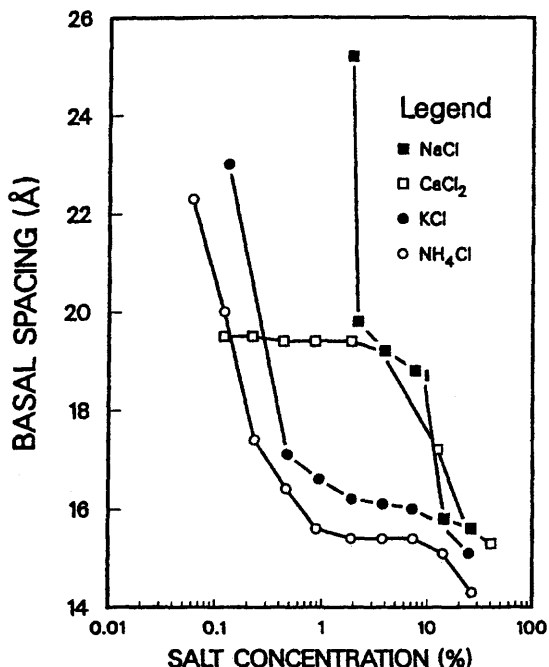


Figure 23-1. Basal spacing of smectite clay vs. concentration of various brines (after Himes et al., ©1991 SPE; reprinted by permission of the Society of Petroleum Engineers).

Cationic Inorganic Polymers (CIP)

In order to provide somewhat permanent clay stabilization, cationic inorganic polymers (CIP) such as hydroxyl aluminum and zirconium oxychloride, have been introduced (Reed, 1974; Valey and Coulter, 1968; Coppell et al., 1973; Himes et al., 1991). These agents provide resistance to cation exchange, but they are applicable for clay stabilization in non-carbonate containing sandstones and the formation should be retreated after acidizing (Himes et al., 1991).

Cationic Organic Polymers (COP)

Quaternary cationic organic polymers (COP) are used for effective and permanent stabilization of clays (especially smectite clays), and controlling fines and sand in sandstone as well as carbonate formations (Himes et al., 1991). They are applicable in acidizing and fracturing treatments.

They provide permanent protection because of the availability of multiple cationic sites of attachment. However, their applicability in tight formations is limited to low concentrations (Himes et al., 1991). They can cause permeability damage by pore plugging because these high molecular weight and long-chain polymers have molecular sizes comparable with the some pore size fractions in porous rock. They can also increase the irreducible water content of porous rock because they are hydrophobic and water-wetting. Their effectiveness is substantially lower in gelled-water solutions used for hydraulic fracturing and gravel-packing as indicated by Table 23-1 by Himes et al. (1991) because of gel competition for adsorption on clay surfaces.

Oligomers

Oligomers are low-molecular-weight, cationic, organic molecules having an average of $0.017\ \mu\text{m}$ length (Penny et al., 1983; Himes et al., 1991). Oligomers offer many potential advantages over the cationic organic polymers for clay stabilization (Himes et al., 1991). Availability of many repeating sites and high affinity for clay surfaces enables better competition of oligomers with gels in water used for hydraulic fracturing and gravel-packing. Because of their smaller size compared to pore size, the treatment-imposed permeability damage is significantly reduced. Because they are only slightly water-wetting (contact angle is 72°), the irreducible water content is also reduced. Zaitoun and Berton (1996) examined the effectiveness of cationic polyacrylamides (CPAM) and nonionic polyacrylamides (PAM) for stabilization of montmorillonite clay by means of the critical salinity concentration method (CSC). As schematically depicted in Figure 23-2 by Zaitoun and Berton (1996), the polymers prevent fines migration by coating over the pore surface and

Table 23-1
Basal Spacing of Smectite Clay Exposed to Various Brines

Solution	Spacing—Dry (Å)
2% KCl + 1% COP	14.8
2% KCl + 0.5% HPG	18.7
2% KCl + 0.5% HPG + 1% COP	17.3
2% KCl + 1% oligomer	14.3
2% KCl + 0.5% HPG + 1% oligomer	14.3

After Himes et al., ©1991 SPE; reprinted by permission of the Society of Petroleum Engineers.

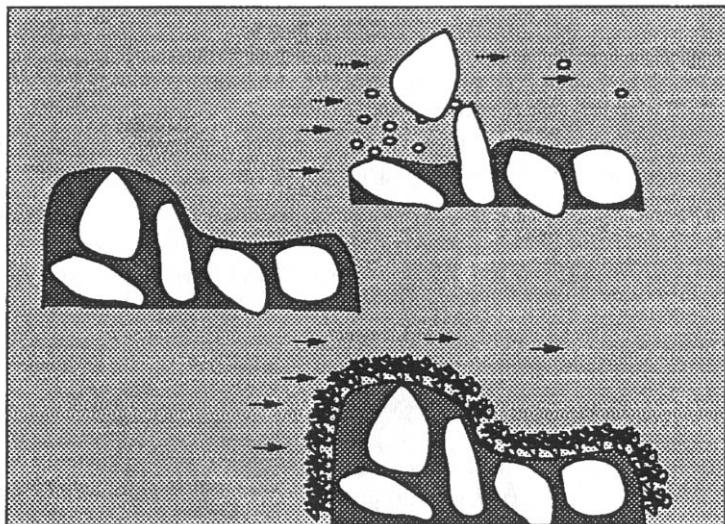


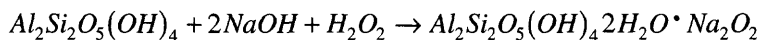
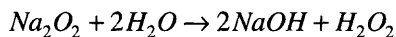
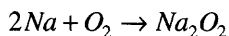
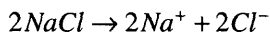
Figure 23–2. Polymer coating of pore surface for clay migration prevention (after Zaitoun and Berton, ©1996 SPE; reprinted by permission of the Society of Petroleum Engineers).

blocking the clay particles. They determined that low-molecular-weight polymers have comparable stabilizing capability to high-molecular-weight polymers and are more advantageous because they cause less treatment-induced permeability damage.

Kalfayan and Watkins (1990) used organosilane compounds as additives to acid systems to prevent the weakening of the rock by acid dissolution. This additive undergoes a hydrolysis reaction to form silanols, which tie to the silanol sites present on siliceous mineral surfaces and forms a polysiloxane coating to bind clay and siliceous fines in place.

***pH*-Buffer Solutions**

Buffering is an effective means of *pH* control by maintaining the hydrogen ion activity constant in spite of the changing conditions. Buffer capacity expresses the sensitivity of *pH* of an aqueous solution to adding a strong base (Gustafsson et al., 1995). Hayatdavoudi (1998) hypothesizes that alteration of kaolinite to dickite, nacrite, and halloysite, through chemical oxidation according to the following reactions, may be responsible for fines generation, at high *pH* in the presence of alkali hydroxides.



Therefore, Hayatdavoudi (1998) recommends buffering the *pH* of brines to 8 or below and avoid aeration of injected fluids to prevent kaolinite comminution-induced formation damage. Hayatdavoudi (1998) also recommends adding ammonium chloride and/or ammonium sulfate buffers to prevent silicate dissolution at high *pH* environments.

Clay and Silt Fines

The fluid selection studies conducted by Thomas et al. (1998) have indicated that:

1. The sandstone formation damage can be treated by fluids that can dissolve the materials causing the damage.
2. The carbonate (limestone) formations are very reactive with acid and, therefore, the damage can be alleviated by dissolving or creating wormholes to bypass the damaged zone. If there is a silt or clay damage, *HCl* should be used to bypass the damage. The damage by calcium fluoride precipitation cannot be treated by *HCl* or *HF* acid treatment.

Formation damaged by silt and clay fines introduced by drilling, completion or production operations require different acid treatment recipes that vary by the formation type, location of damage and temperature (Thomas et al., 1998). Recipes recommended for acidizing of carbonate (limestone) formations are outlined in Figure 23–3 by Thomas et al. (1998).

Motta and Santos (1999) proposed that certain blends of fluosilicic acid (H_2SiF_6) with hydrochloric acid (*HCl*) or an organic acid, such as acetic acid (*HAc*) can dissolve clays and feldspars without reacting with the quartz. These systems remove deep clay damage in sandstone formations, without the usual adverse effects of the secondary precipitation reaction encountered in conventional acidizing by *HF* or H_2SiF_6 alone. Motta and Santos (1999) have determined that properly designed acid blends can substantially reduce the skin in the field. Gdanski and Shuchart (1996) have shown that the equilibrium condition between fluosilicic acid and

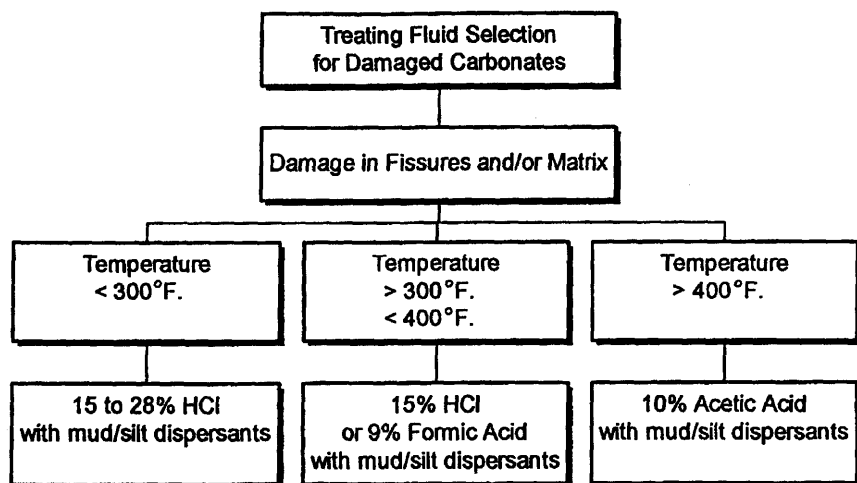


Figure 23–3. Fluid selection for carbonate acidizing (after Thomas et al., ©1998 SPE; reprinted by permission of the Society of Petroleum Engineers).

hydrochloric acid controls the extent of the primary and secondary reactions of hydrofluoric acid with the aluminum silicates.

Fluoboric acid (HBF_4) is a retarded acid, which reacts with the alumina layers of clays to form a borosilicate film. The borosilicate film prevents the migration of in-situ clay and silt fines at high shear-rates of flow because the borosilicate film stabilizes the fine particles in petroleum-bearing formations (Thomas and Crowe, 1978; Colmenares et al., 1997). The fluoboric acid can be effective for applications extending 3 to 5 feet from the wellbore (Ezeukwu et al., 1998).

Bacterial Damage

Bacteria growth in injection wells can cause many problems including plugging of the near-wellbore formation. Johnson et al. (1999) recommend the use of 10-wt% anthrahydroquinone disodium salt in caustic to control the growth of sulfate-reducing bacteria (SRB) combined with the traditional biocide treatment for control of other types of bacteria. For example, bacteria-induced formation damage in injection wells can be treated using a highly alkaline hypochlorite solution, followed by a HCl overflush for neutralization of the system (Thomas et al., 1998).

Inorganic Scales

Scales can be removed by various methods. Carbonate scales can be dissolved by *HCl*, organic acids, and dihydrogen ethylenediamine tetraacetic acid. Iron scales can be dissolved using *HCl* and an iron stabilizer. When *FeS* is present, iron reducing and chelating (or sequestering) agents should be added to the treatment fluid to avoid any precipitation (Thomas et al., 1998). Chelating agents chemically bind the hydrated metal ions and change the reactivity of these ions and, therefore, prevent precipitation of iron (III) hydroxide at $pH > 2.5$ (Brezinski, 1999). The reaction of ferric ion with hydrogen sulfide causes sulfur precipitation. Reaction of ferrous iron with H_2S above $pH = 1.9$ causes *FeS* precipitation. Scale inhibitors may also interfere with the crystallization phenomena by blocking the sites available for crystal growth and prevent the adhesion of scales to metal surfaces (Meyers et al., 1985). Brezinski (1999) has demonstrated that some of the frequently used chelating agents, such as ethylenediaminetetra acedic acid (EDTA) and nitrilotriacetic acid (NTA), may not be effective in downhole temperature conditions because they may decompose at temperatures at or above 250°F. Therefore, Brezinski (1999) recommends removing H_2S using a hydrogen sulfide scavenger as the only method of preventing *FeS* production.

Scale inhibitor squeeze method is resorted to prevent the precipitation of inorganic salts, including barium/strontium/calcium sulfates, calcium/barium/magnesium carbonates, and calcium fluoride. The effectiveness of the scale inhibitors is severely reduced at high temperature and pressure environments prevailing at most wellbore conditions because of thermal decomposition. In fact, the thermal stability studies with several inhibitors, such as penta and hexa-phosphonates, phosphino polycarboxylate (PPC), polyvinyl sulfonate (PVS), and sulfonated polyacrylate copolymer (SPC), conducted by Graham et al. (1997), indicate that they are stable up to 175°C. Hydroxide scales can be dissolved by *HCl* and organic acids, sulfate scales can be dissolved gradually by *EDTA*, chloride scales can be dissolved by aqueous solutions of weak *HCl* or brine, and silica scales can be dissolved using mud acids (Thomas et al., 1998).

Organic Deposits

Organic deposits, such as paraffins and asphaltenes, can be dissolved with aromatic solvents, mutual solvents, blends of aromatic and mutual solvents or their dispersion in water (Thomas et al., 1998).

Asphaltine flocculization and deposition can be prevented by adding resins and aromatics (Leontaritis et al., 1992). Samuelson (1992) has

demonstrated that combined non-aromatic solvents yield the best solvent performance. Barker et al. (1999) tested solvent treatment for removal of the paraffin deposits and applied crystal modifier squeezing to prevent paraffin crystallization.

Mixed Organic/Inorganic Deposits

Mixed organic/inorganic deposits can be dissolved using acid dispersed in an organic solvent (Thomas et al., 1998).

Formation Damage Induced by Completion-Fluids and Crude-Oil Emulsions

Foxenberg et al. (1998) tested some blends of solvents and surfactants and demonstrated that certain blends are effective in providing compatibility between completion-fluids and crude-oils for gravel-packing applications.

Polymer-specific damage associated with drilling, completion, stimulation, and workover operations can be treated by breaking long-chain molecules to short-chain molecules by means of suitable enzymatic degradation reactions.

Filter-cake forming agents can be typically used to prevent the invasion of fines and filtrates of drilling muds and hydraulic fracturing fluids into the reservoir formation by forming an impermeable filter cake over the sand face.

Zhang et al. (1998) propose the use of alpha- and beta-methyl glucosides (*MEG*). These are chemical derivatives of glucose produced from corn starch and, therefore, are environmentally acceptable. These low interfacial tension pore-bridging substances can form low-permeability filter cakes over the sand face of low- and high-permeability formations.

Wettability Alteration and Emulsion and Water Blocks

Wettability change, converting the formation toward oil-wet condition, can be reversed using mutual solvent, blends of mutual solvent and surfactant, and surfactants (Thomas et al., 1998).

Water external emulsions can be decomposed by aqueous solutions of mutual solvents, blends of solvents and surfactants, and alcohol and mutual solvent mixtures (Thomas et al., 1998). Oil external emulsions can be decomposed by means of the blends of aromatic and mutual solvents, such as toluene and xylene (Thomas et al., 1998).

Water blocks can be removed using mutual solvents, blends of aromatic and mutual solvents, blends of alcohol and mutual solvents, and non-aqueous acetic acid containing 10% glacial acetic acid in diesel (Thomas et al., 1998).

Intense Heat Treatment

Jamaluddin et al. (1998) proposed intense heat treatment for enhancing the damaged near-wellbore formation by clay swelling and water block. They show that intense heat treatment works using several mechanisms. Intense heat application dehydrates the clays and destroys the clay lattices, vaporizes the blocked water, and creates microfractures by thermally-induced stress generation in the near-wellbore region.

Stimulation by Hydraulic Fracturing

Stimulation by hydraulic fracturing is an effective technique for circumventing well damage. The productivity improvement is usually adversely affected because of the matrix damage by water block, fines invasion during leak-off, and clay swelling, especially in low permeability formations (Keelan and Koepf, 1977). However, the fractured-well productivity can be increased substantially using compatible fluids and properly selected leak-off control additives (Keelan and Koepf, 1977).

Summary

Summary of the formation treatment methods for various purposes is given in Table 23-2 on the following pages.

References

- Amaefule, J. O., Ajufo, A., Peterson, E., & Durst, K., "Understanding Formation Damage Processes," SPE 16232 paper, SPE Production Operations Symposium, 1987, Oklahoma City, Oklahoma.
- Barker, K. M., Sharum, D. B., & Brewer, D., "Paraffin Damage in High Temperature Formations, Removal and Inhibition," SPE 52156 paper, SPE Mid-Continent Operations Symposium, March 28–31, 1999, Oklahoma City, Oklahoma, 10 p.
- Bennion, B., "Formation Damage—The Impairment of the Invisible, by the Inevitable and Uncontrollable, Resulting in an Indeterminate Reduction of the Unquantifiable!" *Journal of Canadian Petroleum Technology*, Vol. 38, No. 2, February 1999, pp. 11–17.
- Bennion, B., "Experts Share Views on Formation Damage Solutions," *J. of Petroleum Technology*, November 1994, pp. 936–940.

(text continued on page 726)

Table 23–2
Formation Damage Treatment and Preventive Recipes

Agent	Function	Remarks	Reference
Inorganic Cations (IC) K^+ and NH_4^+	Clay stabilizer	<ol style="list-style-type: none"> 1. Nonresistant to cation exchange 2. Not permanent 3. Active above a certain concentration 	Himes et al. (1991)
Cationic Inorganic Polymers (CIP) hydroxyl aluminum and zirconium oxychloride	Clay stabilizer	<ol style="list-style-type: none"> 1. Resistant to cation exchange 2. Permanent 3. Applicable for clay stabilization in non-carbonate-containing sandstones 4. Formation needs to be re-treated after acidizing 	Reed (1974) Valey and Coulter (1968) Coppel et al. (1973) Himes et al. (1991)
Quaternary Cationic Organic Polymers (COP) (5,000 to over 1,000,000 molecular weight long-chain organic polymers, with 1.1 μm average length)	Clay stabilizer Fines control Sand control Water-wetting	<ol style="list-style-type: none"> 1. Stabilizer for smectite clays 2. Contain multiple cationic sites of attachment 3. Acid-resistant and placeable from acidic solutions 4. Unaffected by carbonates 5. Applicable for clay stabilization in carbonate formations 6. Not applicable for permeabilities below 30 md 7. Applicable in acidizing and fracturing 8. Large molecular size of polymer restricts applications in tight formations to low concentrations of the polymer to avoid treatment imposed-permeability damage by pore plugging 9. Water-wetting can increase the irreducible water saturation and lower the relative permeability to oil 	Brown (1956) McLaughlin et al. (1976) Borchardt et al. (1984) Himes et al. (1991)

10. Less effective in gelled-water solutions used for fracturing and gravel-packing			
Oligomer (a low-molecular-weight, cationic, organic molecule, with 0.017 μm average length)	Clay stabilizer	<ol style="list-style-type: none"> 1. Contains many repeating sites and has a high affinity for clay surfaces 2. Applicable in tight formation without creating a treatment-imposed permeability damage 3. Slightly water-wetting (contact angle is 72°) and therefore less irreducible water saturation 4. No significant loss of wash-off by brine or acid 5. Also effective in gelled-water solutions used for fracturing and gravel-packing 	Himes et al. (1991) Penney et al. (1983)
Alpha and beta-Methylglucosides (MEG) (a chemical derivative of glucose produced from corn starch, a low interfacial tension pore-bridging substance)	Shale inhibitor and stabilizer	<ol style="list-style-type: none"> 1. Added to drilling mud 2. Form a low permeability filter cake over sand face to prevent invasion of mud fines and filtrate 3. Applicable to both low and high permeability formations 	Zhang et al. (1998)
Pentaphosphonate (penta-P), hexaphosphonate (hexa-P), phosphinopolycarboxylate (PPC), polyvinyl sulfonate (PVS), sulfonated polyacrylate copolymer (SPC)	Scale inhibitor Scale-control	<ol style="list-style-type: none"> 1. Prevent inorganic precipitates, such as barium/strontium/calcium sulfates, calcium/barium/magnesium carbonates, and calcium fluoride 2. High temperature and pressure environments strongly effect the performance of the inhibitors 3. Proper inhibitor selection is important because inhibitor efficiency usually diminishes at high temperatures because of thermal degradation 4. The PVS inhibitor resists thermal degradation up to 200°C 	Graham et al. (1997)

Table 23–2 (continued)

Agent	Function	Remarks	Reference
		<p>The phosphonate inhibitors become unstable at and above 175°C</p> <p>The PPC inhibitors are stable at 175°C and better than the PPC inhibitors</p>	
Blends of solvents/surfactants	<ol style="list-style-type: none"> 1. Provide completion-fluid and crude-oil compatibility 2. Soluble in the brines and prevents emulsion forming with the crude-oil 	<ol style="list-style-type: none"> 1. Certain blends effective in CaCl_2, $\text{CaCl}_2/\text{CaBr}_2$, and ZnBr_2 brines 2. Applicable in gravel-packing 	Foxenberg et al. (1998)
Buffer solution	<ol style="list-style-type: none"> 1. Provide pH control 	<ol style="list-style-type: none"> 1. Buffering the pH of the brine to 8 at the maximum to prevent kaolinite comminution-induced damage 2. Addition of ammonium chloride and/or ammonium sulfate buffers can prevent dissolution of silicates at high pH solution 	Hayatdavoudi (1998)
8-wt % of water solution of tetra sodium salt of ethylene diamine tetraacetic acid (Na_4EDTA)	<ol style="list-style-type: none"> 1. Dissolves gypsum (CaSO_4) at high temperatures 2. Produces calcium disodium salt of ethylenediamine tetraacetic acid (CaNa_2EDTA), which is soluble in water 	Used for opening of plugged perforations	Číkeš et al. (1990)

Blends of fluosilicic acid (H_2SiF_6) with hydrochloric acid (HCl) or an organic acid, such as acetic acid (HAc)	Dissolves clays and feldspars, but does not react with quartz	<ol style="list-style-type: none"> 1. Removes deep clay damage in sandstone formations 2. The usual adverse effects of the secondary precipitation reactions are effectively eliminated 3. The equilibrium condition between fluosilicic acid and HCl controls the primary and secondary reactions of HF with aluminosilicates 	Motta and Santos (1999) Gdanski and Shuchart (1996)
Cationic polyacrylamides (CPAM) and nonionic polyacrylamides (PAM)	<ol style="list-style-type: none"> 1. Polymer coating by adsorption 2. Stabilize montmorillonite clay 	CPAM better stabilizes clays than PAM but PAM is preferred because of less treatment-imposed permeability damage	Zaitoun and Berton (1996)
Organosilane compound OR $\begin{array}{c} \\ \text{RO} - \text{Si} - \text{OR} \\ \\ \text{R}'\text{NH}_2 \end{array}$ (R and R' are suitable hydrolyzable organic groups)	<ol style="list-style-type: none"> 1. Prevents migration of clay and non-clay siliceous fines and controls dissolution of formation minerals by sandstone acidizing 2. Forms a polysiloxane coating to bind clay and siliceous fines in place 	<ol style="list-style-type: none"> 1. Added to acidizing solutions, such as HCl/HF acid 2. Prevents the reduction of rock strength and formation collapse during acidizing 	Kalfayan and Watkins (1990)
Fluoboric acid (HBF_4) (a retarded acid)	Reacts with the alumina layers of clays to form a borosilicate film, which permanently stabilize the clays	<ol style="list-style-type: none"> 1. Used for matrix treatment to prevent clay fines-induced formation damage 2. Effective for applications 3 to 5 ft from the wellbore 	Thomas and Crowe (1978) Colmenares et al. (1997) Ezeukwu et al. (1998)

Table 23–2 (continued)

Agent	Function	Remarks	Reference
Resins, aromatic solvents (toluene, xylene, heavy aromatic naphthas), combined non-aromatic solvents, polymeric dispersants, asphaltene inhibitors, multi-aromatic natural solvents, condensates	Prevent asphaltene flocculation	Combined solvents work better	Leontaritis et al. (1992) Samuelson (1992) Bouts et al. (1995) King and Cotney (1996)
Enzyme degradants	Enzymatic degradation of long chain to short chain polymers	Treats guar, starch, and cellulose-based residual polymer-specific damage associated with drilling, completion, stimulation, and workover operations	Tjon-Joe-Pin et al. (1993) Tjon-Joe-Pin et al. (1998)
Crystal modifiers, oil/solvent/ chemical treatment, paraffin dispersant	Paraffin removal and inhibition	Solvent treatment removes the deposits and crystal modifier squeezing prevents crystallization of paraffins	Barker et al. (1999)
Anthrahydro quinone disodium salt in caustic (10-wt% concentration) combined with biocide treatments	Controls the growth of sulfate-reducing bacteria (SRB) and other bacteria	Prevents bacteria growth and inhibit sulfate reduction in wells	Johnson et al. (1999)

Intense heat treatment	<ol style="list-style-type: none"> 1. Remediates clay-related damage by dehydration of the clay and by destroying clay lattices 2. Vaporizes blocked water 3. Creates microfractures in the near-wellbore region by the thermally-induced stresses 4. Increases near-wellbore formation permeability 	Structural changes of clay minerals depend on temperature	Jamaluddin et al. (1998)
------------------------	--	---	--------------------------

(text continued from page 719)

- Bennion, D. B., Thomas, F. B., & Bennion, D. W., "Effective Laboratory Coreflood Tests to Evaluate and Minimize Formation Damage in Horizontal Wells," Third International Conference on Horizontal Well Technology, Houston, Texas, November 1991.
- Bennion, D. B., & Thomas, F. B., "Underbalanced Drilling of Horizontal Wells: Does it Really Eliminate Formation Damage?," SPE 27352 paper, SPE Formation Damage Control Symposium, Lafayette, Louisiana, February 1994.
- Bennion, D. F., Bietz, R. F., Thomas, F. B., & Cimolai, M. P., "Reductions in the Productivity of Oil & Gas Reservoirs due to Aqueous Phase Trapping," CIM Annual Technical Conference, Calgary, May 1993.
- Borchardt, J. K., Roll, D. L., & Rayne, L. M., "Use of a Mineral-Fines Stabilizer in Well Completions," SPE 12757 paper, SPE California Regional Meeting, April 11–13, 1984, Long Beach, California.
- Bouts, M. N., Wiersma, R. J., Muijs, H. M., & Samuel, A. J., "An Evaluation of New Asphaltene Inhibitors: Laboratory Study and Field Testing," *J. of Petroleum Technology*, September 1995, pp. 782–787.
- Brezinski, M. M., "Chelating Agents in Sour Well Acidizing: Methodology or Mythology," SPE 54721 paper, Proceedings of the SPE European Formation Damage Conference, May 31–June 1, 1999, Hague, The Netherlands, pp. 127–131.
- Brown, W. E., "Treatment of Clays," U.S. Patent No. 2,761,835, September 4, 1956.
- Cikes, M., Vranjesevic, B., Tomić, M., & Jamnicky, O., "A Successful Treatment of Formation Damage Caused by High-Density Brine," *SPE Production Engineering*, May 1990, pp. 175–179.
- Colmenares, F. J., Padron, A., & Bennaceur, K., "Evaluation of Treatments for Control of Fines Migration in the Ceuta Field in Venezuela," SPE 38596 paper, SPE Annual Technical Conference and Exhibition, October 5–8, 1997, San Antonio, Texas, pp. 317–325.
- Coppell, C. P., Jennings, H. Y., & Reed, M. G., "Field Results from Wells Treated with Hydroxy-Aluminum," *J. of Petroleum Technology*, September 1973, pp. 1108–1112.
- Ezeukwu, T., Thomas, R. L., & Gunnerød, T., "Fines Migration Control in High-Water-Cut Nigerian Oil Wells," *J. of Petroleum Technology*, March 1998, pp. 88–89.
- Foxenberg, W. E., Ali, S. A., Ke, M., Shelby, D. C., & Burman, J. W., "Preventing Formation Damage Caused by High-Density Completion-Fluid/ Crude-Oil Emulsions," *J. of Petroleum Technology*, November 1998, pp. 60–61.

- Gdanski, R. D., & Shuchart, C. E., "Newly Discovered Equilibrium Controls HF Stoichiometry," *J. of Petroleum Technology*, February 1996, pp. 145-149.
- Graham, G. M., Jordan, M. M., Graham, G. C., Sablerolle, W., Sorbie, K. S., Hill, P., & Bunney, J., "Implication of High-Pressure/High-Temperature Reservoir Conditions on Selection and Application of Conventional Scale Inhibitors: Thermal-Stability Studies," *J. of Petroleum Technology*, June 1997, pp. 632-633.
- Gustafsson, T. K., Skrifvars, B. O., Sandström, K. V., & Waller, K. V., "Modeling of pH for Control," *Ind. Eng. Chem. Res.*, Vol. 34, 1995, pp. 820-827.
- Hayatdavoudi, A., "Controlling Formation Damage Caused by Kaolinite Clay Minerals: Part II," SPE 39464 paper, SPE International Symposium on Formation Damage Control, February 18-19, 1998, Lafayette, Louisiana, pp. 421-429.
- Himes, R. E., Vinson, E. F., & Simon, D. E., "Clay Stabilization in Low-Permeability Formations," *SPE Production Engineering*, August 1991, pp. 252-258.
- Jamaluddin, A. K. M., Vandamme, L. M., Nazarko, T. W., & Bennion, D. B., "Heat Treatment for Clay-Related Near-Wellbore Formation Damage," *Journal of Canadian Petroleum Technology*, Vol. 37, No. 1, January 1998, pp. 56-63.
- Johnson, M. D., Harless, M. L., Dickinson, A. L., & Burger, E. D., "Chemical Mitigation of Sulfide in Water-Injection Systems," *J. of Petroleum Technology*, March 1999, pp. 75-76.
- JPT, "Experts Share Views on Formation Damage Solutions," *J. of Petroleum Technology*, November 1994, pp. 936-940.
- Kalfayan, L. J., & Watkins, D. R., "A New Method for Stabilizing Fines and Controlling Dissolution During Sandstone Acidizing," SPE 20076 paper, 60th California Regional Meeting, April 4-6, 1990, Ventura, California, pp. 539-546.
- Keelan, D. K., and Koepf, E. H., "The Role of Cores and Core Analysis in Evaluation of Formation Damage," *J. of Petroleum Technology*, May 1977, pp. 482-490.
- Khilar, K. C., & Fogler, H. S., "The Existence of a Critical Salt Concentration for Particle Release," *J. Colloid Interface Sci.*, Vol. 101, No. 1, September 1985, pp. 214-224.
- King, S. R., & Cotney, C. R., "Natural Solvents for Paraffin and Asphaltene Problems," *J. of Petroleum Technology*, August 1996, pp. 723-724.
- Leontaritis, K. J., Amaefule, J. O., & Charles, R. E., "A Systematic Approach for the Prevention and Treatment of Formation Damage Caused by Asphaltene Deposition," SPE 23810 paper, SPE International Symposium on Formation Damage Control, Lafayette, Louisiana, February 26-27, 1992, pp. 383-395.

- McLaughlin, H. C., Elphinstone, E. A., & Hall, B. E., "Aqueous Organic Polymers for Treating Clays in Oil and Gas Producing Formations," SPE 6008 paper, SPE Annual Technical Conference and Exhibition, October 3–6, 1976, New Orleans, Louisiana.
- Meyers, K. O., Skillman, H. L., Herring, G. D., "Control of Formation Damage at Prudhoe Bay, Alaska, by Inhibitor Squeeze Treatment," *J. of Petroleum Technology*, 1985, pp. 200–215.
- Motta, E. P. D., & Santos, J. A. C. M. D., "New Fluosilicic Acid System Removes Deep Clay Damage," SPE 54729 paper, SPE European Formation Damage Conference, May 31–June 1, 1999, The Hague, The Netherlands, pp. 239–245.
- Mungan, N., "Discussion of An Overview of Formation Damage," *J. of Petroleum Technology*, Vol. 41, No. 11, p. 1224, Nov. 1989.
- Odanski, R. D., & Shuchart, C. E., "Newly Discovered Equilibrium Controls HF Stoichiometry," *J. of Petroleum Technology*, February 1996, pp. 145–149.
- Penny, G. S. et al., "Enhanced Load Water-Recovery Technique Improves Stimulation Results," SPE 12149 paper, SPE Annual Technical Conference and Exhibition, September 5–8, 1983, San Francisco, California.
- Porter, K. E., "An Overview of Formation Damage," *J. of Petroleum Technology*, Vol. 41, No. 8, 1989, pp. 780–786.
- Reed, M. G., "Formation Permeability Maintenance with Hydroxy-Aluminum Solutions," U.S. Patent No. 3,827,500, August 6, 1974.
- Samuelson, M. L., "Alternatives to Aromatics for Solvency of Organic Deposits," SPE 23816 paper, SPE International Symposium on Formation Damage Control, February 26–27, 1992, Lafayette, Louisiana, pp. 447–454.
- Thomas, R. L., & Crowe, C. W., "Matrix Treatment Employs New Acid System for Stimulation and Control of Fines Migration in Sandstone Formations, 1978.
- Thomas, R. L., Saxon, A., & Milne, A. W., "The Use of Coiled Tubing During Matrix Acidizing of Carbonate Reservoirs Completed in Horizontal, Deviated, and Vertical Wells," *SPE Production & Facilities*, August 1998, pp. 147–162.
- Tjon-Joe-Pin, R., Brannon, H. D., & Rickards, A. R., "Remedial Treatment for Polymeric Damage Removal Provides Improved Well Productivity," SPE 25214 paper, SPE International Symposium on Oilfield Chemistry, March 2–5, 1993, New Orleans, Louisiana, pp. 65–75.
- Tjon-Joe-Pin, R., DeVine, C. S., & Carr, M., "Cost Effective Method for Improving Permeability in Damaged Wells," SPE 39784 paper, SPE Permian Basin Oil and Gas Recovery Conference, March 25–27, 1998, Midland, Texas, pp. 297–305.

- Valey, C. D., & Coulter, A. W., "Treatment of Earthen Formations Comprising Argillaceous Material," U.S. Patent No. 3,382,924, May 14, 1968.
- Zaitoun, A., & Berton, N., "Stabilization of Montmorillonite Clay in Porous Media by Polyacrylamides," SPE 31109 paper, SPE Formation Damage Control Symposium, February 14–15, 1996, Lafayette, Louisiana, pp. 423–428.
- Zhang, Y., Chen, Z., & Yan, J., "Investigation of Formation-Damage Control of the Methylglucoside Fluids," *J. of Petroleum Technology*, November 1998, pp. 58–59.

Index

A

Absorption rate, water, 28
Acid treatment of wells, 582
Acoustic techniques (at), 111
Activity-activity charts, 342, 362
Adsorption reactions, 332, 405
Alkali flooding, 592
Alteration, flow functions,
 capillary pressure, relative
 permeability, 72
Alteration, wettability, 66
Analysis of laboratory and field
 tests, 552
Aqueous phase reactions, 328
Aqueous speciation models, 337
Aqueous species of the Fe-O-
 H₂O systems, 367
Aqueous species of the Fe-O-
 H₂O-S systems, 370
Aqueous O-H₂O systems, 372
Area open for flow, 53
Asphaltene adsorption, 405
Asphaltene deposition, two-phase,
 dual-porosity model, 428
Asphaltene phase behavior and
 deposition envelopes, 392
Asphaltene precipitation, single-
 phase, empirical algebraic
 model, 410
Asphaltenic oils, characteristics
 of, 382
Assessment of the formation

 damage potential, 455
Attachment mechanisms, forces,
 147

B

Bacterial damage, 716
Bi-modal distribution, 59
Born repulsion force, 148
Brine, 571
Buffer solutions, pH, 714

C

Cake filtration, mechanisms,
 parameters, modeling, 195,
 262
Cake porosity, thickness-
 averaged, 304
Calcite deposition model, 674
Calcite dissolution with the mud
 cleaning acid, 513
Capillary pressure, alteration, 72
Carbon dioxide flooding, 591
Carbonates, saturation index
 charts, 357
Carman-Kozeny equation, flow
 units, modified, 83
Carman-Kozeny equation, porous
 media altered by deposition,
 modified, 84
Carman-Kozeny hydraulic tubes

- model, 80
 - Cation exchange capacity, 111
 - Cationic inorganic polymers, 712
 - Cationic organic polymers, 712
 - Centrifugal force, 146
 - Cernansky and Siroky model, 199, 220, 535
 - Characteristics, asphaltenic oils, 382
 - Characteristics, petrographical, 49
 - Characterization, formation damage, 9
 - Characterization, porous media processes, formation damage, 127
 - Characterization, reservoir rock, 9, 102
 - Chemical equilibria, graphical description, of rock-fluid, 339
 - Clay content, graphical representation of, 42
 - Clay expansion, coefficient, time-dependent, 33
 - Clay fines, control, 715
 - Clay minerals, saturation index charts, 351
 - Clay stabilization, 711
 - Clay swelling
 - coefficient, 31
 - mechanisms, 22
 - models, 25
 - water content, 32
 - Coefficient, clay expansion, time-dependent, 33
 - Coefficient, clay swelling, 31
 - Colloidal release and mobilization, 155, 250
 - Compartments-in-series ordinary differential model, 197
 - Completion fluids, formation damage, control, 718
 - Composition, petroleum-bearing formations, 12
 - Compressive cake filtration
 - including fines invasion, 291, 536
 - Constant-flow-rate tests, 226
 - Constant-pressure-difference tests, 232
 - Constituents, sedimentary, rocks, 11
 - Continuous real time series
 - analysis, detection and monitoring formation damage, 698
 - Control, emulsion, formation damage, completion-fluids and crude-oil emulsions, 718
 - Control, formation damage, 706
 - Core flood tests, 478, 511
 - Core holders, special purpose, 461
 - Core preparation and characterization, 470
 - Critical interstitial fluid velocity and pH for hydrodynamic detachment of fines in porous media, 491
 - Crude-oil emulsions, formation damage, control, 718
 - Crystal growth in porous media, 164
 - Crystal surface displacement by dissolution and precipitation, 178
 - Crystallization, 166
 - kinetics, 171
- D**
- Damage, depth of, 693
 - Damage by formation fines migration, 251
 - Damage by mud filtration, 255
 - Damage by particle invasion, 253
 - Damage ration, 687
 - Deposition
 - calcite, model, 674

Deposition (*continued*)

- Carman-Kozeny equation,
 - altered porous media, modified, 84
- externally introduced particles, 191, 301
- envelopes, asphaltene and wax, 392
- indigenous particles, 193
- porosity and permeability, effect of, 95, 303
- sulfur, model, 669
- Deposits, mixed organic/inorganic, control, 718
- Depth of damage, 693
- Detachment mechanisms, forces, 147
- Detection, continuous real time series analysis, formation damage, 698
- Diagnosis, formation damage, 679
- Diagnostic charts, 192, 279
- Diagnostic equations, formation damage, 191, 279
- Diagnostic type curves, water injectivity tests, 639
- Diffusion force, 146
- Dissolution, permeability, porosity, effect of, 94
- Dissolution, porosity and permeability, effect of, 95
- Distribution
 - bi-modal, 59
 - fractal, 60
 - log-normal, 56
 - pore and pore throat size, 56
- Drilling mud filtrate and solids invasion and mud cake formation, 608
- Dual-porosity model for simultaneous asphaltene-paraffin deposition, 428

E

- Efficiency, flow, 84
- Electrostatic double-layer force, 148
- Emulsion, formation damage, completion-fluids and crude-oil emulsions, control, 718
- Emulsion block
 - viscosity variation index, 687
 - wettability alteration, 718
- End-point saturation, 72
- Error analysis, propagation, impact, estimation, 556
- Experimental data, model assisted analysis, 213
- Experimental set-up, formation damage testing, 459, 564
- Expert system, formation damage, 702
- Evaluation, formation, 103
- Evaluation, formation damage, laboratory, 456, 478
- Evaluation of drilling mud, 482
- Evaluation of hydraulic fracturing fluids, 488
- Evaluation of workover and injection fluids, 488
- Evaluation of workover damage and remedial chemicals, 491

F

- Fabric, 50
- Factors, formation damage, 4
- Fair-Hatch equation, modified, 93
- Field diagnosis and measurement of formation damage, 680
- Field tests, analysis and interpretation of, 552, 607, 641
- Filter cake formation, 251

- Filtration coefficient, 637
- Finite differences method, 538
- Flow, area open for, 53
- Flow efficiency, 84, 691
- Flow functions, alteration,
 - capillary pressure, relative permeability, 72
- Flow functions, parameters,
 - petrophysics, 66
- Flow units concept, Carman-Kozeny equation, modified, 83
- Flow-units equation, power-law, 94
- Fluid, brine, 571
- Fluid, hydraulic fracturing, 488
- Fluid, preparation, 473
- Fluid, selection, reservoir-compatible fluids, 459
- Fluid, selection, treatment, 710
- Fluid, transport, 241
- Fluid, workover and injection, 488
- Force
 - acting upon particles, 145
 - attachment mechanisms, 147
 - Born repulsion, 148
 - centrifugal, 146
 - detachment mechanisms, 147
 - diffusion, 146
 - electrostatic double-layer, 148
 - friction-drag, hydrodynamic thinning, 147
 - gravity, 145
 - hydrodynamic, 146
 - inertia, 145
 - London-van der Waals, 147
 - shearing, 147
 - transport mechanisms, 145
- Formation
 - brine, 571
 - composition, petroleum-bearing, 12
 - evaluation, 103
 - heterogeneity, 575
 - origin, petroleum-bearing, 11
 - petrography and texture, 49
 - sensitivity, mineralogy, 10, 14, 571, 575
- Formation damage, 1
 - bacterial, 716
 - completion-fluids and crude-oil emulsions, control, 718
 - control and remediation, 706
 - diagnostic equations, 191
 - experimental set-up for testing, 459
 - expert system, 702
 - field diagnosis and mitigation of, 679, 680
 - by fines migration and clay swelling, single-phase, 183
 - by fines migration, two-phase, 238
 - fundamental processes, 458
 - geochemical, inorganic scaling, 323
 - guidelines and program for laboratory testing, 470
 - laboratory evaluation, 456, 478
 - measures of, 684
 - model equations, 529
 - models, numerical solution of, 532
 - monitoring, detection,
 - continuous real time series analysis, 698
 - by organic deposition, 379
 - by particulate processes, 182
 - potential, assessment of, by simulation, 455, 570, 580
 - pseudo-damage, 684
 - reporting, tests, 478
 - by scale deposition, 669
- Forward geochemical modeling, 338

Fractal distribution, 60
Friction-drag force and
hydrodynamic thinning, 147

G

Generalization, cross correlation
of rock properties, 40
Geochemical, formation damage,
inorganic scaling, 323
Geochemical, solid mineral-
aqueous phase interactions,
charts, model assisted
analysis, 344
Geochemical phenomena,
classification, formulation,
modeling, software, 326
Gradual pore reduction by surface
deposition and sweeping,
193
Grain nucleation, growth, and
dissolution, 167
Graphical description of the
rock-fluid chemical
equilibria, 339
Graphical representation of clay
content, 42
Gravel design criteria, 651
Gravel-pack damage, 647
Gravel-pack, sand retention
model, 664
Gravity force, 145
Gruesbeck and Collins model,
201, 224, 421
Guidelines for laboratory
formation damage testing,
470

H

Hayatdavoudi hydration index,
43
Heat treatment, 719

Hydrodynamic detachment,
critical interstitial fluid
velocity and pH for fines
in porous media, 491
Hydrodynamic force, 146
Hydrodynamic thinning, 147
Hydration index, 43
Hydraulic erosion and
mobilization, 156, 250
Hydraulic fracturing fluids, 488,
719
Hydraulic tubes model, Carman-
Kozeny, 80

I

Incompressive cake filtration,
265, 536
Index, hydration, 43
Inertia force, 145
Injectivity, waterflooding wells,
627
Injectivity ratio, 628
Inorganic cations, 711
Inorganic precipitation, 164, 322
Inorganic scaling, geochemical
formation damage, control,
323, 717
Instrumental techniques,
characterization of reservoir
rock, 102
Interconnectivity of pores, 54
Intense heat treatment, 719
Interfaces, particle transfer across
fluid-fluid interfaces, 158
Interpretation of laboratory and
field tests, 552
Inverse geochemical modeling, 338
Ion exchange reactions, 332

K

Khilar and Fogler model,
compartments-in-series

ordinary differential model,
197

Kinetics, crystallization, 171

L

Laboratory techniques,
characterization of reservoir
rock, 102

Laboratory evaluation, formation
damage, 456, 478, 552

Leontaritis model, simplified
analytic model, asphaltene-
induced formation damage
in single-phase, 414

Linear filter cake model, 266,
281, 284, 296

Liquid block problem, 481

Log-normal distribution, 56

London-van der Waals force, 147

M

Macroscopic transport equations,
multi-species and multi-
phase, 133

Measurement error, 554

Mechanism, cake filtration, 195,
262

Mechanism, clay swelling, 22

Mechanism, forces related to
transport, 145

Mechanism, formation damage,
4

Mechanism, heavy organic
deposition, 388

Measures of formation damage,
684

Mineral-aqueous phase
interactions, 344

Mineral quantification,
characterization, analyses,
120, 344

Mineral reactions, 330

Mineral species of the Fe-O-H₂O
systems, 369

Mineral species of the Fe-O-
H₂O-S systems, 370

Mineral stability charts, 339

Mineralogy, sensitivity,
petroleum-bearing
formations, 10, 14

Mixed organic/inorganic deposits,
718

Mitigation, formation damage,
6, 679

Model

calcite deposition, 674

cake filtration, 195, 262

clay swelling, 25

field applications, 607

geochemical phenomena, 326

massive sand production, 658

multi-parameter regression, 92
network, 92

sand retention in gravel-packs,
664

simultaneous asphaltene-
paraffin deposition, two-
phase and dual-porosity
model, 428

sulfur deposition, 669

validation, refinement, and
parameter estimation, 564

Model, asphaltene precipitation

single phase empirical
algebraic model, 410

single phase plugging-
nonplugging pathways
model, 421

single phase simplified
analytic model, 414

single-porosity and two-phase,
438

Model assisted analysis

experimental data, 213, 251,
344, 443

- Model assisted analysis
(*continued*)
 - interpretation of laboratory and field tests, 552
 - near-wellbore permeability alteration using pressure transient data, 694
- Model assisted estimation of skin factor, 694
- Modified Carman-Kozeny equation incorporating the flow units concept, 83
- Mobilization, indigeneous particles, 193
- Monitoring, continuous real time series analysis, formation damage effects, 698
- Mud damage problem, 482, 542
- Multi-parameter regression model, 92
- Multi-phase and multi-species transport in porous media, 128

N

- Near-wellbore permeability alteration, model-assisted analysis, pressure transient data, 694
- Network models, 92
- Nuclear magnetic resonance spectroscopy, 110
- Numerical solution of formation damage models, 532

O

- Ohen et al. model, clayey formation swelling, indigeneous and external particles, 208

- Oil-acid compatibility, 521
- Oligomers, 713
- Ordinary differential equations, 533
- Organic deposition, mechanisms, 388
- Organic deposition, single-porosity and two-phase model, 438
- Organic precipitation, deposits, control, 165, 322, 717
- Origin, formation, petroleum-bearing, 11
- Osmotic repulsive pressure, 27

P

- Paraffin deposition, two-phase and dual-porosity model, 428
- Parameters, cake filtration, 262
- Parameters, estimation with history matching of models, 566
- Parameters, estimation with linearized models, 566
- Parameters, flow functions, petrophysics, 66
- Parameters, textural, 61
- Partial differential equations, 538
- Particle, forces acting, 145
- Particle, pore throats, dislodgment and redeposition, 153
- Particle, transfer across fluid-fluid interfaces, 158
- Particle growth and dissolution in solution, 174
- Particulate processes, porous media, 140, 141
- Particulate processes, porous matrix, rate equations, 148
- Parallel pathways model,

- plugging-nonplugging, 87
- Parity equations, 566
- pe-pH charts, 343, 367
- pH-buffer solutions, 714
- Permeability alteration, pressure
 - transient analysis, near-wellbore, 694
- Permeability
 - effect of deposition/dissolution and stress, 95
 - effect of dissolution/precipitation, 94
 - porosity relationships, 80, 251, 303, 430
 - reduction by swelling, 38
 - temperature effect, 95
 - variation index, 687
- Petrographic image analysis, 109, 500
- Petrographical characteristics, 49
- Petrography, petroleum-bearing formations, 49
- Petroleum-bearing formations
 - composition, 12
 - origin, formation, 11
 - petrography and texture, 49
 - sensitivity, mineralogy, 10
- Petrophysics, flow functions, parameters, 66
- Phase behavior, deposition
 - envelopes, asphaltene and wax, 392
- Plugging-nonplugging parallel pathways model, 87
- Plugging-nonplugging parallel pathways partial differential model, 201, 421
- Polarized light microscopy, 109
- Pore
 - blocking, 195
 - filling after pore throat plugging, 149
 - interconnectivity of, 54
 - size distributions, 56
 - space, spherical approximation, 50
 - throat size distributions, 56
 - throats, plugging, dislodgment and redeposition of particles, 153, 248
- Porosity, 50
 - effect of deposition/dissolution and stress, 95
 - effect of dissolution/precipitation, 94
 - temperature effect, 95
 - thickness-averaged, 304
 - reduction, by swelling, 36
- Porous media, crystal growth and scale formation, 164
- Porous media, macroscopic
 - transport equations, multi-species and multi-phase, 133
- Porous media, multi-phase and multi-species transport, 128
- Porous media, particulate processes, 140, 141
- Power-law flow-units equation, 94
- Precipitation
 - inorganic, 164
 - organic, 165
 - permeability, porosity, effect of, 94
- Pressure-flow relationships, 298
- Pressure
 - osmotic, 27
 - thickness-averaged, 304
 - transient analysis, near-wellbore permeability alteration, 694
- Problems, formation damage, 4
- Program, laboratory formation damage testing, 470

Pseudo-damage, formation damage, 684

R

Reactions in porous media, 328

Reaction-transport geochemical modeling, 339

Real time series analysis, formation damage, monitoring, detection, continuous, 698

Radial filter cake model, 274, 282, 290, 293

Reduction, permeability, by swelling, 38

Reduction, swelling, porosity, 36

Regression, multi-parameter models, 92

Random error, 555

Rate equations, particulate processes in porous matrix, 148

Relationships, permeability, 80

Relative permeability, alteration, 72

Remediation, formation damage, 706

Reporting, formation damage tests, 478

Reservoir properties, from resistivity versus total dissolved solids and temperature relationship, 577

Resistivity versus total dissolved solids and temperature relationship, 577

Rock, composition, 12

Rock, constituents, sedimentary 11

Rock-fluid chemical equilibria, graphical description, 339

Rock, properties, cross

correlation, generalization, 40

Rock, sensitivity, mineralogy, 10, 14

Rock, texture, 49

S

Sand

control, 648

migration, sanding tendency, prediction, control, 647

production, massive, model, 658

retention in gravel-packs, model, 664

Sanding conditions, prediction of, 655

Saturation, end-point, 72

Saturation index charts, 339, 346

Scale formation and dissolution at pore surface, 176

Scale formation in porous media, 164

Scaling from laboratory to bottom hole, 499

Scanning electron microscope, 108

Sedimentary, rocks, constituents, 11

Selection of reservoir-compatible fluids, 459

Selection of treatment fluids, 710

Sensitivity, analysis, stability and conditionality, 561, 568

Sensitivity, mineralogy, petroleum-bearing formations, 10, 14

Shearing force, 147

Silt fines, control, 715

Simplified partial differential model, 199

Simulator development, 528

Single-phase formation damage
 model by fines migration
 and clay swelling, 183
 Single-phase formation damage
 model, clayey formation
 swelling, indigeneous and
 external particles, 208
 Single pore blocking, 195
 Size distributions, pore and pore
 throat, 56
 Skin factor, definition,
 estimation, 685, 694
 Species transport, 241
 Spherical pore space
 approximation, 50
 Stabilization, clay, 711
 Stimulation by hydraulic
 fracturing, 719
 Stress, formation damage,
 sanding tendency,
 prediction, control, sand
 migration, gravel-pack
 damage, 647
 Stress, porosity and permeability,
 effect of, 95, 303
 Surface deposition, 149, 248
 Surface deposition and
 sweeping, gradual pore
 reduction, 193
 Sulfates, saturation index charts,
 357
 Sulfur deposition model, 669
 Swelling
 clay, coefficient, 31
 clay, water content,
 generalization, 32, 40
 mechanisms, clay, 22
 models, clay, 25
 permeability reduction,
 generalization, 38, 40
 porosity reduction,
 generalization, 36, 40
 Systematic error, 556

T

Temperature, effect on porosity
 and permeability, 95
 Test procedures, 475
 Testing, formation damage,
 experimental set-up for, 459
 Textural parameters, 61
 Texture, 50
 Texture, petroleum-bearing
 formations, 49
 Thickness-averaged fluid pressure
 and cake porosity, 304
 Thin section petrography, 109
 Thin slice algebraic model,
 model formulation, 184
 Time-dependent, coefficient, clay
 expansion, 33
 Time series analysis, formation
 damage, monitoring,
 detection, continuous, 698
 Tortuosity, 54
 Total dissolved solids, 577
 Treatment, fluids, selection, 710
 Transition time, 632
 Transport, mechanisms, forces,
 145
 Transport, porous media, multi-
 phase and multi-species,
 128
 Transport, porous media,
 macroscopic equations,
 multi-species and multi-
 phase, 133
 Two-phase formation damage by
 fines migration, 238
 Two-phase model, simultaneous
 asphaltene-paraffin
 deposition, 428

V

Viscosity variation index, 687

W

Water, absorption rate, 28
Water analyses, 346
Water block, wettability alteration, 718
Water content, clay swelling, 32
Water, mixing paths on mineral stability charts, 346
Waterflooding, 585
Waterflooding wells, injectivity of, 627
Wax phase behavior and deposition envelopes, 392
Wettability, 117
Wettability alteration, 66

Wettability alteration, emulsion and water blocks, 718
Wettability transformation and interface transfer of particles, 247
Wojtanowicz et al. Model, 184, 214, 410, 533

X

X-ray CT scanning, 107
X-ray diffraction, 107
X-ray fluoroscopy, 108

Z

Zeta-potential, 116



About the Author

Faruk Civan, Ph.D., is a professor and associate director of reservoir engineering at the School of Petroleum and Geological Engineering at the University of Oklahoma, Norman, Oklahoma, U.S.A. He worked in the chemical engineering department at the Technical University of Istanbul, Turkey, before joining the University of Oklahoma in 1980.

Dr. Civan received an Advanced Engineering degree from the Technical University of Istanbul, Turkey in 1971, an M.S. degree from the University of Texas at Austin, Texas in 1975, and a Ph.D. degree from the University of Oklahoma, Norman, Oklahoma in 1978. All of his degrees are in chemical engineering.

Dr. Civan specializes in formation and well damage modeling, diagnosis, assessment, and mitigation; reservoir and well analyses, modeling, and simulation; natural gas engineering, measurement, processing, hydrates, transportation, and storage; petrophysics and reservoir characterization; improved reservoir recovery techniques; corrosion protection in oil and gas wells; and filtration and separation techniques.

He has co-authored one book chapter, published 68 technical articles in refereed journals, 67 technical articles in various conference proceedings, presented 25 technical papers (unpublished) at various technical meetings, and presented 38 invited seminars and lectures at various companies and universities. Additionally, he has written numerous reports on his funded research projects. Dr. Civan's publications have been cited frequently in various publications, as reported by the Science Author Citation Index.

Dr. Civan has received many honors and awards, including five distinguished lectureship awards. He is a member of the Society of Petroleum Engineers of AIME and the American Institute of Chemical Engineers. Dr. Civan serves as an associate editor for the *Elsevier Journal of Petroleum Science and Engineering*, and the *Turkish Oil and Gas Journal*. He has served in 36 petroleum and chemical engineering, and other related conferences and meetings in various capacities, including as committee chairman and member, session organizer, chair or co-chair, instructor, and as member of the editorial board of the *Society of Petroleum Engineers Reservoir Engineering Journal* and the special authors series of the *Journal of Petroleum Technology*.